14th IEEE International Semiconductor Laser Conference

N00014-94-1-0981

September 19 - 23, 1994

Hyatt Regency Maui
Maui, Hawaii, USA

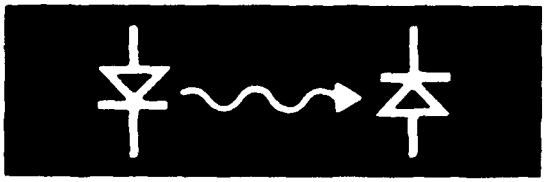

Sponsored by
The IEEE Lasers and
Electro-Optics Society

Supported by:

Advanced Research Projects Agency

Air Force Office of Scientific Research

National Aeronautics and Space Administration (NASA) Jet Propulsion Laboratory

National Institute of Standards & Technology

Office of Naval Research

Sandia National Laboratory

US Air Force Phillips Laboratory

IEEE Catalog #94CH3379-5 Library of Congress #93-80486

14th IEEE
International Semiconductor Laser Conference

September 19 - 23, 1994

Hyatt Regency Maui
Maui, Hawaii, USA

Sponsored by
The IEEE Lasers and
Electro-Optics Society

Supported by:

Advanced Research Projects Agency

Air Force Office of Scientific Research

National Aeronautics and Space Administration (NASA) Jet Propulsion Laboratory

National Institute of Standards & Technology

Office of Naval Research

Sandia National Laboratory

US Air Force Phillips Laboratory

IEEE Catalog #94CH3379-5 **Library of Congress #93-80486**

The papers in this book comprise the digest of the meeting mentioned on the cover and title page. They reflect the author's opinions and are published as presented and without change in the interest of timely dissemination. Their inclusion in this publication does not necessarily constitute endorsement by the editors, the Institute of Electrical and Electronics Engineers, Inc.

IEEE Catalog Number:	94CH3379-5	
ISBN:	0-7803-1754-8	Softbound Edition
	0-7803-1755-6	Casebound Edition
	0-7803-1756-4	Microfiche Edition
Library of Congress:	93-80486	

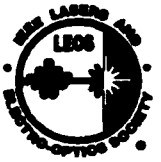

Table of Contents

TUESDAY, SEPTEMBER 20, 1994

WEDNESDAY, SEPTEMBER 21, 1994

THURSDAY, SEPTEMBER 22, 1994

SESSION Th2 – High Speed Lasers II

SESSION Th3 – New Structures and Characterization Approaches

SESSION Th4 – High Power Edge and Surface Emitting Lasers

General Chair Foreword

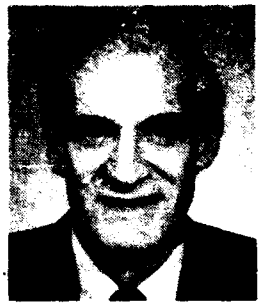

Aloha.

Welcome to sunny Maui, Hawaii, USA and to the 14th IEEE International Semiconductor Laser Conference. Our Conference has convened before in Brazil, Canada, Japan (three times), Mexico, Switzerland, the United Kingdom, and the mainland United States (five times), but this is the first of our Conferences to be held in a tropical mid-Pacific island setting. I trust that you will find the Conference site appealing, but hope that Maui's pleasures will not distract you too much from the week's excellent technical activities.

This year's Conference again begins with three invited Review talks. Each is aimed at exploring an area of importance to the semiconductor laser community: high power lasers, blue-green laser diodes, and optical feedback phenomena. The reviews are presented by D. Welch, SDL, A. Ishibashi, Sony, and K. Petermann, Technical University of Berlin. The core of the technical program features both oral and poster presentations of contributed papers. Of the record 200 papers submitted from 22 countries, 123 were selected for presentation. To permit this large number of presentations, the program includes a Poster Session preceded by a Poster Preview in which the presenters will have a brief opportunity to advertise their wares. One session has been set aside for Post-deadline presentations, often one of the most exciting parts of any technical conference. The program is rounded out by an evening of rump sessions aimed at continuing the technical debate in a less formal atmosphere.

In addition to the regular technical program, three pre-Conference Short Courses, each taught by a technical expert, provide an excellent opportunity for attendees to become current in the field. A Friday morning post-Conference Workshop consisting of two 2-hour sessions follows the formal technical program. This Workshop, open to all conferees, will permit the informal discussion of new results and ideas which were stimulated by the regular technical program. Two guest co-editors, Dan Botez and Rod Tucker, have agreed to put together a special issue of the IEEE Journal of Quantum Electronics on semiconductor lasers in conjunction with the Conference. I strongly recommend that Conference presentations be submitted for publication in this special issue.

Many people deserve special credit for making this 14th IEEE International Semiconductor Laser Conference a real success. It has been my great pleasure to work closely with Chris Harder, Technical Program Chair, over the past two years. I also want to express my appreciation to all of the other members of the Technical Program Committee, and especially to the three regional subcommittee chairs, Tom Koch, James Whiteaway and Yasuhiko Arakawa, for their efforts. The other Conference Committee members, Gary Evans, Joanne LaCourse and Tom Paoli, skillfully handled finance, publicity, and local arrangements. The members of the Advisory Committee provided invaluable guidance in the planning of the Conference. We all thank the U.S. Government agencies which provided partial financial support for the Conference. Finally, my special appreciation goes to Samantha Phillips of the IEEE/LEOS staff for attending to all of the many organizational details.

I know that as an attendee you will be stimulated by what you hear and learn at Maui. I hope that you also will have an opportunity to enjoy the social events and the sights and sounds of this lovely Conference site. Aloha.

Martin A Pollack

Technical Program Chair Foreword

Welcome to ISLC '94, the 14th IEEE International Semiconductor Laser Conference in Maui, Hawaii. The ISLC provides the most comprehensive biennial international forum for recent advances in the field of semiconductor lasers.

The Technical Program Committee has selected 123 presentations contributed by researchers throughout the world to be presented in regular sessions from Monday, September 19, until Thursday, September 23, 1994. In addition, there will be three pre-conference tutorials on Sunday, taught by distinguished instructors, and four post-conference workshops on most the pressing current issues on Friday morning. The regular conference has kept to the traditional format: Three invited review talks, 123 paper and poster presentations (preceded by poster previews), post-deadline papers, and a rump session, all without parallel sessions.

The conference starts with invited review talks by Dr. D. Welch, Spectra Diode Laboratories, A. Ishibashi, Sony Corporation, and Prof. K. Petermann, Technische Universitaet Berlin. These presentations will review progress over the past few years and will help provide attendees with a common technical base. Then we will hear in the paper sessions about extraordinary advances, especially on high-power, high-speed, low-threshold lasers and on longitudinal as well as lateral mode control. At the ISLC '92 in Takamatsu, a special rump session was dedicated to carrier transport and dynamics, and this time you will hear a full paper session on the most recent technical results in this controversial field. The poster session will make informal interaction with the authors possible as well as in-depth discussion of the results. The post-deadline session will supplement the regular papers with late-breaking achievements. At a rump session on Wednesday evening, we will all have a chance to participate in an informal discussion on the most pressing issues of semiconductor lasers.

This year, the two guest editors, Dan Botez and Rodney S. Tucker, will put together the IEEE Journal of Quantum Electronics Special Issue on Semiconductor Lasers in conjunction with this conference, following a long-standing tradition. I strongly recommend that conference presentations be submitted for publication in this special issue, which will be published in June of '95. I trust that, as in the past, it will serve as a most useful reference.

For over a quarter of a century, the Semiconductor Laser Conference has provided an important and unique technical forum on the rapidly expanding field of devices, and it has witnessed revolutionary advances of laser diodes. I would like to thank the many scientists and engineers who are instrumental to the technical success of this conference as well as all attendees who contribute interesting results and who join informal discussions.

It has been my pleasure to work closely during the past two years with Martin Pollack, Conference General Chair, on the preparation of this conference. Finally, let me thank the members of the Technical Program Committee, especially the three regional subcommittee chairs, Yasu Arakawa, Tom Koch and James Whiteaway, for their efforts and cooperation in assembling the technical program.

Christoph S. Harder

Committees

Conference Committee

General Chair
Martin A. Pollack
AT&T Bell Laboratories Crawford Hill Laboratory
Holmdel, NJ 07733-0400 USA
Tel: 908-888-7233
Fax: 908-888-7007
email:map@big.att.com

Technical Program Chair
Christoph S. Harder
IBM Research Division
Saumerstrasse 4
Ruschlikon, CH-8038 Switzerland
Tel: +41 1 724 8339
Fax: +41 1 724 1789
email: cha@zurich. ibm.com

Finance Chair
Gary Evans
Southern Methodist University
School of Engineering & Applied Science
Dallas, TX 75275 USA
Tel: 214-768-3032
Fax: 214-768-3883

Local Arrangements Chair
Thomas L. Paoli
Xerox PARC
333 Coyote Hill Road
Palo Alto, CA 94304 USA
Tel: 415-812-4174
Fax: 415-812-4105

Publicity Chair
Joanne LaCourse
GTE Laboratories
40 Sylvan Road
Waltham, MA 02254 USA
Tel: 617-466-2494
Fax: 617-890-9320

Advisory Committee

P. Eliseev
R. Goodfellow
K. Iga
T. Ikegami
I.P. Kaminow
T. Kamiya
T.-P. Lee
H. Melchior
M.H. Pilkuhn
D. Scifres
A. Yariv

Technical Program Sub-Committee

Americas

Chair: Thomas L. Koch
AT&T Bell Laboratories, 4E338
101 Crawfords Corner Road
Holmdel, NJ 07733-3030, USA
Tel: 908-949-1248
Fax: 908-949-8988
e-mail: tlk@holite.ho.att.com

J.H. Abeles
David Sarnoff Research Center, Princeton, NJ

D.P. Bour
Xerox PARC, Palo Alto, CA

J.E. Bowers
University of California, Santa Barbara, CA

C.J. Chang-Hasnain
Stanford University, Stanford, CA

J.J. Coleman
University of Illinois, Urbana, IL

K.-Y. Lau
University of California, Berkeley, CA

N.B. Patel
Unicamp-IFGW, Campinas, Brazil

W.C. Rideout
GTE Laboratories, Waltham, MA

W.-T. Tsang
AT&T Bell Laboratories, Murray Hill, NJ

D.F. Welch
Spectra Diode Laboratories, San Jose, CA

Committees

Technical Program Sub-Committee

Europe, CIS, Africa, Middle East

Chair: James E.A. Whiteway
BNR Europe Ltd.,
London Road
Harlow, Essex, CM17 9NA
United Kingdom
Tel: +44-279-402343
Fax: +44-279-453658
e-mail: j.e.a.whiteaway@bnr.co.uk

R.G. Baets
University of Gent,
Gent, Belgium

G. Eisenstein
Technion
Haifa, Israel

S.A. Gurevich
Russian Academy of Sciences,
St. Petersburg, Russia

I. Henning
British Telecom Laboratories, Ipswich, UK

E. Kapon
Swiss Federal Institute of Technology,
Lausanne, Switzerland

C. Kazmierski
CNET, Bagneux, France

K. Petermann
Technical University of Berlin, Berlin, Germany

B. Stegmueller
Siemens AG, Muenchen, Germany

B. Tromberg
TDR, Horsholm, Denmark

A. Valster
Philips Research Labs, Eindhoven, The Netherlands

Asia and Australasia

Chair: Yasuhiko Arakawa
University of Tokyo
7-22-1 Roppongi, Minato-Ku
Tokyo 106, Japan
Tel: +81-3-3478-1139
Fax: +81-3-3402-5078
e-mail: arakawa@kappa.iis.u-tokyo.ac.jp

S. Arai
Tokyo Institute of Technology, Tokyo, Japan

N. Chinone
Hitachi Ltd, Tokyo, Japan

G.I. Hatakoshi
Toshiba Corporation, Kanagawa, Japan

K. Ikeda
Mitsubishi Electric Corporation, Hyogo, Japan

H. Ishikawa
Fujitsu Laboratories, Atsugi, Japan

K. Kobayashi
NEC Corporation, Kanagawa, Japan

K. Oe
NTT, Kanagawa, Japan

R.S. Tucker
The University of Melbourne, Parkville Vic, Australia

W. Wang
Chinese Academy of Sciences, Beijing, China

Journal of Quantum Electronics Guest Editors

Dan Botez
Univ. of Wisconsin - Madison
1415 Johnson Drive
Madison, WI 53706 USA
Tel: 608-265-4643
Fax: 608-265-4623
email: botez@engr.wisc.edu

Rodney S. Tucker
The University of Melbourne
Gratton Street
Parkville Vic, 3052
Australia
Tel: +61-3-344-7688
Fax: +61-3-344-7412
email: rst@mullian.ee.mu.oz.au

Monday
September 19, 1994

SESSION M1
Review of Recent Advances in Semiconductor Lasers

SESSION M2
Mode Locking

SESSION M3
Strained QW Lasers

SESSION M4
Integrated Sources

8:40am - 9:20am (Invited)
M1.1

Progress in High Power Semiconductor Lasers

David F. Welch

SDL, Inc.

Summary

Advances in high power semiconductor laser diodes have resulted in both dramatic demonstrations of laser diode characteristics and of innovative systems designs based on these semiconductor sources. As a measure of the capabilities of the semiconductor laser diodes; monolithic laser diode sources have been fabricated which operate to greater than 120 W cw from a 1 um by 1 cm emitting aperture. As a result of such high power demonstrations, the application base of laser diodes can be expanded from the low power, few milliwatt, applications to applications that require kilowatts of power. As a result laser diodes have become the visionary technology for almost all laser based systems.

The advances in high power laser sources can be roughly categorized into four technology areas; i) higher power output, ii) greater reliability, iii) increased coverage of the spectrum and iv) the development of high power diffraction limited sources. In addition to the development of high power diode lasers, much of the recent advances include areas of hybrid technologies where the coupling of high power semiconductor laser diodes with complimentary technologies have further advanced the state of the art in laser sources. The following discussions will try to cover the advances in the four categories by reviewing the key demonstrations in the development of high power sources.

Higher Power Output

The development of several key technologies enabled diode lasers to advance from there typically few milliwatt output. These include growth technologies, packaging technologies, elimination or reduction of catastrophic failure mechanisms, higher efficiency device designs, low optical loss materials enabling low thermal resistance device designs, and large aperture size devices. As a result of technical advances in all of these areas the diode laser increased its output power 100x for a comparable emitting aperture and greater than 20,000x when the aperture size was increased. Maximum output powers of 120 W (Figure 1) have been demonstrated while total efficiencies have exceeded 60%.

Reliability

One of the most noteworthy demonstrations in high power device development is the increased reliability of these sources. Typically reliability in diode lasers has been associated with InP based materials but recent processing and growth advances have resulted in high reliability of AlGaAs materials. Lifetest data of 100 um wide aperture devices operating at 500 mW cw has resulted in lifetimes in excess of 10^6 hours. Similarly with the development of high power sources in the Er doped fiber amplifier (EDFA) market high reliability 980 nm and 1480 nm sources operating up to 200 mW cw have been demonstrated and are commercially available.

Wavelength Access

The development of strained layer active regions have dramatically impacted the wavelength access of diode lasers. Recent developments in the AlGaInP and InGaAsP materials systems through the introduction of strained active regions have resulted in the demonstration of high power operation of diode lasers nearly continuously from wavelengths from 630 nm to 2.05 um. Powers of 90 W cw at 680 nm, 6 W cw at 630 nm, and 8 W cw at 2 um have all been demonstrated (Figure 2). Current work on ZnSe and GaN based materials will potentially extend these wavelengths throughout the visible spectrum and into the near UV.

Diffraction Limited Emission

Significant effort over the past decade has been expended in the development of diffraction limited diode lasers at output powers exceeding 1 W cw. This work has been performed at a number of laboratories where a wide variety of concepts and designs have been investigated. Due to the nature of the presentation I will concentrate only on the two or three most successful demonstrations, these include monolithically integrated MOPAs, unstable resonators, and anti-guide laser arrays. These sources have demonstrated greater than 1 W cw with diffraction limited output beams. In addition the MOPA technology has demonstrated up to 3 W cw diffraction limited output. These demonstrations have resulted in the development of high power sources that couple the attributes of the master oscillator and facilitate the amplification to output powers in excess of 1 W average power. For instance MOPAs have been fabricated with high speed modulators, tunable oscillators, and mode locked oscillators. In addition the technology has been applied to wavelengths from 680 nm to 1.9 um (Figure 3). The design and operation of these sources will be discussed in detail.

λ	Single Mode	100 μm Aperture	1 cm Bar
630	60 mW	1.4 W	6 W
680	295 mW	1.7 W	90 W
830-860	300 mW	5.0 W	120 W
980	300 mW	5.0 W	---
1017	200 mW	---	---
1.8 - 2.0 μm	30 mW	0.5 W	8 W

Table 1: CW Power vs. Wavelength

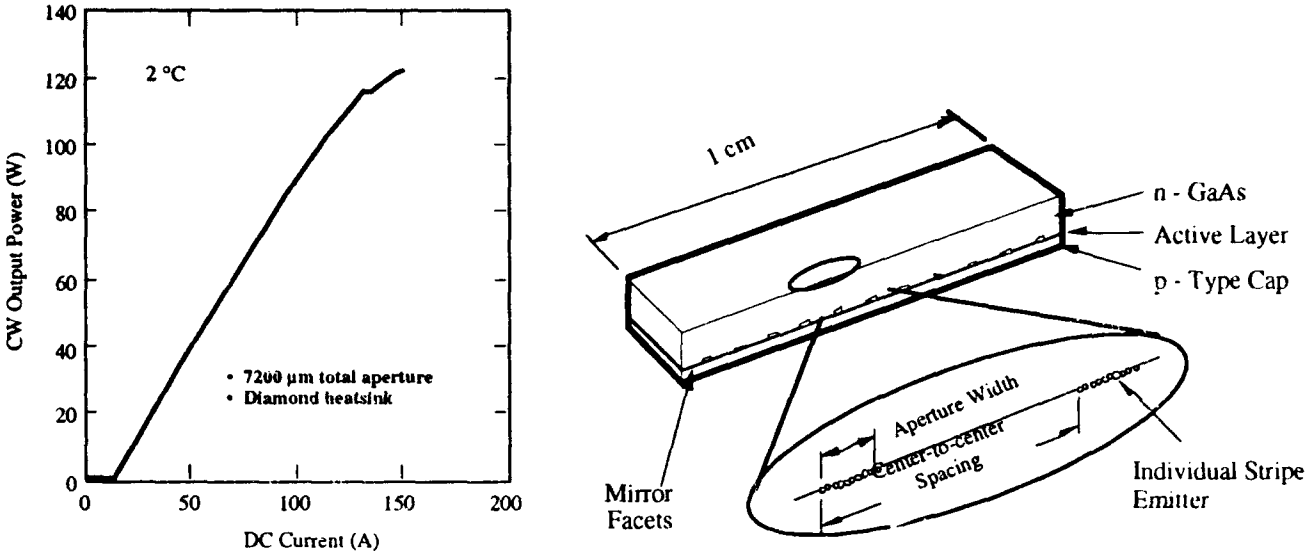

Figure 1: 120 W CW, 1 cm Wide Laser Array

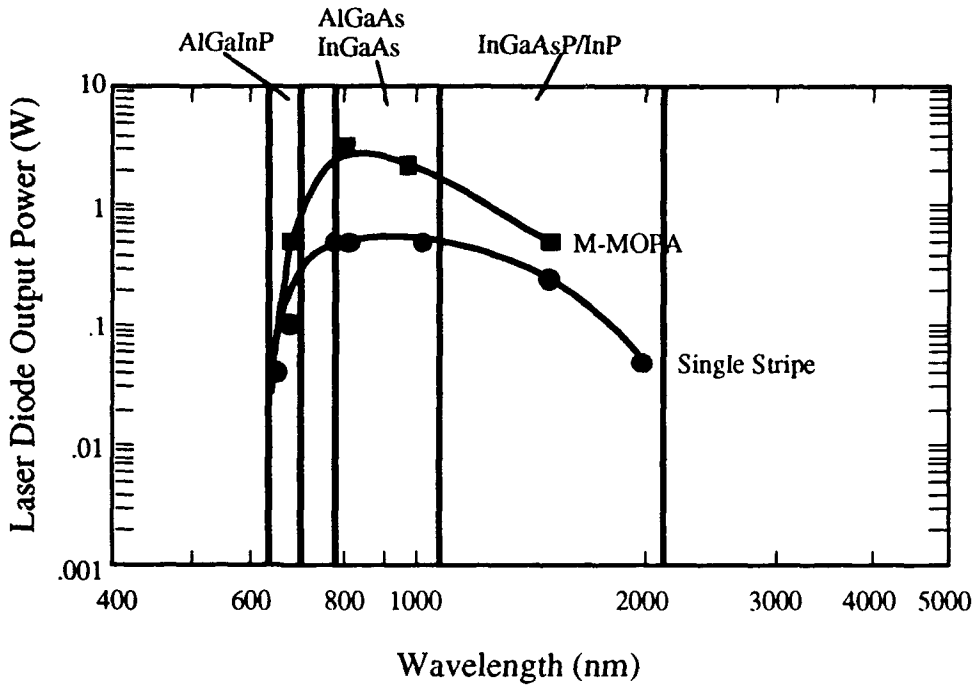

Figure 2: High Power Coherent Laser Diodes

9:20am - 10:00am (Invited) Blue-Green Laser Diodes
M1.2

Akira Ishibashi

Sony Corporation Research Center

174 Fujitsuka-cho, Hodogaya-ku, Yokohama 240, Japan

Semiconductor laser diodes (LDs) have been playing a central role in many systems, such as high transmission-rate communication systems, high power energy source systems, and optical or magneto-optical memory systems, e.g., consumer audio Compact Disc (CD) ROM systems, Mini-Disc (MD) ROM/RAM systems with AlGaAs infra-red LDs, and high definition MUSE disk systems with AlGaInP red-emitting LDs. The research and development, or the evolution, of the semiconductor LDs will be two-fold. One is to integrate the conventional LDs, which have already been established as a discrete chip, into monolithic highly-functional devices. The AlGaAs/GaAs-based LDs have been in this phase. The other is to establish a discrete chip that achieves challenging targets, such as a super high power, an extremely rapid response, and a short wavelength. As the next generation of conventional LDs, the short wavelength, green and blue, LDs have been needed for higher density disk systems. It is straight forward that the shorter the wavelength becomes, the higher the density of those optical disks can be, leading to either a long time or a high definition recording. Furthermore, with the green and the blue LDs we are entering a new paradigm where RGB full-color all-solid-state light-sources are at hand in an inexpensive, mass productive, and highly compact manner.

Since Haase et al. reported the first semiconductor blue-green LD operation at 77K based on ZnCdSe/Zn(S)Se, II-VI wide gap semiconductor LDs have been a focus of attention. The early II-VI wide gap semiconductor LDs based on ZnCdSe/Zn(S)Se have intrinsic problems caused by a small energy-gap difference between the ZnCdSe active layer and the Zn(S)Se cladding layer. This fact makes operation at a high temperature or

at a short wavelength difficult due to insufficient confinement of injected carriers. The ZnMgSSe, on the other hand, being fully lattice-matched to GaAs (001) substrates with ıergy gap tunable up to as high as ~ 4.5 eV, forms a type I heterostructure with ZnSe erve as optimum cladding layers for the blue and the green LDs. The ZnMgSSe has ıed to a successful demonstration of room temperature pulsed operation of a blue LD with a wavelength down to 471 nm, based on a Zn(Cd)Se/Zn(S)Se/ZnMgSSe separate-confinement heterostructure (SCH) structure. Continuous wave (CW) operation of both a green LD with a wavelength up to 531 nm and a blue LD with a wavelength down to 489.9 nm have been achieved at room temperature. Also demonstrated are CW operation up to 353K at 1mW, room temperature CW operation up to 30mW, a threshold voltage of 4.7 V, and a device lifetime of about 9 minutes with gain-guided blue-green SCH LDs. The device characteristics of the II-VI wide gap LDs are becoming as good as the established III-V materials-based LDs except the device lifetime, which is the next target of current research and development. We need to analyze the degradation mechanism and brush up the device reliability. The blue and the green LDs will play a central role in establishing the future high-density recording and the future active display devices just in the same way as advanced micro-processors/memory-chips do for future high performance computers. It is expected that the ZnSe/ZnMgSSe-based II-VI heterostructure devices blossom in near future just like the GaAs/AlGaAs-based III-V heterostructure devices.

10:30am - 11:10am (Invited)
M1.3

Optical feedback phenomena in semiconductor lasers

Klaus Petermann
Technische Universität Berlin,Institut für Hochfrequenztechnik, Einsteinufer 25, 10587 Berlin, Germany

Introduction

Optical feedback phenomena in semiconductor lasers attracted considerable interest during the last decade /1-39/. It has been recognized quite early, that the linewidth can be reduced considerably with optical feedback /10-13/ and external cavity lasers are routinely used if linewidths down to a few kHz are required /40-42/. However, optical feedback phenomena have been found to be responsible also for mode hopping /43/, for strong excess noise in the coherence collapse regime /18/ and other regimes have been identified with stable microwave oscillations /44/.

Feedback regimes

It is customary to describe weak optical feedback by a feedback Parameter C /6/

$$C = \sqrt{f_{ext}}\,\frac{2\,|C_e|\,\tau_{ext}}{\tau_L}\,\sqrt{1+\alpha^2} \qquad (1)$$

where f_{ext} denotes the power ratio between light fed back into the laser and the light emitted from the laser. τ_{ext} denotes the external round trip time, τ_L is the internal roundtrip time within the laser diode, α denotes the linewidth enhancement factor, and C_e describes the coupling between the laser to the cavity /45, 46/.

Feedback regimes have been identified in /22/ and they may be explained by considering the linewidth in Fig. 1.

For relatively low feedback with $C \approx 1$ already a considerable linewidth broadening up to about $\Delta\nu \approx 1/\tau_{ext}$ may occur /36, 47, 48/ which must be considered for designing coherent receivers.

For increasing feedback multiple cavity modes may exist (region II). If feedback is increased further (region III) it is now well recognized that the lowest linewidth mode becomes most stable /27,34/ until the coherence collapses yielding the coherence collapse regime IV /18,22/ if f_{ext} exceeds a critical level $f_{ext,C}$. Below this critical feedback level, the RIN (relative intensity noise) remains low, but the modulation characteristics may be considerably distorted /49,50/. .

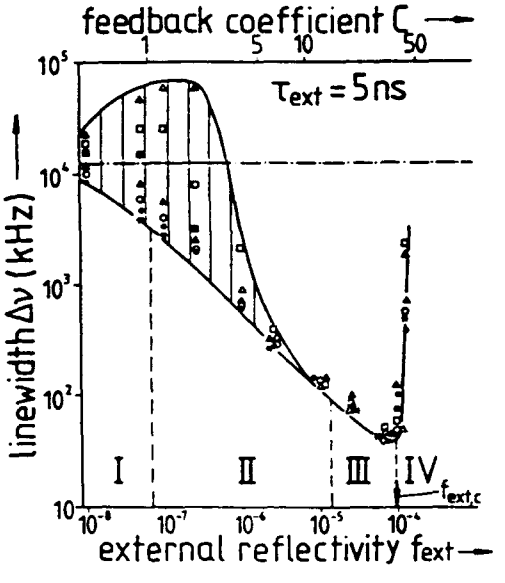

Figure 1: linewidth vs feedback for a semiconductor laser

In particular, for $f_{ext} = f_{ext,C}$ a pole develops in the modulation characteristics for the lowest linewidth mode at a modulation frequency close to the relaxation resonance $f \approx f_r$, from which $f_{ext,C}$ may be determined /30,51/, yielding

$$f_{ext,C} = \frac{{\tau_L}^2}{16\,|C_e|^2}\,\left[K \cdot {f_r}^2 + 1/\tau_e\right]^2 \left(\frac{1+\alpha^2}{\alpha^4}\right)$$

with K — the modulation K-factor and τ_e — the electron lifetime. Efforts are underway to shift $f_{ext,C}$ to higher values. Obviously, a high bias level /31,52/ (yielding a high f_r) and a low α are desirable. Furthermore, long lasers (τ_L large) yield a large $f_{ext,C}$ /53/ and $|C_e|$ should be small which can be accomplished for large κL in DFB-lasers, as long as no significant spatial hole-burning occurs /39/.

It has been reported that gain-coupled DFB-lasers exhibit a larger $f_{ext,C}$ than index-coupled lasers /54/, even though the coupling coefficient C_e is shown to be nearly identical for gain- and index- coupled lasers /55/ for similar $\kappa \cdot L$-values. However, high $\kappa \cdot L$-gain-coupled lasers exhibit a better mode stability /56/, yielding useful devices as long as scattering losses may be kept low.

Vertical-cavity surface emitting lasers also exhibit a very low C_e however, due to the low τ_L the ratio $\tau_L / |C_e|$ is similar as for edge-emitting devices, yielding a similar feedback sensitivity /57/.

After f_{ext} surpasses $f_{ext,C}$, instabilities first occur around f_r and further increasing f_{ext} finally yields a chaotic state and the route to chaos has been studied extensively /30,33,34,38/. Even in this chaotic state the relative intensity noise does not increase beyond a certain limit /32,58/ given by

$$RIN_{max} = \left(K \cdot f_r^{\,2} + 1/\tau_e\right)^{-1} \tag{3}$$

If this RIN_{max} is sufficiently low, systems may operate also without isolators.

Short external cavities

The critical feedback level according to eq. (2) is independent of the external cavity length, as long as $\tau_{ext} \geq 1/f_r$. For short external cavities with $\tau_{ext} < 1/f_r$ one obtains a strongly increasing $f_{ext,C}$ /59/, yielding relatively stable external cavity lasers, which themselves are again relatively stable to additional external feedback /60/.

If a short external cavity laser is designed with sufficiently high feedback to surpass $f_{ext,C}$ a stable output pulsation up to the millimeter-wave region may occur for specific feedback phases, the microwave frequency being controlled by the amount of feedback /44/. On this basis, optical microwave sources are feasible similar to devices with segmented DFB-sections /61/.

After all, a good understanding of optical feedback phenomena has meanwhile been obtained enabling design-guidelines for feedback-tolerant semiconductor laser devices.

References

/1/ R.F. Broom, E.Mohn, C. Risch and R.Salathé: Microwave self-modulation of a diode laser coupled to an external cavity; IEEE J. Quant. Electron., Vol QE-6, pp. 328-334, June 1970

/2/ T. Morikawa, Y. Mitsuhashi, J. Shimada and Y. Kojima: Return-beam-induced oscillations in self-coupled semiconductor lasers; Electron. Lett., Vol. 12 pp. 435-436, 19th Aug. 1976

/3/ I. Ikushima and M. Maeda: Self-coupled phenomena of semiconductor lasers caused by an optical fiber; IEEE J. Quant.Electron., Vol. QE-14, pp. 331-332, May 1978

/4/ I. Ikushima and M. Maeda: lasing spectra of semiconductor lasers coupled to an optical fiber; IEEE J. Quant.Electron.., Vol.QE-15, pp. 844-845, Sept. 1979

/5/ O. Hirota and Y. Suematsu: Noise properties of injection lasers due to reflected waves; IEEE J. Quant.Electron., Vol. QE-15, pp. 142-149, March 1979

/6/ R.P. Salathé: Diode lasers coupled to external resonators; Appl. Phys., Vol 20, pp. 1-18, 1979

/7/ R. Lang and K. Kobayashi: External optical feedback effects on semiconductor injection laser properties; IEEE J. Quant. Elctron., Vol QE-16, pp. 347-355, March 1980

/8/ O. Hirota, Y. Suematsu and K.-S. Kwok: Properties of intensity noises of laser diodes due to reflected waves from single-mode optical fibers and its reduction; IEEE J. Quant. Electron., Vol. QE-17, pp. 1014-1020, June 1981

/9/ R. Ries and F. Sporleder: Low frequency instabilities of laser diodes with optical feedback; Proc. 8th Europ. Conf. on Opt. Comm., pp. 285-290, Cannes, France, Sept. 1982

/10/ L. Goldberg, H.F. Taylor, A. Dandridge, J.F. Weller and R.O. Miles: Spectral characteristics of semiconductor lasers with optical feedback; IEEE J. Quant. Electron., Vol. QE-18, pp. 555-564, Apr. 1982

/11/ K. Kikuchi and T. Okoshi: Simple formula giving spectrum narrowing ratio of semiconductor-laser output obtained by optical feedback; Electron. Lett., Vol. 18, pp. 10-12, 7th Jan. 1982

/12/ E. Patzak, A. Sugimura, S. Saito, T. Mukai and H. Olesen: Semiconductor laser linewidth in optical feedback configurations; Electron. Lett., Vol. 19, pp. 1026-1027, 24th Nov. 1983

/13/ P. Spano, S. Piazolla and M. Tamburrini: Theory of noise in semiconductor lasers in the presence of optical feedback; IEEE J. Quant. Electron., Vol. QE-20, pp. 350-357, Apr. 1984

/14/ G.P. Agrawal: Line narrowing in a single-mode injection laser due to external optical feedback; IEEE J. Quant. Electron., Vol. QE-20, pp. 468-471, May 1984

/15/ B. Tromborg, J.H. Osmundsen and H. Olesen: Stability analysis for a semiconductor laser in an external cavity; IEEE L. Quant. Electron., Vol. QE-20, pp. 1023-1032, Sept. 1984

/16/ G.A. Acket, D. Lenstra, A.J. de Boef and B.H. Verbeek: The influence of feedback intensity on longitudinal mode properties and optical noise in index-guided semiconductor lasers; IEEE J. Quant.Electron., QE-20, pp. 1163-1169, 1984

/17/ H. Sato, T. Fujita and K. Fujito: Intensity fluctuation in semiconductor lasers coupled to external cavity; IEEE J. Quant. Electron., QE-21, pp. 46-51, Jan 1985

/18/ D. Lenstra, B.H. Verbeek and A.J. den Boef: Coherence collapse in single-mode semiconductor lasers due to optical feedback; IEEE J. Quant. Electron., Vol. QE-21, pp. 674- 679, June 1985

/19/ J. Mark, E. Bodtker and B. Tromborg: Measurement of rayleigh backscatter-induced linewigth reduction; Electron. Letters, Vol. 21, pp. 1008-1009,1985

/20/ J. Mark, E. Bodtker and B. Tromborg: Statistical characteristics of a laser diode exposed to rayleigh backscatter from a single-mode fibre; Electron. Letters, Vol. 21, pp. 1010-1011, 1985

/21/ H. Olesen, J.H. Osmudsen and B. Tromberg: Nonlinear dynamics and spectral behaviour for an external cavity lasr; IEEE J. Quant. Electron., Vol. QE-22, pp. 762-773, June 1986

/22/ R.W. Tkach and A.R. Chrapeyvy: Regimes of feedback effects in 1,5 μm distributed feedback lasers; J. Lightwave Techn., Vol. LT-4, pp. 1655-1661, Nov, 1986

/23/ K.Kikuchi and T.P. Lee: Spectral stability of weakly coupled external-cavity semiconductor lasers; J. Lightwave Techn., Vol. LT-5, pp. 1269-1272, Sept. 1987

/24/ G. Duan, P. Gallion and G. Debarge: Analysis of frequency chirping of semiconductor lasers in the presence of optical feedback; Opt. Letters, Vol. 12, pp. 800-802, 1987

/25/ B. Tromborg, H. Olesen, X. Pan and S. Saito: Transmission line description of optical feedback and injection locking for fabry-perot and DFB lasers; IEEE J. Quant. Electron.,QE-23, pp. 1875-1889, 1987

/26/ M. Shikada, S. Takano, S. Fujita, I. Mito and K. Minemura: Evaluation of power penalties caused by feedback noise of distributed feedback laser diodes; J. Lightwave Techn., Vol. 6, pp. 655-659, May 1988

/27/ N. Schunk and K. Petermann: Numerical analysis of the feedback regimes for a single-mode semiconductor laser with external feedback; IEEE J. Quant. Electron., Vol. QE-24, pp. 1242-1247, July 1988

/28/ J.S. Cohen and D. Lenstra: Spectral properties of the coherence collapsed state of a semiconductor laser with delayed optical feedback; IEEE J. Quant. Electron,. Vol QE- 25, pp. 1143-1151, 1989

/29/ J. Helms and K. Petermann: A simple analytic expression for the stable operation range of laser diodes with optical feedback; IEEE J. Quant. Electron., Vol 26, pp. 833-836, May 1990

/30/ B. Tromberg and J. Mork: Nonlinear Injection locking dynamics and the onset of coherence collapse in external cavity lasers; IEEE J. Quant. Electron., Vol. QE-26, pp. 642-654, 1990

/31/ S.L. Woodward, T.L. Koch and U. Koren: The onset of coherence collaps in DBR lasers; IEEE Photonics Techn. Lett., Vol. 2, pp. 391-194, 1990

/32/ J. Wang and K. Petermann: Noise analysis of semiconductor lasers within the coherence collapse regime; IEEE J. Quant. Electron., Vol 27, pp. 03-09 and p. 2365, 1991

/33/ J.S. Cohen and D. Lenstra: The critical amount of optical feedback for coherence collapse in semiconductor lasers; IEEE J. Quant. Electron., Vol 27. pp. 10-12, 1991

/34/ J. Mork, B. Tromborg and J. Mark: Chaos in semiconductor lasers with optical feedback: theory and experiment; IEEE J. Quant. Electron., Vol. 28, pp. 93-108, 1992

/35/ A.J. Lowery: A two-port bilateral model for semiconductor lasers; IEEE J. Quant. Electron., Vol. 28, pp. 82-92, 1992

/36/ W.A. Hamel, M.P. van Exter and J.P. Woerdman: Coherence properties of a semiconductor laser with feedback from a distant reflector: experiment and theory; IEEE J. Quant. Electron., Vol. 28, pp. 1459-1469, 1992

/37/ P. Besnard, B. Meziane and G.M. Stephan: Feedback phenomena in a semiconductor laser induced by distant reflectors; IEEE J. Quant. Electron., Vol. 29, pp. 1271-1284, 1993

/38/ H. Li, J. Ye and J.G. McInerney: Detailed analysis of coherence collapse in semiconductor lasers; IEEE J. Quant. Electron., Vol 29, pp. 2421-2332, 1993

/39/ H.-J. Wu and H.-C. Chang: Analysis of external optical feedback in distributed-feedback semiconductor lasers above threshold; IEEE Photonics Techn. Lett., Vol 5, pp. 1168- 1170, 1993

/40/ R. Wyatt and W.J. Devlin: 10 kHz linewidth 1,5 μm InGaAsP external cavity laser with 55 nm tuning range; Electron. Lett., Vol. 19, pp. 110-112, 3rd Feb. 1983

/41/ R. Wyatt: Spectral linewidth of external cavity semiconductor lasers with strong frequency-selective feedback; Electron. Lett., Vol. 21, pp. 658-659, 18th July 1985

/42/ C.A. Park, C.J. Rowe, J. Buus, J. Hankey, N. Weston and B.T. Debney: External cavity lasers for coherent systems; Proc. OFC-IOOC'87, paper TuG3, Reno, Nevada, USA, 1987

/43/ J.W.M. Biesterbos, A.J. den Boef, W. Linders and G.A. Acket: Low-frequency mode-hopping optical noise on AlGaAs channeled substrate lasers induced by optical feedback; IEEE J. Quant. Electron., Vol. QE-19, pp. 986-990, June 1983

/44/ A.A. Tager and K. Petermann: submitted to IEEE J. Quant. Electron

/45/ F. Favre: Theoretical analysis of external optical feedback on DFB semiconductor lasers; IEEE J. Quant. Electron., Vol. QE-23, pp. 81-88, Jan. 1987

/46/ T. Hirono, T. Kurosaki and M. Fukuda: A novel analytical expression on sensitivity to external optical feedback for DFB semiconductor lasers; IEEE J. Quant. Electron., Vol 28, pp. 2674-2677, 1992

/47/ R.W. Tkach and A.R. Chraplyvy: Line broadening and mode splitting due to weak feedback in single-frequency 1,5 μm lasers; Electron. Lett., Vol. 21, pp. 1081-1085, 7th Nov. 1985

/48/ J. Helms, Ch. Kurtzke and K. Petermann: External feedback requirements for coherent optical communication systems; J. Lightwave Techn., Vol. 10, pp. 1137-1141, 1992

/49/ J. Helms and K. Petermann: Microwave modulation of laser diodes with optical feedback; J. Lightwave Techn., Vol. 09, pp. 468-476, 1991

/50/ J. Helms: Intermodulation and harmonic distortions of laser diodes with optical feedback; J. Lightwave Techn., Vol. 09, pp. 1567-1575, 1991

/51/ H. Helms and K. Petermann: A simple analytic expression for the stable operation range of laser diodes with optical feedback; IEEE J. Quant. Electron., Vol. 26, pp. 833-836, 1990

/52/ N. Schunk and K. Petermann: Measured feedback-induced intensity noise for 1-3 μm DFB laser diodes; Electron. Lett., Vol. 25, pp. 63-64, 1989

/53/ T. Kurosaki, T. Hirono and M. Fukuda: Distributed-feedback laser with a high endurance level against optical feedback; Proc. OFC'92, pp. 273-274, San José, Feb. 1992

/54/ Y. Nakano et. al.: Reduction of excess intensity noise induced by external reflection in a gain-coupled distributed feedback semiconductor lasr; IEEE J. Quant. Electron., Vol. 27, pp. 1732-1735, 1991

/55/ F. Favre: Sensitivity to external feedback for gain-coupled DFB semiconductor lasers; Electron. Lett., Vol. 27, pp. 433-435, 1991

/56/ K. David, G. Morthier, P. Vankwickelberge and R.G. Baets: Gain-coupled DFB lasers versus index-coupled and phased-shifted DFB lasers: A comparison based on spatial hole burning corrected yield; IEEE J. Quant. Electron., Vol. 27, pp. 1714-1723, 1991

/57/ H.M. Chen et. al.: Instability in surface emitting lasers due to external optical feedback; J. Appl. Phys., Vol. 73, pp. 16-20, 1993

/58/ H. Tischer and B. Borchert: Intensity noise measurements for 1.55 μm multi-quantum-well DFB laser diodes with external optical feedback; Proc. ECOC'92, pp. 253-256, Berlin, 1992

/59/ N. Schunk and K. Petermann: Stability analysis for laser diodes with short external cavities; IEEE Phot. Technol. Lett., Vol. 1, pp. 49-51, 1989

/60/ J. Helms, N. Schunk and K. Petermann: Stable operation range for laser diodes with an integrated passive cavity in the presence of external optical feedback; IEEE Phot. Technol. Lett., Vol. 1, pp. 409-411, 1989

/61/ U. Feiste, D.J. As and A. Ehrhardt: 18 GHz all-optical frequency locking and clock recovery using a self-pulsating two-section DFB-lasers; IEEE Phot. Techno. Lett., Vol. 6, pp.106-108, 1994

Generation of 1.54 THz Pulse Train by Harmonic Passive Mode-Locking in DBR Lasers

Shin ARAHIRA, Saeko OSHIBA, Tatsuo KUNII, Yasuhiro MATSUI, and Yoh OGAWA
Semiconductor Technology Laboratory, OKI Electric Industry Co., Ltd.
550-5 Higashiasakawa, Hachioji, Tokyo 193, JAPAN

Abstract : We report on the first demonstration of THz-rate pulse generation by harmonic passive mode-locking in DBR lasers. The mechanism of stable generation of harmonic pulses is discussed concerning the spectral filtering property of the Bragg reflector.

Generation of ultrafast optical pulses with semiconductor laser diodes (LDs) [1] is of considerable interest for the new generation optoelectronic applications such as high speed optical communication systems. Such ultrafast pulses can be generated from a mode-locked LD with a short cavity, however, it sacrifices the output power due to a large mirror loss. Harmonic mode-locking is an alternative method to generate ultrafast pulses without using a short cavity. In this paper, we report, for the first time, THz-rate pulse generation by harmonic passive mode-locking in distributed Bragg-reflector (DBR) lasers.

Figure 1 shows a schematic structure of the DBR laser used in this study. The laser has four sections : a saturable absorber section (75 μm), a gain section (750 μm), a phase control section (150 μm) and a DBR section (120 μm). Both gain and absorber sections consist of three compressively strained InGaAs quantum wells separated by 130 Å-thick InGaAsP barriers. An InGaAsP (λ_g=1.3 μm) is used for the waveguides of the phase control and the DBR sections. The absorber facet is high-reflectivity (~90%) coated, leading to a self-colliding pulse operation. The DBR facet is as-cleaved. The output light from the DBR facet was measured by an SHG autocorrelator and an optical spectrum analyzer.

A light-current characteristics exhibited optical bistability around the threshold (I_{th}~70 mA) when the absorber section was reverse biased. Fundamental passive mode-locking occurred around the threshold at a repetition rate of 38.8 GHz [2]. At higher bias level, harmonic passive mode-locking occurred [3]. We observed three different harmonics depending on the bias condition of the gain section : 400 GHz, 800 GHz, and 1.54 THz. The repetition rate became higher and the pulse width reduced as the bias current increased. Figure 2 shows an SHG correlation trace and a time-averaged optical spectrum of the 1.54 THz pulses. The spectrum has a good purity in that the only three modes separated by 12.5 nm (=1.5 THz) are enhanced but the other longitudinal modes are suppressed. The observed correlation trace (solid line in Fig. 2(a)) was in good agreement with a calculated one (open circle) from the Fourier transformation of the optical spectrum, and it is concluded that the output pulses are transform-limited. The pulse width was estimated to be 260 fs from the calculation. The high average output power of 16 mW was obtained. The transform-limited condition and the high output power was satisfied in the other harmonics (400 and 800 GHz).

We observed the only multiple harmonics of the 400 GHz repetition rate. This is supposed to come from the spectral filtering property of the DBR section. Figure 3 shows a calculated reflectivity profile of the 120 μm-long DBR section. The reflectivity profile of a short DBR section with a finite facet reflectivity has several peaks including the main peak around the Bragg wavelength, and the peak separation is almost equal to the mode spacing of the Fabry-Perot etalon with the same length. The DBR section forms a coupled cavity with the extended cavity, and therefore it is assumed to work as a frequency filter which enhances only the frequency components of optical pulses that coincide with its peak separation (400 GHz in this device), but suppresses the other frequency components, leading to stable operation of harmonic mode-locking. Such a resonance in the Bragg reflector is achieved by adding tuning currents to the phase control and/or the DBR sections, even if there is slight difference between the peak separation of the Bragg reflectivity and the harmonic of the fundamental round trip frequency of

the extended cavity.

In conclusion, THz-rate pulse generation has been demonstrated by harmonic passive mode-locking in DBR lasers for the first time. Transform-limited subpicosecond pulses at high repetition rates of 400, 800 GHz and 1.54 THz have been obtained with high output power over 10 mW. The repetition rate is determined by the DBR length, and a resonance of harmonic pulses in the Bragg reflector contributes to the stable generation of harmonic pulses.

References

[1] Y. K. Chen et. al., *Appl. Phys. Lett.* 58, 1253 (1991).

[2] S. Arahira et. al., *IEEE Photon. Technol. Lett.* 5, 1362 (1993).

[3] S. Arahira et. al., *Appl. Phys. Lett.* (to be published).

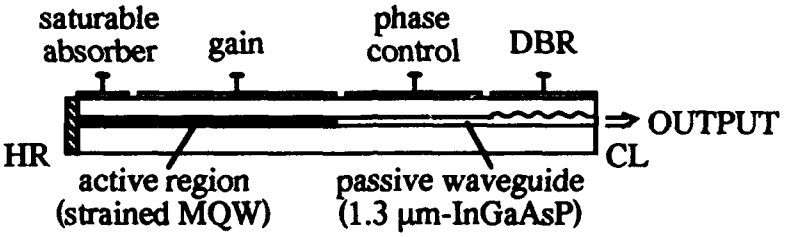

Fig. 1 Schematic structure of the DBR laser used in this study.

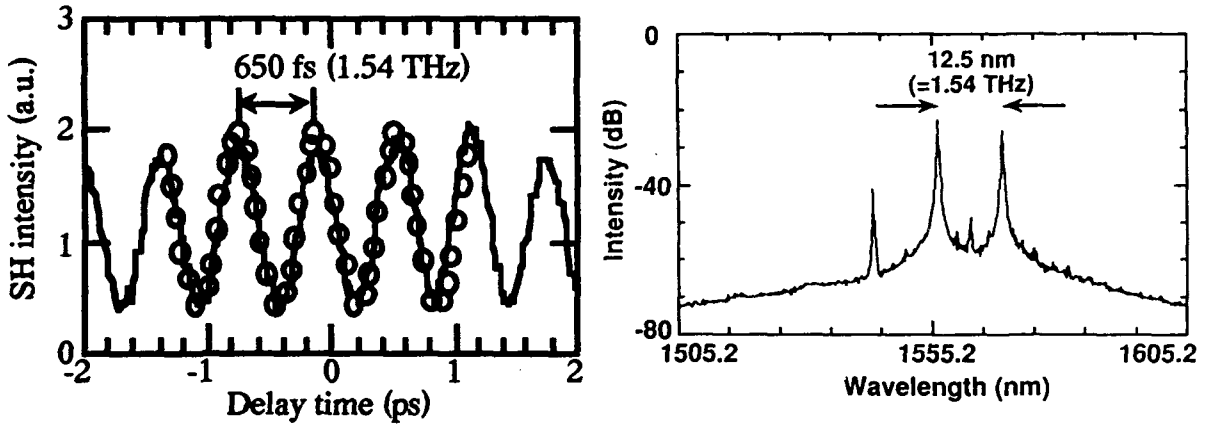

(a) SHG correlation trace (b) Optical spectrum

Fig. 2 SHG correlation trace and optical spectrum of 1.54 THz pulses.

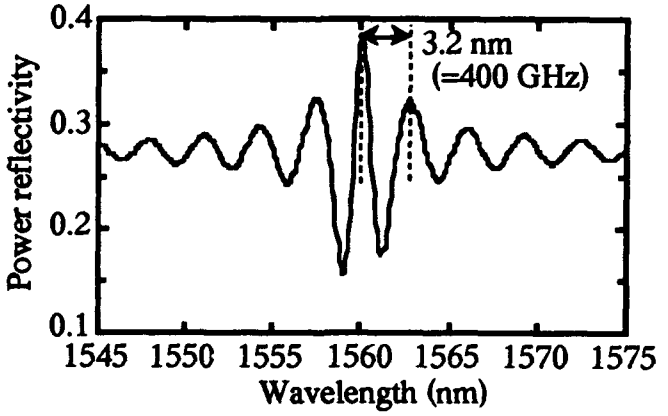

Fig. 3 Calculated reflectivity profile of 120 μm DBR section.

High-Power, Mode-Locked External-Cavity Tunable Semiconductor Laser

Lew Goldberg
Naval Research Laboratory
Washington, DC 20375
(202) 767-9380

David Mehuys and David F. Welch
SDL, Inc.
San Jose, CA 95134
(408) 943-9411

Abstract: A novel, external-cavity tapered-contact laser is mode-locked using a narrow, single-stripe amplifier and emits up to 16 W peak power and 450 pJ pulse energy, in pulses as short as 12 ps.

High-peak power, short-pulse optical sources have significant applications to free-space and fiber optical communications, to materials characterization, and to nonlinear frequency conversion. Large increases in the peak output power as compared to cw diode laser output have been achieved through mode-locking [1,2]. Mode-locked pulses, directly generated by narrow-stripe semiconductor lasers and amplifiers, however, are limited to average powers of approximately 10 mW, pulse energies below 10 pJ, and peak powers below 1 Watt. Higher peak powers, above 1 Watt, may be generated by following the mode-locked low-power master oscillator with a discrete power amplifier [3,4]. Alternatively, in a novel configuration described in this paper, a high-power laser chip can be mode-locked directly using a low-power amplifier as an external modulator.

Recently, broad area tapered-contact gain chips have been successfully used to increase beyond 1 Watt the cw, diffraction-limited power available from semiconductor lasers and amplifiers [5,6,7]. Similar devices have been configured into external-cavity, wavelength-tunable, diffraction-limited sources emitting up to 1 Watt average power [8]. The external-cavity geometry lends itself well to mode-locking, and in this paper, such a high-power external-cavity tapered laser is mode-locked to produce peak powers of 16 W, pulse energies of 450 pJ, and pulse lengths as short as 12 ps. This peak power and pulse energy are more than an order of magnitude greater than those produced by narrow-stripe mode-locked semiconductor lasers.

Figure 1 presents the novel compound mode-locked laser cavity used to generate the high-energy pulse trains. The cavity uses a tapered amplifier gain element (as reported in [8]) for generation of high-average-power, diffraction-limited output, while a second narrow-stripe gain element is used to achieve active mode-locking of the compound cavity through RF modulation of its current. In this way, low-power RF modulation (less than 1 Watt) is used to modulate the approximately 0.5 Watt average output of the compound cavity. The 1.5 mm long tapered amplifier was antireflection coated on both facets [8] and the narrow-stripe amplifier was 500 μm long, with an antireflection-coated front facet and a high-reflectivity rear facet so as to be used in double-pass. Between the two gain element chips were two collimating/focussing lenses and a diffraction grating used in first order, which can provide center wavelength tuning [8]. The total cavity length was adjusted to provide a fundamental cavity round-trip frequency near 500 MHz.

Pulse measurements were carried out to a maximum tapered amplifier current of 1.5 A, or 1.6 I_{th}, where the average power output was 0.5 Watts. The narrow-stripe amplifier was dc-biased at 10-20 mA, upon which the RF modulation (P_{rf} = 1 Watt) was superimposed using a bias tee. The temporal output is displayed in Figure 2(a) and 2(b) for narrow-stripe amplifier currents of 10 and 20 mA respectively. RF modulation was carried out initially at 1 GHz, twice the fundamental cavity frequency. The average power in the two cases is 270 mW and 500 mW respectively. More accurate determination of the temporal pulse characteristics was carried out with collinear autocorrelation measurements, from which pulse widths of 12 ps and 17 ps were extracted for the results of Figure 2. Finally, by

reducing the RF modulation to the fundamental cavity frequency of 500 MHz, peak powers of 16 W and pulse energies of 450 pJ were observed.

In summary, a novel mode-locked external-cavity laser is demonstrated, from which high peak power (16 Watts) and pulse energies (450 pJ) were demonstrated. Such systems have applications to communications systems and nonlinear frequency conversion.

References

[1] S. Corzine, J. Bowers, G. Przybylek, U. Koren, B. Miller, and C. Soccolich, Appl. Phys. Lett. **52**, 348 (1988).

[2] N. Stelmakh and J. Lourtioz, Electron. Lett. **29**, 160 (1993).

[3] P. Delfyett, L. Florez, N. Stoffel, T. Gmitter, N. Andreadakis, Y. Silberberg, J. Heritage, and G. Alphonse, IEEE J. Quantum. Electron. **28**, 2203 (1992).

[4] A. Mar, R. Helkey, J. Bowers, D. Mehuys, and D. Welch, Technical Digest of IEEE LEOS Annual Meeting, San Jose (1993).

[5] E. Kintzer, J. Walpole, S. Chinn, C. Wang, and L. Missagia, IEEE Photon. Tech. Lett. **5**, 605 (1993).

[6] R. Parke, D. Welch, A. Hardy, R. Lang, D. Mehuys, S. O'Brien, K. Dzurko, and D. Scifres, IEEE Photon. Tech. Lett. **5**, 297 (1993).

[7] L. Goldberg, D. Mehuys, M. Surette, and D. Hall, IEEE J. Quantum Electron. **29**, 2028 (1993).

[8] D. Mehuys, D. Welch, and D. Scifres, Electron. Lett. **29**, 1254 (1993).

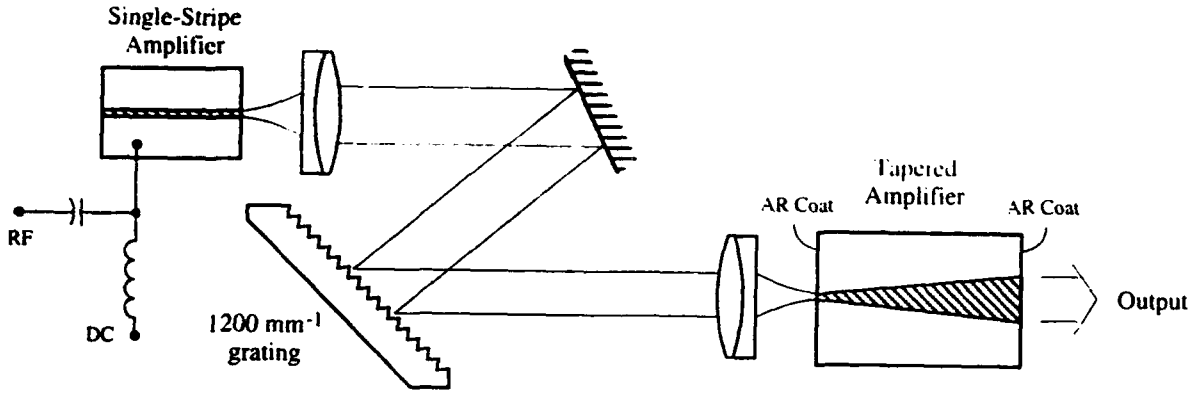

Figure 1 Schematic diagram of the mode-locked, external-cavity tapered laser.

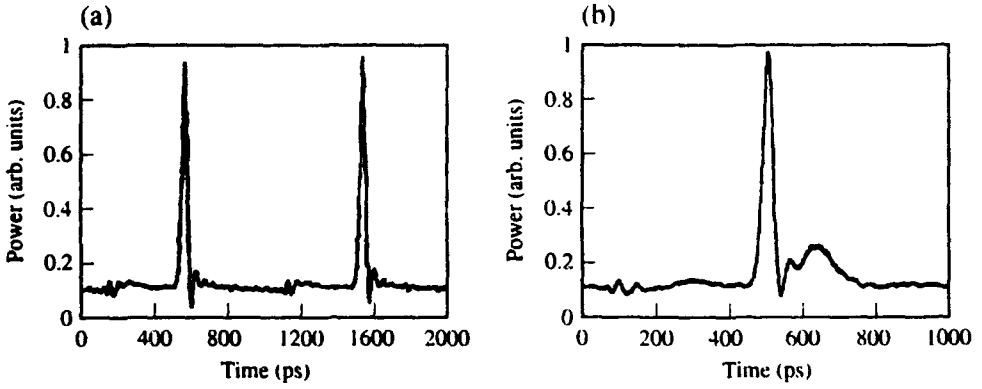

Figure 2 Mode-locked output at tapered amplifier current of 1.5 A, for narrow-stripe bias currents of (a) 10 mA, and (b) 20 mA.

11:40am - 11:55am
M2.3

High repetition rate by multiple colliding pulse mode-locked operation of a semiconductor laser

J. F. Martins-Filho, E. Avrutin and C. N. Ironside
Dept. of Electronics and E. Engineering
University of Glasgow
Glasgow, G12 8LT, UK.
Tel +44 41 339 8855 ex 4796
Fax +44 41 330 4907
Email Ironside@elec.gla.ac.uk

Abstract

The multiple colliding pulse operation where 2, 3 or 4 ultrashort pulses are present simultaneously within a laser resonator is discussed both experimentally and theoretically. In 4 pulse operation, pulse widths of 1.3 ps at repetition rates of 240 GHz have been observed from a 600 μm long laser.

Summary

Semiconductor laser mode-locking at harmonics of the cavity round trip frequency allows the generation of very high repetition rate train of pulses. In this paper we present a modified CPM laser configuration which can generate 2, 3 or 4 pulses in the cavity, giving the second, third or fourth harmonic of the repetition rate. The laser is flexible in the sense that its operation can be switched between 2, 3 or 4 pulses depending on the bias (forward or reverse) applied to each of its 3 independent sections, changing the position and number of saturable absorbers in the cavity. The laser is an extension of the normal colliding pulse laser described in [1] which consists of a gain section with one saturable absorber placed in the centre. In the present laser more saturable absorber sections have been added. However, the basic type of operation is the same, pulses collide at each saturable absorber.

The four sectioned monolithic CPM laser is illustrated in figure 1. The laser has a contiguously electrically connected gain section and 3 separated sections placed at every quarter of the cavity length. The laser wafer structure consists of four 10 nm GaAs wells spaced by 10 nm $Al_{20}Ga_{80}As$ barriers in separate confinement structure. It is described in detail in ref [1].

Figure(1)

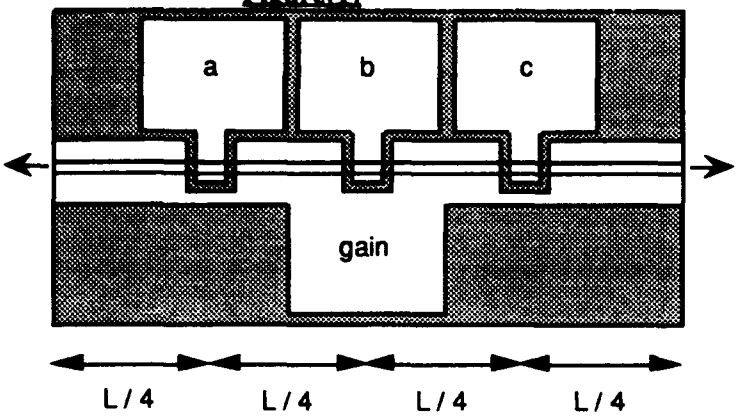

Caption: Top view diagram of the monolithic 4 section passive CPM quantum well laser. Arrows indicate laser output at the waveguide facets.

The total length of the laser is 600 μm and each one of its 3 sections (a, b and c in figure 1) is 30 μm long. The laser operates on CW regime and when it is fully forward biased the threshold current is 36 mA. The multiple pulse operation of the CPM laser is observed for a gain current of 54 mA. We used a cross-correlation technique [2] to perform time domain measurements of the laser, obtaining pulse width and repetition rate measures. The cross-correlator is a Michelson interferometer that can cross-correlate adjacent pulses from a high repetition rate pulse train. The interferogram is then produced by a low-speed photodiode and a lock-in amplifier. Two pulse CPM operation is obtained when the central section of the laser (section b in figure 1) is reverse biased whereas the others (sections a and c) are forward biased by connecting them to the gain section. This configuration corresponds to the normal CPM lasers, which have one saturable absorber in the middle of the cavity [1]. Figure 2-a shows the optical spectrum for 2 pulse CPM operation when -0.37 V reverse bias is applied to section b. It can be seen that three longitudinal modes are locked and the mode space is 0.3 nm which is twice the original cavity mode space (0.15 nm). It indicates that 2 pulses are circulating in the cavity and colliding in the saturable absorber. The cross-correlation measurement gives 1.5 ps pulse width and 120 GHz repetition rate, which corresponds to the second harmonic of the repetition rate. The time-bandwidth product is 0.45.

Figure(2)

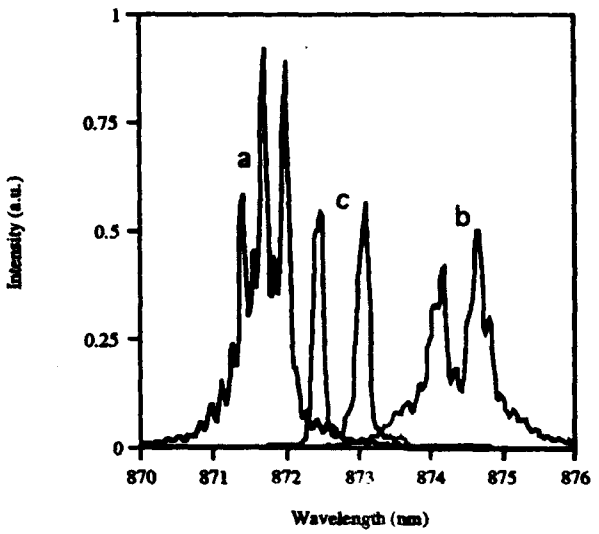

Caption: Figure (2)Optical spectra of the laser operating a) 2 pulse, (b) 3 pulse and (c) 4 pulse mode.

Figure(3)

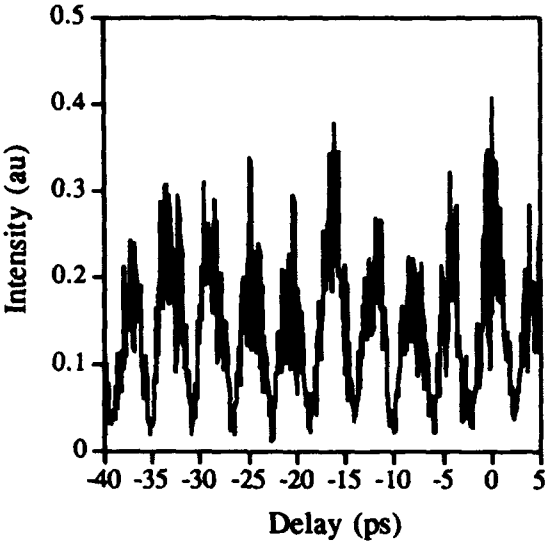

Caption Figure(3) The cross-correlation interferomogram for four pulse opertaion

Three pulse CPM laser operation occurs when the sections a and c (see figure 1) are reverse biased and the section b is forward biased. In this configuration the laser has two saturable absorbers in the cavity. Figure 2-b shows the optical spectrum for three pulse operation when -0.74 V reverse bias is applied to sections a and c. It can be seen that in this case the longitudinal mode separation of the two locked modes is 0.45 nm, which is three times the original cavity mode space. We measured 1.6 ps pulse width and 180 GHz repetition rate, which is the third harmonic of the cavity round trip frequency. The time-bandwidth product is 0.5. The explanation of how can 3 pulses co-exist in the laser cavity is as follows; two of them collide at every 1/3 of the cavity length, while the other is 2/3 of the cavity length distant from them, at the facet. Hence the cavity round trip is 2L/3. Although the collision points do not correspond to the exact position of the saturable absorbers, the pulses are wide enough (120 μm long inside the laser) to overlap in the saturable absorber section. Therefore the pulses still collide in the absorber sections.

The four pulse CPM operation is achieved when the three sections (a, b, and c) are reverse biased. As a result the laser has three saturable absorbers in the cavity. Figure 2-c shows the optical spectrum for -0.33 V reverse bias applied to the three sections. The longitudinal mode separation is 0.6 nm. Figure 3 shows the cross-correlation interferogram for four pulse operation. The pulse width measured from the interferogram must be divided by a factor of 2 to give the actual pulse width at FWHM [2]. It is 1.3 ps and the repetition rate is 240 GHz, which is the fourth harmonic of the repetition rate. The time bandwidth product is 0.38. This configuration has four pulses circulating in the cavity and they collide exactly in the saturable absorber sections. Two of them collide with other two pulses in sections a and c, and after moving a quarter of the cavity length two pulses collide in the section b, while the other two pulses are at each facet of the laser. Therefore the cavity round trip is L/2, which gives the longitudinal mode separation and the repetition rate measured.

A frequency-domain passive mode locking model was applied to interpret the experimental data. The geometrical position of the absorber enters such a model via spatial overlap integrals ξ_m which scale the strength of nonlinear coupling between modes m inverse roundrip periods apart from each other. Calculating the values of ξ_m, one finds that modes separated by 2, 3, and 4 inverse roundrip periods are, indeed, expected to interact most strongly for respective geometries close to those studied in the experiments. The agreement between the measured and calculated results is improved if one supposes that: a) the actual absorber region stretches somewhat beyond the electric contact made to it and b) fast effects in the saturable absorber (possibly exciton saturation and transient gratings) play a significant part in the properties of the device.

We reported the fabrication and characterisation of a monolithic four sectioned passive CPM quantum well laser which can have one, two or three saturable absorbers in the cavity, generating the second, third or fourth harmonic of the repetition rate. The operation of the laser can be switched between harmonics depending on the order and the number of sections reverse biased to produce saturable absorption. The number and the position of the saturable absorber sections in the cavity seem also to affect the width and the spectral purity of the generated pulses. Due to its flexibility and operation characteristics this device is promising for studies of fundamental aspects of mode-locking operation in semiconductor lasers. It may also find application in the generation of microwaves above 100 GHz as well as in an ultrahigh repetition rate ultrashort pulse width optoelectronics.

References

[1] Martins-Filho, J. F., Ironside, C. N. and Roberts, J. S., "Quantum well AlGaAs/GaAs monolithic colliding pulse mode-locked laser", Elect. Lett. 29, 1135-1136, 1993.

[2] Choi, K. N. and Taylor, H. F., "Novel cross-correlation technique for characterization of subpicosecond pulses from mode-locked semiconductor lasers", Appl. Phys. Lett. 62, 1875-1877, 1993.

1:30pm - 1:45pm
M3.1

Sub-milliampere threshold InGaAs/GaAs/AlGaAs laser array elements by single step growth on nonplanar substrates

H. Zhao, M. H. MacDougal, K. Uppal, and P. D. Dapkus
Department of Electrical Engineering
University of Southern California
Los Angeles, CA90089-0483

Abstract--Ultra-low-threshold current InGaAs/GaAs lasers are made by single-step MOCVD growth on nonplanar substrates. Active region widths ranging from 1.6 to 0.2 μm have been studied. Uncoated laser threshold currents as low as 0.5mA has been obtained.

We have developed a technique to make low threshold buried heterostructure InGaAs/GaAs quantum well lasers by one step MOCVD growth on nonplanar substrates[1]. In this technique, active region widths as narrow as 0.2 μm can be fabricated[Fig. 1]. We have studied the threshold current dependence on the active region width as shown in Fig. 2[2]. Room temperature CW threshold currents as low as 0.5 mA for a uncoated double quantum well InGaAs/GaAs/AlGaAs laser are obtained.

The epitaxial growths were performed in an atmospheric pressure MOCVD reactor. The substrate nonplanarity is introduced by chemical etching of mesas with (100) tops and (111)A sidewalls. The growth properties of InGaAs/GaAs/AlGaAs on the mesa top and the mesa sidewall are strongly influenced by the sidewall orietation, growth temperature and V/III ratio[3]. By controlling these variables during the lower cladding layer growth, the mesa top width is reduced by 1 to 2μm depending on the growth conditions. The InGaAs quantum well growth rate on the (111)A mesa sidewall is 4 times smaller than on the (100) mesa top, resulting in a CL emission wavelength on the mesa sidewall that is about 100nm shorter than on the mesa top. This lateral effective bandgap variation will create a BH structure on the mesa top [4]. The width of this active region is controlled by the starting mesa width and the growth of the $Al_{0.6}Ga_{0.4}As$ lower cladding layer. Current confinment in this laser is provided by orietation-selective doping properties of the undoped $Al_{0.6}Ga_{0.4}As$ cladding layer which results in p-type doping on the (100) mesa top and n-type doping on the sidewalls [1,3].

The laser structure shown in fig. 1 has tight optical and current confinement. Fig. 2 shows the L-I curve of a SQW laser with 0.6μm wide active region. The RT CW threshold current for uncoated SQW lasers is 0.7mA and for uncoated DQW lasers is 0.5mA. These lasers have excellent external quantum efficiency of 80-85%. HR/HR coated 120μm long SQW lasers with 0.9μm wide active region showed a RT CW threshold current of 0.28mA. These lasers also exhibit exellent threshold and quantum efficiency uniformity and high yield because of the simple growth and processing procedures. Fig. 3 shows the threshold currents of 1 mA laser array elements on a single bar. Fig. 4 shows the threshold current dependence on the active region width for 250μm long DQW lasers as compared to the theoretical result from [2]. The minium threshold current occurs when the active region is about 0.4 μm wide. So far, the experimental results are generally 0.3 mA higher than the theoretical predictions for a perfect low threshold BH laser with no leakage. These lasers also have high modulation bandwidth at low bias currents.

In conclusion, we have developed a new technique to fabricate extremely low threshold current lasers by single step MOCVD growth on nonplanar substrates. Lasers made by this technique have the advantage of simple growth and processing procedure, good uniformity, high quantum efficiency and low threshold current. In this paper we will describe the growth and properties of these sub-milliampere laser elements and arrays made from them. The dependence of the device properties on the active region width, facet coating, and device length will be discussed.

References:

References:
[1] H. Zhao, M. H. MacDougal, N. C. Frateschi, P. D. Dapkus, S. Siala, and R. N. Nottenburg, IEEE Photonic Technology Lett., Vol. 6, No. 4, 1994
[2] J. S. Osinski, K. M. Dzurko, S. G. Hummel, and P. D. Dapkus, Appl. Phys. Lett., Vol.56, p2487, 1990
[3] H. Zhao, K. Uppal, M. H. MacDougal P. D. Dapkus, H. T. Lin, and D. H. Rich, to appear on J. Crystal Growth, Proceedings of the VII MOVPE conference, May, 1994
[4] E. Kapon, S. Simony, R. Bhat, D. M. Hwang, Appl. Phys Lett. 55, 2715 (1989); K. M. Dzurko, E. P. Menu, C. A. Beyler, J. S. Osinski, and P. D Dapkus, IEEE J. Quantum Elelctron. 25, 1450 (1989).

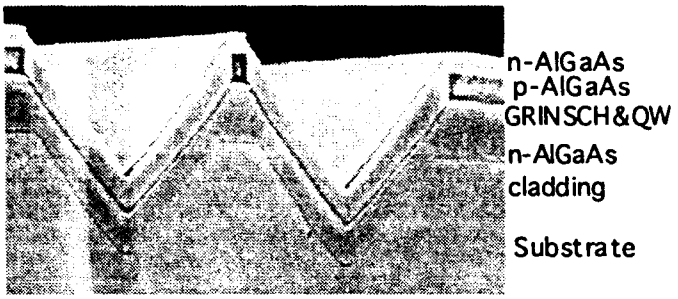

Fig1: SEM picture of the InGaAs/GaAs/AlGaAs laser structure. DQW active region is about 0.5 μm wide.

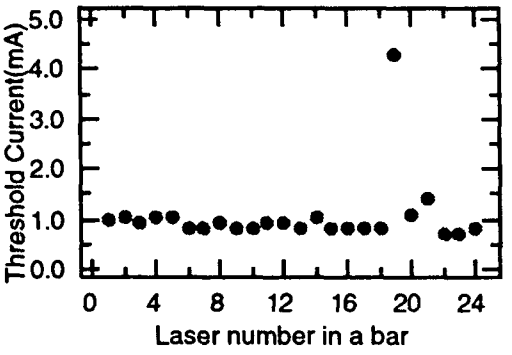

Fig3: Threshold currents of a laser array.

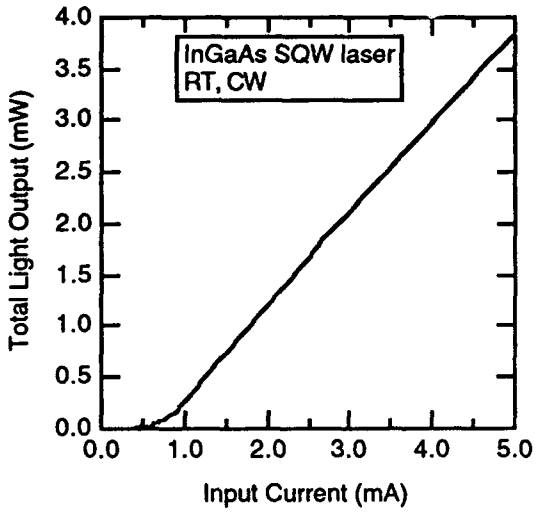

Fig.2: The L-I curve of a SQW laser with a 0.6μm wide active region.

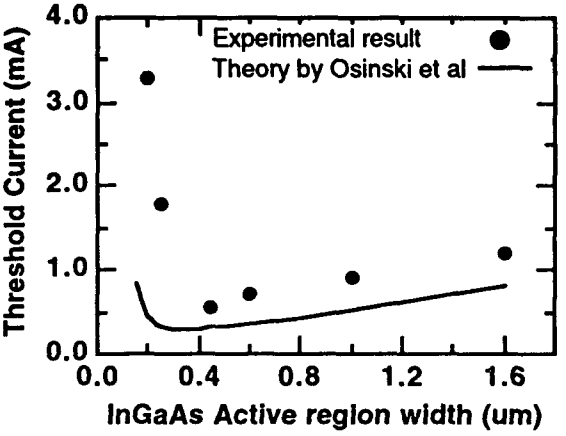

Fig. 4:Threshold current vs active region width.

1:45pm - 2:00pm

M3.2

Ultralow-Threshold (0.56 mA) 1.35-μm InGaAsP/InP Compressive-Strained-MQW Lasers

K. Uomi, T. Tsuchiya, M. Komori, A. Oka*, K. Shinoda, and A. Oishi*
Central Research Laboratory, Hitachi Ltd., *Fiberoptics Division, Hitachi Ltd.
1-280 Higashi-Koigakubo, Kokubunji, Tokyo 185, Japan

Abstract *Extremely low threshold currents of 0.56 mA (pulsed) and 0.58 mA (CW) have been obtained in a 1.35-μm InGaAsP/InP strained-MQW laser, at room temperature. These values are the lowest ever reported for long-wavelength lasers.*

Ultralow-threshold (<1 mA) lasers are required for many applications such as parallel high-throughput optical interconnections. Numerous reports have recently demonstrated that strained multi-quantum well (MQW) structures are very attractive for improving threshold current [1]-[3]. So far, a few studies have been done on submilliampere operation (0.98 mA [3], 0.80 mA [4]) of long-wavelength lasers without cooling, and below room temperature (as in [5]). In this paper, we report on a record-low threshold current of 0.56 mA, at room temperature, in long-wavelength semiconductor lasers, which was achieved by optimizing strained MQW active structure and by employing a short cavity with HR-coated facets.

Figure 1 shows a schematic cross section of a 1.35-μm strained-MQW-CBPBH (Constricted Blocking layer on p-substrate Buried Heterostructure) laser, grown by three-step MOVPE. The MQW active layer consists of five compressive-strained 5-nm InGaAsP wells, separated by 10-nm InGaAsP barriers. The active region was made 1.0-μm wide to reduce the threshold current based on our theoretical model [6]. The fabrication of CBPBH for lateral confinement has been described in detail previous literature [7], [8]. The amount of strain was optimized at 1.4%, to decrease the threshold current, by using a 200-μm-long HR-coated laser, as shown in Fig. 2. The increase in threshold at 2.0% strain was caused by misfit dislocation. Figure 3 shows the dramatic effect of decreasing cavity length L and increasing front facet reflectivity Rf on threshold current calculated for a 1.35-μm 1.4%-strained-MQW laser. In this calculation, the rear facet reflectivity Rr was assumed to be 0.985. As can be seen in Fig. 3, threshold current of about 0.5 mA is possible when Rf is made larger than 0.95 in order to reduce the mirror loss of short cavity (L=100 μm) lasers.

Figure 4 shows typical results of measured light-current characteristics of a 100-μm-long laser with different Rf and with Rr of 0.985 under pulsed operation (800 ns, 100 kHz) at 25°C. Figure 5 shows how measured threshold current depends on Rf for a number of devices; it also shows the calculated threshold current. Note that the extremely low threshold current of 0.56 mA was achieved by increasing Rf to 0.96. The estimated threshold current for this laser from the measured threshold current density is 0.53 mA, which indicates that the leakage current in the CBPBH structure is negligible. The CW threshold current was as low as 0.58 mA at 20°C, as shown in Fig. 6. Moreover, even at 90°C, CW threshold was only 1.62 mA. These are the lowest values ever reported for long-wavelength lasers, to our knowledge. These improvements were essentially attained by the optimization of the strained-MQW active layer and by employing a short cavity with HR-coated facets, as discussed earlier. The characteristic temperature was 68 K in the temperature range of 20-90°C. Further reduction in threshold current should be possible by using optimal design.

In conclusion, we demonstrated superior low-threshold 1.35-μm InGaAsP/InP strained-MQW lasers. Record threshold currents of 0.56 mA (pulsed) and 0.58 mA (CW) for a long-wavelength laser were obtained, at room temperature.

References

[1] H. Temkin et al., Appl. Phys. Lett., 57, 1610 (1990). [2] P. J. A. Thijs et al., IEEE J. Quantum Electron., QE-27, 1426 (1991). [3] C. Zah et al., IEEE J. Quantum Electron., QE-27, 1440 (1991). [4] J. S. Osinski et al., IEEE Photon. Tech. Lett., PTL-4, 1313 (1992). [5] P. J. A. Thijs et al., Electron. Lett., 28, 829 (1992). [6] K. Uomi et al., IEEE J. Quantum Electron., QE-29, 1426 (1993). [7] S. Yamashita et al., IEEE Photon. Tech. Lett., PTL-4, 954 (1992). [8] A. Oishi et al., ECOC'93, post deadline paper, ThC12.6 (1993).

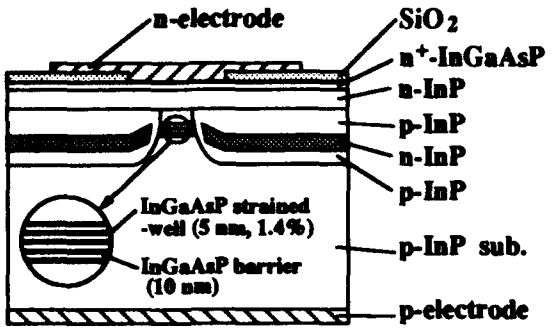

Fig. 1 Schematic diagram of a 1.35-μm compressive-strained MQW-CBPBH laser.

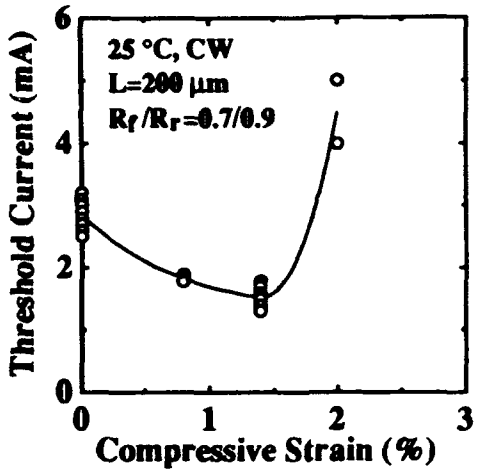

Fig. 2 Strain dependence of measured threshold current for 200-μm-long MQW lasers.

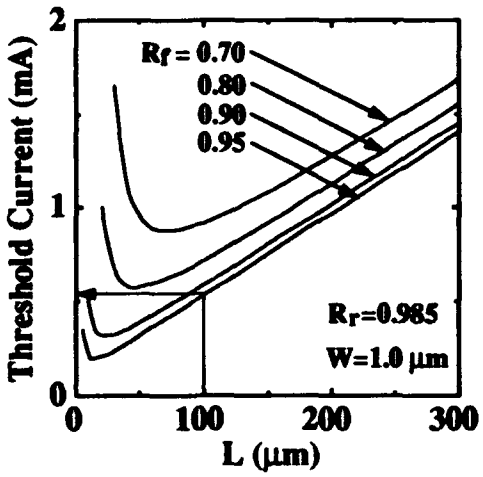

Fig. 3 Calculated threshold current for a 1.35-μm strained-MQW laser with various cavity lengths and facet reflectivities.

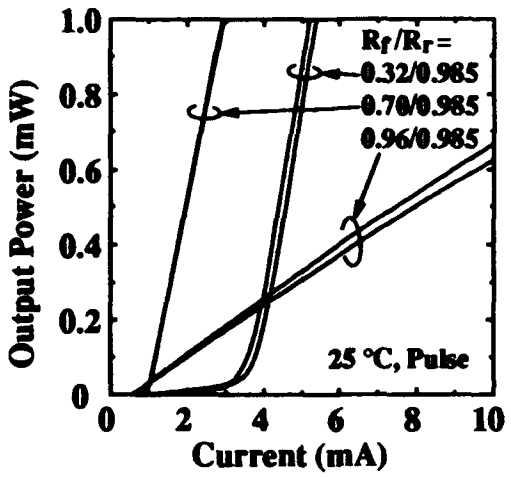

Fig. 4 Light-current characteristics of a 100-μm-long laser with different facet reflectivities.

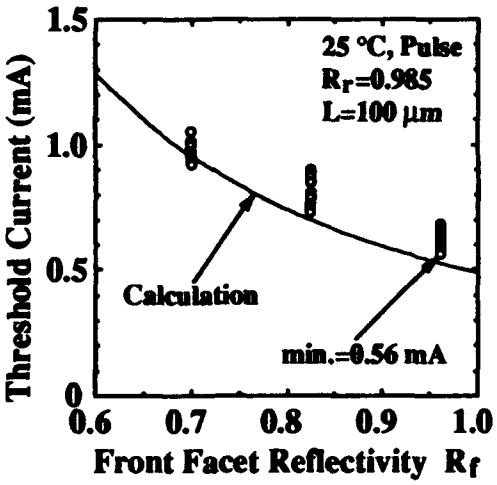

Fig. 5 Measured (o) and calculated threshold current as s function of front facet reflectivity.

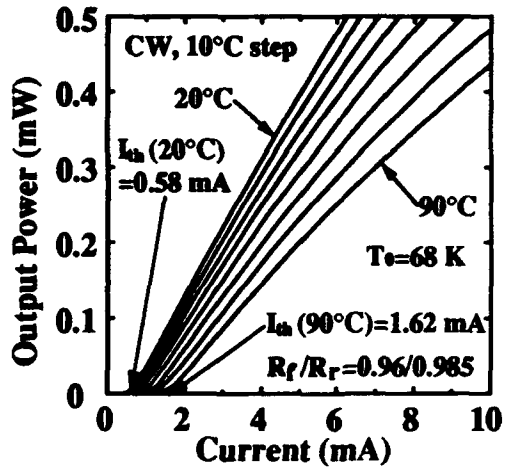

Fig. 6 Temperature dependence of CW light-current characteristics of a 100-μm-long (Rr=0.96, Rr=0.985 coated) laser.

2:00pm - 2:15pm
M3.3

InGaAs/InGaAsP Strained SQW LD Grown on $In_{0.05}Ga_{0.95}As$ Ternary Substrate

H. Shoji, T. Uchida, T. Kusunoki, M. Matsuda, H. Kurakake,
S. Yamazaki, K. Nakajima, and H. Ishikawa
Fujitsu Laboratories Ltd., 10-1 Morinosato-Wakamiya, Atsugi 243-01, Japan

Abstract: A uniform $In_{0.05}Ga_{0.95}As$ ternary substrate was grown and InGaAs/InGaAsP SQW LDs were fabricated on the substrate for the first time. Low threshold current density of 222 A/cm^2 and excellent characteristic temperature of 221 K were achieved.

High performance 1.3 μm laser is strongly required for future optical access systems and optical interconnection systems. Performance of 1.3 μm laser on InP substrate is, however, inferior to that of 0.98 μm laser on GaAs substrate especially in temperature characteristics. By using ternary $In_xGa_{1-x}As$ substrate, we can design deeper potential well such as realized on GaAs substrate, which would lead to higher optical gain and better temperature characteristics in 1.3 μm lasers [1]. This time, we have grown a ternary bulk crystal of $In_{0.05}Ga_{0.95}As$ and fabricated InGaAs/InGaAsP SQW laser on the ternary substrate. Low threshold current density of 222 A/cm^2 and excellent characteristic temperature of 221 K were obtained in the laser emitting at 1.03 μm. Although higher In content of around 0.25 is required for 1.3 μm lasers, we could successfully fabricate SQW LD on the ternary substrate as the first step.

An $In_{0.05}Ga_{0.95}As$ ternary crystal was grown by using liquid encapsulated Czochralski (LEC) technique with a method of supplying GaAs source material [2, 3]. As shown in Fig. 1, a ternary bulk crystal with a diameter of 1.5 cm was obtained. On the ternary substrate, a DH structure shown in Fig. 2 was grown by using MOVPE. Active layer consists of 7 nm-thick $In_{0.25}Ga_{0.75}As$ strained SQW (λ_{act} = 1.03 μm) sandwiched by 100 nm-thick InGaAsP SCH layers (λ_{SCH} = 0.845 μm). After the growth, mesa-stripe of 20 μm width was formed by C_2H_6-RIE. Coplanar structure was employed for current injection because no impurity was introduced in the substrate. Fig. 3 shows light output and voltage versus injected current characteristics of a 600 μm-long laser at 25 °C. Threshold current of 26.7 mA and the corresponding threshold current density of 222 A/cm^2 were obtained. The emission wavelength was 1.03 μm. Temperature dependence of the threshold current is shown in Fig. 4. Characteristic temperature T_0 was as high as 221 K, which was comparable or superior to that of 0.98 μm laser on GaAs substrate. These results indicate that the ternary substrate has sufficient quality for laser fabrication and that increased In content will enable 1.3 μm lasers with excellent temperature characteristics.

References:

[1] H. Ishikawa, *Appl. Phys. Lett.*, **63**, 712 (1993).
[2] K. Nakajima, C. Takenaka, and T. Kusunoki, *J. Crystal Growth*, **113**, 485 (1991).
[3] T. Kusunoki, C. Takenaka, and K. Nakajima, *J. Crystal Growth*, **115**, 723 (1991).

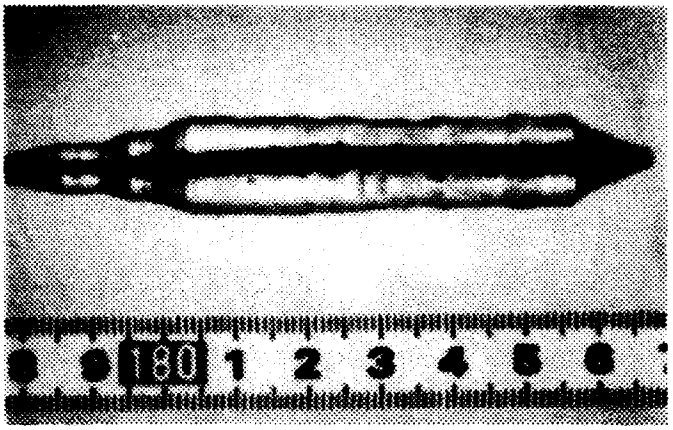

Fig. 1 $In_{0.05}Ga_{0.95}As$ ternary bulk crystal grown by using LEC technique with a method of supplying GaAs source material. Diameter is about 1.5 cm. No impurity is introduced.

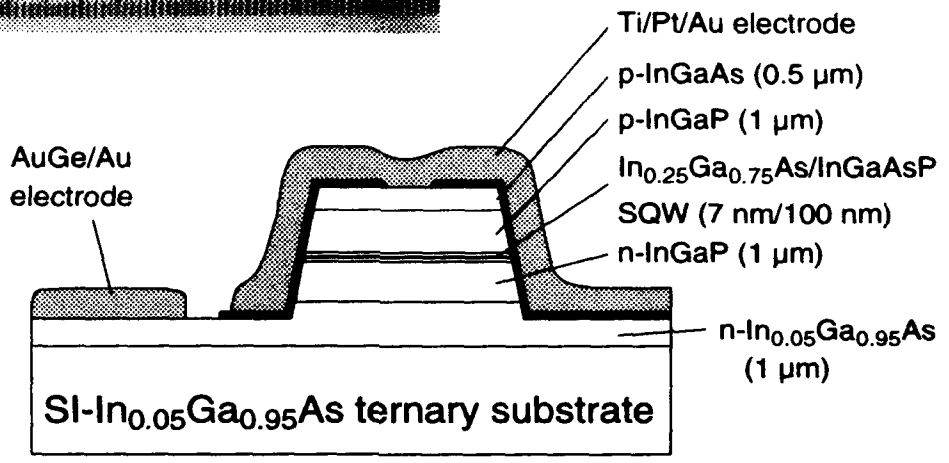

Fig. 2 Cross-sectional view of $In_{0.25}Ga_{0.75}As$/InGaAsP SQW LD grown on SI-$In_{0.05}Ga_{0.95}As$ ternary substrate. Width of mesa-structure is 20 μm.

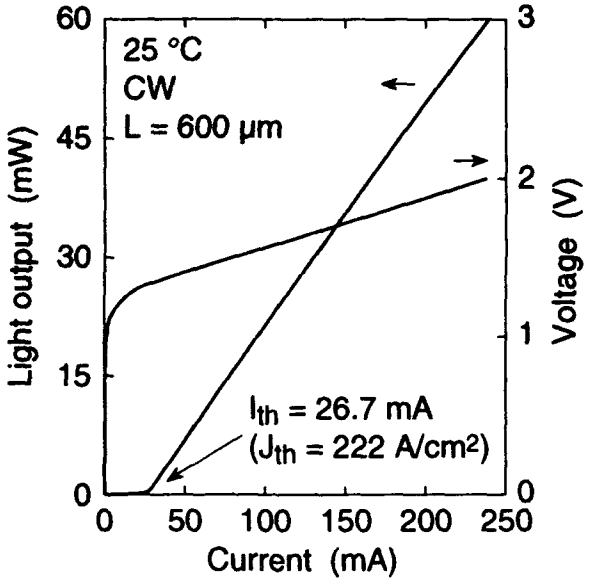

Fig. 3 L-I and V-I characteristics at 25 °C under cw condition. Cavity length is 600 μm and both facets are as-cleaved.

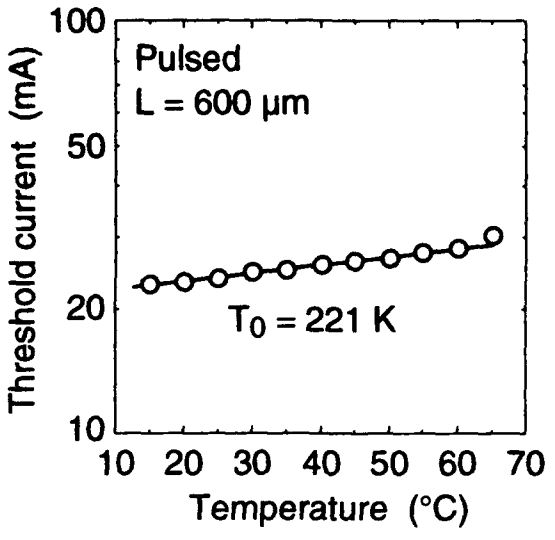

Fig. 4 Temperature dependence of threshold current. Characteristics temperature T_0 is 221 K.

2:15pm - 2:30pm

M3.4

High T_0 1.3 μm InGaAs Strained Single Quantum Well Laser with InGaP Wide Band-Gap Clad Layers

H. Kurakake, T. Uchida, K. Kubota, S. Ogita, H. Soda, and S. Yamasaki

Fujitsu Laboratories Ltd.

10-1 Morinosato-Wakamiya, Atsugi 243-01, Japan

1.3 μm laser simulation taking hot carriers into account indicated the effectiveness of wide band-gap clad layers for improving laser. Lasers fabricated with InGaP cladding layers based on these calculations exhibited the high T_0 of 100K.

The poor temperature characteristic of InGaAsP/InP lasers, remains to be solved after the introduction of strained active layers has drastically improved the threshold current and efficiency. Taking into consideration carrier leakage, we demonstrate theoretically and experimentally that wide band-gap clad layers are effective for increasing the gain coefficient and characteristic temperature without an increasing the threshold current.

To accurately model the carrier leakage, we are the first time to introduce the hot carrier phenomenon into the conventional laser simulations. In our simulation, energy conservation equations for both electrons and holes were solved with a self-consistent set of Poisson equation, current continuity equations, and optical rate equation [1]. Figure 1 shows calculated carrier temperatures Tc at Ith and 7 times Ith for an InGaAs single quantum well laser with InGaP clad layers (Eg=1.52 eV). Carrier heating induces carrier leakage in the waveguide and clad layers as shown in Fig. 2, and reduces a differential efficiency. It was found that the carrier leakage depends on the threshold carrier density and band gap of the clad layers. Figure 3 shows dependence of the injection efficiency on mirror loss for InP and InGaP clad SQW lasers. The injection efficiency η was defined as a ratio of the stimulated emission photon numbers to total carriers injected and obtained from the calculated differential quantum efficiency. The InGaP clad laser showed higher injection efficiency and the weak mirror loss dependence, due to the large band discontinuity between waveguide and clad layers and tight optical confinement. These calculated results predict that use of wider bandgap clad layers will increase gain coefficient and an insensitive threshold current for changes of mirror loss or temperature.

Figure 4 shows the designed and grown laser wafer structure based on our calculated results. The laser wafer was grown by MOVPE on a n-GaAs substrate. To grow $In_{0.3}Ga_{0.2}P$ wide band-gap clad layers we used a 2.4 μm thick compositional graded InGaAs buffer layer and a 1 μm thick $In_{0.3}Ga_{0.7}As$ buffer layer lattice matched to the wide band-gap clad layers. An $In_{0.4}Ga_{0.6}As$ strained active layer was sandwiched between two 100 nm thick nondoped-$In_{0.4}Ga_{0.6}As_{0.8}P_{0.2}$ waveguide layers. We fabricated metal-stripe lasers with a 80 micron-wide electrode from this wafer to evaluate the lasing characteristics. The lasing wavelength was 1.27 μm at room temperature. Figure 5 shows the measured threshold current densities J_{th} for various cavity lengths from 300 μm to 900 μm. The gain coefficient of our InGaAs/InGaP lasers (G_0=1530cm^{-1}) was found to be twice as high as that of InGaAs/InP lasers (G_0=823cm^{-1}) with almost same well volume. This result agrees well with the calculated increase in the injection efficiency. Figure 6 shows the temperature dependence of the threshold current density for HR/HR coated InGaAs/InGaP laser with a 20 nm thick well. As expected, a high T_0 of 100K is obtained between 15°C and 55°C because the injection efficiency is insensitive the increase in the threshold carrier density.

In summary we have calculated and demonstrated the effectiveness of wide band-gap InGaP clad layers for high performance 1.3 μm lasers with high characteristic temperatures.

Reference

[1] H. Kurakake, T. Inoue, S. Kubota, T. Higashi, and H. Soda: IEICE (OQE) in Japan vol. 93, 7(1994)

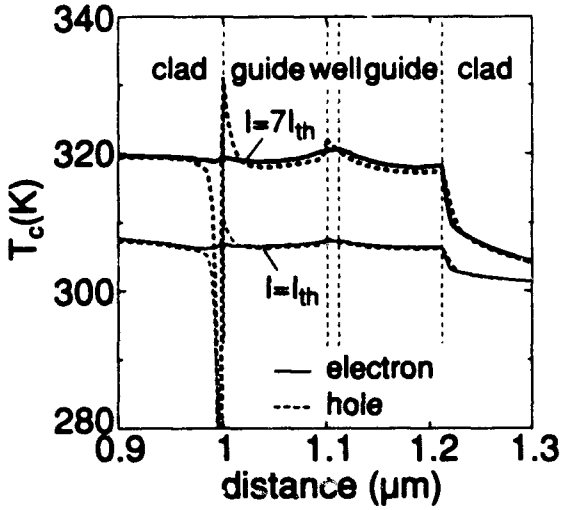

Fig.1 Carrier temperature for InGaAs/InGaP laser

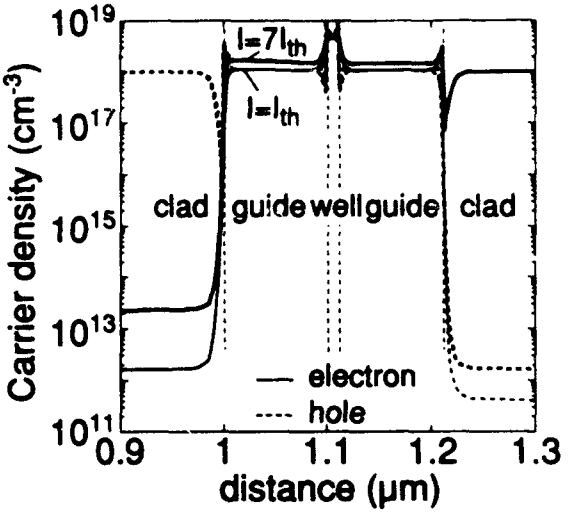

Fig.2 Carrier distribution for InGaAs/InGaP laser

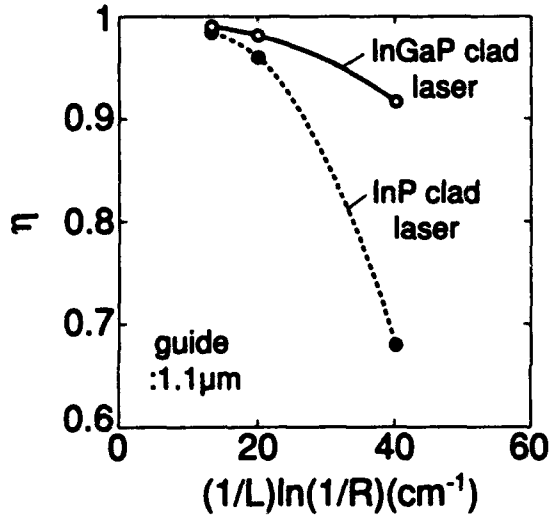

Fig. 3 Calculated injection efficiency dependence on mirror loss (12nm thick InGaAs single quantum well and 100nm thick InGaAsP waveguide layers :λ_g=1.1 μm)

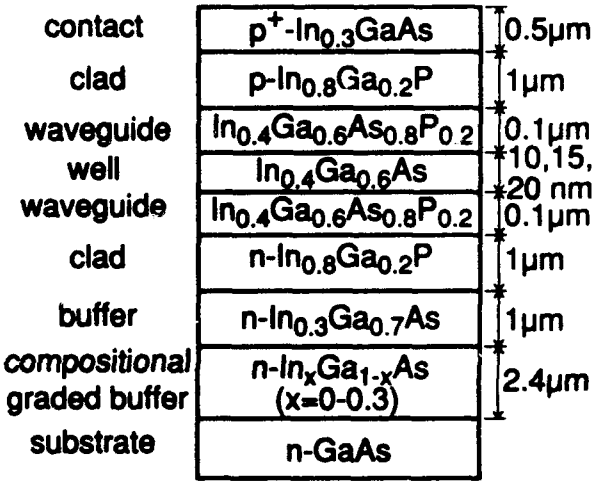

Fig. 4 A schmatic layer structure of fabricated InGaAs/InGaP laser

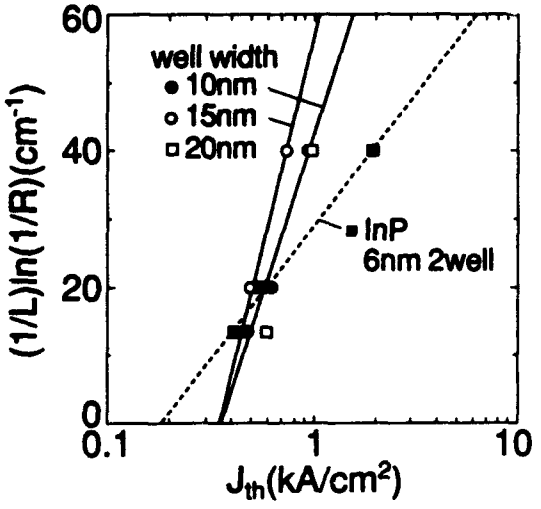

Fig. 5 Cavity length dependence of measured threshold current density

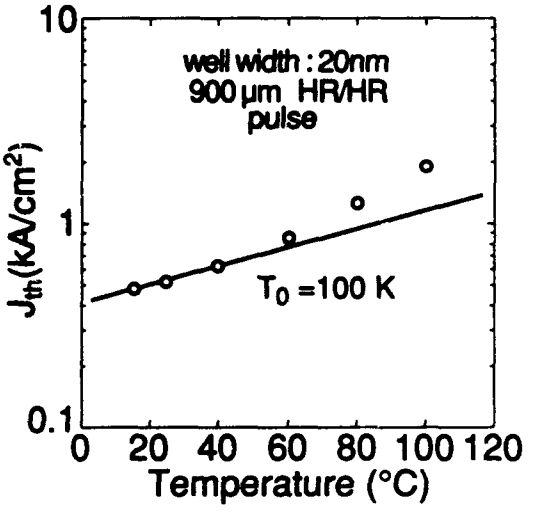

Fig. 6 Temperature dependence of threshold current density J_{th}

2:30pm - 2:45pm

M3.5 1.55μm Strained GaInAs/AlGaInAs MQW Lasers with a Multi-Quantum Barrier

H. Shimizu, T. Fukushima, K. Nishikata, Y. Hirayama and M. Irikawa
The Furukawa Electric Co., Ltd., Yokohama R&D Laboratories
2-4-3 Okano, Nishi-ku, Yokohama 220 , Japan

Abstract: We have fabricated 1.55μm strained GaInAs/AlGaInAs MQW lasers with a multi-quantum barrier (MQB). A reduction of carrier leakage upon incorporation of the MQB structure was demonstrated experimentally in long-wavelength lasers for the first time.

Summary: The MQB [1] has been proposed as a method to suppress electron leakage. In the 0.6μm MQB-loaded AlGaInP lasers, improved lasing performances have been experimentally demonstrated [2]. On the other hand, in long-wavelength lasers, the effect of the MQB has not been demonstrated experimentally in spite of the theoretical predictions on the electron wave confinement effect of the MQB [3,4].

We have grown 1.55μm GaInAs/AlGaInAs MQW lasers a) with MQB at the SCH layer and b) without MQB, on n-InP substrates by MBE, which consisted of p-, n-AlInAs cladding, quaternary SCH (λ_g=1.15μm), 1% compressively strained MQW active layer and p-GaInAs contact (Fig.1(a), 1(b)). The MQW active region consisted of 1% compressively strained four 3.4nm $Ga_{0.32}In_{0.68}As$ quantum wells with 15nm quaternary barrier layers of the same composition as SCH. The MQB structure consisted of an AlGaInAs first barrier (d=80ML) and a multilayer with lattice matched undoped GaInAs wells (10MLx3, 8MLx2, 7MLx4) and undoped AlInAs barriers (8MLx3, 5MLx5). The optical confinement factors for both structures are equal. The structures were confirmed by TEM and X-ray measurements.

Figure 2 shows cavity length dependence of threshold current densities. The measurement was performed on 150μm-wide metal stripe lasers. Both structures had equivalent threshold current densities J_{th} within experimental errors, 1.3kA/cm^2 at L=400μm, 1.08kA/cm^2 at L=800μm, respectively. Values for the strained MQW lasers are comparable to the MBE-grown results reported earlier [5]. Since both structures show equivalent log(current)-voltage curves, carrier injections were not interfered at the MQB heterointerfaces.

Ridge waveguide lasers with the mesa width of 4μm were fabricated. The *L-I* characteristics were investigated at various temperatures. Characteristic temperature T_O values for both structures were around 60K in the range of 25~50°C. However, the degradation rate of external differential efficiencies (η_d) with increasing temperature shows an obvious difference between the two structures (fig.3). The degradation rate of η_d for the lasers with MQB was smaller than that for the lasers without MQB. To clarify the origin of this difference, spontaneous emissions under the laser threshold were measured at various temperatures. Figure 4 shows the spontaneous emission spectrum of the lasers at 100°C and 80mA. A second peak due to carrier overflow emerges around

1.15μm, which corresponds to the band-gap wavelength of the AlGaInAs confinement layers. The second peak is more clearly visible in the lasers without MQB than those with MQB, indicating that a large reduction of carrier leakage occurs upon incorporation of the MQB structure to the SCH layer. This reduction in carrier leakage will further improve laser performance such as high-speed operation and small turn-on delay [6].

In summary, we have fabricated 1.55μm strained GaInAs/AlGaInAs MQW lasers with MQB. The reduction of carrier leakage and improvement on the temperature dependence of slope efficiencies upon incorporation of the MQB were demonstrated in long-wavelength lasers for the first time.

References: (1) K.Iga et al., Electron.Lett.22(1986)1008 (2) K.Kishino et al., Appl.Phys.Lett.58(1991)1822 (3) H.Uenohara et al., IEICE Jpn.J70-C(1989)No.6,851 (4) M.Irikawa et al., Jpn.J.Appl.Phys.31(1992)L1351 (5) M.J.Mondry et al., Electron.Lett. 28(1992)1471 (6) T.Fukushima et al., J.Quantum Electron.,29(1993)1536

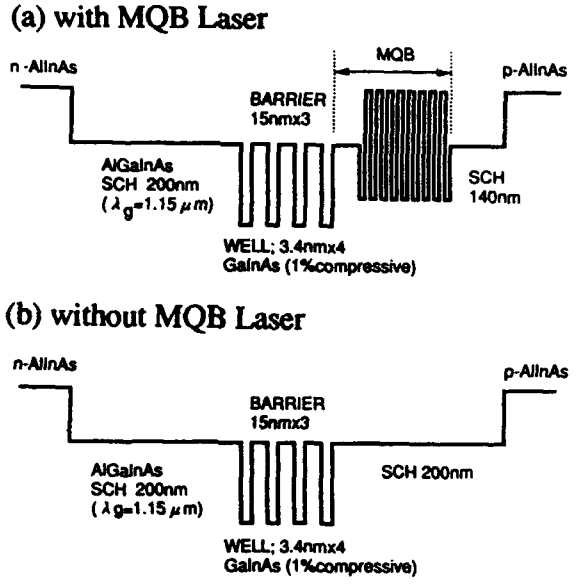

Figure 1 Schematic band diagrams of the lasers

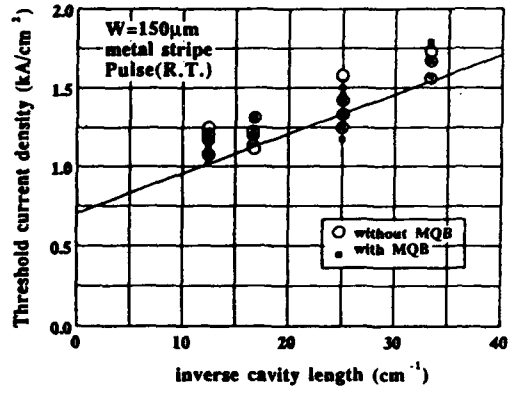

Figure 2 Inverse cavity length dependence of threshold current densities

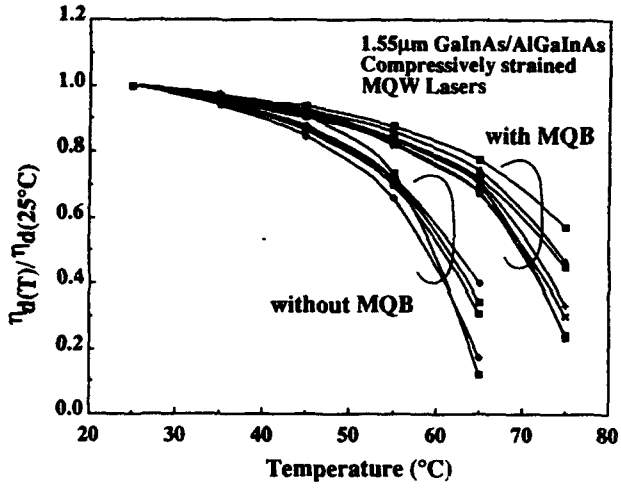

Figure 3 Temperature dependence of normalized external differential efficiencies

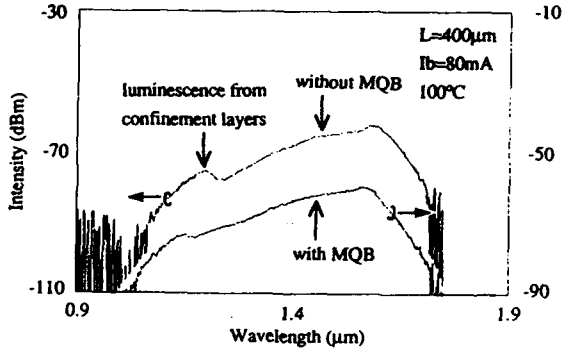

Figure 4 Spontaneous emission of SCH lasers at 100°C, I_b=80mA

2:45pm - 3:00pm
M3.6

InAsSb/AlAsSb Double-Heterostructure and InAsSb/InAlAs Quantum-Well Diode Lasers Emitting at ~4 μm

H. K. Choi, G. W. Turner, and Z. L. Liau
Lincoln Laboratory, Massachusetts Institute of Technology
Lexington, MA 02173-9108, U.S.A.

InAsSb/AlAsSb double-heterostructure lasers emitting at 3.9 μm operated pulsed up to 170 K and cw up to 105 K, with cw power of 30 mW at 70 K. InAsSb/InAlAs quantum-well lasers emitting at 4.5 μm operated pulsed up to 85 K.

Semiconductor diode lasers emitting in the mid-infrared (2 – 5 μm) band are being developed to provide efficient sources for applications such as laser radar, remote sensing, pollution monitoring, and molecular spectroscopy. Diode lasers with GaInAsSb active layers and AlGaAsSb confining layers grown on GaSb substrates are promising for high-performance sources in this spectral region. For lasers emitting at ~ 2 μm, we have achieved significant improvements in room-temperature performance by employing a GaInAsSb/AlGaAsSb quantum-well (QW) active region and AlGaAsSb cladding layers. Broad-stripe lasers have exhibited pulsed threshold current density J_{th} as low as 143 A/cm^2 and single-ended cw output power as high as 1.3 W [1]. For lasers emitting at 4 μm, we reported double-heterostructure (DH) lasers with a ternary InAsSb active layer and AlAsSb cladding layers, that operated pulsed up to 155 K and cw up to 80 K [2]. Even though these lasers exhibited better performance than any other III-V diode lasers with emission wavelengths longer than 3.5 μm, the performance was limited by substantial lattice mismatch in the laser structure. The output power at 80 K was less than 1 mW. In this paper, we report improved InAsSb/AlAsSb DH lasers emitting at ~3.9 μm. These devices have operated pulsed up to 170 K and cw up to 105 K, with single-ended cw power of 30 mW at 70 K. In addition, we report preliminary results on the first InAsSb/InAlAs QW lasers emitting at 4.5 μm.

The laser structures were grown on GaSb substrates by molecular beam epitaxy. The DH structure has a 0.8-μm-thick nominally undoped InAsSb active layer, sandwiched between 3-μm-thick AlAsSb cladding layers. Double-crystal x-ray diffraction measurement of the laser structure showed that the lattice match was better than 2.5×10^{-3}.

Broad-stripe lasers 60 or 100 μm wide and 500 μm long were fabricated by SiO_2 patterning. Figure 1 shows the pulsed J_{th} of a 100-μm-wide device for temperatures between 60 and 170 K. At 60 K, the value of J_{th} is 36 A/cm^2. The characteristic temperature T_0 for the entire temperature range is 20 K, which is higher than 17 K observed for the previous InAsSb/AlAsSb DH lasers [2]. At the maximum operating temperature of 170 K, the value of J_{th} is 8.5 kA/cm^2, which is substantially lower than 24.4 kA/cm^2 obtained for the previous DH lasers at 155 K [2]. We believe that these improvements are mostly due to careful lattice matching and better growth conditions.

Figure 2 shows the cw output power vs current curves for a 60-μm-wide laser at heatsink temperatures from 80 to 105 K. The maximum power at 80 K is 12.5 mW/facet, with initial differential quantum efficiency of 19% from both facets. Another device 100 μm wide was coated to have high (~ 90%) and low (~ 10%) reflectivity on the back and front facets, respectively. The maximum power from this device at 70 and 80 K is 30 and 24 mW, respectively.

In order to increase the emission wavelength and improve device performance, we grew a QW structure that has an active region consisting of 15 pairs of compressively

strained InAsSb wells and tensile-strained InAlAs barriers, surrounded by AlAsSb cladding layers. Calculation of band positions by including strain effects shows that InAlAs provides potential barriers to both electrons and holes. Figure 3 shows the pulsed J_{th} vs temperature of a QW laser. The minimum J_{th} is 320 A/cm^2 at 50 K, and the maximum operating temperature is 85 K. The value of T_0 is 26 K for temperatures between 50 and 70 K. As shown in Fig. 4, the emission wavelength is 4.5 μm, which is the longest value obtained for III-V diode lasers, except for InSb homojunction lasers that operated only at 10 K [3]. Much higher performance is expected for lasers grown under optimum conditions.

This work was sponsored by Phillips Laboratory, the Department of the Air Force.

REFERENCES

[1] H. K. Choi, G. W. Turner, and S. J. Eglash, IEEE Photon. Technol. Lett. **6**, 7 (1994).

[2] S. J. Eglash and H. K. Choi, Appl. Phys. Lett. **64**, 833 (1994).

[3] I. Melngailis, R. J. Phelan, and R. H. Rediker, Appl. Phys. Lett. **5**, 99 (1964).

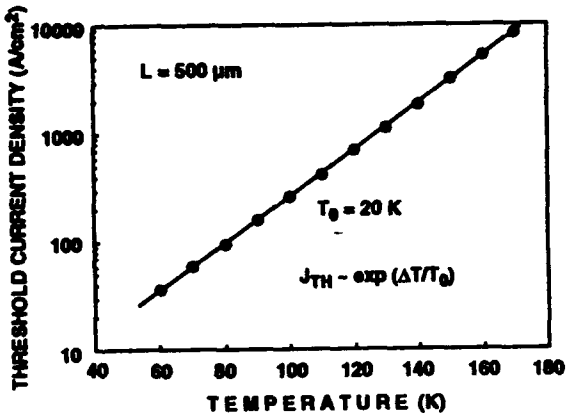

Fig. 1. Pulsed threshold current density of InAsSb/AlGaAsSb DH laser.

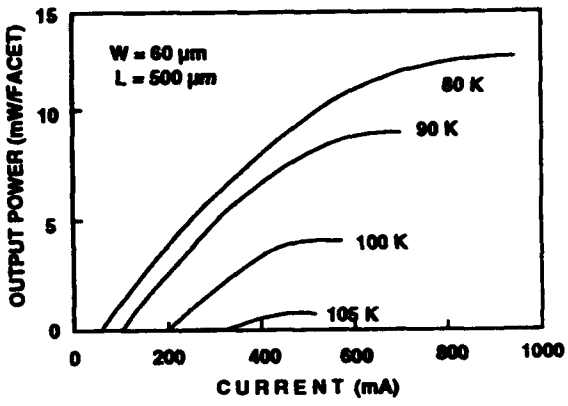

Fig. 2. CW power vs current of InAsSb/ AlAsSb DH laser at several heatsink temperatures.

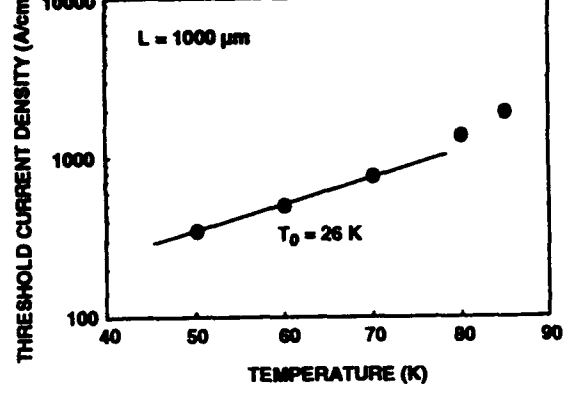

Fig. 3. Pulsed threshold current density of InAsSb/InAlAs QW laser.

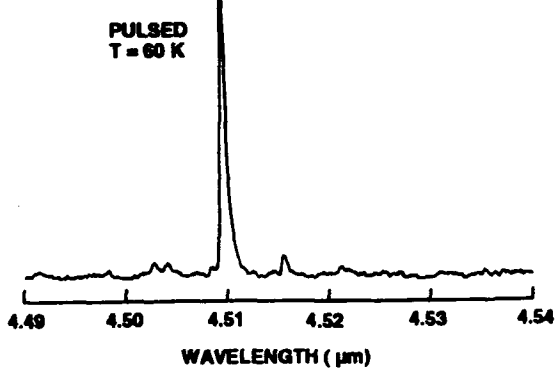

Fig. 4. Emission spectrum of InAsSb/ InAlAs QW laser.

3:30pm - 3:45pm
M4.1

Integration of a Tunable 4-Section DBR Laser within Polarization Diversity Heterodyne Receiver PICs

R. Kaiser, F. Fidorra, D. Trommer, S. Malchow
P. Albrecht, D. Franke, H. Heidrich, W. Passenberg, H. Schroeter-Janßen, R. Stenzel, W. Rehbein
Heinrich-Hertz-Institut für Nachrichtentechnik Berlin GmbH
Einsteinufer 37, D-10587 Berlin, Germany,Tel: +49 30 31002 256; Fax: +49 30 31002 558

Abstract:
Polarization div heterodyne receiver PICs including a tunable 4-section DBR laser as a local oscillator have been successfully fabricated for the first time. PIC design and fabrication are described and characteristics of the integrated laser components are presented.

Introduction:
The availability of low cost photonic integrated circuits (PICs) is expected to become very important for the economic installation of future optical communication systems. Due to its nearly ideal filter characteristics the heterodyne receiver (HR) is a promising candidate for exploiting the full fibre capacity within optical frequency division multiplexing (OFDM) networks. The advantages of a monolithically integrated HR (including the local oscillator) are its compactness, the elimination of an expensive optical isolator, and the fact that only a single fibre needs to be attached to the chip. In this paper we report on the first fabrication of GaInAsP/InP polarization diversity heterodyne receiver PICs (PDHR) and basic balanced heterodyne receiver PICs (BBHR) including a tunable 4-section DBR laser as a local oscillator. Both receiver chips have been fabricated on 2" semi-insulating InP:Fe wafers and represent - to our knowledge - the most complex optoelectronic integration concerning the number of different semiconductor devices based on InP so far.

PIC Design:
The structure PDHR-PIC is shown schematically in Fig. 1. The device consists of 16 elements: A tunable 4-section buried heterostructure DBR laser with a passive polarization rotator, a signal input port, a polarization diversity waveguide network (two TE/TM-mode splitters, two TE/TM-mode filters, and two 3-dB couplers), and a detector unit in a balanced receiver configuration (four photodiodes, two junction field effect transisitors (JFETs), and two load resistors). Even the somewhat simpler BBHR-PIC (DBR laser, 3-dB coupler, balanced photodiodes, JFET, and load resistor) is more complex than other laser integrated HRs reported to date /1,2/.

Laser Technology within the PIC Fabrication:
The tunable laser is the most complicated element in these receiver circuits facing the most technological challenges and encompasses about two third of the total effort for the PIC fabrication. The laser has an GaInAsP (λg = 1.3 µm) stripe waveguide and is butt coupled to the low loss strip loaded semi-insulating GaInAsP:Fe (λg = 1.05 µm) waveguide of the passive polarization diversity network. The butt coupling scheme was chosen because it offers the chance to change and optimize independently the design of both the laser and network components. The chip processing starts with the growth of the basic laser layer stack by MOVPE including an n-contact layer and etch stop layers for vertical structuring /3/. The next main processing steps are as follows: 1) Formation of a 400 µm long gain section, a 300 µm long high reflector Bragg section near the PIC cleaved facet, a 110 µm phase section, and a 150 µm partial Bragg reflector internal to the chip, - 2) grating overgrowth, - 3) formation of a laser island by a special two step etching process,- 4) nearly planar selective area regrowth of the semi-insulating waveguide layer stack around the laser island by employing an improved two step MOVPE which is necessary for the polarization rotator fabrication /4/,- 5) formation of the laser stripe by etching deep trenches down to the n-contact layer using a special etching procedure, - 6) planar selective area regrowth of current blocking layers on both sides of the laser stripe , - 7) growth of the laser p-cladding and formation of the laser into a mesa ,- 8) growth of the GaInAs detector layers using MBE and removal of these layers in the laser and waveguide regions, - 9) etching of a laser n-contact window, - 10) formation of the p- and n-contacts for the laser and detector unit simultaneously, - 11) etching and metallization of the polarization diversity waveguide network. The entire fabrication process involves at present 7 epitaxial growths (3 selective and 4 full wafer growth steps) , 23 photolithographic exposures, and about 150 processing steps altogether.

First Results on Integrated Laser Components:

The threshold currents are 15-25 mA. The laser tuning ranges are ≤5.5 nm (680 GHz) at center wavelengths λo between 1547 and 1551 nm (c.f. Fig. 2). At λo the side mode suppression ratio (SMSR) and linewidth are 30 dB - 38 dB and ≤ 50 MHz, respectively. In case of an optimum butt coupling between laser and network waveguide we found coupling losses of 2-3 dB /3/. The waveguide facet power-current characteristic of a DBR laser/polarization rotator subcomponent chip - cleaved from the PIC wafer - is depicted in Fig. 3 for TE-, TM-, and un-polarized light. From measurements on single polarization converters rotation angles of 40°-42° were obtained. The average loss of the polarization rotator was estimated to be 1.4 dB which is the lowest value for this kind of polarization converter reported to date. The photocurrent-laser current characteristic of a BBHR-PIC at the cross output port of the 3 dB-coupler is shown in Fig. 4. First optical heterodyne beat spectra with unmodulated input light have been recorded from the BBHR-PICs.

References:

/1/ T.L. Koch et al., Electronics Lett., Vol. 25, No. 24, pp. 1621-1623, 1989.

/2/ H. Takeuchi et al., IEEE Photon. Technol. Lett., Vol. 1, No. 11, pp.398-400, 1989.

/3/ R. Kaiser et al., Proc. of InP & Rel. Materials Conf., pp. 476-479, Santa Barbara,USA, 1994.

/4/ H. Heidrich et al., IEEE Photon. Technol. Lett., Vol. 4, No. 1, pp. 34-36, 1992.

Fig. 1. Schematic of the PDHR-PIC.

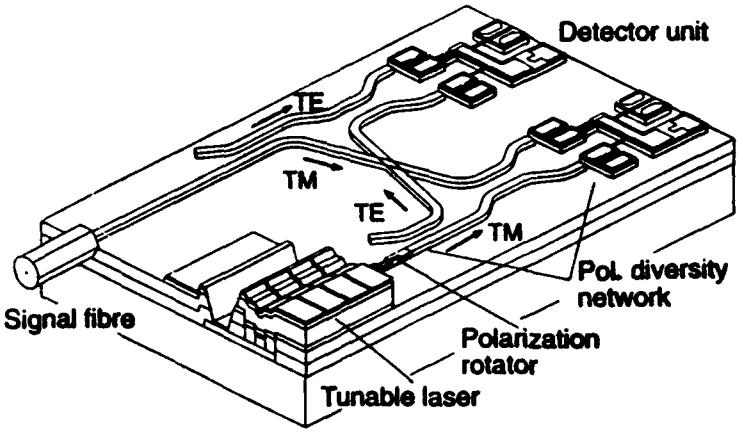

Fig. 2.
Selection of 11 single mode channels over a 5.4 nm laser tuning range.

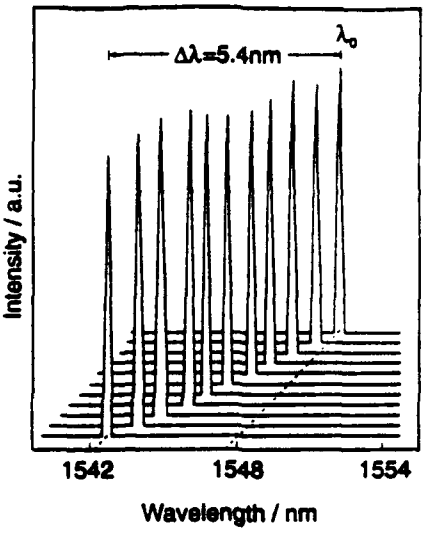

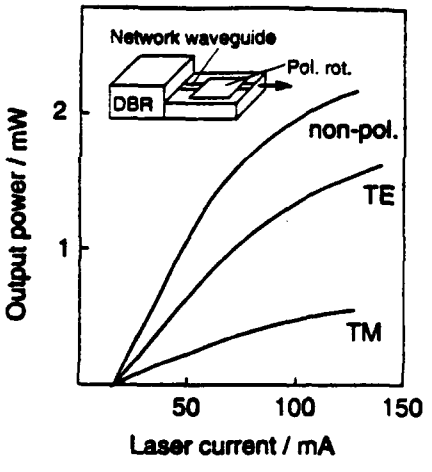

Fig. 3. Power-current characteristics of an integrated laser/pol. rot. submodule.

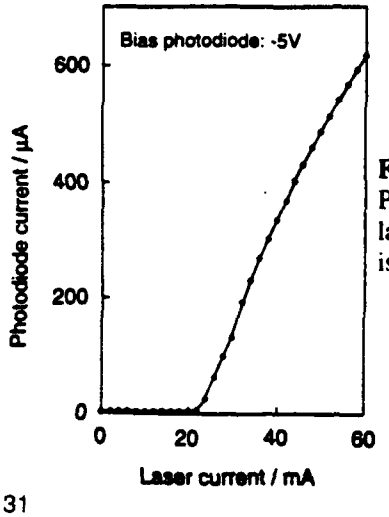

Fig. 4.
Photodiode current - laser current characteristic on the BBHR-PIC.

3:45pm - 4:00pm

M4.2 Complete Single Mode Wavelength Coverage over 40 nm with a Super Structure Grating DBR Laser.

M. Öberg, P.-J. Rigole, S. Nilsson, T. Klinga, L. Bäckbom, K. Streubel and J. Wallin

Laboratory of Photonics and Microwave Engineering, Department of Electronics,
Royal Institute of Technology, Electrum 229, S-164 40 Kista, Sweden

T. Kjellberg

Department of Optoelectronics and Electrical Measurements
Chalmers University of Technology, 412 96 Göteborg, Sweden

Abstract: We experimentally show that every wavelength in an interval of 40 nm can be reached with a side-mode suppression usually better than 30 dB using a super structure grating (SSG) DBR laser.

Wavelength tunable single mode semiconductor lasers are important components in fibre optical communication networks as well as in measurement and sensor applications. Widely tunable lasers have been demonstrated with tuning range exceeding 50 nm. Examples are the Y-laser [1], sampled (super structure) grating DBR lasers [2,3], and the vertical Grating assisted codirectional Coupler laser with rear Sampled grating Reflector (GCSR) laser [4]. So far however, gaps in the wavelength-tuning current characteristics are normally seen and not every wavelength in the total tuning span can be reached with a reasonable side mode suppression. We show that for a carefully designed super structure grating DBR laser every wavelength in a tuning interval exceeding 40 nm can be reached without changing the gain current or the laser temperature.

The SSG-DBR laser consists of 4 sections: 2 SSG reflector sections with different sampling period, providing multiple reflection peaks, a gain section, and a phase section for fine tuning. The SSG reflector is designed to provide low ripple reflection in a 60 nm wide window with reflection peaks separated by 7 nm. The reflector design was realised using a matrix based program [5]. The broadband reflection characteristic was obtained by mixing gratings with five different grating periods as shown in Fig 1. Fig 2 shows the reflection of the 400 μm long SSG-DBR with no waveguide loss. The grating coupling coefficient is estimated to 110 cm^{-1}.

The fabrication of the laser includes five epitaxial steps. The active material is bulk InGaAsP (λ_g=1.58 μm). The super structure gratings are written by e-beam lithography with sampling periods of 44.4 μm in the front Bragg section and of 49.4 μm in the rear Bragg section. The gain section is 250 μm long, the phase tuning section is 150 μm, the rear Bragg section is 680 μm and the front Bragg section is 390 μm long. Both ends of the laser are anti-reflection coated (R<1%) to avoid unwanted Fabry-Perot reflections.

All the wavelength tuning measurements were made with a fixed current of 160 mA into the gain section and at a fixed heat sink temperature of 20°C. In Fig. 3 are shown the tuning characteristics of the laser when one Bragg current is changed at a time and the other is zero. The wavelength steps are given by the reflection peak distances of the super structure Bragg gratings. The total tuning range is around 60 nm limited by the designed difference in sampling periods. The side-mode suppression is better than -30 dB for all wavelengths except close to the mode jumps. In order to reach the missing wavelengths in between the reflectivity peaks both Bragg section currents are increased together so that the two reflection peaks of the lasing mode are tuned at the same speed towards shorter wavelengths. This tuning scheme can be appplied at every wavelength by pre-biasing one of the Bragg sections to the desired reflection peak pair and then increasing both Bragg section currents simultaneously. The rate at which the two Bragg currents are increased is higher for the section with the pre-bias since the tuning efficiency decreases at larger currents. As can be seen in Fig. 4 almost all the longitudinal modes between 1533.8 and 1574.5 nm wavelength can be reached with this method. The tuning range of one peak is limited by the maximum obtainable refractive index change to 7.3 nm. Gaps are still observed in the tuning characteristics corresponding to longitudinal mode jumps. These missing wavelengths can easily be reached by using the phase tuning section of the laser. Thus all the wavelength between 1533.8 and 1574.5 nm can be covered.

References
[1] W. Idler et al., Electron. Lett., vol 27, no 24, pp. 2268-2270, Nov. 1991.
[2] Y. Tohmori et al., Electron. Lett., vol 29, no 4, pp. 352-354, Feb. 1993.
[3] V. Jayaraman et al. 13th IEEE Int. Semiconducteur Laser Conf., Takamatsu, Japan, paper PD-11, Sept., 1992.
[4] M. Öberg et al, IEEE Photon. Technol. Lett., vol. 5, no 7, pp. 735-738, July 1993.
[5] G. Björk and O. Nilsson, J. Lightwave Technol., LT-5, no.1, pp.140-146, Jan. 1987.

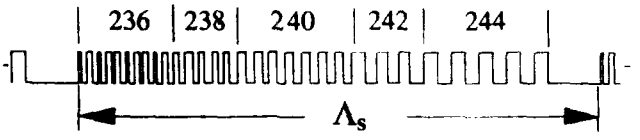

Fig. 1 One sampling period of the SSG-DBR. The length of the region with 236,238,240,242, 244 nm grating periods are 12.98, 2.38, 13.20, 2.42 and 13.42 μm.

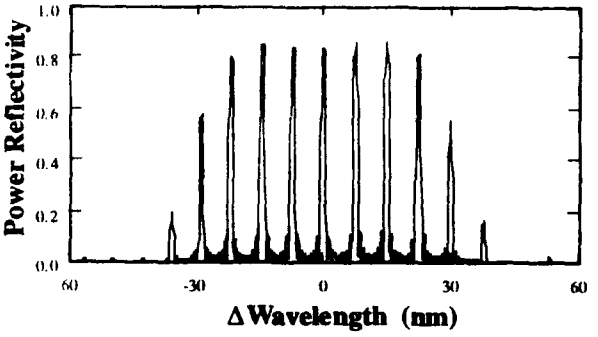

Fig. 2 Calculated reflectivity for 9 sampling periods as defined in fig. 1. Λ_S = 44.4 μm

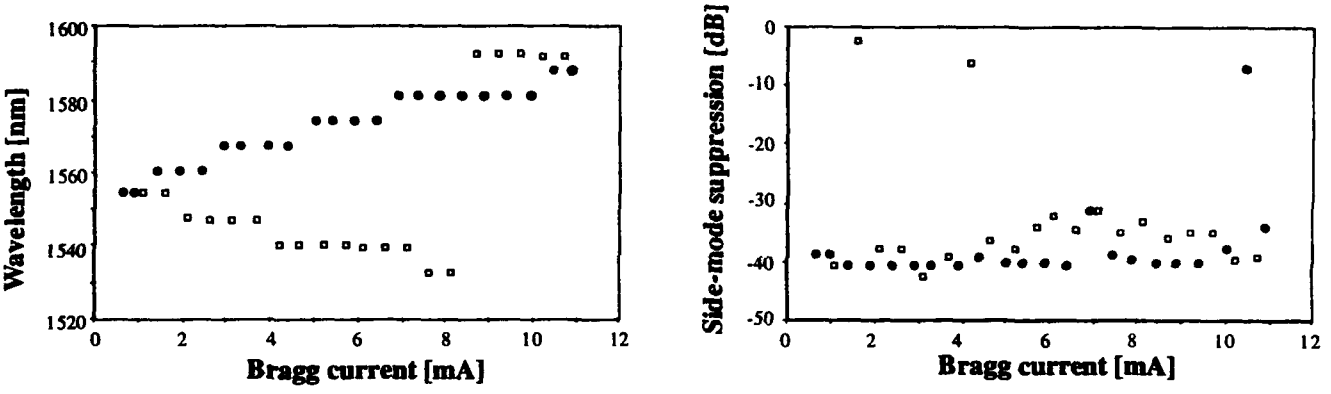

Fig. 3 Measured tuning response when changing the front (squares) or the rear (circles) Bragg current. (a) wavelength. (b) Side-mode suppression.

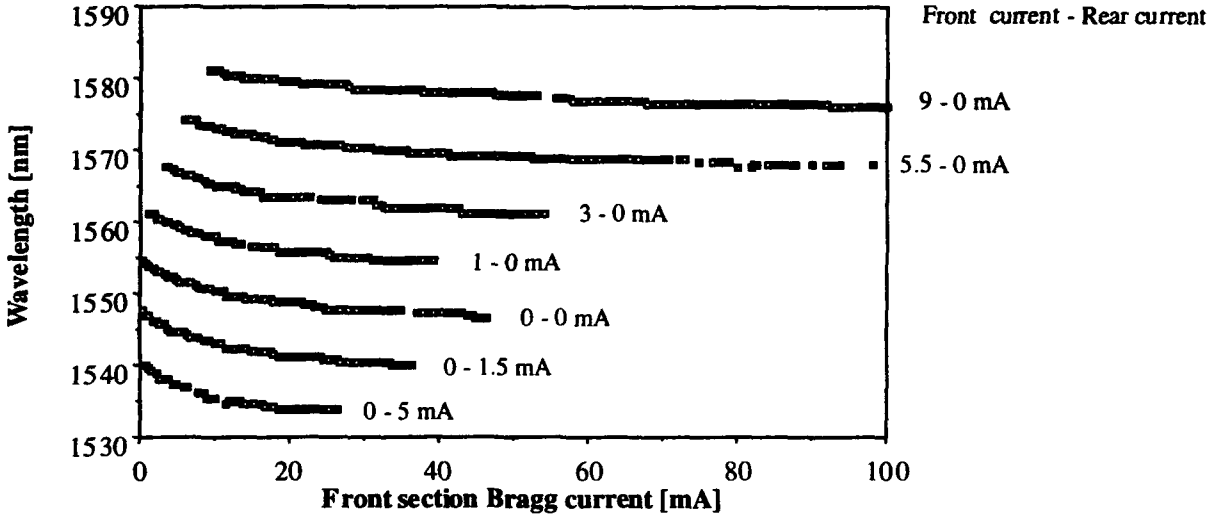

Fig. 4 Wavelength measured when stepping simultaneously the front and rear Bragg currents at different starting biais lavel

4:00pm - 4:15pm
M4.3

Wide Wavelength Tuning with Narrow Spectral Linewidth in Thermally Tunable Super-Structure-Grating DBR Lasers

H. Ishii, F. Kano, Y. Tohmori, Y. Kondo, T. Tamamura, and Y. Yoshikuni

NTT Opto-electronics Laboratories
3-1, Wakamiya, Morinosato, Atsugi-shi, Kanagawa, 243-01 Japan

Abstract

Thermal wavelength tuning characteristics of super-structure-grating DBR lasers with integrated heaters are demonstrated. A quasi-continuous tuning range of 40 nm is obtained while keeping the spectral linewidth below 400 kHz.

Introduction

Wavelength tunable laser diodes will play important roles in future wavelength-division-multiplexed (WDM) networks and optical measurement systems. We have developed super-structure-grating (SSG) DBR lasers to enlarge the tuning range[1-3]. A common method of wavelength tuning in DBR lasers is electrical tuning which utilizes the carrier plasma effect. However, the electrical tuning causes the spectral linewidth to broaden. For coherent optical communication and coherent optical measurement system applications, narrow linewidth operation is important. Hence, narrow spectral linewidth is required as well as wide tunability for such systems. Thermal tuning is a attractive way to avoid broadening the linewidth[4,5]. This paper reports both wide tunability and narrow spectral linewidth operation in thermally tunable SSG DBR lasers.

Device Structure

The device structure is shown schematically in Fig. 1. It consists of an active (300 μm), a phase-control (150 μm), and front and rear SSG DBR regions (400, 600 μm). The 1580-nm-bandgap strained MQW (1% compressive, 6 wells) is introduced in the active region, and 1300-nm-bandgap passive layers are butt-jointed to the active region. A 5-step MOVPE was used for the fabrication. The 1.2-μm-wide laser stripe was buried by p-n current-blocking layers. Phase-shift configurations in the SSGs were numerically optimized to realize uniform reflection peaks[6] and were patterned using electron-beam lithography. Anti-reflection films were formed on both end facets to reduce the SSG peak variation. P-side electrodes are separated from each other by a groove formation. Pt heaters for thermal tuning were integrated into the device over the phase-control and the SSG-DBR regions, where the heaters and p-side electrodes are isolated from each other by SiO_2 film. In this device, both electrical and thermal tuning is possible.

Characteristics

The electrical and the thermal wavelength tuning characteristics respectively are shown in Fig. 2 (a) and (b). When we were taking our measurements, the current to the active region was constant at 100 mA, and heat-sink temperature was controlled to 25°C with a Peltier device. The lasing wavelength is changed with discrete steps of SSG peak spacing (~5 nm) by injecting a SSG current or by heating the SSG region. Stable single-mode oscillations in 8 SSG modes were observed for both electrical and thermal tuning. Although tuning characteristics are almost equivalent, the behavior of the spectral linewidth clearly differs between the two tuning method. The current injection remarkably broadens the linewidth, however the thermal tuning doesn't change the linewidth. In addition to the discrete tuning shown above, the device can continuously cover the tuning range if three tuning ports are simultaneously controlled. Figure 3 shows the linewidth and the mode suppression ratio (MSR) under quasi-continuous tuning, where the linewidth and the MSR are shown by 1-nm steps. We obtained a narrow linewidth of less than 400 kHz and a MSR of more than 35 dB in the 40-nm wavelength range.

Conclusion

A quasi-continuous tuning range of 40 nm with a narrow spectral linewidth of less than 400 kHz was obtained from thermally tunable SSG DBR lasers.

Acknowledgment

The authors are grateful to H. Tsuchiya and M. Yamamoto for their supports and discussions.

References

[1] Y. Tohmori, et al., IEEE J. Quantum Electron., vol. 29, pp. 1817-1823, 1993.
[2] F. Kano, et al., IEEE Photon. Technol. Lett., vol. 5, pp. 611-613, 1993.
[3] H. Ishii, et al., IEEE Photon. Technol. Lett., vol. 5, pp. 613-615, 1993.
[4] S. Sakano, et al., IEEE Photon. Technol. Lett., vol. 4, pp. 321-323, 1992.
[5] T. Kameda, et al., IEEE Photon. Technol. Lett., vol. 5, pp. 608-610, 1993.
[6] H. Ishii, et al., Extended Abstract of SSDM'93, pp. 1038-1040, 1993.

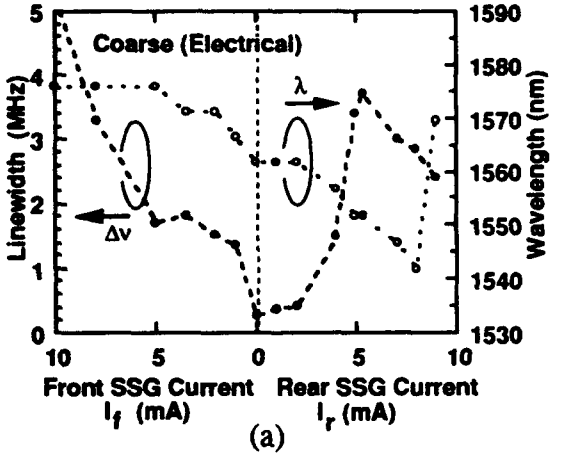

(a)

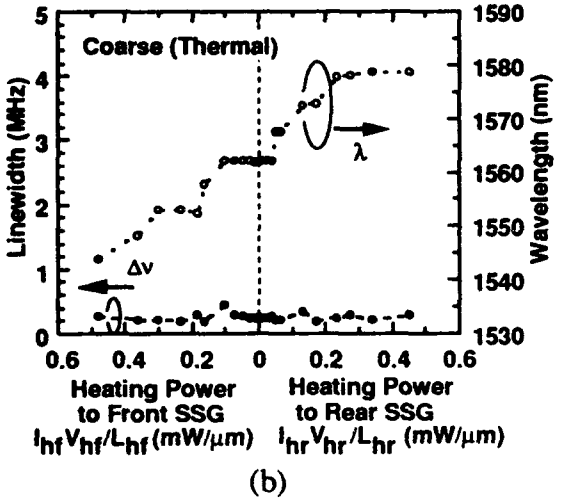

(b)

Fig. 2 Lasing wavelength and spectral linewidth tuned by : (a) injecting the front or rear SSG current, and (b) heating the front or rear SSG.

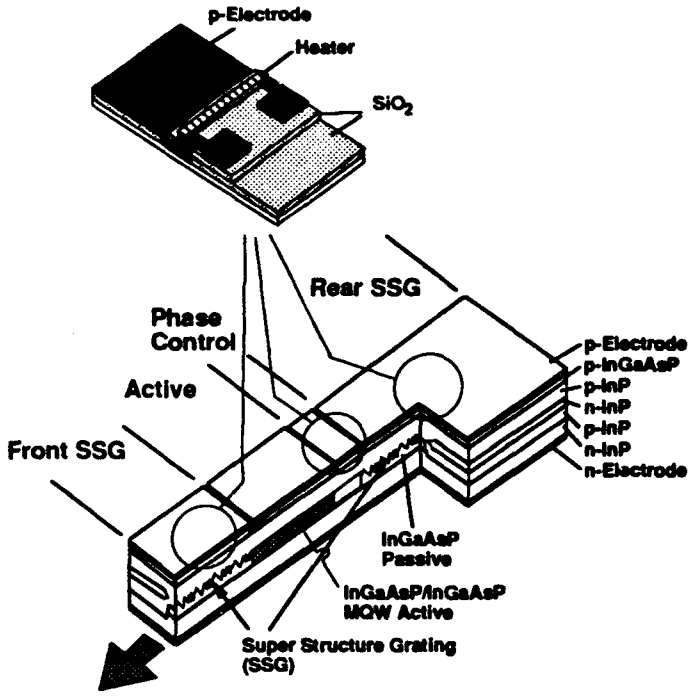

Fig. 1 Schematic of the device structure.

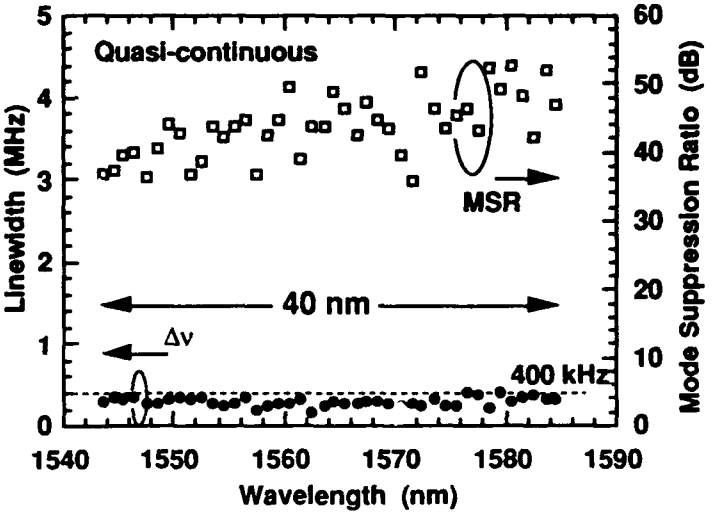

Fig. 3 Spectral linewidth and mode suppression ratio for a lasing wavelength tuned by 1 nm steps.

4:15pm - 4:30pm
M4.4

A Multiwavelength Waveguide Grating Router Laser

M. Zirngibl, B. Glance, L.W. Stulz, C.H. Joyner, G. Raybon, I.P Kaminow
AT&T Bell Laboratories, Holmdel, NJ, 07733

Abstract: Measurements on a multiwavelength laser source are reported. The source can emit cw simultaneously on 11 frequencies that are precisely spaced by 3.2 nm. Laser oscillation occurs on a single longitudinal mode with a 5 MHz linewidth. The 18 mm long cavity limits the direct modulation rate to 155 Mbps.

Lasers, that are based on the integration of a waveguide grating router with amplifiers are capable of producing a set of frequencies that are spaced very precisely and are therefore attractive for WDM systems. Here, we report on the performance of such a packaged WGR laser (WGRL) identical to the device in Ref. (1).

For single channel measurements, the laser reaches threshold at 80 mA total current (40 mA per amplifier). Up to 1 mW of power could be coupled into a fiber when the laser was biased with 400 mA total current. The laser operates on a single longitudinal mode for most biasing conditions. Near threshold conditions; small sidemodes appear, spaced from the main mode by 5 GHz. If pumped even lower, the main mode separates into about 15 modes equally spaced by 2.5 GHz. The linewidth of the lasing mode was found to be 5 Mhz. The laser is capable of emitting cw on several channels simultaneously as shown by the spectra in fig. 1 which were obtained by pumping every second wavelength channel (top curve) and all wavelength channels (lower curve).

A network analyzer was employed to investigate the small signal response of the device, which is displayed in Fig.2. The 3 dB point is around 700 MHz. We can clearly see strong resonance's at 2.5 GHz and 5 GHz which correspond to the round-trip frequency and 2nd harmonic of the 1.8 cm long laser cavity. The strong resonance at 2.5 GHz suggest that this laser may be a candidate for modelocking to generate a train of soliton pulses.

Finally, we used the WGRL for a digital data transmission experiment. The applied signal was a random bit stream at 155 Mbps. In Fig. 3, we plot the bit-error rate versus received power. For 10^{-9} bit error rate, the received power was -39 dBm. In the inset of the figure is shown the eye diagram. We can clearly distinguish the effect of the slow turn on time of the laser which gives rise to the timing jitter at the onset of the non-return-to-zero (NRZ) pulse. This time delay is about 2 ns. The system could run up to 250 Mbps, at the expense of a large power penalty of 10-15 dB .

In the present configuration, we cannot modulate several wavelengths simultaneously. Since all channels go through the same output amplifier, crosstalk due to gain saturation is important. Even though this is bad news for the potential use of this device as a multifrequency transmitter, this behavior may be exploited for other applications.

The present limitations of our device in terms of bit-rate and gain crosstalk can be circumvented. Gain crosstalk can be eliminated by using a purely passive output port. If one wants to overcome the limitations imposed by the long cavity round-trip time, the device would have to be integrated with external modulators and a second multiplexer would have to remultiplex the signals. The actual modulation speed of 155 Mbps may not be sufficient for point-to-point transmission systems. For local loop applications, however, this rate may be adequate.

(1) M. Zirngibl, C.H. Joyner, Postdeadline paper PD16, OFC'94, San Jose, 1994.

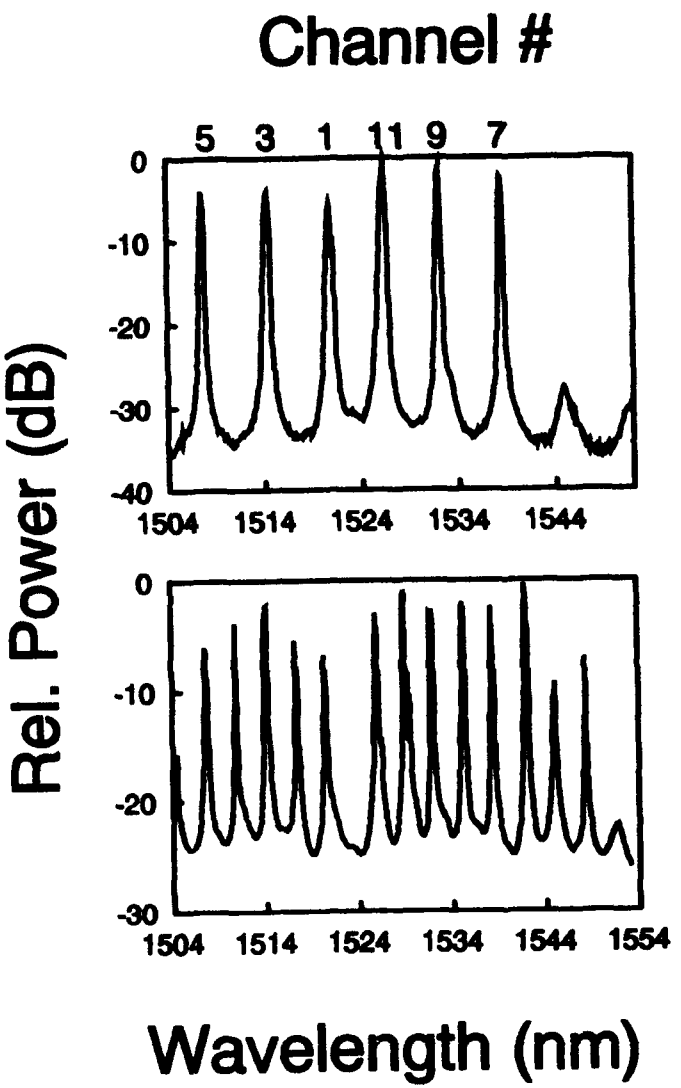

Fig. 1: Multifrequency emission of the WGRL.

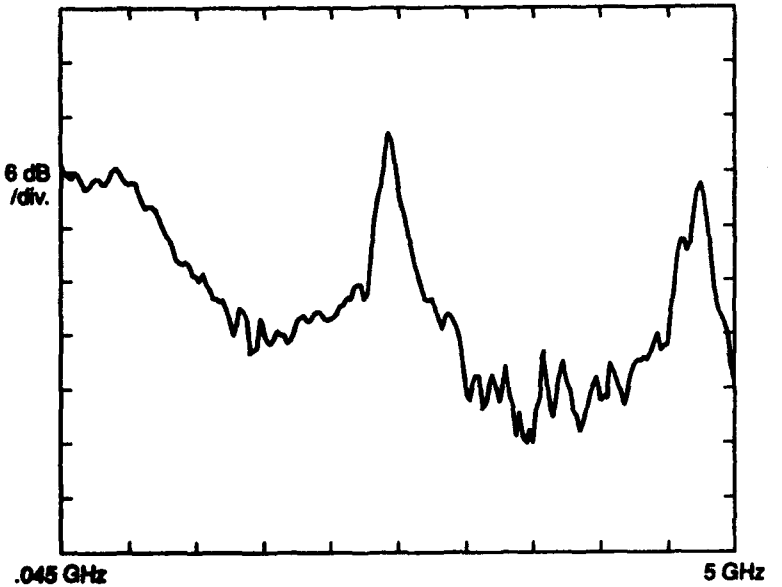

Fig. 2: Small signal response of WGRL.

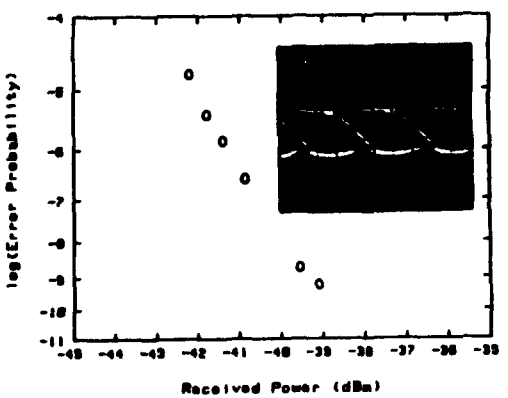

Fig. 3: Bit-error rate versus power. Inset: Eye diagram.

4:30pm - 4:45pm
M4.5

A fast switching N-Frequency laser integrated with an electroabsorption modulator.

U Koren,B. Glance, N.K. Shankaranarayanan, B.I. Miller, M.G. Young, M. Chien
AT&T Bell Laboratories, Holmdel, N.J. 07733

The use of N-frequency tunable distributed Bragg reflector (DBR) lasers has been suggested for WDM switching and routing networks [1,2]. Such networks employ different optical frequencies to enhance the transmission capacity, and to direct optical signals to different destinations. For example, it is possible to use passive demultiplexers such as WDM routers [3] to direct packets of information to different destinations according to their optical frequency.
For such applications, lasers which can be switched between a set of predetermined frequencies, while using external $LiNbO_3$ modulators for data encoding have been demonstrated [4]. In the present work we describe the performance of an integrated device which combines a fast frequency switching laser, and an external electroabsorption modulator for data encoding, on the same semiconductor chip.
The schematic structure of the device is shown in Fig. 1. The gain section has been cleaved to a precise length to achieve tuning mode spacing of 50 GHz with better than 0.5% precision. The device structure and fabrication process have been previously described [5]. In the present configuration, a 40 μm long window section has been included, to suppress residual reflections from the AR coated front facet. The superimposed spectra of 18 tuning modes, using an optical spectrum analyzer and applying a linear ramped current signal to the tuning section is shown in Fig. 2. Although the number of channels is limited to 18 by the tuning range of this device, similar devices with 23-24 channels have been made with 50 GHz channel spacing. The modulator was biased at -0.94 Volt and driven with a 2 Volt peak to peak RF signal, using 1 Gbit/sec, non return to zero (NRZ) pseudo random bit stream (PRBS), with 2^{15} -1 pattern length. Under these conditions the extinction ratio of the modulator was about 10 dB. The tuning section was driven by a fast arbitrary waveform generator and also by a fast function generator and a matching resistor network. The optical output of the packaged device was demultiplexed using a commercial Mach Zender (MZ) interferometer with nominal channel spacing of 49.5 GHz. Fig. 3. shows the device under modulation and being switched between channels 17 and 0. The optical signal is directed to the different ports of the MZ demultiplexer (traces (b) and (c)), according to whether the channel number is even or odd. The switching time is shorter than 10 nsec and limited by the tuning driving voltage, as shown in trace (a). A pseudo random switching sequence through channels 17,0,15,4,13,6,5,16,7,12,9,2,3,10,11,8,1,14,17 is shown in fig. 4. with channel holding time of 25 μsec. As seen, the modulated signal is directed, without errors, to the two output ports according to the parity of the channel number. In conclusion, we demonstrate a fast switching multi-frequency laser with an integrated electroabsorption modulator used for data encoding.

REFERENCES;

1. B. Glance et al, Electronics Lett. 27,pp 1381,(1991).
2. I.P. Kaminow et al, Optical fiber communication conf. paper WD1, San Jose Ca (1994).
3. C. Dragone et al IEEE Photonic Tech. Lett, 3, 812, (1991).
4. N.K. Shankaranarayanan et al, Optical fiber communication conf. paper Tul2, San Jose, Ca (1994).
5. U. Koren et al, Optical fiber communication conf. paper WG5, San Jose, Ca (1992).

4:45pm - 5:00pm

M4.6 **Novel high performance strained layer MQW monolithically integrated DFB laser-electroabsorption modulator using one identical single active layer**

A Ramdane, A Ougazzaden, F Devaux, F Delorme, M Schneider*, J Landreau and A Gloukhian

France Telecom, CNET/PAB, BP 107, Bagneux Cedex, 92225 France
* CNRS, Laboratoire de Microstructures et de Microélectronique, BP 107, Bagneux Cedex, 92225 France

Abstract: A novel and very simple approach is demonstrated for strained layer MQW distributed feedback laser-electroabsorption modulator monolithic integration with very high performance at 1.5 μm (13.6 dB extinction ratio at 1.5 V operating voltage for a 70 μm long modulator)

Introduction: Monolithic integration of a single longitudinal mode laser such as a distributed feedback (DFB) laser and an external electroabsorption modulator based on the quantum confined Stark effect (QCSE) has become a very attractive route to provide for high speed and low chirp light sources in the 1.55 μm wavelength range. The first integration schemes involved multi-epitaxy growth of distinct active layers for the two devices (1). Critical epitaxial steps are then required especially to achieve efficient optical coupling between the two waveguides. Selective area growth was recently successfully applied to laser-modulator monolithic integration (2). This method is based on the variation of the bandgap of multiple quantum well (MQW) material in the same plane with one single growth over masked substrates. In this case however, substrate preparation prior to the epitaxy remains critical. We have more recently demonstrated another simple planar method to integrate a DFB laser and an external modulator (3). In this latter, selective disordering of a particular MQW stack is performed after standard growth of one single active layer, where adverse thermal wavelength shifts during the regrowth step have to be taken into account. In this work a novel yet much simpler approach is proposed and demonstrated for laser-modulator monolithic integration.
The principle: Here the two devices are made of one ***identical*** single active layer and the approach is based upon the positive detuning, i.e. to longer wavelength, of the DFB laser Bragg wavelength relative to that of the optical gain spectrum peak (4).The amount of detuning that ensures optimal wavelength compatibility is achievable thanks to the inherently wide gain spectrum exhibited by strained layer MQW material (5).
The success of the method also relies on a sharp excitonic absorption curve as well as on the ability to pin the Bragg wavelength to the required value, for which modulator insertion loss is kept minimal.
Device growth and fabrication: A novel structure that minimizes intermixing between well and barrier material has been adopted (6). An InGaAsP/InGaAsP MQW stack, for which both barriers and wells have the same group V (As/P) composition, has been grown by atmospheric pressure MOCVD in a T-shaped reactor. It consists of ten compressively strained 9 nm wide wells surrounded by tensile-strained 9 nm wide barriers. After grating formation in the laser section, a standard buried ridge stripe structure is processed. Electrical isolation of the pin laser diode and that of the modulator is achieved by means of proton implantation.
Device results: Figure 1 shows the optical absorption spectrum of the active layer measured at room temperature. The peak at 1540 nm corresponds to the heavy hole -electron excitonic transition. The DFB grating was hence designed for laser emission to occur at a wavelength of minimal absorption.This is illusrated in the inset which shows single mode operation at 1584 nm. Integrated device threshold currents ranged between 40 and 50 mA, to be compared with 35 mA measured for discrete Fabry-Perot laser made on the same wafer. Up to 3 mW optical power is available at modulator output. The modulation performances of integrated devices have been assessed by coupling the output power from the modulator facet to a pin photodetector through a single mode fiber. The results are shown in figure 2 for a 400 μm long laser and only 70 μm long modulator. An on-off ratio of 13.6 dB is achieved for a bias voltage of 1.5 V. Optical insertion losses have been measured for cleaved discrete modulators at different wavelengths using an F-center laser. At 1.58 μm they amount to 4.4 dB/100 μm.

This corresponds to 3 dB for a 70 μm long modulator and thus very acceptable for transmission applications.
In summary we have proposed a novel and very simple approach for laser-modulator monolithic integration, necessitating only standard growth and processing. Very high performance (13.6 dB extinction ratio at a voltage of only 1.5 V) is demonstrated for a very short (70 μm long) modulator, which further implies bandwidths in excess of 20 GHz.

Acknowledgements: We are grateful to M Carré, F Huet and G Le Mestreallan for technical assistance, Ph Krauz for proton implantation and A Carenco, C Kazmierski, A Mircéa for fruitful discussions.This work was partially supported by the EEC under the RACE 2006-WELCOME project.

References

(1)-M Suzuki et al., J. of Lightwave Technology LT-5, 1987, 1277
(2)-M Aoki et al., Electronics Letters 27, 1991, 2138
(3)- A Ramdane et al., Proceedings of the Int. Conf. on Lasers and Electro-Optics (CLEO), Anaheim CA, May 1994
(4)-A Ramdane et al., France Telecom French Patent , 1993
(5)-see e.g. CE Zah et al., Electronics Letters 28, 1992, 824
(6)-A Mircéa et al., J. of Crystal Growth 124, 1992, 737

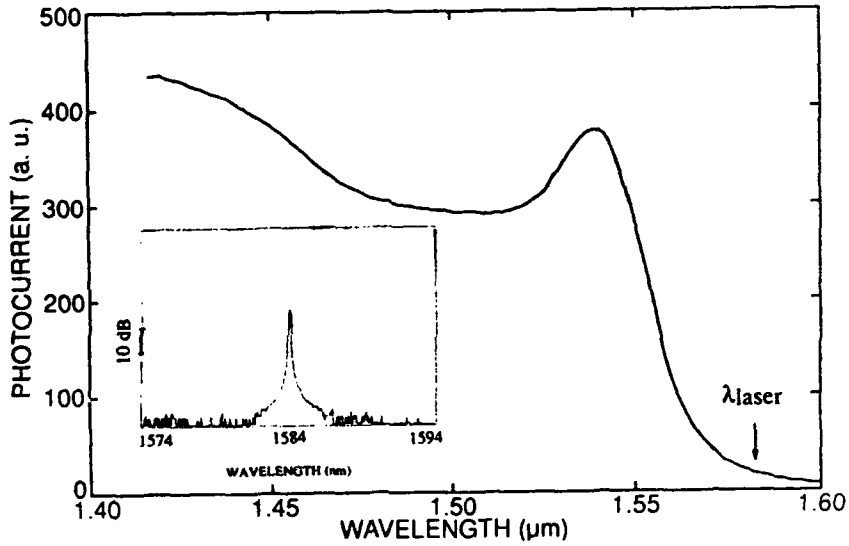

Fig. 1: Optical absorption spectrum of the active layer. The inset illustrates single mode operation at 1584 nm.

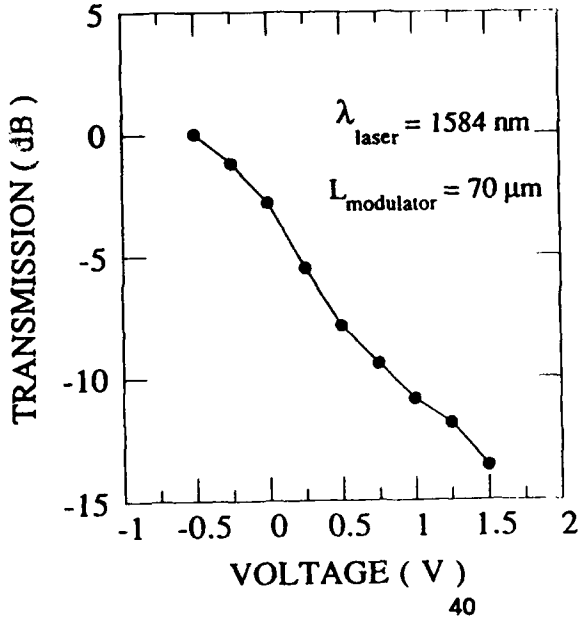

Fig. 2: Modulation performance of an integrated device as a function of reverse applied bias.

5:00pm - 5:15pm
M4.7

Low-Chirp Integrated EA-Modulator/DFB Laser Grown by Selective-Area MOVPE

J. E. Johnson, T. Tanbun-Ek, Y. K. Chen, D. A. Fishman* , R. A. Logan, P. A. Morton, S. N. G. Chu, A. Tate, A. M. Sergent, P. F. Sciortino, Jr., and K. W. Wecht

AT&T Bell Laboratories
600 Mountain Ave., Murray Hill, NJ 07974

2.5 Gbit/s transmission over 517 km of standard fiber is reported using a monolithically integrated EA modulator/DFB laser by selective-area MOVPE. A low chirp of 0.13 Å peak-peak and good reliability are shown.

Monolithically integrated external electroabsorption-modulator/DFB lasers (EMLs) are expected to be key components in future long-haul lightwave transmission systems using existing installed fiber and erbium-doped fiber amplifiers (EDFAs), due to their low chirp, compact size, low drive voltage and long-term stability. EMLs have been demonstrated using etch-and-regrow [1] or butt-joined [2] processes, but these processes are complex and unsuited for high-yield manufacturing, and the introduction of additional regrown interfaces internal to the device poses reliability concerns. In this paper, we report on an EML fabricated using the selective-area MOVPE growth (SAG) technique [3, 4], which results in a device with a continuous active layer and simplified processing. These devices show good reliability as well as excellent transmission performance.

Fabrication of the SAG-EML is by low pressure MOVPE. First, an etched grating is formed on the InP substrate, followed by a patterned SiO_2 layer, which is used to selectively protect the grating in the active region during mass transport smearing of the exposed grating, followed by removal of the SiO_2 and growth of an n-InP spacer layer. Next, another SiO_2 layer is deposited and patterned with two parallel stripes separated by a gap in the active region. The separate confinement waveguide and MQW active layers, consisting of 5 InGaAsP quantum wells and 1.28Q InGaAsP barriers, are formed during the SAG growth step, with the enhanced In concentration between the SiO_2 stripes resulting in a difference in bandgap energy between the laser and modulator. This is followed by the conventional capped-mesa buried heterostructure (CMBH) formation. Reactive ion etching is then used to electrically isolate the laser and modulator. Finally, ohmic contacts are formed, the chips are separated, and an AR coating is applied to the modulator facet. The completed SAG-EML is shown schematically in Fig. 1. The lengths of the DFB laser, isolation gap and modulator are 350, 100 and 200 μm.

The DFB laser threshold current is 12 mA (10-20 mA typical), and 1555 nm output power at I_{las} = 100 mA and

* AT&T Bell Laboratories, Holmdel, NJ

V_{mod} = 0 V into a broad area detector is 2.5 mW (2-6 mW typical). The extinction ratio is better than 12 dB for V_{mod} = -2 V. Reliability of the SAG process has been confirmed by operating SAG-EMLs at 100 °C and I_{las} = 200 mA for 24 hours with less than 2 mA increase of I_{th}. Longer-term burn-in studies at 60 ° C are underway. The time-resolved wavelength chirp of the unpackaged SAG-EML was measured using a microscope objective to couple the light into single-mode fiber. With 2.5 Gbit/s NRZ modulation at I_{las} = 90 mA, V_{mod} = -1.3 V(DC) and 2.5 V(peak-peak), the chirp was only 0.07 Å peak-peak. After packaging with an AR-coated lensed fiber, the chirp increased to 0.13 Å, indicating that there is a small reflection from the fiber tip back into the laser. The transmission performance was then measured over 517 km of standard fiber, with EDFAs spaced every 100 km. The dispersion penalty is only 1.2 dB at a BER of 10^{-10}, as shown in Fig. 2. To conclude, we have fabricated monolithically integrated EA modulator/DFB lasers, using the selective-area MOVPE technique, which results in devices with high reliability, ease of manufacturing, and very low chirp.

References

[1] T. L. Koch, and U. Koren, IEEE J. Quantum Electron. **27**, 641 (1991).

[2] T. Tanbun-Ek, S. Suzaki, S. Wang, Y. Suematsu, F. Koyama, and S. Arai, IEEE J. Quantum Electron. **20**, 131 (1984).

[3] M. Aoki, H. Sano, M. Suzuki, M. Takahashi, K. Uomi, and A. Takai, Electron. Lett. **27**, 2138 (1991).

[4] Y. D. Galeuchet, and P. Roentgen, J. Crystal Growth **107**, 147 (1991).

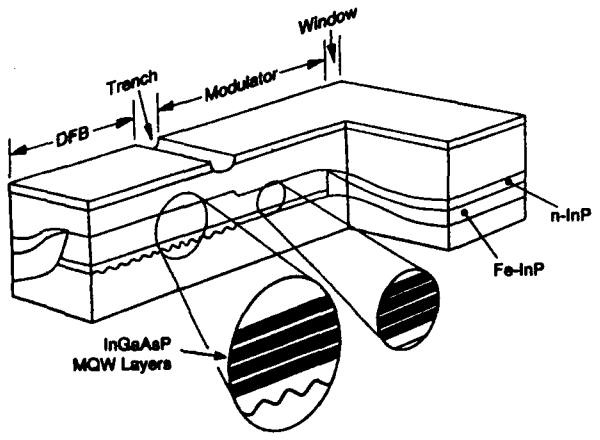

Fig. 1. Schematic illustration of the integrated EA modulator/DFB laser.

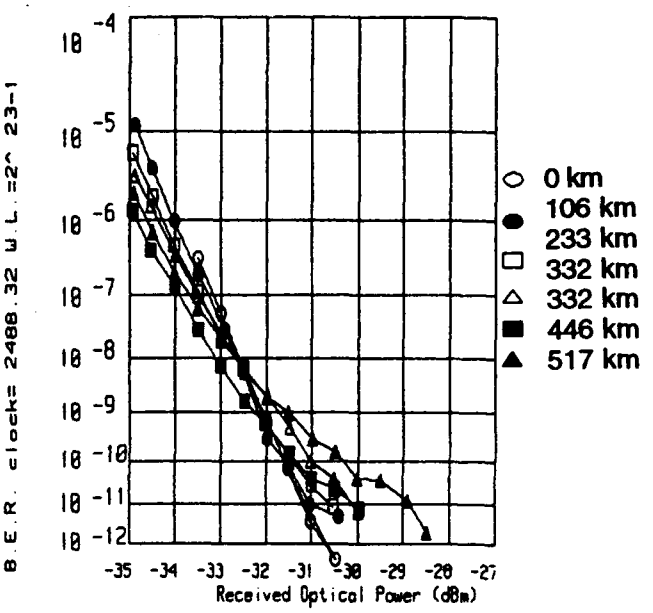

Fig. 2. BER measurement at 2.5 Gbit/s over standard fiber.

5:15pm - 5:30pm
M4.8

Digitally encoded optical pulse generation from an integrated DBR laser-modulator

G. Raybon, N. M. Froberg, U. Koren, B. I. Miller, M. G. Young, M. Chien,
A. M. Johnson, P. B. Hansen, C. A. Burrus, J. J. Veselka, A. H. Gnauck

AT&T Bell Laboratories, Crawford Hill Laboratory
Holmdel, NJ 07733, U.S.A.
(908) 888-7221

Abstract: We demonstrate a novel modulation scheme in which both data-encoding and pulse generation are achieved using a single integrated semiconductor laser/modulator. Data-encoded, near-transform limited 66 ps pulses are obtained at 2.5 Gbit/s and BER performance is reported.

Recently, picosecond soliton pulse generation using sinusoidally driven electroabsorption modulators has been reported using both discrete [1] and integrated modulators [2]. In contrast to mode-locked lasers, the repetition rate of modulator based pulse generation can be tuned continuously over the limit of the modulator bandwidth and is not limited to a fixed resonant frequency. In order to encode data on the pulse stream, the intensity is modulated either by an external modulator or by integrating a second modulator [3]. In this paper, we demonstrate a potentially low-cost single-chip pulse transmitter consisting of a DBR laser integrated with one electroabsorption modulator. The DBR laser is directly modulated at 2.5 Gbit/s generating an optical non-return-to-zero (NRZ) signal out of which the sinusoidally driven integrated modulator carves a *pulsed* data-encoded signal. We report near transform-limited 66 ps pulse output and the bit-error-rate (BER) performance of the transmitter in a back-to-back transmission experiment.

The integrated DBR laser-modulator [4] shown in Fig. 1, consists of a strain-compensated strained-layer (SCSL) multiple quantum well laser which is tunable by local heating of the grating section via a surface resistor. The modulator, which is regrown on top of a 1.3/1.1 μm quaternary passive guiding layer, is a bulk electroabsorption modulator and is followed by a 45 μm window region. An anti-reflection coating is applied to the facet. The choice to integrate a DBR laser enables wide wavelength tunability and a 6.5 nm tuning range near 1.55 μm is obtained. Optical pulses are carved out of the data-encoded light from the directly modulated DBR laser by biasing the modulator near full extinction and applying a sinusoidal voltage which temporarily reduces the attenuation. At 2.5 GHz, 66 ps pulses are obtained for a DC bias of -4.5 V and an RF power of 25 dBm applied to the modulator.

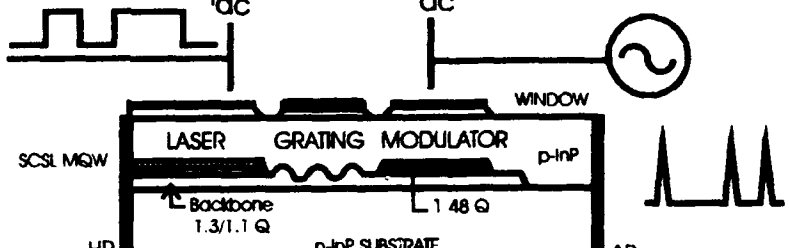

Fig. 1: Experimental configuration for data-encoded pulse generation using the integrated laser/modulator transmitter.

Digital data is encoded by on-off modulation of the DBR laser as shown schematically in Fig. 1. The laser is biased near threshold and a 2.5 Gbit/s pseudorandom 2^{23}-1 NRZ signal is applied to the laser contact with a peak-to-peak voltage of 0.7 V. The phase of the sinusoidal drive to the

modulator is optimized to align the peak amplitude of the sine wave to the center of the NRZ bit period. Figure 2 shows the optical spectra as measured using a high finesse scanning fiber Fabry Perot for the pulses with (a) and without (b) digital modulation of the laser. The measured time bandwidth-product of the pulses is 0.36. Data encoding by direct modulation of the laser broadens the spectrum by approximately 25% from 5.4 GHz to 7.3 GHz.

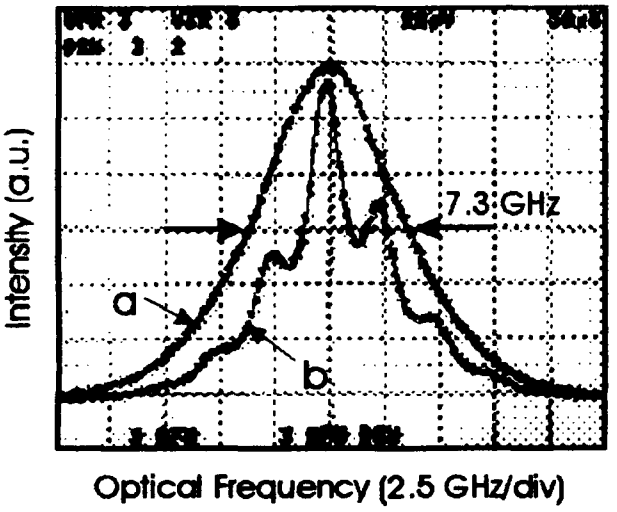

Fig. 2: Time averaged optical spectrum of (a) data-encoded pulses and (b) pulses only measured on scanning Fabry Perot.

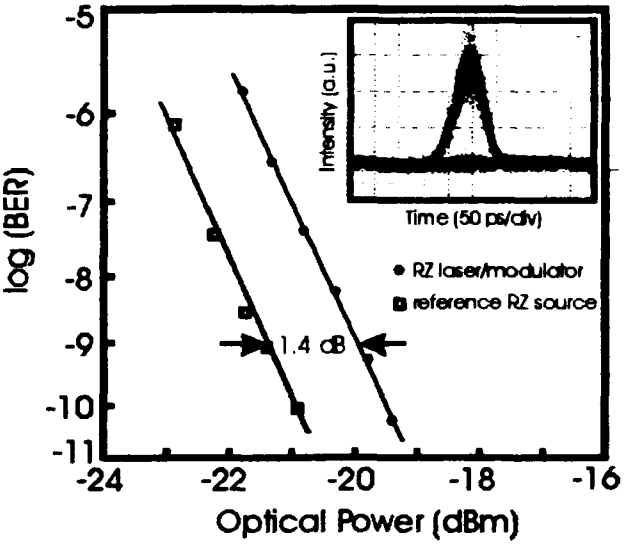

Fig. 3: BER measurement at 2.5 Gbit/s of RZ laser/modulator compared to a source with an external modulator. Inset: RZ eye diagram of laser/modulator.

The performance of the laser/modulator as a transmitter was evaluated in a back-to-back (< 1km of fiber) transmission experiment using an Erbium-doped fiber amplifier in the transmitter to boost the optical power and a PIN detector as the receiver. Figure 3 shows the measured bit-error-rate (BER) as a function of received optical power for the integrated laser/modulator transmitter and a reference RZ source. The reference source consists of the laser/modulator operating solely as a pulse source, followed by a dual drive $LiNbO_3$ Mach Zehnder modulator. At a BER of 10^{-9}, a 1.4 dB penalty is observed for the laser/modulator compared to the reference RZ source. The eye diagram is shown in the inset of Fig. 3. Timing jitter, measured on the rising edge of the eye using a digital oscilloscope differs by only 2 ps between the two sources. The power penalty in the BER measurement originates mostly from the amplitude fluctuation of the bits caused by direct modulation of the laser.

In conclusion, a semiconductor optical pulse transmitter is demonstrated by directly modulating a DBR laser and carving pulses with a sinusoidally driven electroabsorption modulator. At 2.5 Gbit/s, 66 ps near transform-limited operation and error-free transmission is obtained. This monolithic device is a potentially low-cost single-chip RZ pulse transmitter for application in soliton and OTDM/WDM type systems.

References:

[1] : M. Suzuki, et. al., Electron. Lett., vol. 28, no. 11, pp 1007-1008, 1992.
[2] : K. Wakita, et. al., Photon. Technol. Lett., vol. 5, no. 8, pp. 899-901, 1993.
[3] : K. Sato, et. al., European Conf. on Optical Comm., 1993, WeC7.2, pp. 313-3316.
[4] : U. Koren, et. al., Opt. Fiber Comm. Conf., paper No. WG5, 1992.

Tuesday
September 20, 1994

SESSION T1
DFB Lasers

SESSION T2
Carrier Dynamics

SESSION T3
Quantum Confined Lasers

SESSION T5
Poster Session

8:30am - 8:45am
T1.1

High Power Quantum-Well Gain-Coupled (GC) DFB Lasers at 1.3μm and 1.55μm

B. Borchert, J. Rieger and B. Stegmüller
Siemens AG, Corporate R&D, Otto-Hahn-Ring 6, 81730 Munich, GERMANY

Abstract: High power characteristics of quantum-well gain-coupled DFB lasers with a loss grating are presented. Among these are record single-mode (SM) values of 115mW at 1.3μm and 95mW at 1.55μm. The SM-yield at 20mW is as high as 66%.

Introduction: High SM power transmitters, i.e. DFB lasers, are often advantageous in optical communication systems, since they enable high sharing factors or efficient pumping of fiber amplifiers. Recently GC-DFB lasers have been demonstrated as promising alternatives to the commonly used index-coupled DFB lasers [1-3]. In the following for the first time very high power SM operation of GC-DFB lasers is presented.

*Design and Fabrication:*For both the 1.3μm and 1.55μm GC-DFB structures a stable high power design was developed. Accordingly a moderate κL-product around 1.5-2 ($\kappa_{index} \approx \kappa_{gain} \approx 20/cm$, L=600μm) was envisaged. The actual device structure is sketched in Fig.1. The anti-phase grating configuration was chosen due to its superior stability behaviours as compared to the in-phase grating [4]. The active layer comprises quaternary strained QW's to ensure enhanced laser performance [5]. The whole laser structure was grown in two epitaxial steps by MOVPE. Subsequently 3μm wide ridge-waveguide (RWG) lasers were processed and mounted episide-up on copper heatsinks. AR/HR coatings were applied to get high power SM operation of the GC-DFB devices with reasonable yield [6].

Results, 1.3μm devices: First, the power dependence of the SM-yield was investigated by statistical bar measurements. The results are shown in Fig.2. The SM-yield drops from 90% slightly above threshold (i.e. 5mW) to 66% at 20mW, a still reasonable value. These results agree fairly with the predictions of [6], showing the potential of GC-DFB lasers for high power SM operation. The decrease of the SM-yield with increasing power is caused by hole burning effects, which may be weaker than in index-coupled DFB lasers, but which are still present. This is indicated by the decrease of the SSR at very high power levels and finally by the onset of multimode emission at still higher levels above 110-115mW, see Fig.3, where the P-I characteristic of an AR-coated 1.3μm GC-DFB laser is shown. Nevertheless at 25°C (15°C) more than 100mW (115mW) SM power are emitted with a SSR>20dB, which is among the highest values for the SM power of solitary laserdiodes reported up to now.

1.55μm devices: Fig.4 shows the SM power of an AR/HR-coated 1.55μm GC-DFB device at different temperatures. More than 90mW were measured at 15°C (SSR around 30dB). Optimization of the lateral waveguiding in the RWG structure and of the detuning of the Bragg wavelength should lead to further improvements especially at higher temperatures. The power dependence of the SM-yield of these devices is comparable to those at 1.3μm.

In conclusion, for the first time very high power SM operation of 1.3µm and 1.55µm GC-DFB lasers was presented. Potential for further improvements has been indicated.

Acknowledgements:

The authors gratefully acknowledge the technical assistance from H.Hedrich, E.Käufl, I.Karger, H.Michel, E.Noack and R.Unger. This work was partly supported by the EEC under the RACE-project R2069.

References

[1] Y. Nakano et al., Techn. Dig. 17th ECOC 1991, Paris, Part Invited Papers, pp.1-8
[2] G. P. Li et al., Electron. Lett., vol. 28 (1992), pp.1726-1727
[3] B. Borchert et al., Electron. Lett., vol. 29 (1993), pp.210-211
[4] J. Zoz et al., Electron. Lett., vol. 30 (1994), pp.39-40
[5] B. Stegmüller et al., Electron. Lett., vol. 29 (1993), pp.1691-1693
[6] Y. Nakano et al., IEEE Photon. Techn. Lett., vol. 4 (1992), pp.308-311

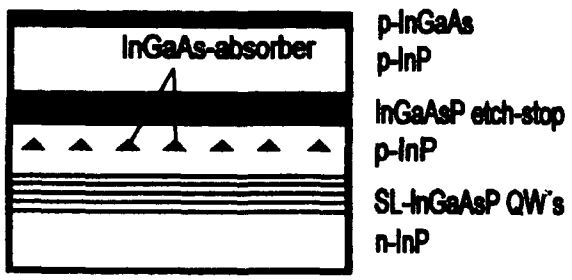

Fig.1: Longitudinal cross-section of 1.3µm and 1.55µm GC-DFB laser structures

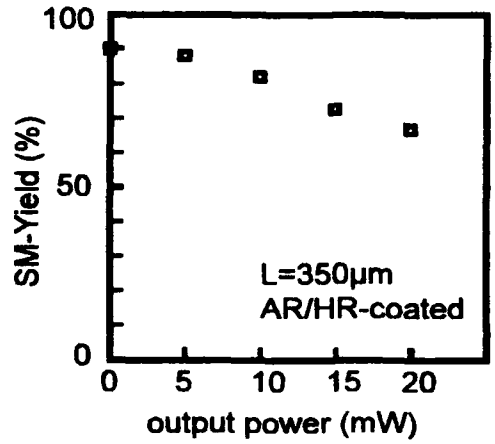

Fig.2: SM-yield of 1.3µm GC-DFB lasers as a function of output power

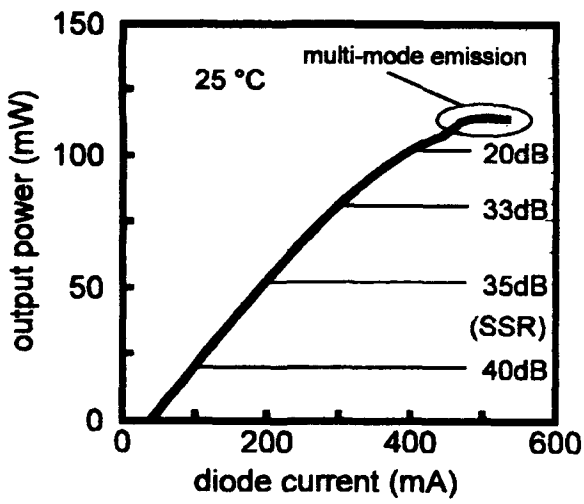

Fig.3: Output power characteristic of 1.3µm GC-DFB laser

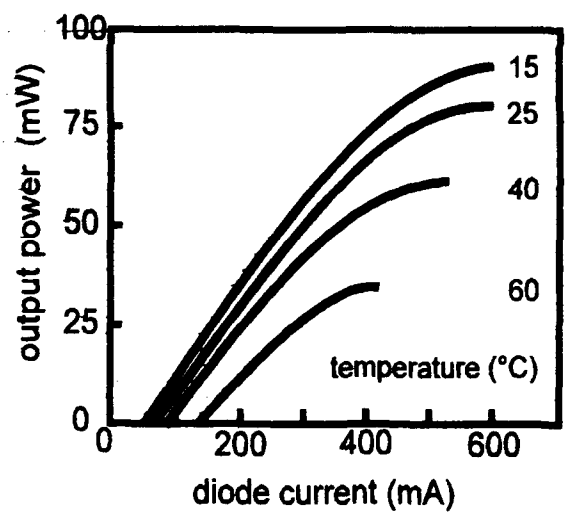

Fig.4: Single-mode output power of 1.55µm GC-DFB-laser at different temperatures

8:45am - 9:00am

T1.2

Complex-coupled λ/4-shifted DFB lasers with a flat FM response from 10 kHz to 17 GHz

M. Okai, M. Suzuki, T. Taniwatari, and N. Chinone
Central Research Lab., Hitachi, Ltd., Kokubunji, Tokyo 185, Japan

Semiconductor lasers with a flat FM response are required for coherent FSK transmission systems. The proposed complex-coupled λ/4-shifted DFB laser gives a flat FM response from 10 k to 17 GHz.

The frequency of lasing light can be modulated directly by modulating the current injected into semiconductor lasers. However FM response decreases in the modulation frequency range of 1-500 MHz due to competition between the thermal red shift dominant in low modulation frequency ranges and the carrier blue shift dominant in high modulation frequency ranges [1]. We proposed a complex-coupled λ/4-shifted DFB laser to obtain a flat FM response by utilizing the self-suppression effect of longitudinal spatial hole-burning [2]. In this paper, we report on device performance of the proposed DFB lasers.

A schematic structure of the complex-coupled λ/4-shifted DFB laser is shown in Fig. 1. λ/4-shifted grating is fabricated on top of the InGaAsP active layer. The active region is embedded by Fe-doped InP and the 6-μm-wide mesa structure fabricated by dry etching to reduce parasitic capacitance. The cavity is 200-μm long and both facets are anti-reflection coated with a sputtered SiN_x thin film.

The longitudinal spatial hole-burning effect is suppressed by increasing the current injected into the laser and wavelength is tuned longer. A flat FM response is expected because both the thermal effect and the carrier effect are red shift in this laser. Figure 2 shows calculated wavelength deviation from the Bragg wavelength (δL) and the normalized threshold field-gain difference between the main mode and the biggest submode ($\Delta\alpha_{th}L$) as a function of normalized driving current (J/J_{th}). The wavelength is tuned longer (δL decreases) and single-mode operation stabilizes ($\Delta\alpha_{th}L$ increases) with the increase in driving current due to the self-suppression effect of the longitudinal spatial hole-burning In this calculation, the normalized coupling coefficient κL is assumed to be 2.0, the normalized gain coupling coefficient $\kappa_g L$ is 0.6, and the linewidth enhancement factor α is 7.0.

FM response as a function of the modulation frequency at a 15-mW output power is shown in Fig. 3. A flat FM response from 10 kHz to 17 GHz is obtained and a high FM response of 1.25 GHz/mA is obtained at a modulation frequency of 1 GHz. The wavelength is tuned longer within the modulation frequency range and response speed is limited by parasitic capacitance. Figure 4 shows the FM response as a function of the output power at a modulation frequency of 1 GHz. Here, the FM response is shown to decrease with increases in the output power as is expected from the calculated results shown in Fig. 2. Spectral linewidth is shown as a function of the output power in Fig. 5. Spectral linewidth is 10.2 MHz at an output power of 15 mW.

[1] S. Kobayashi *et al.*, IEEE J. Quantum Electron., vol. QE-18, pp. 582-595, 1982.
[2] M. Okai, Electron. Lett., vol. 29, pp. 1497-1498, 1993.

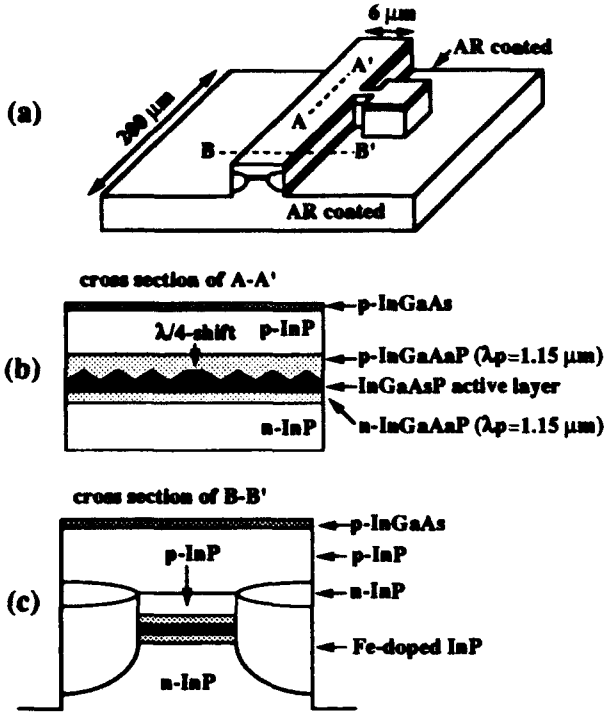

Fig. 1
A schematic view of the complex-coupled λ/4-shifted DFB laser.
(a) Side view (b) Cross section of A-A'
(c) Cross section of B-B'.

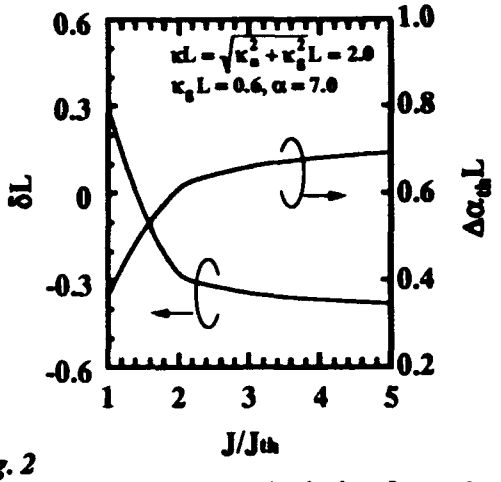

Fig. 2
Calculated wavelength deviation from the Bragg wavelength (δL) and the normalized threshold field-gain difference between the main mode and the biggest submode ($\Delta\alpha_{th}L$) as a function of normalized driving current (J/Jth).

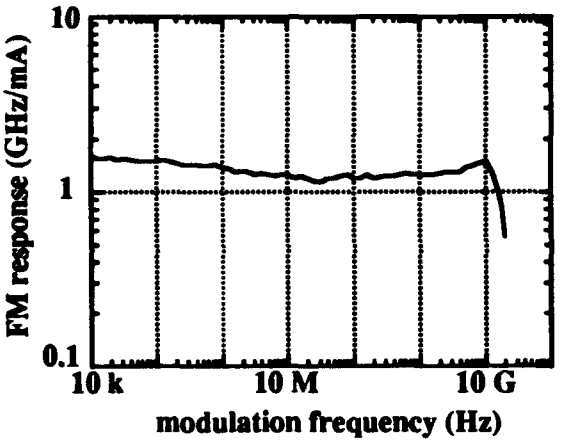

Fig. 3
FM response as a function of the modulation frequency at 15-mW output power.

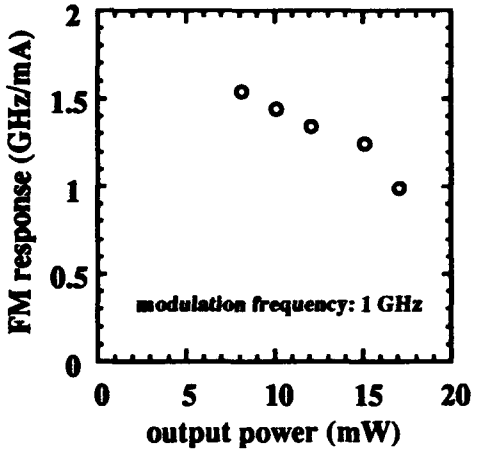

Fig. 4
FM response as a function of the output power at the modulation frequency of 1 GHz.

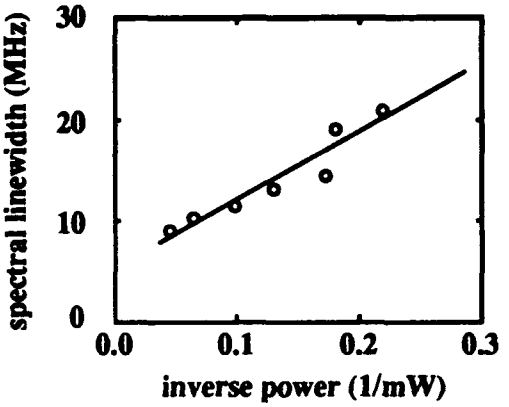

Fig. 5
Spectral linewidth as a function of the inverse output power.

9:00am - 9:15am
T1.3

High-power and high-speed performance of gain-coupled 1.3 μm strained-layer MQW DFB lasers

H. Lu, C. Blaauw, B. Benyon, and T. Makino
Bell-Northern Research, P. O. Box 3511, Station C, Ottawa, Canada K1Y 4H7

Abstract- High power and high modulation bandwidth 1.3 μm DFB lasers with gain coupling in a strained-layer MQW active region are reported for the first time. Due to the nature of the gain coupling effect, devices show lasing spectra with a consistently high single mode yield.

Dynamic single mode 1.3 μm DFB lasers with narrow spectral linewidth and high modulation bandwidth are highly desirable for long haul and high bit-rate optical communications using normal single mode fiber because of zero dispersion at this wavelength. Also, recently there is an increasing demand for high speed and high power lasers to satisfy broadcast requirements to many channels in data interconnect and switching applications.

1.55 μm DFB lasers with pure gain-coupling [1], partial gain-coupling [2],[3], and loss-coupling [4] have been demonstrated to have many advantages over conventional index-coupled DFB lasers such as high single mode selectivity, less sensitivity to external reflections, high modulation bandwidth and reduced wavelength chirp. However, there are no reports of such devices operating at 1.3 μm wavelength.

In this paper, we present for the first time the fabrication and the lasing performance of partly gain-coupled 1.3 μm DFB lasers, for which a high single mode yield and high output power with high quantum efficiency and high modulation bandwidth are the main performance objectives.

Fig. 1 shows a TEM of the layer structure, which was fabricated by two-step MOCVD. An active region containing nine strained quaternary quantum wells (0.7 % compressive strain) was grown in the first MOCVD stage. A first order grating pattern was formed by holographic exposure and chemical etching through the top five quantum wells followed by a second overgrowth to produce both gain and index coupling. The ratio $\kappa_{gain}L/\kappa_{index}L$ is estimated to be around 1/50 to 1/100 for devices with cavity length L of 150 μm to 400 μm; this gain coupling fraction is supplement to effectively increase the threshold gain margin between the two Bragg modes in favor of single mode operation at the long wavelength side of the stop band.

Fig. 2 shows the typical light-current curves for ridge waveguide lasers with different values of L at 30°C. The threshold currents I_{th} typically vary between 18 mA and 32 mA for devices with L = 150 μm to 375 μm. The slope efficiencies were approximately 0.40 mW/mA and 0.20 mW/mA for devices with L = 150 μm and 375 μm, respectively. Good linearity of light-current curves over 50 mW was achieved for devices with L = 200 μm and longer, where the lasing spectra maintained single modes. Fig. 3 shows the lasing spectra at a current below I_{th} and at 20 mW output power for two devices with short and long cavity lengths. The stop band was measured to be around 3.3 - 3.6 nm, which corresponds to κ_{index}= 200 cm^{-1}. The dominant longitudinal mode is on the long wavelength side of the stop band as the gain coupling favors this mode. The side mode suppression ratio is greater than 50 dB for both short and long cavity devices. The internal loss and internal quantum efficiency were estimated to be around 15 cm^{-1} and 0.83, respectively, from FP lasers with a similar structure.

To investigate the laser dynamic characteristics, RIN measurements were carried out. High resonance frequency and high intrinsic bandwidth were obtained with typical f_r ~ 12 - 14 GHz at 10 mW output power and very low RIN (below -155 dB/Hz measured at 2.5 GHz). The typical small signal frequency response of these 1.3 μm gain-coupled DFB lasers at different bias currents is shown in Fig. 4 for a device with L = 250 μm; I_{th} is around 22 mA for this device. The

measured -3 dB bandwidth is 18 GHz at 85 mA bias current for this gain-coupled DFB laser. Because of the high damping characteristics and the high bandwidth, the device shows a good eye opening of the optical output waveform 10 Gbit/s speudorandom NRZ modulation.

In conclusion, we have demonstrated high power with single mode operation up to 50 mW of partly gain-coupled 1.3 μm DFB lasers. The devices showed very low RIN and a high measured bandwidth of 18 GHz, which makes them suitable for long haul high bit-rate optical communication systems. They are also suitable for 10 Gbit/s optical data switching and interconnect and analog applications when the high power, low distortion and low RIN lasers are required.

[1] Y. Nakano, K. Tada, Y. Luo, H. Hosomatsu, T. Oki, H. Iwaoka, Proc. of ECOC/IOOC'91, Paris, pp. 1-8, 1991.

[2] G.P. Li, T. Makino, R. Moore, N. Puetz, K. Leong, H. Lu, IEEE J. Quantum Electron., vol. QE-29, pp. 1736-1742, 1993.

[3] H. Lu, S. McGarry, G.P. Li, T. Makino, Electron. Lett., vol. 29, pp. 1369-1370, 1993.

[4] B. Borchert, K. David, B. Stegmuller, R. Gessner, M. Beschorner, D. Sacher, G. Franz, IEEE Photon. Technol. Lett., vol. 3, pp. 955-957, 1991.

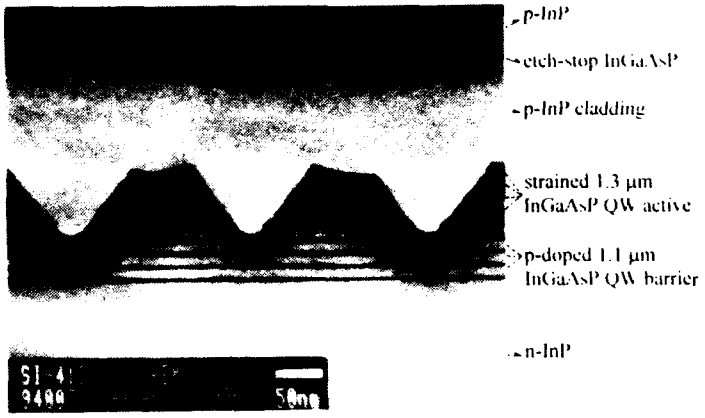

Fig. 1 TEM of the layer structure of gain-coupled DFB lasers.

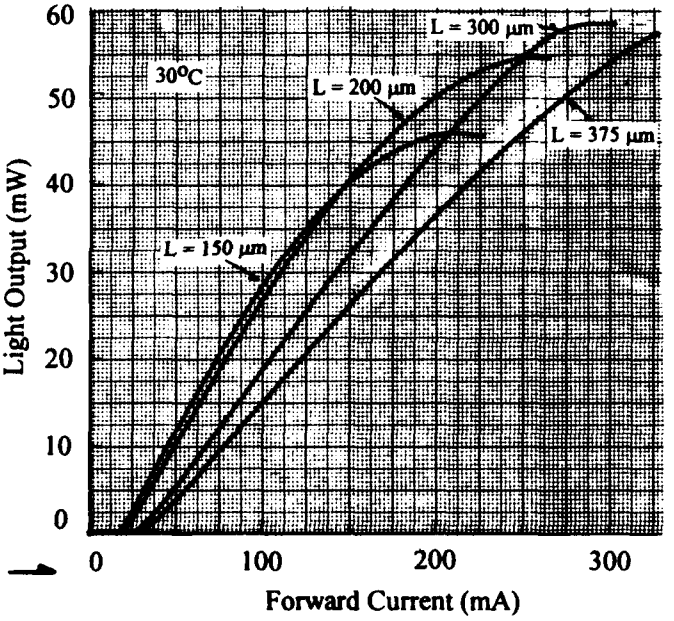

Fig. 2 Light-current characteristics of gain-coupled DFB lasers with L as a parameter.

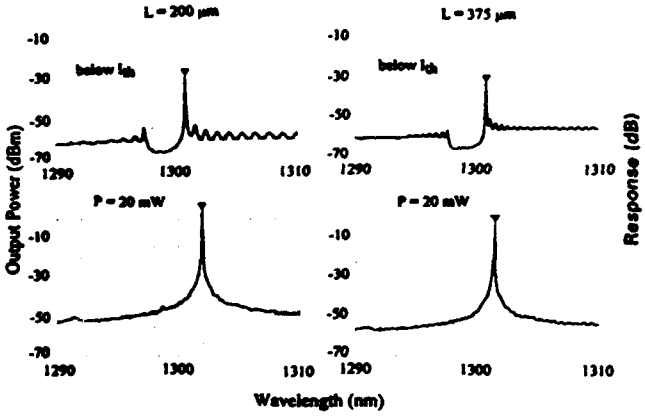

Fig. 3 Lasing spectra at below I_{th} and at high power for two devices with different L.

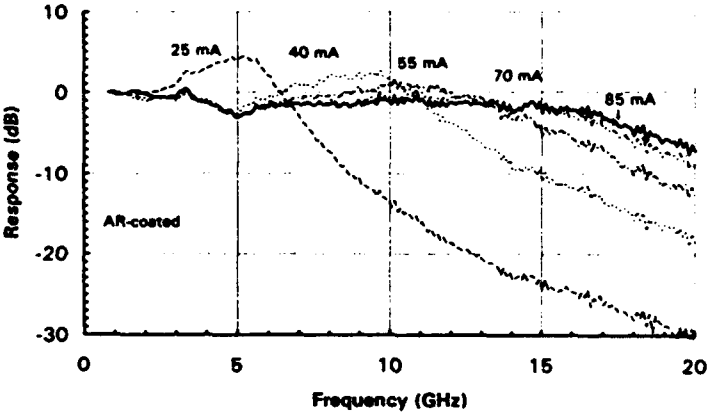

Fig. 4 Small signal frequency response at various bias currents.

9:15am - 9:30am
T1.4

Anomalous Dynamic Wavelength Chirp in Gain-Switched Short Optical Pulses from Absorptive-Grating Gain-Coupled DFB Lasers

Tsurugi K. Sudoh, Yoshiaki Nakano, Kenio Tada, and Takaaki Hirata*

Department of Electronic Engineering, University of Tokyo
7-3-1 Hongo, Bunkyo-ku, Tokyo, 113, Japan
Phone: +81-3-3812-2111 ext. 6777, Facsimile: +81-3-5802-3313

Abstract- Instantaneous wavelength shifts in gain-switched short optical pulses from absorptive-grating gain-coupled (GC) DFB lasers were measured and compared with those of Fabry-Perot lasers. The GC DFB laser showed characteristic wavelength shifts which resulted in much smaller chirping. Its mechanism is discussed.

One important advantage of the gain-coupled (GC) distributed feedback (DFB) semiconductor laser is its capability of generating nearly-transform-limited short optical pulses by simple gain switching configuration.[1-3] This is particularly useful for soliton transmission systems. In order to clarify its mechanism, a preliminary experiment was conducted where time-resolved spectra of the gain-switched optical pulses were observed.[4] This paper describes further investigation in this respect, emphasizing comparison with conventional lasers with the same layer structure.

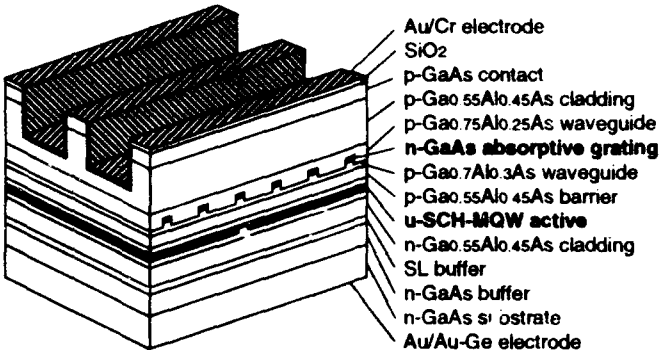

Fig. 1. Schematic drawing of the MQW GC DFB laser with a GaAs absorptive grating.

Figure 1 shows a schematic of the GC DFB laser fabricated by two-step OMVPE[5] and measured here. Thin GaAs periodically allocated above the MQW active layer provides periodic absorption, thus producing gain coupling. Pitch and duty cycle of the GaAs absorptive grating are 374nm (3rd order) and approximately 25%. A 4μm-wide ridge waveguide is formed on the epitaxial wafer. It is cleaved into 200μm-long devices whose facets are left uncoated. Typical threshold current and differential efficiency were 15mA and 0.5W/A/facet at 20°C. Lasing wavelength was around 840nm. The gain- and index-coupling coefficients were estimated to be 30cm^{-1} and 20cm^{-1}, respectively. Fabry-Perot (FP) lasers measured here for comparison were fabricated in exactly the same manner, except that the GaAs absorptive layer was removed entirely before the regrowth.

The devices were driven by current pulses of 130ps width, about 300mA peak amplitude, and 100MHz repetition rate, which were added on a DC bias current. Generated short optical pulses were observed by a streak camera. Figure 2 shows bias-current dependence of output pulse energy and pulse width in the GC DFB laser. The pulse energy increases monotonously with the bias while the pulse width decreases once and then increases. The minimum width in this particular case was 30ps.

Next, time-resolved spectra were taken by placing a grating monochromator before the streak camera. Typical streak images of the FP and GC DFB lasers showing instantaneous wavelength shifts are illustrated in Figs. 3 and 4, together with intensity profiles (their time-width is stretched because of path-length difference in the monochromator). The FP laser was biased at I_{th}, and the GC DFB laser was biased at 0.38 I_{th} (a) and I_{th} (b). Pulse energies were 17.8pJ, 4.8pJ, and 13.2pJ, respectively. As is common, multi-mode oscillation is observed in the FP laser. The GC DFB laser shows complete dynamic single-mode oscillation at any bias level.

*Devices Laboratory, Yokogawa Electric Corporation, 2-9-32 Naka-cho, Musashino-shi, Tokyo, 180, Japan.

At the beginning of the optical pulse, the instantaneous wavelength of both the FP and GC DFB lasers shifts toward longer wavelength (red shift). However, in the GC DFB laser the shift rapidly becomes smaller as the intensity reaches its maximum. This results in much smaller chirping. By contrast, the wavelength still shifts toward the longer side in the FP laser. Furthermore, we notice that the wavelength shift has bias dependence in the GC DFB laser. In Fig. 4 (a) the wavelength slightly moves back toward shorter side (blue shift) around the pulse peak while it shows a slight red shift in Fig. 4 (b).

To explain this anomalous behavior, we need to consider photon-density-dependent absorption (saturable absorption) of the GC DFB laser grating. From the output pulse energy and the coupling coefficients, the photon density in the absorptive regions is estimated to be in the order of $10^{18}cm^{-3}$, which is sufficient for saturation of the absorber. In the FP laser, the monotonous red shift is due to the monotonous decrease in carrier density throughout the optical pulse duration. In the GC DFB laser, the refractive index of the absorptive grating becomes lower due to saturation as photon density increases, so that the red shift can be canceled at high photon density regime.

In Fig. 4 (a), this blue shift overcomes the original red shift near the pulse peak. When the pulse energy is relatively high in Fig. 4 (b), the absorptive region is almost bleached and the refractive index does not change much. Therefore, we observe net red shift around the pulse peak. In between these two extremes, there is an optimum pumping where we can obtain chirp-compensated optical pulses. Pulse width could be narrower at the same time as understood from Fig. 2.

1) Y. Luo et al., Appl. Phys. Lett. **59**, 37 (1991).
2) Y. K. Chen et al., CLEO '92, CTuF4.
3) C. E. Zah et al., OFC / IOOC '93, TuM4.
4) T. K. Sudoh et al., CLEO '94, CWJ5.
5) Y. Nakano et al., Jpn. J. Appl. Phys. **32**, 825 (1993).

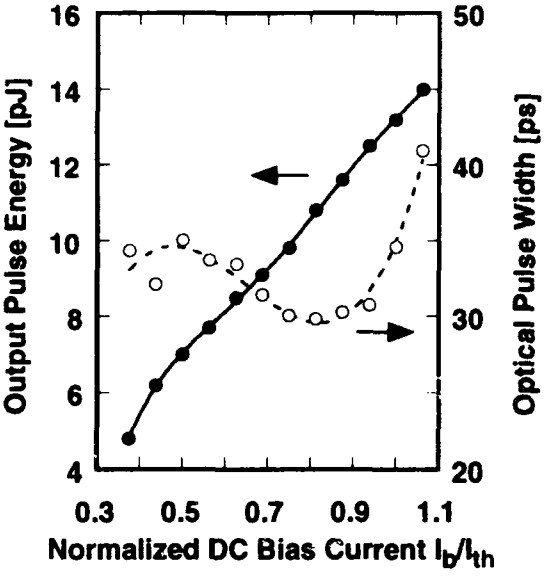

Fig. 2. Energy and width of gain-switched optical pulse from the GC DFB laser as functions of DC bias current.

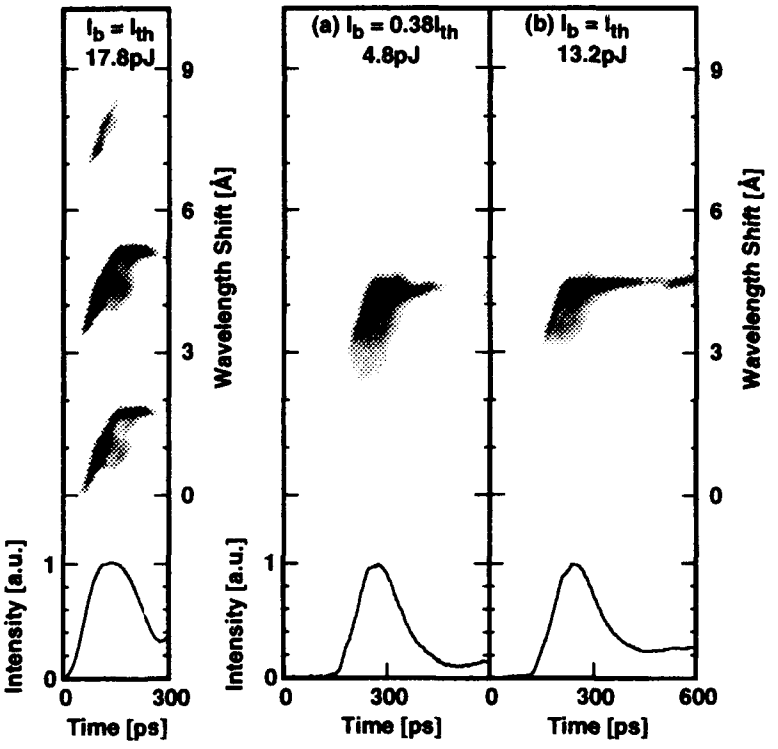

Fig. 3. Time-resolved spectrum of gain-switched optical pulse from the FP laser along with pulse intensity profile.

Fig. 4. Time-resolved spectra of gain-switched optical pulses from the GC DFB laser at DC bias levels of 0.38 I_{th} (a) and I_{th} (b).

9:30am - 9:45am
T1.5

Tailored DFB laser properties by individually chirped gratings using bent waveguides

H. Hillmer, H.-L. Zhu, S. Hansmann, A. Grabmaier, K. Magari*, H. Burkhard
Deutsche TELEKOM, Forschungszentrum, P.O.Box 100003, 64276 Darmstadt, Germany
* NTT Integrated Opto-electronics Laboratories, Atsugi, Kanagawa Pref. , 243-01 Japan

Abstract: DFB lasers with quasi-continuously and arbirtrarily chirped gratings of ultra-high spatial precision were realized by an economically interesting method using bent waveguides. Several application possibilities are discussed.

Chirped DFB gratings (CDGs) are very attractive to fit individual laser properties with respect to the requirements of advanced lightwave communication systems. In recent years CDGs were studied and applied rarely, since a realization method providing arbitrary chirping functions [pitch length variation $\Lambda(z)$] was not available [1-4]. We use a method based on bent waveguides superimposed on homogeneous grating fields (Fig. 1) capable to generate arbitrary and quasi continuous chirping functions with ultrahigh spatial precision [5]. The local Λ is defined by the local tilt angle of the waveguide with respect to the grating. Choosing individually tailored bending functions y(x), individual $\Lambda(z)$ are generated, providing the following attractive laser applications: realization of axially arbitrarily distributed phase-shifts, reduction of axial spatial hole-burning to stabilize Bragg-mode, optical output power increase, linewidth reduction, yield increase, improved high-frequency properties and enhanced wavelength tuning range.

Now experimental and theoretical application examples are shown: InGaAs/InAlGaAs QW DFB lasers were realized with bent waveguides to provide the chirping functions shown in Fig. 2. Fig. 2a corresponds to a bending function similar to that shown in Fig. 1. Transfer matrix model calculations show a considerably reduced photon pile-up in Fig. 3 for a distributed $\lambda/4$ distributed phase-shifted laser (Fig. 2b) compared to an abrupt $\lambda/4$ phase-shifted laser. This results in higher output power, reduced spatial hole-burning and Bragg-mode stabilization. Fig. 4 depicts lower linewidth at the highest output power before the device turns out to become multimode for the same CDG laser compared to the abrupt phase-shifted laser. The $\Lambda(z)$ function shown in Fig. 2c was optimized for wavelength tunability: $\Lambda(z)$ is optimized to provide several neighbouring modes of nearly identical threshold gain. A single mode is selected by multi-sectioning. Fig. 5 shows the wavelength variation covering 5.5nm, maintaining a constant output power and a side mode suppression larger than 30dB over the total unbroken wavelength range.

References : 1. A. Katzir, A. C. Livanos and A. Yariv, Appl. Phys. Lett. **30**, 225 (1977).
2. A. Suzuki and K. Tada, Thin Solid Films **72**, 419 (1980).
3. P. Zhou, and G. S. Lee, Appl. Phys. Lett. **58**, 331 (1991).
4. G. Morthier, K. David, P. Vankwikelberge, R. Baets, IEEE Phot. Tech. Lett. **2**, 388 (1990).
5. H. Hillmer, K. Magari, and Y. Suzuki, IEEE Photonic Technol. Lett., **5**, 10 (1993).

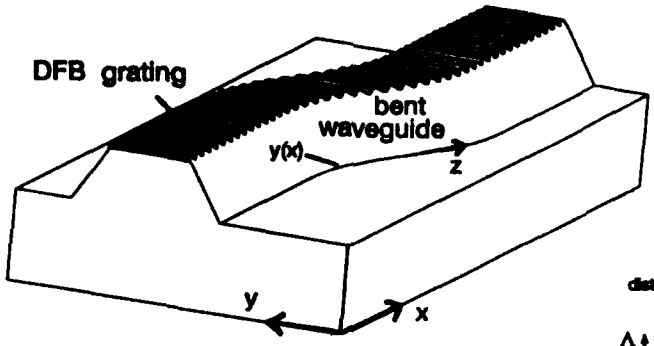

Fig. 1: Bent waveguide DFB laser

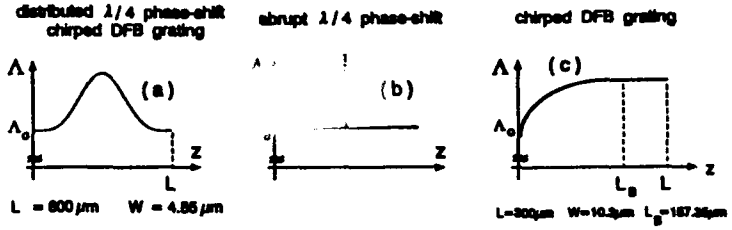

Fig. 2: Three different axial pitch length variations

$$(a) \qquad \Lambda = \Lambda_0 \sqrt{1 + \frac{4W^2}{L^2}\left(\cos\frac{2\pi z}{L} - 1\right)^2}$$

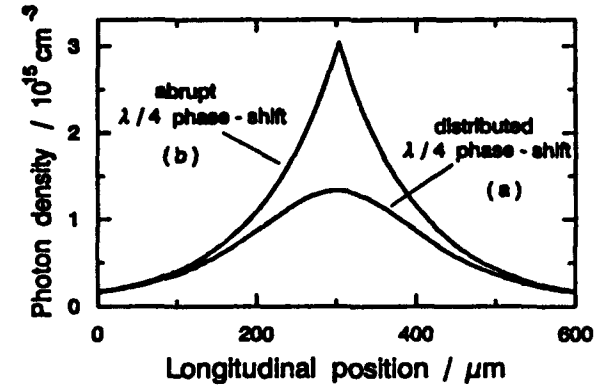

Fig. 3: photon ditribution for a distributed (a) and an abrupt (b) λ/4 phase-shifted DFB laser.

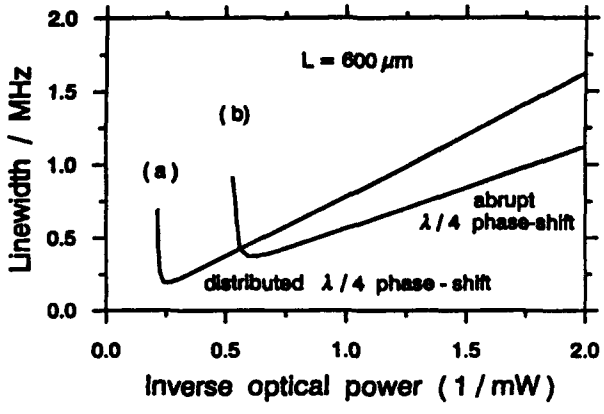

Fig. 4: Linewidth versus inverse power for lasers (a) and (b), [K·L~3].

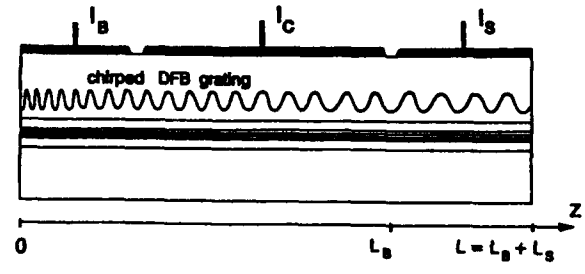

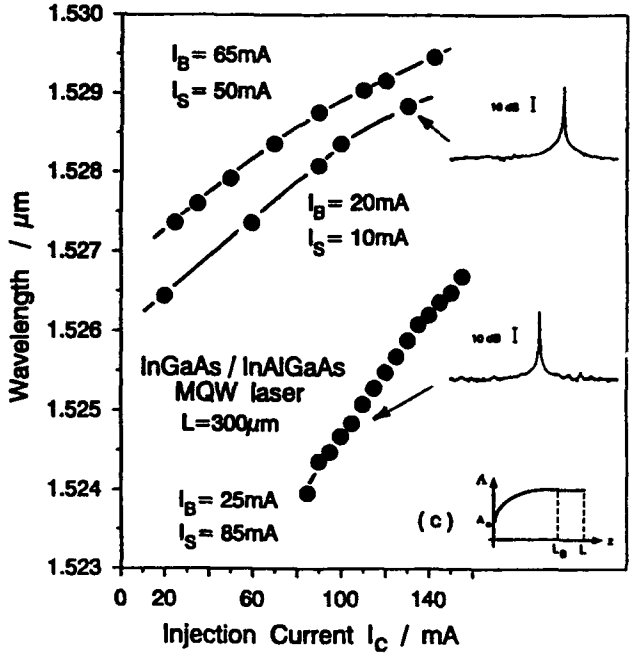

Fig. 5: Top: Three-section DFB laser.
Bottom: exper.wavelength tunability.

9:45am - 10:00am

T1.6

The S-bent waveguide distributed feedback laser

J. Salzman[1], H. Olesen, A. Møller-Larsen, O. Albrektsen,

J. Hanberg, J. Nørregaard and B. Tromborg

Tele Danmark Research, Lyngsø Allé 2, DK-2970 Hørsholm, Denmark

Abstract: We analyzed the above threshold behaviour of pitch-modulated DFB cavities seeking optimum design for high power dynamic single-mode operation. Implementation of such lasers by S-bent waveguides is reported.

A DFB laser with a discrete $\lambda/4$ phase shift is the optimum cavity for achieving oscillation at the Bragg frequency with a large side-mode suppression ratio (SMSR) [1]. Above threshold, however, these lasers exhibit longitudinal spatial holeburning with the subsequent degradation in SMSR. In order to achieve dynamic single-mode operation up to high output powers different grating designs have been proposed, including multiple phase shifts [2], chirp [3], and corrugation-pitch-modulation (CPM) [4]. High output powers in a single mode with record values of narrow linewidth were reported from CPM lasers [5].

Recently, we have shown that discrete phase-shifted and pitch-modulated DFB lasers are not equivalent, and that threshold considerations are not sufficient to realize a good cavity design for high power operation [6]. In addition to that, variations of the grating period with the required resolution may impose stringent technological limitations in the fabrication procedure.

Here, we propose a novel and simple fabrication method to implement chirped or pitch-modulated DFB lasers, and optimize the design for high power single-mode operation. The method consists of bending the laser waveguide, so that the Bragg wavenumber is varied controllably along the laser cavity. The feasibility of the proposed method is demonstrated by the fabrication of a sinusoidally bent waveguide DFB laser (S-DFB) with a high coupling coefficient, κ, operating in a single mode up to a very high current above threshold.

In Fig. 1(a) the effect of tilting the laser waveguide with respect to a background grating field is shown [7]-[8]. Figs. 1(b)-(d) show how this effect can be used in order to implement chirped and pitch-modulated DFB cavities. For example, the previously reported CPM-DFB design [4] could be fabricated as in Fig. 1(b), with a tilt of $\Theta = 1.48°$ in the central section.

Variations in the waveguide parameters due to fabrication tolerances may introduce deviations in the local Bragg wavelength and thus affect the filter properties of the modulated grating. In order to optimize and to check the robustness of the proposed design, we used our simulation program [9] to study the above threshold behaviour of various DFB cavities (with constant electrode potential). As an example, Fig. 2 shows the power limit, where the roundtrip gain for the side mode exceeds 0.8 [9], versus $(\beta_c - \beta_o)/\kappa$ for different relative center section lengths. β_c and β_o are the Bragg wavenumbers of the center and outer sections. The input parameters in the simulation leading to Fig. 2(a) are those of a CPM cavity (as in Fig. 1(b)), while S-DFB lasers (as in Figs. 1(c)-(d)) were considered in Fig. 2(b). From these calculations we may conclude, that: (i) Optimal design for high power single-mode operation requires $l_c/l \simeq 0.5$ and $\kappa \lesssim \beta_c - \beta_o \lesssim 1.5\kappa$. This cavity design does not, in general, correspond to a distributed $\lambda/4$-shift. (ii) The cavity with a constantly detuned center section and that with a sinusoidally bent waveguide exhibit qualitatively similar behaviour, with highest power for single-mode operation in the same region in spite of the different input parameters. Note, that although Refs. [4]-[5] included a larger grating pitch in the center section, our calculations show that a positive center section detuning (*shorter* grating pitch) leads to the highest power single-mode operation.

[1]On leave from TECHNION, the Israel Institute of Technology, Haifa 32000, Israel.

Similar results were obtained for other chirped-grating cavities, showing that the design rules derived from Fig. 2 are robust against microfabrication related uncertainties. We have also calculated the linewidth versus output power of various cavities and concluded, that the narrowest linewidth for a particular (attainable) operating power requires a different design than that for high power single-mode operation.

In order to demonstrate the feasibility of the proposed method we have fabricated S-DFB ridge waveguide SCH-MQW lasers with $\kappa l \simeq 6.5$, $l = 800$ μm, $l_c/l = 0.5$, and $\beta_c - \beta_o \simeq \kappa$. The lasers were processed on a conventional holographic grating and AR-coated on both facets. In Fig. 3 we show, as a preliminary result, the spectra from $I_{th} = 20$ mA up to $I = 5I_{th}$, maintaining a side-mode suppression of more than 40 dB in the whole range tested. Further characterization of these lasers is being performed.

References

1. H. A. Haus and C. V. Shank, *IEEE J. Quantum Electron.*, QE-12, 532, 1976.
2. S. Nilsson et al., *J. Lightwave Technol.*, (in press).
3. X. Pan et al., *Digest of CLEO'91*, CWF15 (1991).
4. M. Okai et al., *IEEE Photon. Technol. Lett.*, 2, 519 (1990).
5. M. Okai et al., *Electron. Lett.*, 29, 1696 (1993).
6. H. Olesen et al., submitted to *CLEO/Europe '94*, (1994).
7. H. Hillmer et al., *IEEE Photon. Technol. Lett.*, 5, 10 (1993).
8. W. T. Tsang et al., *IEEE Photon. Technol. Lett.*, 5, 978 (1993).
9. H. Olesen et al., *IEEE J. Quantum Electron.*, 29, 2282, (1993).

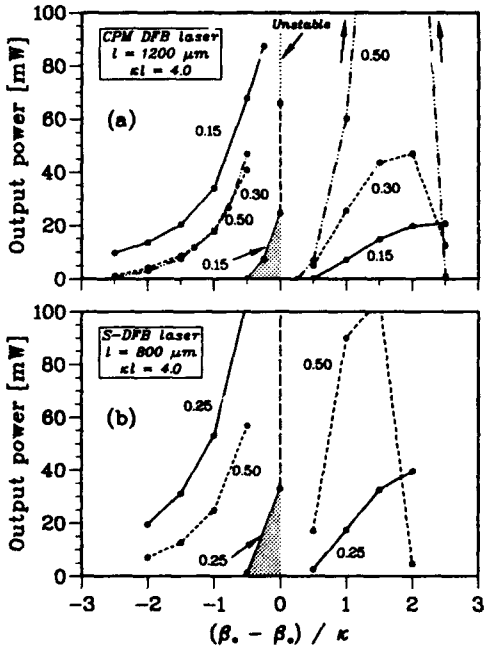

Fig. 2 Calculated power limits of single-mode operation for (a) CPM DFB lasers and (b) S-DFB lasers with sinusoidal bends. The curve labels indicate the relative length of the center section l_c/l. The horizontal axis shows the normalized Bragg deviation between the center and outer sections (for S-DFB lasers the RMS-deviation is used). Nearly uniform lasers show poor side-mode suppression close to threshold (shaded area).

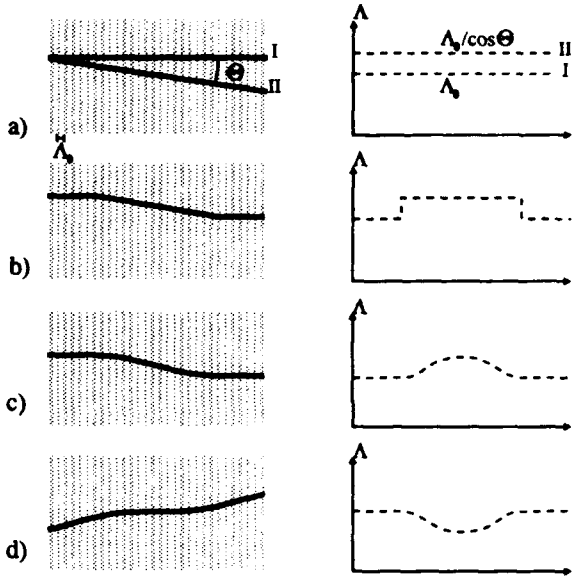

Fig. 1 Schematic illustration of tilted or bent waveguides on a uniform grating. Left column: Different waveguide layouts, right column: the corresponding variation of the grating pitch along the cavity. b) corresponds to a CPM DFB laser, whereas c) and d) are referred to as S-DFB lasers.

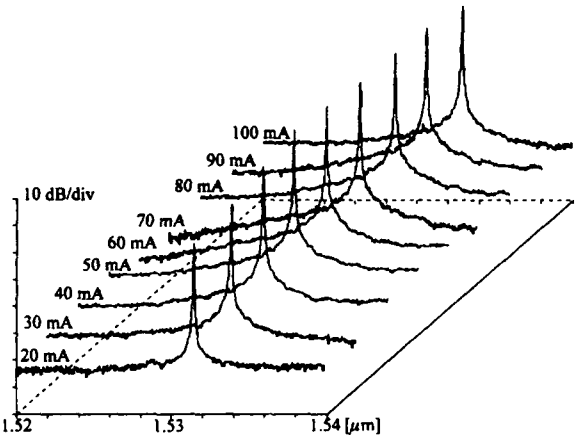

Fig. 3 Example of spectral behaviour for a fabricated S-DFB laser. More than 40 dB side-mode suppression is maintained up to 5 times threshold.

10:30am - 10:45am
T2.1

Unambiguous Determination of Quantum Capture, Carrier Diffusion and Intrinsic Effects in Quantum Well Laser Dynamics Using Wavelength - Selective Optical Modulation

Dan Vassilovski, Ta-Chung Wu, Sidney Kan[1], and Kam Y. Lau

Abstract

A novel wavelength -dependent optical modulation technique is described which is capable of delineating quantum capture, carrier diffusion and other intrinsic effects in quantum well laser dynamics. Dependence of these mechanisms on device structure will be discussed.

Limitations in the modulation bandwidth of quantum well lasers imposed by damping is generally represented by a K-parameter. The physical mechanisms responsible for the damping currently consist of the following candidates: intrinsic quantum capture, carrier diffusion and intrinsic effects including carrier heating and spectral hole burning. Except in certain devices of atypical structures specially fabricated to highlight some of these mechanisms individually, in most typical QW laser structures it is most likely that all three mechanisms are at play. For these devices, the conventional method of extracting the damping parameter through electrical modulation response measurements generally sheds little light on the relative role of each of these mechanisms, since they all give quantitatively (and sometimes qualitatively) similar consequences. We report here a novel modulation measurement technique that can unambiguously delineate the intrinsic quantum capture effect and the carrier diffusion effect from the rest of the intrinsic mechanisms. These results are very useful in the design of a real-life high speed laser.

The experimental approach is shown in Fig. 1. The test laser is electrically DC biased and optically modulated using a separate laser which is directly modulated by the RF output of a network analyzer [1]. By varying the wavelength of the modulating laser, one can modulate directly carriers either in the quantum well (in-well), or in the separate-confinement heterostructure region (out-of-well). By comparing the in-well modulation response to the out-of-well response, the intrinsic quantum capture effects can be isolated, while comparison of the out-of-well response to the direct current modulation response yields the effects of diffusion. Results of a detailed analysis (shown below) will confirm these assertions.

Quantitative analysis of the three modulation schemes described above is based on the semiclassical capture model (SCC) which is a space-time model incorporating both spatial diffusion in the SCH region and quantum capture at the QWs [2]. In the limit of a short quantum capture time and a long diffusion length relative to the barrier width (which is almost always the case for typical QW lasers), the SCC model reduces to the following modulation responses:

modulation method	**modulation response**	τ^E_{cap}	$\mathbf{R^E}$
optical, in-well	$\dfrac{1}{(-\omega^2 + j\omega\gamma + \omega_R^2) - \dfrac{\omega^2 R^E}{(1 + j\omega\tau^E_{cap})}}$	$\tau^Q_{cap}\dfrac{L_{SCH}}{L_{QW}}$	$\dfrac{\tau^Q_{cap}}{\tau^Q_{esc}}\dfrac{L_{SCH}}{L_Q}$
optical, out-of-well	$\dfrac{1}{(-\omega^2 + j\omega\gamma + \omega_R^2)\,(1 + j\omega\tau^E_{cap}) - \omega^2 R^E}$		
electrical		$\tau^Q_{cap}\dfrac{L_{SCH}}{L_{QW}} + \dfrac{L^2_{SCH}}{8D}$	$\dfrac{\tau^E_{cap}}{\tau^Q_{es}}$

1. Present address: Hong Kong University of Science and Technology

These three different responses are shown schematically in Fig. 2. Thus, by comparing and observing the corner frequencies of the poles of the response functions, each of the three contributing mechanisms can be delineated. Figure 3 shows a typical optical modulation measurement result for a single quantum well 1.55 μm laser. The measured effective quantum capture time is shown in Fig. 3b as a function of optical power.

To delineate the contribution of intrinsic damping effects such as carrier heating and spectral hole burning, one needs to independently measure the ratio R^E. This can be done in a straight-forward manner by spontaneous emission measurements as in Ref. [3]. With this information, we can obtain the damping rate due to quantum capture alone. By comparing this damping rate to the total measured damping rate, the contribution of intrinsic effects can thus be obtained.

This talk will describe the details of these measurement techniques as well as comparison of experimental results of different quantum well structures. Physical significance of various amount of contribution to damping in different laser structures will be discussed.

References:

[1] Vahala and Newkirk, Appl. Phys. Lett., Vol. 53, pg. 1141 (1988)

[2] Kan et al., Appl. Phys. Lett., Vol. 61, pg. 752 (1992).

[3] Hirayama et al., IEEE J. Quant. Electron., QE-30, pg. 54 (1994)

Figure 1a: Optical Modulation

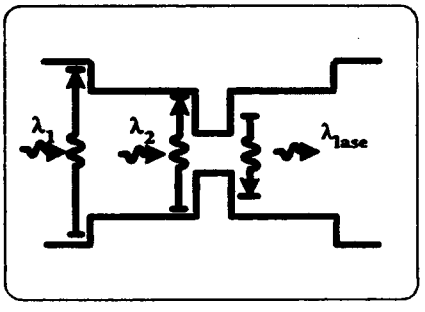

Figure 1b: Experimental Apparatus

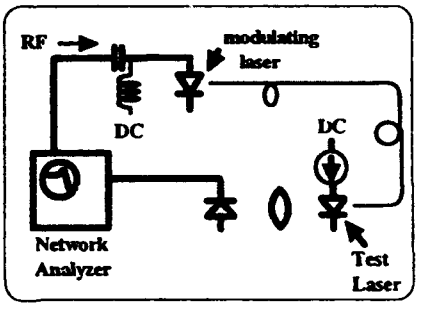

Figure 2: Theoretical Calculation of in-well, out-of-well and electrical modulation response functions

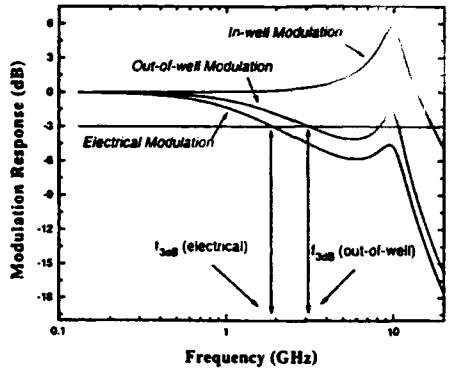

Figure 3a: Experimentally obtained in-well and out-of-well optical modulation response

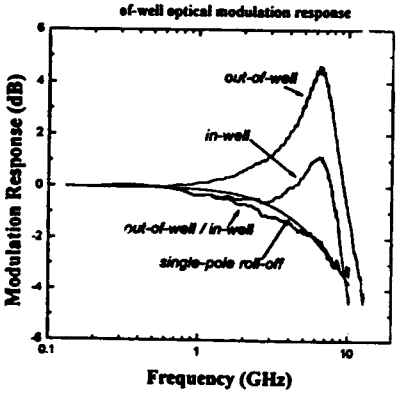

Figure 3b: power dependence of τ_{cap}^{E}

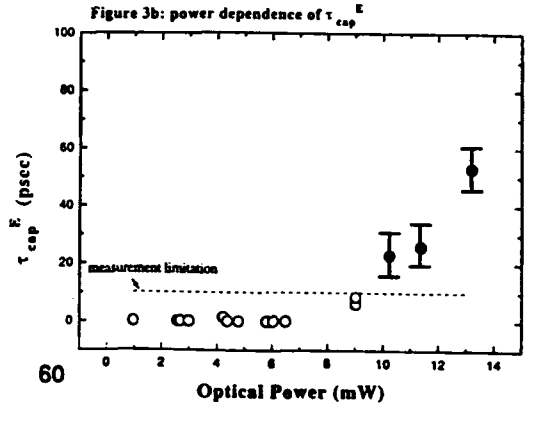

10:45am - 11:00am

T2.2 **Anomalously slow carrier-phonon interaction in InGaAs/InGaAsP multi-quantum-well investigated by time-development of carrier temperature**

Masaaki Nido and Akira Suzuki
Opto-Electronics Research Laboratories, NEC Corporation
34 Miyukigaoka, Tsukuba, Ibaragi 305, Japan

Extremely large electron-LO phonon intrasubband scattering time (8ps) was obtained, by the rate-equation analysis for the experimental time-development of the carrier temperature in a 1.5μm-band multi-quantum-well (MQW) laser amplifier. Consequently, pronounced optical output power saturation was predicted in the MQW laser.

Carrier-LO phonon interaction plays an essential role in the MQW carrier dynamics, and its influence on MQW laser (LD) characteristics has been discussed [1], [2]. However, the interaction time constant is still unclear. In this paper, the time-development of the carrier temperature in an InGaAs/InGaAsP MQW was investigated, by time-resolved spectroscopy [3], together with a calculation in an extended rate-equation model. The interaction time constant was found to be one order of magnitude larger than the predicted theoretically. Consequently, pronounced optical output power saturation was predicted in the MQW-LD.

The investigated MQW was composed of four $In_{0.53}Ga_{0.47}As$ QWs (7nm thick) and 1.15μm composition InGaAsP barriers (10nm thick), sandwiched by 1.15μm composition InGaAsP optical confinement layers (200nm thick). The experimental method for the time-development of the carrier temperature is schematically drawn in Fig. 1. The TE polarized optical pulse (1542nm wavelength, 2ps width, and 80mW peak power) was introduced to the biased MQW-LD amplifier. The carrier temperature at a fixed time (with the time-resolution of 2ps) was estimated from the high-energy tail of the TM polarized amplified spontaneous emission (ASE) [3]. The experimental time-development of the carrier temperature for the bias current I_B of 150mA is shown in Fig. 2 as full squares. The time origin was the optical pulse peak time. The time-development was calculated using rate equations, which took into account almost all possible carrier flow processes (radiative and Auger recombination, carrier capture/escape between the QW and the barrier). The capture/escape and the QW carrier energy emission/absorption processes were expressed as LO phonon emission/ absorption, whose rates were determined by the intrasubband electron-LO phonon scattering time τ_{ph}. The hot-phonon effect was also considered using the LO phonon lifetime τ_{LO}, which corresponds to the LO phonon-acoustic phonon scattering time.

The calculated time-development of the carrier temperature, using τ_{ph} of 1 and 8ps with fixed τ_{LO} (20ps), are shown in Fig. 2 as thin and thick solid lines. The experimental time-development was close to the calculated one with τ_{ph} of 8ps, which was one order of

magnitude larger than the theoretically predicted τ_{ph} of 0.8ps after the consideration of the Coulomb screening effect. The calculated time-development was found to be weakly dependent on τ_{LO}, showing the minor role of the hot-phonon effect. The experimental time-development for I_B of 50 and 100mA was also close to the calculated one with τ_{ph} of 8ps, showing the weak dependence of τ_{ph} on I_B. Figure 3 shows the current-light output (I-L) characteristics for the MQW-LD with the same MQW structure investigated, calculated using the rate equations with τ_{ph} of 1 and 8ps. By taking the obtained value of τ_{ph} (8ps), pronounced I-L saturation, due to the carrier temperature increase, was predicted.

[1] S. C. Can et al., IEEE Photon. Technol. Lett. 4, 428 (1992).

[2] C. Y. Tsai et al., Appl. Phys. Lett. 63, 3408 (1993).

[3] M. Nido and A. Suzuki, Appl. Phys. Lett. 64, 681 (1994).

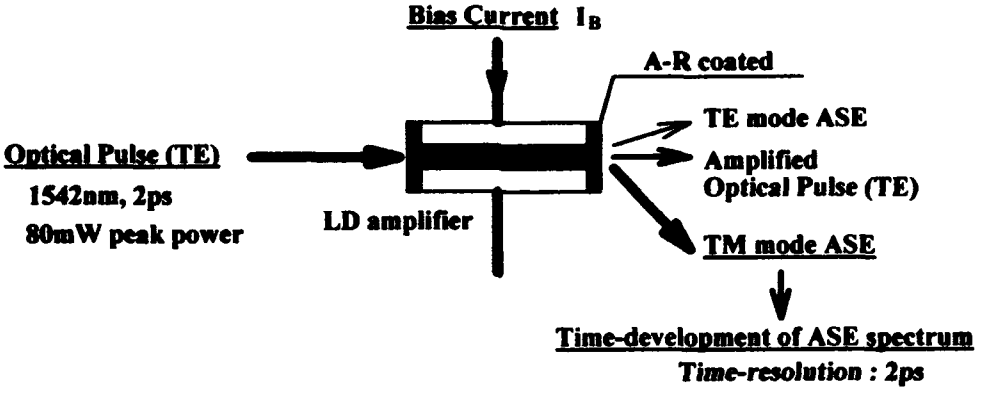

Fig. 1 : Experimental method

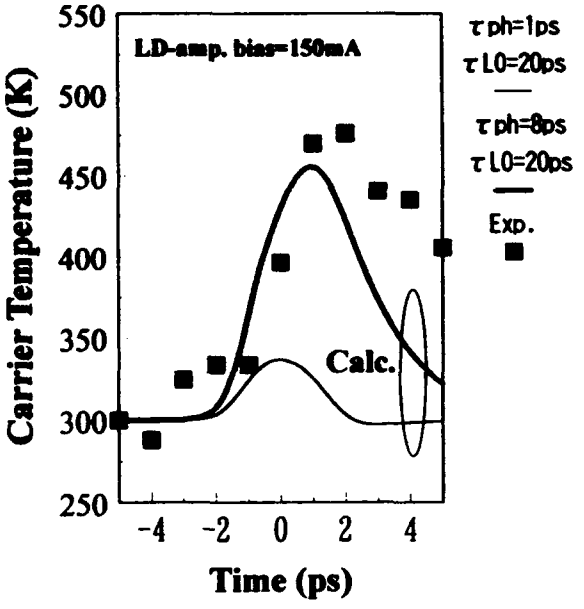

Fig. 2 : Time-development of the carrier temperature

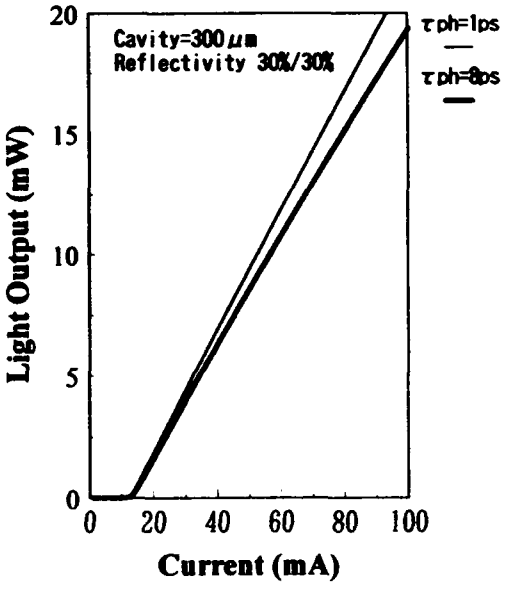

Fig. 3 : Calculated I-L characteristics for the MQW-LD

11:00am - 11:15am

T2.3 **Ultrafast gain and refractive index dynamics of semiconductor amplifiers measured by four-wave mixing**

A. D'Ottavi, E. Iannone, A. Mecozzi, S. Scotti, P. Spano
Fondazione Ugo Bordoni - Via B. Castiglione 59 - 00142 Rome - ITALY

R. Dall'Ara, G. Guekos, J. Eckner
Institute of Quantum Electronics - Swiss Federal Institute of Technology
8093 Zurich - Switzerland

Abstract - Measurements of four-wave mixing in traveling wave semiconductor optical amplifiers are extended up to frequency detunings between pump and probe as high as 4.3 THz. The 35 fs equivalent time resolution is, to our knowledge, the highest achieved to date. Experimental evidence of nonlinear processes faster than spectral hole burning is obtained for the first time by using a frequency domain technique.

Nonlinear optical effects in semiconductor active devices have been studied as a tool for investigating the mechanisms behind the modulation limitations of laser diodes and for their potential use in photonic devices for advanced optical communication networks. Optical nonlinearities have been investigated both in time [1, 2] and in frequency domain [3, 4]. These techniques underline the presence of different nonlinear processes behind the interaction of the electric field with the population of the electronic bands. Time domain experiments have shown that carrier depletion (CD), carrier heating (CH), spectral hole burning (SHB), and a quasi instantaneous effect ascribed to two photon absorption (TPA) are responsible for the nonlinear gain dynamics. CD, CH and a quasi-instantaneous process ascribed to Kerr effect (KE) are instead responsible for the nonlinear index dynamics. These processes are characterized by different time constants τ_{CD}~200 ps, τ_{CH}~700 fs, τ_{SHB}~100 fs. CH is also characterized by a delay time equal to τ_{SHB}. Frequency domain experiments based upon four-wave mixing (FWM) confirmed the presence of CD, CH and SHB, but the quasi instantaneous processes were never observed.

In this paper, we report a FWM experiment extended up to 4.3 THz. The 35 fs equivalent temporal resolution permits to detect the fastest processes for the first time.

Two optical fields, the pump at the fixed wavelength of 1.5469 μm and the probe, are mixed and injected into the semiconductor traveling wave amplifier. The pump power coupled to the waveguide is 120 μW, the probe power is <10 μW. The amplifier has a bulk structure with a ridge geometry. Its maximum gain is 25 dB at a bias current of 250 mA. The conjugate field, generated by the modulation of the optical gain and index induced by the pump-probe beating, is detected by a double-grating spectrometer. In fig. 1 the experimental values of the ratio between conjugate and probe output powers are reported vs. the pump-probe frequency detuning. Close and open circles refer to positive and negative pump-probe detunings. Solid lines are obtained by the theory of [5] by best fit of the experimental data. The contribution of the instantaneous effects is considered in analogy with what done in [5] for CH. The asymmetry between positive and negative detunings is due to the superposition of the processes producing the FWM response that combine with a different phase in the two branches. Each mechanism is characterized by a gain saturation coefficient P_s^{-1}, ε_{CH}, ε_{SHB} and ε_{INST} and index coefficient αP_s^{-1}, $\beta\varepsilon_{CH}$ and $\beta'\varepsilon_{INST}$. To first order, SHB affects only the gain [6]. The FWM efficiency of each nonlinear process decreases 20 dB per decade at frequency detunings $\Delta f >> (2\pi\tau)^{-1}$, where τ is its characteristic time constant. At frequency detuning larger than few THz, CH is no more effective, and the two curves of fig. 1 should approach to each other if SHB is the only process responsible for FWM. Consequently, the asymmetry between positive and negative detunings is the signature of the presence of the instantaneous process that interferes with SHB. The parameters

obtained by best fit are reported in Table 1. It is worth noting that the value and sign of β' and the value of ε_{INST} are in agreement with the values obtained by time domain measurements [2,6]. To clarify the role of the different nonlinear processes to the FWM efficiency, the ratio between the conjugate output power and probe input power is shown in fig. 2 as it is if only one process would have been present.

Work carried out in the framework of the agreement between Fondazione Ugo Bordoni and the Italian PT Administration, partial support has been given by the Italian National Research Council (CNR) in the framework of the Telecommunication Project. The investigation is carried out in the frame of the European Project COST 240. The support by the Swiss office for education and science is acknowledged.

References

[1] K. L. Hall et al. "Femtosecond gain dynamics in InGaAsP optical amplifiers" Appl. Phys. Lett., **56**, pp. 1740-1742, 1990.

[2] J. Mark and J. Mørk "Subpicosecond gain dynamics in InGaAsP optical amplifiers: Experiment and theory" Appl. Phys. Lett., **61**, pp. 2281-2283, 1992.

[3] L. Tiemeijer "Effects of nonlinear gain on four-wave mixing and asymmetric gain saturation in a semiconductor laser amplifier" Appl. Phys. Lett., **59**, pp. 499-501, 1991.

[4] K. Kikuchi et al. "Analysis of origin of nonlinear gain in 1.5 mm semiconductor active layers by highly nondegenerate four-wave mixing" Appl. Phys. Lett., **64**, pp. 548-550, 1994.

[5] A. Mecozzi et al. "Four-wave mixing in traveling-wave semiconductor amplifiers" submittet to J. Quantum Electron.

[6] K. L. Hall et al. "Femtosecond index nonlinearities in InGaAsP optical amplifiers" Appl. Phys. Lett., **62**, pp. 1320-1322, 1993.

Table 1

P_s^{-1} (mW^{-1})	α	ε_{CH} (mW^{-1})	β	ε_{SHB} (mW^{-1})	ε_{INST} (mW^{-1})	β'
0.14	4	$6.7\ 10^{-3}$	.9	$2\ 10^{-3}$	$1.2\ 10^{-4}$	-2

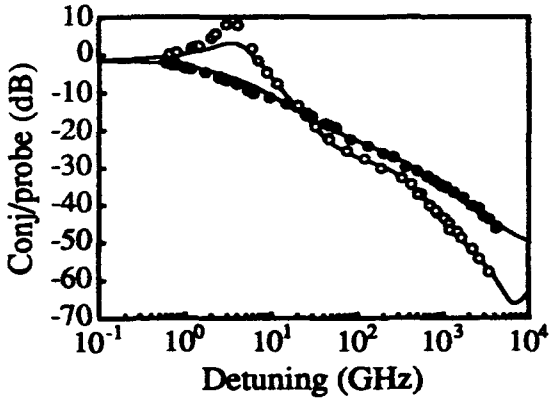

Fig. 1 - Ratio between the conjugate and probe power at the output of the amplifier vs. the pump-probe frequency detuning ν_{pu}-ν_{pr}. Close and open circles refer to positive and negative pump-probe detunings.

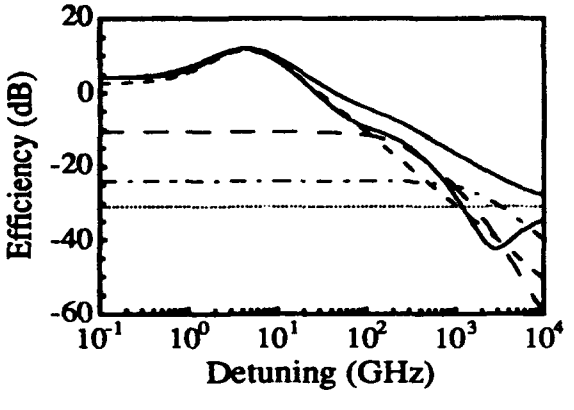

Fig. 2 - Contribution to the efficiency of the various nonlinear terms. Short dashed curve refers to CD, long dashed to CH, dashed-dotted to SHB, dotted to instantaneous effects. Continuous lines represent the theoretical efficiency calculated with the parameters reported in Table1.

11:15am - 11:30am

T2.4

Four-Wave Mixing in Semiconductor Optical Amplifiers at THz Detuning Frequencies: Experiment and Theory

J. Mørk, A. Uskov, J. Mark
Tele Danmark Research
Lyngsø Allé 2, DK-2970 Hørsholm, Denmark

M. C. Tatham, G. Sherlock
BT Laboratories, Martlesham Heath, Ipswich, IP5 7RE, U.K.

Abstract: Highly non-degenerate four-wave mixing processes in semiconductor optical amplifiers are analyzed by comparing experimental data at detuning frequencies up to 3 THz with numerical calculations based on microscopic density matrix equations.

The study of four-wave mixing (FWM) processes in active semiconductor waveguides is important for basic spectroscopy [1,2], as well as for applications in wavelength conversion [3], dispersion compensation based on phase conjugation [4], and self-frequency locking in lasers. Recent experimental studies achieved detuning frequencies up to 2 THz and were analyzed by comparison with simple semi-phenomenological models [1,2]. We here extend the experimental detuning frequency to about 3 THz and by comparison with numerical calculations based on density matrix equations (DME) we conclude on the physical nature of the FWM processes. These same DME have been succesfull in explaining sub-picosecond pump-probe dynamics in laser amplifiers [5].

In the experiments, light from two tunable, narrow linewidth, semiconductor lasers, with frequencies f_0 and f_1, is coupled into a buried heterostructure InGaAsP traveling wave amplifier with bulk active region. These pump and probe beams, having comparable power $P_1 = 0.10$ mW and $P_0 = 0.25$ mW, are amplified as they co-propagate along the amplifier and generate conjugate signals at the low frequency side, $f_2 = 2f_0 - f_1$, and high frequency side, $f_3 = 2f_1 - f_0$. The FWM efficiency, measured as a function of the pump-probe detuning, $f_1 - f_0 > 0$, with f_1 maintained close to the gain peak of the amplifier, is shown in Fig. 1(a).

In the modelling, propagation of the four waves is described by Maxwell's equations with induced polarization components calculated from DME. The DME include, in a unified manner, the effects of carrier density pulsations (CDP), carrier heating (CH) due to stimulated emission as well as free carrier absorption, and spectral holeburning (SHB) [5]. The main approximation, and the one which avoids the solution of a complicated many-body problem, is the use of phenomenological relaxation time *constants*; this approach has already been shown to work very well for describing ultrafast temporal dynamics under similar conditions [5].

The numerical results, also shown in Fig. 1(a), provide a good, quantitative, explanation of the experimental observations. Main parameter values are (c: conduction band, v: heavy-hole valence band): Intraband carrier-carrier scattering times $\tau_{1c} = \tau_{1v} = 30$ fs; temperature relaxation times due to carrier-LO phonon scattering $\tau_{hc} = 650$ fs [5], $\tau_{hv} = 200$ fs [5]; ratio of real and imaginary parts of third-order susceptibilities due to changes in carrier density $\alpha_N = 7$ and carrier temperatures $\alpha_{Tc} = \alpha_{Tv} = 5$. The small τ_1 values are attributed to the high injection conditions in the present experiment, i.e., a bias current of 115 mA corresponding to an estimated carrier density of $3.4 \cdot 10^{24}$ m^{-3}. The α_T values are subject to some uncertainty, but generally $\alpha_T \sim \alpha_N$, due to the similar energy dependencies of perturturbations of the carrier distributions due to changes of the Fermi level and the carrier temperature. The corresponding α-parameter value for spectral holeburning extracted from DME is less than 0.1 and not significant.

In Figs. 1(b) and 1(c) we investigate the contributions to FWM from the different physical pro-

cesses. Fig. 1(b), artificially neglecting SHB, already shows qualitative agreement with experiment, but the asymmetry between the high and low-frequency signals is too small in the calculated curves; this is an effect of the relation $\alpha_T \sim \alpha_N$, which minimizes interference effects between the CDP and CH contributions. In contrast, the combination SHB and CDP, Fig. 1(c), shows strong interference effects due to the large difference in α-parameters, that are not experimentally observed. In the combination of all processes, Fig. 1(a), it is mainly the interference effects that introduce an asymmetry between the high and low frequency signals. The bending of the dotted curves for CDP at large frequency detunings, Figs. 1(b) and (c), is due to the finite intraband scattering time, and the asymmetry between the high and low frequency signals is due to the frequency dependence of the gain.

From the material parameters extracted from the FWM data we calculate nonlinear gain suppression factors (at the gain peak) $\epsilon_{CH} = 2.8 \cdot 10^{-24}$ m^3 and $\epsilon_{SHB} = 1.4 \cdot 10^{-24}$ m^3, i.e., the contribution from CH is twice as large as that from SHB. This is in contrast with the results in [2] where SHB was found to be approximately ten times more important than CH; one reason for the discrepancy may be the large detuning from the gain peak (towards the long wavelength side) employed in [2]. More generally, however, we find from the density matrix approach that simple models like those used in [1,2] only are applicable in the sub-THz regime; for larger detunings it is important to take into account the interrelated nature of the scattering processes relaxing the spectral hole, the carrier temperature and the interband polarization.

[1] J. Zhou, N. Park, J. Dawson, K. Vahala, M. Newkirk, and B. Miller, Appl. Phys. Lett., **63**, 1179 (1993).
[2] K. Kikuchi, M. Amano, C.E. Zah, and T.P. Lee., Appl. Phys. Lett., **64**, 548 (1993).
[3] R. Schnabel, W. Pieper, M. Ehrhardt, M. Eiselt, and H.G. Weber, Electron. Lett., **29**, 2047 (1993).
[4] M. C. Tatham, G. Sherlock, and L. D. Westbrook, In Proc. of ECOC'93, paper ThP 12.3 (1993).
[5] J. Mark and J. Mørk, Appl. Phys. Lett., **61**, 2281 (1992).

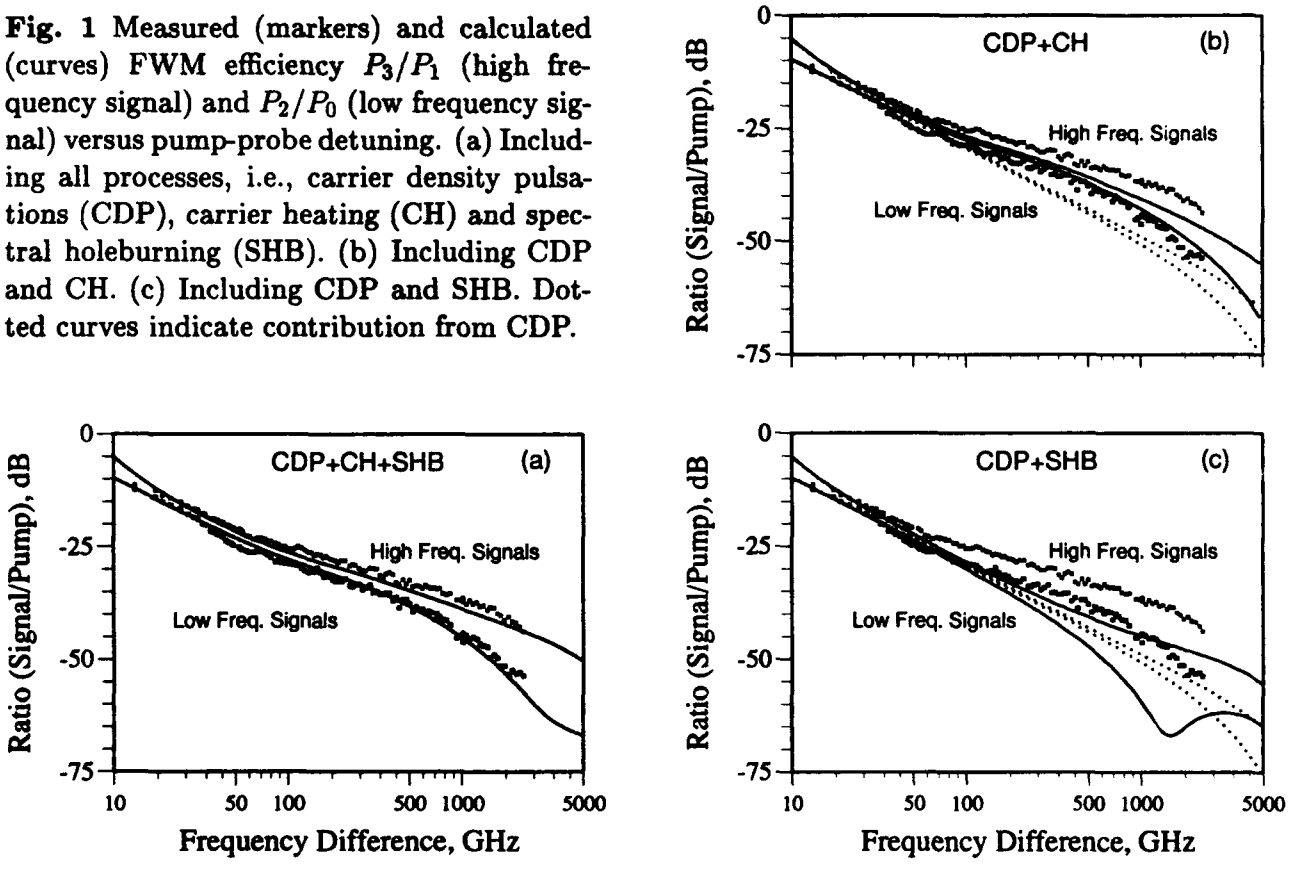

Fig. 1 Measured (markers) and calculated (curves) FWM efficiency P_3/P_1 (high frequency signal) and P_2/P_0 (low frequency signal) versus pump-probe detuning. (a) Including all processes, i.e., carrier density pulsations (CDP), carrier heating (CH) and spectral holeburning (SHB). (b) Including CDP and CH. (c) Including CDP and SHB. Dotted curves indicate contribution from CDP.

11:30am - 11:45am
T2.5

Temperature And Output Power Dependence of Carrier Overflow And Internal Loss In InGaAs/InGaAsP Multiple Quantum Well Lasers

N. Tessler, V. Mikhaelashvili, R. Nagar, G. Eisenstein
Electrical Engineering Dept. TECHNION Haifa 32000 ISRAEL
A. G. Dentai, C. H. Joyner, S. Chandrasekhar
AT&T Bell Laboratories Crawford Hill Lab, Holmdel New Jersey 07733
Tel. +972 4 294 694 FAX +972 4 323 041

ABSTRACT

We demonstrate temperature and output power dependence of internal loss in multiple quantum well lasers resulting from carrier overflow effects.

SUMMARY

The implication of carrier occupation in waveguide states of quantum well (QW) lasers (carrier overflow) to differential gain, internal efficiency, modulation bandwidth and the structure dependent gain nonlinearity coefficient has received significant attention in the past few years [1]. A related topic, the carrier overflow dependent internal loss, has received surprisingly little attention [2]. This paper demonstrates that this loss mechanism is both temperature and output power dependent so that in addition to reducing the differential gain, it enhances the gain nonlinearity, increases the temperature dependence of laser parameters and imposes a limit on output power.

The effects we consider are modeled by means of a three level model [3]whose parameters are corrected using a more detailed model [4]. We calculate the population of both confined (2D) and unconfined (3D) carriers as a function of temperature and output power. The main contribution to internal loss is associated with inter-valance-band absorption [5] by both confined and unconfined holes. The energy band diagram of the laser structure we tested is shown in the insert of Fig. 1a. The calculated dependencies of the internal loss on temperature and on output power are shown in Fig. 1a and Fig. 1b, respectively. Figure 1a, which is calculated at threshold, shows that the loss due to 3D carriers increases rapidly as the temperature rises and occupation of 3D states becomes larger. The loss increase due to 2D carriers is more moderate. Figure 1b shows the calculated loss dependence of 2D and 3D carriers on photon density for two temperatures, 20 °C and 50 °C. Again, we see the larger effect due to 3D carriers, particularly at the higher temperature. From the slope of the power dependence of the 3D holes mediated internal loss we deduce the structure dependent enhancement of the nonlinear gain as : $\varepsilon = (\delta\alpha_{3D} / \delta S)g_{th}^{-1}$ which takes the values of 1.2×10^{-18} cm^{-3} and 2.8×10^{-18} cm^{-3}, for 20 °C and 50 °C, respectively, a non negligible fraction of documented values for the nonlinear gain coefficient ($\sim 10^{-17}$ cm^{-3}).

Experimental verification of the model predictions were obtained by a systematic study of the temperature dependent internal loss. All tested lasers were cleaved from the same bar into different lengths and mounted on copper studs. The stud temperature was controlled to within 0.1°C and the lasers were biased by 0.5μsec long pulses at a 0.5% duty cycle so as to ensure that the junction temperature equals the heat sink temperature. Measurements of the inverse of

the differential efficiency versus the cavity length are shown for several temperatures in Fig. 2. The straight lines are the best linear fits for each temperature.

Using $\eta_{ext}^{-1} = \eta_{int}^{-1}\{1 - \alpha L / \ln R\}$, the intercept with the y axis yields the inverse of the internal efficiency while the slope is a measure of the internal loss. Figure 3 shows the temperature dependent internal loss, as deduced from Fig. 2, along with the prediction of the model for the 3D carriers (see Fig. 1a). Note the good agreement between the experiment and the calculation. The 2D carriers contribute little if any loss due to strain in the quantum wells. Further details of the influence on this loss mechanism of the transport time and barrier height will be given at the presentation.

REFERENCES

[1] R. Nagarajan et. al., IEEE JQE (1992) 1990
[2] K. Tanaka et. al., IEEE PTL 5 (1993) 602
[3] N. Tessler R. Nagar and G. Eisenstein, IEEE JQE 28 (1992) 2242
[4] N. Tessler and G. Eisenstein, IEEE JQE 29 (1993) 1586
[5] H. C. Casey and P. L. Carter, Appl. Phys. Lett. 44 (1984) 82

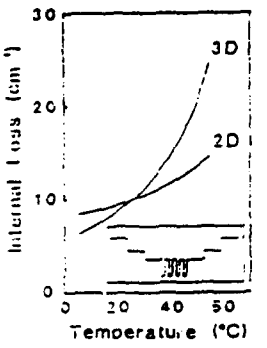

Fig. 1a - Calculated temperature dependent of loss of 2D and 3d carriers

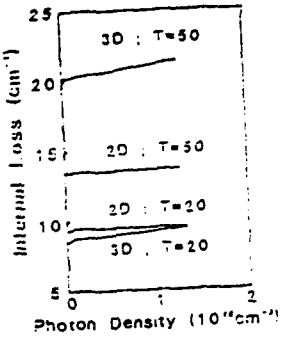

Fig. 1b - Calculated photon density loss 2D and 3d carriers at 20°C, and 50°C

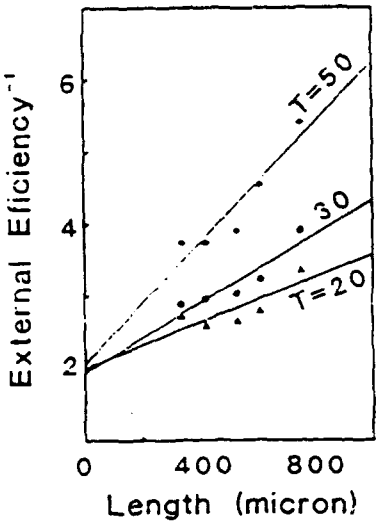

Fig. 2 - Measured length dependence of the inverse external efficiency

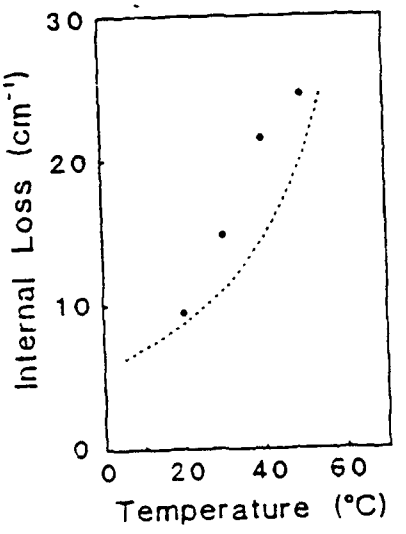

Fig.3 Measured temperature dependent loss for various temperatures

11:45am - 12:00noon
T2.6

The effect of dynamic spatial hole burning on the second and third order intermodulation distortion in DFB lasers

Masahiro Kito, Hisanao Sato, Nobuyuki Otsuka, Naoki Takenaka, Masato Ishino and Yasushi Matsui

Semiconductor Research Center
Matsushita Electric Industrial Co., Ltd.
3-1-1 Yagumonakamachi, Moriguchi, Osaka 570, Japan
Tel: +81-6-906-4921, Fax: +81-6-906-8100

Abstract: Analysis of second and third order intermodulation distortion characteristics is, for the first time, performed including dynamic longitudinal spatial hole burning effect in DFB lasers.

Introduction: Low distortion DFB lasers are widely used in Sub-Carrier Multiplexed (SCM) scheme, such as AM-FDM transmission for CATV. We have developed 1.3μm strained MQW-DFB lasers which can transmit 100 channel TV signals in AM-FDM scheme [1]. This result has been realized due to their low distortion characteristics over wide band frequency range resulted from their high relaxation oscillation frequency (f_r) characteristics [2]. However, in order to explain various distortion characteristics in actual devices, it is necessary to take account of the effect of longitudinal spatial hole burning (LSHB). The analysis of intermodulation (IM) distortion caused by dynamic LSHB has not yet done, though the static approximation using L-I characteristics has been reported [3]. In this paper, we propose a new theory of dynamic LSHB and discuss experimental results of IM distortion.

Theory: An investigated DFB laser model is shown in Fig.1. We assume that optical fields instantaneously follow the carrier distribution and, therefore, the field distributions are derived from the static coupled-mode equations. The carrier distribution obeys the local rate equation, while the field intensity is determined from the rate equations for average photon density. From this assumption, the power, P(L,t), from the output facet (z=L) is represented by the product of the average photon density, S(t), and the optical field at z=L as follows:

$$P(L,t) = v_g (1-R_L)(1+R_L)^{-1} S(t)\Psi(L,t)\left(L^{-1}\int_0^L \Psi(z,t)dz\right)^{-1}$$

$$= P_0(L) + P_1(L,t) + P_2(L,t) + P_3(L,t)$$

$$\Psi(z,t) = \left[|E_A(z,t)|^2 + |E_B(z,t)|^2\right]\left[|E_B(0,t)|^2\right]^{-1}$$

where, v_g is the group velocity, $E_A(z,t)$ and $E_B(z,t)$ are the amplitudes of forward and backward propagation waves, respectively, R_L is the reflectivity at the output facet and P_i represents i -order value of the output power. Second IM distortion (IM_2) and third IM distortion (IM_3) are given by $20\log|P_2(L,t)/P_1(L,t)|$ and $20\log|P_3(L,t)/P_1(L,t)|$, respectively.

Theoretical and experimental results: Figure 2 and 3 show calculated curves of IM_2 and IM_3 as a function of distortion frequency (f_1+f_2 and $2f_1-f_2$), respectively under the modulation depth of 20% and the injection current of 30mA. In the calculation the following material and structure parameters are assumed: differential gain; $6.0\times10^{-12}m^3/s$, coefficient for refractive index change; $-2.0\times10^{-26}m^3$, confinement factor; 0.07, total well thickness; 60nm, gain-suppression coefficient; $3.0\times10^{23}m^{-3}$, internal loss; $20cm^{-1}$, cavity length (L); 200μm, normalized coupling coefficient (κL) ; 0.6,1.2, phase of facets (Ω_0 and Ω_L); π/2 and π/2. In Fig.2 and Fig.3, IM_2 and IM_3 values in relatively low frequency range are steeply degraded with increase in κL as compared with the calculated curve without LSHB, and in high frequency range near f_r (~10GHz) are limited by relaxation oscillation independently of κL. One of the notable points of this analysis is that IM_3 takes on smaller values at certain frequency ranges than those calculated without LSHB.

Figure 4 shows calculated curves and experimental data (plots) of IM_3 as a function of relaxation oscillation frequency with the distortion frequency ($f_d=2f_1-f_2$) as a parameter. The f_r values were varied by the injection current. In the experiment, a 1.3μm MQW-DFB laser (10 wells, L=200μm) was used. The distortion frequencies were 0.95GHz, 1.5GHz and 1.9GHz, which are used in the SCM transmission system for mobile communication. In the calculation, κL value was 0.6 and other parameters were the same as used in Fig.2 and Fig.3. The experimental data decrease with f_r and become smaller than those of the calculated curves without LSHB. The calculated curves with LSHB well explain the experimental results. It indicates that very low distortion can be realized even in frequency range of several GHz.

Conclusions: We have clarified, for the first time, that the effect of dynamic spatial hole burning on the second and third order intermodulation distortion. We have theoretically shown that the IM_3 values can be smaller than the calculated curve without LSHB, which is confirmed with the experiments.

References:

[1] M. Ishino et al., Technical Digest of IEDM '93 (1993).
[2] M. Kito et al., Electron. Lett., 28, p.891 (1992).
[3] T. Okuda et al., IEEE Photon. Technol. Lett., 6, p.27 (1994).

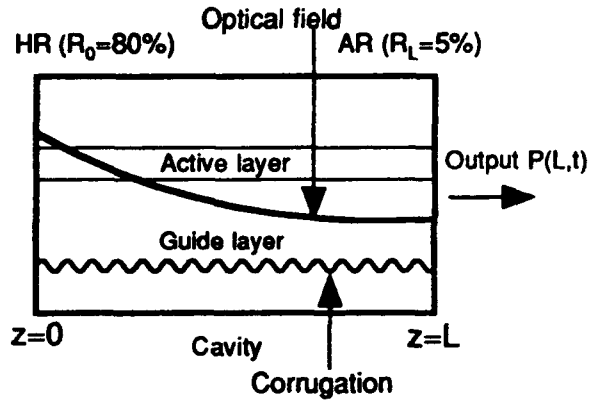

Fig. 1 An investigated DFB laser model.

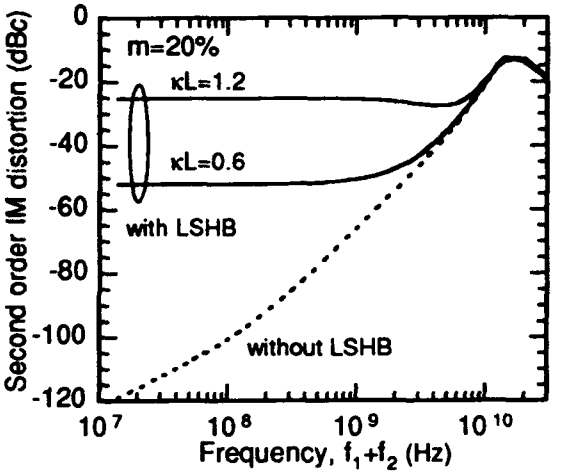

Fig. 2 The calculated curves of second order intermodulation distortion as a function of distortion frequency.

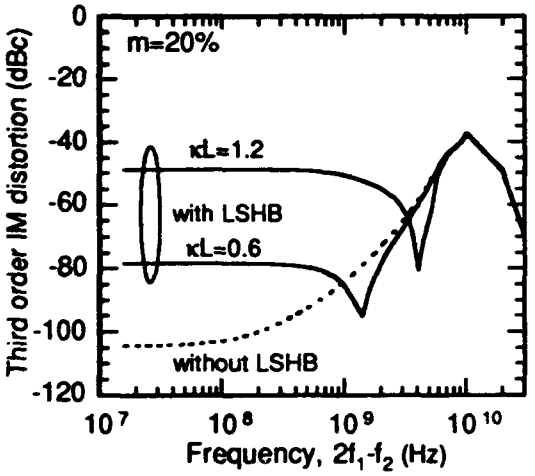

Fig. 3 The calculated curves of third order intermodulation distortion as a function of distortion frequency.

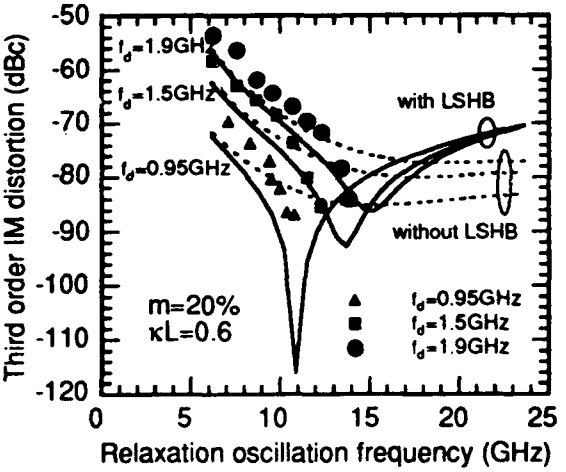

Fig. 4 The calculated curves and experimental data of third order intermodulation distortion as a function of relaxation oscillation frequency with the distortion frequency as a parameter.

Quantum Cascade Laser: A Unipolar Intersubband Semiconductor Laser

F. Capasso, J. Faist, D. L. Sivco, C. Sirtori,
A. L. Hutchinson, S. N. G. Chu and A. Y. Cho

AT&T Bell Laboratories
600 Mountain Ave.,Murray Hill,NJ 07974

ABSTRACT

A new semiconductor injection laser (Quantum Cascade Laser) which differs in a fundamental way from diode lasers has been demonstrated. It relies on only one type of carrier (it is a unipolar semiconductor laser), and on electronic transitions between conduction band energy levels of quantum wells.

Intersubband lasers were originally proposed 25 years ago,[1] but despite considerable effort this is the first structure to achieve laser action. The present device operates at a wavelength of 4.26 microns, but since the wavelength is entirely determined by quantum confinement, it can be tailored from the mid-infrared to the submillimeter region using the same heterostructure material. Electrons streaming down a potential staircase sequentially emit photons at the steps. The latter consist of coupled quantum wells in which population inversion between discrete conduction band excited states is achieved in a 4-level atomic like laser scheme using tunneling injection (Fig. 1). The AlInAs/GaInAs structure grown by MBE comprises 25 stages, each consisting of a graded gap n-type injection layer and a three coupled-well active region, cladded by waveguiding layers. The undoped active region includes 0.8 nm and 3.5 nm thick GaInAs wells separated by 3.5 nm AlInAs barriers. The reduced spatial overlap between the states of the laser transition and the strong tunnel-coupling to a nearby 2.8 nm GaInAs well ensure population inversion. The samples were processed into mesa etched ridge waveguides and the laser facets were obtained by cleaving. Powers $\simeq$ 20 mW in pulsed operation (20 ns pulses with a 10^{-3} duty cycle) have been obtained at 80 K. Operating temperatures up to 125 K have been achieved with 5 mW of power (Fig. 2). A dramatic narrowing of the emission spectrum provides direct evidence of laser action (Fig. 3). An outstanding feature of this laser is that the gain is much less sensitive to temperature than conventional semiconductor lasers. A preliminary study of the temperature dependence of the threshold indicates a T_0 = 110 K. In addition, the intrinsic linewidth of these lasers in cw single mode operation is expected to be Schawlow-Townes limited, similar to atomic lasers, without the linewidth enhancement factor typical of diode lasers. Fig. 4 shows the high resolution spectrum at two different currents. Well defined longitudinal modes are observed. The mode spacing 2.175 cm^{-1} is in good agreement with the calculated one ($\frac{1}{2nL}$ = 2.13 cm^{-1} with n = 3.26). The linewidth of the dominant mode is presently limited by heating effects and mode hopping during the pulse. At higher currents additional transverse mode emerge.

For a preliminary account of the operation of this laser at 10 K see Ref. 2.

1. R. F. Kazarinov and R. A. Suris, Sov. Phys. Semicond. *5*, 207 (1991).
2. J. Faist, F. Capasso, D. L. Sivco, C. Sirtori, A. L. Hutchinson and A. Y. Cho, Science, April 22, 1994.

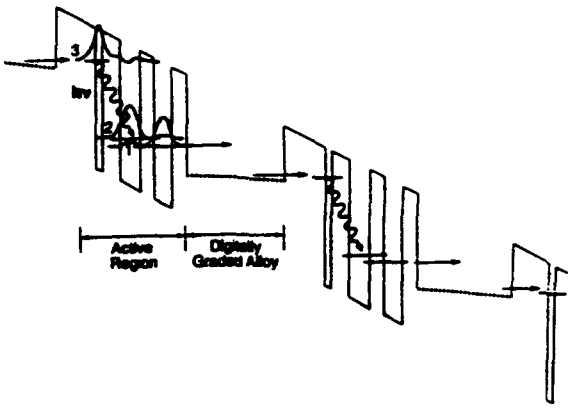

FIGURE 1
Energy diagram of the QC laser showing the laser transition (wavy arrow).

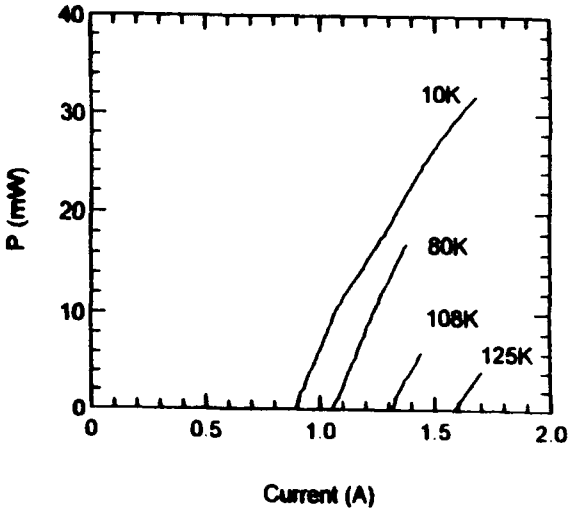

FIGURE 2
Optical power vs. current for a 720 μm cavity length laser at various temperatures. The threshold at 80 K is 14 kA/cm^2.

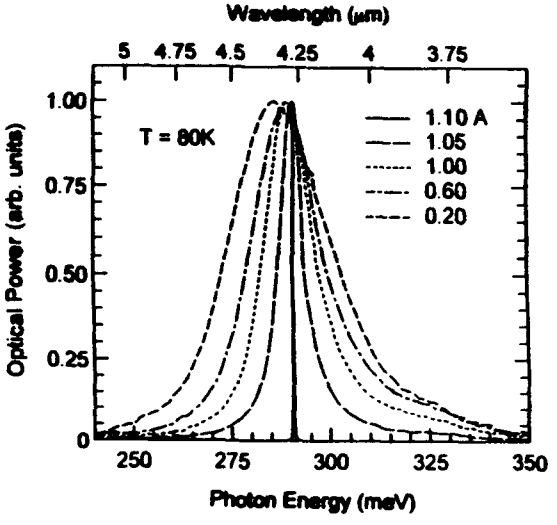

FIGURE 3
Normalized emission spectrum at various currents.

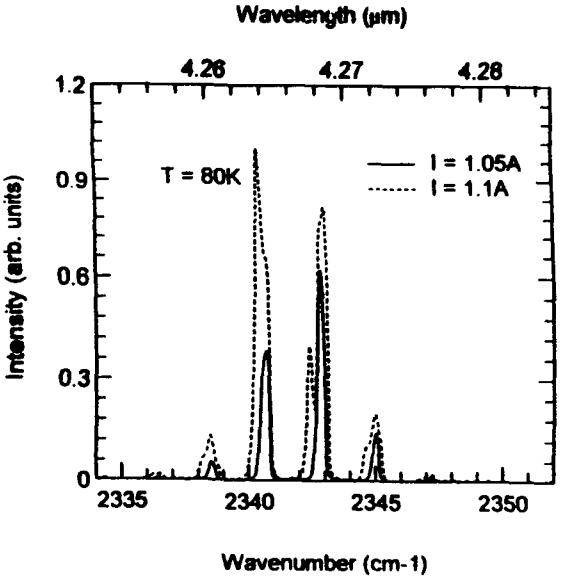

FIGURE 4
High resolution spectrum for two different currents (cavity length 720 μm).

1:45pm - 2:00pm
T3.2

Room Temperature CW Operation of GaInP/AlGaInP Multiple Quantum Wire Visible Lasers (MQWR-LD)

Junji YOSHIDA and Katsumi KISHINO
Department of Electrical and Electronics Engineering
Sophia University
7-1 Kioi-cho, Chiyoda-ku, Tokyo 102, Japan
Tel. +81-3-3238-3323 Fax. +81-3-3238-3321

Abstract: The first successful room temperature (r.t.) cw operation of GaInP/AlGaInP multiple quantum wire visible lasers was obtained, with the maximum cw temperature of 70 °C. For uncoated facet condition at 20 °C, the threshold current density (Jth) was 294A/cm^2, the output power 50 mW/facet, and the differential quantum efficiency 37%. The low pulse Jth value of 277A/cm^2 was obtained.

Summary:

Strained quantum wire lasers (SQWR-LD) are theoretically superior to strained quantum film lasers (SQWF-LD) in terms of very low threshold current density [1], high device efficiency, and high To values [2]. We have already reported getting a low threshold pulsed operation of GaInP/AlGaInP SQWR-LDs with 345A/cm ^{2} [3] .

In this talk, the first room temperature cw operation and lowering pulse Jth values of the SQWR-LDs are described. The investigated lasers are schematically shown in Fig.1, in which quantum wire structures were fabricated during crystal growth through in-situ process, here using the strain induced lateral-layer ordering scheme [4]. In the lasers, quantum wire behaviors, such as the strong Jth value anisotropy as a factor of 7 and the lasing mode difference in TE and TM between [011] and [01$\bar{1}$] crystal direction were observed .

Figure 2 shows the inverse cavity length dependencies of pulse threshold current density given in square root, in which circle points indicate data for GaInP/AlGaInP MQWR-LDs (Q-Wire), while the dashed line that for GaInP/AlGaInP compressively strained quantum film (CS-Q-Film) lasers. As easily noted here, a slope of Q-Wire was smaller than that of CS-Q-Film, probably reflecting higher differential gain of Q-Wire compared with that of CS-Q-Film. The lowest Jth value of MQWR-LDs was 277A/cm^2 at cavity length of 794μm .

The r.t. cw operation of GaInP/AlGaInP MQWR-LDs was achieved. Figure 3 shows the cw light output versus current characteristics and the lasing spectrum observed at 20 °C for the 50μm striped laser with the cavity length of 569μm. The Jth value was 294A/cm^2 and the lasing wavelength was 747nm. Under uncoated facet condition, the light output of 50mW/facet was obtained with the differential quantum efficiency of 37% . The temperature dependency of cw light output versus current characteristics is shown in Fig. 4 . The maximum cw temperature was 70 °C .

References

[1] S.Ueno, Y.Miyake, and M.Asada, Jpn. J. Appl. Phys. 31,286 (1992)
[2] Y.Arakawa and H.Sakaki, Appl.Phys.Lett., 40, 939, June. 1982
[3] J.Yoshida and K.Kishino, CThR6, CLEO'94, May. 1994
[4] K.Y.Cheng, K.C.Hsieh, and J.N.Baillargeon, Appl.Phys.Lett., 60, 2892, June. 1992

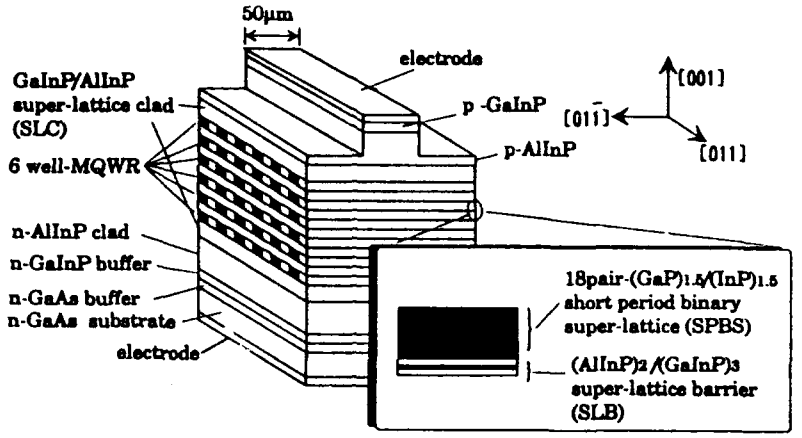

Fig.1 Schematic Structure of a GaInP/AlGaInP MQWR laser

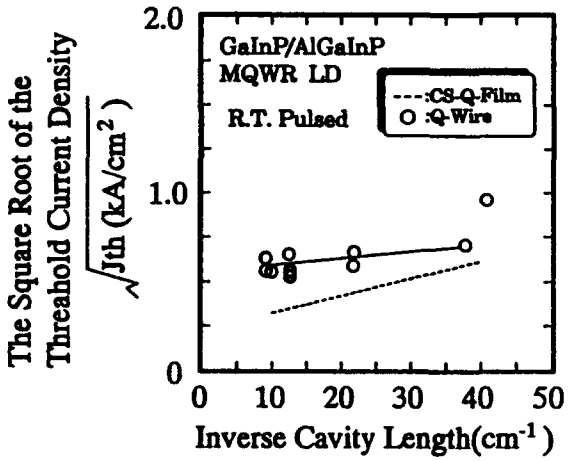

Fig.2 Inverse Cavity Length Dependence of Square Root of the Threshold Current Density

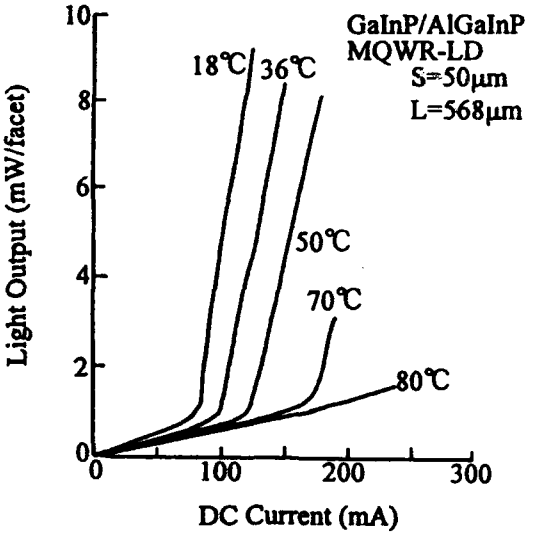

Fig.4 Temperature Dependency of CW Light-current Characteristics

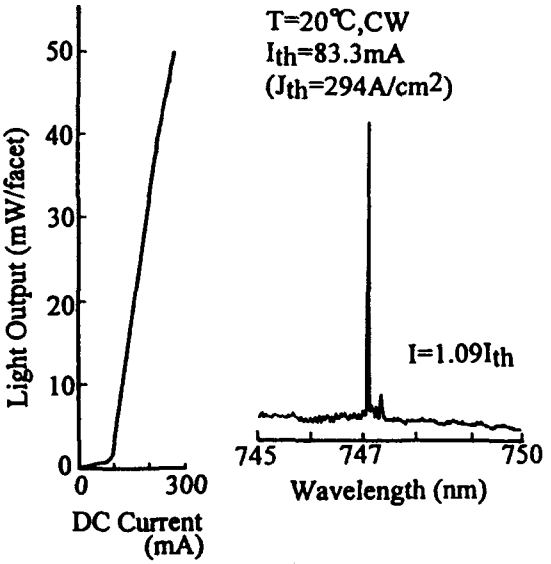

Fig.3 CW Light-current Characteristics and Lasing Spectra

2:00pm - 2:15pm

T3.3 First Demonstration of Extremely Low-Threshold AlGaAs/GaAs Quantum Wire-Like Lasers Grown on V-Grooved GaAs/Si Substrates

Y. Hasegawa [a], T. Egawa [b], T. Jimbo [b] and M. Umeno [a, b]
[a] Department of Electrical and Computer Engineering,
[b] Research Center for Micro-Structure Devices,
Nagoya Institute of Technology, Gokiso-cho, Showa-ku, Nagoya 466, Japan
Fax: +81-52-732-2761

Abstract: We report first demonstration of extremely low-threshold AlGaAs/GaAs quantum wire-like lasers grown on V-grooved GaAs/Si substrates. Threshold current as low as 9.8 mA and 16 mA were realized under room-temperature pulsed and continuous-wave conditions, respectively.

Low-threshold and reliable GaAs-based lasers grown on Si substrates are key devices in high density applications such as optical interconnects in future optoelectronic integrated circuits (OEIC's). However, a high dislocation density ($>10^6$ cm^{-2}) and a large residual thermal stress (~10^9 dyn/cm^2), which are introduced by the ~4 % lattice mismatch and the ~250 % difference in the thermal expansion coefficients between GaAs and Si, cause the rapid degradation of GaAs-based lasers on Si [1]. On the other hand, very low-threshold AlGaAs/GaAs lasers with quantum wire active regions have been recently demonstrated using the growth technique on nonplanar GaAs substrates by metalorganic chemical vapor deposition (MOCVD) [2, 3].

In this study, using this method, we demonstrate an extremely low-threshold AlGaAs/GaAs quantum wire-like laser grown on a V-grooved GaAs/Si substrate by MOCVD for the first time. This quantum wire-like laser is a completely different approach for the realization of reliable GaAs-based lasers on Si. Because this laser has much attractive advantages such as low-threshold operation and low-dislocation number which are caused by the reduction of the active regions. In our another experiment, we found that the growth velocity of <100> dark-line defects (DLD's) increases drastically with increasing the injected current (the growth velocity was estimated to be ~50 μm/h at 50 mA). This indicates that low-threshold operation contributes to the improvement in the reliability of GaAs-based lasers on Si.

Figure 1 shows the scanning electron microscope (SEM) micrograph of the overall AlGaAs/GaAs quantum wire-like laser grown on a V-grooved GaAs/Si substrate. The active layers in this laser consist of three 3-nm-thick GaAs quantum wells separated by 5.5-nm-thick $Al_{0.3}Ga_{0.7}As$ barrier layers, and 60-nm-thick $Al_{0.3}Ga_{0.7}As$ lower and upper optical confining layers. It can be seen that the active layers are sharply formed by defining along the V-groove with (111)A side-walls. Figure 2 shows the high-resolution SEM micrograph of the vertically-stacked GaAs quantum wires near the center of the V-groove in Fig. 1. The crescent-shaped quantum wires are 11-15 nm thick at its center and 83-127 nm wide. This very narrow width of the quantum wire results in the reduction of the dislocation number in the active regions. For example, the dislocation number of this quantum wire laser is approximately 1/100 of that of the conventional quantum well lasers on Si with 10-μm-wide stripe contact windows. The light versus current characteristic and lasing spectrum of this laser under the room-temperature pulsed condition (0.2 μs pulses at 5 kHz repetition rate) are shown in Fig. 3. For the 123-μm-long laser, the threshold current (I_{th}) and external differential quantum efficiency were 9.8 mA and 21 %, respectively. The lasing wavelength was 859 nm at 2.0 X I_{th}. In addition, the laser beam was mainly polarized parallel to the (100) substrate plane (TE-like mode). For the room-temperature continuous-wave operation, the distribution of I_{th} of this laser was 16-20 mA for the 150-380 μm cavity length. These remarkable improvements in I_{th} are due to the reduction of the volume of GaAs active regions by use of the quantum wire-like structure.

In summary, an extremely low-threshold (9.8 mA) AlGaAs/GaAs quantum wire-like

laser grown on a V-grooved GaAs/Si substrate was demonstrated for the first time. This technique is promising for the fabrication of low-threshold and reliable GaAs-based lasers on Si.

References:

[1] T. Egawa, Y. Hasegawa, T. Jimbo and M. Umeno, Jpn. J. Appl. Phys., **31**, 791 (1992).

[2] E. Kapon, D. M. Hwang and R. Bhat, Phys. Rev. Lett., **63**, 430 (1989).

[3] S. Simhony, E. Kapon, E. Colas, R. Bhat, N. G. Stoffel and D. M. Hwang, IEEE Photon. Technol. Lett., **2**, 305 (1990).

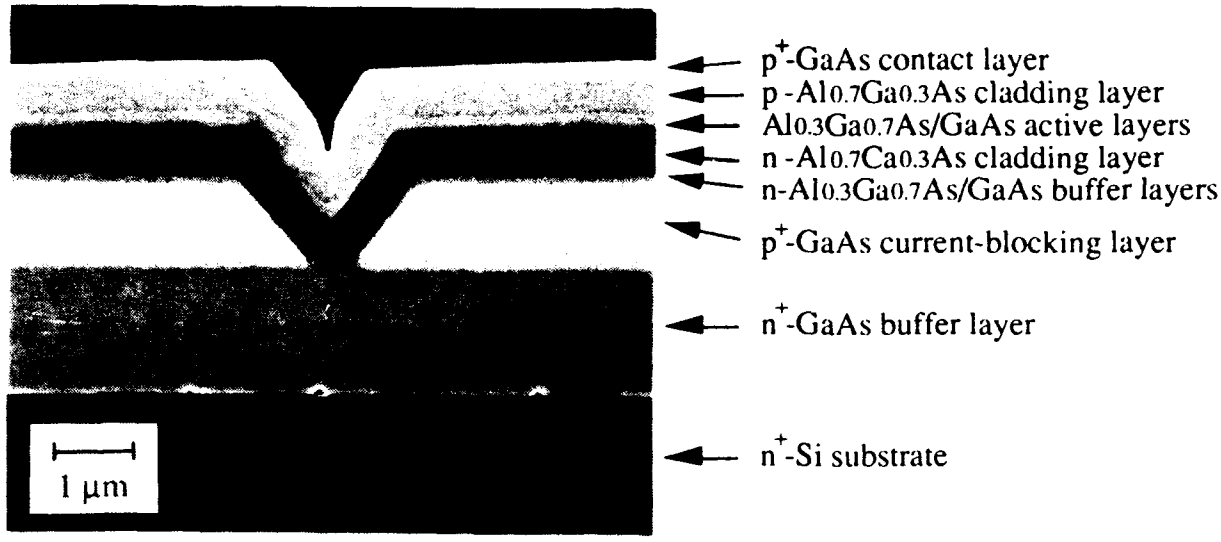

Fig. 1. SEM micrograph of the overall quantum wire-like laser on V-grooved GaAs/Si substrate.

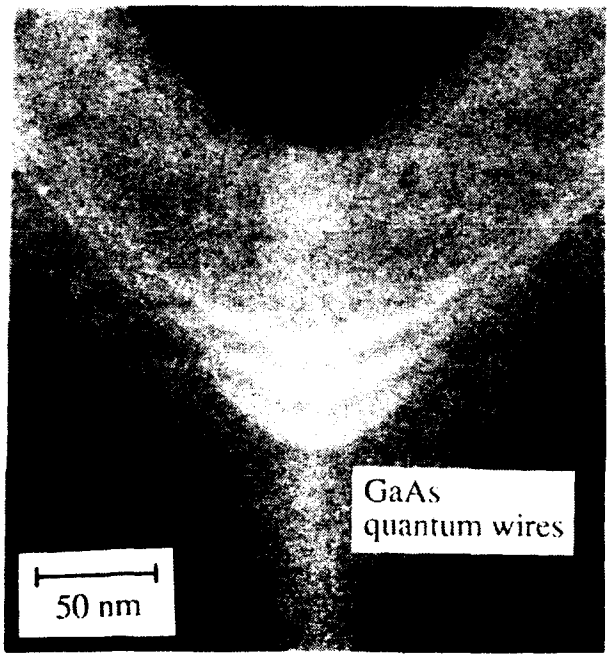

Fig. 2. SEM micrograph of the vertically-stacked GaAs quantum wires.

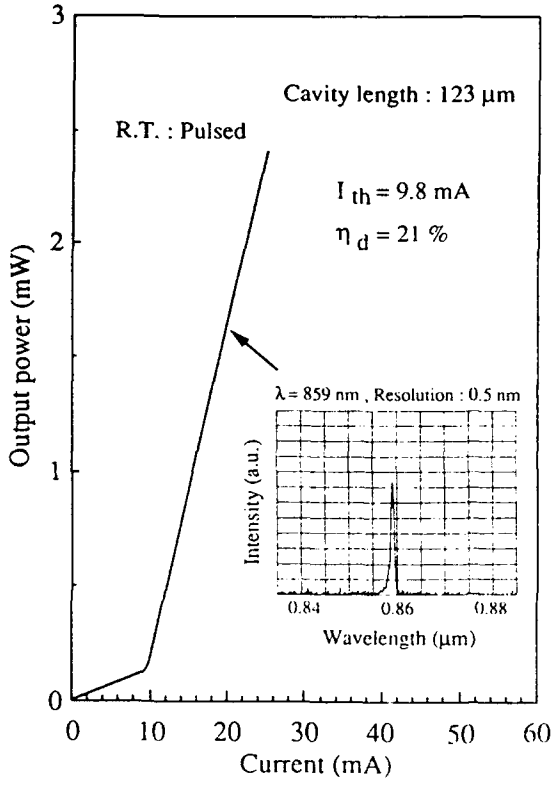

Fig. 3. Light versus current characteristic and lasing spectrum under the room-temperature pulsed condition.

2:15pm - 2:30pm
T3.4

Threshold Current and Modulation Dynamics in Quantum Dot Lasers

H. Nakayama and Y. Arakawa

Institute of Industrial Science, University of Tokyo
7-22-1 Roppongi, Minato-ku, Tokyo 106, Japan

Abstract: Threshold current and modulation dynamics are theoretically discussed taking into account the detailed behavior of carrier dynamics related to the bottleneck problem. The results indicate that extremely low threshold current and high modulation frequency devices can be realized if the quantum dot structure is correctly designed.

It has been predicted that the use of quantum dots leads to substantial improvement of lasing characteristics in semiconductor lasers[1,2]. Against this optimistic prediction, however, an important problem was pointed out: the phonon bottleneck causes degradation of luminescence and dynamic properties of carriers[3,4]. This bottleneck occurs when the energy difference ΔE between the energy level of the quantum dots and that of the barrier region is larger than the energy of LA-phonon and LO-phonon. Without phonon assisted coupling, carrier injection is inhibited.

In this paper, we theoretically discuss threshold current and dynamic properties of the quantum dot lasers considering this bottleneck problem. The effect of the quantum dot structure on the carrier capture time, dephasing time of the dipole moment, gain and differential gain are carefully examined. The results demonstrate that the bottleneck can be almost eliminated if the laser structure is appropriately designed. It is shown that quantum dot lasers can achieve a sub-μA threshold current and a modulation bandwidth wider than 100GHz.

To eliminate the bottleneck, we propose two structures shown in Fig.1 (a) and (b). In Fig. 1(a), the quantum dots are coupled to each other so that carriers relax from the excited mini-band state to the ground level of the quantum dots by LO-phonon emission. On the other hand, in the second structure of Fig. 1(b), the ground energy level of the quantum dots is sufficiently close to potential barrier in order to realize direct carrier relaxation from the barrier to the ground level of the quantum dots. Here we focus on the structure of Fig. 1(b). Figure 2 shows a simple illustration for the quantum dot lasers with these structures. Carrier relaxation from the upper levels to the ground state of the quantum dots is calculated. Figure 3 shows the capture rate into the quantum dots plotted as a function of ΔE. In this calculation, the energy dispersion of the LO-phonon and the wavefunctions of the initial and final states are considered.

We calculated the threshold current of the quantum dot lasers. In this calculation, we assumed the carrier escape time from the ground state is determined by absorption of the LO-phonon and is equal to the dephasing time of the optical dipole moment. We also assumed a Lorentzian-type lineshape function of the gain and ignored inhomogeneous broadening. The laser structure is a vertical cavity with mirror reflectivity of 0.99. Rate equations are solved in the system where the energy level inside the quantum dot and mini-band levels in the barrier region are formed as indicated in Fig.4. Figure 5 shows the threshold current and the dephasing time as a function of the size of the quantum dots. The result shows that sub-μA threshold current can be obtained if the size of the quantum dots are appropriately chosen. The total number of the quantum dots is optimized so that threshold current is the minimum.

Figure 6 shows the calculated modulation bandwidth of the quantum dot lasers as a function of photon density for different mirror reflectivity. The results show that modulation band width as wide as 100GHz can be achieved. The nonlinear gain effect has also been calculated, although this effect is not included in the figure. Note that the discussion here is to clarify the intrinsic effects of carrier relaxation, so carrier diffusion is neglected.

In conclusion, we discussed threshold current and modulation bandwidth in quantum dot lasers clarifying detailed behavior of carrier dynamics and dephasing time. The results indicate that the carrier relaxation process due to electron-phonon interactions is not a bottleneck if the active region including quantum dot structures are correctly designed.

References

[1] Y. Arakawa and H. Sakaki, Appl. Phys. Lett., **40**, 939 (1982)

[2] Y. Arakawa, K. Vahala, and A. Yariv, Appl. Phys. Lett., **45**, 950 (1984)

[3] H. Benisty, C. M. Sotomayor-Torrès and C. Weisbuch, Phys. Rev., **B44**, 10945 (1991)

[4] P. D. Wang, C. M. Sotomayor-Torrès, H. Benisty, C. Weisbuch, S. P. Beaumont, Appl. Phys. Lett., **61**, 946 (1992)

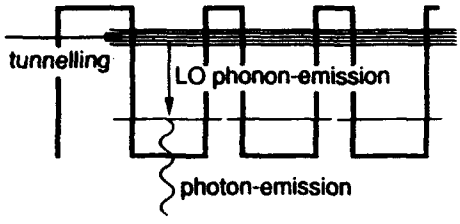

(a) coupled quantum dots

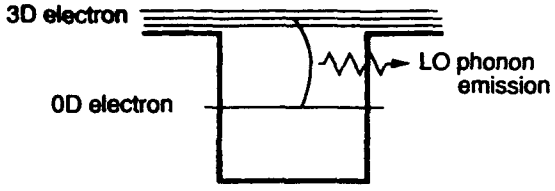

(b) direct injection

Fig.1:Quantum dot structures to eliminate the bottleneck

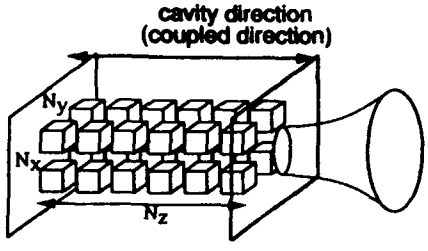

Fig.2:Scematic illustration of quantum dot lasers

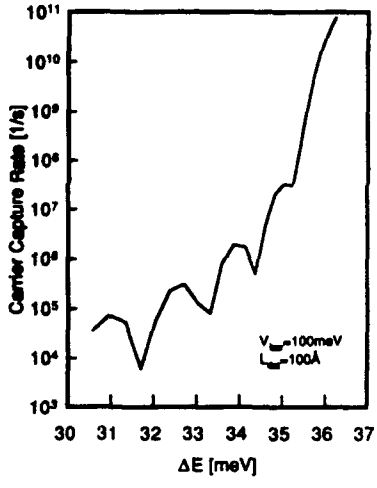

Fig.3:Carrier capture rate due to LO-phonon emission

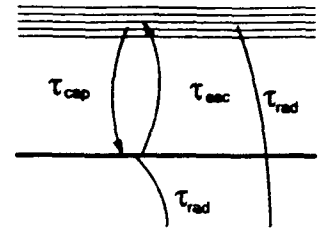

Fig.4:Energy levels and transition and relaxation rates

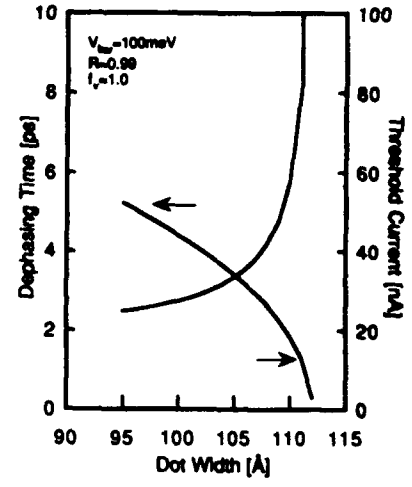

Fig.5:Threshold current and dephasing time as a function of the size of quantum dots

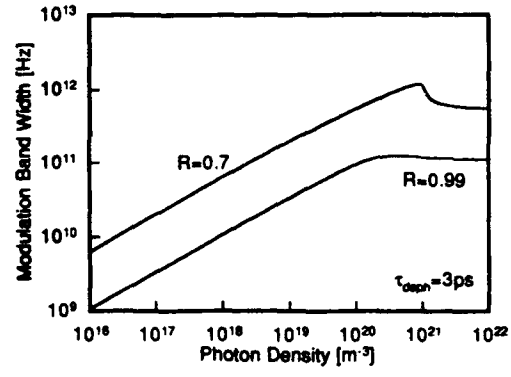

Fig.6:Modulation bandwidth as a function of photon density for two diffrent mirror reflectivity

2:30pm - 2:45pm
T3.5

Limitations to Controlling Spontaneous Emission in Microcavities with Distributed Mirrors

Rajeev J. Ram, Dubravko I. Babić, Robert A. York and John E. Bowers
Dept. of Electrical & Computer Engineering, University of California, Santa Barbara 93106

Limitations introduced by diffraction penetration depth and mirror pass band on controlling spontaneous emission in planar and post microcavities are investigated. Analytic expressions for the emission rate and coupling factor are presented and verified by exact numerical calculations as well as millimeter wave experiments.

The primary limitations to controlling spontaneous emission for planar and post semiconductor microcavities are the broad emission linewidth, the diffraction in the DBR and the finite mirror band stop. While the effects of broad emission linewidth have been discussed in the literature [1,2], the influence of diffraction and finite band stop have not been treated explicitly. Recently, an equivalent hard mirror construction was used to study modal reflectivity in surface emitting lasers. The diffraction equivalent distance (L_D) characterizes the modal diffraction and can be specified analytically [3,4]. The diffraction penetration depths in the two mirrors add to the physical cavity length resulting in a larger effective resonator length (Fig. 1).

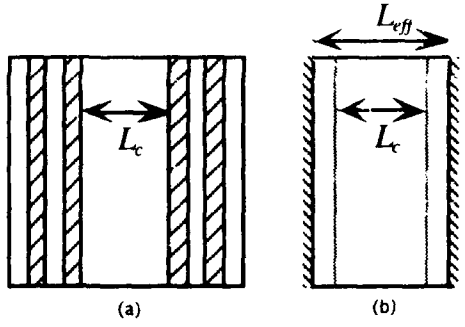

Fig.1 (a) A symmetric DBR resonator with (b) its equivalent hard mirror resonator.

In small resonators the dipole radiation interferes strongly with the time-retarded reflections. For this reason, finite-Q microcavity devices typically consist of λ or $\lambda/2$ cavities. However, penetration of radiation into the DBRs increases the effective resonator length. Fig. 2 shows the normalized emission rates for a dipole adjacent to a single DBR where the dipole is oriented parallel to the plane of the mirror. We see that as L_D increases, the achievable inhibition or enhancement decreases significantly. We also see that different material systems have significantly different potential for observing microcavity effects. A physical cavity length of λ gives an effective cavity length of more than 3λ for GaAs/AlAs DBRs and almost 6λ for InGaAsP/InP DBRs! Diffraction within the DBR is an extremely important limit to realizing microcavity effects in most practical semiconductor materials.

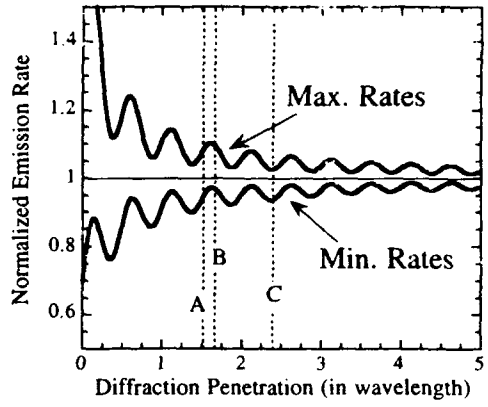

Fig. 2 The near-maximum and near-minimum emission rates for a dipole adjacent to a DBR. The dashed lines represent various mirror systems in use today. A) AlAs/GaAs at 980 nm, B) SiO_2/SiN_4 at 1300 nm C) InGaAsP/InP at 1550 nm.

In order to test the validity of the penetration depth concept for treating spontaneous emission, millimeter wave experiments were performed. The millimeter wave DBR consisted of 5.5 periods of air and Rexolite 1422 (a nearly lossless dielectric with an

index of refraction of 1.56). The Bragg wavelength for this DBR was 8.08 cm (3.71 GHz). The peak reflectivity was 0.9848 (assuming no losses) and $L_D = 2.343$cm. The radiation resistance was compared to the results of the induced EMF method [5] using a two element array (the physical dipole and its image) modeled using the equivalent hard mirror. We see that, for a separation greater than a quarter wavelength, the diffraction penetration depth describes the modified dipole radiation. So even with an infinitesimal linewidth the achievable alteration of spontaneous emission in a DBR microcavity is limited.

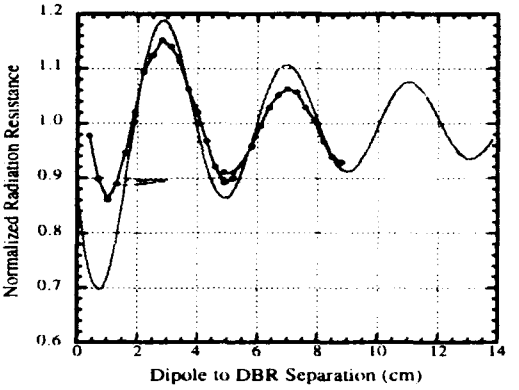

Fig. 3 The experimental versus theoretical readiation resistance of a dipole antenna in front of a DBR versus the dipole-to DBR distance.

In addition, we observe that since the DBR angular pass band represents a region of lowered reflectivity, the spontaneous emission is not significantly altered from the free space value. Let us assume that the DBR has a reflectivity given by the equivalent hard mirror within the band stop and by *zero* reflectivity within the pass band. In order to test the applicability of this approximate boundary, we compare how the DBR and approximate mirror modify the power carried in various plane wave components as a function of the angle. The results for a symmetric AlAs resonator embedded in GaAs utilizing two 17-period GaAs/AlAs DBRs and the equivalent boundary are shown in Fig. 4.

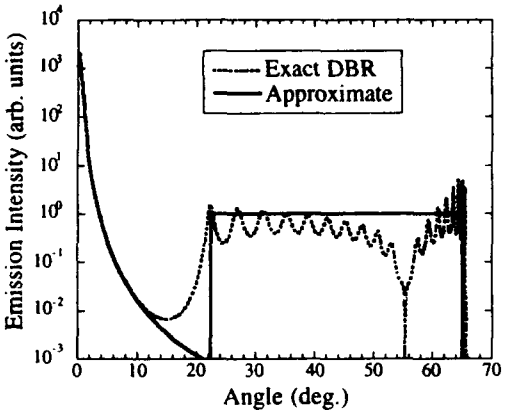

Fig. 4 The approximate and exact spontantaneous emission intensity for an isotropic source a in half-wavelength resonator utilizing two 17-period GaAs/AlAs DBRs and the hard mirror equivalent. The intensity is plotted versus the angle in the GaAs in which the resonator is embedded.

We see that the analytic spontaneous emission intensity approximates the exact intensity for all angles in a piece wise manner. The agreement between the approximate and exact intensities suggests that it is only within the band stop of the DBR that the dipole emission properties are being altered significantly. Also, since the angular extent of the pass band and diffraction equivalent distance can be specified analytically, the approximate boundary allows us to obtain analytic expressions for the spontaneous emission rates, spontaneous emission coupling factor and spontaneous beam divergence in semiconductor microcavities.

The approximate boundary highlights the influence of diffraction penetration depth and pass band as key limiting factors to controlling spontaneous emission in semiconductors. It also allows us to obtain simple analytic expression for all of the relevant optical parameters.

References:

[1] T. Baba, T. Hamano, F. Koyama and K. Iga, *IEEE J. Quantum Electron.*, vol. 27, no. 6, pp. 1347-1358, 1991.
[2] G. Björk, Y. Yamamoto, S. Machida and K. Igeta, *Phys. Rev. A*, vol. 44, no. 1, pp. 669-681, 1991.
[3] D. I. Babić, Y. C. Chung, N. Dagli and J. E. Bowers, *IEEE J. Quant. Elect.*, vol. 29, no. 6, pp. 1950-1962, 1993.
[4] D. I. Babić, R. J. Ram, J. E. Bowers, M. R. Tan and L. Yang, to appear in *Appl. Phys. Lett.*, vol. 64, no. 14, 1994.
[5] R. J. Ram and R. A. York, to appear in *IEEE Trans. on Antennas. and Prop.* , vol. 42, no. 3, 1994.

2:45pm - 3:00pm
T3.6

Ultralow Threshold Lasers - How low is low enough ?

D.M. Cutrer and K.Y. Lau
Dept. of EECS, University of California at Berkeley, Berkeley, CA 94720

Abstract

Ultralow threshold (I_{th}<100 μA) lasers can be used in bias-free digital optical modulation. Even though the pulse drive current may be many times I_{th}, reducing the latter to 50-100 μA is essential in minimizing the total driver power.

Intense interest in recent years in ultralow threshold lasers, through a combination of quantum-confined and/or microcavity VSEL structures, was motivated mainly by their potential for optoelectronic integrated circuits (OEICs) due to their low electrical power requirements. Lasers with a threshold in the 100 μA range already exist. This is already small compared to the drive current above threshold needed to generate the typical required optical power for high data rate communication. It thus *appears* that continued research effort to further lower the threshold will have little impact on the laser driver requirements of the OEICs. We show in this paper that this is NOT TRUE when one fully considers the switching dynamics of semiconductor lasers in an OEIC environment, particularly at multi-gigabit data rates.

We base our analysis on the presumption that the laser is digitally modulated and *zero-bias* modulation format [1,2] is used. This modulation format is a highly favorable one in OEICs since it eliminates the need for optical monitoring and feedback control of the bias point of each individual laser - a logistic complication, particularly for VSELs due to their unique geometry, that consumes both power and on-chip real estate. It is well known that zero-bias on/off switching produces data-dependent turn-on delays that result in a degradation of the data. This is illustrated in Fig. 1 for the time evolution of the electron density and optical output under a pseudorandom pulse modulation. When the optical data stream is fed into a typical digital receiver, the resulting timing jitter introduces a bit-error-rate (BER) degradation. This degradation depends on the relative magnitude of the time delay compared to the bit rate. Considering that the turn-on delay is nominally the time required for the drive current to fill the electron density up to the threshold level, a laser with lower threshold will require less drive current in order to achieve a certain turn-on delay, and thus reducing the power requirement for the laser driver overall.

Since the turn-on delay is data dependent and is thus random, we must describe it in terms of a statistical distribution with the assumption that the modulation current pulses follow a truly random digital pattern. Under this assumption, the following turn-on delay distribution is obtained:

$$p(T_{on}) = CB\left[\frac{I_m}{I_{th}}\right]\left[1-\frac{T_{on}}{\tau}\frac{I_m}{I_{th}}\right]^{CB\tau-1} \qquad (1)$$

Where B is the bit rate, c is a normalization factor, τ is the carrier lifetime, I_m is the electrical drive current, and T_{on} is the turn-on time for the laser. Note that this distribution depends only on the ratio I_m/I_{th}. In order to quantify the requirements for drive current for satisfactory laser modulation performance, we assume that the optical pulse stream is fed into a thermal noise dominated simple photodiode receiver (50 Ω load) through 6dB of optical loss (a typical number in short-distance optical interconnect). The resulting BER is given by:

$$BER = \frac{1}{2}\left\{Q\left(\frac{D}{\sigma\sqrt{2}}\right)+\int_0^{t_o} p(T_{on})\,Q\left(\frac{h(t_{on})-D}{\sigma\sqrt{2}}\right)d(T_{on})\right\} \qquad (2)$$

Where Q is the standard gaussian Q function, D is the decision level, σ is the thermal noise variance, h(t) is the received photocurrent after equalization, and t_o is the turn-on time for the laser with no initial carriers in the active region. The decision level is numerically chosen to minimize the BER under each condition. By requiring a BER of 10^{-9}, we compute from Eq. (1) and (2) the required drive current, I_m as a function of laser threshold current, I_{th} for various bit rates. We have assumed that the DQE of the laser is 0.3 W/A in all cases, a typical number for low threshold lasers, and a carrier lifetime of 1 ns. We compute the average electrical power consumption for the laser, given by $P_E = (0.5)(I_m V_{on} + I_m^2 Z_o)$ where we choose V_{on} = 1.5 Volts and Z_o = 5Ω. This is shown in Fig. 2. It can be seen from Fig. 2 that the need for sub-100 μA threshold lasers depends on the modulation bit rate. The lowest threshold which still yields a drive power advantage is between 50 μA for 5 Gb/s to 100 μA for 0.1 Gb/s. It should be noted that the above results are for a specific link loss and receiver configuration. Therefore, the answer to the question "how low a threshold is low enough" depends not only on the modulation bit rate but on the interconnection link configuration.

References:

[1] K.Y. Lau, N. Bar-Chaim, P.L. Derry, and A. Yariv, Applied Physics Letters. 51, 69 (1987).

[2] T. Odagawa, K. Nakajima, K. Tanaka, H. Nobuhara, T. Inoue, N. Okazaki, and K. Wakao, Journal of Quantum Electronics. QE-29, 1682 (1993).

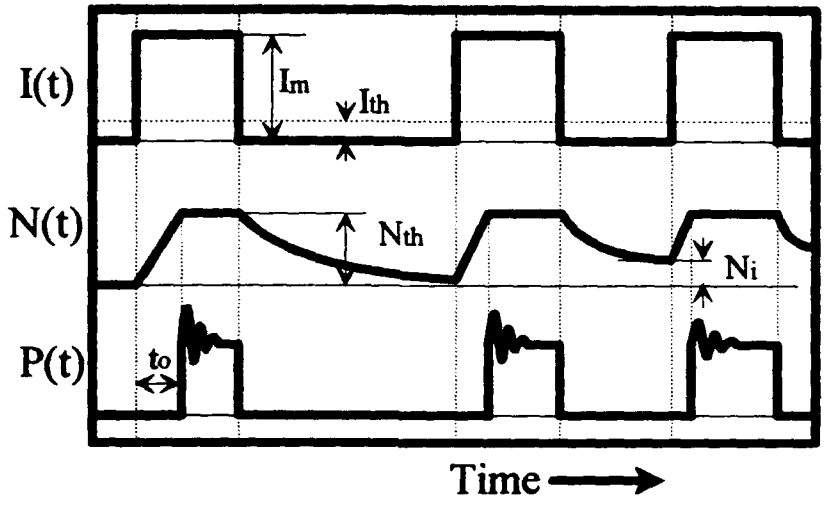

Figure 1: Pseudorandom bit stream, the corresponding carrier density in the laser, and the resulting optical bits.

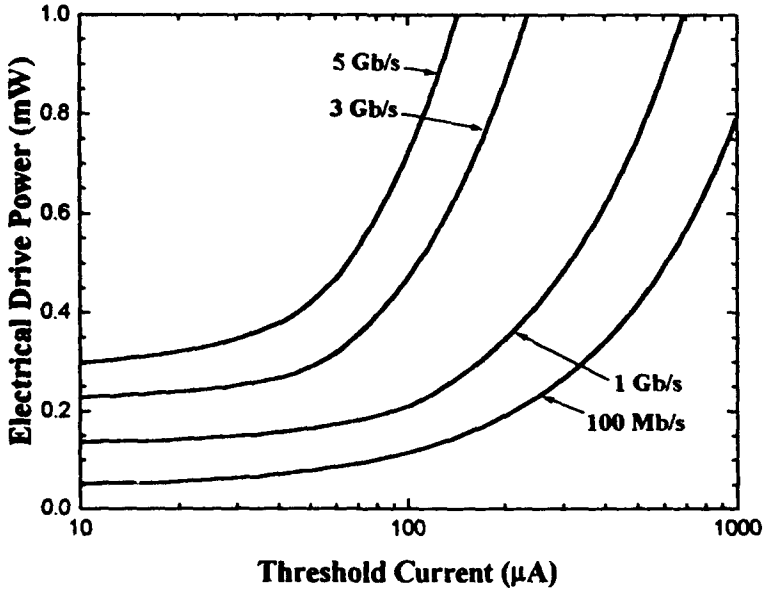

Figure 2: Calculated electrical drive power to the laser to achieve a $BER = 10^{-9}$ at the receiver as a function of the laser threshold current for different bit rates.

P1

SINGLE-MODE TUNABLE FIR PULSED p-Ge LASER

A. V. Muravjov, S. G. Pavlov, V. N. Shastin
Institute of Physics of Microstructures, Russian Academy of Sciences,
603600, Nizhny Novgorod, Russia
E. Bründermann, H.-P. Röser
Max-Planck-Institut für Radioastronomie, D-53121 Bonn, Germany

Abstract

A mechanically tunable selective resonator was developed and introduced in the far-infrared $p-Ge$ laser cavity. It leads to a continuous wavelength tunability from 75 to 110 μm. High resolved heterodyne mixing spectroscopy was used to measure the linewidth and mode structure of the $p-Ge$ laser radiation.

1. Introduction

The far-infrared pulsed semiconductor lasers based on the transitions between the light and heavy hole subbands of $p-Ge$ in crossed electric and magnetic fields $\vec{E}\perp\vec{H}$ at cryogenic temperatures cover a very broad spectral range (75–200 μm) [1]. The amplification of radiation on direct optical $l \rightarrow h$ transitions takes place in a wide frequency range lying below the energy of the optical phonon. As the result, the $l \rightarrow h$ laser with a nonselective, quasi-optical cavity has an anomalously wide radiation spectrum with a typical width about 10-20 cm^{-1} which can be tuned by applied $\vec{E}\perp\vec{H}$ fields in the range 80-135 cm^{-1} (λ=80-125 μm) with a typical output power up to 10 W during the laser pulse (several μsec).

There are a lot of methods to design a selective laser resonator in order to reach a single or quasi-single mode operation. Several attempts to select the modes and to tune the radiation frequency by different groups can be found in references [1-4]. We have designed a high-Q intracavity selector to get a very narrow-band tunable laser.

The active body of the laser is a sample of monocrystalline Ge doped by Ga with an acceptor concentration $(5-7)\times10^{13}$ cm^{-3}. The length is about 50 mm with a rectangular cross-section of 5×7 mm^2. The lateral sides of the sample are prepared in order to suppress radiation reflections. A silicon plane-concave spacer with an evaporated metal mirror is attached to one of the end faces. This element serves as an output mirror. On the opposite end of the p-Ge sample another silicon spacer with an evaporated metal semi-transparent mirror in the form of metal stripes or a chess desk is attached. This element serves as a coupling element. A total reflecting metal mirror closes the resonator. The vacuum gap enclosed between this end mirror and the coupling element is the passive Fabry-Perot type resonator with changeable thickness h, which is coupled with the active laser part, and serves as the tunable frequency selector.

2. Experimental results

In the experiments to analyse the output characteristics of the selective laser we used optical and heterodyne type spectrometers. The experimental setup consists of the p-Ge laser with a pump power supply and the receiving part. The latter includes either a grating far-infrared monochromator IRS-31 with a cooled Ge:Ga photodetector or a Schottky diode detector-mixer with a spectrum analyser.

The pulsed electric field $\mathbf{E_{ap}} = 0.5-2.0$ kV/cm is applied to the lateral surfaces 50×5 mm^2 through evaporated Al ohmic contacts. All resonator elements are fixed by a special holder to provide the optical coupling and the orthogonality of all elements. The holder is placed in a superconductive solenoid with a magnetic field $\mathbf{H}$ = 5–20 kOe oriented along the long axis of the resonator, thus $\vec{E}_{ap}\perp\vec{H}$. The whole system is immersed in liquid helium. The laser radiation is directed out of the helium cryostat by a 10 mm diameter metal waveguide which leads to the registration part of the setup.

Direct optical measurements of the radiation spectrum from the selective p-Ge laser by the IRS-31 showed that the laser spectrum is transformed to a narrow spectral line with a full width at half maximum (FWHM) not exceeding 0.077–0.080 μm, which is almost an order less than the spectral linewidth of the other known constructions of $p-Ge$ lasers [3,4]. The estimation of the linewidth maximum with respect to the grating spectrometer resolution limit gave a value about 0.02 μm. There is practically no change of the total laser power with the inserted intracavity frequency selector. The power is in the order of several watts, i.e. the power spectral density increases at the resonant line at least by three orders in

comparison with the broad-band regime of generation. The construction of the selective element allows the continuous wavelength tunability in the range 75–110 μm, tuned by a wheel, allocated outside of the liquid helium cryostat at room temperature.

To investigate the fine structure of the $p-Ge$ laser spectrum we have used the method of homodyne and heterodyne mixing spectroscopy with $n-GaAs$ Schottky diode mixer [5]. The signal from the $p-Ge$ laser was detected by the diode and the intermediate frequency (IF) signal from the diode was registrated by a spectrum analyser. The IF spectrum consisted of beat frequencies from different p-Ge laser modes. The main line in the frequency spectrum (458 MHz) equals to the fundamental intermode spacing $\Delta f = c/(2L)$, where c is the velocity of light and L is the optical length of the whole resonator. The FWHM for this line is about 1-2 MHz for a laser pulse duration $T = 2-3\mu$sec, that approaches the physical limit FWHM $\times T = Const$. The additional stray resonant lines in the IF spectrum are connected with disturbances of the internal transparency. As it was discovered in [5] the IF spectrum, obtained by mixing the nonselective p-Ge laser with the FIR CW gas laser on the wavelengths 117.7, 118.8 μm, has a time evolution, i.e. there is a shift of the $p-Ge$ laser modes during the laser pulse up to 25 MHz to low frequencies. This can be explained by an increase of the optical length of the laser resonator due to sample heating by the applied electric field pulses.

3. The results of numerical computations of the resonator

To analyse the described resonator we used the method based on solving the Fresnel-Kirchkoff surface integral [6]. It was found that the wave field (called the mode TEM_{mnq}) is close to known quasi-Gaussian form for the low loss level modes and differs from it for the case of high loss level modes. The eigenfrequencies are similiar to the spectrum of a hemi-spherical cavity [6]. The calculated loss level of the resonant frequencies (about 10^{-4} cm^{-1}) gives high-Q resonant lines upto $\frac{\delta\nu}{\nu} = \frac{1}{Q_{00}} = 3.2 \times 10^{-7}$ with FWHM about 1 MHz. The calculations for high-order modes (TEM_{10q} and higher) show that the proposed selector effectively separates higher transverse modes because of higher diffraction losses.

The main advantage to use an intracavity selection is the progressive increase of the gain — loss frequency differences, introduced by the selector. The most effective spectral narrowing arises for the linear regime of the stimulated emission when the intensity of the laser mode grows on the exponential low. Basing on it and knowing the time of the linear regime [7], we can estimate the FWHM about 0.030–0.037 cm^{-1} for the output lasing spectrum.

4. Discussion

So both the experimental and theoretical investigations discover the spectrum structure of the realized selective tunable p-Ge laser. The lasing spectrum consists of a single-mode type radiation TEM_{00q} with not more than 2–3 eigenfrequency oscillations. The frequency envelope of the lasing is about 0.02–0.03 cm^{-1} (600–900 MHz) and the FWHM of the carrier lines is about 1 MHz. The performed calculations gives the optimal dimensions for the resonator to reach a single frequency laser operation. Thus the quality of the radiation line $Q = \frac{\nu}{\delta\nu}$ may be within the limits $5 \times 10^3 - 6 \times 10^6$ with a coefficient of wavelength tunability $\eta = (140-90)(\text{cm}^{-1})/\delta\nu = Q/2$. The lossless concentration of the total laser power from a 500 GHz (17 cm^{-1}) wide frequency interval into the selected line evidently requires the accent on the frequency interaction processes, i.e. on a nonlinear regime of laser generation.

References:

1. Special Issue on Far-infrared Semiconductor Lasers, *Optical and Quantum Electronics*, **23**(2) (1991).
2. A. V. Murav'ev, I. M. Nefedov, S. G. Pavlov, V. N. Shastin, *Quantum Electron.* **23**(2) (1993) 119.
3. S. Komiyama, H. Morita, I. Hosako, *Jpn. J. Appl. Phys.*, **32** (1993) 4987.
4. L. E. Vorobjev et al., *Optical and Quantum Electronics*, **25** (1993) 705.
5. E. Bründermann et al. *Conf. Digest of Int. Conf. on MM and SubMM Waves MM and SubMM Waves and Applications, San Diego, USA*, SPIE **2250** (1994) 43.
6. A. G. Fox and T. Li, *Bell System Techn. J.* **40**(2) (1961) 453.
7. S. Komiyama and S. Kuroda, *Solid State Commun.* **59** (1986) 167.

P2

Analysis on Tu..g Range of Enhanced-Plasma-Effect Lasers

Motoyasu Morinaga, Masayuki Ishikawa, and Nobuo Suzuki

Materials and Devices Research Laboratories
Research and Development Center, Toshiba Corporation

1 Komukai Toshiba-cho, Saiwai-ku, Kawasaki 210, Japan

Abstract — We show wide and rapid tuning characteristics of the Enhanced-Plasma-Effect (EPE) lasers, which are new frequency tunable lasers having a thick carrier reservoir. Using the EPE lasers, continuous tuning range of more than 10 nm is predicted.

Frequency tunable lasers with rapid tunability and wide continuous tuning range are essential for coherent optical frequency-division-multiplexed networks. Recently we proposed the Enhanced-Plasma-Effect (EPE) lasers [1], which are novel multiquantum-well (MQW) distributed-feedback (DFB) lasers having a very thick p-side carrier reservoir. Carrier density change is enhanced by the thick reservoir because of the carrier-transport effect [2][3]. Therefore the fast blue frequency shift due to the plasma effect is strikingly enhanced and surpasses the slow red thermal frequency drift. We demonstrated rapid tunability (< 5 ns) and strong thermal frequency drift suppression (1/10) in the EPE DFB laser with a 600-nm-thick carrier reservoir [1]. In this paper, we also demonstrate theoretically wide continuous tuning range of the EPE lasers.

Figure 1 shows the schematic band diagram of the EPE lasers. The fre... hifts were calculated in consideration of the carrier transport time, the carrier lifetime in ... reservoir τ_a, and heat generation owing to nonradiative current. The carrier density dependence of the τ_a and the thermal dependence of the gain were also considered. Figure 2 shows the experimental and calculated results of the frequency-modulation (FM) efficiency at 20 MHz, which equals the initial blue frequency shift per unit current due to the plasma effect. The FM efficiency increased with reservoir thickness but was reduced by the influence of τ_a. The calculated and experimental results show good agreement.

Figure 3 shows the calculated results of the optical frequency shift at steady state, which was influenced by the red thermal drift, for different reservoir thicknesses. The frequency shift increased at lower current levels but decreased rapidly at higher levels because of increased heat generation. Therefore there was maximum frequency shift that indicates the CW tuning range for each reservoir thickness. Figure 4 shows the calculated results of the CW tuning range for two supposed values of thermal resistance R_{th}. The values 100 and 20 K/W were for hypothetical junction-up and junction-down mounts, respectively. The maximum tuning range of 460 GHz (3.6 nm) was considered to be realized with a 760-nm-thick reservoir when R_{th} = 100 K/W. The 1350-GHz (10.8-nm) tuning range could be realized with an 800-nm-thick reservoir if R_{th} were reduced to 20 K/W. This 10-nm tuning range covers the bandwidth of Erbium-Doped Fiber Amplifiers.

In conclusion, we have demonstrated wide and rapid tunability of the EPE lasers. The key to expand the tuning range is reduction of the thermal resistance. Over 10-nm continuous

rapid tuning was predicted with optimized reservoir thickness.

References

[1] M. Morinaga *et al.*, in *Conference on Optical Fiber Communication*, 1994 Technical Digest Series, vol. 4, paper ThB4.

[2] R. Nagarajan *et al.*, *IEEE J. Quantum Electron.*, vol. 28, pp. 1990–2008, 1992.

[3] H. Yamazaki *et al.*, *IEEE Photon. Technol. Lett.*, vol. 5, pp. 396–398, 1993.

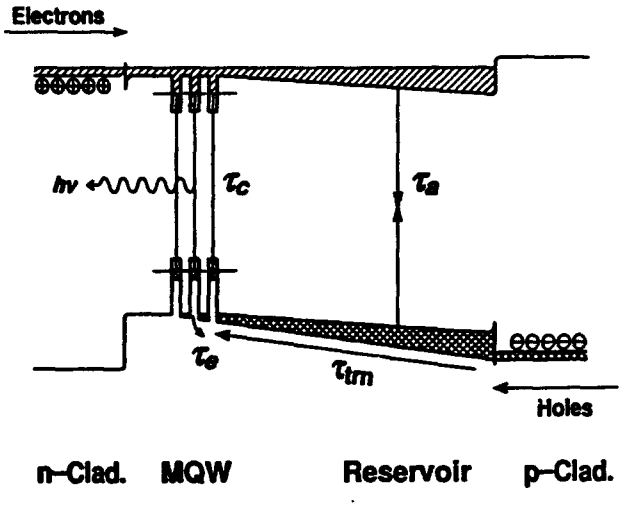

Fig. 1. Schematic band diagram of the EPE lasers.

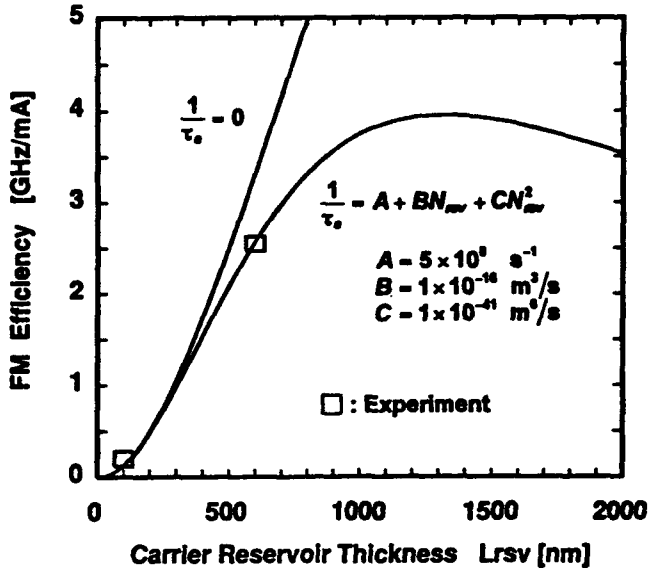

Fig. 2. FM efficiency versus carrier reservoir thickness in the EPE lasers.

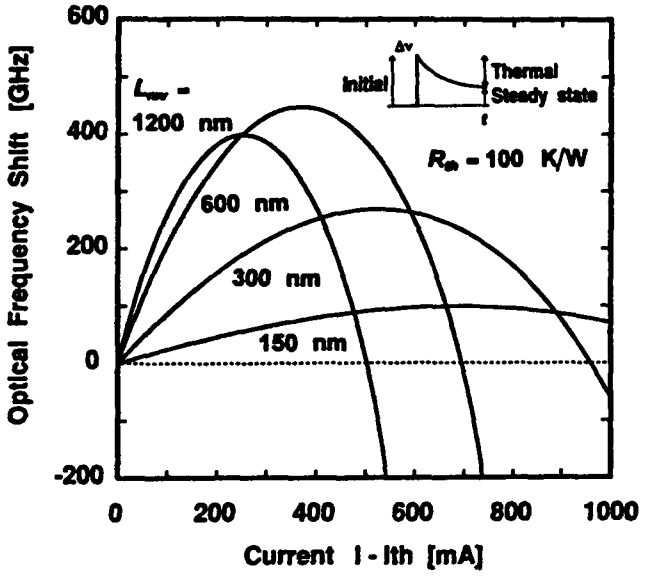

Fig. 3. Optical frequency shift at steady state in the EPE lasers for different reservoir thickness.

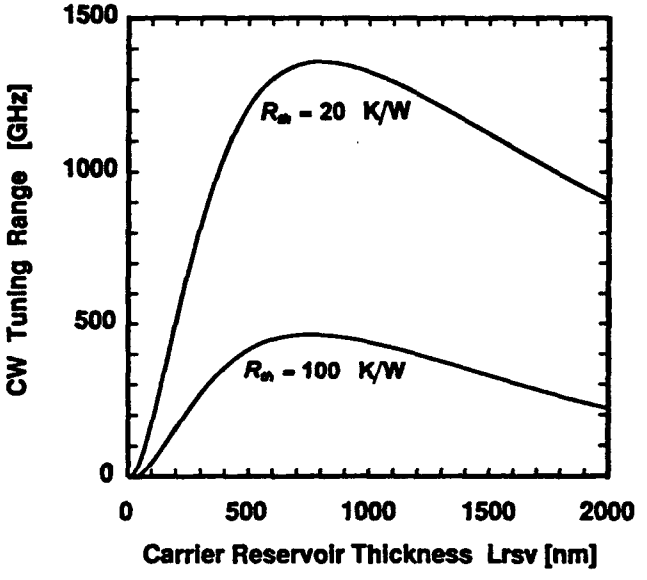

Fig. 4. CW tuning range of the EPE lasers for junction-up mount (R_{th} = 100 K/W) and junction-down mount (R_{th} = 20 K/W).

P3

Improved performance of semiconductor ring lasers with multi-mode interference output couplers

T.Krauss, P.J.R.Laybourn and R.M.DelaRue

Optoelectronics Group, Department of Electronics and Electrical Engineering, The University, Glasgow, G12 8LT, Scotland, U.K.

We present strip-loaded ring lasers in GaAs/AlGaAs that operate with a threshold current of 140mA for a total pumped device length of 4.5mm and a quantum efficiency of 7% (per output), to our knowledge the highest efficiency for such lasers reported to date.

Semiconductor ring resonator lasers offer a range of advantages over other geometries that employ cleaved facets or gratings for optical feedback. They are easily integrated and naturally offer themselves for mode-locked configurations [1], because of the inherent symmetry and because the device dimensions are defined by lithography which allows precise control over the resonator length and repetition frequency.
Here, we present devices that use a strip-loaded geometry [2] to overcome the degradation problems previously encountered with deeply etched structures in the GaAs/AlGaAs material system [3]. The curvature radius is 400μm and we compare three different types of output coupler in order to identify the influence of the coupling geometry on the performance of such lasers. Ring lasers employing multi-mode interference (MMI) couplers show significantly better characteristics than devices with Y-junctions and directional couplers (Fig.1).

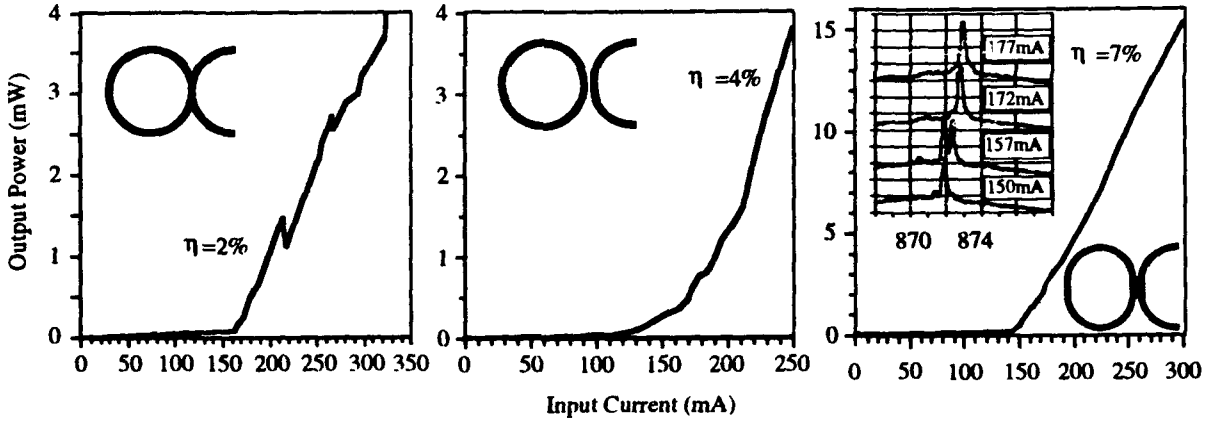

Figure 1 L-I curves of semiconductor ring lasers with three different types of output coupler; **a)** Y-junction; **b)** Directional coupler; **c)** MMI coupler. The spectrum shown in **c)** indicates the correlation between kinks in the L-I curve and mode hops, indicating coupled cavity effects. The scale is 2nm/div (horizontal), 10dB/div (vertical).

The good performance of the strip-loaded MMI coupler section is an essential requirement for this improvement. Despite the reduced number of modes in the interference section compared to deeply etched structures, strip-loaded couplers also produce a 3dB coupling ratio and virtually no loss [Fig.2a].
The reason for the improved performance of the ring laser devices that employ these couplers is that the coupling ratio is very tolerant to changes in mode position, refractive index and wavelength that occur during operation. This is illustrated in Fig.2b, where we show two characteristics of MMI couplers that are beneficial to ring laser operation. Firstly, the distorted input field caused by the curvature of the ring laser waveguide does not significantly alter the coupling ratio because of the imaging properties of the device. Secondly, if the mode position shifts during operation (due to the fact that the refractive index change caused by

injected carriers is of the same order as the contrast due to strip loading), the coupling ratio is maintained and the fraction of light coupled into the output path remains unchanged, an essential requirement for a linear L-I curve. This invariance of the coupling ratio to small changes of the input field does not apply in the same way to Y-junctions and directional couplers, which is the reason for the superior output characteristic of MMI coupler lasers. The same applies to fabrication tolerances, where small changes do not influence the device operation significantly, as shown by the almost identical results that we obtained for ring lasers with coupler lengths of 280μm, 300μm and 320μm. The devices operated cw at typically 140mA threshold current with a differential quantum efficiency of 7% (per output), which we believe is the highest value reported to date for lasers of this type.
The output curve is almost linear [Fig.1c], but some kink-like features remain between 150mA and 180mA. We attribute these kinks to coupled cavity effects, which indicates that the output waveguide, despite the small reflection coefficiant of the 4° tilted output facets, clearly affects the overall mode-structure of the laser. This assumption is supported by the spectral behaviour, which shows a mode-hop accompanying the kink at 160mA, a typical result for a coupled cavity [4].

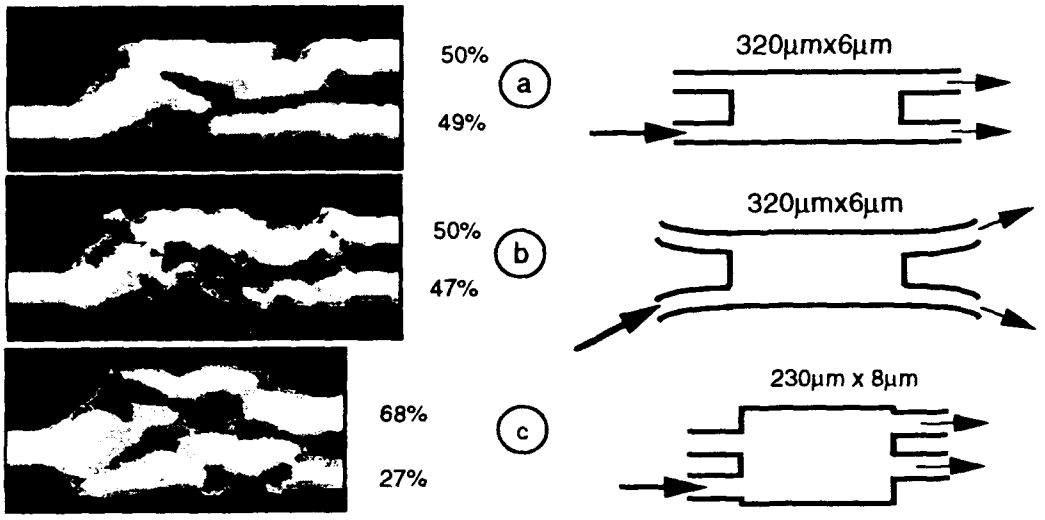

Figure 2 Intensity distribution in 2x2 MMI couplers modelled using the Finite Difference BPM; **a)** showing that strip-loaded couplers perform equally well as deeply etched ones, despite the reduce number of modes (6-8) in the interference section; **b)** illustrating that the coupling ratio is mostly independent of the shape of the input field; **c)** proposing an asymmetric coupler to increase the fraction of light coupled into the output path.

The efficiency can be further increased by employing an asymmetric coupler configuration as shown in Fig.2c. Feeding the coupler off-centre excites the modes in the interference section at a different ratio and the resulting self-images are not of equal brightness. In consequence, a higher fraction of the input field can be coupled into the output path and the external efficiency be increased. We acknowledge J.S.Roberts, Sheffield University, for material growth and the SERC for financial support.

1.J.P.Hohimer and G.A.Vawter, "Passive mode locking of monolithic semiconductor ring lasers at 86 GHz", Appl.Phys.Lett., vol.63, pp.1598-1600, Sep.1993.
2.T.Krauss, R.DelaRue, P.Laybourn, J.S.Roberts, "Strip-loaded semiconductor ring lasers employing multi-mode interference (MMI) output couplers" accepted for Appl.Phys.Lett.
3.T. Krauss and P.J.R. Laybourn, "Very low threshold operation of semiconductor ring lasers", IEE Proc.(J), vol 139, pp.383-387, Dec.1992.
4.R.Lang and K.Kobyashi, "External optical feedback effects on semiconductor injection laser properties", IEEE J.Quant.El., vol. QE-16, pp.347-355, Mar.1980.

P4

Reduction of Size Fluctuation Effect in GaInAs/GaInAsP Quantum-Box Lasers Using Tensile-Strained Active Region

Hideki HIRAYAMA and Masahiro ASADA

Department of Electrical and Electronic Engineering
Tokyo Institute of Technology
2-12-1 O-okayama, Meguro-ku, Tokyo 152, Japan
Telephone:+81-3-5734-2564 FAX:+81-3-5499-4791

Abstract: We show theoretically the reduction of quantum-box (QB) size fluctuation effect in GaInAs/GaInAsP QB lasers using tensile-strained active region. Tensile-strained QB laser is shown to be highly advantagous for 1.5μm low threshold laser.

Strained Quantum-box (QB) lasers are theoretically expected to exhibit various high performances such as high quantum efficiency, high power, ultralow threshold current due to large 0-dimensional confined effect. We have already achieved the lasing operation of a GaInAs/GaInAsP tensile-strained QB laser[1] and observed the 0-dimensional size effect in strained QB structures[2]. In this paper, we show the influence of size fluctuation, which has been the most severe problem in QB lasers, can be relaxed by tensile-strained active region.

Figure 1 shows the strain effect to carrier distribution in GaInAs/GaInAsP QB structures. By introducing compressive- or tensile-strain into QB region, quantum levels largely split due to the reduction of lateral hole effective mass which leads to the efficient hole concentration in lasing level. In addition, in tensile-strained case, electron level is only one even in relatively large QB size due to small conduction band discontinuity which leads to the efficient electron concentration into the lasing level and low transparent carrier density. The coupling between dipole moment and light field is also large in tensile case. The strain effect in QB laser is summarized in table 1.

Size fluctuation effect on optical gain is determined by the emission peak energy broabening with the change of QB size. For unstrained and compressive-strained QB, threshold current increase due to QB size fluctuation is large because of large emission energy brodening with the change of QB size due to small optimal QB size and small electron and hole effective masses. On the other hand, the fluctuation effect is reduced dramatically in tensile-stained QB because of small emission energy broadening due to small conduction band discontinuity.

Figures. 2 shows the threshold current densities of QB lasers as a function of QB density for optimal QB size with and without QB size fluctuation. Tensile-strained QB laser shows the lowest threshold current density as well as less influence of size fluctuation.

Refererences:

[1] H. Hirayama et al. *Electron. Lett.*, vol. **30**, no. 2, p. 142, Jan. 1994.
[2] H.Hirayama et al., to be published in Jan. J. Appl. Phys..

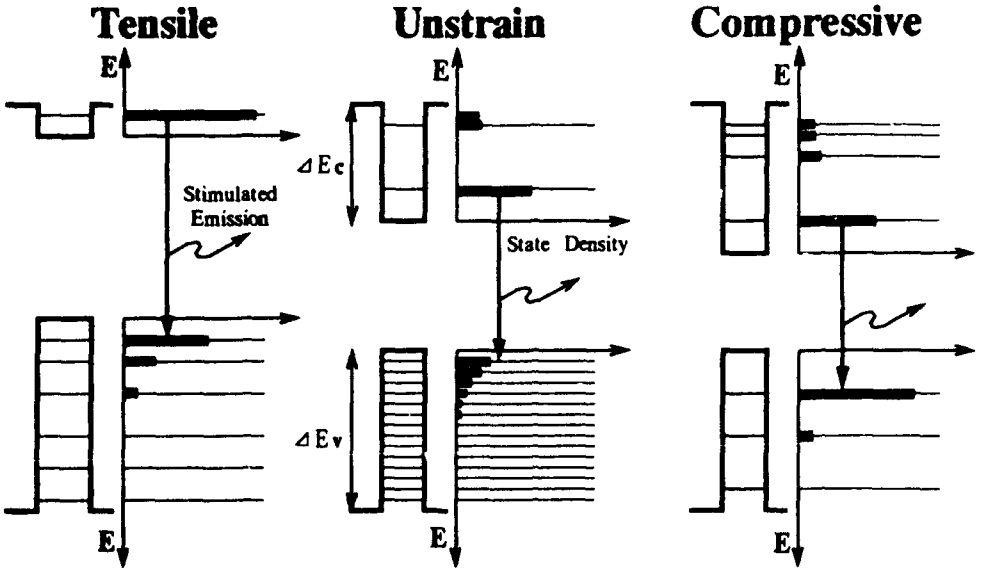

Fig.1. Carrier distribution in GaInAs/GaInAsP strained QB structures.

Q-Box	Tensile	Unstrain	Compressive
Modal Gain $\xi \cdot g$ (J=30A/cm²)	80cm^{-1}	29cm^{-1}	65cm^{-1}
Wavelength	1.47 μm	1.43 μm	1.67 μm
Efficient Hole Consentration to 1st Level	○	×	◎
Efficient Electron Consentration to 1st Level	○	△	△
Coupling Between Dipole Moment and Light Field	△	×	×
Size Fluctuation Effect	◎	×	×
Threshold Current Density	◎	△	○

◎ – excellent ○ – good × – bad

Table 1. Strain effect on QB lasers.

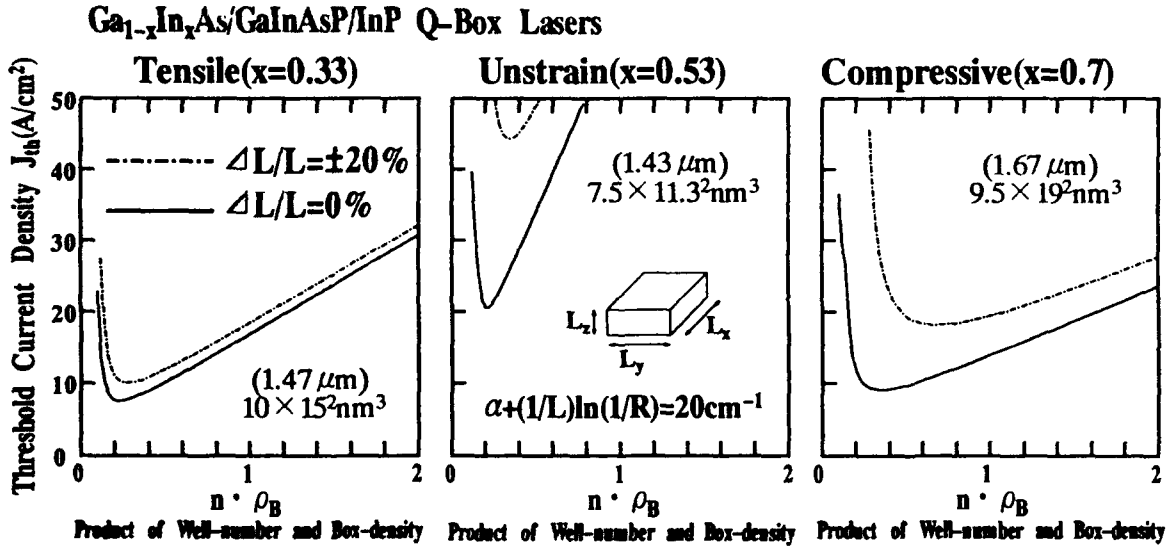

Fig.2. Threshold current densities of QB lasers as a function of QB density for optimal QB size with and without QB size fluctuation. Size fluctuation effect is much reduced using tensile-strained active region.

P5

Submilliampere Threshold Buried-Heterostructure InGaAs/GaAs Single Quantum Well Lasers Grown by Selective-Area Epitaxy

R.M. Lammert, T.M. Cockerill, D.V. Forbes, G.M. Smith and J.J. Coleman

Microelectronics Laboratory
Materials Research Laboratory
University of Illinois
208 N. Wright St.
Urbana, IL 61801 USA

Abstract - Submilliampere threshold strained-layer InGaAs-GaAs-AlGaAs single quantum well buried heterostructure lasers grown by selective-area MOCVD are described. Low threshold currents, high differential slope efficiencies and high output powers are reported.

Buried heterostructure (BH) lasers are desirable because of the strong lateral index guiding and current confinement provided by the heterostructure discontinuity in the lateral direction. These features allow the BH laser to operate with low threshold current and high efficiency. Fabrication of BH laser structures containing AlGaAs can be difficult because the formation of a stable native oxide often results in poor quality interfaces upon regrowth. Low threshold BH lasers containing AlGaAs have been fabricated using liquid phase epitaxy (LPE) for the regrowth in order to melt-back the oxidized interface [1]. Impurity-induced layer disorder (IILD) has also been used to fabricate low threshold BH lasers [2] but has the disadvantage of a long anneal at high temperatures which can lead to interdiffusion at the InGaAs-GaAs interface. Recently, a three step selective-area epitaxy has been demonstrated [3] that eliminates much of the difficulty associated with regrowth over exposed AlGaAs. This process also permits wavelength "tuning" over the wafer, allowing for a single wafer containing BH lasers which operate at various wavelengths. In this talk, we report the fabrication of optimized strained-layer, InGaAs-GaAs-AlGaAs single quantum well (SQW) BH lasers by three-step selective-area growth using only atmospheric pressure metalorganic chemical vapor deposition (MOCVD). These lasers exhibit extremely low threshold currents for as-cleaved facet devices (I_{th} = 2.65 mA) and submilliampere thresholds for HR coated devices (I_{th} = 0.97 mA).

Selective-area MOCVD growth utilizing a patterned silicon dioxide mask was used to fabricate the strained-layer InGaAs-GaAs-AlGaAs SQW BH lasers [3]. No deposition takes place on the silicon dioxide and the

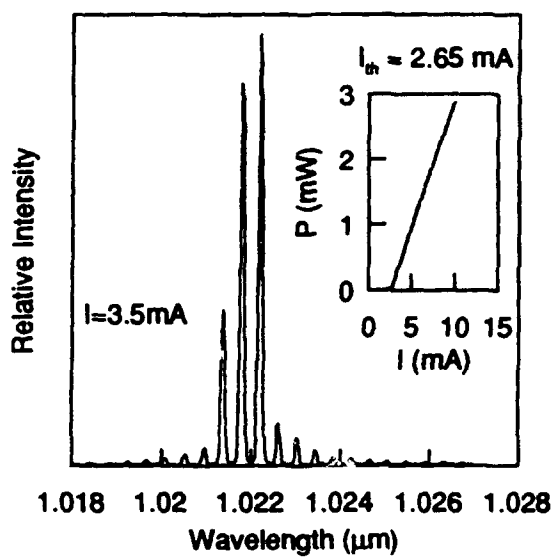

Figure 1. Longitudinal mode spectrum with the output vs. current (inset) of a three step selective-area epitaxy buried heterostructure laser with as-cleaved facets operating pulsed at room temperature (λ_{peak} = 1.022 μm, I_{th} = 2.65 mA).

growth rate everywhere else is enhanced. The amount of this enhancement and, hence, quantum well thickness and composition, is determined by the geometry of the mask pattern. For these devices, a dual oxide stripe ge-

ometry is employed with the oxide stripe width defining the emission wavelength and the spacing between stripes defining the lateral waveguide width. The three-step growth process begins with growth of a buffer layer, a 1 μm $Al_{0.60}Ga_{0.40}As$ lower cladding and a thin (150 Å) GaAs layer to prevent oxidation. The sample is removed from the chamber and a 600Å SiO_2 mask is deposited on the sample and patterned by standard lithography methods and an H_2SO_4:H_2O (1:80) etch is used to remove process contamination before the sample is returned to the reactor for the selective growth of the active region. The oxide mask was removed and another H_2SO_4:H_2O (1:80) etch is performed before the final growth consisting of a 50 Å GaAs layer, a 1 μm $Al_{0.60}Ga_{0.40}As$ upper cladding and a 0.15 μm GaAs p^+ cap.

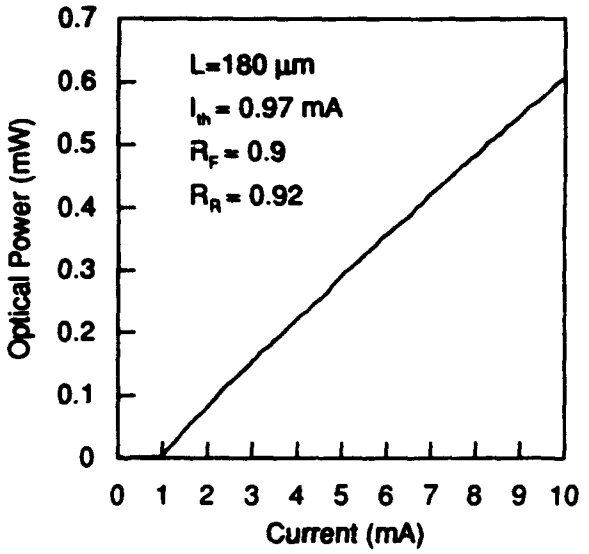

Figure 2. Pulsed output vs. current at low current levels for one facet of a three step selective-area epitaxy buried heterostructure laser (I_{th} = 0.97 mA, length 180 μm, active region stripe width 2 μm)

Fig. 1 shows the longitudinal mode spectrum of a 330 μm long, 2 μm wide BH laser (λ_{peak} = 1.022 μm) with as-cleaved facets operating just above threshold at room temperature. The inset of Fig. 1 shows the L-I characteristic of this device. A threshold current of 2.65 mA (401 A/cm^2) and a differential slope efficiency of 0.392 (W/A) per uncoated facet was observed from this device which had a calculated effective lateral index step of 0.19. With the application of HR coatings, a submilliampere (0.97 mA) threshold current is obtained on a similar 180 μm long BH laser, shown in Fig. 2. Shown in Fig. 3 is the L-I characteristic for one facet of a 760 μm long 4 μm wide BH driven to higher currents (I_{th}=7 mA, J_{th}=230 A/cm^2, λ_{peak} = 1.032 μm). The peak optical power of this device (170 mW/facet) was limited by the onset of COD.

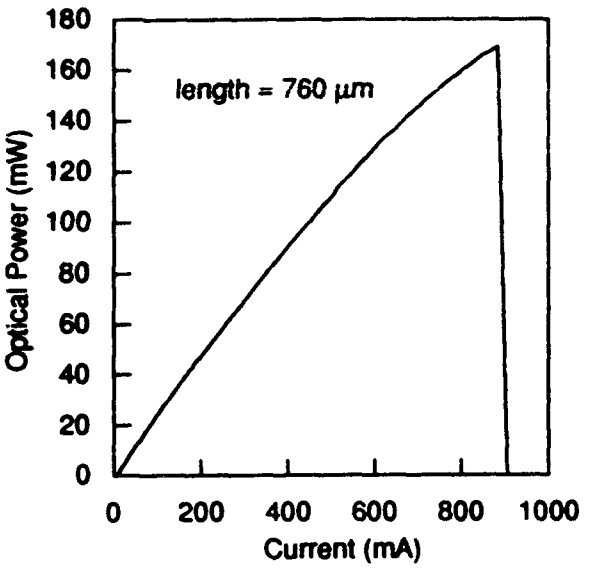

Figure 3. Pulsed output vs. current at higher current levels for one facet of an uncoated three step selective-area epitaxy buried heterostructure laser (I_{th} = 7 mA, J_{th} = 230 A/cm^2, λ_{peak} = 1.032 μm, P_{max} = 170 mW)

The selective-area process allows the wavelength across the sample to be varied from 0.956 to 1.032 μm. These results indicate low threshold, wavelength tunability, and high optical power are obtainable for selective-area epitaxy buried heterostructure lasers.

[1] T.R. Chen, L.E. Eng, B. Zhao, Y.H. Zhuang, and A. Yariv, "Strained Single Quantum Well InGaAs Lasers with a Threshold Current of 0.25 mA," *Appl. Phys. Lett.*, vol. 63, p. 2621, 1993.

[2] D.G. Deppe, K.C. Hsieh, N. Holonyak, Jr., "Low-Threshold Disorder-Defined Buried-Heterostructure $Al_xGa_{1-x}As$-GaAs Quantum Well Lasers," *J. Appl. Phys.*, vol. 58, p. 4515, 1985.

[3] T.M.Cockerill, D.V. Forbes, H. Han, B.A. Turkut, J.A. Dantzig, I.M. Robertson and J.J. Coleman, "Wavelength Tuning in Strained-Layer InGaAs-GaAs-AlGaAs Quantum well lasers by Selective-Area MOCVD," *J. Electronic Mater.* vol. 23, p. 115, 1994.

P6

Monolithic Integration of a Laser Diode with a Polymer-Based Waveguide for Photonic Integrated Circuits.

N.Bouadma, J.Liang, R.Pinsard-Levenson, A.Talneau, G.Hervé-Gruyer

France Telecom, CNET/PAB/BAG
196 avenue Henri-Ravera BP 107
92225 Bagneux cedex France

In the rapidly developing field of photonic integrated circuits (PICs), monolithic integration of active and passive optoelectronic components is becoming increasingly important as a tool to produce low cost and high funtionality optical modules with applications in a wide range of systems. One of the key elements in these PICs is the connection of the laser diode to an external waveguide in a monolithical way. Various schemes, involving particularly III-V materials for the waveguide structure, have been already reported to achieve such integration. More recently promising approaches using glass or polymer materials for light waveguiding have been intensively studied with a view to develop optical interconnects[1]. These kinds of materials have intrinsically very low-loss in the infrared region. Attempts to integrate hybrid components with silica based waveguides onto silicon motherboard has shown very good losses figures and high thermal stability[2]. However the resulting optical coupling efficiency is fairly low and the assembly techniques are expansive and time consuming. In this paper a monolithic integration of a laser diode with a polymeric based waveguide is reported as a first step in developping a monolithically integrated multi-wavelength DFB laser array with a passive polymeric optical power combiner. This alternative approach based on polymeric materials offers the advantages of the potentially low optical losses and high and easy processability, and the capability of preparation of active and passive components on III-V wafers with already processed devices.

The monolithically integrated laser/waveguide device shown schematically in Fig. 1. was prepared via a two distinct process stages : first, the laser wafer with buried ridge stripe structure (BRS) was fabricated using MOVPE and reactive ion beam etching (RIBE) technique[3]. After the p and n contact metallization, the Fabry-Perrot laser mirrors have been made by $CH_4/H_2/Ar$ based RIBE[4]. Single mode waveguides were then fabricated using the polyimides by spin coating, conventional photolithographic patterning and reactive ion etching (RIE). An under-cladding layer of PMMA (n=1.48, 1.5μm thick and cured at 170°C) and a core layer of polystyrene (n=1.6, 1μm thcik cured at 200°C) were spin coated onto the substrate. Care has been taken to butt-joint couple the laser to the waveguide active layer in order to improve the coupling efficiency. The core ridge was then fabricated by photolithographic patterning and RIE using oxygen. Finally the ridge was embedded into a teflon AF upper cladding layer. Fig. 2 shows the light absorption spectrum of the polystyrene we used as core material. Only one peak at 1.65μm is observed int he near infrared region which is attributed to the second harmonics of the stretching vibration of the C-H bond. There are no absorption peaks at 1.3 and 1.55μm where the absorption is less than 1 dB/cm. Fig.3 shows the light output power versus current characteristics of the integrated device measured at the cleaved laser facet and at the end of the waveguide. The laser cavity and the waveguide lengths were respectively 250 μm and 600 μm. The optical power output from the laser and the waveguide facets were typically 11 mW and 5 mW at 100mA. The difference between the optical powers stems from the coupling loss at the joint, the propagation losses and the out-coupling losses at the end of the waveguide. Significant improvement may be expected by optimizing the processing steps. Single mode operation of the waveguide is identified by the near field patterns (Fig.3). Moreover the integrated device shows high thermal stability against temperature after heating at 250°C for 1 h, with no significant decrease in the waveguide power output.

Furthermore, this proposed integration scheme could be a particularly suitable builing block for the fabrication of various PICs. As first example, Fig. 4 shows an SEM photograph of a monolithically integrated multi-wavelengths DFB lasers array with a passive optical power combiner as well as a 2 D BPM simulation of the optical combiner. The total length of such combiner is 800 μm and the angles between waveguides are 22°. Due to the low refractive index of the core and the refractive index difference between core and cladding (~ 0.2), wide branching angles are allowed. The total optical losses of such a device have been estimated to be less than 10 dB.

1.3μm Buried Ridge Structure lasers and polymer-based waveguides have been monolithically integrated using high performance and low cost technology. The main applications are passive components such as optical combiners for WDM devices, splitters switches and other various PICs.

References: **[1]** C.Rompf, B.Hilmer, W.Kowalsky ECOC 93, paper N° WeP7.5. **[2]** C.A.Jones et al. Electron. Lett. 1994, **30**,(3). **[3]** N.Bouadma, C.Kazmierski and J.Semo Appl. Phys. Lett.**59**, 1 (1991). **[4]** N.Bouadma and J.Semo to be published in IEEE J. Lightwave Technol.

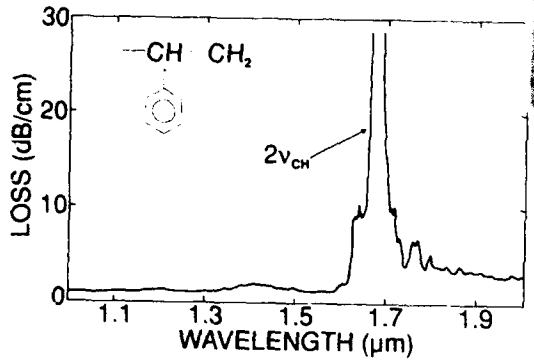

Fig.1: Light absorption spectrum of polystyrene cured at 200°C.

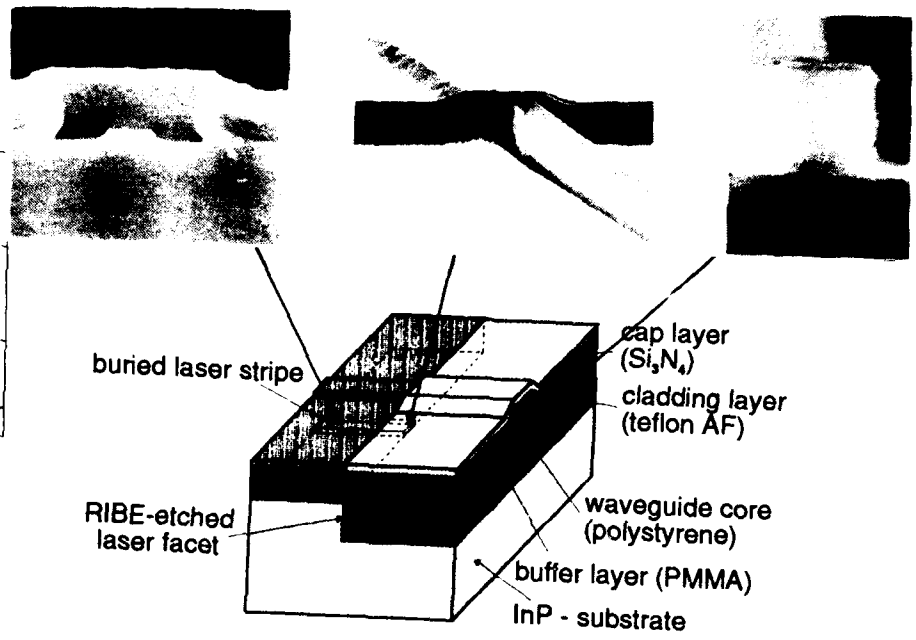

Fig.2: Schematic diagram and SEM photoraphs of monolithically integrated laser/waveguide structure.

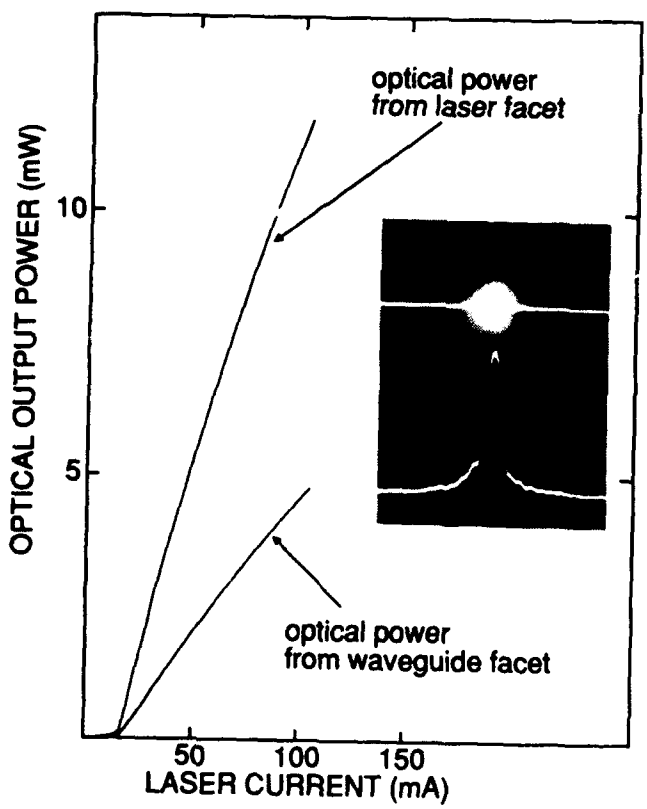

Fig.3: Light/current characteristics of the integrated laser/polymer waveguide and near field pattern of the waveguide.

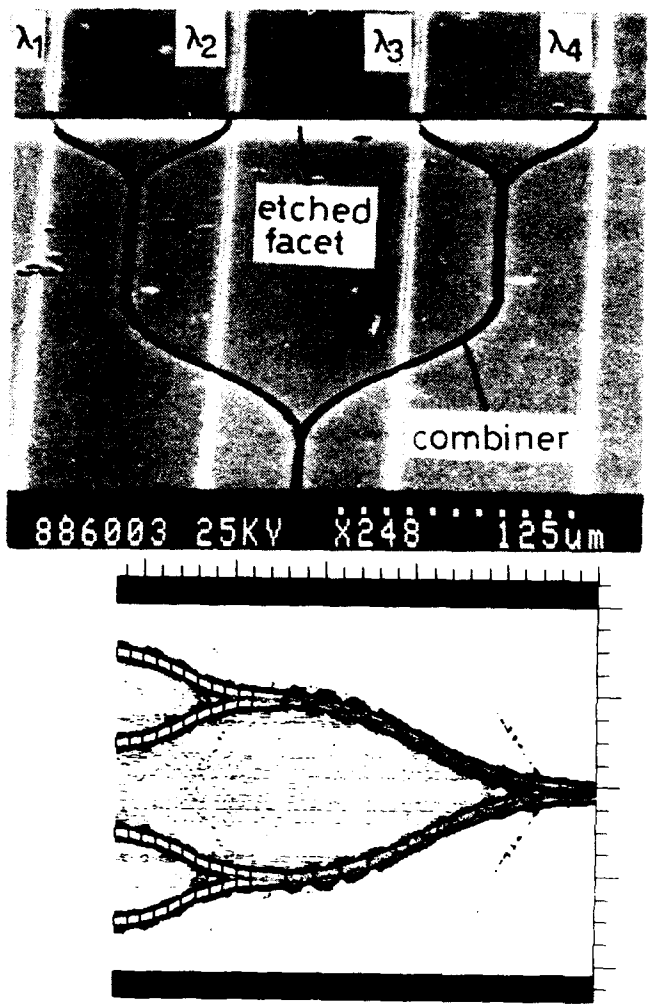

Fig.4: SEM micrograph and 2 D BPM simulation of monolithically integrated multi λ laser with optical combiner.

P7

EXTREMELY SMALL ACTIVE STRIPE LASER DIODES(EXSAS-LDs) FOR 17-CHANNEL LOW THRESHOLD ARRAY

Shotaro KITAMURA, Tatsuya SASAKI, Keiro KOMATSU, and Mitsuhiro KITAMURA

Opto-Electronics Research Labs.
NEC Corporation
34 Miyukiga-oka, Tsukuba, Ibaraki 305, JAPAN

ABSTRACT

Uniform 17-channel array of low threshold(3.5mA,av.) 1.3μm wavelength lasers was realized with submicron wide bulk active layers grown by selective MOVPE technique.

INTRODUCTION

Optical parallel interconnection is a promising technology for high-speed, high capacity computing and transmission systems, where multi-channel laser arrays with uniform characteristics and low threshold current are required[1]. So far, ten-channel laser arrays with 1.8mA threshold current have been reported[2]. However, there still exist problems to be solved for multi-channel arrays, with regard to broad area uniformity and reproducibility. In this report, we propose a new type of low threshold laser array with quite simple structure, having submicron wide bulk active layers. The proposed laser array was fabricated by selective MOVPE technique[3,4]. Uniform 17-channel laser array, which corresponds to 2-bytes data and 1bit control signals, was demonstrated with low threshold current.

DEVICE STRUCTURE AND FABRICATION

Figure 1 shows the extremely small active stripe laser diode(EXSAS-LD) of the array. A bulk InGaAsP active layer of 1.3μm wavelength composition was buried in InP layers. The active layer was designed to be 0.5μm wide and 0.3μm thick and the cross sectional SEM image is shown in Fig.2. This nearly square cross sectional dimensions have such a large optical confinement of 40%, while commonly taken dimensions of 1.5-2.0μm width and 0.1μm thickness for BH lasers have only 15% though they have equivalent cross sectional area. Therefore, low threshold current due to high optical modal gain was expected. The device length was 210 μm and the spacing between channels was 250μm. The facets were coated with Al_2O_3/a-Si multi-layers to have 70% and 90% of reflectivity for front and rear facets, respectively.

In order to form so narrow active layers as 0.5μm, selective MOVPE technique has been employed. In this fabrication technique, extremely small semiconductor stripes including active layers were successfully grown on submicron wide center spacings between pairs of SiO_2 masks[4]. Submicron mask pattering was easily realized by a projection printer. Therefore, the small active layer dimensions were precisely controlled, so that the laser array with low threshold current and excellent uniformity was realized.

DEVICE CHARACTERISTICS

Figure 3 shows the measured CW light output characteristics of the 17-channel array. The 17-lasers showed uniform characteristics of threshold current of 3.0-4.5mA and slope efficiency of 0.13-0.17W/A. The average threshold and efficiency are 3.5mA and 0.15A/W, respectively. Temperature dependence of the light output characteristics is shown in Fig.4. Even at high temperature of 80°C, the laser still has low threshold of 8mA and 0.12W/A slope efficiency. The characteristic temperature T_0 was 60K between 25-80°C, which is typical value for BH lasers.

Excellent characteristics have been achieved, even though the laser structure has not been fully optimized yet. The measured characteristics demonstrates the potentiality of this proposed laser array.

CONCLUSION

A new type of laser array for parallel interconnection was proposed, and uniform 17-channel array with low threshold current was demonstrated by selective MOVPE technique.

ACKNOWLEDGEMENT

The authors would like to thank K.Kobayashi and I.Mito for their encouragement and supports.

REFERENCES
[1]J.W.Goodman, et.al., Proc. IEEE, Vol.72 pp.850-865(1984)
[2]A.Oishi, et.al., ECOC'93 Proc. Vol.3 Post deadline papers, ThC12.6 pp21-24(1993)
[3]T.Sasaki and I.Mito, OFC/IOOC'93, Technical Digest, ThK1 pp.210-212(1993)
[4]S.Kitamura, et.al., OAA'93, Technical Digest, SuB3 pp.12-15(1993)

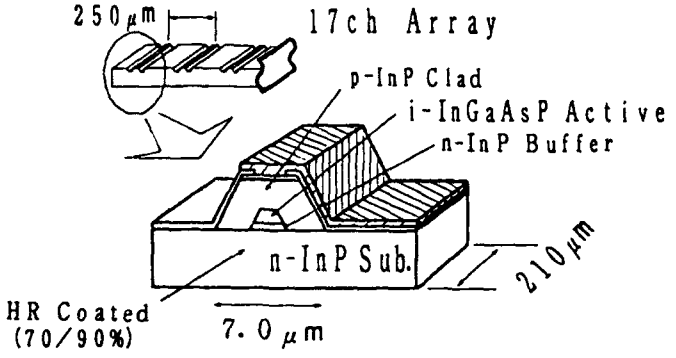

Fig.1 Structure Diagram of Laser Array

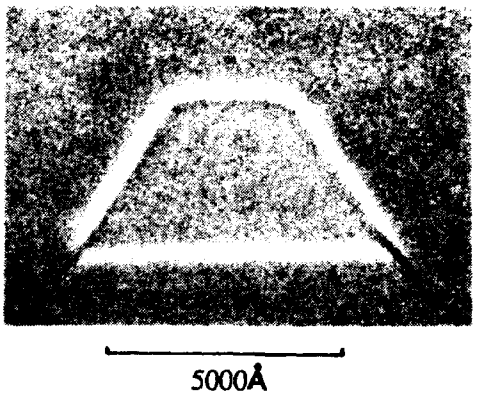

Fig.2 Cross Sectional SEM Image of Active Layer

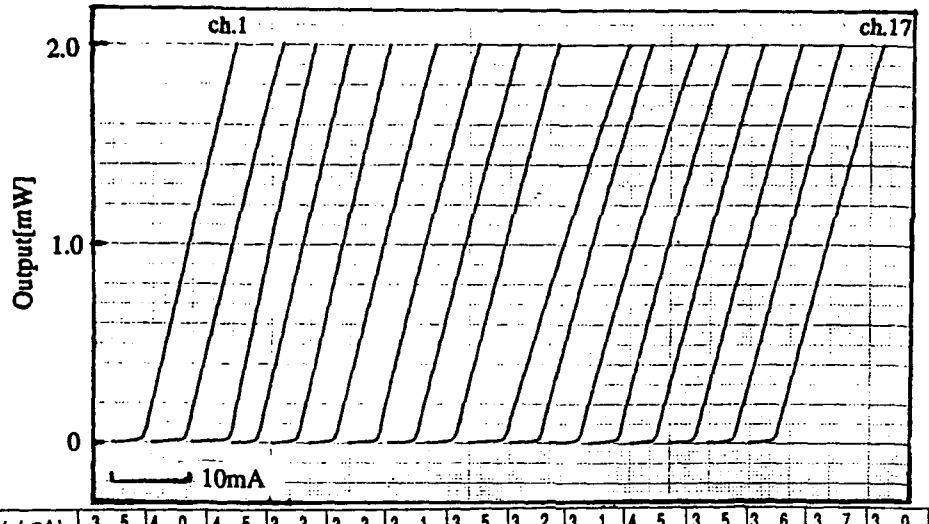

Ith [mA]	3.5	4.0	4.5	3.3	3.3	3.1	3.5	3.2	3.1	4.5	3.5	3.6	3.7	3.0	3.0	3.0	3.1
η [W/A]	0.16	0.16	0.17	0.17	0.17	0.15	0.15	0.15	0.15	0.13	0.14	0.14	0.14	0.15	0.14	0.15	0.15

Fig.3 Light Output versus Current Curves for 17-channel Laser Array

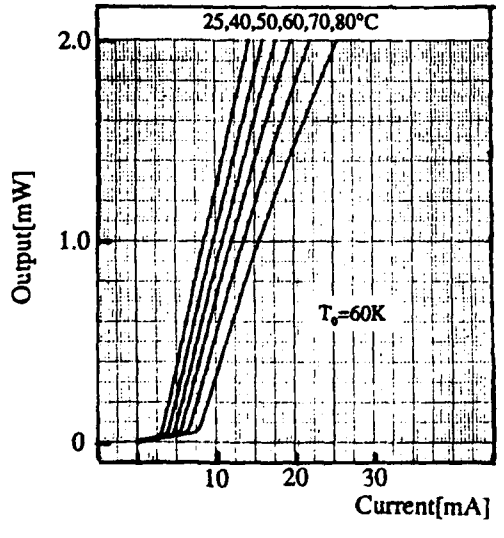

Fig.4 Temperature Dependence of Light Output

P8 Hydrogen Effect on 670nm AlGaInP Visible Laser during High Temperature Operation

Won-Jin Choi, Ji-Ho Chang, Won-Taek Choi, Seung-Hee Kim, Jong-Seok Kim, Shi-Jong Leem, and Tae-Kyung Yoo

GoldStar Central Research Laboratory, 16 Woomyeon-Dong , Seocho-Gu, Seoul 137-140, Korea

Abstract

It has been shown that characteristics of AlGaInP lasers are improved after a short-term aging test. It is proposed based on SIMS measurement that this phenomenon is due to the redistribution of atomic hydrogens during the operation.

During the accelerated aging test, we have found that AlGaInP laser diodes show a typical phenomenon that the characteristics are improved at the beginning of the aging test. This phenomenon has been shown in the previous papers[1-3], but its origin has not been explained clearly.

In this paper, we studied on aging characteristics of AlGaInP laser, especially on that phenomenon. An index guided strained multi-quantum well (SMQW) AlGaInP laser with the wavelength of 670nm and the threshold current of 35mA at 250μm cavity length has been fabricated by metalorganic vapor phase deposition(MOCVD). Growth conditions in detail were reported in another paper[4]. Aging test was carried out on automatic power control(APC) for 3mW at 50°C. Fig.1a) shows aging characteristics of index guided SMQW GaInP/AlGaInP visible laser diode with those of 860nm LPE grown index guided GaAs/AlGaAs laser diode for a comparison. For AlGaInP visible laser diodes we found the operating current decreased gradually from the starting point to about 50 hours and then stabilized. Fig.1b) and Fig. 1c) show the changes in series resistances and threshold currents of the laser diodes after the aging test starts. From Fig.1a), it can be expected that the output power would not vary under a constant current condition at room temperature(RT) as well as the aging temperature. Fig. 2 shows the increase of lasing output power when the current is maintained constantly at RT. Therefore, we assumed that the changes are related with atomic hydrogens in epi-layers of the laser because sources for MOCVD can supply epi-layers with a lot of atomic hydrogens[5]. In semiconductors, it is well known that the atomic hydrogens passivate shallow dopants, deep levels, and defects in bulk and at interface[6]. Hydrogen passivation could effect on the decrease of nonradiative centers and the increase of the radiative recombination lifetime[7]. Thus, hydrogen passivation could reduce the acceptor activation[9] and increase luminescence efficiencies[6-8]. So it is expected that any behavior of the atomic hydrogen would effect on the characteristics of a laser diode.

To investigate the hydrogen effect on a laser diode structure, we fabricated SMQW GaInP/AlGaInP visible light emitting diode(LED) which has the same structures in the clad and active region that the laser diode has. We examined the change of the hydrogen profile of each layer by secondary ion mass spectroscopy(SIMS) before and after the aging test done in the similar condition that laser diodes were tested in. Before aging, the hydrogen concentration of p- AlGaInP layer was relatively higher than those of the active layer and n-AlGaInP layer as shown in Fig. 3. The hydrogen concentration of the active region was the lowest among those of three layers. But, after aging test, the hydrogen concentration of p- AlGaInP layer decreased and reached nearly the same level of n-AlGaInP layer. And, the hydrogen concentration of the active region increased and the lowest concentration point was shifted toward the n- AlGaInP layer after aging test.

In conclusion, we proposed that the reduction of the series resistance of the laser diode and the improvements of the threshold characteristic and the output power with a short-term of the aging test are attributed to the reduction of hydrogen concentration in the p-AlGaInP layer and the passivation of defects both in bulk and at interface of the active region respectively.

References

[1] A. Gomyo, K. Kobayashi, S. Kawata, I. Hino, and T. Suzuki, Electron. Lett., **23**, 85(1987).

[2] K. Itaya, M. Ishikawa, H. Okuda, Y. Watanabe, K. Nitta, H. Shiozawa, and Y. Uematsu, Appl. Phys. Lett., **53**, 1363(1988).

[3] M. Ishikawa, H. Okuda, K. Itaya, H. Shiozawa, and Y. Uematsu, Jpn. J. Appl. Phys.,**28**, 1615(1989).

[4] H.-C. Ko, J.-S. Kim, W.-J Choi, K.-W. Chung, and T.-K. Yoo, Extended Abstracts of the 1992 Meeting IEEE Korea Section (Seoul) **10**, 279(1992).

[5] G. R. Antell, A. T. R. Briggs, B. R. Butler, S. A. Kittching, and J. P. Stagg, A. Chew, and D. E. Sykes, Appl. Phys. Lett., 53, 758(1988).

[6] J. I. Pankove and N. M. Johnson, Eds., Semiconductor and Semimaterials(Academic, New York, 1991),

vol. 34.
[7] L. Pavesi, F. Martelli, D. Martin, and F. K. Reinhart, Appl. Phys. Lett., 54, 1522(1989).
[8] S. M. Lord, G. Roos, and J. S. Harris, Jr., N. M. Johnson, J. Appl. Phys., 73, 740(1993).
[9] M. Ishkawa, M. Suzuki, Y. Nishikawa, K. Itaya, G. Hatakoshi, Y. Kokubun, and Y. Uematsu, Int. Symp. GaAs and Related Compounds, Karuizawa, Japen, 1989, p. 575.

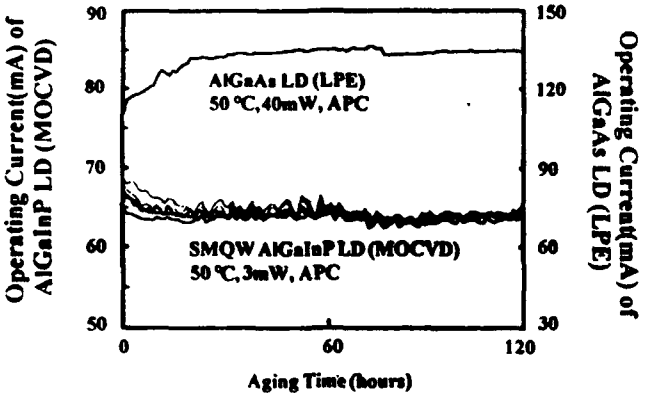

(a)

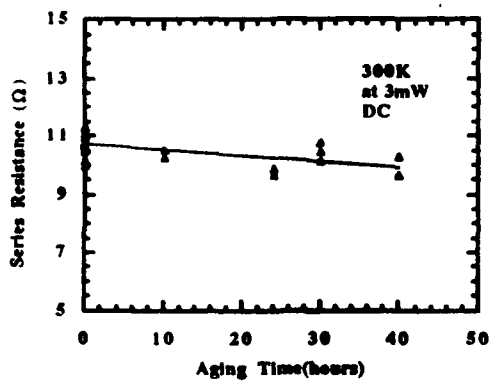

(b)

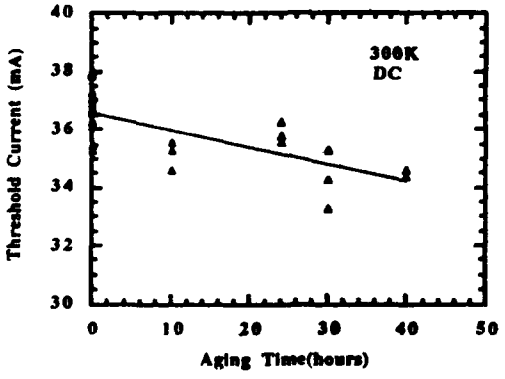

(c)

Fig. 1. Aging characteristics of GaInP/AlGaInP LDs

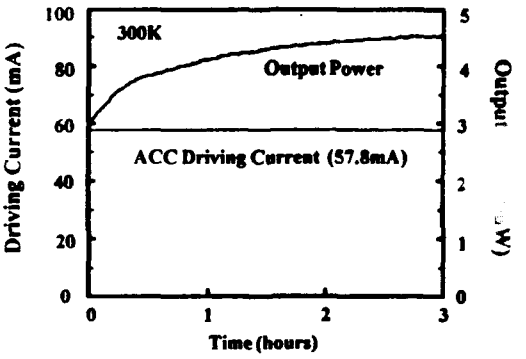

Fig. 2. Increase of the optical power with operating time at room temperature

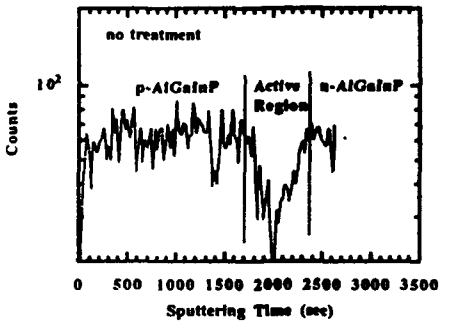

(a)

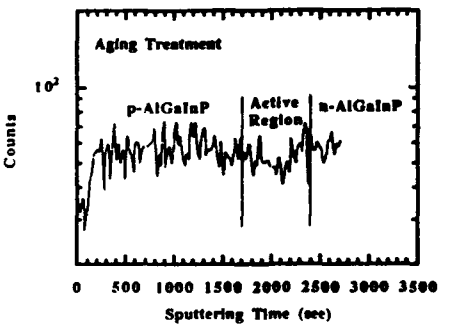

(b)

Fig. 3. Hydrogen profiles of clad and active layers before and after aging test

P9

High temperature and reliable operation of 630nm-band InGaAlP tensile-strained multiquantum-well laser diodes

Minoru Watanabe, Hatsumi Matsuura, Naohiro Shimada, and Hajime Okuda

Semiconductor Group, Toshiba Corporation, 72, Horikawa-cho, Saiwai-ku, Kawasaki 210, Japan

Abstract

High temperature and reliable operation of 635 nm tensile strained multiquantum-well laser diodes has been achieved. An output power level of 10 mW was sustainale up to 80 °C and stable operation of over 1000 hours, for an output of 5 mW, at 50 °C, was observed.

Summary

630 nm-band semiconductor laser diodes are attractive as substitutes for He-Ne lasers. We have previously reported that the operation characteristics of InGaAlP multiquantum-well (MQW) laser diodes with tensile-strained quantum wells are superior to those of conventional unstrained MQW laser diodes, and the practical development of such MQW lasers has now been achieved.[1] In this report, we describe the design of 630 nm-band tensile-strained MQW lasers for high temperature and reliable operation, and outline the optimum structure.

The tensile-strained MQW laser diodes used in this work, were prepared by low pressure metalorganic chemical vapor deposition (MOCVD) techniques, all having an MQW-separate confinement heterostructure (MQW-SCH) which consisted of 1.0 μm p and n-$In_{0.5}(Ga_{0.3}Al_{0.7})_{0.5}P$ cladding layers, two $In_{0.5}(Ga_{0.5}Al_{0.5})_{0.5}P$ confinement layers, and an MQW active region with tensile-strained InGaP wells and 4 nm $In_{0.5}(Ga_{0.5}Al_{0.5})_{0.5}P$ barriers. Si doped GaAs (100) substrates, 15° misoriented towards the [011] direction, were used.[2] These transverse-mode stabilized MQW lasers had a selectively buried ridge waveguide (SBR) structure with $\lambda/2$ coated facets, and a stripe width of 5 μm for a 600 μm cavity length.

Fig. 1 shows temperature dependence of light output power vs. continuous wave (cw) current of the lasers with (a)two and (b)four 8 nm $In_{0.38}Ga_{0.62}P$($\Delta a/a$=-0.75%) wells. At 20 °C these lased, at 633 and 635 nm, respectively, with threshold currents of 61 and 68 mA. Their characteristic temperatures, T_0, below 50 °C were found to be 55 K and 81 K, respectively. The four well (8 nm, -0.75%) lasers were found to operate up to 80 °C, whereas, the two well(8 nm, -0.75%) lasers could not operate at all above 60 °C. This indicates that increasing the well number is an effective method to improve the temperature characteristics. The lasers with three 11 nm $In_{0.36}Ga_{0.64}P$($\Delta a/a$=-0.93%) wells, fabricated to investigate the effect of strain upon operation characteristics, were found to have threshold currents as low as 49 mA at 20 °C. These lasers had a characteristic temperature

below 50 °C, of 74 K and could operate at temperature as high as the four well(8 nm, -0.75%) laser. Fig.2 shows life test data for (a)the four well(8 nm, -0.75%) lasers and (b)the three well(11 nm, -0.93%) lasers, respectively. The four well(8 nm, -0.75%) lasers have been operating stably, at 5 mW at 50 °C, for more than 1000 hours with no degradation. However, the three well(11 nm, -0.93%) lasers show signs of some degradation under the same test conditions. This is thought to be due to the fact that, in the three well(11 nm, -0.93%) case, the overall active region thickness exceeds the critical thickness value for lattice relaxation, according to the theory of Matthews et al..[3]

In conclusion, it has been found that, to improve the temperature and reliability characteristics of tensile-strained MQW lasers, an increase in well number, well width, and tensile strain within the critical thickness criteria is effective. The MQW structure with four 8 nm wells (-0.75%) was found to be optimum.

[1] M.Watanabe et al., Appl.Phys.Lett. 63,1486(1993)
[2] M.Watanabe et al., Electron.Lett. 29,250(1993)
[3] J.W.Matthews et al., J.Cry.Growth, 27,118(1974)

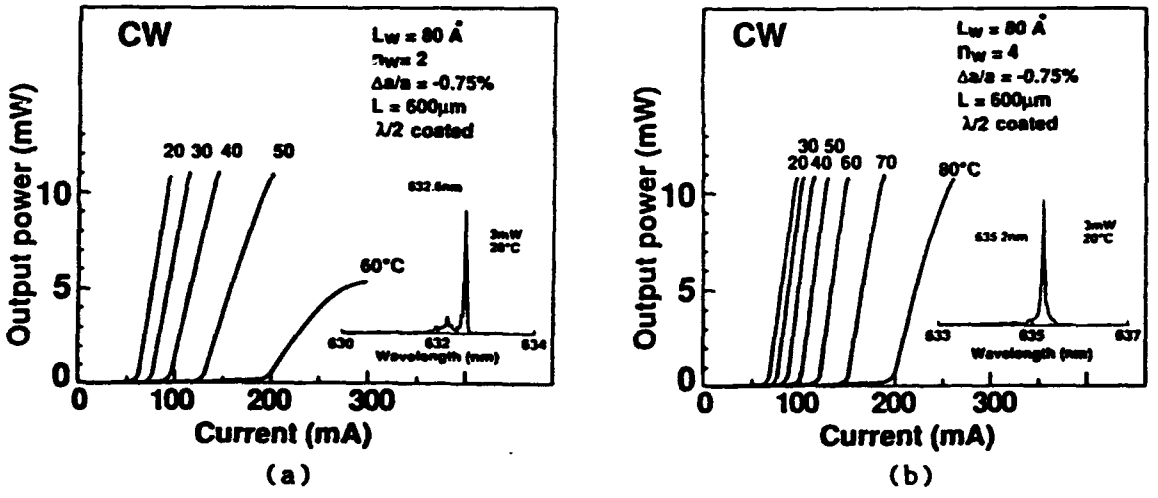

(a) (b)

Fig.1 Temperature dependence of light output power vs. cw current

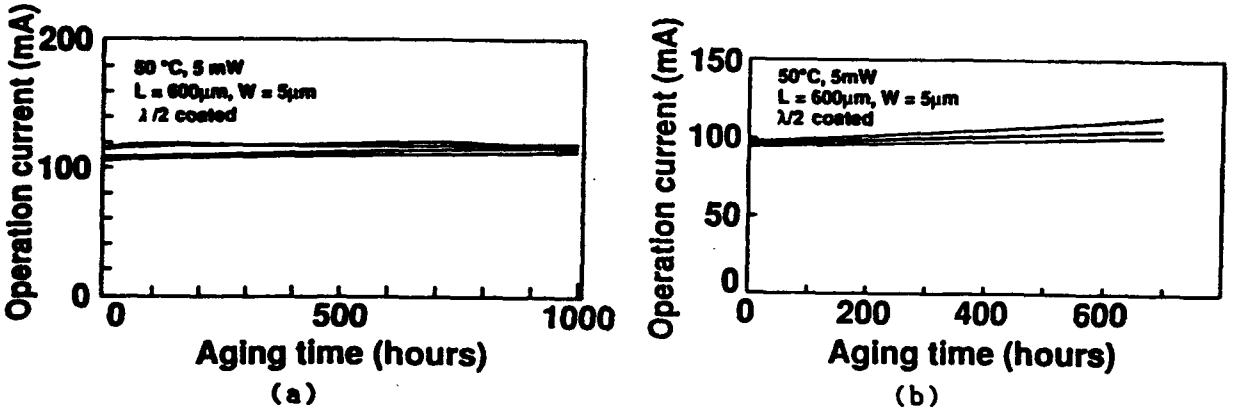

(a) (b)

Fig.2 Life test data for (a)the four well(8 nm, -0.75%) and (b)the three well(11 nm, -0.93%) lasers

P10

High Efficiency Visible Single Mode Laser Diodes

Randall S. Geels, William E. Plano, David F. Welch
Spectra Diode Laboratories, 80 Rose Orchard Way, San Jose, CA, 95134
Ph.: (408) 943-9411, Fax: (408) 943-9411

Abstract

We report low threshold and high efficiency operation of 660 nm band single mode laser diodes. The threshold currents are as low as 13 mA. External differential quantum efficiencies greater than 80% are reported.

Summary

Visible laser diodes are of considerable interest for applications in printing, optical data storage, medicine, bar code reading, and laser pointing. Recent progress includes demonstration of high temperature, high power lasers at short wavelengths[1-3] and low threshold currents in the vicinity of 670 nm.[4] For applications in battery operated devices and other low power applications it is important to minimize the operating current. In this work we report single mode visible laser diodes which simultaneously achieve low threshold current and high slope efficiency to obtain greater than 20 mW at operating currents less than 30 mA.

The visible laser epitaxial structure is grown by metal organic chemical vapor deposition (MOCVD) on a GaAs substrate. Cladding layers of AlInP surround waveguiding layers of AlGaInP. The active layer consists of a single compressively strained InGaP quantum well. The use of a single quantum well minimizes the threshold current and the use of compressive strain also serves to decrease the threshold current and insure high efficiency operation. Also, the use of AlInP cladding layers maximizes the carrier confinement in the active region. Material characterization is performed by fabricating broad area lasers and testing them under cw operation. Threshold current densities in the 200-250 A/cm^2 range are routinely obtained. External differential quantum efficiencies (η_D) are as high as 83%.

Index guided single mode visible laser diodes are fabricated and mounted junction side down onto heatsinks for cw testing. Both uncoated and AR/HR coated laser diodes were tested. The AR/HR coatings consisted of an approximately 10% AR coating on the front and a 90% HR coating on the rear facet. Fig. 1 shows the light current characteristics of an AR/HR coated 250 μm laser diode. As shown in the inset, the lasing wavelength is 662 nm. The threshold current is 13 mA and the slope efficiency is 1.4 W/A which corresponds to an external differential quantum efficiency of 74%. For a longer, 500 μm cavity device the threshold current increases to 22 mA and the slope efficiency decreases to 1.2 W/A as shown in Fig. 2. Also shown in Fig. 2 is the total output power vs current of an uncoated 500 μm cavity device from the same location in the wafer. As is evident from the figure, the external efficiency before coating is 83%, whereas after coating the efficiency is decreased. The parallel far field pattern from a 500 μm cavity laser diode is illustrated in Fig. 3. The far field is well behaved with no significant beam steering or broadening. The far field pattern of the 250 μm cavity lasers is similarly well-behaved. The temperature characteristics of the lasers are shown in Fig. 4.

In summary, we report low threshold visible single mode lasers with threshold currents as low as 13 mA under room temperature cw operation. External differential efficiencies greater than 80% are indicated by uncoated test data.

References

[1] R.S. Geels, D.F. Welch, D.P. Bour, D.W. Treat, and R.D. Bringans, "Low threshold, high power 624 nm laser diodes," *IEEE LEOS Annual Mtg*, paper SCL9.2 San Jose, Nov., 1993.

[2]T. Tanaka, H. Yanagisawa, S. Yano, and S. Minagawa, "Tensile strained QW structure for low-threshold operation of short-wavelength AlGaInP LDs emitting in the 630 nm band," *Electron. Lett.*, Vol. 29, p. 606, 1993.

[3]M. Watanabe, J. Rennie, M. Okajima, and G. Hatakoshi, "High temperature (77°C) operation of 634 nm InGaAlP multiquantum-well laser diodes with tensile-strained quantum wells," *Appl. Phys. Lett.*, Vol. 63, p. 1486, 1993.

[4]C. Anayama, H. Sekiguchi, M. Kondo, H. Sudo, T Fukushima, A. Furuya, and T. Tanahashi, "One-step-metalorganic-vapor-phase-epitaxy-grown AlGaInP visible laser using simultaneous impurity doping," *Appl. Phys. Lett.*, Vol. 63, p. 1736, 1993.

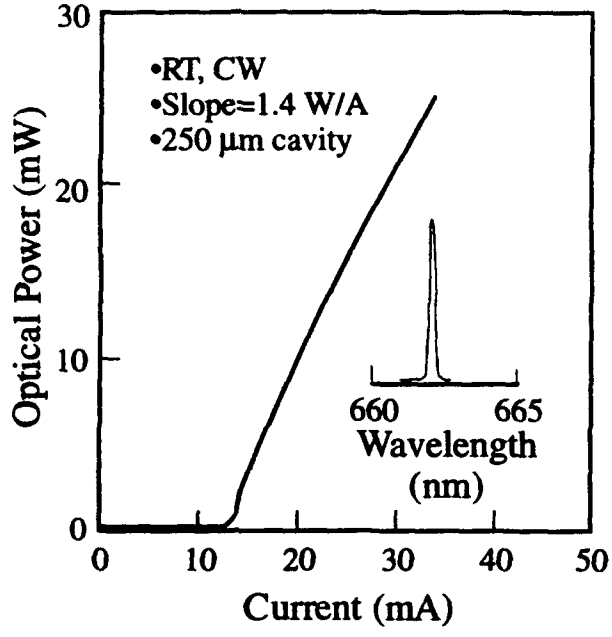

Figure 1 Light-current characteristics of 250 μm laser.

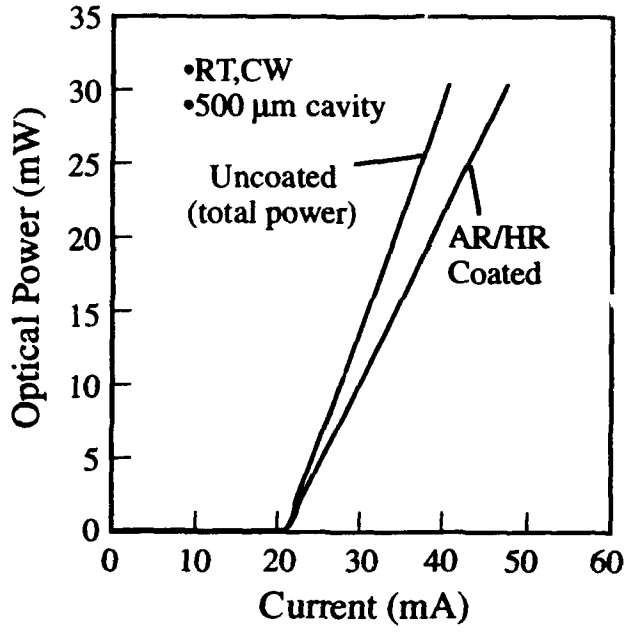

Figure 2 Light-current characteristics of 500 μm laser

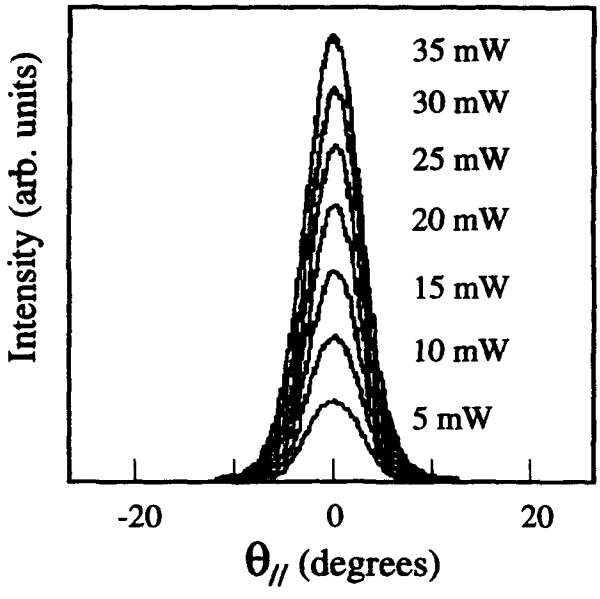

Figure 3 Far field pattern from 500 μm laser.

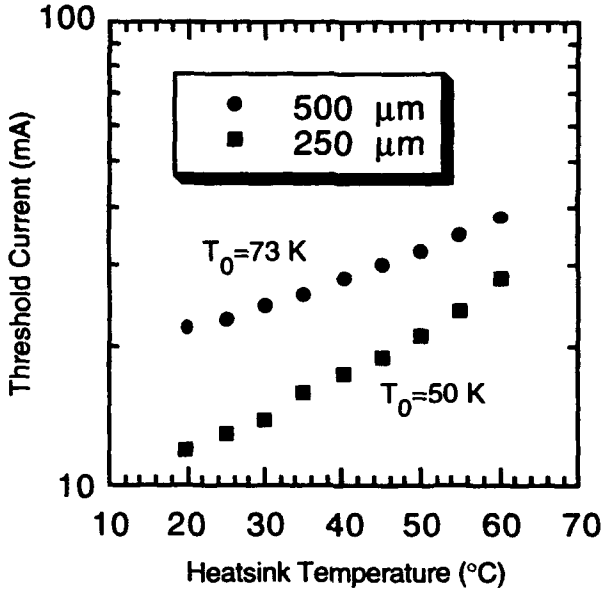

Figure 4 Threshold current vs temperature.

P11

IMPROVING PULSES FROM 2-CONTACT SELF-PULSATING DFB SEMICONDUCTOR LASERS

A.J. Lowery, P.C.R Gurney
Photonics Research Laboratory, Department of Electrical and Electronic Engineering
The University of Melbourne, Parkville, VIC 3052, Australia

Abstract: We propose that short pulses from a self-pulsating DFB laser will be shortened and stabilised by optical filtering and optical feedback. Simulations predict 60 ps pulses at 2.5 GHz with a contrast ratio >10 dB.

Introduction: Möhrle *et al.* [1] have measured multi-mode self-pulsations in 2-contact 1535-nm DFB lasers when the contact current densities were unequal. The pulsations were at around 3 GHz, making them useful for clock pulses in Gbit/s optical transmission systems. Similar pulsation have been observed by Phelan *et al.* [2] in three-contact lasers. Bandelow *et al.* [3] have modelled self-pulsating in 2-contact lasers using a single-mode model.

In this paper, we show that the pulsations are a result of mode-hopping between an unstable asymmetric mode [4] and a non-dominant symmetrical mode [4] using a detailed *multi-mode* laser model [5]. We have found that the rate of pulsation can be increased by increasing the current inhomogeneity, which is an advantage over single-contact devices. Furthermore, the strongest output pulsations will occur at the facet with the largest current density, unlike single-contact devices where strong pulsations appear at one or other facet randomly. We show that three improvements can be made to the device as a clock source. These are: (a) to antireflection (AR) coat the laser facets to achieve short pulse generation over a wide operating range of currents; (b) to filter the output pulsations in order to achieve shorter output pulses with an increased contrast ratio; (c) to feed back a small proportion of the filtered output to the laser to reduce timing jitter.

Results: We simulated a 1550-nm uniform grating AR-coated DFB laser with a bulk active region and a Bragg coupling of 4.0 using the transmission-line laser model (TLLM) [5]. The front contact was driven at 60 mA and the rear contact at 45 mA. Strong pulsations (Fig.1a) appeared at the front facet, and weak pulsations at the rear facet (Fig.1b). The repetition frequency was 2.5 GHz and could be increased by increasing the contact current difference.

The method of pulse generation is similar to that in single-contact devices driven at high currents [5]. Analysis [4] shows that a single-contact device can have an *unstable* asymmetric mode and a *stable* but higher-threshold symmetrical mode, when biassed at high currents. Thus neither mode is indefinitely stable, leading to self-pulsation [5]. In the 2-contact device the asymmetric mode is favoured at lower total currents because of the unequal current injection densities. Our simulations show that a high-power pulse will rapidly reduce any asymmetry in the carrier density, and so is quickly quenched. The device will then lase in the symmetrical mode until an asymmetric mode regrows due to the current density asymmetry.

Our simulations predict pulsations for a wide range of current combinations, unlike in the uncoated device in [1]. However, if 1% facet reflectivities were used, the number of current combinations causing self-pulsation decreased considerably. This could explain why the currents for self-pulsation were so critical in [1], and shows that AR coating is desirable.

The optical spectrum from the front facet (Fig.2) shows a heavily chirped lower-frequency mode and a narrower upper-frequency mode, as seen in [2]. The large chirping suggests that the lower frequency mode is a train of very short pulses. Thus, the short pulses can be recovered by optical band-pass filtering of the lower mode. The front facet output after a 25-GHz FWHM filter (Fig.3) shows an improved contrast ratio, and pulse shortening to approx. 60 ps from 130 ps.

Because the low-frequency (asymmetric) mode grows from a low power, its timing will be influenced by noise. Thus, injection locking should improve the timing jitter. Fig.4 shows the RF spectra of the laser without feedback, and with feedback from the filtered output (0.01% with

266 ps delay). The width of the spectral peaks is reduced by the feedback, suggesting a reduced amplitude and/or timing jitter. Surprisingly, the repetition frequency is also reduced.

Conclusions: We show that 2-contact DFB lasers can be used as stable pulse sources and that their characteristics can be improved by AR coating, filtering the output, and feeding back a small proportion of the filtered output to the laser.

We acknowledge the support of the Australian Photonics Cooperative Research Centre.

[1] MÖHRLE, *et al.*: *Photon. Technol. Lett.*, 1993, **4**, pp.976-978
[2] PHELAN,P., *et al.*: *IEE Proc. J: Optoelectron.*, 1994, **30**
[3] BANDELOW,U.,*et al.*: *Photon. Technol. Lett.*, 1993, **4**, pp.1176-1179
[4] TROMBORG,B., *et al.*: *Photon. Technol. Lett.*, 1992, **28**, pp.985-988
[5] LOWERY, A.J., *Electron. Lett.*, 1993, **29**, pp.1852-1853

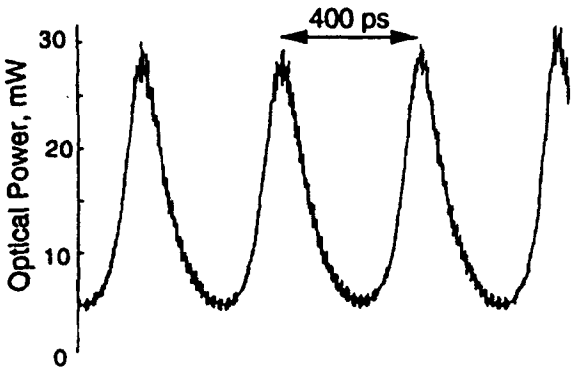

Fig.1a: *Optical output from front facet.*

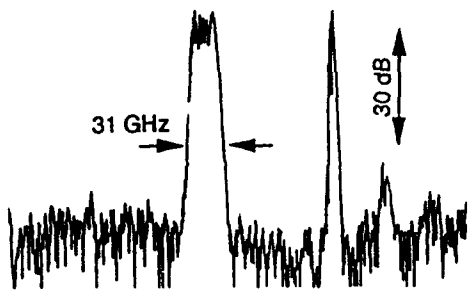

Fig.2: *Optical spectrum from front facet.*

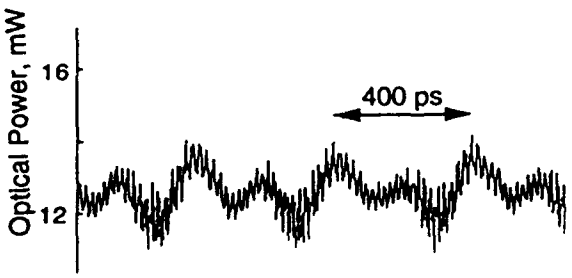

Fig.1b: *Optical output from rear facet.*

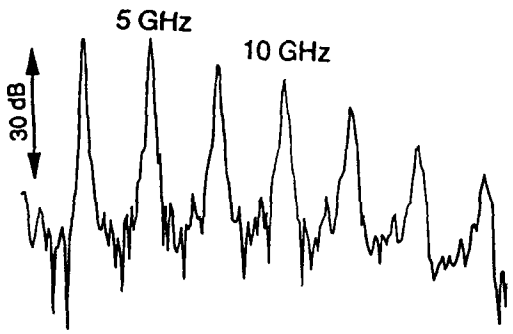

Fig.4a: *RF spectrum without feedback.*

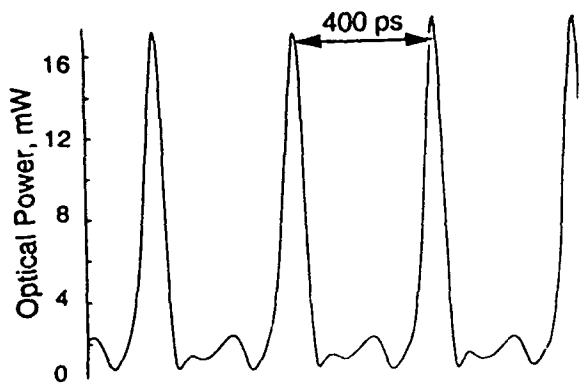

Fig.3: *Filtered front facet output.*

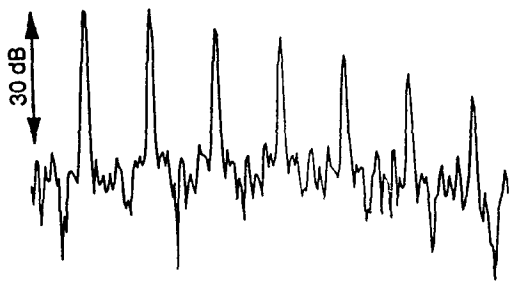

Fig.4b: *RF spectrum with feedback.*

P12

Temperature Dependent Efficiency and Modulation Characteristics of Al-free 980 nm Laser Diodes

R. F. Nabiev, E.C. Vail, C.J. Chang-Hasnain

E.L. Ginzton Laboratory, Stanford University
Stanford, CA 94305-4085
Tel: (415)725-8426

Abstract: Temperature dependent efficiency and modulation characteristics of laser diodes of various design are analyzed using self consistent carrier transport analysis including stimulated emission.

Introduction. InGaAs/InGaAsP/InGaP 980 nm lasers are promising for pumping optical fibers and as sources for local area networks. High temperature, high efficiency, and high modulation frequency operation are important for these applications. The increase of threshold current in quantum well (QW) lasers at higher temperatures has been attributed to the decrease of differential gain [1, 2], recombination in separate confinement heterostructure (SCH) regions [2]; and the decrease of differential efficiency to the leakage of carriers over barriers (visible lasers and 1.3 μm InP based lasers) [3,4] and absorption in the SCH region [2]. The processes of band filling [5] and carrier transport in SCH region [6, 7] have been shown to be important for high speed operation. In this paper, we present for the first time, to our knowledge, an analysis of temperature behavior of efficiency and modulation properties of 980 nm lasers of various designs. The analysis and general conclusions should be applicable for lasers operating at other wavelengths.

Model. Carrier transport across SCH QW laser is governed by the continuity equations for electron (*e*) and hole (*h*) currents and the Poisson equation for electrostatic potential. Self-consistent solution of these equations based on Scharfetter-Gummel numerical scheme [8] results in distributions of carriers, electric field, and *e*- and *h*- currents in the laser structure. Spontaneous recombination rate and optical gain in strained QW for different pumping levels are calculated using 4x4 Hamiltonian for complex valence band structure [9]. Stimulated emission rate is included in the continuity equations as well. Our calculations show that optical gain scales linearly with quasi-Fermi level separation. We then obtained the laser modulation response using small signal analysis based on the above equations. Thus, the effects the carrier transport and carrier filling in the SCH region are inherently incorporated. Carrier capture and escaping processes are presently not included and will be incorporated at the time of presentation.

Results and discussion. Fig. 1 shows calculated band diagrams of lasers with SCH single QW (SQW), linearly graded index (GRIN) SCH and 5QW structures at high current injection (above lasing threshold). The SCH laser structures include doped InGaP claddings (E_g=1.85 eV), quaternary SCH region of width W = 0.2 μm (E_g=1.458 eV), and 8 nm wide InGaAs QWs. The conduction band/valence band off-set ratio is chosen to be $\Delta E_c/\Delta E_v = 0.65/0.35$. Because of the high energy barrier seen by the minority carriers (see Fig. 1), their leakage currents are small even at 450 K (see Fig. 2). As the quasi-Fermi levels of electrons f_e and holes f_h approach the corresponding bands of the SCH region, the increased carrier density in SCH region causes increased absorption of light. In the SQW laser, free carrier absorption in the SCH and QW regions has a strong temperature dependence (Fig. 3a) whereas GRINSCH structure demonstrates much less absorption. We believe that this absorption is the main reason for the reduction of the differential efficiency of SQW laser at high temperature (Fig. 3b).

The modulation response of SCH SQW laser is determined by diffusion in SCH region. Laser with a wider SCH region (W=0.4μm) has considerably narrower bandwidth (Fig. 4) which agrees well with experimental results [10]. GRINSCH laser shows faster response which can be attributed to the enhanced drift current component in SCH region due to the residual built-in electric field [3]. A SQW structure with highly doped SCH region (doping ends in the QW) shows similarly fast response as the GRINSCH laser because carriers need to diffuse only over QW width. But the free carrier loss is increased in this case. The 5QW laser has even better modulation characteristics which is caused by higher differential gain and less distance for holes to diffuse to the first QW from P-cladding. At high temperatures, the modulation bandwidth is considerably reduced, mainly because of increased threshold gain and the decrease of differential gain (Fig. 4).

In conclusion, the decrease of the differential efficiency of 980 nm laser diodes with temperature is found to be caused by an increased modal loss attributed to the free carrier absorption, while modulation characteristics are determined mainly by drift-diffusion in SCH region. At high temperatures modulation bandwidth is reduced because of the decrease in differential gain. GRIN SCH lasers show superior efficiency and modulation behavior at high temperatures.

References:
1. Y. Zou et al. IEEE J. of Quantum Electron. 29, 1565 (1993)
2. E.C. Vail et al. Paper FA2 in *Integrated Photonics Research*, 1994, pp. 168-170.
3. D.P. Bour et al. IEEE J. of Quantum Electron. 29, 1337 (1993)
4. D.Z. Garbuzov et al. Sov. Phys. - Semiconductors, 25, 560 (1991)
5. B. Zhao et al. Appl. Phys. Lett. 62, 1200 (1993)
6. T.C. Wu et al. Appl. Phys. Lett. 63, 441 (1993)
7. N. Tessler et al. IEEE J. of Quantum Electron. 29, 1586 (1993)
8. D. L. Scharfetter, H.K. Gummel. IEEE Trans. on Electron Dev., ED16, 64 (1969)
9. D. Ahn et al. J. Appl. Phys. 64, 4056 (1988). S. L. Chuang. Phys. Rev. B 43, 9649 (1991)
10. R. Nagarajan et al. Electron. Lett., 29, 1688 (1993)

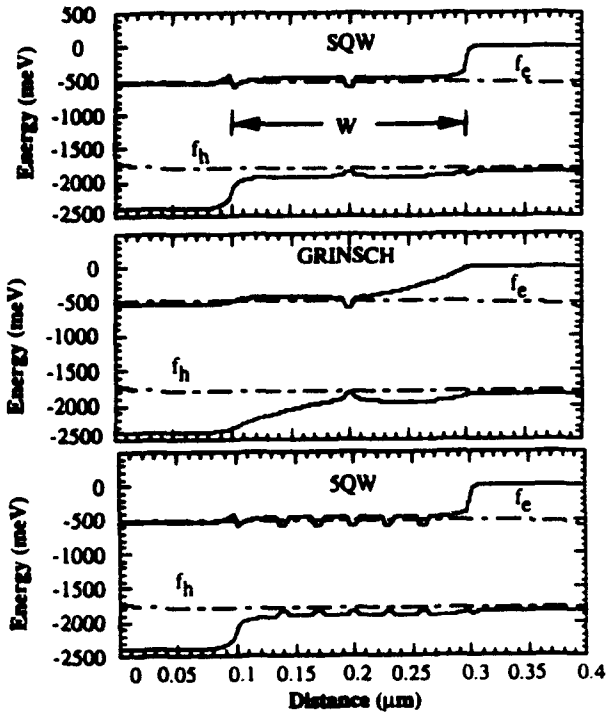

Fig. 1. Band diagrams of SCH structures above lasing threshold.

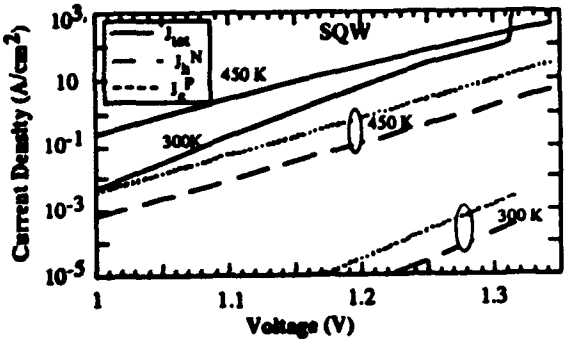

Fig. 2. Current-voltage characteristics of SCH SQW structure at 300 and 450 K. The jumps in curves for total current J_{tot} correspond to lasing. Leakage currents of minority carriers are J_e^P and J_h^N in P- and N-type claddings, respectively.

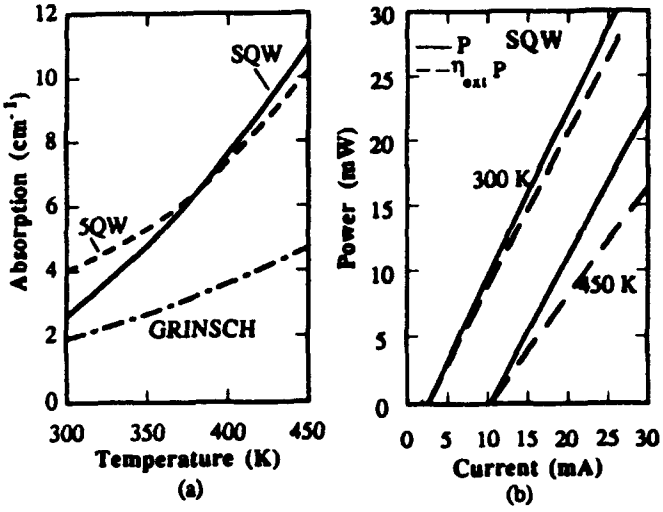

Fig. 3. (a) Temperature dependence of the free carrier absorption in SQW, GRINSCH and 5QW lasers. Cross sections of absorption are 3.10^{-18} and 7.10^{-18} cm^2 for *e* and *h*, respectively.
(b) Light-current (LI) characteristics of SCH SQW laser. Laser area is 400x5 μm^2. Mirror loss is 30 cm^{-1}. Solid and dashed lines show the LI curves without and with inclusion of free carrier absorption.

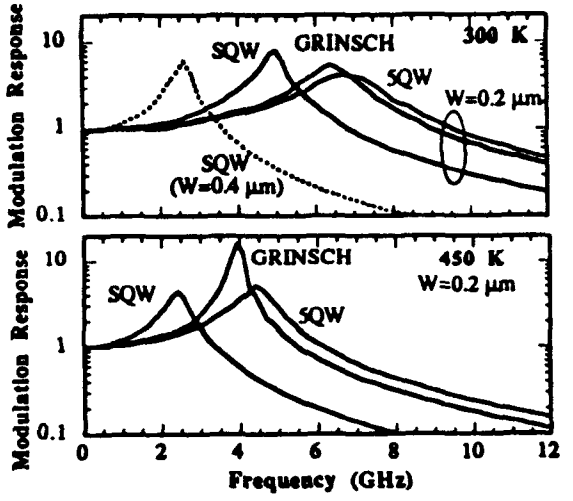

Fig. 4. Modulation response characteristics for SQW, GRINSCH and 5QW lasers at 40 mW optical power at 300 and 450 K.

P13

Generation of High Repetition Frequency Subpicosecond Pulses at 1.535 μm by Passive Mode-Locking of InGaAsP/InP Laser Diode with Saturable Absorber Regions Created by Ion Implantation

A.G. Deryagin, D.V. Kuksenkov, V.I. Kuchinskii, E.L. Portnoi, I.Yu. Khrushchev*, J. Frahm†
A.F.Ioffe Physico-Technical Institute, Polytechnicheskaya 26, St.Petersburg 194021 Russia.
* Institute of General Physics, Vavilova 38., Moscow, 117942 Russia.
† WITEGA Laboratories, Berlin 12489 Germany

Abstract. We report obtaining optical pulses 0.64 ps wide at a 104 GHz repetition rate from a passively mode-locked InGaAsP/InP laser diode. The laser emission spectrum corresponds to the amplification band of erbium-doped fiber amplifiers.

In our experiments, we use commercial InGaAsP/InP lasers with a cavity length of about 400 μm. The lasers are implanted into both facets by O^{3+} ions with the energy of 17 MeV, corresponding to the average penetration depth of 10 μm. Such a technique was previously shown to form regions of fast saturable absorber, necessary for mode locking [1]. Here, we investigate laser samples implanted with different dosages. The optimal implantation dosage value is found to be $\Phi=5\times10^{12}$ cm^{-2}. During the first several hours of operation, we have observed a gradual increase in the average output power due to partial annealing of the defects created by the ion implantation. During approximately 50 hours of subsequent operation under cw pumping in the cource of measurements, no significant change in the laser parameters is detected. The implantation is also found to cause a red shift of the lasing wavelength of about 5-10 nm, so for our experiments samples initially lasing at 1.525-1.53 μm are chosen.

Pure mode locking operation is shown to exist within a limited range of pumping current values above the threshold. Near the threshold, the laser diode operates in a free-running cw regime (Fig.3A). The transition to a mode locked regime is accompanied by the appearance of a modal chirp, caused by self-phase-modulation in the gain region and increasing in value with the pumping current (Fig. 3B,C). Self-starting of mode locking manifests itself also in a kink in the derivative *dP/dI* of the light-current characteristic (Fig.1). Cooling the sample down enables one to observe another kink in this curve, at a higher current value, corresponding to the transition to a combined mode-locking/Q-switching regime (not shown in Fig.1). The results described here are in contradiction with some of the predictions of the theory [2], which we believe to be due to the high optical density of the saturable absorber in our case. It should be noted also that the lasing spectrum becomes visibly assymetric as mode locking develops (Fig. 3D). This fact, along with the implantation-induced red shift of the emission wavelength, can be explained by the absorbtion saturation being easier for longer wavelengths.

The autocorrelation profile of the pulse train is shown in Fig. 2. The repetition rate of 104 GHz and the trace width of 1 ps for an individual pulse are measured. Assuming the pulse shape to be sech^2, one can calculate the pulse duration as 0.64 ps. The autocorrelation contrast is about 5 in the pumping current range of 150-170 mA, indicating that the mode locking is not complete. The spectrum width is 6.2 nm, giving $\Delta\tau\Delta\nu = 0.51$. A considerable up-chirp in the instanataneous frequency of the emission pulses is detected. The origin of this chirp may be strong group velocity dispersion in the (bulk) active region of the samples, as well as fast gain nonlinearities, eg dynamic carrier heating effect. Further compression of the pulses should be possible anyway in a medium with a properly chosen dispersion.

Amplification of the signal from a passively mode-locked laser diode in a two-cascade erbium-doped fiber amplifier produces 0.8 ps-long, apparently transform-limited optical pulses with a peak power of about 3.5 W. The soliton propagation regime is demonstrated in an auxiliary 1.3 km piece of fiber.

[1] E.L.Portnoi, A.V.Chelnokov, Digest, 12th IEEE Semicond. Laser Conference, pp.140-1 (1990)
[2]J. Paslaski, K.Y. Lau, Appl. Phys. Lett., V. 59, No.1, pp. 7-9 (1991).

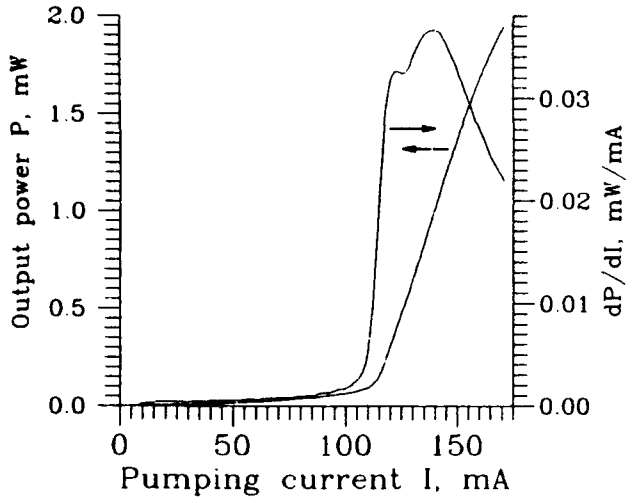

Fig.1 The L-I characteristic and its derivative at heat sink temperature T=16° C.

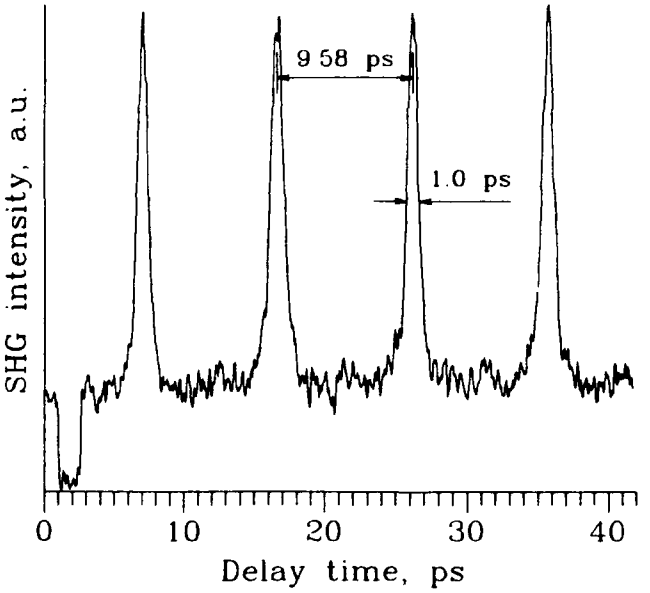

Fig.2 Autocorrelation trace of the optical pulses, I_p=150 mA, T=16° C.

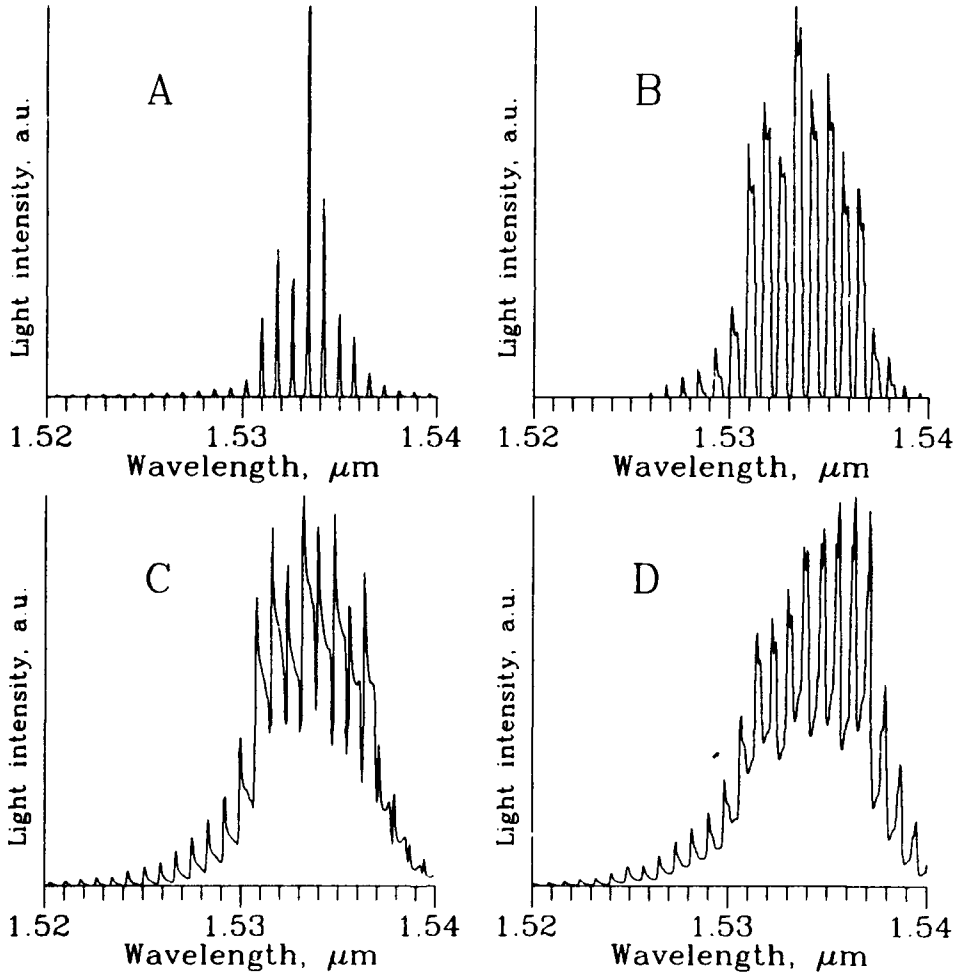

Fig.3. Laser spectrum evolution with the increase of the pumping current; I_p=125 mA (A); 135 mA (B); 145 mA (C) and 170 mA (D); T=16° C.

P14

Dynamics of injection locking of mode locked semiconductor lasers

M. Margalit, M. Orenstein, G. Eisenstein and V. Mikhaelshvili
Department of Electrical Engineering
Technion
Haifa, 32000,Israel
Tel. 972-4-294696; Fax: 972-4-323041

Abstract

We report the first observation of synchronous injection locking of a mode locked semiconductor laser. Locking ranges, both in the time and in the frequency domains, were measured, as well as noise parameters. Experimental results were compared to a model, with an emphasis on possible instabilities.

Summary

Injection locking of Continuos Wave (CW) semiconductor lasers was thoroughly studied both as a mean of externally stabilizing (fixing) an optical lasing frequency[1] and as a generic source for interesting nonlinear dynamics and instabilities in the optical regime[2]. On the other hand, mode locked lasers typify a unique class of infinite dimensional oscillators, with the possibility of displaying their own wide range of dynamic behavior[3,4]. Past research has noted the similarity between injection locking, mode locking, and phase locking in semiconductor laser arrays[5,6]. However the dynamic behavior of an integrated scheme comprised of a synchronous coherently injected input and a mode locked laser has not been addressed yet. This integration is of possible practical implication in the field of fast synchronization of optical clocks and optical signal regeneration and is of a basic interest because of the rich variety of expected dynamic behavior

We model this scheme by employing a unification of models describing mode locking[3] and injection locking[1]. The set of equations describing the dynamics of a unidirectional coupling of two mode locked lasers was then solved numerically to track the evolution of the pulse. When the coherent injected signal was turned on, the mode locked operation of the slave semiconductor laser was enhanced (narrower pulse), and the laser parameters were pulled towards those of the injected pulse. Above a critical coupling level, instability and pulse breaking were obtained (Figs. 1,2).

These effects were confirmed experimentally (Fig 3). An actively mode locked laser was based on extended cavity InGaAs/GaAs quantum well diode laser, operating near 980nm. A mode locked Ti/Sapphire laser served as the source for the low intensity injected signal. The latter, coherently locked the operation of the mode locked diode laser (Fig. 4 and 5). Possible incoherent interactions were ruled out by using proper wavelength and polarization discrimination. Locking ranges of: 150 psec. in the time domain; 1 nm of optical frequency and 2 KHz of modulation frequency were measured.

In summary, we present an analysis of the dynamic behavior of a mode locked semiconductor laser with synchronous coherent pulse injection. Both model and experimental results confirm, the significant effects on the operation of mode locked lasers while being subjected to the locking interaction. The limitations on the temporal and frequency locking range as well as the inherent instabilities at the high coupling regime will be discussed.

References
[1] R. Lang, IEEE. JQE. Vol. QE-18 p976, 1982.
[2] H. Zeghlache, V. Zehnl'e, Phys. Rev. A. Vol. 46 p6015, 1992.
[3] H. Haken, M. Pauthier, IEEE. JQE. Vol. QE-4 p454, 1968.
[4] H. A. Haus , Y Silberberg, IEEE. JQE. Vol. QE-22 p325, 1986.
[5] P. A. Morton, R. J. Helkley, J. E. Bowers, IEEE, JQE. Vol. QE-25 p2621, 1989.
[6] S.S. Wang, H. G. Winful, APL. Vol. 52 p1774, 1988.

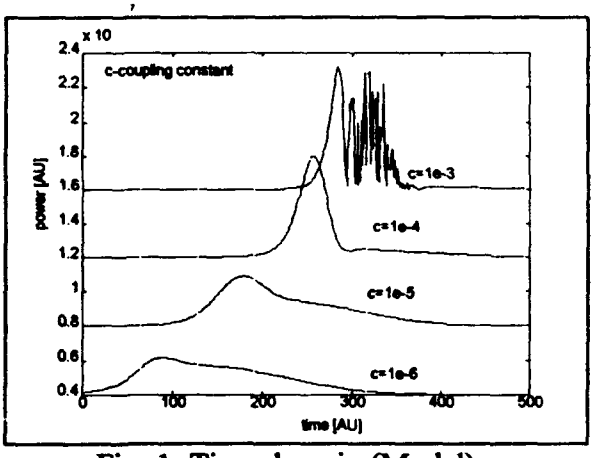

Fig. 1. Time domain (Model)

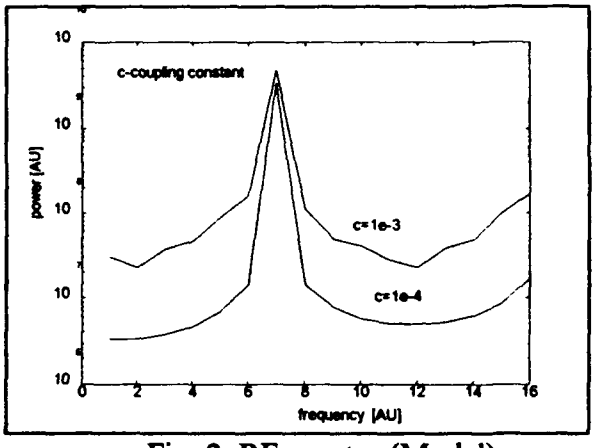

Fig. 2. RF spectra (Model)

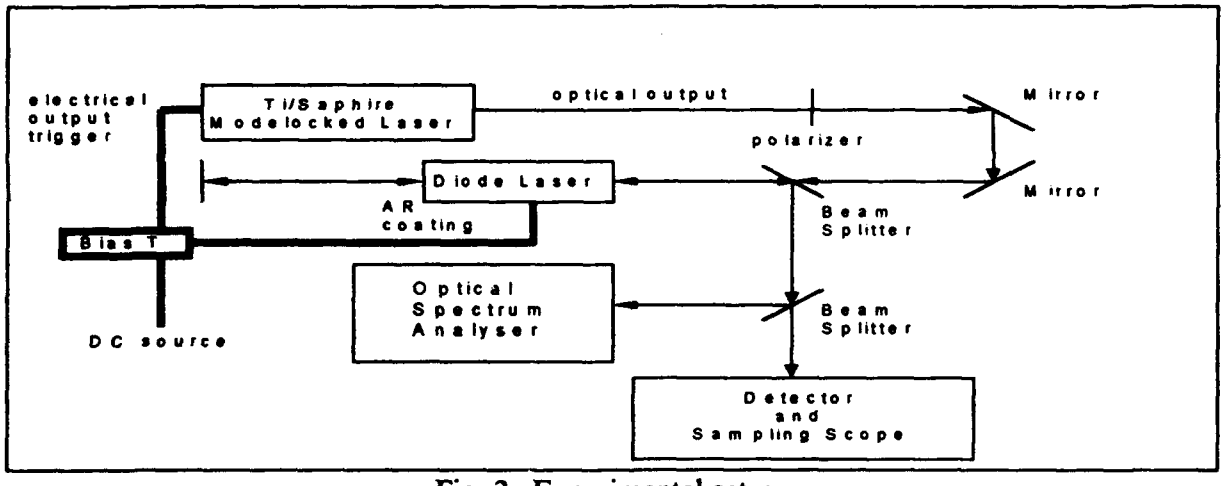

Fig. 3 Experimental setup.

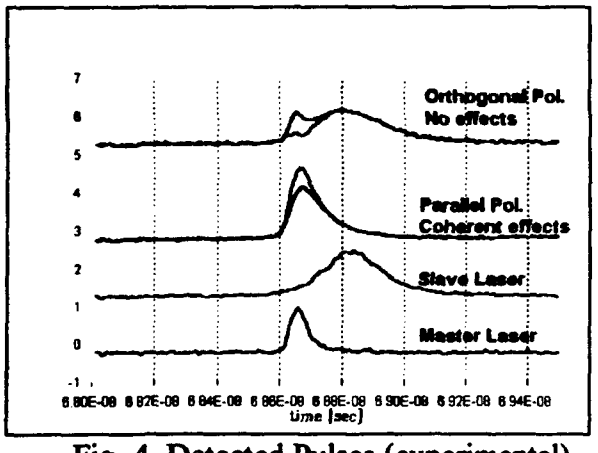

Fig. 4. Detected Pulses (experimental)

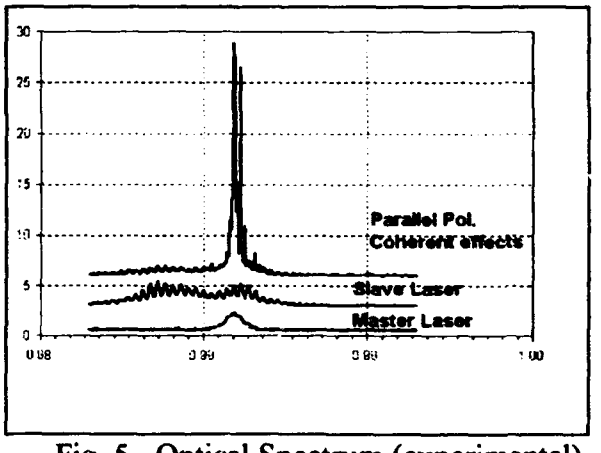

Fig. 5. Optical Spectrum (experimental)

P15

High-Frequency Operation of SQW Diode Laser Modulated by Dual Optical Confinement Factor and Pumping Current Density Control.

S.A.Gurevich, I.E.Chebunina, M.S.Shatalov, G.E.Shtengel and V.B.Gorfinkel*

A.F.Ioffe Physical-Technical Institute of Russian Academy of Sciences,
26 Politechnicheskaya st., St. Petersburg, 194021, Russia
**University of Kassel, 73 Wilhelmshöher Allee, D-34121, Kassel, Germany*

Abstract. We demonstrate high-frequency operation of AlGaAs/GaAs SCH SQW four-terminal ridge-guide diode laser modulated by dual optical confinement factor and pumping current control. 20 ps switching time was observed at 3 mW output power.

Recently, there has been considerable interest in dynamic behaviour of diode lasers governed not by pumping current variations but rather by controlling the optical gain [1], photon lifetime [2] and optical confinement factor [3]. The dual modulation schemes based on simultaneous variations of these parameters in combination with pumping current were considered as well [4]. These new modulation techniques were shown theoretically to afford considerable expansion of laser modulation bandwidth when compared with that corresponding to conventional direct modulation (DM). In this paper we report on high-speed operation of a diode laser modulated by dual governing of optical confinement factor and pumping current density.

The laser structure studied is shown in Fig.1. This is AlGaAs/GaAs SCH SQW four-terminal ridge-guide laser with two electrodes for pumping (ridge top and substrate) and two side contacts for modulation by high-frequency signal. The 6-μm ridge was defined by dry-etching of two parallel grooves, each 4 μm in width, with further dielectric coating and contact metallization.

Fig.2 shows the lateral near field distributions obtained in steady-state conditions when the laser was pumped below the threshold by 30 mA current and potentials of various amplitude and polarity were applied between the side contacts and central ridge electrode. As indicated in Fig.2, forward or reverse bias at the side contacts results in considerable lateral redistribution of carrier density which is associated with the corresponding redistribution of the pumping current flow in the laser structure. Above the threshold, side contact potentials initiate the same carrier and current redistribution while the lateral optical mode shape is fixed by the ridge geometry. Under this condition, the modulating signal governs simultaneously the overlap of lateral optical mode with the carrier (gain) distribution as well as the pumping current density in the area of the mode.

The small signal analysis of this dual optical confinement factor (Γ) and pumping current density (J) modulation yields the frequency dependence of laser output response which is quite different from that commonly obtained for DM. Fig.3 shows two modulation responses calculated with the parameters characteristics for the described ridge-guide laser structure, the output power being 20 mW. The important feature is that at high frequencies (f) Γ&J response drops as f^{-1} while DM response is proportional to f^{-2}. Owing to this the 3 dB modulation bandwidth is about 70 GHz for Γ&J modulation and 10 GHz for DM.

In high-frequency experiment the laser was driven to about 3 mW output power and short electrical pulses with the amplitude of -2 V and 20 ps rise time were applied to the side contacts, resulting in reduction of the laser output power (see Fig.2). Fig.4 displays the temporal dependence of the laser output showing 20 ps switching time at the forward front. For

comparison, the period of relaxation oscillations in which the laser is involved after the end of modulating pulse is about 300 ps.

In conclusion, novel Γ&J modulation scheme was realized in four-terminal ridge-guide diode laser. Very short, 20 ps, switching time of laser emission observed at fairly low, 3 mW, output power proofs the possibility of very high-speed laser operation under Γ&J modulation. Further optimization of the laser structure and reduction of parasitics should result in practical laser capable for operation in picosecond time scale.

References.

1. V.B.Gorfinkel, et al., Int.J.of Infrared & MM Waves, **12**, n.6, p.649, (1991).
2. E.A.Avrutin et al., Appl.Phys.Lett., **63**, n.18, p. 2460, (1993).
3. V.B.Gorfinkel et al., Proc.of 20th Int. Symposium on GaAs and Related Compounds, Freiburg 1993, to be published.
4. V.B.Gorfinkel et al., Proc. of 1993 Int. Semiconductor Device Research Symposium (ISDRS), Charlottesville, Virginia, USA, Dec.1-3, 1993, p.723.

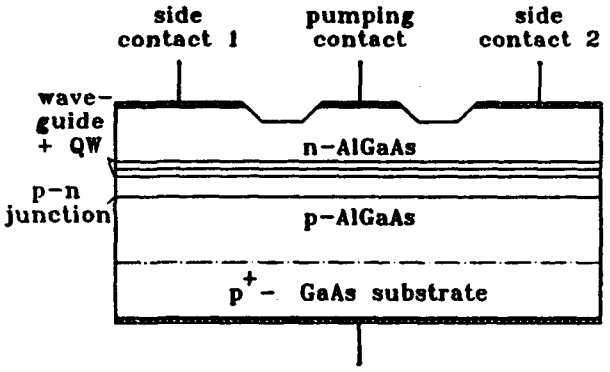

Fig.1. Schematic cross-section of the laser diode.

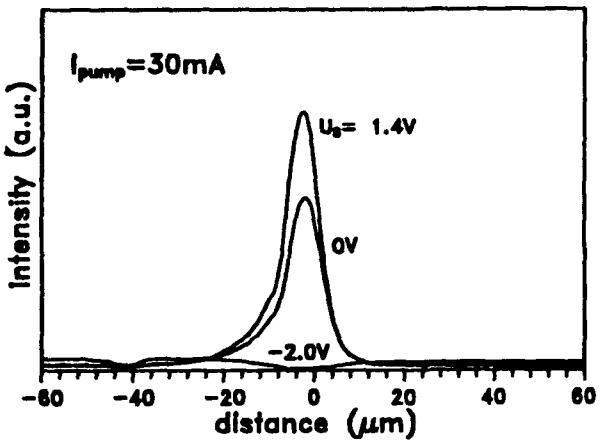

Fig.2. Near field patterns, recorded with various voltages at the side contacts.

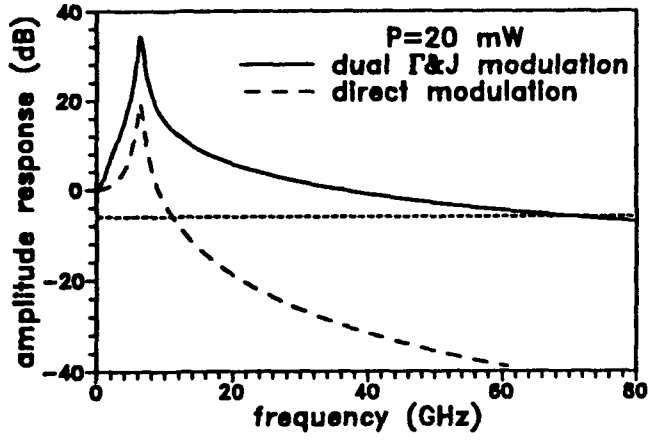

Fig.3. Calculated modulation responses.

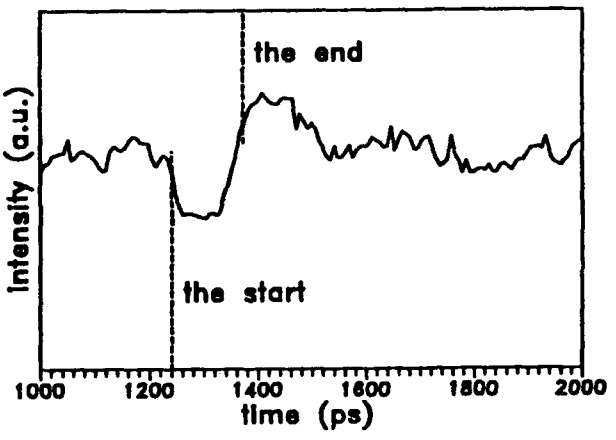

Fig.4. Streak-camera trace of the laser output. The start and the end of modulating pulse are indicated.

P16

Multi-Longitudinal-Mode Two-Dimensional Analysis of Self-Sustained Pulsating Laser Diodes

Masaaki Yuri, Toru Takayama*, Osamu Imafuji*, Hideyuki Sugiura*, Hiroki Naito*, Masahiro Kume*, Kunio Itoh*, Takaaki Baba*, and James S. Harris, Jr.**

Solid State Electronics Laboratory, Stanford University, Stanford CA 94305, USA
*Electronics Research Laboratory, Matsushita Electronics Corp., Takatsuki, Osaka 569, JAPAN

Abstract- The structural dependence of self-sustained pulsation in AlGaAs laser diodes is quantitatively analyzed for the first time, with the incorporation of the two-dimensional distribution of carriers and photons into the multi-longitudinal-mode rate equations.

Self-sustained pulsation (SSP) in laser diodes is an important phenomenon that is utilized to reduce the feedback noise due to reflected light in optical disk systems[1].

Since the lasing spectrum under SSP operation involves multiple longitudinal modes[2], it is important to employ a precise gain function for each mode, which has a great effect on transient behavior. Although many theoretical investigations on SSP have been reported, all of them assumed a single longitudinal mode and a simplified linear gain model[3]. Moreover, the time evolution of the optical field has often been ignored for simplicity. These simplifications have made difficult a quantitative simulation for a given device structure and an operating condition.

We have incorporated the two-dimensional distribution of both carriers and photons into the multi-longitudinal-mode rate equations, using a precise gain function for each mode. With this simulator, we have successfully analyzed the structural dependence of SSP in a quantitative manner for the first time. The calculation was carried out for narrow-stripe, self-aligned AlGaAs laser diodes, and the simulated results are verified experimentally in terms of the pulsation frequency and optical spectra as well as *IL*-characteristics and far field patterns.

One of the important results about the mechanism for SSP is that the oscillation of the optical field width during the pulsation enhances the saturable absorbing effect of the active layer. It is found that this process is the driving force of SSP.

In a conventional laser structure whose current blocking layer is composed of GaAs, there is a trade-off between SSP and low threshold current[3]. Our numerical analysis clearly showed that this problem can be eliminated by replacing the blocking layer with an AlGaAs layer. This structure was found to be very suitable for SSP lasers with low threshold current enabling the current width and the optical width to be controlled separately.

The principles behind the simulation and the approaches to design the SSP lasers will be discussed in detail along with experimental results.

[1] S.Matsui et al., Appl. Phys. Lett., 43, p.219, 1983
[2] S.Yamashita et al., IEEE J. Quantum Electron., 25(6), p.1483, 1989
[3] M.Yamada, IEEE J. Quantum Electron., 29(5), p.1330, 1993

** on leave from Electronics Research Laboratory, Matsushita Electronics Corp., Takatsuki, Osaka 569, JAPAN

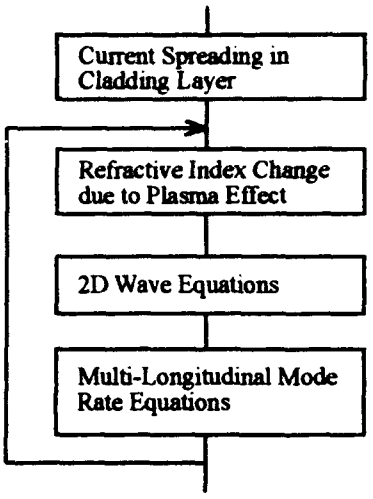

Fig. 1 Flow diagram of our numerical approach.

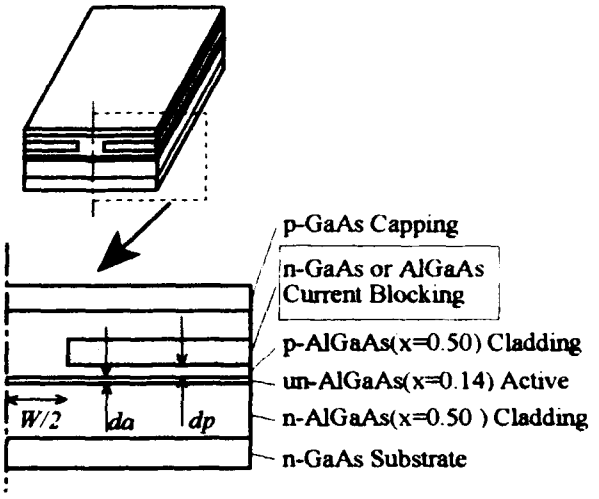

Fig. 2 Schematic diagram of the device structure.

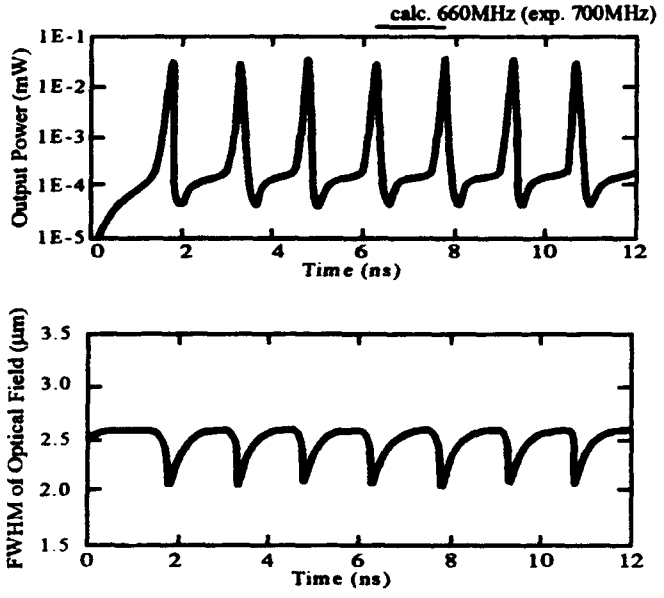

Fig. 3 Calculated pulsation of output power and FWHM of the optical field. (x_B=0.60, I=30mA)

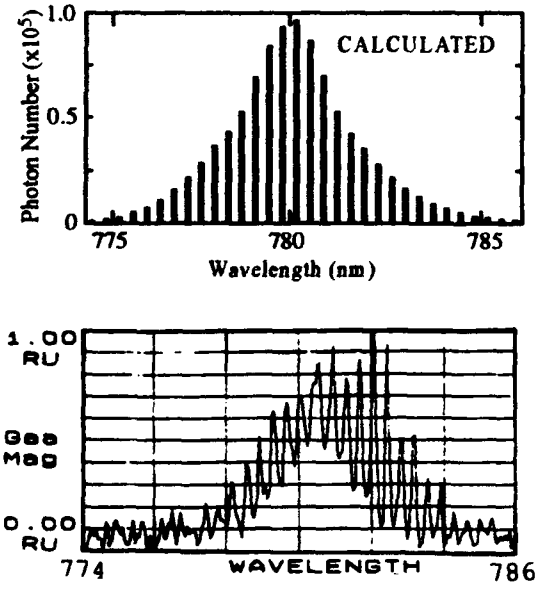

Fig. 4 Calculated and experimented lasing spectrum during the pulsation.

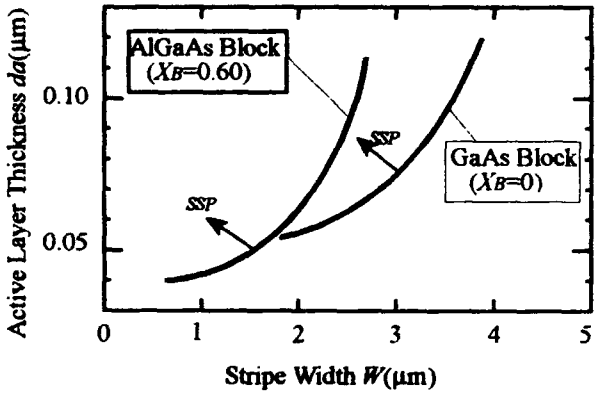

Fig. 5 Calculated structural dependence of the pulsation. An AlGaAs current blocking layer enables a thinner active layer to provide the pulsation condition.

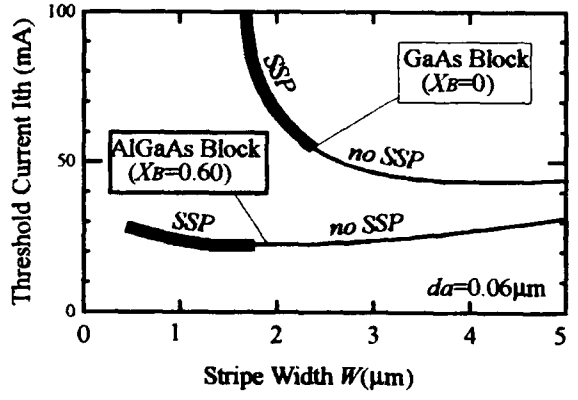

Fig. 6 Calculated threshold current versus stripe width. An AlGaAs current blocking layer provides much lower *Ith* in the pulsation region than a GaAs one.

P17

Modelocking of Low Threshold VCSEL with Pigtailed Fiber Resonator

U. Fiedler, E. Zeeb, K. Panzlaff, C. Jung, K.J. Ebeling
University of Ulm, Dept. of Optoelectronics, Albert-Einstein-Allee 45,
89081 Ulm, Germany

Abstract. *We have generated 24 ps pulses using a modelocked VCSEL with a fiber optic resonator. CW threshold current of the modelocking configuration is as low as 1.8 mA. The timing jitter of the pulses remains below 1 ps.*

Optical and electrical gain switching experiments [1] show the potential of vertical cavity surface emitting laser diodes (VCSEL) for short pulse generation but impose a relatively large jitter on the pulses [2]. We use sinusoidal modulated VCSEL to demonstrate a new technique of modelocking in the compound system of a short cavity cw-lasing VCSEL and an fiber optic external resonator and show that the coupled resonator oscillates on quasi equidistant modes even though the reflectivity of the inner mirror exceeds 98%.

Fig. 1 shows the resonator system. The amplitude reflection coefficients of the top and bottom Bragg reflector are 99.75% and 99.25%, respectively. Due to the VCSEL-fiber coupling efficiency of 90% pigtailing the 12 μm active diameter VCSEL to a gold coated (r_{Gold}=93%) 4.5 μm core diameter fiber end reduces the threshold current to 1.8 mA (Fig. 2). The phase condition to determine the modes of a two-resonator system is derived in [3] and can be seen as the intersection points of the functions given in Fig. 3. The very short cavity length of the VCSEL yields a linear function Φ_1 that is about 200 times smaller than for edge emitting laser diodes. Hence, Φ_1 intersects the arctan-function in the vicinity of its zeros. This leads to quasi equidistant modes. Point A is physically meaningless because it denotes $\Phi_2 = \pi$. Fig. 4 illustrates the calculated frequency deviation from equidistant modes and the corresponding threshold gain. For lower reflectivities r_2 the equidistant spectrum broadens but the trade off is an increased threshold gain. Modelocked pulses depicted in Fig. 5 are achieved by prebiasing the laser at 3 mA and superimposing a sinusoidal signal of 25 dBm at f_0=821 MHz, the inverse roundtrip time of the fiber optic resonator. The pulses have a FWHM of 24 ps, a spectral width of 35 GHz and yield a time bandwidth product of 0.84. Jitter measurement is performed by recording the RF spectrum at the 10th harmonic [4] shown in Fig. 6. Integration over the noise band leads to a jitter of 0.95 ps.

We have shown that the high top surface VCSEL to single-mode fiber coupling efficiency offers the use of an external fiber resonator for modelocking. This technique avoids the use of gratings for frequency filtering, eases mechanical stability problems and allows compact hybrid integration of amplifier and external cavity sections. The short VCSEL cavity length gives the opportunity of using a two-resonator system as modelocking source with quasi equidistant modes and timing jitter below 1 ps. No longer the inner reflectivity of the coupled cavities needs to approach zero to generate short pulses.

References:

[1] B. Möller et al., Proc. ECOC, Montreux, Switzerland, 1993, 409-412.
[2] J. M. Wiesenfeld et al., IEEE J. Quant. Electr. 29 (1993), 1996-2005.
[3] A. Clsson et al., IEEE J. Quant. Electr. 17 (1981), 1320-1323.
[4] A. J. Taylor et al., Appl. Phys. Lett. 49 (1986), 681-683.

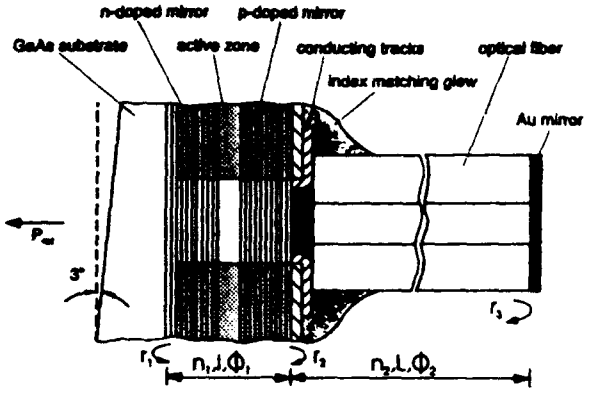

Fig. 1: Modelocking configuration consisting of VCSEL with a pigtailed gold coated (r_{Gold}=93%) 4.5 μm fiber.

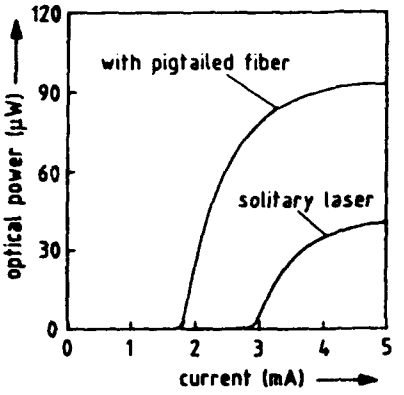

Fig. 2: Bottom output characteristics of solitary and pigtailed 12 μm diameter VCSEL. Max. power in fiber is 0.3 mW.

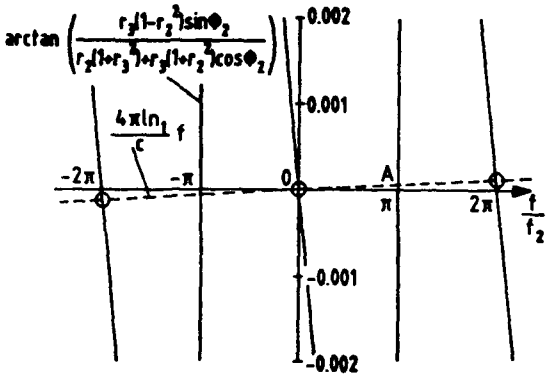

Fig. 3: Solution of phase condition in three mirror system for r_1=99.75%, r_2=99.25%, r_3=80%, $n_1 l$=3.6 μm and $n_2 L$=18.22 cm.

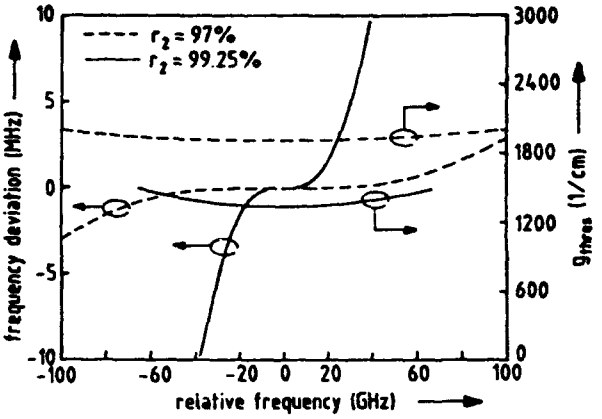

Fig. 4: Deviation Δf from equidistant modes and corresponding threshold gain for modes of the compound cavity.

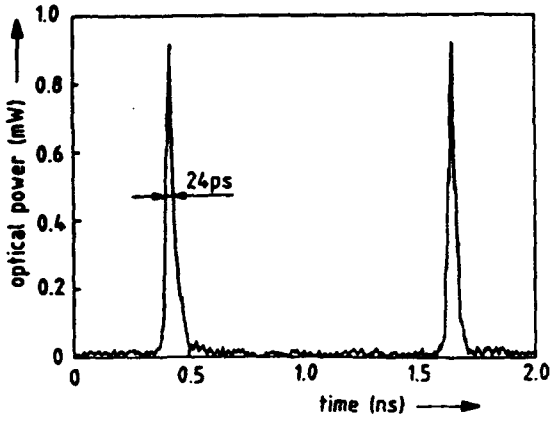

Fig. 5: Modelocked pulse train at f_0=821 MHz. Power through bottom mirror.

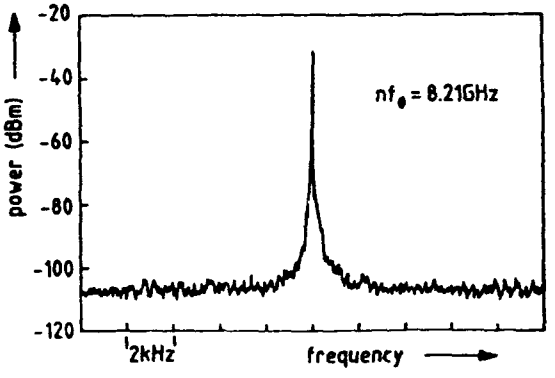

Fig. 6: RF spectrum at 10th harmonic nf_0=8.21 GHz. The resolution bandwidth is 30 Hz.

P18

Ultrafast Dynamics in Waveguide Saturable Absorbers

A.V. Uskov, J.R. Karin, R. Nagarajan, J.E. Bowers
Department of Electrical & Computer Engineering, University of California, Santa Barbara, California 93106

J. Mørk
Tele Danmark Research, Lyngsø Allé 2, DK-2970 Hørsholm, Denmark

Abstract: The results of a model of differential transmission measurements in waveguide saturable absorbers indicate that high field effects, spectral hole burning and carrier heating are important mechanisms governing absorption dynamics.

Semiconductor saturable absorbers are used in many types of mode-locked lasers, including semiconductor, fiber, Ti:sapphire, color center and dye lasers. It is commonly believed that as an optical pulse passes through the absorber, it quickly saturates and then recovers monotonically with a lifetime of ~1 ns. In fact, in reverse-biased absorbers the recovery of the saturable material is much more complicated, and typically has femtosecond transients followed by changes on a time scale of several picoseconds[1]. In this paper, we explain this time dependence of absorption for a waveguide saturable absorber that is used for mode locked semiconductor lasers. We describe a model which includes spectral hole burning (SHB), as well as carrier heating (CH) due to the electric field (EFH), two photon absorption (TPA) and free carrier absorption (FCA).

In pump-probe experiments, a large pump pulse is coupled into the saturable absorber. The transmission of a weak probe pulse is measured as a function of the delay between the two pulses. Figure 1 shows differential transmission data for a bulk GaAs/GaAlAs p-i-n waveguide saturable absorber with different pump energies[1]. The pump pulse generates carriers and changes their energy distribution and temperature. The large electric field (from the built-in potential and applied bias) leads to drift current as well as heating of the carriers, which also affect the carrier distributions.

Our model is based on the density matrix approach (after refs. [2-4]). We consider the absorption coefficient α as a function of the carrier density N, the electron and hole temperatures T_e and T_h, and the photon density S, i.e. $\alpha = \alpha_0(N,T_e,T_h,S)$. The dependence of α on S is a result of SHB. The dynamics of N, T_e and T_h under the action of the optical pump pulse S(z,t) are described by the rate equations for carrier density, N, and electron and hole energy densities, $U_e(N,T_e)$ and $U_h(N,T_h)$. The pump pulse changes N through single photon absorption (SPA) and TPA[4]. Carrier removal from the i-region via thermionic emission and tunneling across the heterojunction also affect N. U_e and U_h vary due to FCA, SPA, TPA and heating of the carriers by the electric field, as well as by relaxation of carriers to the lattice temperature. It should be noted that heating by the field must be taken into account in this case, since the fields are very high in reverse biased absorbers. This is in contrast to models of gain dynamics in amplifiers[3,4], where under forward bias the effect of heating by the field is negligible.

The drift of the photogenerated carriers across the absorbing i-region also leads to screening of the electric field. Carriers accumulate at the heterojunction barriers and create a space charge field which eventually cancels the built-in and applied potential. We model the field screening by considering that the charge accumulated near the barriers is proportional to the drift current, which is in turn given by the field. Thus our model includes equations for carrier density and temperature, and for electric field in the absorbing region. These 'material' equations are supplemented with propagation equations for the pump S(z,t) and probe p(z,t) pulses[3,4].

Figure 2 shows the calculated effect of SHB and CH on the transmission through the waveguide structure used in [1]. The pump pulse energy is 5 pJ, with a pulse width of 150 fs. The relaxation times of T_e and T_h are 0.65 ps and 0.2 ps, and the intraband relaxation times are 50 fs. The dotted curve is the response with no CH or SHB, just simple absorption saturation and recovery with an assumed carrier removal time of 10 ps. The dashed curve includes SHB, along with carrier cooling due to the generation of cold carriers by the pump via single photon

absorption. The inclusion of TPA, FCA and electric field effects in the calculation results in the solid curve, which exhibits features similar to that seen in the experimental data. The ultrafast transient is due primarily to SHB, and the rapid fall time comes from heating by TPA, FCA and EFH. Subsequent cooling leads to the delayed, slowly rising second peak. Figure 3 shows the calculated response, including all the above mechanisms, at three different pump pulse energies. The behavior of the curves is in accordance with the experimental data in Fig.1, and is explained by the increase in CH and SHB effects with increasing pulse energy.

In conclusion, we have presented a model to explain the features in the absorption recovery of reverse-biased waveguide saturable absorbers. The results of the model indicate that carrier heating due to high electric fields and two-photon and free-carrier absorption, along with spectral hole burning, may be responsible for the observed dynamics. We will present the details of the calculation, including the implementation of SHB, FCA, TPA and EFH, as well as other mechanisms such as field screening and intervalley scattering. We will discuss the agreement between our model and experimental results, the important differences between bulk and quantum well absorbers, and the implications for pulse shaping in modelocked semiconductor lasers.

References

[1] J.R. Karin, R.J. Helkey, D.J. Derickson, R. Nagarajan, D.S. Allin, J.E. Bowers and R.L. Thornton, Appl. Phys. Lett., **64**, 676 (1994)

[2] M. Willatzen, A. Uskov, J. Mørk, H. Olesen, B. Tromborg and A.-P Jauho, IEEE Photon.Technol. Lett., **3**, 606 (1991)

[3] J. Mark and J. Mørk, Appl. Phys. Lett., **61**, 2281 (1992)

[4] J. Mørk, J. Mark and C.P. Seltzer, Appl. Phys. Lett., **64**, No. 17 (1994)

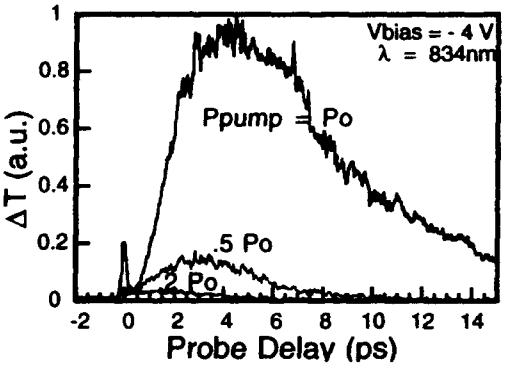

Figure 1: Experimental differential transmission data at three different pump powers in a bulk GaAs /GaAlAs waveguide saturable absorber. Assuming 10% coupling efficiency, Po corresponds to ~2 mW average power coupled into the device, at 109 MHz repetition rate.

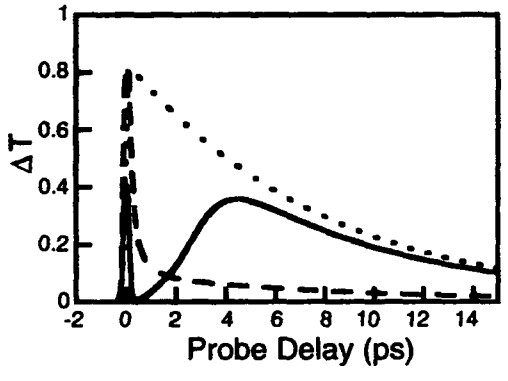

Figure 2: Results of calculation for simple absorption saturation (dots); carrier cooling and spectral hole burning (dashes); carrier cooling, SHB, plus heating by two-photon and free-carrier absorption and electric field (solid line).

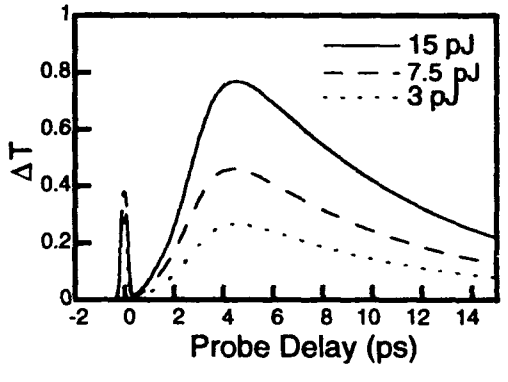

Figure 3: Calculated change in transmission coefficient at three different pump pulse energies.

P19

High Speed All-Optical Functional Elements Using Injection Locked Semiconductor Lasers

J. Hörer, K. Weich, M. Möhrle, E. Patzak, B. Sartorius

Heinrich Hertz Institute for Information Technology, Berlin GmbH, Berlin, Germany, Fax: +49 30 31002 558

Abstract: The speed of all-optical switching using injection locked lasers is analyzed. A model describing two-section lasers is developed yielding a speed above 20 Gb/s. The function of a decision unit is experimentally demonstrated at 10 Gb/s.

Background: Ultrafast operation is a crucial prerequisite for the use of all-optical functional elements in optical signal processing. A high operation speed can be achieved taking advantage of the short gain recovery time at high photon densities in semiconductor optical amplifiers. Using this approach wavelength conversion at 10 and 20 Gb/s (NRZ-coded, corresponding to 5 and 10 Gb/s RZ-coded) has been reported (1,2). However the attainable extinction ratio is relatively poor.

Our approach combines the short gain recovery time at high photon densities with the strong nonlinearity of injection locking (IL). Thus we are able to perform even regenerative switching at high data rates (3,4).

Principle of operation: If an optical signal (probe signal) is injected into a Fabry-Perot (FP) laser with a wavelength λ_p only slighty different from a FP mode, its gain depends strongly on the detuning. Fig.1 shows the measured dependence of the output power on the detuning for different values of input power. For high input powers a jump in the output exists. The corresponding critical detuning $\Delta\lambda_{crit}$ separates the IL region with high output powers from the unlocked region with small values. A small change of the probe detuning around $\Delta\lambda_{crit}$ leads to a nearly digital jump in the gain of the probe signal. This behaviour can be well explained by the IL model of Lang (5).

For all-optical switching we inject the probe signal with a detuning slightly larger than $\Delta\lambda_{crit}$, and a second optical signal (the control signal) at a wavelength λ_c, which has a small positive detuning with respect to another FP mode (Fig. 2). The incoming control signal lowers the carrier density rapidly due to injection-locked stimulated emission. Due to the coupling between the carrier density and the refractive index the probe detuning is shifted below $\Delta\lambda_{crit}$, and the output at the probe wavelength switches digitally from its low-level to the high-level.

Experimental realization: In order to verify the high speed capability of this mechanism a 10 Gb/s RZ PRBS data signal at λ_c=1564nm (P=2mW) is injected into a two-section 1.55μm ridge waveguide FP laser (6) driven by DC currents I_1 and I_2. The probe is formed by a clock signal adjusted to λ_p=1533nm with a power of 0.8mW. The laser output is filtered by an optical bandpass centered at λ_p. Then the output bit pattern at λ_p is a retimed and reshaped replica of the input pattern at λ_c. Compared to the input eye pattern (Fig. 3a) the eye at the output (Fig. 3b) shows an increased opening and a reduction of jitter and noise (extinction ratio: 8 dB). Pulse shaping and retiming have been achieved with an input jitter of up to 60% of the bit duration.

Modelling: The speed potential of this kind of all-optical switching is mainly determined by the dynamics of the mode shift. The response of the shift to an injected data signal has been modelled by a numerical integration of rate equations. For this purpose the IL-model of Lang (5) has been extended to include

- two sections
- two injected wavelengths

Parameters describing the experimental device are used. Under optimized current conditions the shift of the mode spectrum and the connected probe detuning follow the injected 20 Gb/s RZ data signal as shown in Fig. 4 (left and center). The dashed line marks the critical detuning $\Delta\lambda_{crit}$. A clock pulse arriving at the laser experiences either high gain (corresponding to a logical '1' at the output) or low gain (logical '0') depending on the momentary detuning (below or above $\Delta\lambda_{crit}$). $\Delta\lambda_{crit}$ depends on the clock wavelength and intensity (Fig.1). As shown in Fig.4 it can be set to give an error-free decision between '0' and '1' bits at a data rate of 20 Gb/s.

Discussion: Three effects contribute to the high attainable data rates: 1.) a high stimulated emission rate leads to the rapid decrease of the probe detuning at the onset of a control pulse; 2.) a fast recovery is achieved after the end of a control pulse; 3.) digital switching is attained with only small changes in carrier density. The first is caused by the high resonant gain for the control signal due to IL. The second is attained by the use of two-section lasers: section 2 does not take part in the light induced dynamic processes, because it is operated near transparency. However it increases the laser threshold. Thus high carrier densities in section 1 can be used for which the gain

recovery time is small. The third effect is caused by the strong nonlinearity of IL (Fig.1): even a small modulation of the carrier density is sufficient to attain a high contrast.

Conclusion: A model describing all-optical switching in injection-locked two-section lasers is developed. It shows that the strong nonlinearity of injection locking in combination with short recovery times leads to a high speed potential. For a specific device a speed limit of 20 Gb/s is calculated. Even higher data rates are expected if the heterostructure and the device geometry are optimized. Regenerative switching at 10Gb/s is experimentally verified. The described mechanism can also be used for other high speed all-optical functions, such as wavelength conversion or demultiplexing.

Acknowledgement: This work is supported by Deutsche Bundespost Telekom.

References:

(1) J.M. Wiesenfeld et al., IEEE Photonics Technol. Lett. vol.5, no.11, pp. 1300, 1993
(2) B. Mikkelsen et al., ECOC 1993, paper ThP12.6, Montreux, Switzerland, 1993
(3) K. Weich et al., Electron. Lett., (in press)
(4) ---, OFC 1994, paper WB5, San Jose, USA
(5) R. Lang, IEEE J. Quantum Electron., QE-18, no.6, pp. 976, 1982
(6) J. Hörer et al., IEEE Photonics Technol. Lett., vol.5, no.11, pp. 1273, 1993

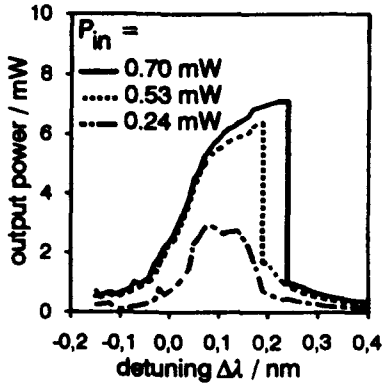

Fig. 1: Output power versus detuning; for high input powers P_{in} a critical detuning exists where the output switches digitally.

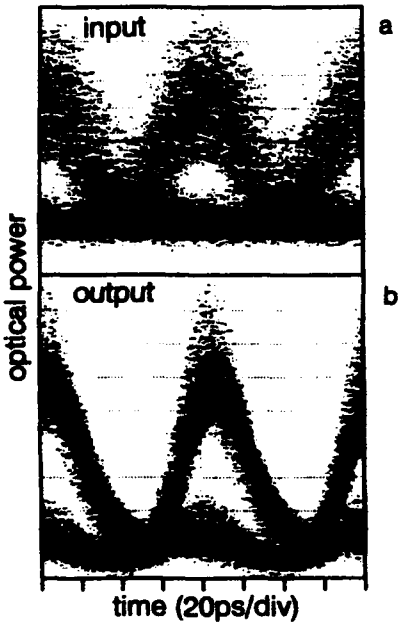

Fig. 3: All-optical regeneration at 10Gb/s (RZ, PRBS) : eye pattern of the input data (a) and the regenerated output data (b).

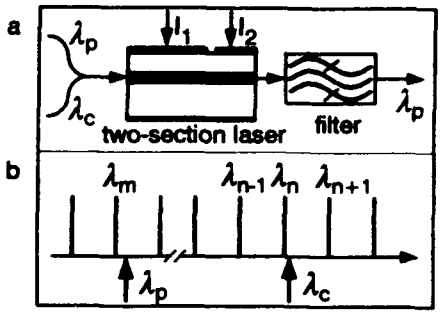

Fig. 2: a) Schematic view of the setup consisting of a two-section laser and an optical bandpass; b) Position of the signal wavelengths relative to the FP modes.

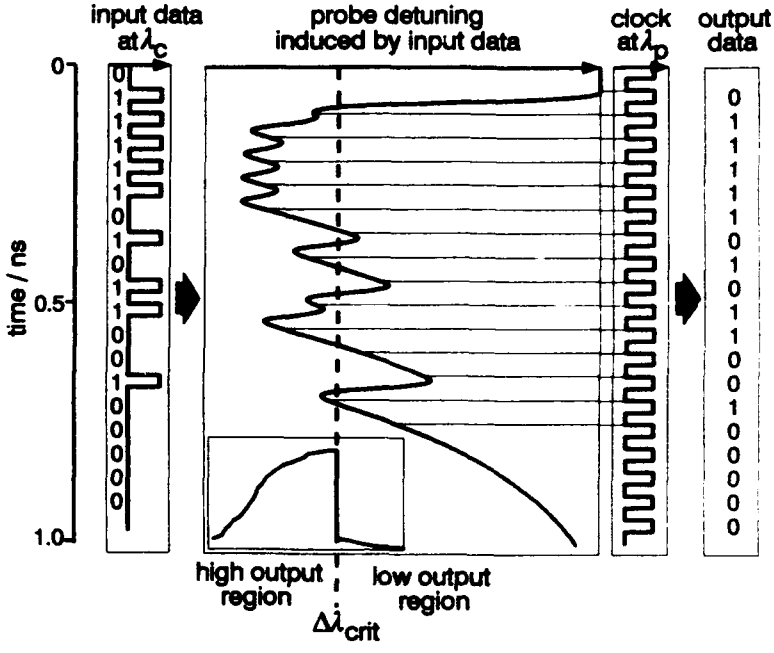

Fig. 4: Modelling results indicating error-free decision at 20 Gb/s. Left: injected 20 Gb/s data stream. Center: response of the detuning. The dashed line marks the critical detuning. Depending on the momentary detuning (probed by the clock) either a '1' or a '0' appears at the output (right).

P20

Aluminum-free InGaAs/GaAs/InGaP Strained-Quantum-Well Lasers with InGaAsP Transition Layers

Hung-Pin Shieo, Wei Lin*, Jian-Guan Chen*, Yuan-Kuag Tu*, and Ching-Ting Lee

Institute of Optical Science, National Central University, Chung-Li, Taiwan, R.O.C.
* Telecommunication Laboratories, Ministry of Transportation and Communications, 12, Lane 551, Min-Tsu Rd. Sec. 3, Yang-Mei, Taiwan 32617, R.O.C.

Abstract Aluminum-free InGaAs/GaAs/InGaP strained quantum well laser with high characteristic temperature of 170 K is reported. The as-cleaved lasers with InGaAsP transition layers show internal quantum efficiency of 87 % and internal waveguide loss of 6.33 cm^{-1}.

Pumping laser of 980 nm has attracted intensive studies due to the importance of erbium-doped fiber amplifiers (EDFAs) in the optical fiber communication. The development of InGaAs/GaAs/AlGaAs strained quantum well separate-confinement-hetero-structure (SQW-SCH) lasers has been accelerated in the past few years. However, the facet oxidation of AlGaAs causes performance degradation and affects its long term reliability [1]. With the inherent advantages of multi-step regrowth, selective chemical fabrication process, and low surface recombination velocity at interface[2], the aluminum-free $In_{0.49}Ga_{0.51}P$ (InGaP) system is considered to replace AlGaAs system for the design and fabrication of high quality and reliable pumping laser[2-5].

Oval defects are usually found in the growth of InGaP layer on (100) GaAs substrate by organometallic vapor phase epitaxy (OMVPE). By growing InGaP epilayer on mis-oriented (100) GaAs substrate or by adopting an InGaAsP transition layer on the exact (100) GaAs substrate prior to the growth of InGaP layer, we can reduce oval defects significantly.

Two laser structures are grown on n-type (100) GaAs (structure A) and n-type (100)4° GaAs (structure B), as shown in Fig. 1, respectively. The active region consists of three quantum wells with 6 nm strained $In_{0.2}Ga_{0.8}As$ well and 20 nm GaAs barrier. The active region and separate-confinement heterostructure (SCH) are cladded by InGaP layers. The SCH of structure A comprises GaAs and $In_{0.22}Ga_{0.78}As_{0.56}P_{0.44}$ (with conduction band almost located at the middle position between GaAs and InGaP). 5 μm wide ridge-waveguide lasers are formed with cavity length of 500 - 1200 μm.

Fig. 2 shows the continuous wave light-current characteristics of p-side up as-cleaved 750 μm-long lasers without any thermal roll-off. The threshold current and the slope efficiency are 20 mA and 0.42 mW/mA for structure A, and 23 mA and 0.37 mW/mA for structure B, respectively. Relationships of the inverse differential quantum efficiencies as a function of cavity length are shown in Fig. 3. The internal quantum efficiency and the internal waveguide loss are 87 % and 6.33 cm^{-1} for structure A, and 77 % and 10.6 cm^{-1} for structure B. The characteristic temperature, derived from the threshold current in various operating temperatures (shown in Fig. 4), is about 170 K and 162 K for lasers in structure A and B, respectively.

In summary, an aluminum-free InGaAs/GaAs/InGaP strained quantum well laser with InGaAsP transition layers grown on exact (100) oriented GaAs substrate has been successfully

grown. The internal quantum efficiency of 87 %, internal waveguide loss of 6.33 cm^{-1}, and characteristic temperature of 170 K in as-cleaved lasers have been demonstrated. Incorporating the InGaAsP transition layers in the device structure can eliminate the oval defects, improve the epilayer interface quality, prevent the cavity mis-alignment, and provide flexible design of laser waveguide and confinement factor.

1. T. Yuasa, et al, *Appl. Phys. Lett.*, **32**, 119-121, 1978.
2. J. M. Olson, et al, *Appl. Phys. Lett.*, **55**, 1208-1211, 1989.
3. J. M. Kuo, et al, *Appl. Phys. Lett.*, **59**, 2781-2783, 1991.
4. Y. K. Chen, et al, *Appl. Phys. Lett.*, **59**, 2929-2931, 1991.
5. M. Ohkubo, et al, *Electron. Lett.*, **28**, 1149-1150, 1992.

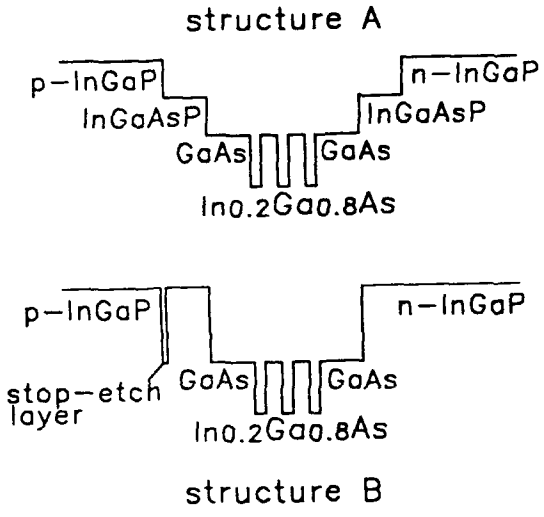

Fig. 1. Schematic conduction band profiles of structure A and B.

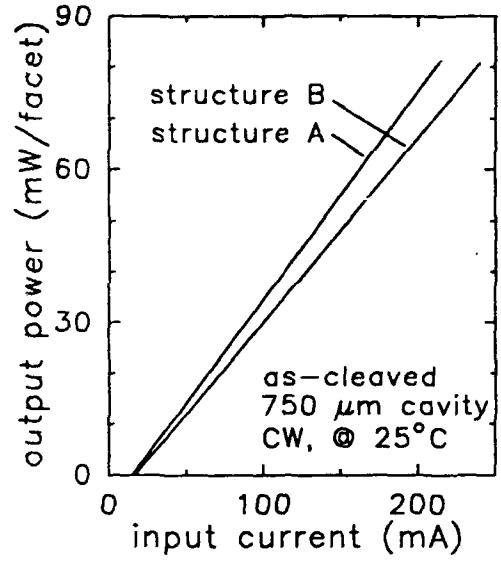

Fig. 2. Continuous wave light-current characteristics of structures A and B with as-cleaved 750 μm long cavity.

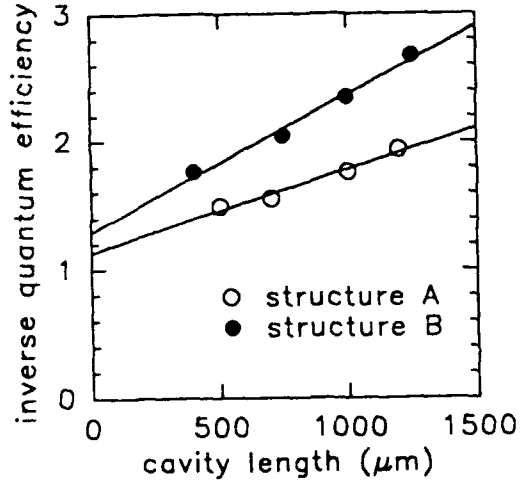

Fig. 3. Relationships between inverse differential quantum efficiency and cavity length for structure A and B.

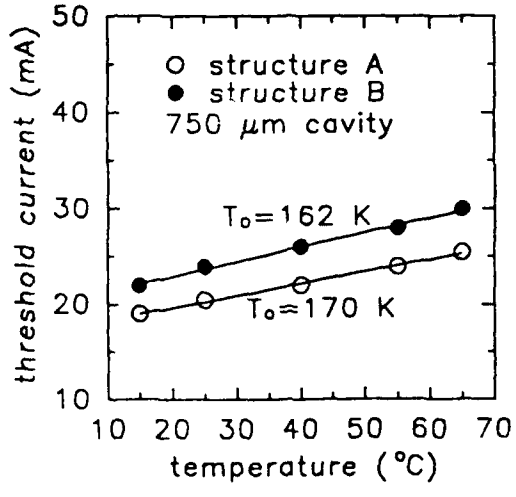

Fig. 4. Temperature dependence of threshold currents of as-cleaved 750 μm long cavity.

P21

GaInP-Crossed-Coupled-Cavity-Laser (XCCL) for Investigation of Strain Effects and GaInP Superlattice Ordering

F. Barth, G. Forstmann, S. Nagel, C. Geng, F. Scholz, H. Schweizer
E. O'Reilly† and M. Pilkuhn
4. Physikalisches Institut, Universität Stuttgart, Paffenwaldring 57
D-70550 Stuttgart, Germany
† *Fraunhofer-Institut für Angewandte Festkörperforschung, Tullastrasse 72,*
D-79108 Freiburg, Germany
On leave from: Department of Physics, University of Surrey, Guildford,
Surrey GU2 5XH, England

An anisotropy of GaInP lasers with CuPt-type superlattice was observed in polarization of laser emission. This effect can be understood with direction dependent transition matrix elements. A XCCL device is used for testing anisotropic properties.

GaInP is well known to form a $CuPt_B$ type superlattice with the group III atoms ordered in different {111} planes under certain growth conditions. Polarization dependent photoluminescence have revealed that ordering affects the conduction to valence band transition matrix element [1,2]. Furthermore an anisotropy for threshold current densities and lasing wavelengths for [011] and [01$\bar{1}$] striped-GaInP lasers have been found [3,4].
We present experimental data and theoretical calculations which show that this anisotropy can be observed in the polarization of laser emission. The measured properties are well explained by a model that includes strain, ordering and band mixing effects [5]. As a possible application of this anisotropy a XCCL for wavelength conversion is presented.
Strained quantum well laser structures have been grown using LP-MOVPE on two types of misoriented (100) substrates: (i) Type A, which is expected to show only a small degree of ordering and (ii) Type B, which is expected to be strongly ordered. The layer sequence is described elsewhere [6]. The Ga-content in the active region varied from x=0.42 to x=0.56. 16μm wide stripe-geometry lasers and XCCLs both with cavity orientation along [011] and [01$\bar{1}$] were fabricated from each sample using standard techniques.
Laser emission from standard devices on type B substrates with cavity orientation along [01$\bar{1}$] and from devices on type A substrates show TE or TM polarization, expected for conventional slab waveguide. By contrast, type B lasers with cavity orientation along [011] emit light with strain-dependent polarization direction tilted towards the plane of ordering (see Figure 1, Figure 2).
Theoretical calculations, which presume ordering along the [1$\bar{1}$1] direction, show the angular dependence of the normalized transition matrix elements for emission with propagation in a) the [011] and b) the [01$\bar{1}$] direction for partially ordered GaInP (see Figure 3). For the [011] direction it can be seen in all three cases that the matrix element is maximised for polarization directions at an angle to the principal [100] axis. With applied compressive (tensile) strain the magnitude of the matrix elements decreases (increases) and the lobes are turned towards the [0$\bar{1}$1] ([100]) direction. Since no cavity length dependence of the polarization could be observed, we conclude that the polarization angle represents the matrix element in the crystal. For the propagation in [01$\bar{1}$] direction the maximum matrix element is oriented along the principal axis as expected for the conventional slab waveguide polarization.
As a possible application of the anisotropy of GaInP we fabricated XCCLs with two intersecting cavities oriented along [0$\bar{1}$1] and [011]. One of the cavities is a conventional stripe laser with a stripe width of 5μm (laser I). The crossed cavity is oriented perpendicular to the first with a stripe width of 64μm (increased for coupling purpose) (see Figure 4). Figure 5 shows the characteristics of the two lasers operated independently. When operated simultaneously, and laser I is above threshold, its output power is reduced when laser II starts lasing, since the carrier density in the intersection is reduced. The two crossed cavities serve as a wavelength as well as a polarization converter with two physically separated optical outputs. Further application

could be the introduction of a semitransparent beam splitter at the cavity crossing point which would enable enhanced polarization dependent beam splitting for purposes of demultiplexing.
More data will be presented at the conference.

[1] A. Mascarenhas *et al.*, Phys. Rev. Lett. **63**, 2108 (1989).
[2] T. Kanata *et al.*, Phys. Rev. B **45**, 6637 (1992).
[3] K. Nakano *et al.*, Appl. Phys. Lett. **61**, 1959 (1992).
[4] H. Fujii *et al.*, Appl. Phys. Lett. **61** 737 (1992)
[5] G. Forstmann *et al.*, to be published
[6] F. Barth *et al.*, Proc. 23rd European Solid State Device Research Conf., 283 (1993).

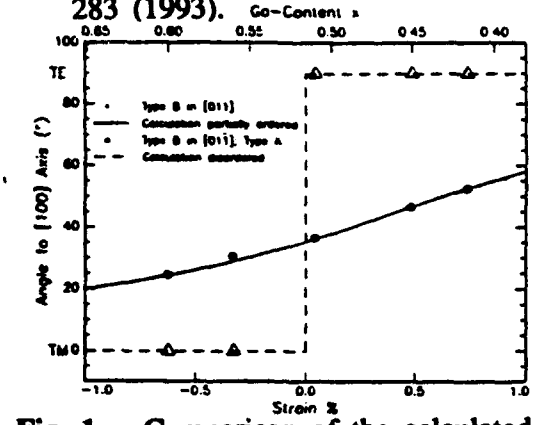

Fig. 1. Comparison of the calculated angle of maximum matrix element with experimental polarization angles of laser emission.

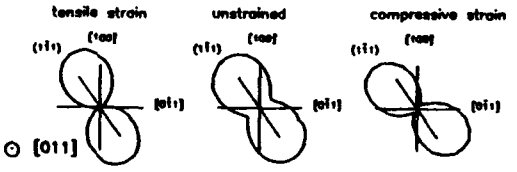

Fig. 2. Polar plot of laser emission for cavity orientation along [011] direction for differently strained lasers.

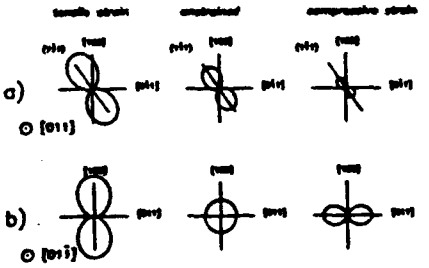

Fig. 3. Direction dependent matrix element for differently strained GaInP for light propagation in [011] and [01$\bar{1}$] direction.

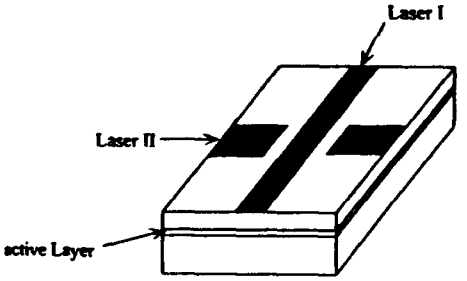

Fig. 4. Schematic structure of the Crossed Cavity Laser

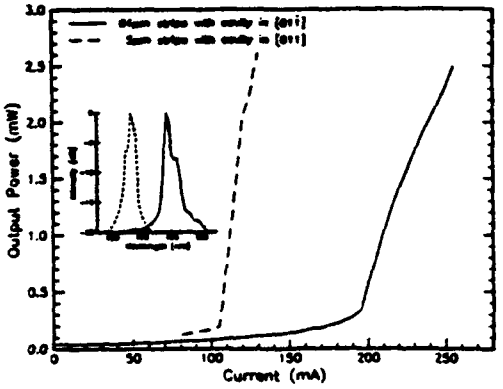

Fig. 5. Output power vs. current and emission spectra of the Crossed Cavity Laser

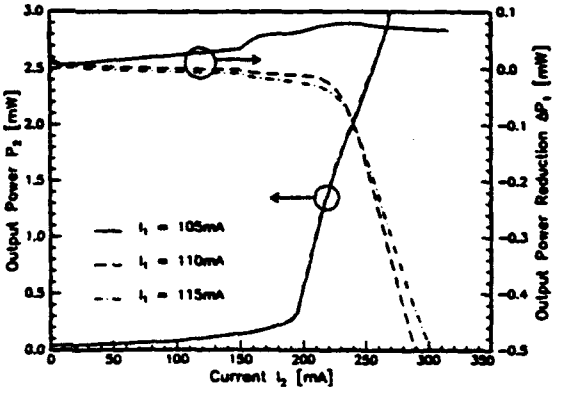

Fig. 6. Modulation of the output power of laser I as a function of the output of laser II

P22 Low-Threshold Strained-Layer Quantum-Well 630-nm AlGaInP LDs and Relative Intensity of Strain-Induced Polarization Mode

T. Tanaka, H. Yanagisawa, S. Kawanaka, and S. Minagawa
Central Research Laboratory, Hitachi Ltd., Kokubunji, Tokyo 185, Japan

Low-threshold CW operation of 630-nm AlGaInP LDs with compressive- or tensile-strained quantum-well structures is investigated. In addition, the correlation between the threshold current and polarization-mode intensity is discussed in terms of strain effects and injected carrier density.

Strained-layer quantum-well (QW) structures have been studied intensively to attain the high performance in semiconductor lasers. Strain-induced reduction of the in-plane hole effective mass and density of states results from energy dispersion and separation of the valence subband structure, which are affected by strain and QW width. Optimizing a design combining strain and quantum confinement effects is indispensable for short-wavelength AlGaInP LDs to attain low-threshold high-temperature operation. Introducing either compressive or tensile strain into GaInP QWs has been evaluated as a way to achieve a low threshold current I_{th} in 633-nm AlGaInP LDs[1]. Consequently, the minimum I_{th} values have been shown to be around ±0.5% for both kinds of strain. However, it's possible to further reduce I_{th} in more detailed strained-layer QW structures by adjusting the number and width of QWs, as well as the optical confinement factor Γ.

Requiring optimum use of the quantum confinement effect leads to narrower QWs for compressive strain and wider QWs for tensile strain. We have investigated the dependence of I_{th} under CW operation at 20°C on both strains in several kinds of QW structures, keeping approximately the same Γ and allowing the oscillation wavelength to range from 630 to 635 nm, as shown in Fig. 1. Quaternary QWs containing Al are applied in the presence of compressive strain to avoid a small carrier confinement and nonuniform carrier injection in a large number of narrower ternary QWs. Tensile-strained ternary QWs with large carrier confinement and uniform injection can be designed, while compressive-strained QWs exhibited these characteristics are not as easy to design. As a result, an I_{th} less than half that of unstrained QW LDs was achieved when a larger tensile strain was introduced into a QW thinner than the critical layer thickness[2]. The lowest I_{th} of 27.7 mA was attained in a SQW LD with $\Delta a/a = -1.1\%$[3]. A low threshold carrier density n_{th} due to strain effects lowers the quasi-Fermi level, and thus the larger heterobarrier suppresses carrier overflow and brings about high-temperature operation.

The separation of valence subbands due to strain intensifies the polarization mode, in addtion to reducing n_{th}. We examined the correlation between I_{th} and the relative intensity $\rho = |I_{TE}-I_{TM}|/(I_{TE}+I_{TM})$ of the polarization mode in various QW structures. The results for ρ at $I/I_{th} = 0.9$ as seen in Fig. 2, corresponding to the tendency of I_{th} relative to strain, suggest that the separation of valence subbands results in a low I_{th}. As I_{th} gets higher, even under a larger compressive strain, the separation seems to decrease due to the large injected carrier density and the rise in the quasi-Fermi level.

To control the ρ in both strains, we evaluated the ρ value relative to various device parameters, such as cavity length, which can vary the carrier density. Figures 3 and 4 show the dependence of ρ on the cavity length for both strains. Under compressive strain, the ρ increases with lengthening the cavity, which decreases the carrier density and lowers the quasi-Fermi level. This results in a large separation of valence subbands and reductions in n_{th}. Note that the ρ decreases with increasing the cavity length under tensile strain, although a large tensile strain is dominant for the large ρ of TM polarization. The ρ becomes small even when the carrier density is lowered by lengthening the cavity, and thus subband separation seems to be reduced. The injection carrier distribution is regarded as being different in tensile and compressive strain cases. This paper will also discuss the distribution of injected holes among the valence subbands with the strain-induced energy dispersion.

References
1. A. Valster et al., 13th IEEE Int. Semiconductor Laser Conf., G-1, 152 (1992).
2. T. Tanaka et al., Electron. Lett., 29, 606 (1993).
3. T. Tanaka et al., Extended Abstracts of the Int. Conf. on SSDM, LC-10, 974 (1993).

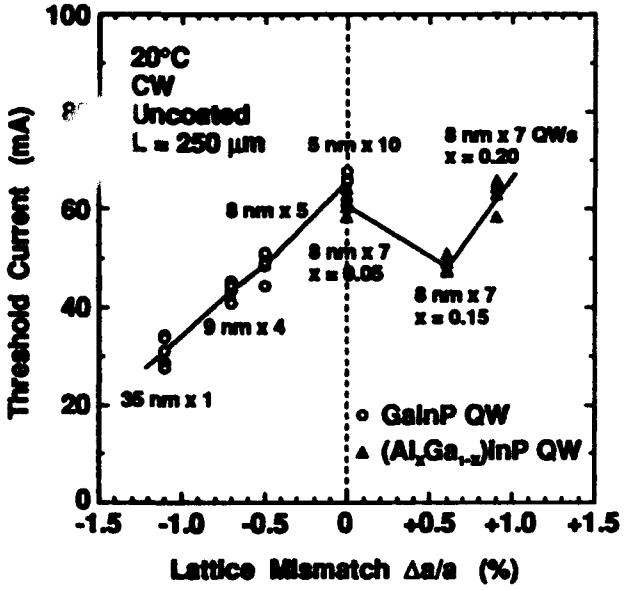

Fig. 1 Threshold currents against lattice mismatch of unstrained, compressive-, and tensile-strained quantum-well lasers

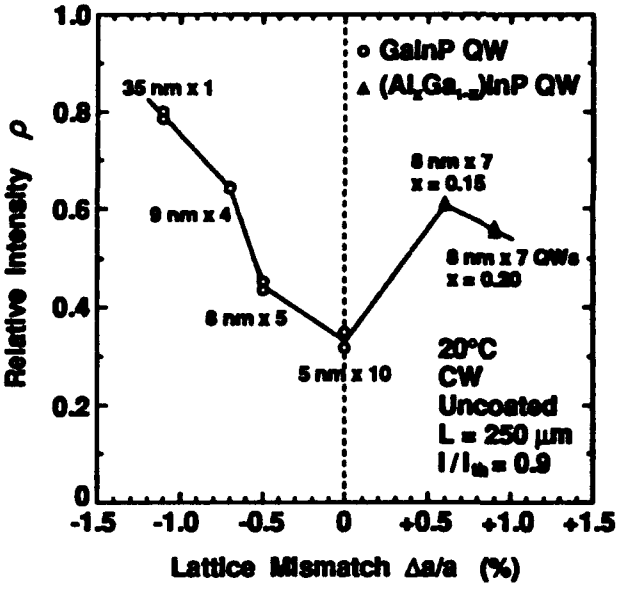

Fig. 2 Relative intensity of polarization mode against lattice mismatch of unstrained, compressive-, and tensile-strained quantum-well lasers

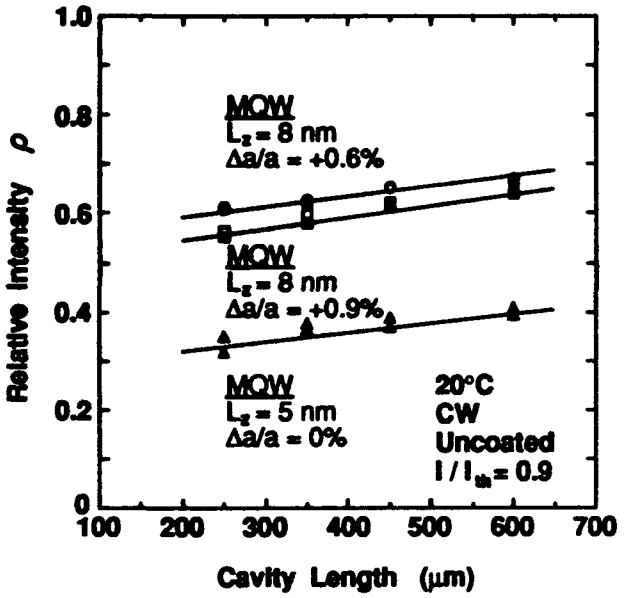

Fig. 3 Dependence of relative intensity of the polarization mode on the cavity length of unstrained and compressive-strained quantum-well lasers

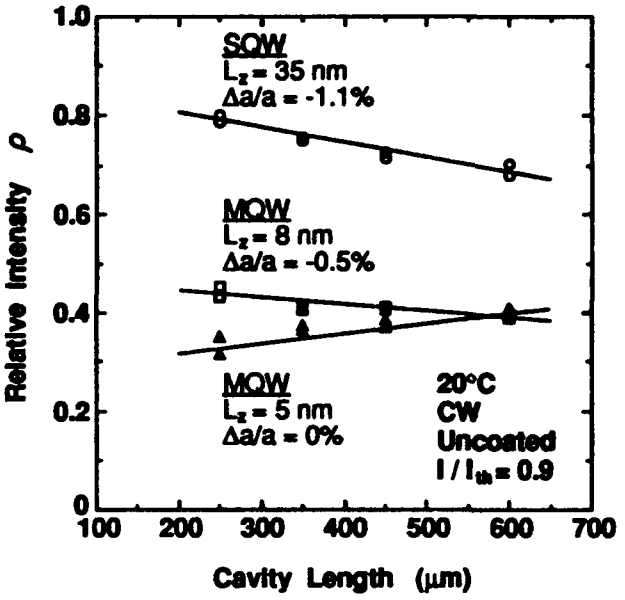

Fig. 4 Dependence of relative intensity of the polarization mode on the cavity length of unstrained and tensile-strained quantum-well lasers

P23

2.5Gb/s parallel transmission without excess bit error rate in a 1.3 μ m strained MQW LD array for optical interconnection

K.Matsumoto, Y.Miyazaki, E.Ishimura, H.Nishiguchi, T.Shiba, K.Goto, A.Takemoto, E.Omura, M.Aiga, and M.Otsubo
Optoelectric & Microwave Devices Laboratory, Mitsubishi Electric Corporation
4-1, Mizuhara, Itami City, Hyogo 664, Japan FAX:+81-727-80-2696

[Abstract] 2.5Gb/s parallel transmission has been successfully demonstrated using a 1.3 μ m strained MQW 10-element LD array. It is shown that the electrical crosstalk between neighboring LD's should be suppressed less than -20dB at 2.5GHz.

Recently, the optical parallel data transmission between electrical instruments is a focus of attention. In order to realize the optical interconnection, the monolithic laser array is a key device. One of the most critical characteristics required in the LD arrays is the least electrical crosstalk between the element LD's in an array to obtain high bit rate (several Gb/s) parallel operation. So far, a bit error rate in the parallel transmission using LD array has not been investigated yet, to the best of our knowledge. In this paper, the effect of the electrical crosstalk on 2.5Gb/s parallel transmission is closely examined. It is shown that the electrical crosstalk between neighboring LD's should be suppressed less than -20dB at 2.5GHz.

A schematic structure of the 10-element LD array is shown in Fig.1. The array consists of ten 1.3 μ m FSBH(Facet-Selective growth Buried-Heterostructure) Fabry-Perot lasers[1]. The separation of the the active region in each element is set to be 250 μ m corresponding the 250 μ m spacing ribbon fibers. The cavity length is 200 μ m and the LD facets are 60%/90% coated. First, an electrical crosstalk between the neighboring elements was measured as follows; two neighboring lasers(LD1 and LD2) were dc-biased and LD1 was superimposed with a small rf signal. Two light output powers were coupled to separate fibers, respectively. An rf signal(P1) from LD1 indicates the frequency response of LD1 and that(P2) from LD2 means the electrical crosstalk. The crosstalk can be defined as 20log(P1/P2). The frequency response of the signal from LD1 and LD2 up to 10GHz are shown in Fig.2. The electrical crosstalk at 2.5GHz was -20dB. To evaluate the effect of the electrical crosstalk on 2.5Gb/s bit error rate characteristics, we made up the condition that the electrical crosstalk was intentionally degraded. The condition was realized as follows; the common electrode of LD array is connected electrically to the earth conductor by a Au wire to increase inductance (shown in Fig.3). The electrical crosstalk at 2.5GHz was degraded to -13dB by this scheme. Next, we investigated 2.5Gb/s bit error rate(BER) characteristics. LD1 and LD2 are biased at 0.6Ith (Ith is the threshold current, 2.5mA), and driven by NRZ, PRBS 2^{23}-1 patterns. Fig.4 shows the BER performance under back-to-back condition. No degradation is observed under the various conditions described in the figure, and BER below 10^{-12} is confirmed. But, in case of the condition that the electrical crosstalk was set to -13dB, serious degradation of BER characteristics is observed. As can be seen, the electrical crosstalk of -20dB in our design is low enough to obtain the 2.5Gb/s parallel transmission.

In conclusion, 2.5Gb/s parallel transmission has been successfully demonstrated using a 1.3 μ m strained MQW LD array. It is shown that the electrical crosstalk between neighboring LD's should be suppressed less than -20dB at 2.5GHz. This array is suitable for light source of high-speed optical parallel data transmission systems.

[References] [1]Y.Ohkura et al.,Electron. Lett., vol.89, No.19, pp.1844-1845,(1992)

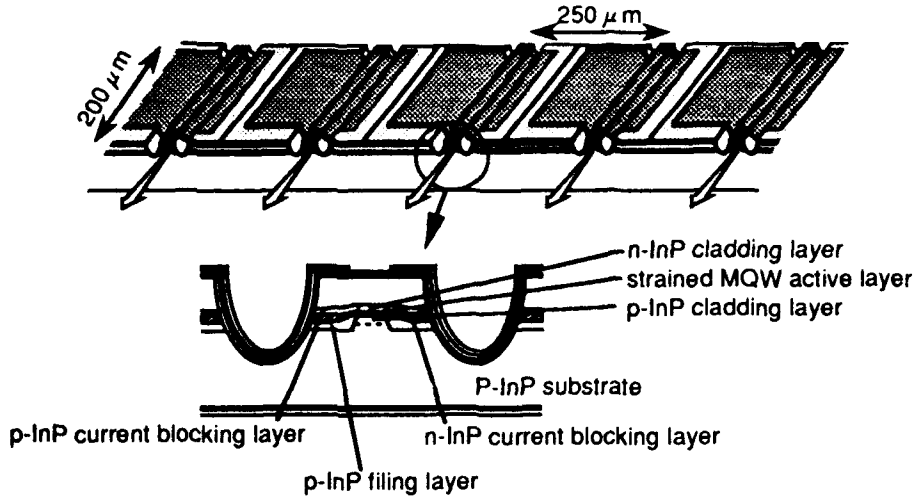

Fig.1 Schematic structure of the 10-element LD array

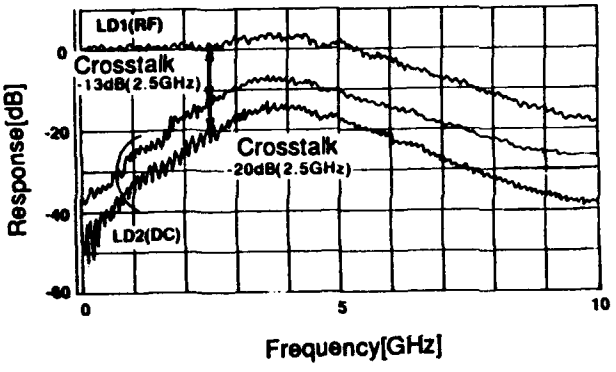

Fig.2 Frequency response of LD1 and LD2

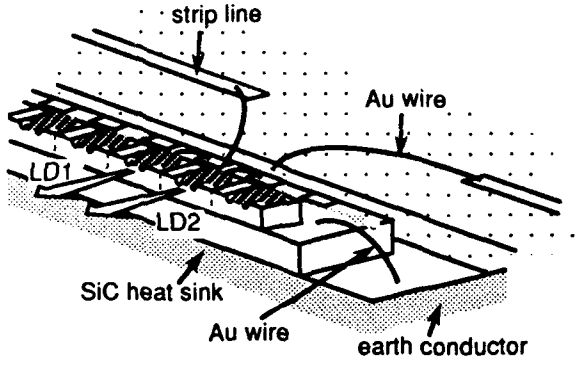

Fig.3 Method of degradation of the electrical crosstalk

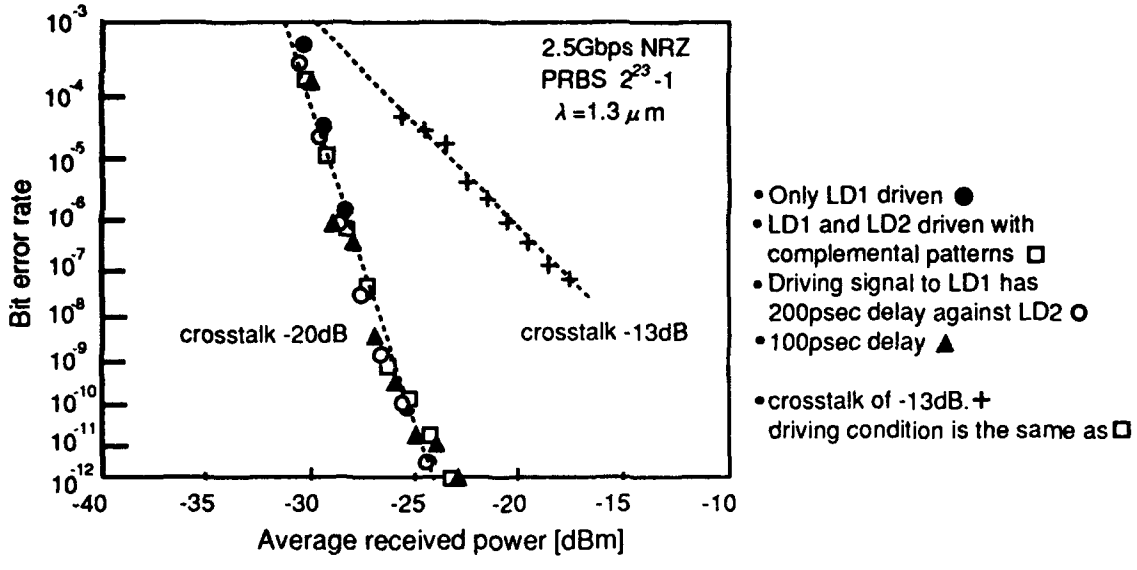

Fig.4 Bit error rate performance

P24

Low Threshold Current 780 nm InAlGaAs/AlGaAs Strained QW Lasers and the Integration with a Passive, Non-absorbing Tapered Mode-size Transformer

G. Vermeire, F. Vermaerke, R. Baets, P. Van Daele and P. Demeester

Department of Information Technology, University of Gent -IMEC
Sint-Pietersnieuwstraat 41 B9000 Gent, Belgium

Abstract

InAlGaAs/AlGaAs QW lasers operating at 780 nm have been realised with threshold currents down to 8.2 mA. The monolithic integration with a passive, non-absorbing mode-size transformer has been demonstrated for the first time.

The impact of strain on the characteristics of III/V semiconductor laser diodes has already been demonstrated several times. InAlGaAs has been introduced since 1991 as a new quaternary compound to realise strained QW lasers on GaAs substrates for a wavelength range between 750 and 900 nm [1]. This wavelength domain related to GaAs/AlGaAs lasers offers several applications such as solid-state pumping, CD-lasers, ... Compared to AlGaAs/AlGaAs QWs, the introduction of indium into the QW results in lower threshold current densities (due to a strongly modified energy band structure) and improved reliabilities (due to lattice hardening). In this paper we present the realisation of InAlGaAs/AlGaAs double QW ridge lasers operating at 780 nm, a wavelength used for optical disk systems. To obtain an emission wavelength of 780 nm the InAlGaAs QWs contain a fairly high aluminium content (22%) because 19% indium is introduced to achieve low threshold currents and high quantum efficiencies. Facet oxidation, related to the high aluminium content, is avoided by providing non-absorbing mirrors through the integration of passive, non-absorbing mode-size transformers, which additionally shape the far-field to become more symmetric.

Untapered lasers are grown by low pressure MOVPE and contain two 4.6 nm thick $In_{0.19}(Al_{0.28}Ga_{0.72})_{0.81}As$ /$Al_{0.28}Ga_{0.72}As$ QWs (T_{gr} = 720 °C) separated by 10 nm $Al_{0.28}Ga_{0.72}As$. The same growth conditions have been applied to grow an identical laser without aluminium in the QW resulting in two 3.5 nm $In_{0.245}Ga_{0.755}As/Al_{0.28}Ga_{0.72}As$ QWs. A third $In_{0.20}Ga_{0.80}As/GaAs$ SQW laser was grown under optimised growth conditions for InGaAs strained layers (T_{gr} = 650 °C) and contains a single 5.6 nm thick $In_{0.20}Ga_{0.80}As$ QW surrounded by 10 nm GaAs. Table 1 lists the exact composition of the waveguiding layers for the 3 lasers together with the measurement results. The InAlGaAs lasers show a minimum threshold current of 8.2 mA (CW) what is to our knowledge the lowest value reported for an InAlGaAs/AlGaAs ridge laser. The maximum external differential quantum efficiency (uncoated facets) is lower compared to the InGaAs QW lasers and is related to the very high cavity losses. Further optimisation will be needed to reduce the cavity losses and hence improve the quantum efficiency. Figure 1 shows the optical spectrum of an InAlGaAs laser operating at 780 nm.

The FWHM of the far-field equals 12° and 50° in the lateral and transverse direction respectively and results in an asymmetric elliptical far-field. A circular laser beam simplifies for instance the accompanying optics for optical disk systems or a narrow lateral and transverse far-field will improve the coupling efficiency into glass fibres or other optical waveguiding structures. In order to reduce the diffraction of the transverse far-field we have "tapered" the waveguiding layers of the InAlGaAs lasers near the facets using the shadow masked growth (SMG) technique [2,3]. As illustrated in figure 2 the optical mode is expanded by reducing the thickness of the core waveguiding layers near the laser facet and hence obtaining a wider near-field distribution at the laser mirror. The thickness reduction of the epilayers has been obtained by growing the laser structure on a shadow masked substrate as shown in figure 2. Due to the diffusion limitation of the MOVPE growth process the epilayer thickness on the GaAs substrate will be reduced as the mask opening width W decreases. The mask itself consists of 1 µm GaAs held at 7 µm above the substrate by an AlGaAs spacer layer, grown on the substrate during a former MOVPE run. After growth, the shadow mask was lifted-off and 5 µm wide ridge lasers were processed. Only the 400 µm untapered uniform part of the laser was provided with a metal p-contact.

The lasers were cleaved at different positions along the tapered section which has a maximum length of 200 µm. Experimental data are presented in figure 3, illustrating the reduction of the FWHM of the transverse far-field from 50° to 30° as the lasers are cleaved further along the passive tapered section. Also the CW threshold current is shown as a function of taper length indicating fluctuations around a mean value of 26 mA (the average differential quantum efficiency was 42 %). There is no clear relation between the taper length and the threshold current fluctuations indicating that they could

not be attributed to absorption in the passive taper section. The thickness reduction of the epilayers along the passive section will additionally result in a bandgap increase through the use of InAlGaAs QWs. The passive tapered section provides the InAlGaAs QW laser with a non-absorbing mirror (NAM) and will alter the reliability at high output power (if NAMs are implemented at both facets of the laser). Further results on the bandgap increase in the tapered section will be presented at the conference.

In conclusion, low threshold current InAlGaAs/AlGaAs QW lasers operating at 780 nm have been realised and far-field shaping by including a passive, non-absorbing tapered section has been successfully demonstrated. The authors want to acknowledge Jan Haes for simulations, Steven Verstuyft for processing and Guy Janssens for measurements. Gerrit Vermeire wants to thank the IWONL for financial support.

[1] : C.A. Wang, J.N. Walpole, H.K. Choi, L.J. Missagia, IEEE Photon. Technol. Lett. 3 pp 4 (1991)
[2] : P. Demeester, L. Buydens, P. Van Daele, Appl. Phys. Lett. 57 pp 168 (1990)
[3] : G. Vermeire et al., Proceedings ICMOVPE '94, Japan

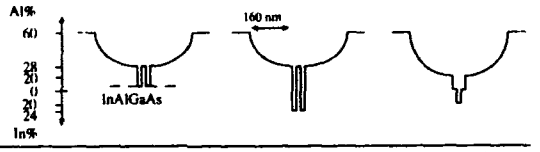

	InAlGaAs/AlGaAs	InGaAs/AlGaAs	InGaAs/GaAs
wavelength (nm)	780	930	980
min. threshold current (mA)	8.2	9.8	7.8
max. external differential quantum efficiency (%)	54	66	68
internal quantum efficiency (%)	74	71	74
internal cavity losses (1/cm)	22	5	3.6

Tabel 1

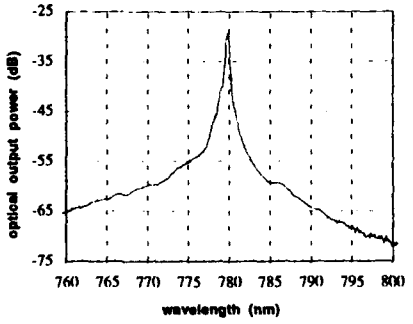

Fig. 1 : emission spectrum of an InAlGaAs/AlGaAs QW laser

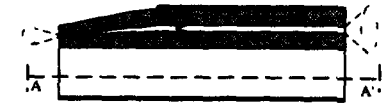

a) cross-section tapered laser

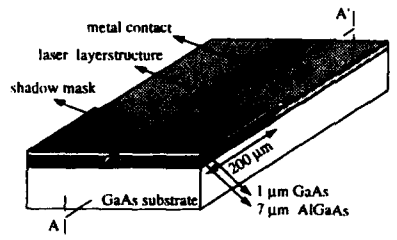

b) fabrication concept tapered laser

Fig. 2 : schematic representation of a tapered InAlGaAs/AlGaAs QW laser

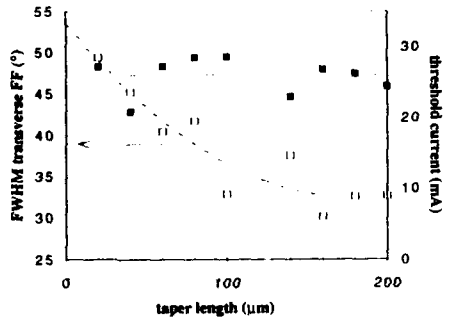

Fig. 3 : variation of the transverse far-field diffraction angle and threshold current as a function of taper length

P25 0.78-0.98μm Ridge-Waveguide-Lasers Buried with AlGaAs Confinement Layer Selectively Grown by Chloride-Assisted MOCVD

A.Shima, A.Takemoto, H.Kizuki, S.Karakida, M.Miyashita,
Y.Nagai, T.Kamizato, E.Omura, and M.Otsubo

Optoelectronic & Microwave Devices Laboratory, Mitsubishi Electric Corporatio
4-1, Mizuhara, Itami City, Hyogo, 664 Japan FAX:+81-727-80-2696

Ridge-waveguide laser diodes (LD's) buried with an $Al_{0.7}Ga_{0.3}As$ confinement layer selectively grown by using the Cl-assisted MOCVD have realized, for the first time, reduction of the operating current, stabilization of the lateral mode and the high reliability in the high-power operation.

A buried ridge LD is highly reliable because it does not have regrowth interfaces in the active region. A loss-guided ridge structure buried with a GaAs confinement layer which controls the lateral optical field and the current spreading, has been widely used for various LD's lasing at the wavelength of shorter than ~0.87μm. However, the external quantum efficiency of the LD's with this structure is relatively low because of the inherently high internal loss. Moreover, in case of the 0.98-1.02μm-LD's for the fiber amp pumping, it may be very difficult for the ridge-waveguide buried with the GaAs confinement layer to realize the fundamental transverse mode, as the GaAs can not absorb the laser light of the wavelength over ~0.9μm (i.e. anti-guide structure). Replacement of the GaAs confinement layer by the lower index material compared to the cladding layer (e.g. polyimide[1], $In_{0.5}Ga_{0.5}P$[2]) has solved these problems. Provided that an $Al_xGa_{1-x}As$ confinement layer can be selectively grown outside the ridge over the wide range of the Al content (especially high Al content), it has possibility to expand the tolerance of the waveguide design for the various LD's formed on the GaAs substrate.

In this paper, we demonstrate the 0.78-0.98μm high-power ridge-waveguide LD's with the $Al_{0.7}Ga_{0.3}As$ confinement layer. Fig.1 shows the structure of the laser chip. The triple quantum well of $Al_{0.1}Ga_{0.9}As$ and the strained double quantum well of $In_{0.16}Ga_{0.84}As$ are applied for the active layers of the 0.78μm-LD and the 0.98μm-LD, respectively. The cladding layers consist of $Al_{0.48}Ga_{0.52}As$. Refractive index step (ΔN) of the stripe region is defined by the difference of the Al content between the upper cladding layer and the confinement layer and the distance between the active layer and the confinement layer controlled by the etching stop layer[3]. As shown in Fig.2, we have solved the deposition of poly-crystal on the SiN mask in the selective growth of the $Al_{0.7}Ga_{0.3}As$ layer by using a Cl-Assisted MOCVD with the HCl gas introduced.

Fig.3 shows the output characteristics of the 0.78μm-LD (a) and the 0.98μm-LD (b). In the 0.78μm-LD, the threshold current and the quantum efficiency are 31.5mA and 1.06W/A, respectively. These values are improved by ~40% compared to those of the loss-guided LD with the GaAs confinement layer. The linear power-current (P-I) characteristics and the stable single lobed far-field patterns (//) are obtained over 150mW. The 0.98μm-LD shows the single lobed far-field patterns up to 300mW and the maximum output power of 458mW.

The aging test result is shown in Fig.4. The operating currents at 60℃, 55mW of the 0.78μm-LD are lower than those of the conventional 0.78μm-LD with the GaAs confinement layer (broken lines) by ~33%. The 0.78μm-LD's and the 0.98μm-LD's (50℃, 100mW) have been operating for over 1,000 hours with little increase of the operating currents.

References

1. Ohkubo et al, J.Quantum Electron. Vol. 29, p.1932, 1993.
2. Ishikawa et al, J.Quantum Electron. Vol. 29, p.1936, 1993.
3. Shima et al, Technical Digest of the 13th Int'l. Semiconductor Laser Conference, p.98, 1992.

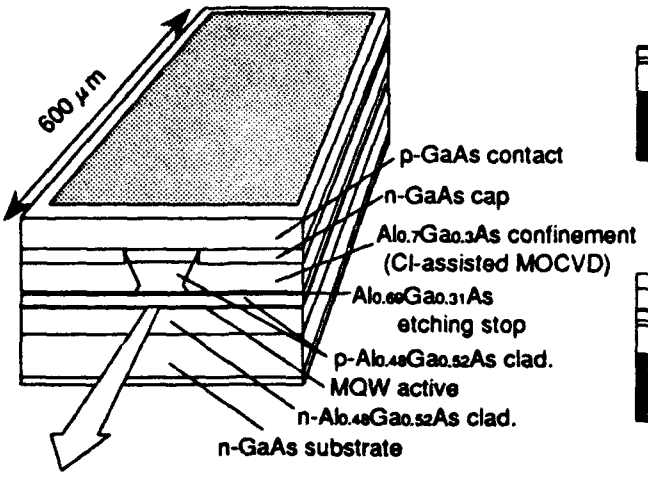

Fig.1 Structure of the laser chip

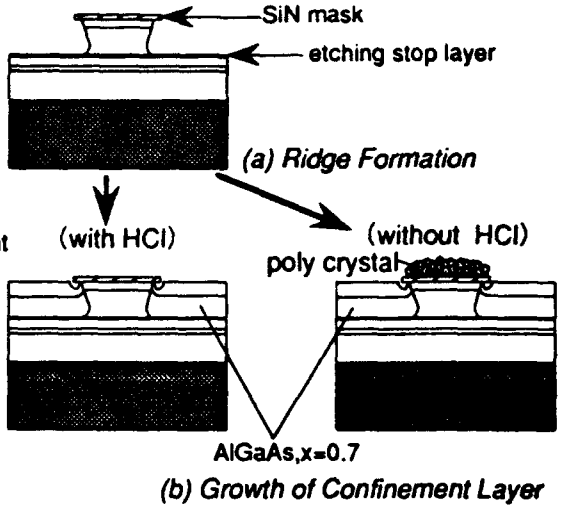

Fig.2 Formation of the waveguide

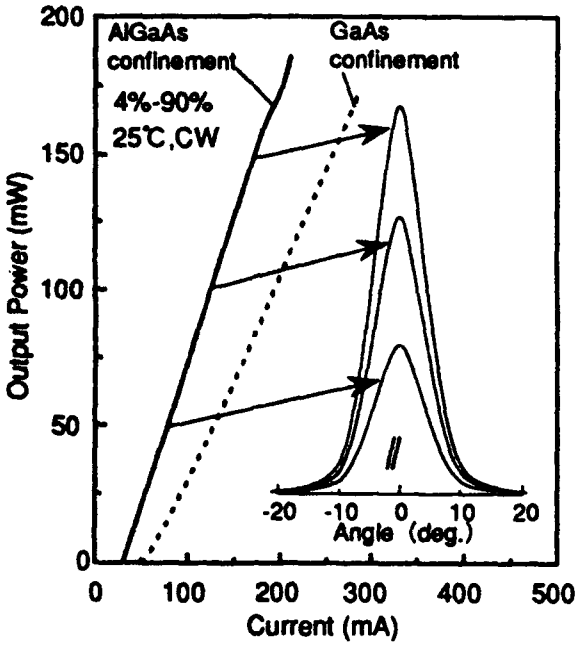

(a) 0.78μm-LD

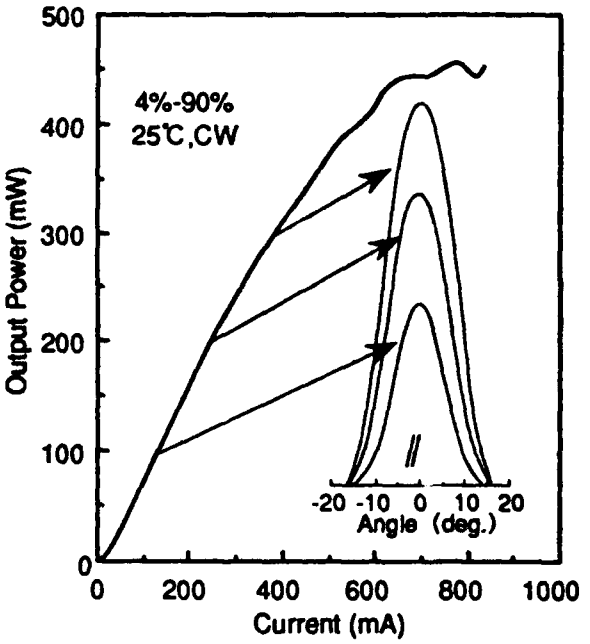

(a) 0.98μm-LD

Fig.3 Output characteristics of the LD's

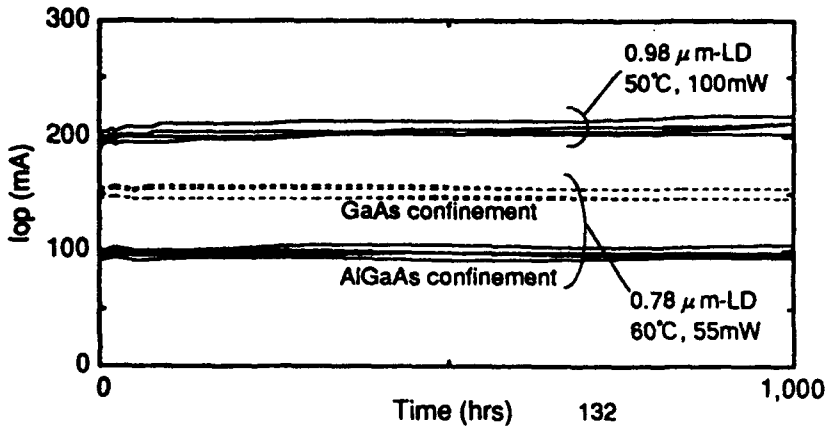

Fig.4
Aging test results

P26

Strained Layer Single Quantum Well InGaAs Lasers with Room Temperature CW Threshold Current 165 μA

T. R. Chen, B. Zhao, L. E. Eng, Y. H. Zhuang, and A. Yariv
T. J. Watson Sr. Laboratories of Applied Physics, 128-95
California Institute of Technology, Pasadena, CA 91125, USA

Abstract

A record low threshold current 165 μA (CW) at room temperature has been demonstrated in a buried heterostructure strained layer single quantum well InGaAs laser with short cavity length and high reflectivity coatings.

In applications such as optical interconnects and parallel data processing, a large number of lasers will be involved to handle huge amount of information. Extremely low threshold current and large modulation bandwidth will be key requirements for laser performance. Progress has been made during the recent years due to the development of quantum well (QW) structure. CW threshold currents as low as ~ 1mA [1-3] for as cleaved lasers and 0.35mA for dielectric coated lasers [2] have been reported.

In this paper, we report on the systematic study on the threshold behavior of single quantum well (SQW) lasers with various cavity length and facet mirror reflectivities. Very low threshold current was demonstrated for short cavity lasers. The lasers used in this work were strained layer (SL) SQW InGaAs/AlGaAs buried heterostructure (BH) lasers made by a two-step hybrid MBE/LPE growth technique [2]. We used a relatively thick QW (80Å) to reduce gain saturation effect and state-filling effect [2,4]. The width of the active stripe is ~ 1.5μm. The lasers displayed very low threshold current ~ 1mA at a cavity length ~ 400μm. However, when the cavity length became shorter, the threshold current increased due to gain saturation, reaching ~ 3mA at a cavity length ~ 100μm. This behavior can be well described by a logarithmic gain saturation function and the threshold current can be derived as [5]

$$I_{th} = \frac{w L}{\eta_i} J_0 \exp\left[\frac{1}{\Gamma G_0}\left(\alpha_i + \frac{1}{2L}\ln\frac{1}{R_f R_r}\right) - 1\right] \qquad (1)$$

where J_0 and G_0 are saturation parameters, α_i is the internal loss, η_i is the internal quantum efficiency, Γ is the optical confinement factor, R_f and R_r are the front and rear mirror reflectivities, w and L are the active stripe width and cavity length, respectively.

To reduce the threshold of various short cavity lasers, we applied high reflectivity coatings to the laser facets. The typical measured threshold currents along with the estimated mirror reflectivities are summarized in Table I. Experimental data are depicted in Fig.1. It is seen that the threshold current for an as-cleaved laser increases when cavity length decreases from 300μm to 90μm. However, the threshold currents of the short cavity lasers drop much more than those of the long cavity lasers when proper high reflectivity coatings are applied to the facet mirrors. A record low threshold current 165μA has been achieved at a cavity length of 125μm (Laser SSQW4). Very similar result was also obtained for a 90μm long laser. The L-I characteristic curves of Laser SSQW4 are shown in Fig.2(a) and Fig.2(b).

In conclusion, CW threshold current 165μA has been demonstrated in a BH SL SQW laser with ~ 125μm cavity length and ~ 0.99 mirror reflectivities.

Reference

[1] Y. K. Sin, H. Horikawa, Y. Matsui, T. Kamijoh, *Electron. Lett.* **29**, 873 (1993)
[2] T. R. Chen, L. E. Eng, B. Zhao, Y. H. Zhuang and A. Yariv, *Appl. Phys. Lett.* **63**, 2621 (1993)
[3] W. X. Zou, T. Bowen, K. K. Law, D. B. Young, J. L. Merz, *IEEE Photon. Technol. Lett.* **5**, 591 (1993)
[4] B. Zhao, T. R. Chen, and A. Yariv, *Appl. Phys. Lett.* **60**, 1930 (1992)
[5] A. Kurobe, H. Furuyama, S. Naritsuka, N. Sugiyama, Y. Kokubun, M. Nakamura, *IEEE J. Quantum Electron.* **24**, 635 (1988)

Laser ID	L (μm)	R_f/R_r	I_{th} (mA) Room T CW
SSQW1	300	0.3/0.3 0.3/0.98 0.75/0.99	1.2 0.68 0.44
SSQW6	225	0.3/0.3 0.3/0.98 0.98/0.98	2.0 0.8 0.37
SSQW4	125	0.3/0.3 0.3/0.99 0.99/0.99	2.8 0.7 0.165
SSQW2	90	0.3/0.3 0.3/0.99 0.99/0.99	3.0 1.4 0.175

Table I. Threshold currents of the SQW lasers under study.

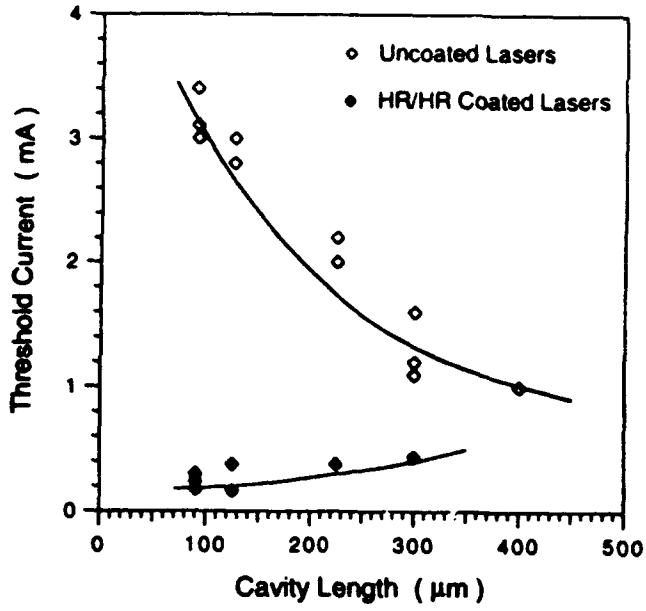

Fig. 1. Threshold current of SQW lasers with various cavity length and mirror coatings.

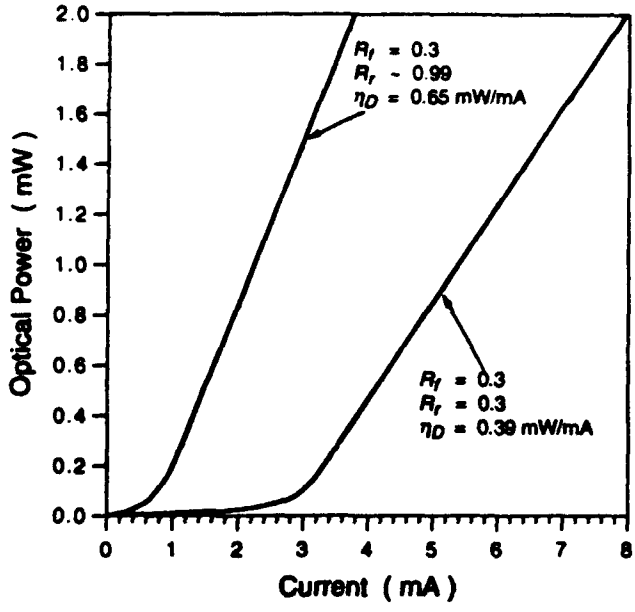

(a)

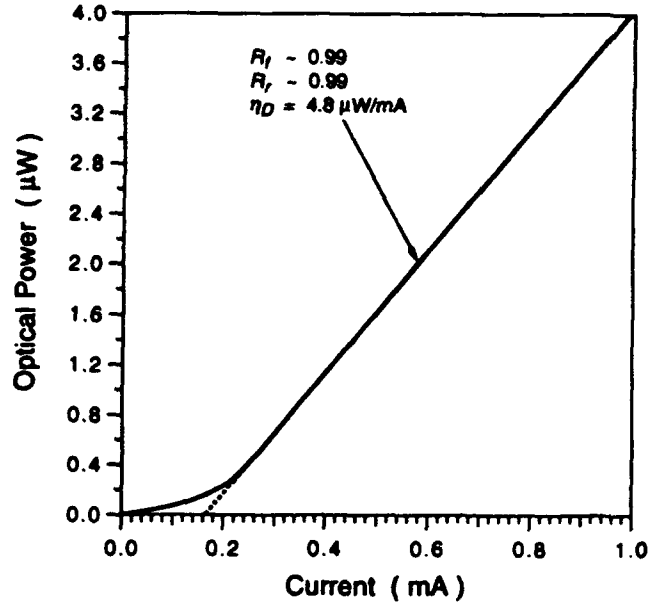

(b)

Fig.2. Light verses current characteristics of Laser SSQW4 (L=125μm).
(a) $R_f = 0.3$, $R_r = 0.3$ and $R_f = 0.3$, $R_r \sim 0.99$
(b) $R_f \sim 0.99$, $R_r \sim 0.99$

P27

The Influence of Valence-Band Well Depth on Optical Gain Uniformity in 1.3-μm InP-Based Strained-Layer Multiple-Quantum-Well Lasers

Shunji Seki and Kiyoyuki Yokoyama
NTT Opto-electronics Laboratories
3-1 Morinosato Wakamiya, Atsugi, Kanagawa, 243-01 JAPAN (FAX +81-462-40-2859)
Paul Sotirelis
Department of Electrical Engineering, Ohio State University,
2015 Neil Avenue, Columbus, OH 43210-1272, USA

Abstract

We compare the optical gain uniformity in 1.3-μm InAsP/InP (ΔEc:ΔEv=0.56:0.44) and InGaAsP/InP (ΔEc:ΔEv=0.40:0.60) compressively-strained multiple-quantum-well (MQW) lasers with a wide-bandgap barrier. We quantitatively demonstrate that the valence-band well depth plays a dominant role in determining the optical gain uniformity in InP-based MQW lasers.

InP-based strained-layer MQW lasers operating at 1.3 μm have attracted much attention for their applications to fiber-in-the-loop, computer interconnects, etc. In these applications, excellent high-temperature characteristics are particularly important. Recent study has shown that a low threshold gain and tight electron confinement in the well are essential to improve the high-temperature characteristics of 1.3-μm lasers [1], [2]. These conditions are easily satisfied in lasers in which the MQW stack consists of a number of thick wells (e.g., 6-10 nm) and wide-bandgap barrier layers (e.g., λg=1.0 μm) . However, an MQW stack with a wide-bandgap barrier brings about an increase in the well depth in the valence band as well as in the conduction band, which may lead to a non-uniform distribution of carriers, thereby the degradation of the optical gain uniformity among the wells. It should be pointed out that an MQW structure provides its full benefits only if each well can generate a similar amount of optical gain, i.e., optical gain is uniform among the wells. In this paper, we study the optical gain uniformity in InAsP and InGaAsP MQW lasers and demonstrate that the valence-band well depth has a significant influence on the optical gain uniformity in InP-based strained-layer MQW lasers.

We analyzed InAsP/InP compressively-strained MQW structures [3] with a separate confinement heterostructure (SCH) region on either side. A strained InGaAsP quaternary material was also used as an active layer for comparison. The MQW stack incorporates six 6-nm wells with barriers of 10-nm InGaAsP (lattice matched to InP, λg=1.0 μm). Valence-band offsets in strained InAsP/InP heterointerfaces were determined by the *ab initio* pseudopotential method within the local density functional approach [4]. Valence-band structures in the InAsP/InP and InGaAsP/InP wells were then obtained by effective mass approximation with a 6x6 Luttinger-Kohn Hamiltonian [5]. Carrier injection in these MQW structures was analyzed by solving Poisson's equation, the Schrödinger equation, and the current continuity equations, selfconsistently. The capture and escape processes into and out of the well were treated as a space-dependent recombination process [6]. The capture and escape rates were calculated by taking into account the carrier–carrier and carrier–LO-phonon interactions on an equal basis within the fully dynamic random phase approximation (RPA) [7]. On the basis of the obtained valence band structures and the carrier distribution, the optical gain spectrum was then calculated for each well.

Figure 1 shows the calculated band positions of an InAsP material system. In contrast with the conventional InGaAsP quaternary system (ΔEc:ΔEv=0.40:0.60), the InAsP material system has a smaller valence-band offset; ΔEc:ΔEv=0.56:0.44. In Fig. 2, variations in peak optical gain with changes in current density are compared for InAsP and InGaAsP MQW lasers. Although both active layers are compressively strained to a similar extent, there is a marked difference in gain characteristics.

To clarify the reason for this difference, the optical gain spectrum was analyzed for each well at the lasing thresholds A and B indicated in Fig. 2. The results are shown in Figs. 3(a) and (b). Although the spectra of total gain exhibit a similar behavior, the status of each well is completely different in these two material systems. In InAsP MQW lasers, each well works as a gain medium, while only two thirds of the wells generate gain in InGaAsP MQW lasers. As shown in Fig. 3, the optical gain uniformity is considerably distorted toward the well labelled QW#1 in the InGaAsP MQW lasers, which suggests that the pile-up of carriers in the well nearest the P-contact becomes more serious when valence-band wells become deeper. These results clearly indicate that the valence-band well depth plays a key role in determining the optical gain uniformity in InP-based MQW lasers. We can conclude that InAsP MQW lasers have a higher potential for high-temperature operation since the electron confinement is easily improved in the InAsP material system without paying any penalty in optical gain uniformtiy.

In summary, we have quantitatively demonstrated that the valence-band well depth plays a dominant role in determining the optical gain uniformity in InP-based MQW lasers. We have also shown that the InAsP material system, which has a smaller valence-band offset, has a higher potential for high-temperature operation than its conventional quaternary counterparts.

Acknowledgment

The authors would like to thank T. Ohno and K. Shiraishi for their help with the band offset calculations.

References

[1] H. Temkin et al., Appl. Phys. Lett., 62, 2402 (1993).
[2] C. E. Zah et al., OFC '94 Tech. Dig., 204 (1994).
[3] N. Tessler et al., IEEE J. Quantum. Electron., 29, 1586 (1993).
[3] M. Yamamoto et al., IPRM '93 Tech. Dig., 232 (1993).
[4] K. Shiraishi et al., Jpn. J. Appl. Phys., 29, L556 (1990).
[5] E. P. O'Reilly, Semicond. Sci. Technol., 4, 121 (1989).
[6] A. Weller et al., Appl. Phys. A, 48, 509 (1989).
[7] P. Sotirelis et al., to be published in Phys. Rev. B.

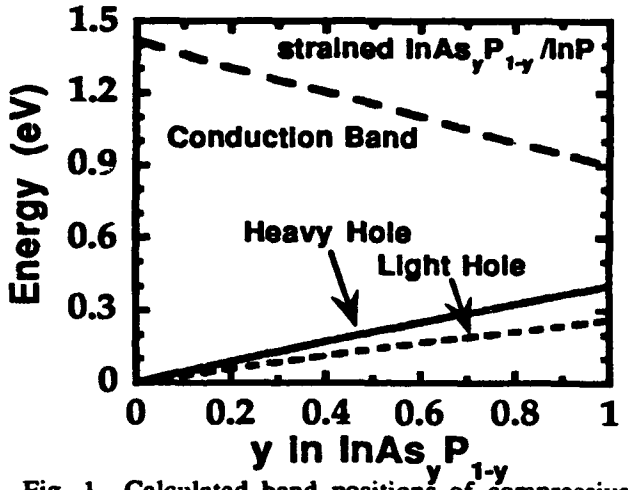

Fig. 1 Calculated band positions of compressively-strained InAsP pseudomorphically-grown on an InP substrate. Energy is referenced to the top of the InP valence band. Valence band positions were determined by the *ab initio* pseudopotential method.

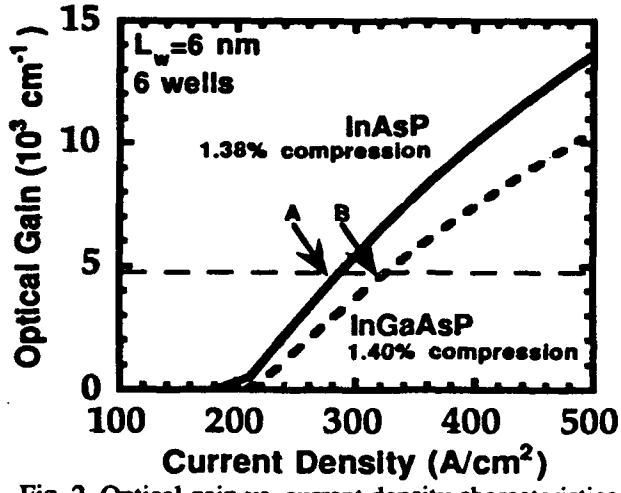

Fig. 2 Optical gain vs. current density characteristics. The results for InAsP (the solid line) and InGaAsP (the dashed line) active layers are compared. A and B are the thresholds for the 300-μm cavity with cleaved facets at both ends.

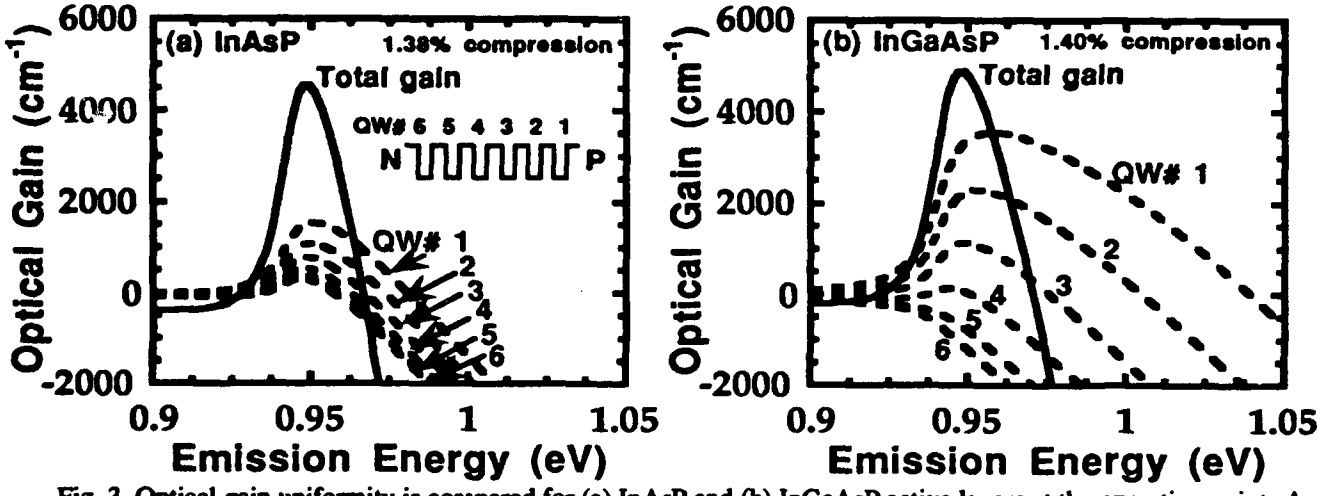

Fig. 3 Optical gain uniformity is compared for (a) InAsP and (b) InGaAsP active layers at the operation points A and B shown in Fig. 2. The dashed lines indicate the optical gain spectrum of each well and the solid line shows the spectrum of total gain. The inset in Fig. 3(a) is a schematic of the MQW structure. P and N indicate the P- and N-contacts, respectively.

P28

0.98μm InGaAs/InGaP Strained Quantum Well Lasers with GaAs/InGaP Superlattice Optical Confinement Layer

M. Usami and Y. Matsushima
KDD R&D Laboratories
2-1-15 Ohara Kamifukuoka-shi, Saitama 356, Japan

ABSTRACT : Improvement of internal quantum efficiency and threshold current density was demonstrated by introducing GaAs/InGaP superlattice optical confinement layer (SL-OCL) into InGaAs/InGaP strained QW lasers. Carrier confinement due to the multiple quantum barrier (MQB) effect in addition to the graded index effect in the SL-OCL was also discussed.

High performance 0.98 μm InGaAs/InGaP laser is a key for realizing low noise Er-doped fiber amplifiers [1,2]. Graded-index separate-confinement-heterostructure (GRINSCH) was one of the most excellent schemes to optimize optical confinement [3], however, the composition of InGaAsP GRIN layer should be carefully controlled. In this paper, we propose GaAs/InGaP superlattice optical confinement layer (SL-OCL) instead of the GRIN layer and confirm the clear improvement of the laser characteristics.

InGaAs/GaAs/SL-OCL/InGaP strained QW lasers were grown by a gas source molecular beam epitaxy. The active region consisted of 6 nm $In_{0.2}Ga_{0.8}As$ strained double quantum wells separated by 10 nm GaAs barrier and 80 nm GaAs optical confinement layers on both sides. P-type and n-type GaAs/InGaP SL-OCLs of about 40nm sandwiched the active layer. Fig. 1 shows the band diagrams for three types of the SCH structures, as follows. Type(A) : with SL-OCL, in which the thickness of each layer is uniform, Type(B) : with SL-OCL, in which the thickness of GaAs in the superlattice layers was gradually increased with getting close to the active layer, and Type(C) : without SL-OCL for reference.

Fig. 2 shows the inverse differential quantum efficiency as a function of the cavity length for the ridge waveguide lasers. The internal quantum efficiency was increased as high as 90% for type(B) by inserting the SL-OCL, although the internal loss was slightly increased, which might be due to a free carrier absorption in the impurity doped SL-OCL. Fig. 3 shows the threshold current density J_{th} as a function of the inverse cavity length. J_{th} was drastically decreased as low as J_{th}=280A/cm^2 at L=900μm in type(B). Modifying the equivalent refractive index profile as well as improvement of the carrier confinement owing to the modified GRIN SL-OCL structure were main reasons both for increasing η_i and lowering J_{th}. Temperature dependence of the threshold current is shown in Fig. 4. The characteristic temperature T_0 around room temperature was increased over 300K by inserting the uniform SL-OCL (typeA). Note that T_0 around 90°C was still kept 125K, while type(C) exhibits abrupt hike of I_{th} over 80°C. This result indicates that the multiple quantum barrier (MQB) effect [4], enhancing the confinement of carriers, is also expected in the SL-OCL structure in addition to the ordinary GRIN effect.

In summary, we have investigated the effect of GaAs/InGaP superlattice optical confinement layer (SL-OCL) inserted in the InGaAs/InGaP strained QW lasers. The internal quantum efficiency as high as 90% and the threshold current density as low as 280A/cm^2 were obtained in a laser with GRIN SL-OCL. The SL-OCL structure is also effective for high power operation under high temperature.

REFERENCES

[1] M. Shimizu et. al., IEEE J. Lightwave Technol., LT-9, (1991), p.291
[2] H. Asonen et. al., IEEE Photon. Technol. Lett., 5, (1993), p.589
[3] M. Ohkubo et. al., IEEE J. Quantum Electron., 29, (1993), p.1932
[4] K. Iga et. al., Electron. Lett., 22, (1986), p.1008

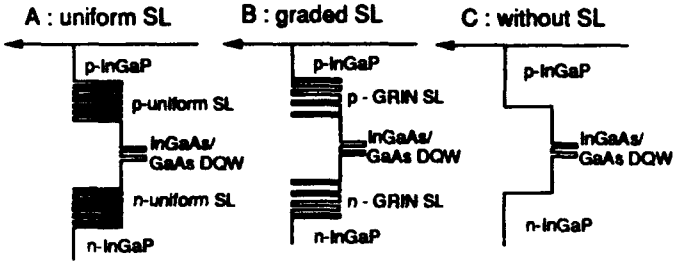

Fig. 1 Band diagram of LDs with SL-OCL (typeA, typeB) and without SL-OCL (typeC).

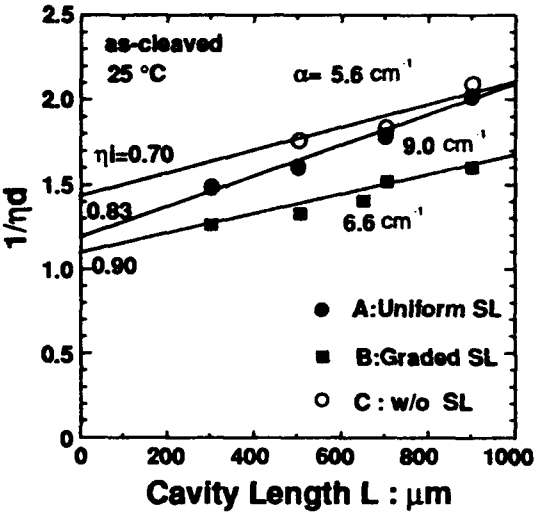

Fig. 2 Inverse differential quantum efficiency versus cavity length.

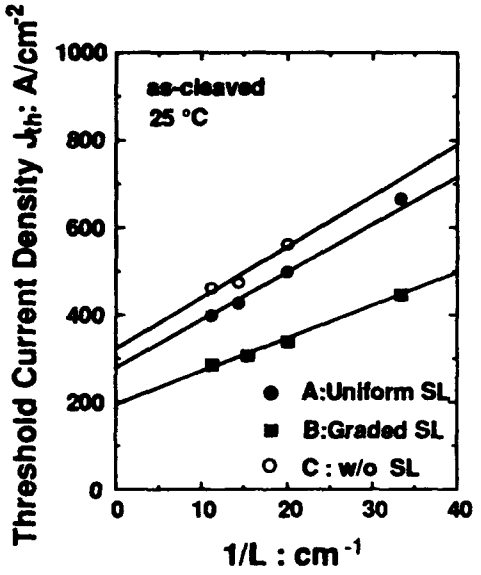

Fig. 3 Threshold current density versus inverse cavity length.

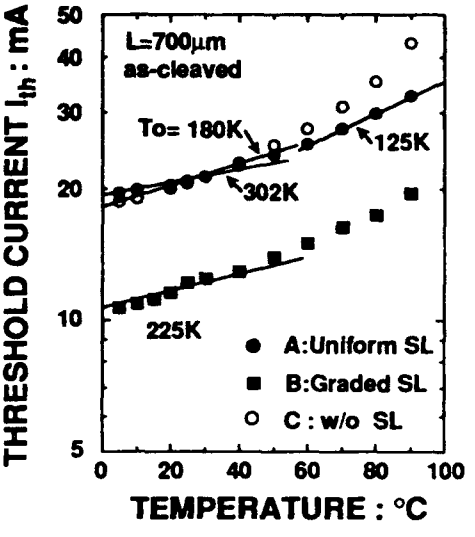

Fig. 4 Temperature dependencc of threshold current.

P29

Optically-Pumped Vertical-Cavity Surface-Emitting Lasers on (110) GaAs Substrates with Stable Polarization Characteristics

D. Sun, E. Towe, J. Grantham†, G. Vansuch† and P. Ostdiek†

University of Virginia, Charlottesville, VA 22903-2442

and

†Engineering Physics, AFIT, Wright-Patterson Air Force Base, OH 45433-7765

Abstract

We report the study of polarization characteristics of optically-pumped vertical-cavity surface-emitting laser devices fabricated from structures grown on (110) GaAs substrates. These devices exhibit stable, well-defined polarization states at room temperature.

The control of the polarization characteristics of vertical-cavity surface-emitting lasers (VCSELs) has recently generated a great deal of interest because of the potential use of these devices in polarization-sensitive applications such as magneto-optic recording and certain fiber-optic coupling experiments [1]. To date, most VCSEL structures have been grown on GaAs substrates oriented in the conventional [001] crystal direction. These devices have generally exhibited random polarization characteristics under both optical and electrical pumping. This is believed to be because of the isotropy of the gain coefficient for structures on the (001) crystal surface [2]. We have recently found that quantum well structures grown on (110) GaAs substrates have anisotropic optical properties [3]; in an effort to explore the use of this anisotropy in the control of the polarization characteristics of VCSELs, we have fabricated devices grown on (110) GaAs substrates. Our room temperature optical pumping experiments show that the [110]-oriented VCSEL structures have stable polarization characteristics.

The VCSEL structures used in our study consist of a bottom distributed Bragg reflector (DBR) made of a stack of 19.5 GaAs/AlAs quarter wave pairs. The active region consists of two $In_{0.20}Ga_{0.80}As$ (80 Å)/GaAs (80 Å) quantum wells in the middle of a one-wave $GaAs/Al_{0.45}Ga_{0.55}As$ spacer region. The top DBR mirror is composed of a stack of 16 GaAs/AlAs quarter wave pairs. These structures were grown by molecular beam epitaxy on semi-insulating (110) GaAs substrates which were vicinally mis-oriented by 6° toward (111)B surface in order to obtain high quality optical material [4]. For purposes of comparison, identical device structures were also grown on the (001) GaAs surface.

We show in Fig. 1, the reflectivity spectrum of the VCSEL structure grown on the (110) GaAs surface; shown in the inset is the lasing spectrum of the device. The optical pumping experiments were carried out at room temperature using a tunable laser source which could be operated in both the pulsed and continuous mode. The state of polarization of the laser was analyzed using a prism polarizer. The output of the device exhibited two orthogonal

polarization states: the polarization state with maximum optical intensity was oriented at a 35-degree angle relative to [001] crystallographic direction. Several spots were tested on the wafer; all of these spots showed similar polarization characteristics. The output intensity as a function of optical pumping power for the two orthogonal polarization states is displayed in Fig. 2. The intensity contrast ratio of the two orthogonal states of polarization for a pumping power of 70 mW incident onto a 10 μm-diameter spot size is about 4. In contrast, the optically-pumped VCSEL devices grown on the (001) GaAs substrate exhibited random polarization directions from spot to spot. We observed no preference of polarization direction for the (001) devices.

In summary, we have studied the polarization characteristics of optically-pumped vertical-cavity surface-emitting lasers fabricated from structures grown on vicinal (110) GaAs substrates. These laser devices showed stable polarization characteristics.

References

[1] T. Mukaihara, F. Koyama and K. Iga, Jpn. J. Appl. Phys. **31**, 1389 (1992).
[2] C. J. Chang-Hasnain *et al.* Electron. Lett. **27**, 583 (1990).
[3] D. Sun, E. Towe, M. Hayduk and R. Boncek, Appl. Phys. Lett. **63**, 166 (1993).
[4] D. Sun and E. Towe, J. Crystal Growth, **132**, 2882 (1993).

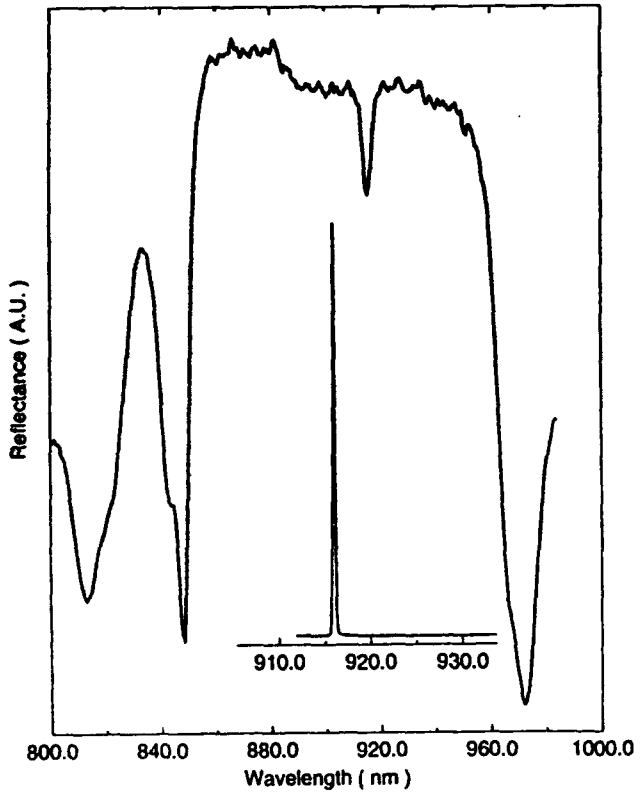

Figure 1. Reflectance spectrum of the VCSEL structure grown on vicinal (110) GaAs; inset: room temperature lasing spectrum of the optically-pumped device.

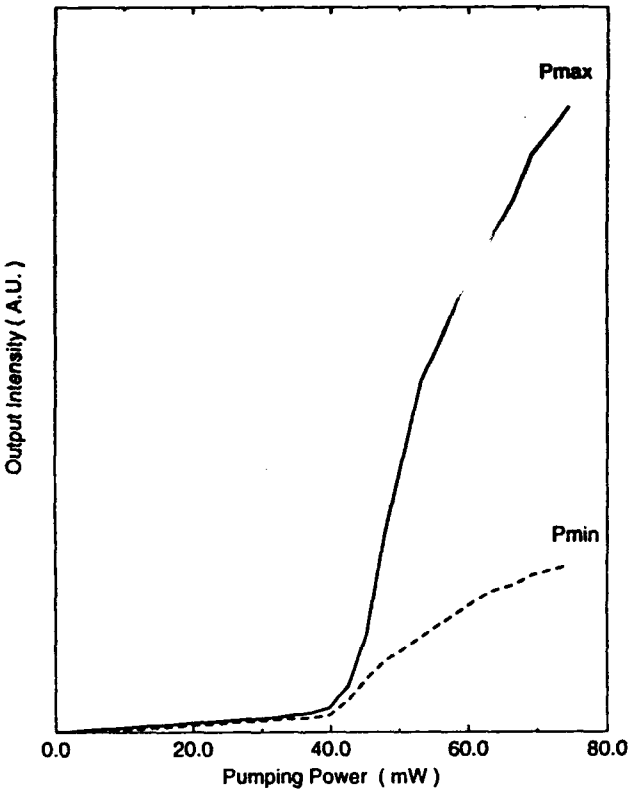

Figure 2. The lasing intensities of orthogonal polarization states as a function of optical pumping power for the VCSEL structure grown on the vicinal (110) GaAs.

P30

Circular-grating surface-emitting distributed Bragg reflector lasers on an InGaAs/GaAs structure for 0.98 μm applications

M. Fallahi, F. Chatenoud, M. Dion, I.M. Templeton, R. Barber and J. Thompson

National Research Council of Canada and Solid State Optoelectronics Consortium, Ottawa, Ontario, Canada, K1A 0R6, Fax : (613) 957 8734

Abstract : InGaAs/GaAs circular-grating surface-emission DBR lasers with a pulsed external efficiency over 11% (power > 100 mW) and a divergence of 1° are obtained. We also demonstrate the first CW operation near room temperature.

Summary : Surface emitting lasers with high power and low divergence are very attractive for a number of optoelectronics applications. Circular-grating surface-emitting distributed Bragg reflector (CG-SE-DBR) lasers are new candidates with great potential to fulfill these requirements.In the last few years, a number of theoretical and experimental studies have been published on CG-SE DFB/DBR lasers [1-5]. In this work, we present our latest results and report the first CW operation of CG-SE-DBR lasers.

Fig. 1 shows a schematic view of our InGaAs/GaAs CG-SE- DBR lasers A circular gain region is defined in the center of the structure. Second-order circular gratings are used in order to provide feedback for resonance as well as surface emission. The active layer is a strained InGaAs/GaAs quantum-well (QW), graded-index, separate-confinement heterostructure (GRINSCH). In order to avoid any regrowth and complication in the process, the passive section has the same layer structure as the gain section and the gratings are defined on the top of the QW layers. The structure was grown by one-step MBE. Gain sections with diameters of 100 μm and less were defined by reactive ion etching (RIE) of GaAs and AlGaAs in BCl_3 : He gas mixture. P-type contacts were then made on top of the mesas. Second-order circular gratings with periods of about 300 nm were defined by electron-beam lithography and etched into AlGaAs above the active region by RIE. The radial extent of the circular gratings surrounding the active region is about 150 μm. Finally, a n-type back contact was evaporated.

Fig. 2 shows the room temperature L-I curve of a 100 μm diameter gain region under pulsed operation with 1% duty cycle. The threshold current is about 80 mA and the external efficiency measured from the surface-emitted power is over 11% with a maximum power of 100 mW. High temperature operation up to 90°C is also obtained [5]. The device operated with almost the same threshold current under a 40% duty cycle pulse. The measurement of the far-field pattern gives a divergence of 1° in all directions with a quasi-circular section which is of a great interest for many optical communication applications. Recently, by optimizing the process steps, the first CW operation of a CG-SE-DBR laser with an 80 μm diameter gain section was obtained near room temperature. Figure 3 shows the CW lasing spectrum of the laser at 10, 15 and 20 °C. The lasing wavelength is about 970 nm with a temperature shift of 1 Å/degree. The measure of the CW L-I curve shows that at 5 °C the threshold current is about 66 mA with an external efficiency of 4%. At 10 °C the threshold current increases to 73 mA and the external efficiency drops to 2.6 %. Further increase of the temperature to 15 °C and above resulted in a drop of the external efficiency. Detailed results will be presented and discussed.

References :

[1] : M. Toda, IEEE J. Quantum Electron., vol. 26, p.473, 1990.

[2] : C. Wu, M. Svilans, M. Fallahi, I.M. Templeton, T. Makino, J. Glinski, R. Maciejko, S.I. Najafi, C. Maritan, C. Blaauw and G. Knight, Electron. Lett., vol. 28, p. 1037, 1992.

[3] : M. Fallahi, M. Dion, F. Chatenoud, I.M. Templeton and R. Barber, Electron. Letters, vol. 29, p. 2117, 1993.

[4] : T. Erdogan, O. King, G.W. Wicks, D.G. Hall, E.H. Anderson, M.J. Rooks, Appl. Phys. Lett., vol. 60, p.1773, 1992.

[5] : M. Fallahi, M. Dion, F. Chatenoud, I.M. Templeton, and R. Barber, accepted for publication in IEEE Photonics Technology Letters, March 1994.

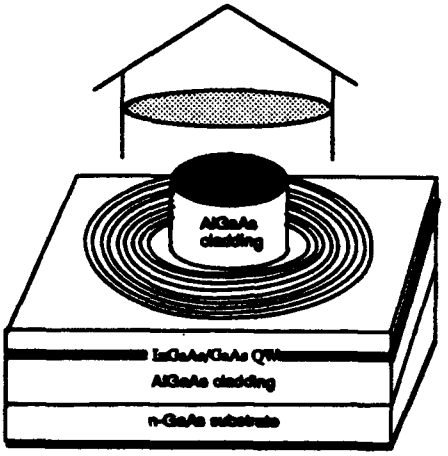

Fig. 1 : Circular Grating Surface Emitting DBR laser

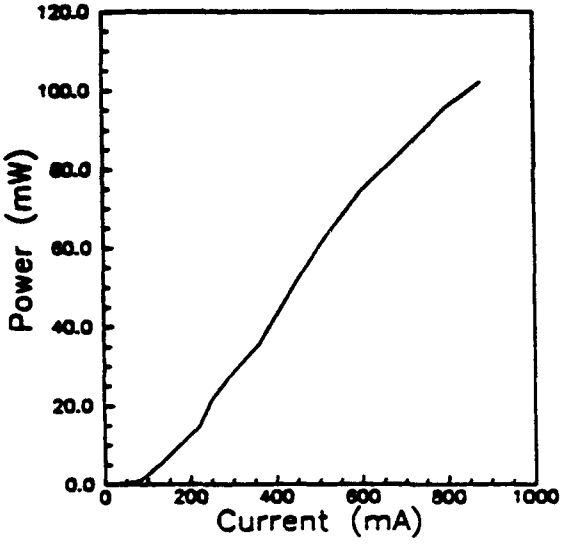

Fig. 2 : L-I curve (pulsed) of a CG-SE DBR laser

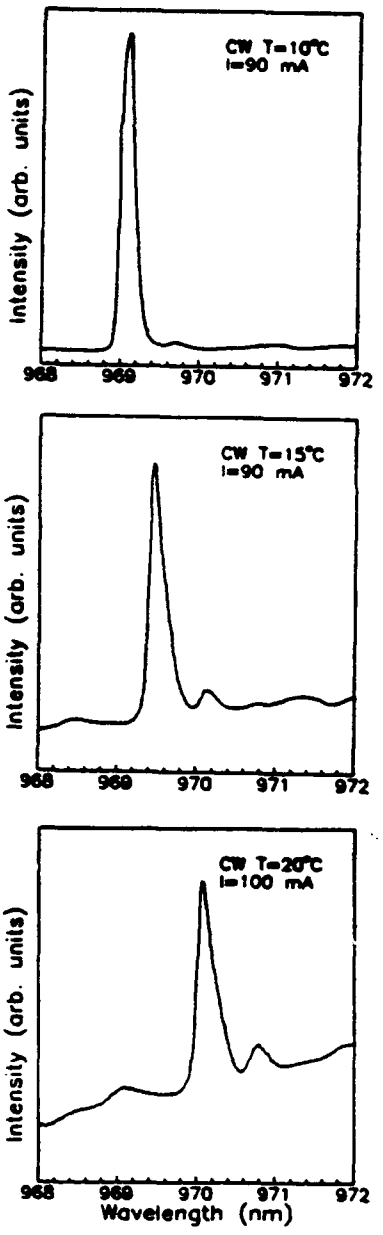

Fig. 3 : CW lasing spectrum at different Temperature

P31

Optimization of Gain and Mode Field Overlap for Efficient Proton Implanted Broad Area Vertical-Cavity Laser Diodes

B. Möller[1], E. Zeeb[1], T. Hackbarth[2], K.J. Ebeling[1]
University of Ulm, Dept. of Optoelectronics, D-89069 Ulm, Germany[1]
Daimler Benz Research Center, D-89013 Ulm, Germany[2]

Abstract: Overlap of gain and mode profiles in conventional planar proton implanted VCSELs is measured to be in the order of 10%. The resulting low device efficiency is considerably increased if a beam transforming layer is integrated.

There is an urgent need for transverse mode control in broad area vertical-cavity surface-emitting laser diodes (VCSELs). To this aim we have performed a detailed study of fundamental and higher order transverse mode behavior in planar VCSELs to better understand the effects of integrated mode filters and lenses on emission characteristics. Near field mode patterns whose overlap with the gain profile greatly affects laser efficiency have been determined precisely.

Experiments presented were performed on a standard VCSEL of 25 μm active diameter. Smaller devices of 12 μm size of the same wafer oscillate single-mode over the whole current range up to 0.45 mW output power with a minimum linewidth of 70 MHz and a record low linewidth-power product of 4.8 MHz·mW. Larger devices of 55 μm diameter oscillate multi-transverse mode and exhibit maximum output powers of more than 12 mW and small-signal bandwidths beyond 10 GHz when mounted on heat sinks. Fig. 1 shows output power characteristics of a non heat sinked 25 μm VCSEL. Indicated are the onsets of higher order transverse modes. Fig. 2 gives threshold currents and mode spacings. Included are theoretical data according to a simple model that assumes parabolic refractive index and gain profiles induced by thermal heating and carrier diffusion. Self-consistent calculations [1] give Laguerre-Gaussian modal eigenfunctions from which near and far field patterns are readily obtained. Fig. 3 shows the measured far field patterns and emission spectra for different driving currents. Solid lines are calculated from the spectra. The agreement between theory and experiment is excellent. Hence, calculated near field patterns in Fig. 4 have to be attributted the same accuracy. The current distribution across the active layer is well approximated by a step function for the planar proton implanted devices studied [2]. The overlap of modal intensity and current density distributions estimates device efficiency. Results plotted in Fig. 5 show that the efficiency typically remains below 20%. However, when a beam transformimg layer correcting for thermal lensing is inserted in the cavity considerable improvement of the device performance can be obtained as is also indicated in Fig. 5.

In summary, precise measurements on high performance planar proton implanted VCSELs show that due to imperfect mode and current overlap device efficiency typically remains below 20%. Integration of an antiguiding layer considerably enhances the efficiency by at least a factor of 3.

[1] A. E. Siegman, *Lasers*, University Science Books, Mill Valley, Carlifonia, 1986.
[2] R. Michalzik and K.J. Ebeling, *IEEE J. Quant. Electron.*, vol. 29, pp. 1963-1974, 1993.

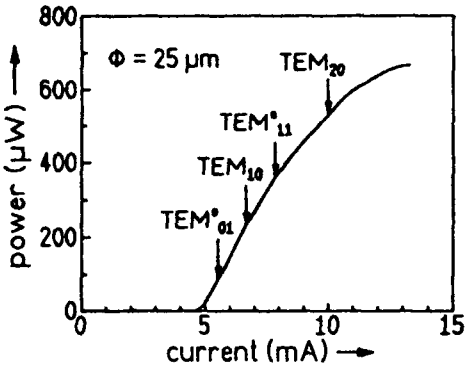

Fig. 1: Light output characteristics of a 25 μm active diameter VCSEL.

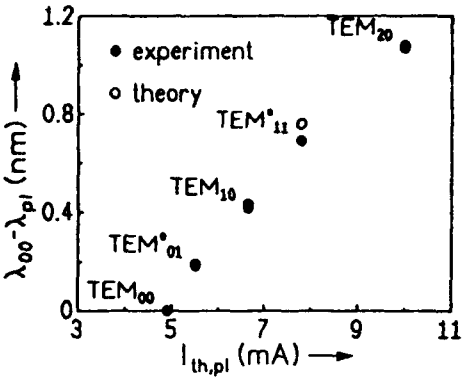

Fig. 2: Threshold currents and emission wavelengths of transverse modes.

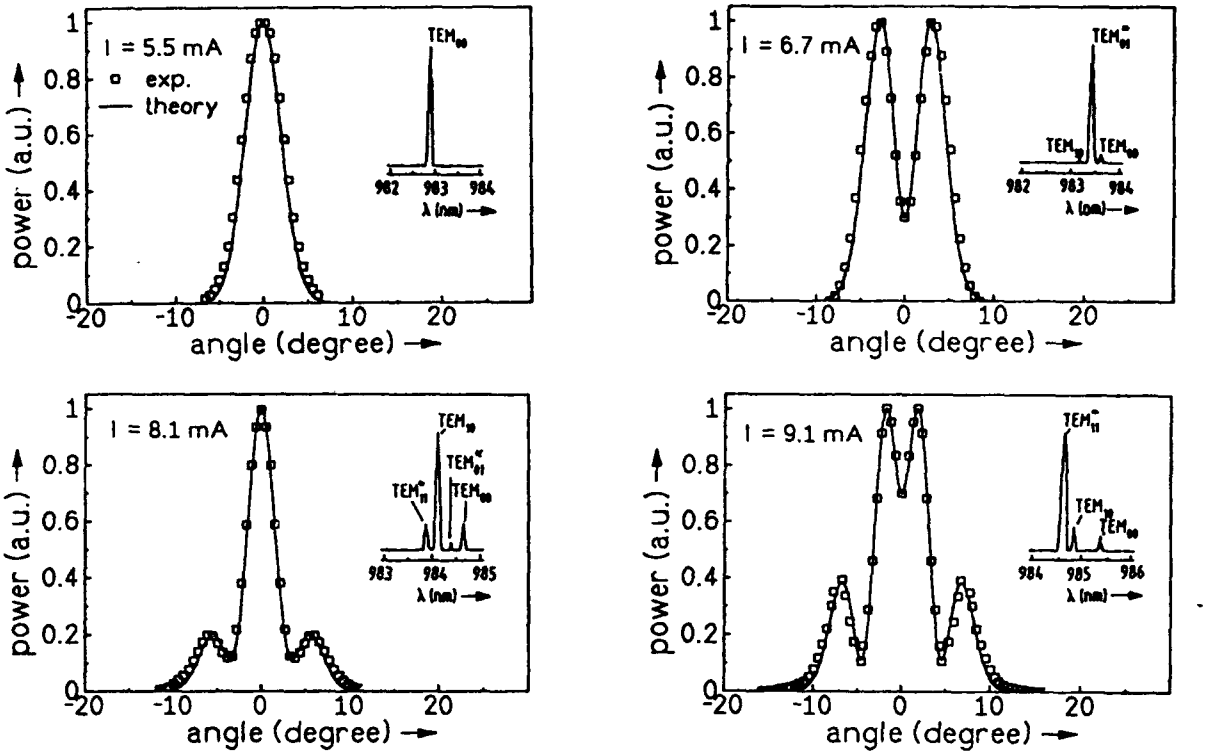

Fig. 3: Measured and calculated far field intensity profiles for driving currents of 5.5 mA, 6.7 mA, 8.1 mA, and 9.1 mA. Corresponding emission spectra in the insets.

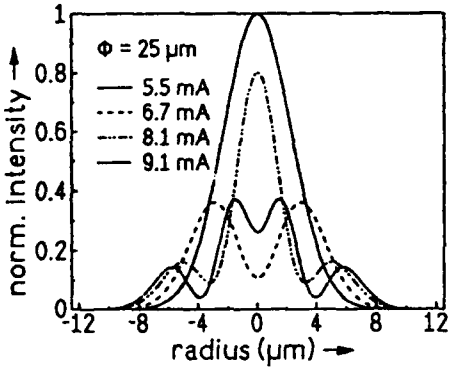

Fig. 4: Radial near field profiles in the active layer.

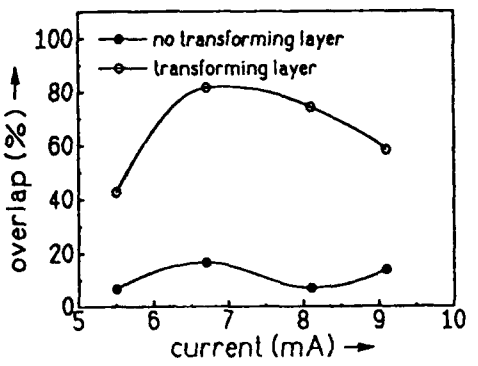

Fig. 5: Overlap of gain and near field profiles.

P32

Polarization Induced Enhancement of Relative Intensity Noise and Modulation Distortion in Vertical Cavity Surface Emitting Lasers

M.S. Wu, L.A. Buckman*, G.S. Li, K.Y. Lau*, C.J. Chang-Hasnain
E.L. Ginzton Laboratory, Stanford University, Stanford, CA 94305
* Department of EECS, University of California at Berkeley, Berkeley, CA 94720

Abstract: Due to the lack of polarization control in proton-implanted vertical cavity surface emitting lasers, increased relative intensity noise and pulse distortion are observed when the laser is modulated and a single polarization direction is selected.

Introduction: Proton implanted vertical cavity surface emitting lasers (VCSELs) are extremely attractive because of their ease of fabrication and high yields. However, they exhibit circular symmetry and consequently, two orthogonal polarization modes can oscillate simultaneously [1]. Polarization selection is determined by unintentional anisotropy of the gain medium. The polarization stability of VCSELs under modulation is thus of critical concern in applications involving polarization sensitive components. These applications include: optical computing, optical interconnects, and optical communications. Previous investigations of polarization stability have considered only continuous-wave (CW) operation [1]-[4]. We report the relative intensity noise (RIN) and pulse shape distortion of VCSELs while modulating the laser up to 2 GHz. We establish three regimes of laser operation: Regime I, single polarization mode (I_{th} - 1.4 I_{th}); Regime II, dual polarization modes/single spatial transverse mode (1.4 I_{th} - 1.7 I_{th}); and Regime III, dual polarization modes/dual spatial transverse modes (> 1.7 I_{th}). A significant increase in RIN and pulse shape distortion were observed in the second and third regimes when a single polarization mode is isolated. Negligible effects were observed in the first regime. The devices considered in this study are GaAs-AlGaAs top-emitting, multi-quantum well VCSELs operating at 0.85 μm [5]. Detailed results from a typical device are presented.

Experimental setup: The laser was biased with a current source and modulated with either a frequency synthesizer or pulse generator through a bias tee. The VCSEL beam was collimated and refocused onto a GaAs photodetector. The RF signal was amplified using a 45 dB gain amplifier with a 3 dB-bandwidth of approximately 3 GHz. The RF signal was then observed on a RF spectrum analyzer or sampling oscilloscope. A polarizer, mounted on a rotation stage and positioned between the collimating and focusing optics, was used to select a single polarization mode.

Results: The CW light-current (LI) characteristics were measured with and without polarization selection. As discussed previously, three distinct regimes of operation were identified. These are illustrated in Figure 1. The LI curve, without polarization selection, clearly shows a nonlinearity at the onset of the second spatial transverse mode (I $\approx$ 1.7 I_{th}). Using an optical spectrum analyzer, this mode is first observed with a suppression ratio of over 30 dB at a bias current of 1.7 I_{th} with 1 mA peak-to-peak modulation.

A pulse generator was used to modulate the laser from 2 Mb/s to 2 Gb/s with 1 mA peak-to-peak modulation. The detected, amplified pulses with and without polarization selection, with the laser biased in each of the three regimes, were observed on a sampling oscilloscope. In the first regime, negligible distortion of the pulses occur when selecting the first polarization mode. In the second and third regimes, the pulse shape was distorted when either polarization mode was selected. This pulse shape distortion was quantified by considering the harmonic distortion introduced by polarization selection when the laser was modulated with a sinusoidal signal. With the laser biased in each regime and modulated at frequencies ranging from 100 MHz to 2 GHz, the power in the second harmonic, with and without polarization selection, was normalized to the power in the fundamental. Figure 2 shows the increase in the normalized second harmonic power when the first polarization mode is selected when compared to the case of no polarization selection. As illustrated in Figure 2, in the first regime less than 2 dB distortion is observed over the entire modulation frequency span. In the second and third regimes, a distortion as high as 4 dB and 12 dB, respectively, was observed at a modulation frequency of 100 MHz. Distortion for both regimes decreases significantly with increasing

modulation frequencies (> 500 MHz).

The RIN spectra, with and without polarization selection, in each of the three regimes with 1.5 GHz modulation is shown in Figure 3. The spectra was observed to be independent of applied modulation. As expected, the RIN decreases with increasing bias and the relaxation peak of the laser modulation response flattens and shifts to higher frequencies. However, substantial RIN enhancement is observed in all regimes at low frequencies when selecting a single polarization mode. As shown in Figure 3, the amount of RIN increase depends on the regime of operation. This low frequency RIN enhancement is most significant in the second and third regimes due to the onset of the additional polarization mode and transverse mode respectively. This type of low frequency RIN enhancement is characteristic of mode partition noise similar to that observed in conventional multi-longitudinal mode edge-emitting lasers [6].

Conclusion: We have shown that due to the random nature of the polarization direction in proton-implanted vertical cavity surface emitting lasers, significant RIN increase and modulation distortion are observed when modulating the laser and selecting a single polarization mode.

References

[1] C.J. Chang-Hasnain et.al., *IEEE J. Quantum Electronics*, vol. 27, no. 6, pp. 1402-1409, June 1991.

[2] F. Koyama et.al.,*IEEE J. Quantum Electronics*, vol. 27, no. 6, pp. 1410-1416, June 1991.

[3] K.D. Choquette et.al.,*IEEE Trans. on Electron Devices*, vol.40, no.11, pp. 2117-2118, Nov. 1993.

[4] A. Chavez-Pirson et.al.,*Appl. Phys. Lett.*, vol.62, no. 24, pp. 3082-3084, June 1993.

[5] G. Hasnain et.al.,*IEEE J. Quantum Electronics*, vol. 27, no. 6, June 1991.

[6] C.B. Su et.al., *Appl. Phys. Lett.*, vol.57, no. 9, pp. 849-851,Aug. 1990.

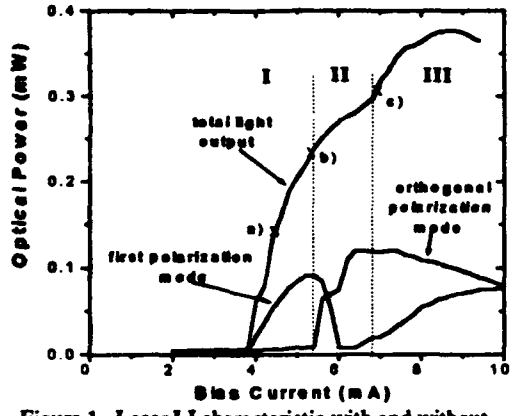

Figure 1. Laser LI characteristic with and without polarization selection. The reduction in the optical power with polarization selection is due to the transmission loss of the polarizer. a) 1.1 Ith b) 1.4 Ith c) 1.7 Ith

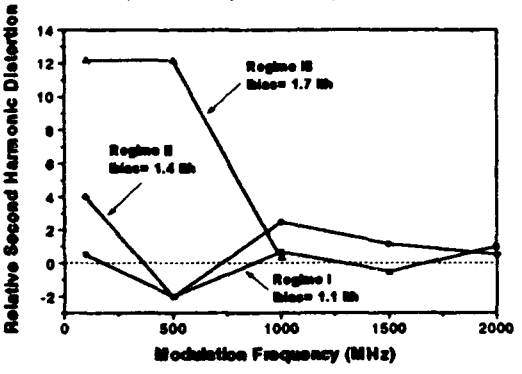

Figure 2. Increase in the normalized second harmonic power when the first polarization mode is selected.

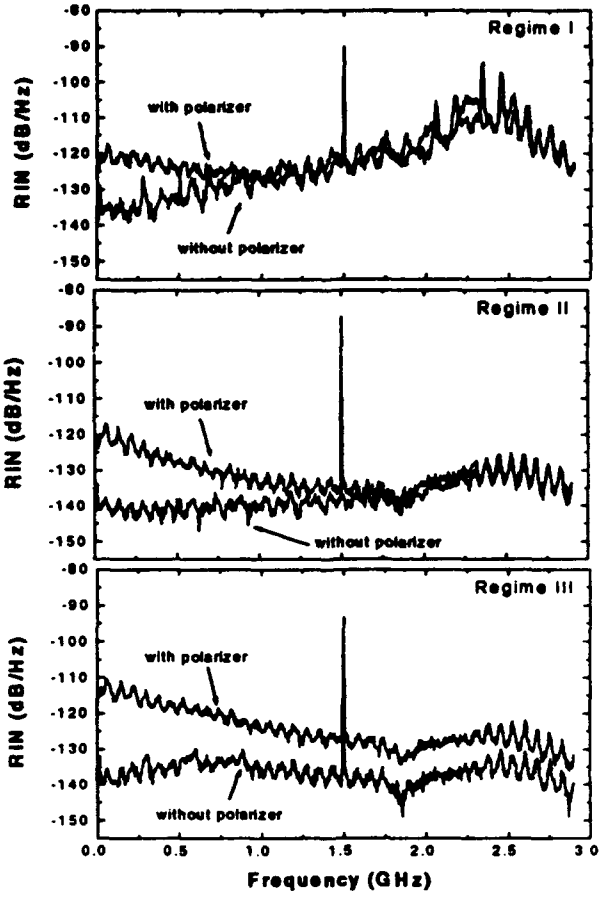

Figure 3. RIN spectra with and without polarization selection in each of the three regimes.

P33

Lateral Mode Behavior of CW Proton-Implanted Vertical-Cavity Surface-Emitting Lasers

G. R. Hadley, K. L. Lear, M. E. Warren
Sandia National laboratories, MS0603
Albuquerque, New Mexico 87185-5800

J. W. Scott
Optical Concepts, Incorporated
432A Commerce Court
Lompoc, CA 93436

S. W. Corzine
University of California at Santa Barbara
Santa Barbara, CA, 93106

ABSTRACT

We employ a highly-sophisticated numerical model to provide the first study of lateral mode competition during cw operation of proton-implanted vcsels. The model is validated by direct comparison with experimental data, and is used to explore new device designs for extending fundamental mode operation to higher powers.

Vertical-cavity surface-emitting lasers (vcsels) are presently the subject of intense research due to their potential as compact, efficient, astigmatic laser sources for a number of important applications. Of special interest are the gain-guided vcsels fabricated by proton-bombardment, which offer ease of fabrication, planar geometry, high efficiencies and inherently high fundamental-mode output powers. The onset of higher-order modes at powers of a few milli-Watts, however, presently limits the wide utilization of these devices and indicates the need for improvements in design. Unfortunately, their complexity precludes optimization based solely upon empirical methods, and points instead to the need for a comprehensive model.

In order to better understand the operation of these lasers and to allow accurate design optimization, we have constructed a highly-sophisticated and complete numerical model that simulates virtually all major device processes. This is the first vcsel simulation to include self-consistently the effects of thermal and carrier transport with a multimode optical model, so as to explore the onset of higher-order lateral modes. In particular, we include the following physical processes modeled in 3D (assuming cylindrical symmetry): (1) The Ohmic transport of carriers through the cladding layers to an active region, including anisotropic conductivities, (2) The transport of heat towards a heat sink beneath the substrate, including source terms from Ohmic dissipation, non-radiative recombination and reabsorbed laser radiation, (3) The diffusion of carriers inside the quantum well, and their recombination via spontaneous emission, stimulated emission, and non-radiative processes (both through traps and Auger transitions), (4) The cw behavior of five different optical cavity modes, denoted by their assumed azimuthal dependences of the form $\exp[\pm im\varphi]$, with $m = 0-4$, and (5) The interaction of each of these modes with carriers in the quantum well through a comprehensive gain model that includes effects arising from the strained band structure of our InGaAs quantum well[1].

The devices used in this study were processed from molecular-beam-epitaxially-grown wafers of AlGaAs mirrors on n-type GaAs substrates with triple InGaAs quantum wells, as described in detail elsewhere[2]. Gain-guided vcsels with circular symmetry and diameters ranging from 10-35 μm were then defined by proton bombardment, resulting in device geometries shown schematically in Fig. 1. We modeled a simplified version of the devices in which the triple quantum wells were assumed to have equal carrier density profiles[3]. Once the electrical resistivities were modified to reproduce the measured device resistance for several device diameters, no other parameter adjustments were employed. The resulting predicted LI curves for the 15-μm-diameter device are shown in Fig. 2 for values of the material parameter dn/dT (the derivative of refractive index w.r.t. temperature) ranging from the commonly accepted value of 4×10^{-4} down to zero. Results obtained using the accepted value predict the onset of two higher-order lateral

modes as shown. These two modes were also observed experimentally, appearing at currents corresponding to the kinks in the curve marked "Experiment" in Figure 2 (and confirmed by near-field and spectral measurements). In addition, the calculated results accurately predict the measured threshold current and differential quantum efficiency, and approximately predict the observed thermal rollover. Further calculations using decreasing values of dn/dT show a decreasing presence of higher-order lateral modes (Fig. 2). These results demonstrate clearly the crucial role played by thermal lensing in determining the cw modal behavior of these devices. The thermal lens acts to pull the higher-order modes into the gain region, where they compete more effectively with the fundamental mode.

Subsequently, our model has been used to investigate the effects of various design parameters (such as the diameter and depth of the implanted region) on the modal discrimination. The resulting implications of these studies on optimum device designs for high-power fundamental-mode operation will be presented.

1. S. W. Corzine, R. H. Yan, L. A. Coldren, App. Phys. Lett. 57, No. 27, 2835(1990).
2. K. L. Lear and S. A. Chalmers, IEEE Phot. Tech. Lett. 5, No. 9, 972(1993).
3. J. W. Scott, S. W. Corzine, D. B. Young and L. A. Coldren, App. Phys. Lett. 62, No. 10, 1050(1993).

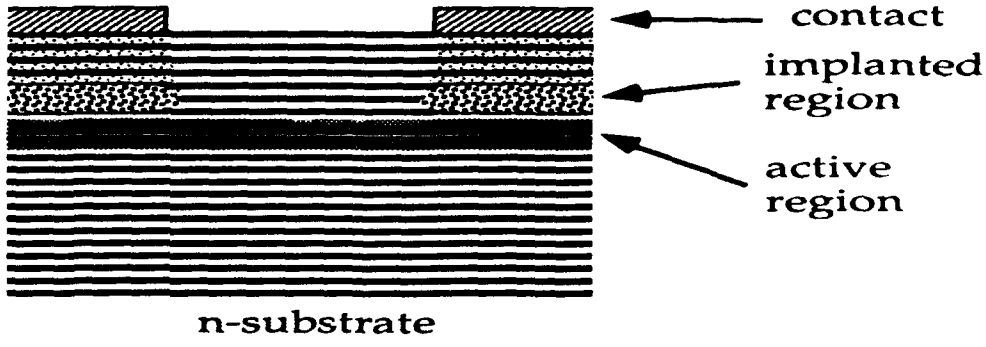

Fig. 1.Schematic of proton-implanted vcsel used in the present study. Heat sinking is through the substrate.

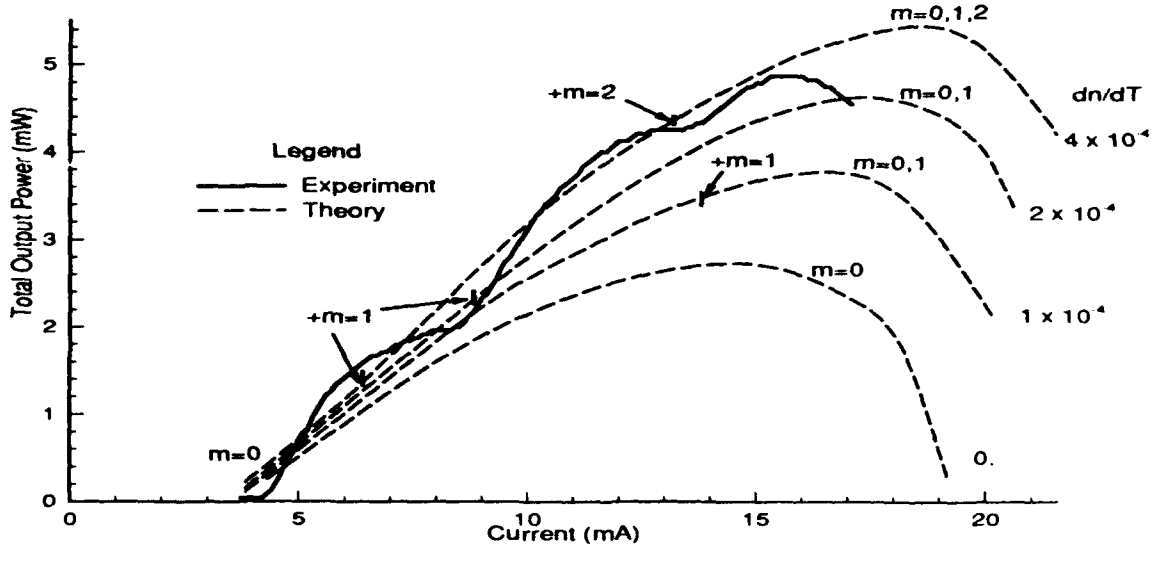

Fig. 2.Measured and calculated LI curves for a 15-μm-diameter vcsel. The predicted onset of higher-order lateral modes is shown by the arrows. Only the top theoretical curve predicts all three modes observed experimentally.

P34

Gain-Dependent Polarization Properties of Vertical-Cavity Lasers

Kent D. Choquette, K. L. Lear, R. P. Schneider, Jr., and R. E. Leibenguth*
Sandia National Laboratories
Albuquerque, NM 87185
*AT&T Bell Laboratories, STC
Breinigsville, PA 18031

Abstract: We show that the power partitioning between orthogonal TE polarization states depends on their relative spectral alignment with the gain spectrum in VCSELs. A simple means of maintaining a dominant eigen polarization for all elements in a VCSEL array is described.

Each electromagnetic field configuration of a vertical-cavity surface emitting laser (VCSEL) possesses two orthogonal TE polarization states which can share the laser output power. What governs the competition between these eigen polarizations in the absence of an intentional gain [1] or cavity [2] anisotropy is unclear. Furthermore, maintaining a single polarization for all devices in a wafer will be critical for the deployment of VCSELs in polarization-sensitive applications. We show the partitioning of power between the orthogonal polarization modes is correlated with the spectral alignment of the cavity resonance of each polarization state with the laser gain spectrum. Based on our findings, a simple means to sustain a single polarization in VCSEL arrays is described.

We have performed the first extensive polarization-resolved light intensity vs. current (L-I) measurements for MOVPE and MBE grown gain-guided ion implanted VCSELs over a wide operating temperature range. The spectral splitting between the eigen polarizations were also determined using a scanning Fabry-Perot interferometer. InGaAs and GaAs quantum well 15 μm diameter VCSELs designed for 950 and 850 nm emission, respectively, were included in our study. InGaAs VCSELs, grown by MOVPE on misoriented substrates, possess eigen polarizations that are always aligned along the <110> crystal directions (denoted as 0° and 90°) over a wide range of temperature. In contrast the GaAs VCSELs, grown by MBE on (100) substrates, exhibit eigen polarizations which are randomly oriented in the plane of the quantum wells and vary with operating temperature [3]. For the InGaAs VCSELs, both quantum well strain and the misoriented substrate likely contribute to the crystallographic polarization alignment.

Figure 1 shows the room temperature L-I curves of InGaAs VCSELs from various locations in one wafer. This MOVPE wafer was not rotated during growth, producing a 5% variation of layer thickness and thus cavity resonance, but only a 1% change in the maximum gain wavelength, along the direction of gas flow. The dominant Gaussian mode polarization varies with location on the wafer as shown in Fig. 1. In Fig. 2 we plot the threshold current, I_{th}, and threshold wavelength vs. wafer position. Near the "thick" front edge of the wafer, corresponding to blue-shifted gain relative to the cavity resonance, the 90° eigen polarization is dominant. Conversely, at the opposite "thin" end of the wafer, corresponding to red-shifted gain, the 0° eigen polarization is dominant. In between near the wafer region exhibiting the minimum I_{th}, the 90° state initially dominates at threshold until an abrupt switching transition where upon the opposite state prevails before the emergence of higher order transverse modes.

In Fig. 3 we plot I_{th} vs. substrate temperature for a GaAs VCSEL. Fig. 3 is similar to Fig. 2 in that the spectral mismatch between the cavity resonance and gain is adjusted by their noncommensurate thermal shifts rather than growth nonuniformity. Again we observe that the eigen polarizations are each dominant on opposite sides of the minimum I_{th}, separated by a region of polarization switching [3]. The inset shows the room temperature spectral splitting of the polarized Gaussian modes for the laser characterized in Fig. 3. The two peaks in the inset, which correspond to the two eigen polarizations, are separated by 0.23 Å under the condition of no applied stress.

The polarization power partitioning and the I_{th} dependence on wafer location or substrate temperature are both related to the relative spectral alignment of the cavity resonance of each polarization mode with the laser gain. In Figs. 2 and 3 the minimum I_{th} occurs at the wafer location or substrate temperature where the cavity resonance and laser gain are optimally aligned. When the gain is blue- or red-shifted relative to the cavity resonance, greater injection is required to achieve lasing. Due to the spectral splitting of the fundamental polarization states, under the condition of blue-shifted gain, the shorter wavelength eigen polarization will enjoy enhanced gain overlap, while for red-shifted gain, the longer wavelength eigen polarization will dominate. Moreover, near gain/cavity resonance alignment, the dominant polarization should abruptly switch by 90° as the gain sweeps through the resonances of the polarization states due to ohmic heating with increasing current injection. Polarization switching is seen explicitly for the Gaussian mode and higher order modes in Fig. 1(b).

The kinks seen in the total output power curves in Fig. 1 (denoted with arrows) indicate the onset of a higher order mode. Note that when the gain is red-shifted relative to the cavity resonances as in Fig. 1(a), the higher order mode tends to be orthogonally polarized to the fundamental, presumably to better utilize the gain [4]. However, for sufficiently blue-shifted gain, the higher order mode arises with the same polarization as the fundamental as in Fig. 1(c). This indicates that spectral hole burning is perhaps of greater consequence under the condition of red-shifted gain. Further, with the tradeoff of higher I_{th}, VCSEL arrays with each element having its gain blue-shifted ≥ 20 nm

from the cavity resonance will provide a single dominant polarization through the onset of multi-mode operation. For array polarization uniformity, it is crucial that the cavity resonances do not span the gain peak maximum.

From examination of several GaAs VCSEL wafers, we find the polarization spectral splitting, such as shown in the inset of Fig. 3, varies only slightly between devices on a given sample, but can be 0.6 to $<10^{-2}$ Å for different samples. Interestingly, the sample with the smallest polarization splitting still exhibits the polarization gain-dependence to the same degree as discussed above. We also find that locally applied stress can effect both the splitting as well as the power partitioning [1] between the eigen polarizations. We will further discuss polarization strain effects and describe the application of polarization switching in novel VCSEL structures.

[1] F. Koyama and K. Iga, *IEEE Photon. Technol. Lett.* **5**, 133 (1993).
[2] K. D. Choquette and R. E. Leibenguth, *IEEE Photon. Technol. Lett.* **6** (1994).
[3] K. D. Choquette, *et. al*, *Appl. Phys. Lett.* **64** (1994).
[4] C. J. Chang-Hasnain, *et. al*, *Electron. Lett.* **27**, 1067, (1991).

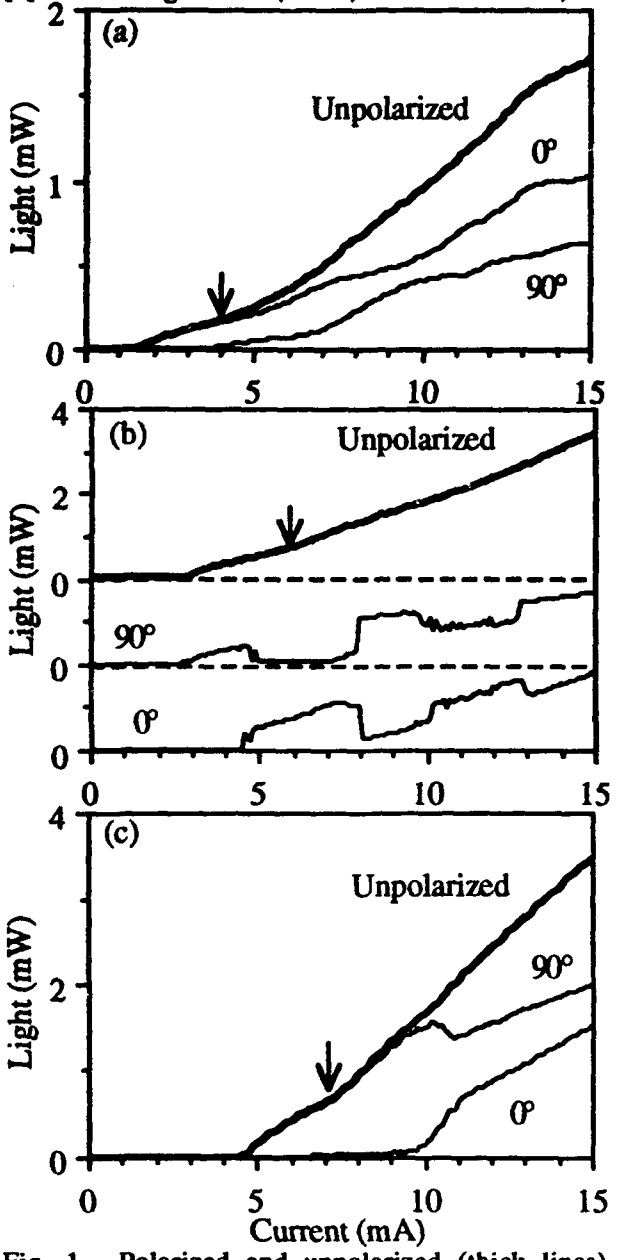

Fig. 1. Polarized and unpolarized (thick lines) emission vs. current at 297 K for three InGaAs VCSELs at different wafer locations; λ_{th}= (a) 943 nm, (b) 965 nm (curves offset for clarity), and (c) 970 nm.

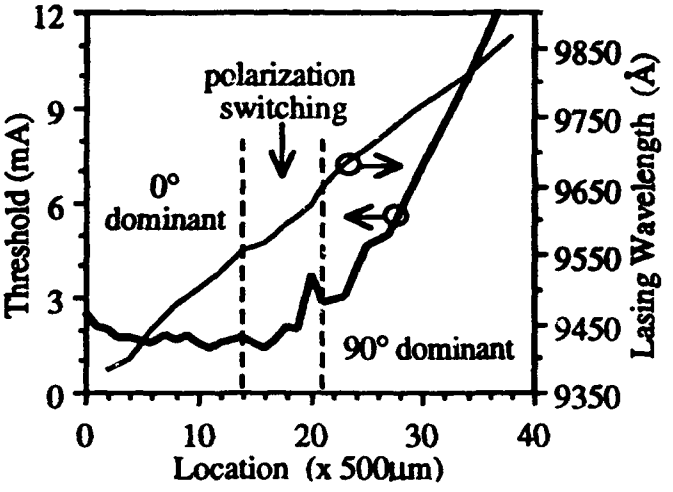

Fig. 2. I_{th} and threshold wavelength vs. wafer position for the InGaAs VCSELs.

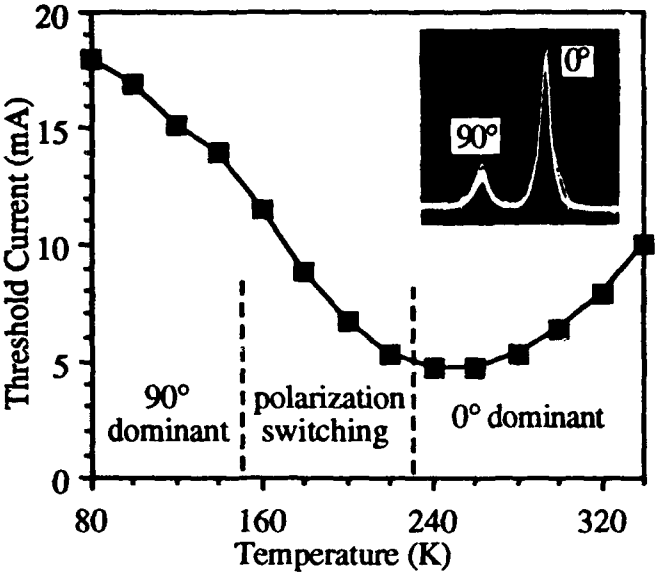

Fig. 3. I_{th} vs. substrate temperature for a GaAs VCSEL. The inset shows the room temperature spectral splitting (0.23 Å) where each peak correspond to an eigen polarization of the Gaussian mode.

P35

Growth Direction Dependence of Polarization Properties in Surface-Emitting Lasers with Strained Quantum Wells

T. Ohtoshi, T. Kuroda, A. Niwa, S. Tsuji, and K. Uomi
Central Research Laboratory, Hitachi, Ltd.
Kokubunji, Tokyo 185, Japan

Abstract—Polarization properties of surface-emitting lasers are analyzed theoretically for various crystallographic directions. In strained quantum wells on ($NN1$) substrates ($N \geq 2$), the polarization can be controlled, facilitating high optical gains.

In this paper we discuss the polarization properties of vertical-cavity surface-emitting lasers (VCSELs) and their dependence on growth direction. The optical anisotropy in (110)-QWs has been analyzed by Kajikawa *et al.*, but only at the Brillouin-zone center ($k_{||}=0$).[1] In this work, we calculate, for the first time, optical gains related to arbitrary growth directions at non-zero $k_{||}$ values to estimate polarization properties in the VCSELs.

The present model is based on the Luttinger-Kohn effective-mass theory [2] for valence bands, taking into account strain-orbit interaction. The conduction band is calculated by Kane's model.[3] The energy-band structures for arbitrary growth directions are obtained by rotating the conventional (001) Hamiltonian H, i.e., $UHU^{\dagger}$ where $U=R_{y'}(\theta)R_z(\phi)$. Here, $R_{y'}(\theta)$ and $R_z(\phi)$ represent the spinor rotations [4] which transform the basis states from (x,y,z) coordinates to (x',y',z') coordinates, as shown in Fig. 1. The z axis corresponds to the primary crystallographic axis [001] and the z' axis is normal to the substrate surface (hkl). The resulting multiband effective-mass equation is solved by means of the finite-difference method to consider the spreading of wave functions inside barrier materials.

Next, we present calculated results for $In_{0.7}Ga_{0.3}As$ (3.5nm)/InP strained-quantum-well (QW) lasers. Figure 2 shows the in-plane dispersions of the valence bands in (001)- and (221)-orientations. It is worth noting that conventional models assuming infinite barriers underestimate the hole effective mass. Figure 3 shows equi-energy patterns in the in-plane wavenumber space, k_1-k_2. Here, k_1 and k_2 denote the in-plane wavenumbers in the (x',y',z') coordinate system. Since (001) and (111) QWs belong to the D4h and D6h point groups, respectively, their optical properties are isotropic in the QW plane. Meanwhile, other orientations, such as (112) and (221), have twofold symmetry, thus the polarization properties are expected to be anisotropic.

The relationship between the gain and the polarization angle α in the QW plane is shown in Fig. 4. The electron and hole densities are assumed to be 5×10^{18} cm^{-3}. It is clear that the maximum gains are obtained at $\alpha = 90°$ for ($NN1$) and at $\alpha = 0°$ for ($11N$) ($N \geq 2$). Therefore, it is possible to fix the polarization in the maximum gain direction. For instance, in the case of VCSELs with (221) QWs, the light must linearly polarize in the [$\bar{1}$10] direction. Moreover, the optical gain in the (221) orientation is larger than for that of the other orientations except (111) because of the reduction in the hole density-of-states, as shown in Fig. 2. From Fig. 4, it is clear

that ($\bar{1}10$) faces are the best facets for edge-emitting lasers with ($NN1$)-oriented QWs.

References —[1] Y. Kajikawa *et al.*: Jpn. J. Appl. Phys. **30** (1991) 1944, [2] J. M. Luttinger *et al.*: Phys. Rev. **97** (1955) 869, [3] E. O. Kane: J. Phys. Chem. Solids **1** (1957) 249, [4] R. P. Feynman *et al.*: *The Feynman Lectures on Physics* (1965) Vol. 3.

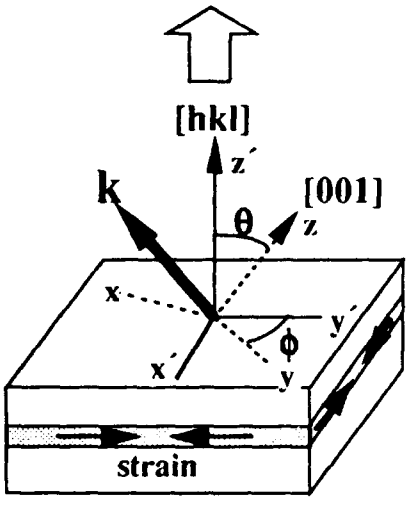

Fig. 1 Configuration of coordinate systems in VCSELs with (*hkl*)-oriented strained QW.

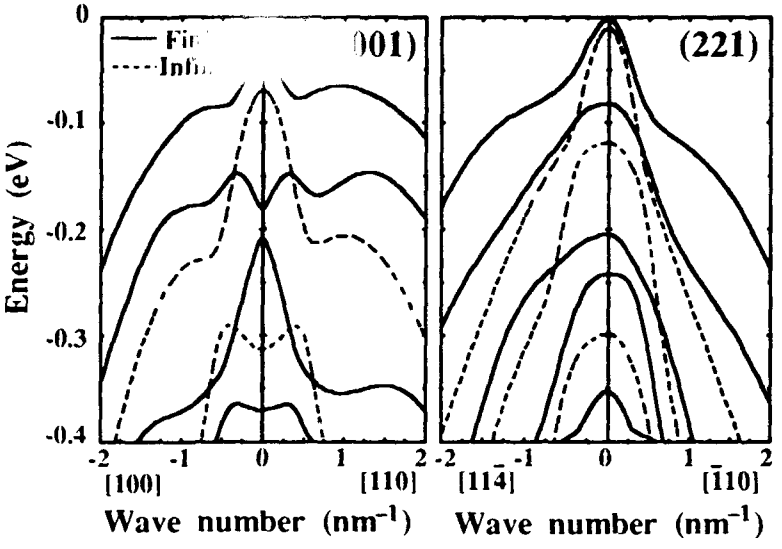

Fig. 2 Valence band dispersion. (solid lines: finite barriers (present work), dashed lines: infinite barriers)

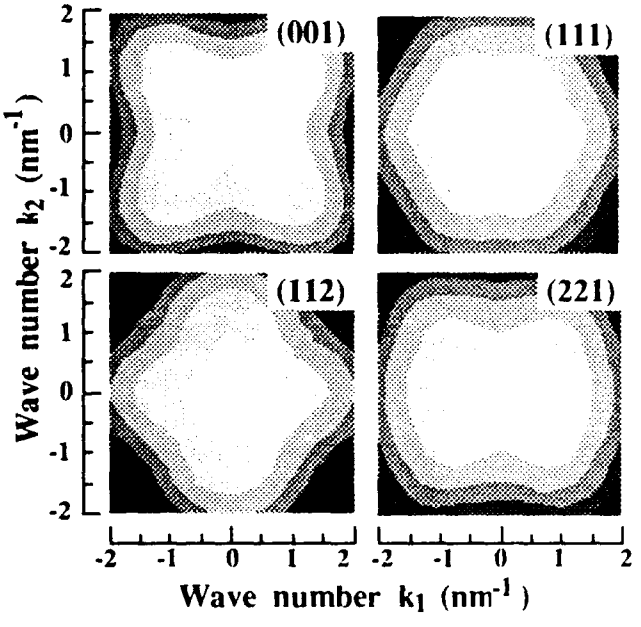

Fig. 3 Equi-energy patterns of the first valence subband in (*hkl*) strained-QW planes.

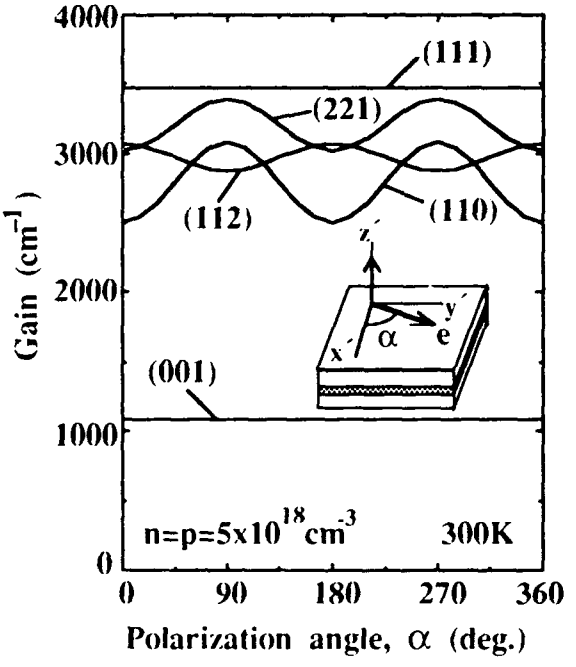

Fig. 4 Polarization dependence of optical gains for five orientations.

P36

980 nm and 850 nm Zone Lasers

Daryoosh Vakhshoori, James D. Wynn and Minghwei Hong

AT&T Bell Laboratories
600 Mountain Avenue
Murray Hill, NJ 07974, USA

Moses Asom and Keisuke Kojima

AT&T Bell Laboratories
Solid State Technology Center
Breinigsville, PA, USA

Vertical cavity zone lasers (Z-lasers) operating at 980 nm and 850 nm have been fabricated. This new class of high power (>100 mW) high efficiency ($\eta_{ext} \approx 36\%$) large area (70 μm diameter) vertical cavity laser has an output that is automatically focused to a spot at a particular distance away from the laser. This is in contrast to the conventional surface or edge emitting array devices that usually have multiple far-field lobes and need external optical components for focusing purposes. Among other applications, the unique properties of 980 nm Z-lasers makes them attractive as a pump laser for fiber amplifier systems.

The operation and the basic structure of these lasers are shown in Fig. 1. The structure consists of different optical zones separated by reactive ion etched trenches. Due to the scattering at the trench sites, the transverse laser mode with the lowest intensity at those points will have the least loss. The designed field profile is indicated in the bottom of the figure. The separation of the trenches is designed in such a way that the optical path difference from the center of these zones and the focal point on the axes of the symmetry of the structure differ by $2n\pi$ where n can be designated as the order of the zones. The focusing nature of the laser beam is similar to the operation of a Fresnel lens.

The 980 nm laser wafer was grown by molecular beam epitaxy (MBE) and consisted of 3 layers of InGaAs quantum wells each 100Å thick sandwiched between two semiconductor Bragg mirrors on each side. For the 850 nm laser the active region consists of GaAs quantum wells and the period of the corresponding Bragg mirrors are changed. The 1 μm wide and approximately 700Å deep trenches were first dry-etched to define the zones. Silver and gold were then evaporated to form the p-contact. Mesa posts of different diameters were then etched passed the active region to isolate the devices. The back side was then polished, anti-reflection coated and windowed *n*-contact was formed to allow the 980 nm laser light to escape through the substrate. For the 850 nm laser the light is emitted from the top.

The 980 nm lasers had a diameter of 70 μm with a pulsed threshold current of 50 mA, output power of 100 mW and external differential efficiency of close to 36%. The output focuses to a spot 8 μm in diameter at the focal plane of the structure. As the device current is increased, the spot becomes larger indicating the reduction of the spatial coherence of the output laser beam. 200 mW output power was obtained from 120 μm dia Z-lasers operating at 850 nm.

The reduction in spatial coherence of the beam is mainly due to thermal nonuniformity across the laser aperature which causes thermal lensing. We will present a finite difference analysis of the temperature profile of the device and show how it is responsible for limiting the spatial coherence of our broad area vertical cavity surface emitting Z-lasers. More on thermal imaging and other issues will be discussed in the presentation.

Zone Laser (Z-Laser)

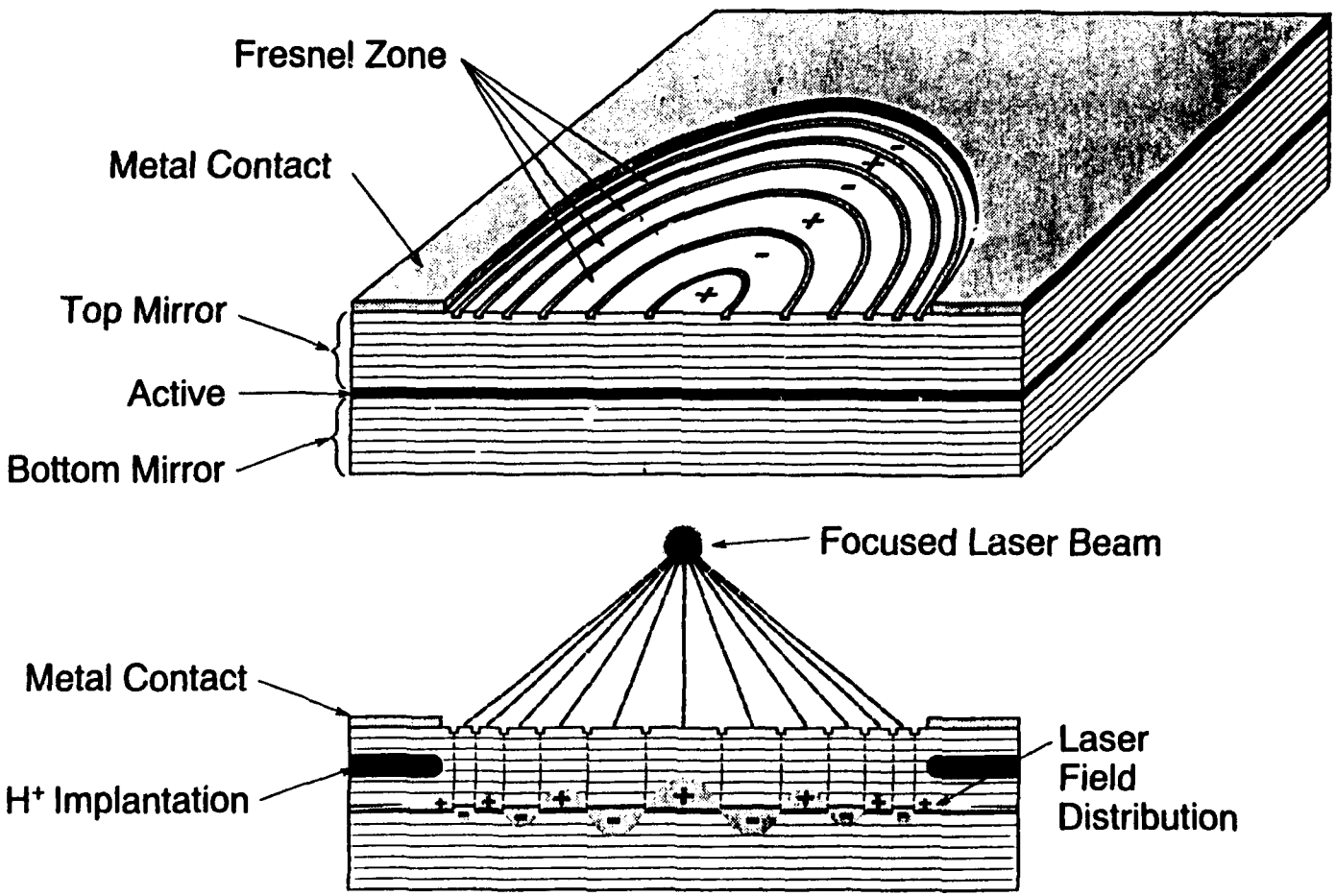

Fig.1. The structure of the Z-laser. The device is a temporally/spatially coherent vertica. cavity laser with output beam that focuses to a spot without the use of external binary grating or lenses.

P37

Novel technique for fabricating Non Absorbing Mirror Laser

Gabgyu Lim, Jaeho Lee, Gueorugi Park, and Taeil Kim
New Material & Device Research Center
Samsung Advanced Institute of Technology
P.O.Box 111, Suwon, Korea 440-600

Abstract : Nonabsorbing mirror for AlGaAs/GaAs laser was achieved by novel and simple method of laser treatment of the cleaved facets. No surface recombination effect at the facet was observed. The COD level was tripled.

The ultimate limit in output power for semiconductor lasers is produced by catastrophic damage at the laser facets. It has been observed that the catastrophic damage is produced by a localized melting of the facets. In order to prevent such effects one has to create a region of higher energy bandgap and low surface recombination at the laser facets. Most of the approaches [1,2] currently being implemented require elaborate processing and/or crystal steps. In this paper we report novel technique for fabricating nonabsorbing mirror(NAM) lasers by Eximer laser treatment of the cleaved laser facets.

For the experiment, single mode, AlGaAs/GaAs V channeled substrate inner stripe (VSIS) lasers were used [3]. The Eximer laser pulse width and wavelength were 17ns and 306nm, and the annealing powers were 60mJ, 100mJ, and 200mJ. Uncoated bars with 250μm long cavity were cleaved. Before laser treatment, threshold current density was measured by bar test. Then both facets of the bars were irradiated using Eximer laser. After cleaving to individual chips, the lasing characteristics of each lasers were measured using low duty cycle pulsed current. The threshold current density and catastrophic damage power with and without laser treatment were compared .

Fig.1 shows the threshold current density dependence of annealing power. Threshold current density was not changed and facet was not damaged by the Eximer laser treatment. Fig.2 shows the peak catastrophic optical damage(COD) power level as a function of the annealing power. The COD power reaches maximum around an annealing power of 60mJ and is three times higher than that of the untreated bars.

In summary, a non-absorbing mirror for AlGaAs/GaAs laser was achieved by a novel and simple method of laser treatment of the cleaved facets. No

surface recombination effect at the facet was observed. The COD level was increased threefold and can be further enhanced by optimizing annealing condition.

References

1. H. Blauvelt, S. Margalit, and A.Yariv, Appl.Phys.Lett. **40**, 1029, 1982
2. R.L. Thornton, R.D. Burnham, and T.L.Paoli, Appl.Phys.Lett.**48**, 7, 1986
3. Song Jae Lee, J.K. Song, J.S. Park, N.H. Kim, W.Y. Song, S.K. Koh, J.Y. Kim, D.S. Shin, J.H. Lee, D.S. Bang, S.H. Lee, K.H. Kim, and Y.W. Huh, Appl. Phys. Lett. **61**, 1507, 1992

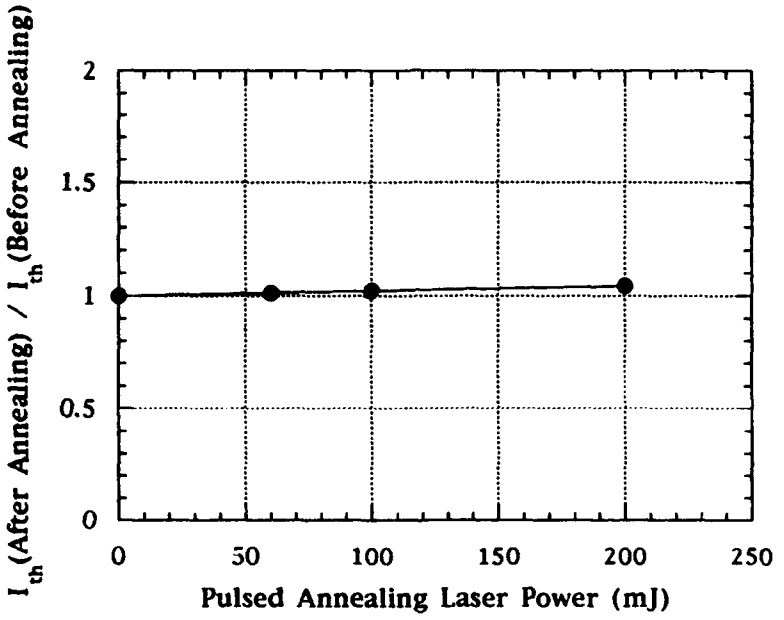

Fig.1 Threshold current density vs annealing power

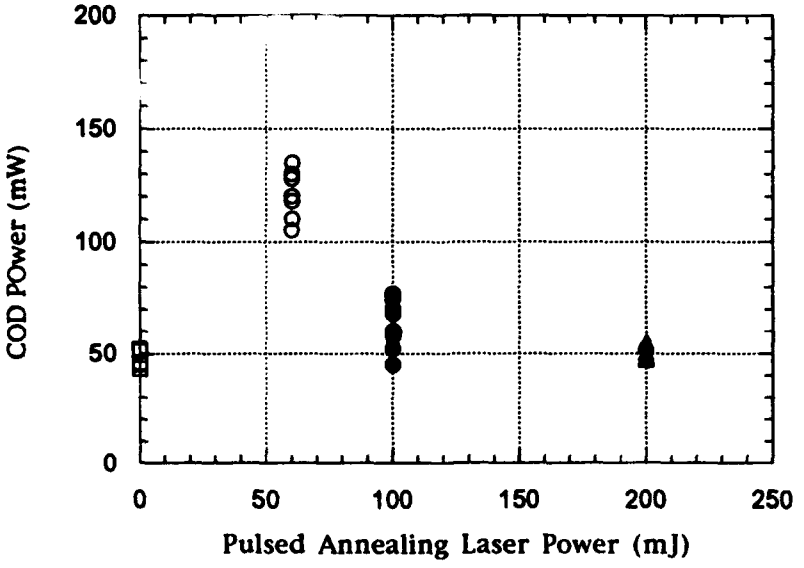

Fig.2 Peak catastrophic optical damage power vs annealing power

P38

Above-Threshold Behavior of High-Power, Single-Mode ARROW-type Diode Lasers

L.J. Mawst, D. Botez
University of Wisconsin-Madison, 1415 Johnson Drive, Madison, WI, 53706

R.F. Nabiev
Stanford University, Stanford, CA, 94305

C. Zmudzinski
TRW Inc., One Space Park, Redondo Beach, CA, 90278

Abstract: Above-threshold analysis of ARROW-type diode lasers is performed for the first time. One key finding is that preferential pumping of the antiguide core dramatically enhances the single-mode power, in good agreement with experiment. Single-spatial-mode operation in a stable beam can be maintained to >10× threshold from large-aperture (6-20μm) devices.

High-output-power, single-spatial-mode diode lasers are of interest for applications such as pump sources for rare-earth-doped fiber amplifiers and/or frequency upconversion schemes. ARROW structures have been extensively studied as passive waveguides[1,2] of large transverse spot size. For ARROW-type lasers[3], the spatial mode is stabilized by a large built-in (lateral) negative index step ($\Delta n \geq 0.05$). Antiresonant cladding layers result in low loss ($\sim 1 cm^{-1}$)for the fundamental mode, and large radiation losses for high-order modes. As a result, InGaAs/GaAs ($\lambda = 0.98\mu m$) ARROW lasers have operated up to 0.5W peak-pulsed and 0.3W CW power in a stable, single spatial mode[3]. So far analysis has been limited to the "cold-cavity" structure[3]. Here we present above-threshold analysis including gain spatial hole burning (SHB) and carrier-induced index depressions. The study reveals the importance of preferentially pumping the low-index core region(s), and projects stable, single-mode operation to high powers for both 6 – 10μm-wide (single-core) devices as well as 20μm-wide (triple-core) devices.

The above-threshold model includes effects of gain-SHB and carrier diffusion as previously done for antiguided arrays[4,5]. A comparison between preferential pumping the low-index core region (6μm wide) and uniform pumping is shown in Fig. 1. Fig. 1a displays the output power, and the imaginary part of the complex propagation constant for the first-order mode, $Im\beta_1$, as a function of the relative drive above threshold. In the case of uniform pumping the index increase that occurs in the core due to (fundamental-mode) gain SHB focuses the first-order mode (Fig. 1c), compared to the "cold-cavity" case (Fig. 1b), thereby reducing its edge losses. (This self-focusing mechanism is consistent with the behavior of nonresonant antiguided array structures.)[4,5] In turn (Fig. 1a) the first-order mode reaches threshold (i.e. $Im\beta_1 = 0$)[4,5] at only about 3.5 × fundamental-mode threshold, a fact observed experimentally[3]. In contrast, for the preferential pumping case, the carrier-induced index depression in the core defocuses the first-order mode (Fig. 1d), thus increasing its edge losses, and placing most of its field in the low-gain outer regions. As a result the first-order mode does not reach threshold even at 10 × fundamental-mode threshold. Furthermore, the fundamental-mode beamwidth is found to remain constant to 10 × threshold (i.e. no self-focusing). These findings are in excellent agreement with experiment[3].

Larger-aperture (10μm) ARROW lasers can also maintain a single mode to 10 × threshold, as shown in Fig. 2. However, due to gain SHB, the fundamental mode self-focuses, which causes a mild broadening of the far-field pattern (i.e. from 4.1° to 5°). To prevent far-field broadening while keeping a large emitting aperture, a triple-core (6μm-wide cores) ARROW device[6] can be used (Fig. 3a). Diffraction-limited-beam operation from 20μm-wide apertures ($\theta_{1/2} = 1.9°$) is obtained to at least 10 × threshold in a stable beam, with 67% of the energy in the main lobe (Fig. 3b). Thus triple-core ARROW devices (with nonabsorbing mirrors), having ~5 times larger aperture than conventional single-mode devices, hold the potential for reliable, stable, single-spatial-mode operation at 1W CW output power.

1. T.L. Koch et al, Electron Lett., 23, 244 (1987)
2. T. Baba et al, IEEE J. Quantum Electron., 28, 1689 (1992)
3. L.J. Mawst et al, IEEE Photon Tech. Lett., 4, 1204 (1992)
4. R.F. Nabiev et al, Appl. Phys. Lett., 62, 916 (1993)
5. R.F. Nabiev et al, OE-LASE '93, Los Angeles, CA, SPIE Proc., Vol. 1850, 23 (1993)
6. C. Zmudzinski et al, CLEO '94, Anaheim, CA, paper CMA2 (1994)

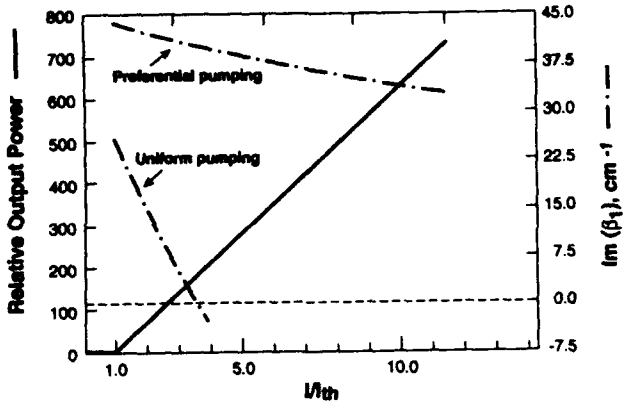

Fig. 1. 6μm-core ARROW laser. (a) Output power and imaginary part of the first-order-mode propagation constant, $\mathrm{Im}\beta_1$, (for uniform pumping and preferential (core) pumping) as a function of the relative drive above threshold, I/I_{th}. Dielectric-constant and first-order-mode near-field intensity profiles: (b) cold-cavity; (c) uniform pumping at 3 I_{th}; (d) preferential pumping at 10 I_{th}. λ_1 is the leaky-wave lateral wavelength.

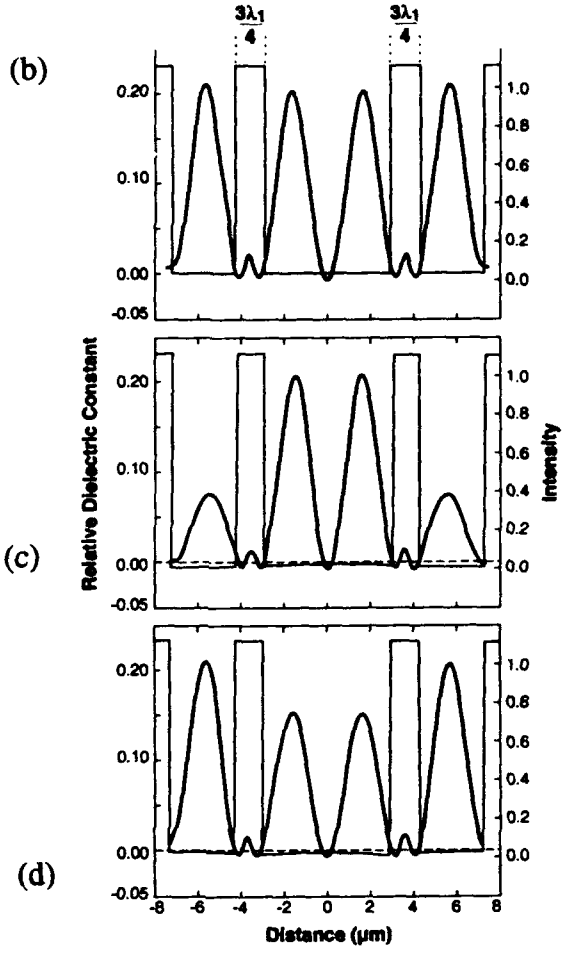

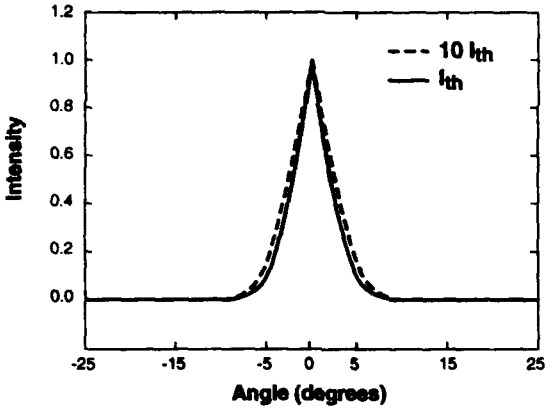

Fig. 2. Far-field pattern of 10μm-core ARROW laser at threshold and 10 × threshold.

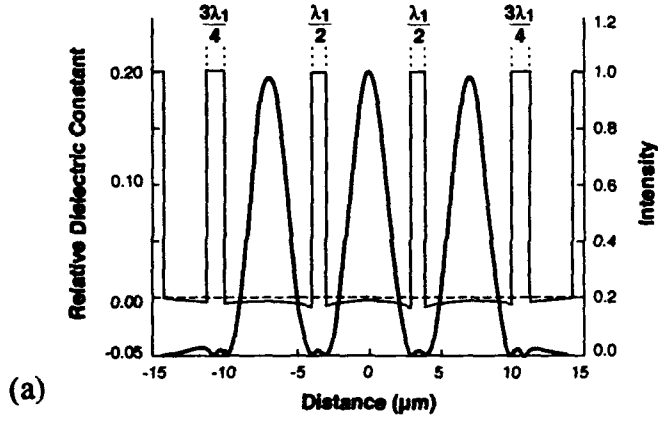

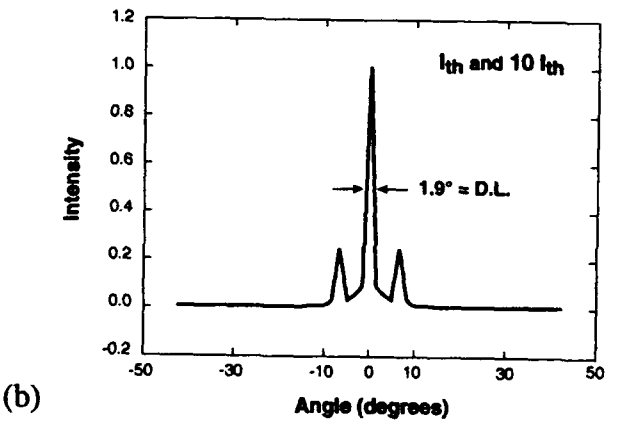

Fig. 3. Triple-core ARROW device: (a) in-phase mode near-field profile, and dielectric-constant profile; (b) diffraction-limited (D.L.) far-field pattern at threshold and 10 × threshold. λ_1 is the leaky-wave lateral wavelength.

P39

Peculiarities of operation characteristics of high-power InGaAsP/GaAs 0.8 μm laser diodes

M. Razeghi, J. Diaz, I. Eliashevich, X. He, H. Yi, M. Erdtman, E. Kolev, L. Wang and D. Garbuzov

Center for Quantum Devices, Department of Electrical Engineering and Computer Science, Northwestern University, Evanston, Illinois 60208

Abstract

GaInAsP high power laser emitting at 808nm with a η_d=1.1 W/A, J_{th}=200 A/cm^2, and T_0=155°C have been grown by LP-MOCVD. Far field divergence of 27°, output power of 3W in pulse- regime, 1.5W in quasi-CW-, and 1W in CW-mode per uncoated facet have been obtained for 1mm long diodes .

High-quality $In_xGa_{1-x}As_yP_{1-y}$-GaAs multilayer structures with composition corresponding to the wavelength range from .75 μm to 1 μm have been grown by LP-MOCVD. High-power Al-free DH and SCH lasers emitting at 808nm have been fabricated. High-power operation of 3 W in pulse mode, 1.5 W in quasi-CW and 1 W in CW per uncoated facet for 1mm long cavity InGaAsP/GaAs 808nm laser diodes has been obtained. Threshold current density of 200 A/cm^2, differential efficiency of 1.1 W/A, and series resistance of 0.04 Ω for 1mm long diodes have been measured. The lasing spectrum has a narrow envelope (FWHM about 1 nm). Measurements of far field distribution in the direction perpendicular to the structure plane gave half width values of 27° in full agreement with the calculated value of Γ. Thermal resistance of the diodes is better than 4 grad/W and overheating does not exceed 20 °C at 3 A driving current.

Investigation of threshold current density and differential efficiency dependencies on cavity length for 808nm SCH laser diodes shows that internal losses may be considered to be independent of current only for diodes with very long cavity lasers. Enhancement of waveguide radiation contribution with increasing current density implies that peculiarities of these dependencies manifesting themselves with decreasing cavity length are caused by current overflow to the waveguide and cladding layers.

Lifetime testing in quasi-continuous wave regime was performed for an uncoated diode bonded n-side down. After 1000 hours of testing at room temperature at driving current 2 A corresponding to output power 400 mW per each facet the decrease in output power was less than 2 %. Reliable high-power InGaAs-GaAs-InGaP single quantum well lasers emitting at 0.98μm were also grown by LP-MOCVD. Threshold current density as low as 80 A/cm^2 and differential efficiency as high as 75% were observed for 1mm cavity length coated lasers. Device lifetime exceeded 2000 hours at 50 °C at 1W output power with degradation less than 20%.

The results achieved at this time demonstrate the advantages of GaInAsP-GaAs system compared to AlGaAs devices since similar results at CW and quasi-CW testing can hardly be obtained for AlGaAs lasers with uncoated absorbing mirrors. This work was supported by ARPA/US Army contract #DAAH04-93-G-004.

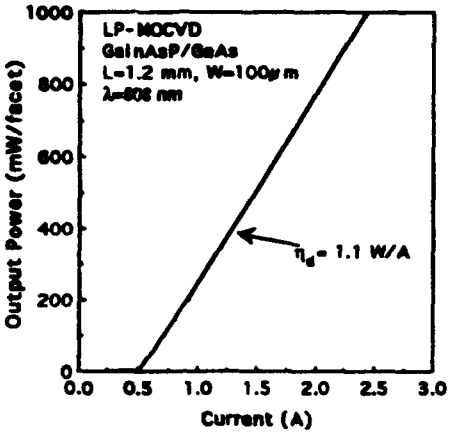

Fig.1 Differential efficiency of 1mm cavity length laser diode with 100μm aperture in pulse region.

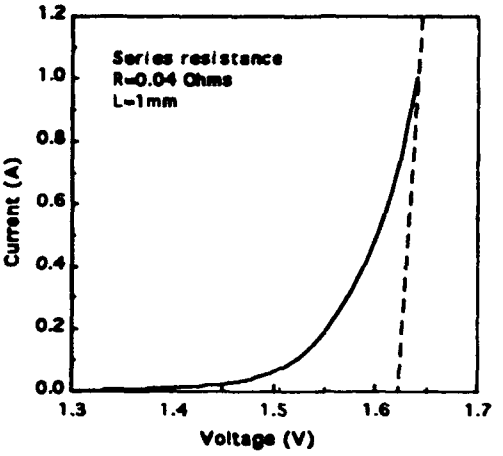

Fig. 2 Current-voltage characteristics for 100μm aperture diode demonstrating 0.04 ohms series resistance.

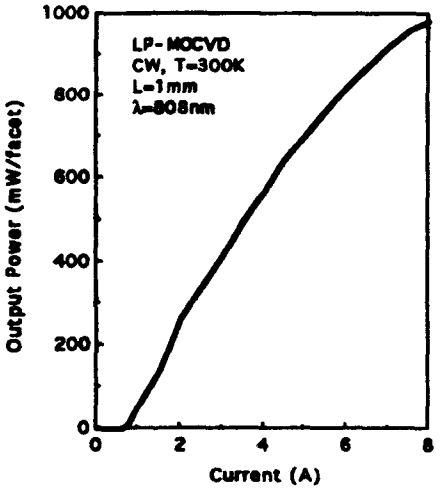

Fig. 3 Continuous wave output power of 1W per uncoated facet for a 1mm long cavity laser diode.

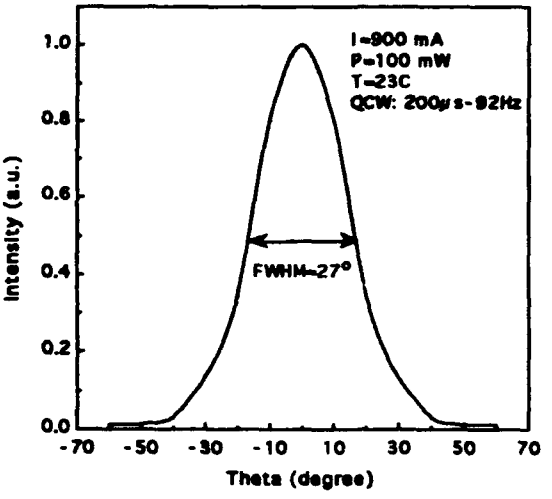

Fig.4 Transverse far-field pattern with FWHM=27 in the perpendicular plane direction.

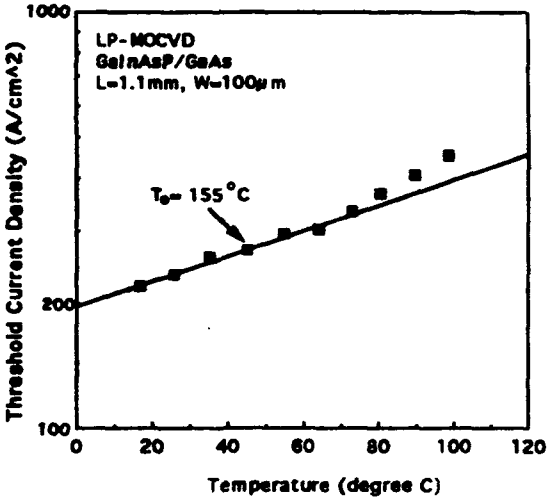

Fig. 5 Threshold current density vs. temperature for bonded 1.1 mm long GaInAsP/GaAs laser exhibiting a temperature characteristics of To = 155C.

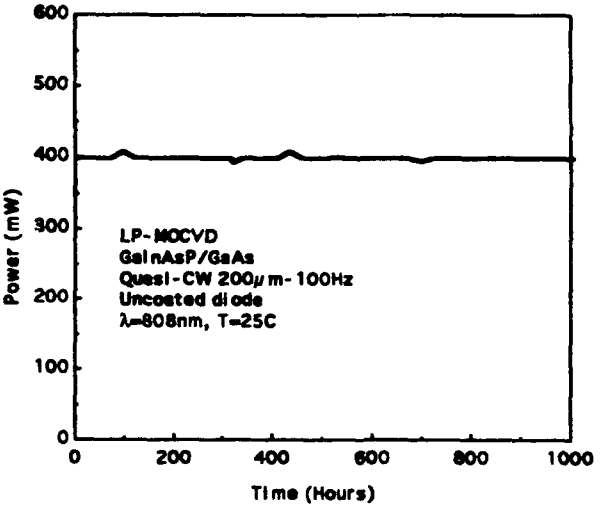

Fig. 6 Preliminary results of lifetime testing in quasi-continuous wave regime for 1000 hours under driving current 2A at room temperature (output power 400 mW per each facet).

P40

Electronically Tunable, 1 W CW, Diffraction-Limited Monolithic Flared Amplifier-Master Oscillator Power Amplifier (MFA-MOPA)

J. S. Osinski, K. M. Dzurko, J. S. Major, Jr., R. A. Parke, and D. F. Welch
SDL, Inc., 80 Rose Orchard Way, San Jose, CA 95134
(408) 943-9411 FAX (408) 943-1070

ABSTRACT: Free-carrier tuning of a master oscillator/power amplifier is demonstrated, operating at 1 W CW. Approximately 20 mA of current tunes the device ~6 Å while maintaining near-diffraction-limited performance.

High-power diffraction-limited semiconductor laser sources are useful for several applications such as FSK free-space communications and frequency doubling. These applications require precise wavelength control of a high-power, single mode laser source. Whereas tunability has been demonstrated in many low-power InP-based semiconductor laser devices, or in high-power external cavity configurations,[1] a monolithically integrated, free-carrier tunable semiconductor laser device has not been made at the power levels useful for the above applications.

Previously, greater than 2 W of continuous diffraction-limited power has been demonstrated in a single monolithic flared amplifier–master oscillator/power amplifier (MFA-MOPA).[2,3] We extend this design to fabricate a current-tunable device at $\lambda \sim 980$ nm by adding an additional contact to the 1000 μm long rear grating of the DBR master oscillator. Carrier injection into this region provides tuning by the free-carrier plasma effect, and is therefore capable of speeds comparable to the carrier lifetime, on the order of 5 nsec.

The MOPA geometry is similar to that in Ref. 2, with a flared amplifier extending from the single-mode DBR master oscillator made in the InGaAs/AlGaAs material system. The exit facet is AR coated to a reflectivity of less than 0.1%. Devices are bonded p-side down onto a patterned submount and tested under CW conditions at 25°C. Power-current characterisitics are shown in Figure 1. The far field of the device, measured according to the procedure described in Ref. 3, is presented in Fig. 1 as well and is single-lobed and nearly diffraction limited over the entire operating range.

Tuning characteristics at an amplifier current of 2 A are shown in Fig. 2. Tuning to shorter wavelengths indicates that this tuning is free-carrier, and not thermal, in nature, although the thermal contribution at higher currents limits the tuning range somewhat. 6 Å (180 GHz) of tuning is obtained in approximately 20 mA of injected current, sufficient for matching the resonance of a non-linear crystal for frequency doubling, for example. The spectrum is predominantly single mode except at the mode-hop regions, and the ~1.3 Å free spectral range of the mode hops correlates properly with the longitudinal modes expected from the DBR master oscillator. Slight (~ 1%) power fluctuations are evident in the output power as the device is tuned through these mode hops, as indicated in Fig. 1, and the far-field quality is virtually unchanged in terms of pointing accuracy and FWHM as tuning current is increased. Addition of a phase control region into the cavity of the DBR laser should provide a straightforward extension to continuous tunability if desired. To obtain higher speeds, reverse biased tuning of this region is feasible as well.

In conclusion, a device that combines fast, integrated tunability with 1 W CW of single-mode, near-diffraction-limited power is demonstrated for the first time in an MFA-MOPA.

This work was supported by NASA Langley.

---

1 D. Mehuys, D. Welch, and D. Scifres, "1 W CW, diffraction-limited, tunable external-cavity semiconductor laser," *Elect. Lett.*, **29**, 1254, 1993.

2 R. Parke, D. F. Welch, A. Hardy, R. Lang, D. Mehuys, S. O'Brien, K. Dzurko, and D. Scifres, "2.0 W CW, diffraction-limited operation of a monolithically integrated master oscillator power amplifier," *IEEE Phot. Tech. Lett.*, **5**, 297, 1993.

3 S. O'Brien, D. F. Welch, R. A. Parke, D. Mehuys, K. Dzurko, R. J. Lang, R. Waarts, and D. Scifres, "Operating characteristics of a high-power monolithically integrated flared amplifier master oscillator power amplifier," *IEEE J. Quant. Elect.*, **29**, 2052, 1993.

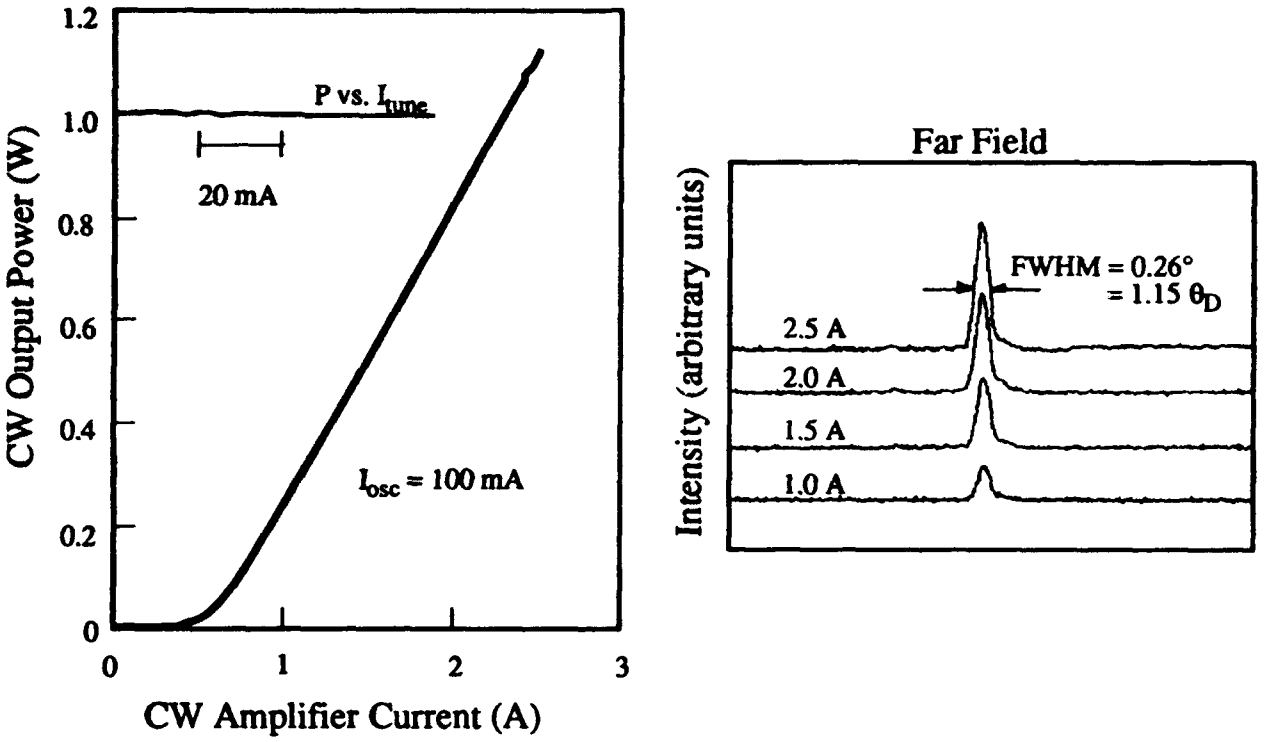

Fig. 1. Power-current (left) and far-field (right) characteristics of the tunable MOPA. Power verses tuning current is also indicated in this figure, for a nominal 1 W operating condition.

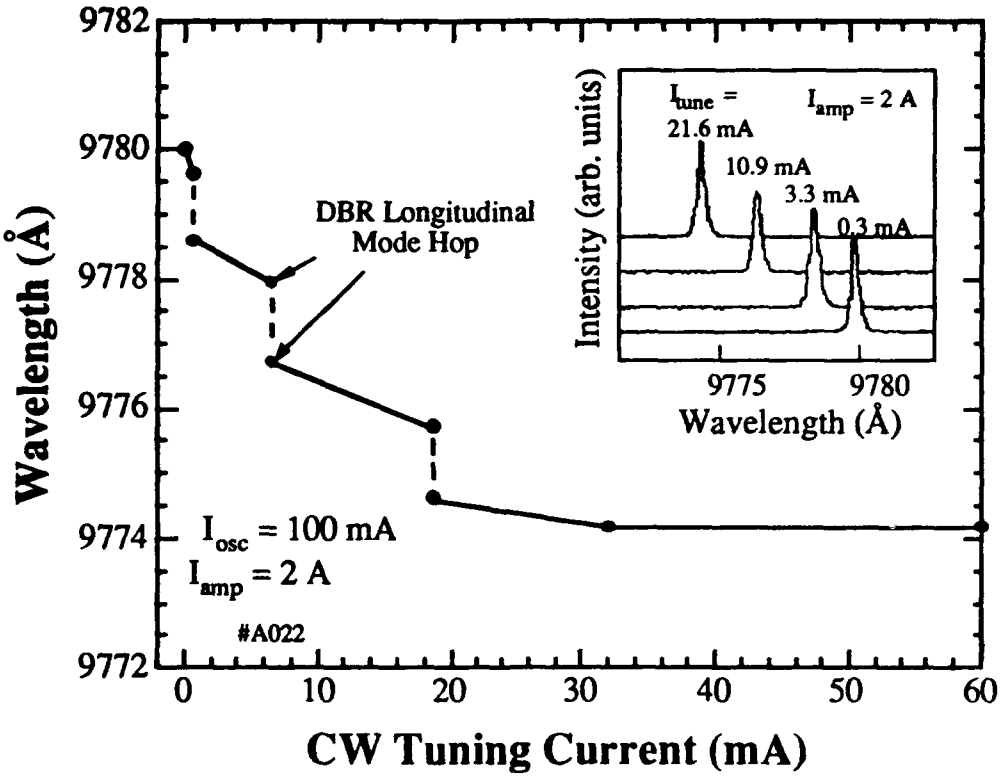

Fig. 2. Tuning and spectral characteristics of the tunable MOPA.

P41 High-Power Highly Reliable Operation (40 mW at 60°C) of Compressively Strained Quantum-Well 680-nm AlGaInP LDs

S. Kawanaka, T. Tanaka, H. Yanagisawa, and S. Minagawa
Central Research Laboratory, Hitachi Ltd., Kokubunji, Tokyo 185, Japan

Optimized thin quantum-well (QW) structures under compressive strain are examined for high-power characteristics suitable for light sources of optical disk systems. As a result, compressively strained triple-quantum-well LDs can operate stably at 40 mW and a high temperature of 60°C for over 1000 hours.

High-power long-term stable operation of AlGaInP LDs at a short wavelength of around 680 nm is needed for use in high-density optical disk systems. To meet this requirement we have investigated the optimum design of high-power AlGaInP LDs by introducing compressively strained quantum structures. In a compressively strained layer, the deep potential of GaInP QWs due to a large In content and small carrier effective mass due to strain-induced valence subband structures are effective in achieving a low density of injected carriers at the threshold. A large potential depth in QWs results in a longer oscillation wavelength, which is important for reducing threshold currents by suppressing overflow carriers[1,2]. On the other hand, the quantum size effect in very thin QWs should be used when a large strain is introduced, retaining the wavelength at around 680 nm[3]. Therefore, MQW structures with thin-layered compressively strained QWs should be optimized in the retained oscillation wavelength of 680 nm.

In this study, we first calculated the threshold current density J_{th} to determine the number of strained QWs. The threshold carrier density n_{th} and the excess carrier density were taken into account in this calculation. Figure 1 shows the dependence of the calculated J_{th} on QW width for each number of QWs. The optimum QW width which accomplishes minimum J_{th} becomes smaller as the number of QWs increases because the optical confinement factor Γ increases with the number of QWs. Lower density of states is strongly expected in thin QWs and this also reduces the n_{th}, resulting in a reduction in overflow current. This shows that MQW structures with QWs that are less than 10-nm thick have high carrier confinement and are suitable for high-power LDs.

We experimentally compared the characteristics of several LDs with various numbers of QWs. Figure 2 shows the threshold current I_{th} for several strained QW structures. In SQW LDs, which have a QW of more than 10-nm thick, reduction in overflow current is mainly magnified by the potential depth in the QW because quantum size effects are relatively small. Thus, the decrease in bandgap energy due to large In content reduces I_{th}, although it results in a lasing wavelength longer than 690 nm. On the other hand, higher carrier confinement can be obtained by introducing larger strain into MQWs. I_{th} reaches a minimum value of about 35 mA both in DQW LDs with 8-nm-thick QWs and in TQW LDs with 6-nm-thick QWs. Reduction in n_{th} due to larger strain suppresses overflow carriers, thus achieving low I_{th} in MQW LDs even at a lasing wavelength shorter than that in SQW LDs. The effect of strain becomes more pronounced at higher temperatures. T_0 and driving current under 40 mW light output at 60°C are plotted in Fig. 3 against the QW width. By decreasing the QW width, we varied the amount of strain introduced in the QWs from 1 to 2%. The lasing wavelength was thus kept nearly constant at 680 nm. T_0 reaches maximum around 6-nm-thick QWs in TQW LDs, while that of DQW LDs decreases according to the QW width. This shows that larger strain in the thinner QWs of TQW LDs enhances reduction in carrier effective mass and the separation between heavy-hole and light-hole subbands, resulting in a lower n_{th} and suppression of excess carriers. As a result, we obtained the lowest driving currents in TQW LDs with 6-nm-thick QWs. The reduction in the driving current reduces the long-term degradation. Figure 4 shows lifetest results for these LDs. Over 1000 hours of stable 40 mW operation has been achieved at a high temperature of 60°C.

References
1. S. Kawanaka et al., Electron. Lett., submitted.
2. S. Kawanaka et al., Jpn J. Appl. Phys., 32, 609 (1993).
3. T. Tanaka et al., Quantum Optoelectronics Technical Digest, QWD2-1, 42 (1993).

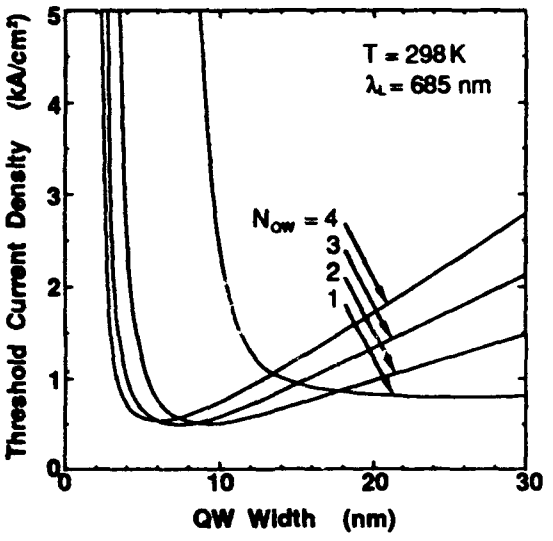

Fig. 1 Calculated results for threshold current density of several strained QW LDs with the same lasing wavelength of 685 nm

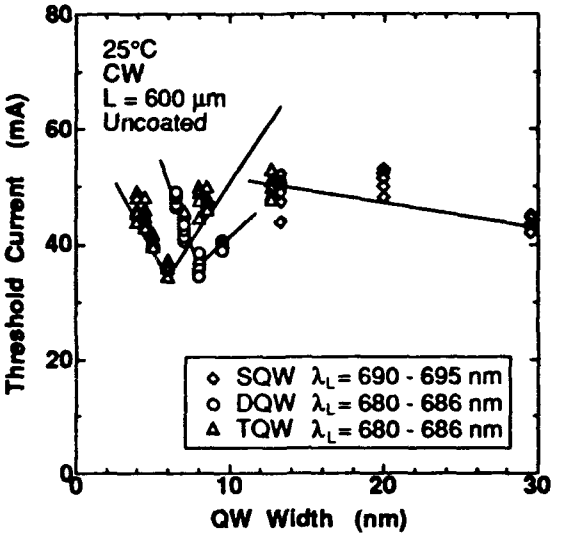

Fig. 2 Measured threshold current of strained SQW, DQW, and TQW LDs with various QW widths

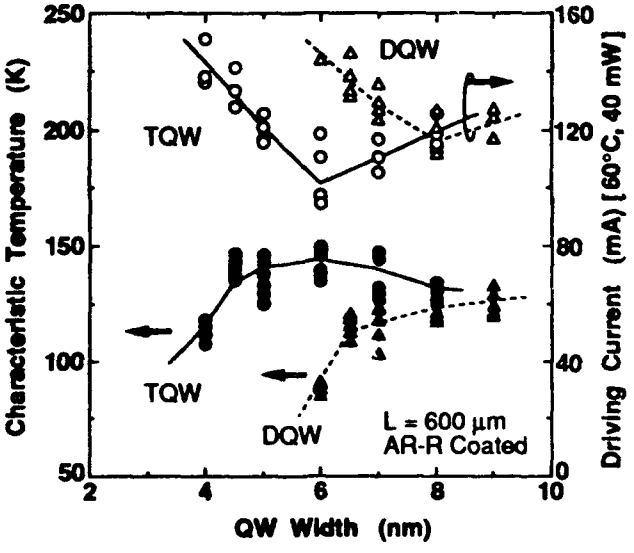

Fig. 3 Comparison between DQW and TQW LDs for characteristic temperatures and driving currents under 40 mW operation at 60°C

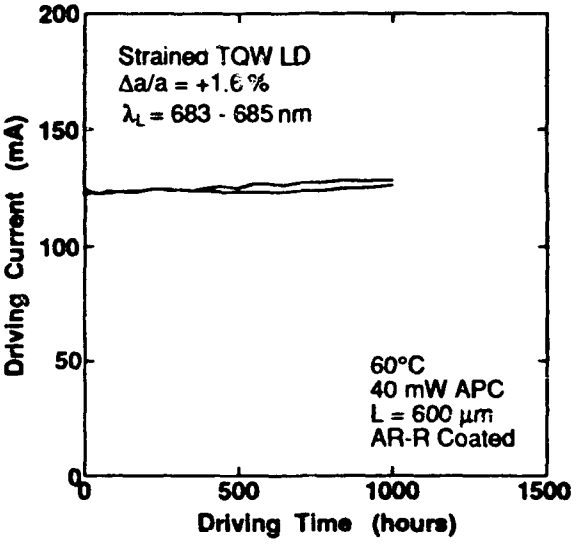

Fig. 4 Lifetest results for strained TQW LDs under 40 mW operation at 60°C

P42 High-power Single-transverse-mode Operation of Narrow-ridge-waveguide 0.98-μm InGaAs/AlGaAs Strained-quantum-well Lasers by *in situ* Monitored RIBE

Hiroaki Chida, Kiich Hamamoto, Kazuo Fukagai, Takashi Miyazaki, and Shin Ishikawa
Opto-electronics Research Laboratories, NEC Corporation
34 Miyukigaoka, Tsukuba-city, Ibaraki, 305 Japan

Abstract Narrow ridge waveguide 0.98-μm InGaAs/AlGaAs quantum-well laser diodes (LDs) fabricated by *in situ* monitored reactive ion beam etching operated in the fundamental lateral-mode up to 254 mW, and fiber-coupled power was as much as 150 mW.

Introduction Strained InGaAs quantum-well LDs emitting at 0.98μm have been developed as pumping light sources for Er^{3+}-doped fiber amplifiers (EDFAs).[1] High fiber-coupled power is required for such sources, and the mesa geometry of buried-ridge-structure LDs must be precisely controlled in order to obtain stable lateral-mode operation and high fiber-coupled power. Reactive ion beam etching (RIBE) is expected to provide excellent process control because etching depth can be monitored by using a laser interference technique.[2,3] In this paper we report 0.98-μm buried-ridge LDs fabricated by *in situ* monitored RIBE. The 150-mW fiber-coupled power attained is to our knowledge, the highest value ever reported.

Structure and fabrication Figure 1 shows a schematic drawing of 0.98-μm LDs fabricated by RIBE, and its energy band diagram of separated confinement hetero-structure (SCH). The epitaxial layers were grown by metal-organic vapor phase epitaxy. The SCH consists of an InGaAs/GaAs double quantum-well (DQW) sandwiched between $Al_{0.2}Ga_{0.8}As$ waveguide layers. The transverse mode is controlled in the ridge waveguide. A p-$Al_{0.1}Ga_{0.9}As$ etch end indicating layer (EEIL),[2] where RIBE should be terminated, was inserted within the p-$Al_{0.33}Ga_{0.67}As$ cladding layer. The ridge waveguides were fabricated by RIBE at a 400-V dc bias. A He-Ne laser was installed for *in situ* etch monitoring, and layer with a different Al content could be distinguished during the RIBE process by the change in the reflective signal pattern. The etching could therefore be terminated accurately at the EEIL. Figure 2 (a) shows the Al or In content profile of the wafer, and Fig.2(b) shows the change of reflectivity during etching.

Characteristics A cw L-I curve for a coated 2-μm-wide ridge waveguide laser is shown in Fig. 4. The threshold current at room temperature is 24 mA, and the slope efficiency is 0.86 W/A. Output power exceeded 300 mW. The temperature dependence of the cw L-I curve, as well as the current dependence of transverse lateral mode from 50 to 300 mA, are shown in Fig. 3 together with a lasing spectrum at 100 mW. The characteristic temperature To measured between 20℃ and 80℃ was 114 K, and the emission wavelength was 0.98 μm. FWHMs of the horizontal and vertical far-field patterns were respectively 6 and 31 degrees. Figure 4 shows LD output and single-mode fiber coupled power as a function of injection current. A fiber-coupling efficiency of 56% was achieved by using a 2-lens coupling system. The fiber output power reached 150 mW, so the fundamental lateral mode operation was maintained up to 254 mW. Figure 5 shows LD performance during a preliminary aging test under 100-mW constant light output at 50℃. Stable operation over 500hr indicates that there is no severe plasma damage to the etched surface.

Conclusion These 0.98-μm buried-ridge LDs fabricated by *in situ* monitored RIBE were newly developed. These have the highest fiber-coupled power of 150 mW and operate stably for more than 500 hr under 100 mW constant ligth output.

References

1) M. Okayasu, T. Takeshita, M. Yamada, O. Kogure, M. Horiguchi, M. Fukuda, A. Kozen, K. Oe, and S. Uehara, Electron. Lett., vol. 25, 1563 (1989).

2) M. Jost, G. L. Bona, P. Buchmann, G. Sasso, P. Vettiger, and D. Webb, IEEE Photo. Technol. Lett., vol. 2, 697 (1990).

3) C. P. Chao, S. Y. Hu, P. Floyd, K-K. Law, S. W. Corzine, J. L. Merz, A. C. Gossard, and L. A. Coldren, IEEE Photo. Technol. Lett., vol. 3, 585 (1991).

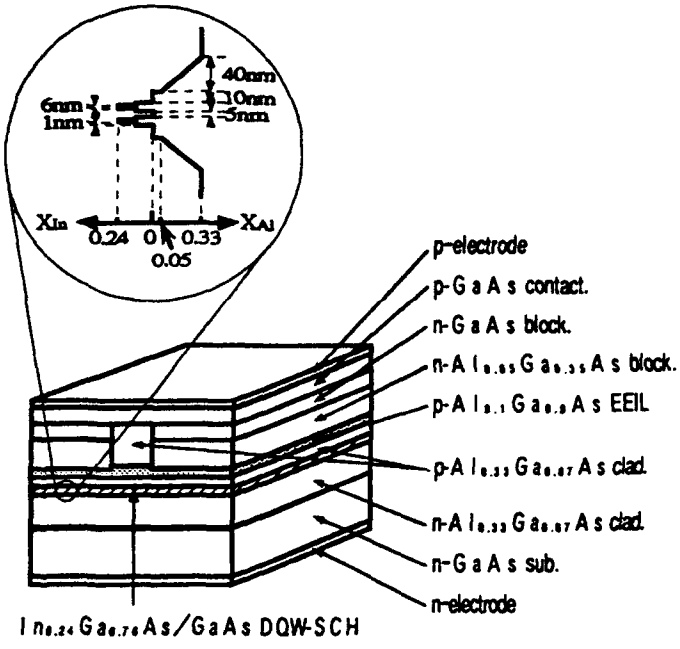

FIG. 1. Schematic drawing of 0.98-μm LDs and its energy band diagram of SCH (circled).

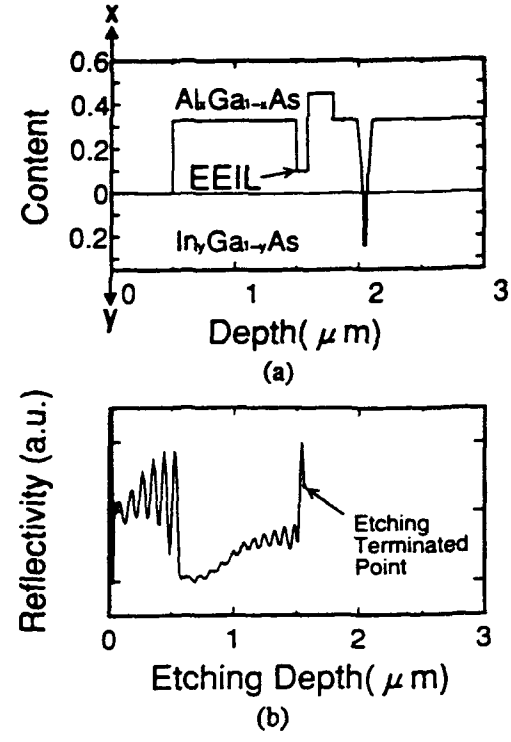

FIG. 2. (a) Content profile of the wafer. (b) Change of reflectivity during etching.

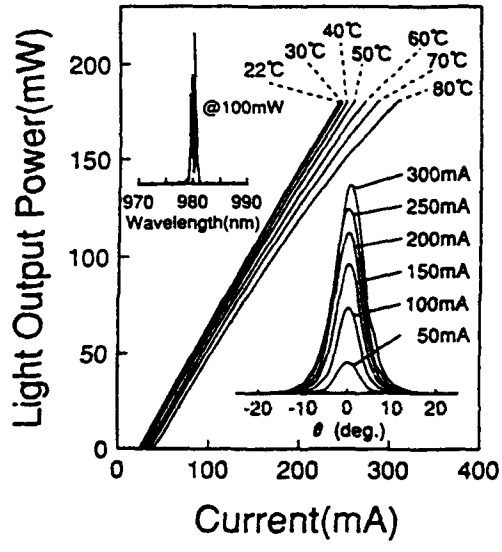

FIG. 3. The temperature dependence of cw L-I curve, the current dependence of the transverse lateral mode, and the lasing spectrum at 100 mW.

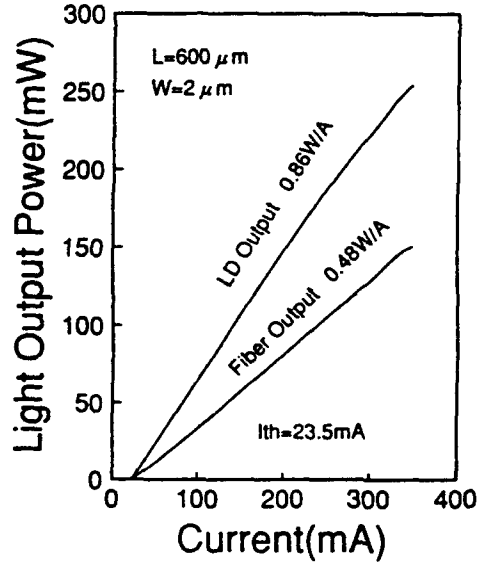

FIG. 4. The LD and fiber output L-I curve.

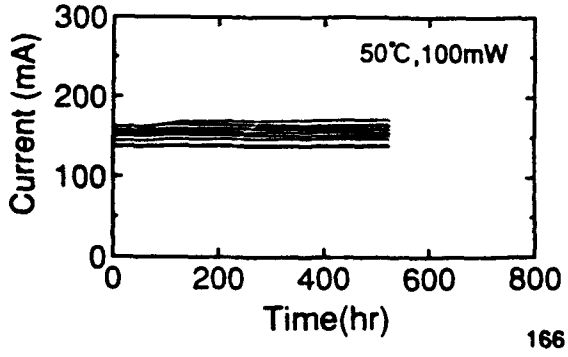

FIG. 5. Preliminary aging test under 100-mW constant light output at 50℃.

P43

Novel method to optimize complex coupling coefficients by sampled gratings

S. Hansmann, H. Walter, H. Hillmer, H. Burkhard
Deutsche Bundespost Telekom, Forschungs- und Technologiezentrum
64276 Darmstadt, P.O.-Box 100003, Germany

We propose and demonstrate the application of sampled gratings for the variation of the coupling coefficient on a single wafer. Using this method the influence of the coupling strength on the performance of gain-coupled InGaAs/InGaAlAs-DFB-lasers is studied.

Complex-coupled DFB lasers [1-4] are attractive light sources for advanced fibre communication systems. To achieve ultimate performance and high yield, however, a careful choice of the complex coupling coefficient is essential. Therefore an efficient method is required to define different values of the coupling coefficient on the same wafer, so that the optimum coupling strength can be determined reliably by experiment. In this paper, we present a powerful method based on a sampled grating structure (fig. 1) which is applied to the variation of the complex coupling constant of loss-coupled InGaAs/InGaAlAs/InP-DFB lasers.

The resulting effective coupling constant κ_{eff} of the sampled grating is given in a good approximation by the product of the coupling coefficient κ of the full grating times the duty cycle of the superstructure. The validity range of this relation is verified by detailed transfermatrix simulations: identical spectra (fig. 2) are obtained for a laser with a full grating (coupling coefficient κ) compared to a grating structure sampled by a duty cycle of 1:4 with a coupling coefficient of $4\,\kappa$. The supermodes caused by the periodic sampling, which appear at a spectral distance of $\Delta\lambda_{sg} = \lambda_B^2/(2\,N_g\,\Delta\Lambda_{sg})$ on both sides of the Bragg-wavelength λ_B are shifted apart from the gain-maximum by choosing a small period $\Delta\Lambda_{sg}$ of the superstructure.

The first order grating structure shown in fig. 1 was defined by electron beam lithography and dry etching in the absorbing InGaAs/InP quantum well. The undercut volume of the fabricated mushroom-type lasers was refilled with s.i. InP. Typical spectra from a $410\mu m$ long device with uncoated facets and a full grating are given in fig. 3 demonstrating a high sidemode supression of $> 46dB$ even at high injection levels. The residual index coupling of about 40cm^{-1} (loss coupling $\approx 20\text{cm}^{-1}$) creates a narrow stopband which vanishes for a device from the same bar (identical length L) with a 1:3-sampled grating reducing the coupling to a third (fig. 4). The coupling coefficients were determined by a detailed comparison between experimental data and theoretical model calculations.

As theoretically expected, the supermodes are strongly suppressed even for devices with a very small duty cycle of the sampled grating (1:7 in fig. 5), since the spectral distance $\Delta\Lambda_{sg}$ turns out to be large enough compared to the width of the gain-curve. Thus, the coupling constant can be varied at least by a factor of 7 on the same wafer. Comparing the sidemode supression of neighbouring devices with equal length $L = 475\mu\text{m}$ and different coupling constant (fig. 6) we found an increasing stability of the monomode emission with increasing coupling strength of the complex grating. Thus, the variation of the coupling coefficient enables systematic design optimizations.

In summary, we have demonstrated theoretically and experimentally, that sampled gratings can be applied to the realization of multiple or even axially varying coupling coeffcients on a wafer. This new method is capable to define laser devices on the same bar with precisely controllable coupling coefficients.

References

[1] Y. Luo, Y. Nakano, K.-Tada, T. Inoue et al., *IEEE J. Quantum Electron.*, **27**, p. 1724, June 1991.
[2] K. David, G. Morthier et al., *IEEE J. Quantum Electron.*, **27**, p. 1714, June 1991.
[3] B. Borchert, B. Stegmüller, R. Gessner, *Electron. Lett.*, **29**, p. 210, January 1993.
[4] W. T. Tsang, F. S. Choa, M. C. Wu, Y. K. Chen et al., *Appl. Phys. Lett.*, **60**, p. 2580, May 1992.

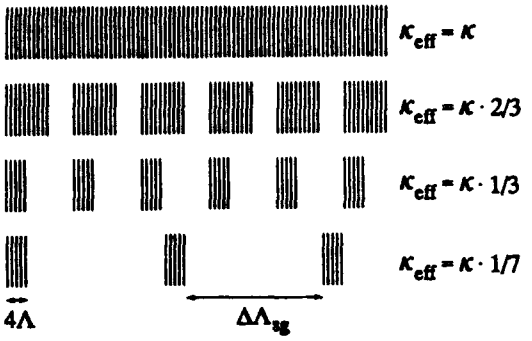

Fig. 1: Sketch of the sampled grating structure realized on the wafer.

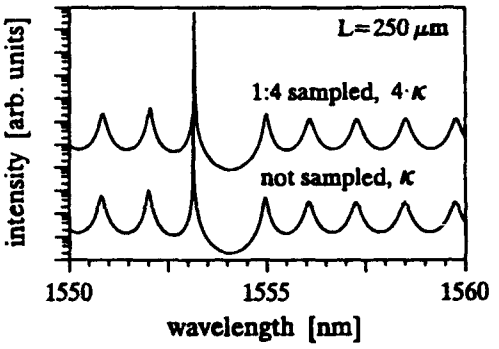

Fig. 2: Calculated spectra for sampled and not sampled DFB gratings.

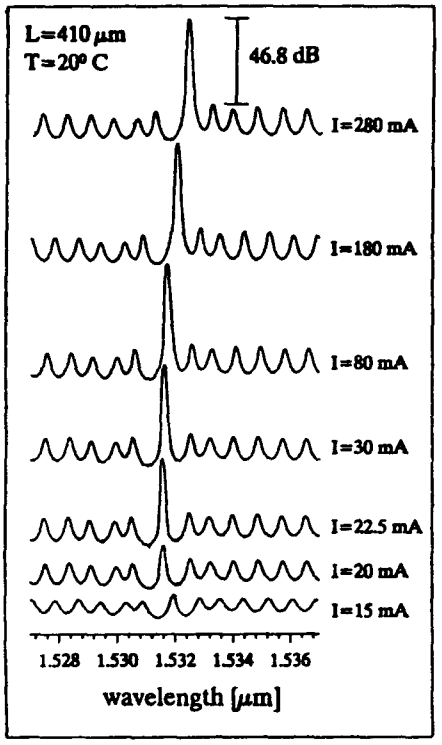

Fig. 3 : Series of measured spectra.

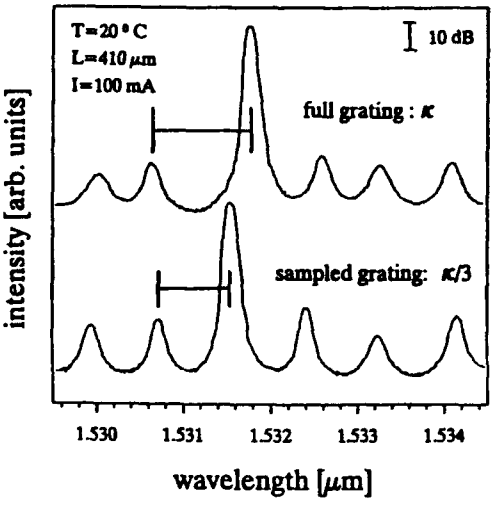

Fig. 4: Spectra from two gain-coupled DFB lasers with full and sampled grating of the same length. The stopband-width of both devices is indicated.

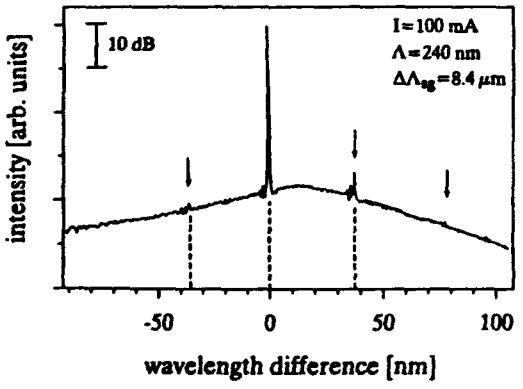

Fig. 5: Suppression of supermodes in the spectrum of a DFB laser with a 1:7 sampled complex grating.

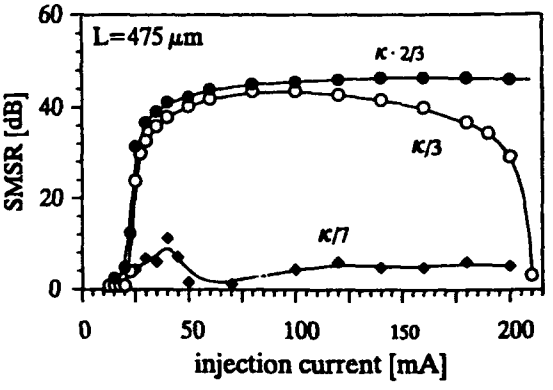

Fig. 6 : Measured sidemode suppression ratio for three gain-coupled devices with identical length L and different coupling from the same wafer .

P44

Influence of gain saturation on the tuning range and tuning rate of three-contact DFB lasers and amplifier-filters : modelling and experiments

H. Nakajima, J. Charil, S. Slempkes, A. Gloukhian,
D. Robein, D. Mathoorasing, S. Cherif, J.-C. Bouley

France Telecom, CNET, Laboratoire de Bagneux, 196 avenue Henri Ravera, BP 107, F-92225 Bagneux Cedex, France

Introduction

Within the EEC RACE 2039 (ATMOS) project, advanced ATM switching nodes are being studied [1]. For the implementation of a demonstrative packet-switching subsystem that is based on a multiwavelength optical-fiber-loop memory, fast tunable wavelength filters based on distributed feedback (DFB) laser amplifier are required to perform dynamic ATM cell selection in the wavelength domain [2]. For this purpose, we have studied DFB laser-amplifiers showing a short switching time, a wide tuning range and a high tuning rate at single current modulation. The DFB laser-amplifiers were designed by taking into account the modal gain saturation due to gain-curve-shift with the carrier density. The aim of the paper is to show impacts of the modal gain saturation on the tuning range as well as the tuning rate of three-contact DFB lasers (and filters) at **single current modulation.**

Modelling

To show the influence of the modal gain saturation on the tuning range, we compare the transmission gain with and without the saturation of a three-contact uniform-grating (kL=2) DFB laser of 200 μm long with a 50 μm long centre section using the same parameters except for the modal gain. Fig.1 shows linear and saturated modal gain curves used in the calculation. The linear gain constant is 3.4×10^{-16} cm^2. The saturated gain curve was obtained from experimental data. The linear parts of these curves are approximately the same. We calculate sub-threshold power transmission spectra using a computer program based on the transfer matrix method [3]. The transmission gain corresponding to the highest peak in a spectrum is plotted as a function of the lateral current density for the linear (dashed lines) and saturated gain (solid lines) in Fig.2. J_c denotes the current density in the centre section. It is clearly shown that with the linear modal gain the lasing occurs for any centre current value. Instead, when the saturation is taken into account, the gain curve describes a resonant profile and no lasing occurs at the highest lateral currents even with a high centre current (J_c=40 kA/cm^2). This is explained by the lasing wavelength excursion over the stop-band where the threshold gain is minimum at the centre. The transmission gain plotted as a function of the wavelength shows the feasibility of single lateral current tuning at a nearly constant gain (output power) for a saturated gain device at both below- and above-threshold (Fig.3, solid lines) which is impossible for a linear gain device (dashed lines). The single current tuning range (-3 dB) of the saturated gain device is 0.8 nm and 0.4 nm for the filter (J_c=25 kA/cm^2) and laser (40 kA/cm^2) respectively. The tuning rate is 5 GHz/mA for the laser.

Experimental Results

1.5 μm three-contact DFB lasers have been fabricated by using standard BRS laser technology with two-step epitaxial growth [4]. The lasers have a 0.11 μm thick InGaAsP bulk active layer and a 100 cm^{-1} coupling coefficient uniform grating. The modal gain saturation is enhanced by up-shifting the Bragg wavelength about 60 nm with respect to the maximum gain. The leakage current through the lateral homojunctions is reduced by proton implantation. The centre electrode is separated from the lateral electrodes, which are connected to each other, by using reactive ion beam etching (RIBE) technique.

We describe one of the best devices in terms of the above-threshold tuning range (as a laser). The 200 μm long device with a 60 μm long centre section has AR coatings on both facets and shows an uniform-injection threshold current of 26 mA. In Fig.4, the emission power level of the highest peak in spectra for different sets of the centre (I_c) and lateral (I_{lat}) currents is plotted as a function of the wavelength. The curves corresponding to sub-threshold spectra (I_c=5 and 5.5 mA) reproduce well the profiles given in Fig.3. For I_c=5 mA, the tuning range corresponding to the -3 dB power is 0.72 nm with lateral current tuning. Note that better results exceeding a 1 nm tuning range were obtained for the devices with a 50 μm long centre section. The curve for I_c=30mA corresponds to the lasing power level (≈ 1 mW) with SMSR > 30 dB. The tuning range corresponding to the -3 dB power is **2.5 nm** with a tuning current swing of 27 mA. The corresponding tuning rate is about 12 GHz/mA. By driving the lateral sections by 15 ns duration current pulses of 100 KHz repetition rate, a thermal effect free tuning rate of **32 GHz/mA** was obtained (Fig.5). The device is biased at I_c=20 mA and I_{lat}=13 mA.

Conclusion

Taking into account the modal gain saturation due to gain-curve-shift, we have demonstrated theoretically and experimentally the feasibility of a wide wavelength tuning (~ 2.5 nm) and a high tuning rate (~ 32 GHz/mA) with a small power change by single (lateral) current tuning in the case of three-contact DFB lasers and filters. We believe that this effect differs from the gain lever effect [5], since it was observed independently on bias conditions.

This work has been supported in part by the EEC RACE 2039 (ATMOS) project.

References

[1] A. de Bosio et al., *in Proc.* ISS'90 (Stockholm, Sweden), 1990.
[2] M. Calzavara et al., *in Proc.* OFC'94 (San Jose, USA), 1994.
[3] P. Correc, Ann. Télécommun. (Paris, France), 47, 125, 1992.
[4] J. Charil et al., Electron. Lett., 25, 1477, 1989.
[5] K.J. Vahala et al., Appl. Phys. Lett., 54, 2506, 1989.

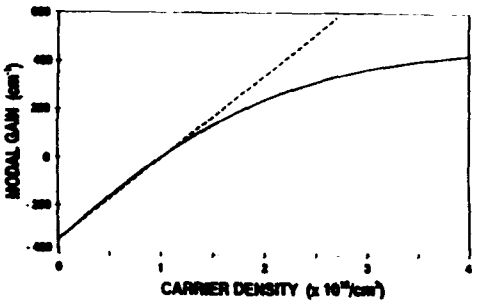

Fig.1 Modal Gain.

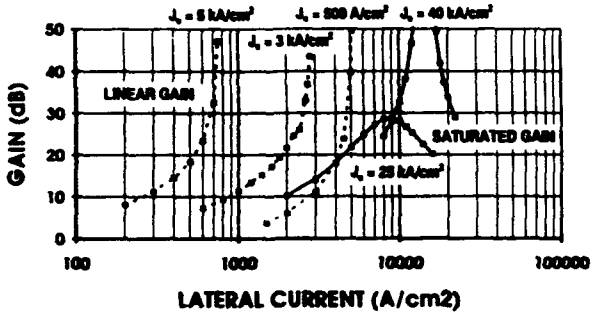

Fig.2 Transmission Gain vs Lateral Current Density.

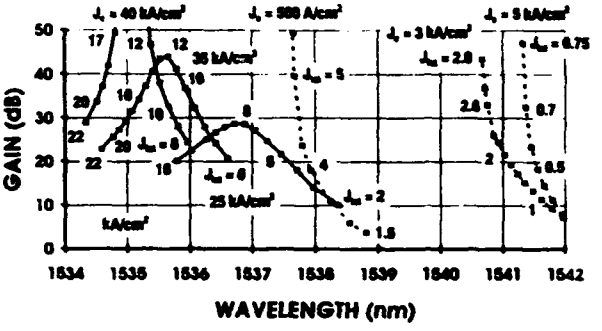

Fig.3 Transmission Gain vs Wavelength.

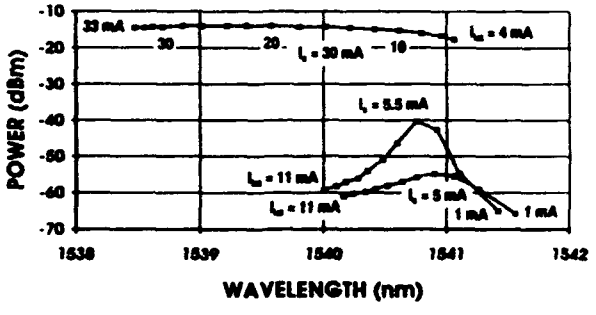

Fig.4 Power Level (arbitrary) vs Wavelength.

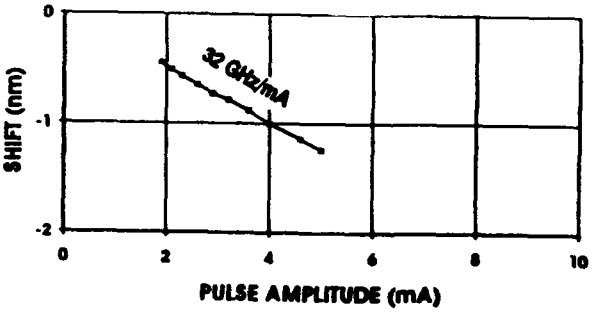

Fig.5 Wavelength Shift Measured by Applying Pulsed Current.

Wednesday
September 21, 1994

SESSION W1
VCSELs

SESSION W2
Coupling Structures for Lasers and Amplifiers

SESSION W3
Visible Lasers

8:30am - 8:45am
W1.1

Arrays of Red VCSELs With Partial Top Dielectric Stack DBRs†

J. A. Lott[a, b], R. P. Schneider, Jr., K. J. Malloy[b], S. P. Kilcoyne, and K. D. Choquette
Sandia National Laboratories, Microelectronics and Photonics Center, Albuquerque, NM 87185
[a]*Air Force Institute of Technology, Wright-Patterson AFB, OH 45433*
[b]*The University of New Mexico, Center for High Technology Materials, Albuquerque, NM 87131*

Abstract

We report arrays (1x64) of red vertical cavity surface emitting lasers (VCSELs) with partial top dielectric stack distributed Bragg reflectors (DBRs). Output powers exceed 0.5 mW at λ_o~660 nm for 15 μm diameter devices with threshold currents below 2 mA.

Visible vertical cavity surface emitting lasers (VCSELs) have several design options which directly impact both device performance and the complexity of the post-growth fabrication process. One design option aimed at improving device efficiency is the replacement of all or part of the p-doped distributed Bragg reflector (DBR) with a hybrid dielectric stack [1-3]. Here, we report the first one-dimensional red VCSEL arrays that use a partial top dielectric DBR stack.

The device structures, shown in Fig. 1, are grown by metalorganic vapor phase epitaxy (MOVPE) [4, 5]. Rotation is not used during growth, such that the Fabry-Perot resonance varies across the 2 inch wafer at a rate of ~0.1 nm/100 μm from front to back along the centerline. The Fabry-Perot resonance at wafer center is λ_o ~660 nm. The bottom DBR is 55.5 periods of (n+)AlAs/$Al_{0.5}Ga_{0.5}As$ with ~biparabolic compositional interface grading. A similar p-doped top DBR stack has just 10 periods, and includes a 10 nm (p+)GaAs contact layer. An 8λ thick AlGaInP optical cavity contains three 6 nm thick $Ga_{0.43}In_{0.57}P$ strained quantum wells.

One-dimensional (1x64) arrays with a pitch of 100 μm are fabricated using standard techniques including proton implantation and mesa etching for isolation. The device apertures are 15 μm in diameter, while the implant diameter is 20 μm. The as-processed resonant cavity light-emitting diodes (RCLEDs) [6] are characterized with L-I-V and electroluminescence (EL) measurements. Then, a SiO_2/Nb_2O_5 dielectric DBR stack is deposited with a low temperature (≤ 50 °C) DC magnetron sputtering process.

The EL and LI characteristics for a device before and after the addition of the top dielectric stack (6 periods) are shown in Figures 2 and 3, respectively. The threshold current versus peak emission wavelength for an example 1x64 array is shown in Fig. 4. The spread in wavelength $\Delta\lambda$ ~6.3 nm and threshold current ΔI_{th} ~ 0.53 mA, are readily improved by using rotation during MOVPE growth, and by properly aligning the Fabry-Perot mode to the quantum well peak spectral gain.

References
[1] C. Lei *et al.*, *J. Appl. Phys.*, vol. 69, pp. 7430-7434, 1991.
[2] H-J. Yoo *et al.*, *Jap. J. Appl. Phys.* , vol. 30, pp. L492-L494, 1991.
[3] A. Scherer *et al.*, *Electr. Lett.*, vol. 28, pp. 1224-1226, 1992.
[4] J. A. Lott and R. P. Schneider, Jr., *Electr. Lett.*, vol. 29, pp. 830-832, 1993.
[5] R. P. Schneider, Jr. and J. A. Lott, *Appl. Phys. Lett, pp.* 917-919, 1993.
[6] J. A. Lott *et al.*, *Phot. Tech. Lett.*, vol. 5, pp. 631-633, 1993.
† This work was supported by the US Dept. of Energy under Contract Number DE-AC04-76DP00789.

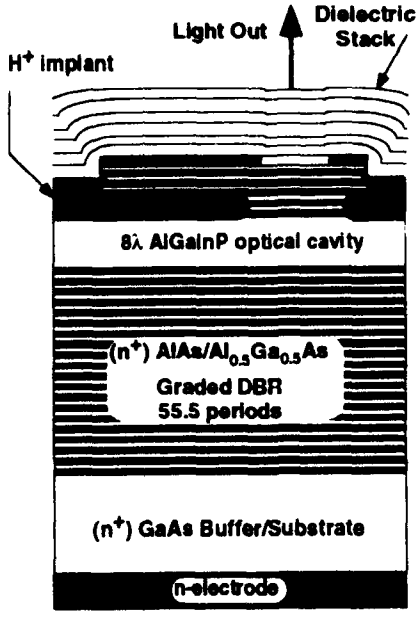

Fig. 1 Schematic of the completed Red VCSEL

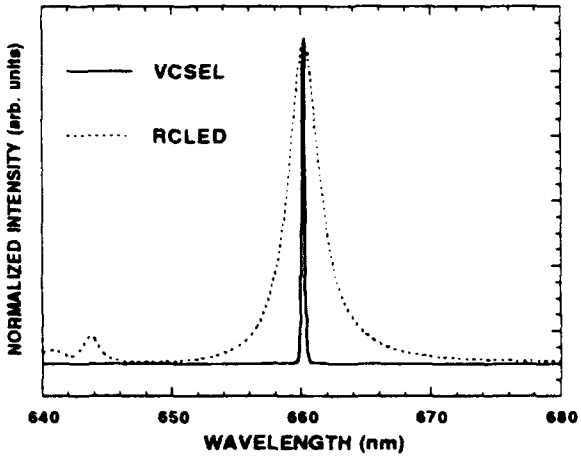

Fig. 2 Normalized EL before and after adding the top dielectric stack

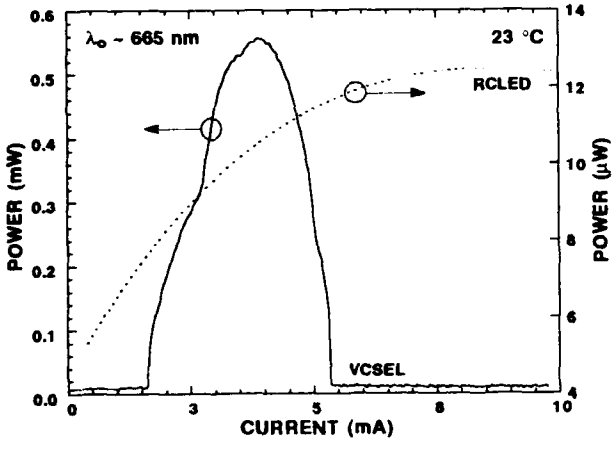

Fig. 3 L-I before and after adding the top dielectric stack

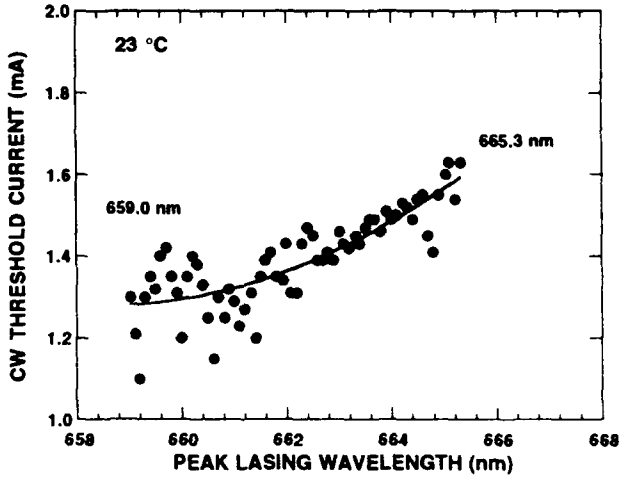

Fig. 4 Threshold current vs. emission wavelength for a 1x64 red VCSEL array

8:45am - 9:00am

W1.2

6 GHz Modulation of Fiber Coupled VCSEL Arrays

E. Zeeb[1], B. Möller[1], G. Reiner[1], M. Ries[1], T. Hackbarth[2], K.J. Ebeling[1]
University of Ulm, Department of Optoelectronics, D-89069 Ulm, Germany[1]
Daimler Benz Research Center, D-89013 Ulm, Germany[2]

Abstract: Fiber coupling of independently addressable 4×8 vertical-cavity top-surface-emitting laser diode arrays with coupling-efficiency above 70 % is reported. Individual lasers show maximum output powers of 1.3 mW and electrical 3 dB modulation bandwidths up to 6 GHz.

Vertical-cavity surface-emitting laser diodes (VCSEL) 2D arrays considerably increase the transmission capacity of multi-wavelength and multi-fiber optical interconnects. Aside from very low threshold currents and single-mode oscillation, large coupling efficiencies into single-mode fibers are achievable [1]. Here we report the fabrication of 4×8 independently addressable VCSEL arrays with low threshold currents and large small-signal modulation bandwiths and a simple method to couple lasers simultaneously into multi-mode fibers.

The laser structure under investigation was grown by molecular beam epitaxy. The undoped active region contains three InGaAs quantum wells and is embedded between two Bragg reflectors consisting of 30.5 n-doped and 20 p-doped AlAs/GaAs quarter-wavelength pairs, respectively. Lateral current confinement and insulation of the individual lasers of 12 μm active diameter is achieved by proton implantation with energies between 60 keV and 300 keV and a total dose of $1.5 \cdot 10^{15}$ cm^{-2}. To enhance the maximum single-mode output power [2] and to improve the ohmic behavior of the TiAu p-contacts the 10 μm diameter emission window is smaller than the active diameter. Lasing elements of an array are grouped in a rectangular matrix with 250 μm pitch size and connected to bonding pads by TiAu feeding lines. Fig. 1 shows a cross-section of the device structure and illustrates butt coupling of the array into a fiber bundle. Fibers are fixed in a 2.5 mm thick plastic matrix with holes of 125 μm diameter arranged to match the VCSEL array. The matrix is adjusted in front of the VCSEL array and light is butt coupled into the flat cut fibers. Fig. 2 shows light output powers in some fibers for various lasing elements. Maximum output powers about 0.75 mW are achieved in all fibers, coupling efficiency is in the order of 70 %.

To measure the modulation characteristics of the lasers the arrays are mounted in high frequency packages and wire bonded to SMA sockets. Typical small-signal modulation responses for various driving currents above threshold are illustrated in Fig. 3. With increasing bias the 3 dB modulation bandwidth increases up to 5 GHz at a single-mode output power of 0.8 mW. Above this level higher transverse modes appear in the emission. At an output power of 1.3 mW 3 dB modulation bandwidth is 6 GHz.

The emission wavelength distribution and a histogram of threshold currents of an array designed for a large wavelength shift across the device is depicted in Fig. 4. Due to wedge shaped epitaxial layers produced intentionally during MBE growth emission wavelengths of individual lasers vary by 20 nm for driving currents of 5 mA. Accordingly threshold currents show a relatively strong variation between 2.2 mA and 3.8 mA. Corresponding diagrams for an array fabricated from a rather homogeneous wafer are shown in Fig. 5. Threshold currents are between 4.1 mA and 4.4 mA.

To conclude, we have fabricated high performance fiber pigtailed 4×8 independently addressable VCSEL arrays of low threshold current and high simultaneous multi-mode coupling efficiency of 70 %. Small-signal modulation bandwidths are 5 GHz for single-mode and 6 GHz for multi-mode VCSEL oscillation.

References

[1] T. Wipiejewski et al., Proc. 19th ECOC, Montreux, Switzerland, Sept. 1993, pp. 333-336.
[2] R.A. Morgan et al., IEEE Photon. Technol. Lett. 4, pp. 374 - 377, (1993).

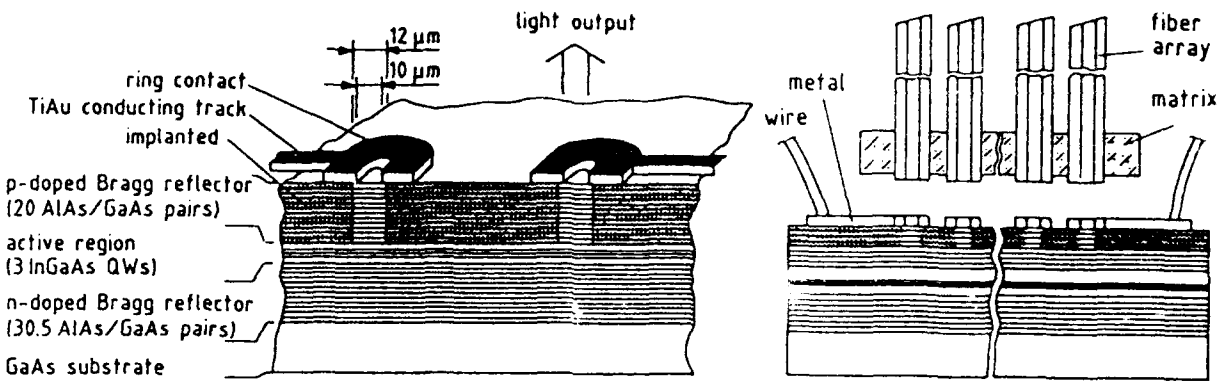

Fig. 1: Cross-section of an array fabricated and schematic of fiber coupling arrangement.

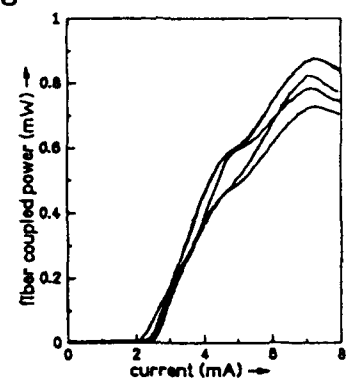

Fig. 2: Power coupled into various fibers.

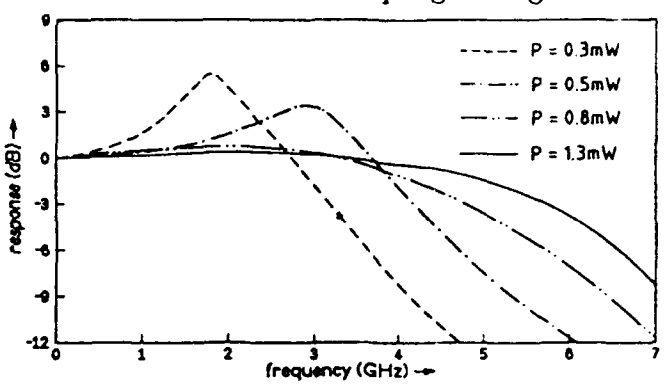

Fig. 3: Modulation response of an individual laser.

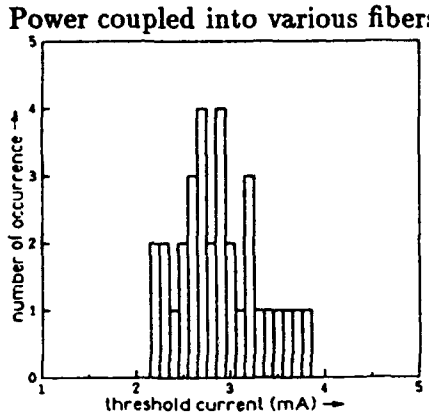

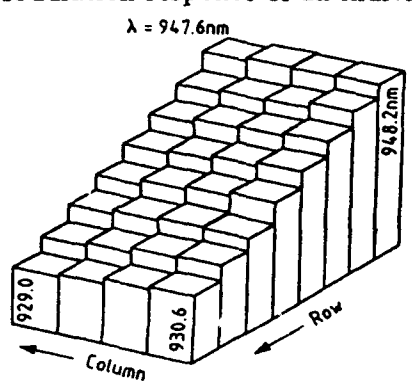

Fig. 4: Wavelength distribution and histogram of threshold currents of wedge shaped array.

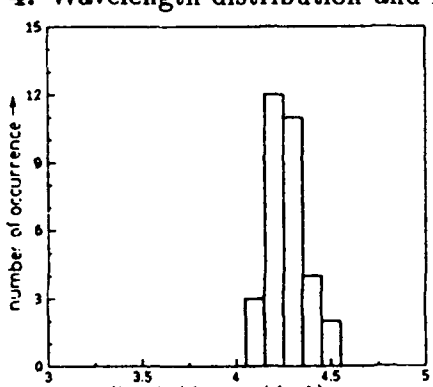

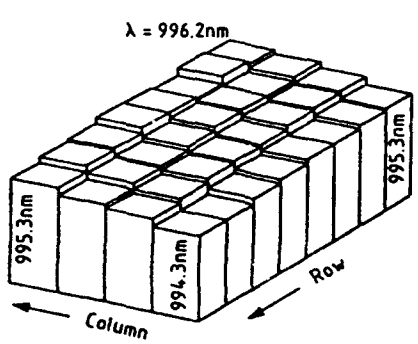

Fig. 5: Wavelength distribution and histogram of threshold currents of homogeneous array.

9:00am - 9:15am
W1.3

Design,Characterisitics and Reliability of a Large Area Surface Emitting Laser (SEL) for Multimode Data Link Applications

M.R.T. Tan, K.H. Hahn, Y.M. Houng and S.Y. Wang
Hewlett-Packard Laboratories
3500 Deer Creek Road, Palo Alto, CA 94303
Albert T. Yuen, Tao Zhang and Chun Lei
Optical-Communication Division
350 W. Trimble Rd, San Jose, CA 95131

Abstract:
For short distance multimode data link systems, the large area surface emitting laser with spectral width of up to 1 nm has been shown to operate in multimode links with RIN less than -120 dB/Hz [1,2]. SELs have been specifically designed for this application. Modal properties, modal stabilities, efficiencies, reliability and details of the bottom emitting 980 nm SEL design will be discussed in this talk.

Application:
Gigabit rate optical data links of under 1 km length are becoming increasingly important as the need for high speed data transmission between high performance workstations becomes necessary. The optical source for such links has been the CD laser operating in the self-pulsating mode to broaden the spectrum in order to minimize the modal noise due to mode dependent loss in the multimode fiber system. Limitations of the CD laser include: the laser has to be pre-selected for its self-pulsating characteristics, and the modulation frequency is limited to approximately one-third [3] of the self-pulsating frequency which is typically ~1.5-2 GHz. A properly designed large area SEL will not have the limitations mentioned above and is an excellent light source for a multimode data link.

Device:

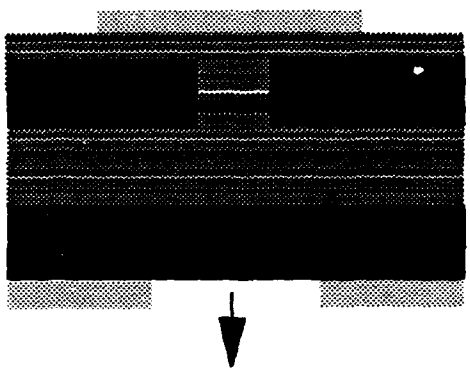

Figure 1. Bottom Emitting SEL structure with a lateral active width of 24 um.

The SEL is a bottom emitting structure with strained InGaAs quantum wells emitting at 980 nm as shown in Figure 1. The SEL consists of 18.5 pairs of n-GaAs/AlAs Bragg mirrors on the output face and 15 pairs of p-GaAs/AlAs together with a Au mirror on the totally reflective face. The cavity length is a single lambda wide and consists of an active region with 3 x 80 angstrom strained InGaAs quantum wells with 100 angstroms GaAs barriers and about 970 angstroms of $Al_{0.3}Ga_{0.7}As$ carrier confining layers. The interface between GaAs and AlAs in the DBR mirrors is digitally graded in 8 steps using a chirped short period superlattice. The final p-GaAs phase matching layer is doped to 3×10^{19} cm^3 to provide a non-alloyed ohmic contact to the hybrid Au mirror which also acts as a p-contact. The GaAs/AlAs Bragg mirrors are uniformly doped to 1×10^{18} cm^3 except for the digital grading region which is uniformly doped to $5 \times 10^{18} cm^3$. The n dopant is Si and the p dopant is carbon which has been shown not to diffuse [4,5] out of the graded region. The epitaxial layers are grown by a gas source molecular beam machine on n^+ GaAs substrate with in-situ monitoring and feedback control of the epitaxial structure [6]. The basic fabrication steps are: hybrid Au mirror deposition, mask photoresist proton implant mask, etch Au field, etch GaAs phase layer, proton implant, Au plate for die-attaching, lap and polish to 5 mils, n-contact deposition and finally anti-reflection coating. SELs with 24 um active diameters have turn on voltages as low as 1.39 V and threshold current of 3.0mA. Wallplug efficiencies of 16% have been demonstrated. The IV and LI curves of the SEL is shown in Figure 2. The kinks in the LI curve are from filamentation and/or higher order spatial modes appearing in the laser cavity as the bias is increased. The 1.39V turn on voltage is only 0.27 V excess above the InGaAs bandgap energy. The series resistence of the device is 20 ohms.

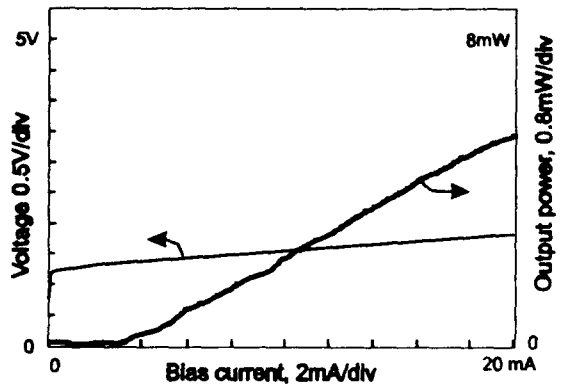

Figure 2. LI and IV characteristics of the SEL. The turn on voltage is 1.39V and the threshold current is 3.0mA. Output power at 6mA is about 1mW.

Spectral width:
A wide spectral width is necessary to reduce the effect of modal noise due to mode selective loss in multimode links. SEL with an active width of 24 um was found to give a spectral width of 0.3-1.0 nm. The wide active region is necessary to allow the accomodation of multiple filaments and/or higher order modes whose simultaneous existence give rise to the wide spectral width. Figure 3 shows the near field pattern of the SEL and the associated spectrum as a function of the bias. BER of better than 10^{-12} at 1 Gb/s with good eye opening and low modal and intensity noise have been obtained with these devices.

Reliability:
The major burn-in failure that we have observed is that of dark line defects (DLD) and dark spot defects (DSD). The burn-in screening investigation showed that a short constant current stress is effective in screening out early failures. The conditions used for the burn-in is 70°C, 10^4 A/cm^2 , for 24 hours. It is believed that the current density and temperature are the major driving forces for the defects and not optical density. The devices which have passed the burn-in screening are now being stressed at 40°C, 60°C and 70°C at 1mW. Lifetime estimates and further failure analysis will be discussed in the talk.

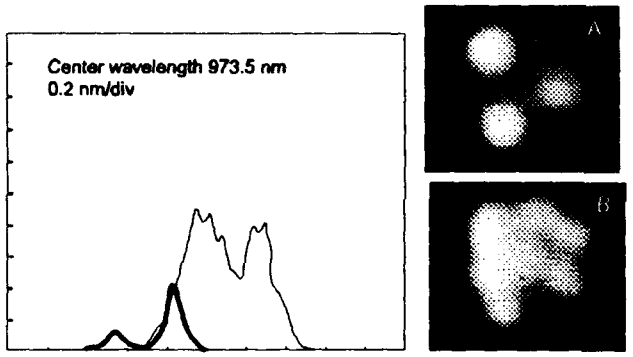

Figure 3. The near field pattern at a bias of approxiamtely 8mA (A) and 20mA (B) is shown together with the spectrum at the respective bias. The curve with the thicker line correspond to condition A.

Aspects of its reliability will also be discussed.

Conclusion:
Large area SELs are excellent candidates as sources for multimode optical fiber data link applications. Wide spectral width and high speed modulation have been shown to be possible.This talk will elaborate on the device design and characteristics desirable for multimode data link applications.

References:

[1] Hahn, K.H., Tan. M.R.T., Houng, Y.M. Wang, S.Y.; Electronics Letters,29, p.1482, 1993.
[2] Hahn, K.H., Tan, M.R.T., Wang, S.Y.; Electronics Letters, 30, p. 139, 1994.
[3] D. Sears, Hewlett-Packard Optoelectronics Division, private communication.
[4] Houng, Y.M., Lester, S.D., Mars, D.E. Miller, J.N.; J. Vac. Sci. Technol. , B11(3), p.915, 1993.
[5] Houng, Y.M., Lee, B.J., Low, T.S., Miller, J.N.; J. Vac. Sci. Technol.,B8(2), p.355, 1990.
[6] Houng, Y.M. , Tan, M.R.T., Liang, B.W., Wang, S.Y., Yang, L., Mars, D.E.; J. Crystal Growth, 136, p. 216, 1994.

9:15am - 9:30am
W1.4

Improved temperature characteristics of a vertical cavity surface-emitting laser with a broad gain bandwidth

Mikihiro Kajita, Takeshi Kawakami, Takashi Yoshikawa, Atsuko Uemura,
Yoshimasa Sugimoto, and Kenichi Kasahara

Opto-Electronics Research Laboratories, NEC Corporation, 34 Miyukigaoka, Tsukuba, Ibaraki 305, Japan

Abstract

A vertical cavity surface-emitting laser with a broad-gain bandwidth was fabricated by using multiple-quantum-well active layers with different bandgap energies, increasing the temperature range by more than 20℃.

Vertical cavity surface-emitting lasers (VCSELs) are being developed as light sources for two-dimensional optical interconnections. These devices need to provide a stable light output at a constant current, even when the temperature increases due to simultaneous device operation or changes in the environment. Extending the operational temperature range of these devices is important, because an increase in temperature can cause a cavity resonant peak to exceed the gain bandwidth limit. This reduces the light output power and increases the driving current. One way to prevent this problem is to use the offset-gain method[1-2]. As another way, we propose a VCSEL with a broad-gain bandwidth fabricated by using multiple-quantum-well (MQW) active layers with different bandgap energies.

The structure of the proposed device is shown in Fig. 1. The top mesa is 6 μm square and produces single lateral-mode oscillation. The quantum wells, QW1, QW2 and QW3, consist of InGaAs with gain peaks of 970, 980 and 990 nm, respectively. The cavity resonant peak is set at 980 nm, the gain peak of QW2. The spacer layers consist of $Al_{0.25}Ga_{0.75}As$. The DBRs consist of AlAs/GaAs quarter-wave stacks with linearly graded transition layers. The pair numbers of the top and bottom DBRs are 15 and 18.5, respectively.

The gain spectrum of this VCSEL as a function of the wavelength difference from the cavity resonant peak λ_c (Fig. 2(b)) was obtained from the emission spectrum of an edge emitter fabricated from a VCSEL wafer. For reference, the gain spectrum of a VCSEL with three quantum-well active layers, each consisting of the same type InGaAs, is also shown in Fig. 2(a). The gain bandwidth of the VCSEL consisting of three different InGaAs MQWs is larger than that of the reference device.

The I-L characteristics of the proposed VCSEL are shown with temperature as a variable in Fig. 3. Threshold current I_{th} and slope efficiency at threshold η_d at 20℃ of this VCSEL were 1.18 ± 0.34 mA and 0.267 ± 0.034 mW/mA, respectively, while those of the reference VCSEL were 1.33 ± 0.25 mA and 0.251 ± 0.027 mW/mA, respectively. The change in the threshold current of the proposed VCSEL remained lower than that of the reference VCSEL as the temperature changed. To clarify this, temperature range ΔT is plotted in Fig. 4 as a function of the change in threshold current from the minimum ΔI; ΔT is defined as the allowable temperature range when ΔI is restricted to a certain range of values from the minimum. The threshold current of both devices reached a minimum at the same temperature, -30℃, where I_{th} was almost the same in both devices. These results indicate that the operational temperature range of a VCSEL consisting of three different InGaAs MQWs is wider than that of a reference VCSEL by more than 20℃. This difference in the range is considered to be

due to the extended gain bandwidth.

The difference in temperature characteristics between the proposed and reference VCSELs is larger at lower temperatures less than room temperature, because the gain spectrum of both devices is almost the same in the high temperature-region (wavelength region below cavity resonant peak λ_c) as shown in Fig. 2. This means that the temperature characteristics at higher temperatures of the proposed VCSEL can be expected to be further improved by combining the offset-gain method with a carrier confinement by using a high-barrier cladding layer[1-2] with a broad-gain bandwidth, as we have proposed.

References

1) D.B. Young et al., IEEE J. Quantum Electron., **29** (1993) 2013.
2) J.M. Catchmark et al., Appl. Phys. Lett., **63** (1993) 3122.

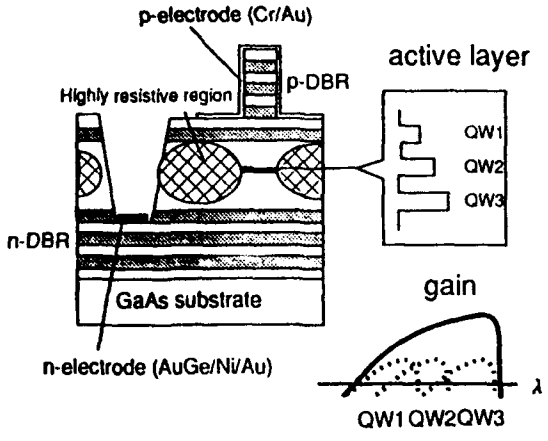

Fig.1. Device structure.

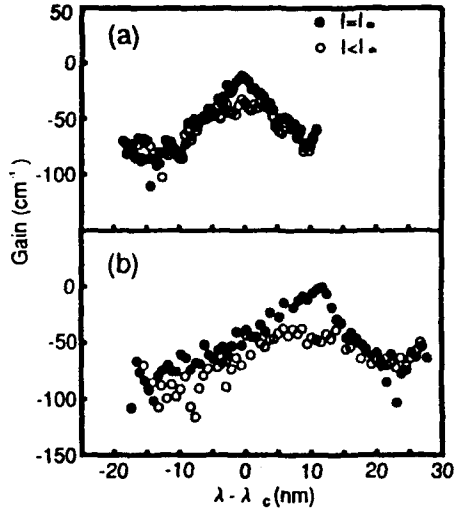

Fig.2. Gain spectra of the (a)reference and (b)proposed VCSEL. λ_c denotes a cavity resonant peak.

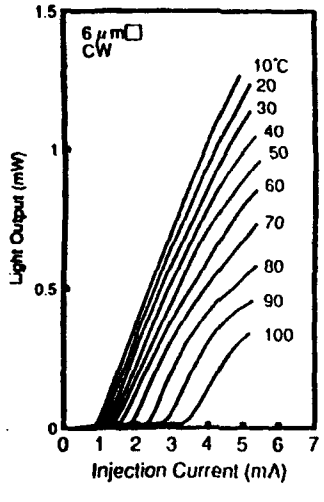

Fig.3. I-L characteristics of a proposed VCSEL consisting of three different InGaAs MQWs.

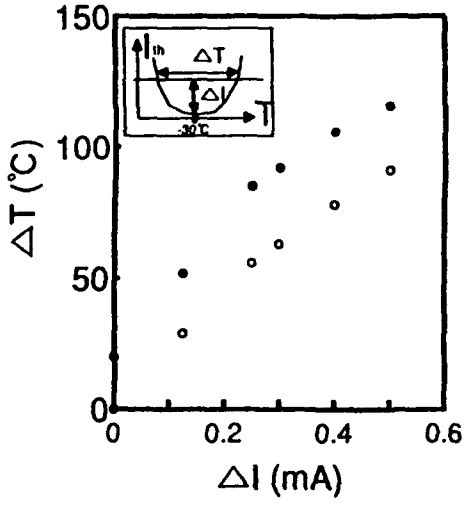

Fig.4. Temperature range (ΔT) vs. change of threshold current from the minimum (ΔI_{th}) plots for the (a)reference (○)and (b)proposed (●) VCSEL.

9:30am - 9:45am
W1.5

Vertical-Cavity Surface-Emitting-Lasers with 21% Efficiency by Metalorganic Vapor Phase Epitaxy

K. L. Lear, R. P. Schneider, Jr., K. D. Choquette, S. P. Kilcoyne, J. J. Figiel, and J. C. Zolper
Sandia National Laboratories, Photonics Research Department
MS 0603 / PO Box 5800 / Albuquerque, NM 87185-0603

Abstract: We have demonstrated vertical-cavity top-surface-emitting lasers by metalorganic vapor phase epitaxy that set record cw performance marks of 21% power conversion efficiency, 1.47 V threshold voltage, 23 mW output power, and 3.7 mW single-mode output power. The enhanced laser performance relies on novel mirror designs and benefits of metalorganic vapor phase epitaxy.

Vertical cavity surface emitting lasers (VCSELs) promise to compete with more conventional laser diodes in an array of applications including parallel optical communications, sensing, printing, and scanning. The viability of VCSELs in these areas is contingent upon both improved performance as well as demonstrated manufacturability. To these ends, we have produced VCSELs by metalorganic vapor phase epitaxy (MOVPE) with record performance in several respects. MOVPE offers beneficial materials capability and high throughput. The results for the lasers presented here, including the first report of power conversion efficiency in excess of 20%, surpass those of previous VCSELs grown by MBE[1,2] or MOVPE. These improvements are attributed to novel low resistance mirror designs with enhanced optical and thermal characteristics as well as advantages inherent in MOVPE technology.

The mirrors were designed to offer low resistance while decreasing the alloy content and thus increasing the thermal conductivity and interfacial reflectivity relative to previous mirror grading designs used in our MBE devices. The MOVPE mirror composition is graded from GaAs to $Al_{0.95}Ga_{0.05}As$ in 28 nm while the MBE mirrors were graded from $Al_{0.1}Ga_{0.9}As$ to $Al_{0.9}Ga_{0.1}As$ in 56 nm. The larger, more abrupt composition step leads to higher interfacial reflectivity as well as decreasing average alloy content thus decreasing alloy scattering of phonons and increasing thermal conductivity. The increased GaAs content also improves lateral electrical conductivity thus enhancing current injection uniformity. Despite the more abrupt grading, low interfacial resistance is fostered by the smoothly varying AlGaAs composition and carbon doping afforded by MOVPE.

The devices studied were proton implanted, top-emitting VCSELs with a nominal wavelength of 950 nm measured as the cavity mode luminescence peak at low current levels. The epitaxial structure was grown by MOVPE at a rate of ~3 μm/hour and had a one-wavelength cavity including three InGaAs quantum wells, a 38-period bottom mirror doped $2x10^{18}$ cm^{-3} with silicon, and a top mirror carbon doped at $1\text{-}2x10^{18}$ cm^{-3} with either 18 or 22 periods. The high growth rate facilitated the growth of the thicker than normal bottom mirror with the additional periods reducing the high reflector transmission loss which was non-negligible in our previous MBE designs that had fewer bottom mirror periods. The samples were implanted with protons masked by 11.5 μm thick photoresist pattern commensurate with a circular aperture in the p-contact ranging from 5 to 50 μm in diameter. The lasers were tested in wafer form on a stage with a controlled temperature of 20 °C. Calibrated cw output power and voltage versus current measurements were made on a variety of devices.

A range of cavity mode wavelengths were present on the samples due to the approximately 5% variation in the layer thickness across the unrotated wafers. Devices lased at wavelengths from approximately 1010 nm to 920 nm. The minimum threshold current and maximum output power occurred for devices with low bias wavelengths of approximately 940 nm and 960 nm respectively. The full range of device sizes from 5 to 50 μm diameters lased in this wavelength range. The maximum cw output power of the 50 μm diameter devices was 23 mW. Figure 1 shows the characteristics of two different 30 μm diameter devices that lased at 943 nm and 951 nm on the sample with the 22 period top mirror. The first device's lasing threshold occurs at 5.1 mA and 1.47 V, only 0.16 volts above the corresponding photon energy at 943 nm. The 951 nm device has a slightly higher threshold current of 6.5 mA, but reached a maximum cw power of 19.5 mW while dropping less than 2 volts over almost the entire useful operating range. The difference in the slope quantum efficiencies of the two devices (27% for the lower threshold 943 nm device, and 41% for the higher power 951 nm device) indicates a variation in relative mirror transmission for the two devices. A slight change in mirror reflectivity may be due to incommensurate changes in the growth rates of the high and low index mirror layers as a function of position. The low threshold current, high slope efficiency, and low voltage drop of the 951 nm laser result in a power conversion efficiency of 21% at 31 mA, the highest efficiency reported for any VCSEL diode.

Many potential VCSEL applications such as fiber communications only require approximately 1 mW of output power. These levels of output power can be attained with less input power by using devices with smaller threshold currents than the 30 μm diameter ones discussed above. The characteristics of some of the smaller devices from 18 period top mirror sample are displayed in Figure 2. The characteristics for a 12 μm diameter device with a 3.1 mA threshold current show that it reaches the 1 mW output level with an electrical drive of 5.1 mA and

1.75 V for a total input power of 8.9 mW. This gives an efficiency of 11.2% at the 1 mW output power level. Even smaller devices on this sample exhibited higher threshold currents, similar to the threshold current vs. size dependence previously reported for our proton implanted MBE VCSELs. However, the maximum single-mode output power does increase with decreasing device size for MOVPE device diameters down to 8 μm. Figure 2b has the characteristics for a 8 μm diameter device that provides up to 3.7 mW of single-mode power, higher than previously reported values[3]. Devices as small as 5 μm in diameter lased with the same threshold current as the 8 μm diameter device, but had higher voltage drops and lower output powers.

In conclusion, we have reported MOVPE 950 nm VCSELs that exhibit record performance in several respects. The devices employ low resistance p-type mirrors that take advantage of the continuous alloy grading and carbon doping afforded by MOVPE. These devices demonstrate that MOVPE is not only well suited for high throughput growth of VCSELs, but can produce near-infrared devices that are superior to previously reported MBE VCSELs in many respects. Work is in progress on bottom-emitting devices that are more amenable to heatsinking and uniform current injection and consequently should deliver even higher power results.

[1] K. L. Lear and S. A. Chalmers, *Photon. Tech. Lett.*, vol. 5, pp. 972--975, 1993.
[2] M. G. Peters et al., *Photon. Tech. Lett.*, vol. 6, pp. 31--33, 1994.
[3] R. A. Morgan et al., *Photon. Tech. Lett.*, vol. 4, pp. 374--377, 1993.

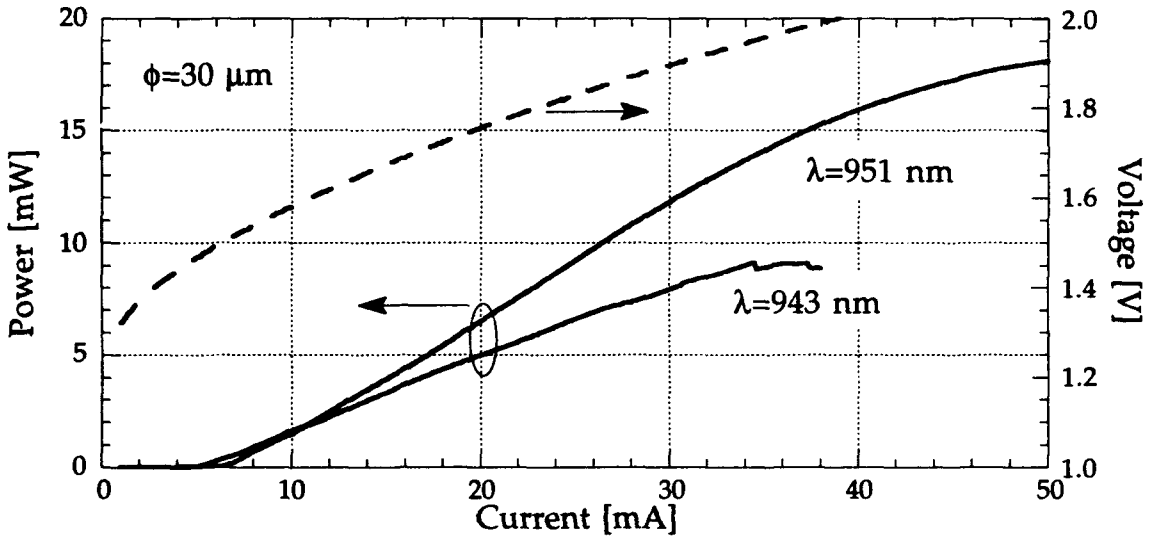

Figure 1. Output power (solid lines) and voltage(dashed line) vs. current characteristics for two 30 μm diameter devices at the indicated wavelengths. The voltage curve is nearly identical for the two devices. The 943 nm laser has a 1.47 V threshold and the 951 nm laser has a maximum power conversion efficiency of 21% occurring at 31 mA.

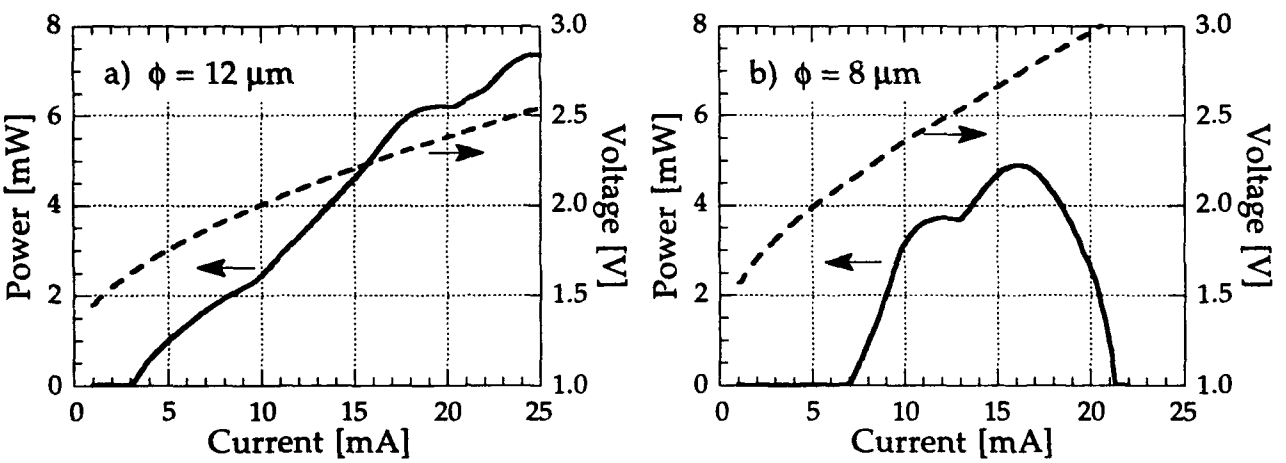

Figure 2. Characteristics for two smaller VCSELs exhibiting (a) 1 mW of output power with 8.9 mW of input electrical power, and (b) a maximum single-mode output power of 3.7 mW.

This work was supported by the United States Department of Energy under contract No. DE-AC04-94AL85000.

9:45am - 10:00am

W1.6 Polarization Control of Vertical-cavity Surface-Emitting Lasers by a Birefringent Metal/Semiconductor Polarizer Terminating a Distributed Bragg Reflector

T. Mukaihara, N. Ohnoki, Y. Hayashi, F. Koyama and K. Iga
Tokyo Institute of Technology, Precision and Intelligence Laboratory,
4259, Nagatsuta, Midoriku, Yokohama, 227, Japan

Abstract: We propose a polarization controlled vertical-cavity surface-emitting laser (VCSEL) using a birefringent metal/semiconductor polarizer on a distributed Bragg reflector. Theoretically, we found that the proposed concept can provide an extremely large polarization selectivity at the resonant cavity wavelength by adjusting the phase condition between two polarization states. Experimentally, we have demonstrated a 0.98μm InGaAs/GaAs VCSEL with an Au/GaAs polarizer exhibiting a fairly good polarization control and maintaining low thresholds.

The performances of vertical-cavity surface-emitting laser (VCSEL)[1] have been dramatically improved in recent years. Sub-milliampere threshold current VCSELs[2,3] have been achieved by employing high reflective mirror stacks. It is important to control the polarization states for low noise operations and for polarization sensitive applications. It is found, however, that no polarization selection is observed in planar isotropic devices except some approaches introducing anisotropy[4,5]. In this paper, we propose a polarization control method by using a birefringent metal/semiconductor polarizer terminating distributed Bragg reflector (DBR) with adjusting the phase condition between two polarization states. The concept is analogous to the method reported previously[6,7]. However, the fabrication process can be simplified by the present method and first installed into real devices.

The laser structure with a proposed polarizer is schematically shown in Fig. 1. Periodic metal/semiconductor layers, which create birefringence for the waves with parallel ($E_{//}$) and perpendicular ($E_{\perp}$) electric fields to the grating, are introduced on a top GaAs/AlAs DBR. Due to its birefringence, we can control the phase to be an antiresonant phase for the $E_{\perp}$ and form a dip of the reflectivity for the $E_{\perp}$ at the cavity resonance wavelength by adjusting the thickness of the polarizer and the cap layer, respectively. We assume, for example, a Au/GaAs polarizer of which lateral width is 400nm for Au and 1μm for GaAs, respectively. We have also assumed that GaAs/AlAs DBR stack is 20 pairs and the cavity resonance wavelength λ is 1.0μm. A calculated reflectivity for each polarization is shown in Fig. 2. By choosing the thickness of a GaAs layer L_1 to be 1.64×λ/4, the reflectivity of the $E_{\perp}$ can be drastically reduced at the resonant cavity wavelength. As shown in Fig. 2, we can obtain 11% reflectivity difference at the wavelength of 1μm, while the reflectivity of the $E_{//}$ maintains being 99.9%. Also, by alternating the thickness of the cap layer, each reflectivity at the resonant cavity wavelength could be changed. Figure 3 shows the reflectivity for two polarization states at the resonant cavity wavelength versus the thickness of cap layer. By dealing with the appropriate design of the cap layer, we can select the hopeful polarization state.

We fabricated MOCVD grown VCSELs with an Au/GaAs polarizer. The structure consists of 3 InGaAs strained quantum wells sandwiched by 22 and 25 period GaAs/AlAs bottom and top mirror stacks, respectively. Also, the Au(1.0μm)/GaAs(200nm) polarizer has been patterned on the top DBR, which is used as a contact. One of tested 25μmϕ diameter devices shows the minimum threshold current of 3.2mA (J_{th}≅ 660A/cm^2). It is found that the polarizer loaded devices show good performances comparable to ordinary VCSELs. Figure 4 shows an I-L characteristics for each polarization. Some of the devices show stable $E_{//}$ polarization. However, the perfect polarization control has not been achieved yet as shown in Table 1, which might be due to the fluctuations in the thickness of the cap layer or the polarizer in the present devices.

In conclusion, we have proposed a polarization control method of VCSELs by a birefringent metal/semiconductor polarizer. We pointed out that the phase matching in the composite mirror of a DBR and a polarizer could provide an extremely large difference in the reflectivity between the two polarization states. By adjusting the thickness of the cap layer, we would obtain the stable polarization control.

References

[1] K. Iga et al., *IEEE J. Quantum Electron.*, **24** (1988) 1845.
[2] T. Numai et al., *Jpn. J. Appl. Phys.*, **32** (1993) L1533.
[3] D B. Young et al., *Electron. Lett.*, 30 (1994) 233.
[4] M. Shimizu et al., *Electron. Lett.*, **27** (1991) 1067.
[5] T. Mukaihara et al., *IEEE Photon. Technol. Lett.*, **5** (1993) 133.
[6] T. Mukaihara et al., *Jpn. J. Appl. Phys.*, **33** (1994) L227.
[7] T. Mukaihara et al., *CLEO '94*, paper No. CMI2.

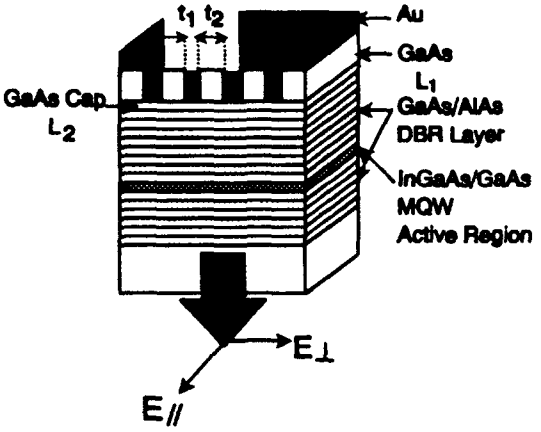

Fig. 1 Schematic of the proposed polarization control VCSEL.

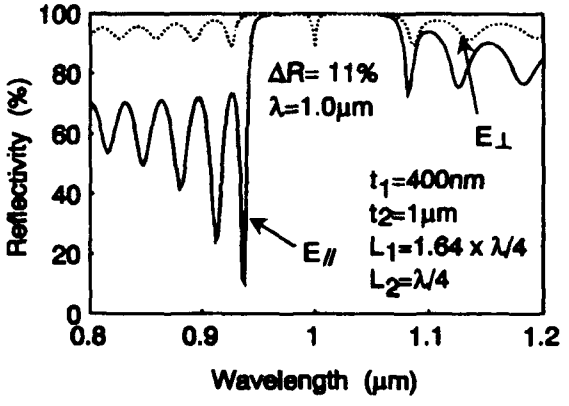

Fig. 2 A calculated reflectivity spectra for two polarizations.

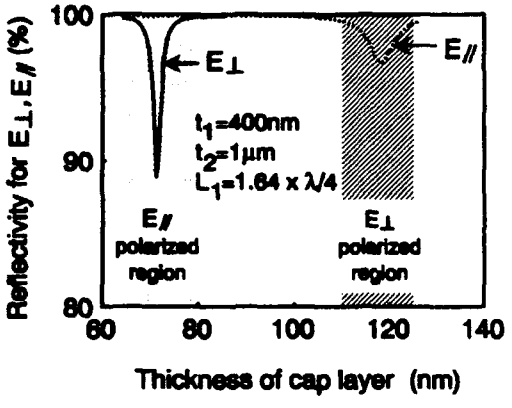

Fig. 3 A reflectivity for $E_{//}$, $E_{\perp}$ versus the thickness of cap layer

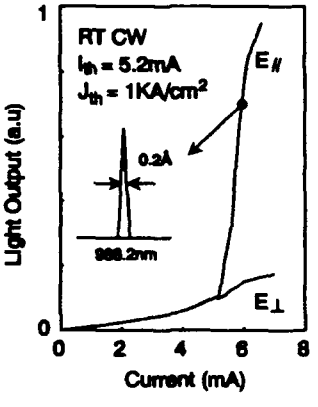

Fig. 4 A I-L characteristics for two polarization state.

Table. 1 Polarization characteristics of tested devices

Polarization direction	$E_{//}$	$E_{\perp}$	Random
Number (CW)	5	2	1
Number (Pulse)	8	0	6

10:30am - 10:45am

W2.1

Clamped Gain Travelling Wave Semiconductor Optical Amplifier for Wavelength Division Multiplexing Applications.

P. Doussiere, A. Jourdan, G. Soulage, P. Garabédian, C. Graver, T. Fillion, E. Derouin and D. Leclerc.
ALCATEL ALSTHOM RECHERCHE Route de Nozay, 91460 Marcoussis (France)

Introduction : Crosstalk induced by gain saturation and short carrier lifetime, intrinsic to the semiconductor medium, can severely limits the application of Semiconductor Optical Amplifiers (SOA) in Wavelength Division Multiplexing (WDM) systems with intensity modulated scheme [1]. Suppression of signal induced gain fluctuations using gain clamping by laser oscillation at a wavelength different from signal bandwidth has already been demonstrated in the case of a semiconductor amplifier with an external wavelength selective reflector [2].
In this paper, we report a new Clamped Gain SOA (CG SOA) structure with an integrated Bragg grating as a wavelength selective reflector and demonstrate crosstalk suppression in case of WDM application at 2.5 Gbit/s.
Device structure and principle : The proposed amplifier structure (Figure 1) is similar to those reported in [3] and is based on 0.5 µm wide square active stripe made of InGaAsP bulk material for polarisation independant operation. The active stripe is lateraly tapered over 70 µm at both ends for reduction of far field divergence and improvement of coupling efficiency to the fiber. Window regions and antireflection coating are used for suppression of cleaved facet reflectivity. The total length of the device is 600 µm.
A distributed Bragg grating is introduced under the active stripe and forms a wavelength selective reflector. The coupling coefficient of the grating is chosen so that it provides a high single pass gain at the oscillation threshold. Assuming homogeneous broadening of semiconductor gain lineshape, the overall gain bandwidth is expected to be clamped once the threshold oscillation is reached. At a wavelength different from the Bragg wavelength, the gain is independent of the signal intensity as long as the lasing oscillation is not switched off through carrier depletion effect. The optical power is, in fact, stored in the lasing wavelength and converted into amplified signal following intensity modulations,with a time response limited by the relaxation oscillation frequency.
Device characteristics and results : Static light / current characteristic of CG SOA is shown on figure 2. Lasing oscillation threshold is clearly observed around 60 mA. The maximum output power is 15 mW per facet at 200mA and is mainly limited by thermal effects. Small signal fiber to fiber gain versus driving current is shown on figure 3 for TE and TM polarisations: thanks to the square active stripe, the TE / TM gain difference is less than 1 dB and gain reaches 15 dB at 60 mA where the oscillation occurs. Figure 3 clearly shows the gain clamping effect due to the distributed grating: at 60 mA the gain saturate strongly and is nearly independant, in the one dB range, on the driving current from 60 up to 200 mA. Taking into account 3 to 4 dB coupling losses per facet, the internal gain is in the 21- 23 dB range.
The spectrum of the light at the output of the amplifier is shown on figure 4 for -25 dBm signal power launched at the input of the device. We can observe the lasing wavelength at 1530 nm, the amplified signal at 1540 nm and the broad-band Amplified Spontaneous Emission (ASE). Note that oscillation is not perfectly singlemode due to the two natural modes of the distributed Bragg grating. Despite the high single pass gain, the ASE curve is free from ripple and suggests negligible reflectivity of the grating, away from the stop band.
Crosstalk has been evaluated at 2.5 Gbit/s using two DFB laser sources at respectively 1550 nm and 1555 nm. Up to four channels were simulated by introducing power unbalance between both reference transmitter and interfering one. Figure 5 shows penalty at 10-9 B.E.R. versus average signal power per channel into the input fiber in case of 1, 2 and 4 channels. First, it is important to note, in the one channel case, the very high dynamic range (18 dB) of input power, corresponding to less than one dB penalty. Compared to the one channel case, penalty due to crosstalk is less than 1 dB as long as the total input power does not extinct the lasing oscillation.
Conclusion: Using new gain clamped TWA SOA structure, we demonstrate suppression of gain saturation induced crosstalk in WDM applications.
References :
[1] N.G. OBERG et al, IEEE J. Quantum Electron., vol. 24, pp. 52-59, Jan. 1988.
[2] J.C. SIMON et al, Electron Let., vol. 30, pp 49-50, Jan. 1994.
[3] P. DOUSSIERE et al., IEEE Photon. Techn. Let., vol 6, Fev 1994.

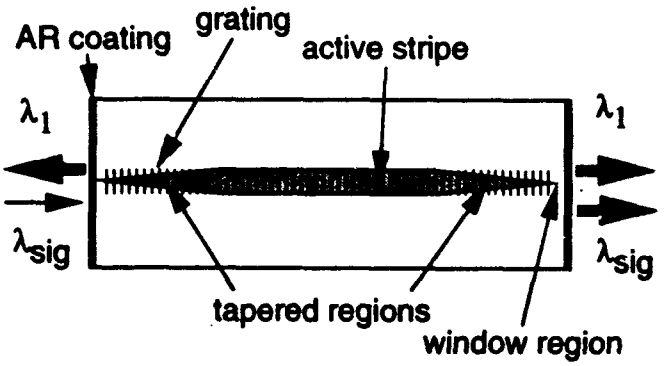

Fig 1: Overview of CG SOA structure

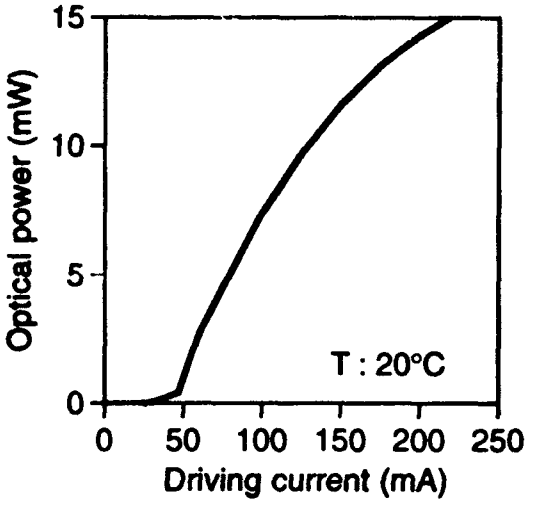

Fig 2 : Ligth / current characteristic of CG SOA

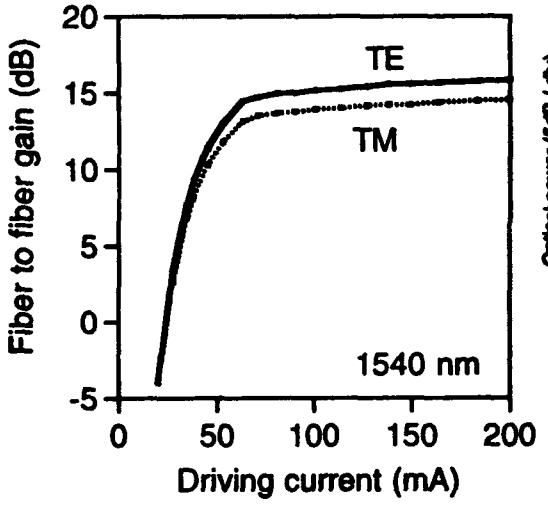

Fig 3 : Gain versus current of CG SOA

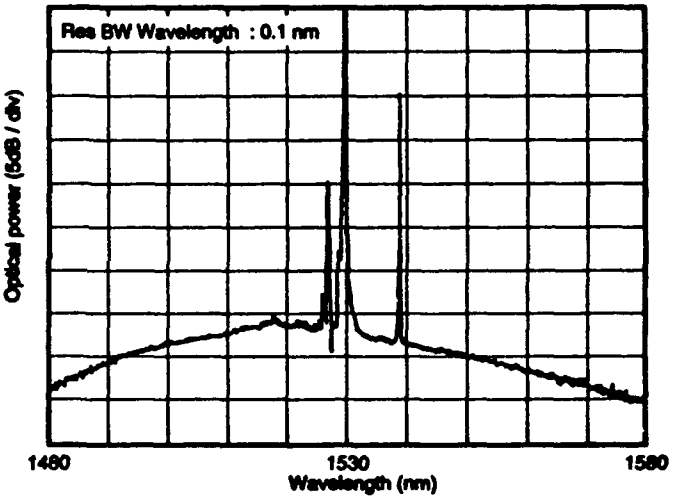

Fig 4 : Output spectrum of CG SOA

Fig 5 : Sensitivity penalty and input power per channel for 1, 2 and 4 channels

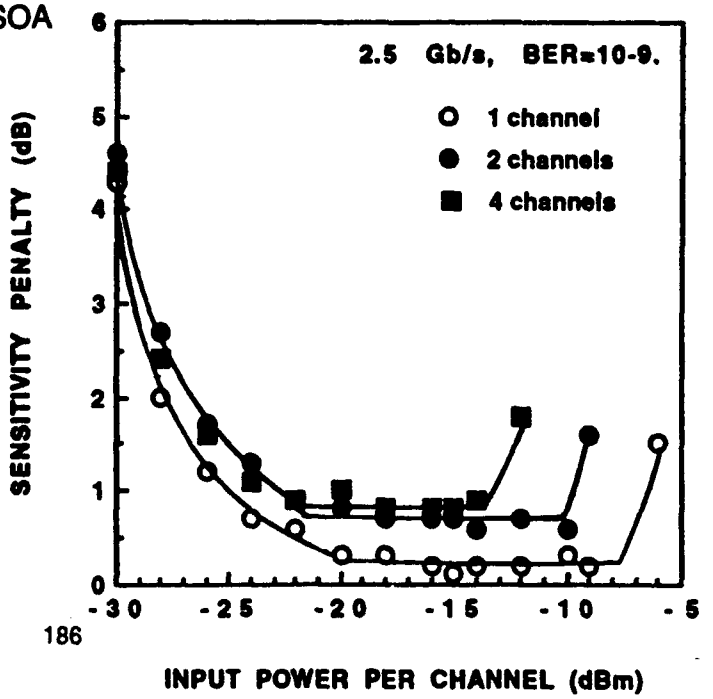

10:45am -11:00am
W2.2

InGaAs/InGaAsP Multiple Quantum Well Laser with An Integrated Tapered Beam Expander Waveguide

R. Ben-Michael, U. Koren, B. I. Miller, M. G. Young, M. Chien, and G. Raybon
AT&T Bell Laboratories, Holmdel, New Jersey 07733

Abstract Integration of a diode laser and a laterally tapered beam expander waveguide, results in narrow beam divergence of 5°×7°, and record fiber alignment tolerance of ±2.6 μm vertically and ±3.1 μm laterally.

The coupling of a diode laser to an optical fiber suffers from relatively high loss, since the optical mode emitted from the laser is too small, and since the optical mode shape is not circular. Optimizing a diode laser for the purpose of efficient coupling to an optical fiber is bound to result in compromises in the overall characteristics of the laser, because small spot size is needed for higher confinement of the optical mode in the active region. This results in low overlap between the emitted optical mode of a diode laser and the optical mode of the fiber. The use of an external waveguide for expanding the optical mode of a laser has been suggested[1], and for fiber-chip coupling[2,3]. However, the external waveguides still need careful alignment. Integration of a diode laser and a beam expander results in a more cost effective method of coupling to a "cleaved" (flat) optical fiber. This approach has been recently demonstrated by integrating vertically step-like tapered waveguide structure and a diode laser into one monolithic device[4,5].

In this work we have modified and integrated the continuously tapered Shani-Henry[1] beam expander inside the laser cavity. The structure of this new Adiabatic Mode Expander Laser Diode (AME-LD) device is shown in Fig. 1. The waveguide consists of two layers. The bottom waveguiding rib is an InGaAsP (λ=1.1 μm) layer, with a constant width of 5 μm. The upper guiding rib is composed of InGaAsP (λ=1.3 μm) layer, tapered continuously from 3 μm to a sharp point. This passive waveguide expands the beam size both laterally and vertically. Lateral broadening is due to the 5 μm broad output waveguide, that is twofold wider than the gain section waveguide. Vertical broadening is achieved by the gradual change from two guiding layers to one guiding layer. This two layer lateral tapered waveguide is made with a newly developed process, that allows for the integration of the waveguide with the active section, and for the formation of the tapered two layer waveguide using selective etch and selective regrowth. The transition between the gain and the passive sections of the AME-LD is similar to that reported previously[6]. The gain section consists of a 2.5 μm wide mesa, buried in semi-insulating Fe doped InP, using MOCVD selective regrowth technique. The same semi insulating blocking layers are used as cladding for the passive beam expanding waveguide.

700 μm long AME-LD's consisting of 400 μm long gain section and 300 μm waveguide section were cleaved and mounted on copper heat sinks for measurements. We also cleaved and mounted gain sections only, to make 400 μm long conventional Fabry Perot cavity lasers. The conventional lasers typically have 15 mA threshold current (uncoated). Typical CW light versus current of an HR coated uncooled AME-LD lasing at 1.55 μm shows threshold current of 12 mA, and external quantum efficiency in excess of 50%, by that showing minor additional losses caused by the integration of the waveguide section in the device.

In order to examine the mode expansion caused by the waveguide section of the AME-LD, the near- and far-field of the laser section only, and of the AME-LD, were measured. The far field pattern of the laser section is measured to be elliptical, with lateral Full Width at Half Maximum (FWHM) of 25°, and vertical FWHM of 45°. The measured far field of the AME-LD is almost circular symmetric, with an extremely narrow far field distribution, that is, to the best of our knowledge, the narrowest achieved out of a single laser diode. The lateral far-field FWHM angle is measured to be only 5°, and the perpendicular angle width is 7°, as can be seen in Fig. 2. The main central lobe is surrounded by weak scattering from the different interfaces of the AME-LD, but most of the energy is centered in the main lobe. The near field measurements support the far-field measurements, accounting for the limited resolution of the near field apparatus. The

lateral spot size was measured to be 4 μm, and the vertical size is 3.1 μm. The near field of the conventional device is measured to be 2.0 μm in the lateral direction, and smaller than 1 μm in the vertical direction.

Coupling efficiency to a cleaved single mode optical fiber is 42% (-3.75 dB). The alignment tolerance for butt coupling into the cleaved fiber is shown in fig. 3. The cleaved fiber was aligned for best coupling, and than translated laterally and vertically to the junction plane. The AME-LD is extremely tolerant for misalignment, both for lateral or vertical translations. Starting at the initial minimum coupling loss of −3.75 dB, the −1 dB excess loss range is as broad as ±2.6 μm vertically, and ±3.1 μm laterally. This is a significant improvement over the previously published results.[4,5].

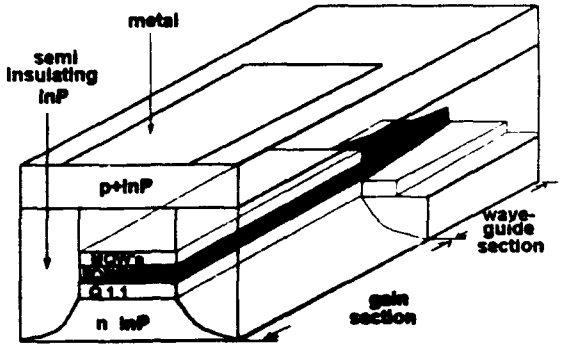

Fig. 1. Schematic description of the AME-LD laser structure

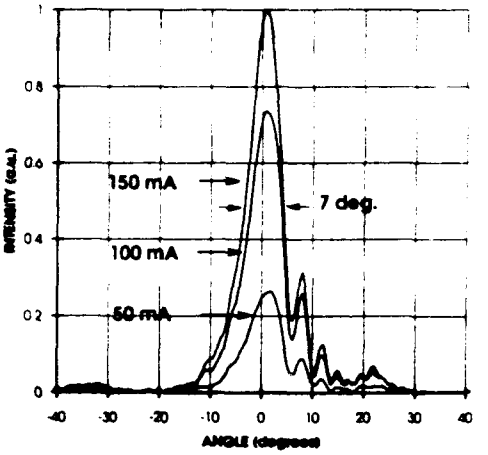

Fig. 2(a). Vertical far-field pattern of the AME-LD, with FWHM of 7°

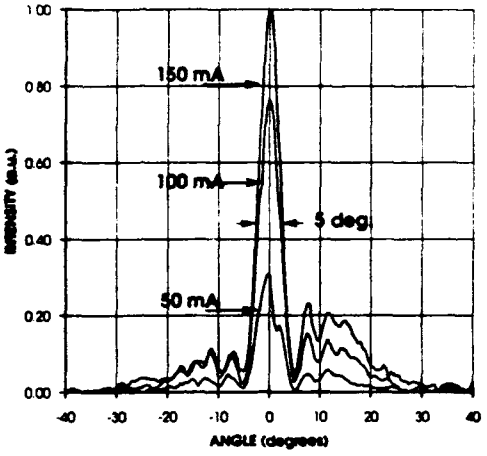

Fig. 2(b). Lateral far-field pattern of the AME-LD, with FWHM of 5°

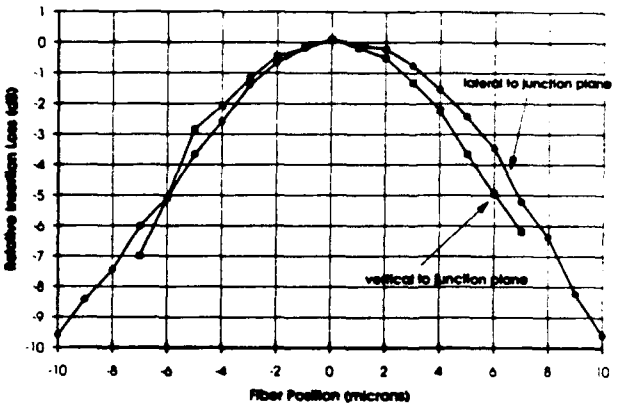

Fig. 3. Tolerance to coupling of the output of the AME-LD into a cleaved single mode optical fiber.

References

[1] Y. Shani, C. H. Henry. R. C. Kistler, K. J. Orlowsky, and D. A. Ackerman, Appl. Phys. Lett., vol. 55, pp. 2389-2391, 1989.

[2] G. Muller, B. Stegmuller, H. Westermeier, G. Wenger, Electron. Lett., vol. 27, pp. 1836-1838, 1991.

[3] R. Zengerle, H. Bruckner, H. Olzhausen, Electron. Lett. vol. 28, pp. 631-632, 1992.

[4] T. L. Koch, U. Koren, G. Eisenstein, M. G. Young, M. Oron, C. R. Giles, and B. I. Miller, IEEE Photon. Tech. Lett. vol. 2, pp. 88-90, 1990.

[5] M. Chien, U. Koren, T. L. Koch, B. I. Miller, M. Oron, M. G. Young, J. L. Demiguel, IEEE Photon. Tech. Lett. vol. 3, pp. 418-420, 1991.

[6] U. Koren, T. L. Koch, B. I. Miller, A. Shahar, paper MDD2, Tech. Dig. of the Topical Meeting on Integrated and Guided Wave Optics, Houston, 1989.

11:00am - 11:15am
W2.3

1.5 μm InGaAsP/InP large mode size laser for high coupling efficiency to cleaved single mode fibre.

I. F. Lealman, M. J. Robertson, L. J. Rivers, M. J. Harlow, S. D. Perrin and C. P. Seltzer.
BT Laboratories, Martlesham Heath, Ipswich, IP5 7RE, UK

Abstract : Increased mode size MQW BH lasers utilising a tapered active region and passive guide have shown cleaved fibre coupling losses down to 4.1 dB with threshold currents of 4.9 mA and 15 mA at 20°C and 80°C respectively.

A key factor in the price of packaged semiconductor lasers is the expensive fibre alignment stage. In order to reduce the cost, simpler fibre fixing and wider alignment tolerances are required. Increasing the spot size of a laser to increase both the coupling efficiency to cleaved fibre and fibre alignment tolerances, has already been demonstrated [1, 2]. Both of these device designs place significant constraints on the active layer thickness and consequently the performance of the device. To overcome these limitations we have developed a laser that employs a flexible twin guide structure [3], in which the active guide is tapered to allow the light to couple into an underlying passive guide. In this device the laser spot size at the output facet is determined solely by the lower passive guide structure. This allows considerable flexibility of active layer design, and devices have been fabricated both with an unstrained 16 well MQW active layer and 8 well compressively strained MQW for low threshold.

The guide structure of the device, fig 1, consists of three sections, the untapered part of the active region, the taper, and a passive region to allow the guided mode to stabilise. The length of the tapered section was calculated to provide a low loss near adiabatic mode expansion. The BH lasers were fabricated using atmospheric pressure MOVPE. The fabrication route was as for a standard BH laser except that a double mesa etch stage was used to pattern the active and passive guides. The laser output spot size, determined solely by the passive guide dimensions, was 3.8 μm wide by 2.8 μm high.

Linear and 3 section tapers with taper lengths of 60 μm, 180 μm, 400 μm and 800 μm were employed and devices cut with 300 μm long untapered active and passive sections. A comparison of the threshold current at 20 °C for unstrained 16 well and strained 8 well low threshold devices are shown in table 1. As can be seen the 8 well devices have room temperature threshold currents of less than half that of the 16 well devices. The threshold current of the 8 well devices remains low at elevated temperatures, with values of ≈ 15 mA being observed for devices with 60 μm and 180 μm tapers at 80 °C, compared to ≈ 13 mA for untapered 300 μm long devices. Farfield measurements for the 8 well strained MQW devices at 50 mA and 20 °C showed a reduction from ≈ 27° to ≈ 11° in both parallel and perpendicular directions between the untapered and tapered devices respectively, fig 2. No significant difference was observed in farfield angle as the taper length was increased, or between the linear and 3 section tapers. Coupling measurements were carried out to 10 μm core cleaved fibre and results are shown in figures 3, with a minimum coupling loss of ≈ 4.1 dB being obtained, and a positional 3dB tolerance of ± 3.6μm in both x and y directions. This compares with ± 1.5μm for a standard device with lensed fibre. No dependence on taper length or design was observed, suggesting the shorter taper lengths are adequate. These results show it is possible to fabricate a cheap fibre pigtailed device using cleaved fibre that has an output power, ex-fibre, of > 1 mW at a drive current of 40 mA or less up to 80 °C.

While these results offer a significant improvement in device performance over untapered devices, further enhancements are possible. These include further increasing the spot size of the laser to reduce the coupling loss to cleaved fibre to 1 dB or less, as demonstrated in passive mode converters [3]. This is a generic design (which does not impose constraints on the active layer

design) whose benefits are not limited to lasers, but could be used to reduce the packaging cost of a range of optoelectronic devices.

Acknowledgement: The authors acknowledge G. Sherlock for developing the software used in a number of these calculations.

References:

[1] Koch T. L. et al , *IEEE Photon. Tech. Lett.*, 1990, **2**, (2), pp. 88-90.

[2] Doussiere P. et al , *Appl. Phys. Lett.*, 1994, **64**, (5), pp. 539-541.

[3] Zengerle R. et al , *Proc. ECOC' 93*, 1993, **2**, pp. 249-251.

Device type	Taper length (μm)				
	None	60	180	400	800
Unstrained 16 well MQW	8.5	11.5	12.6	14.0	20.7
Strained 8 well MQW	4.2	4.8	4.9	5.8	7.0

Table 1. Comparison of unstrained 16 well and strained 8 well MQW laser threshold currents at 20 °C in mA vs. taper length for devices with a 300 μm long untapered active section.

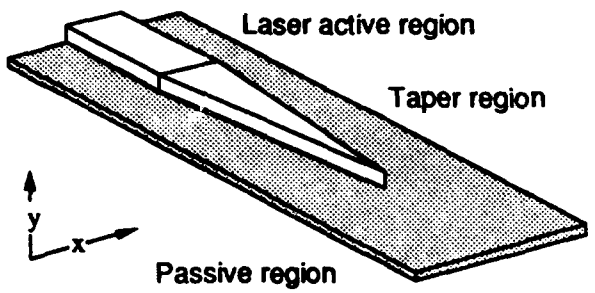

Fig 1. Schematic diagram of the two guide structure of the large spot size laser.

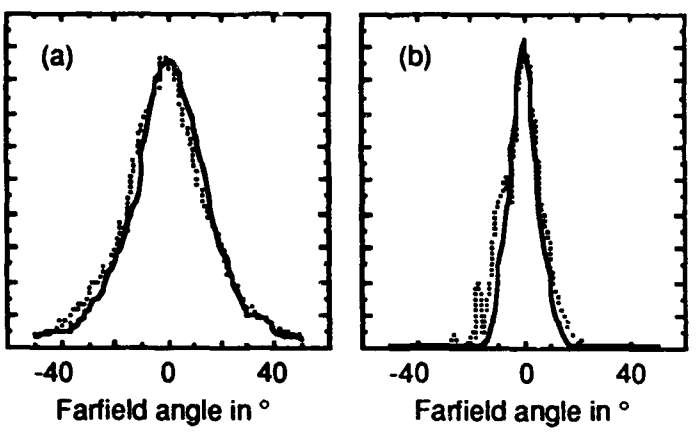

Fig 2. Farfields of an (a) untapered and (b) tapered active (180 μm taper) layer devices at 50 mA drive current and 20 °C.
——— Parallel farfield
- - - - - Perpendicular farfield

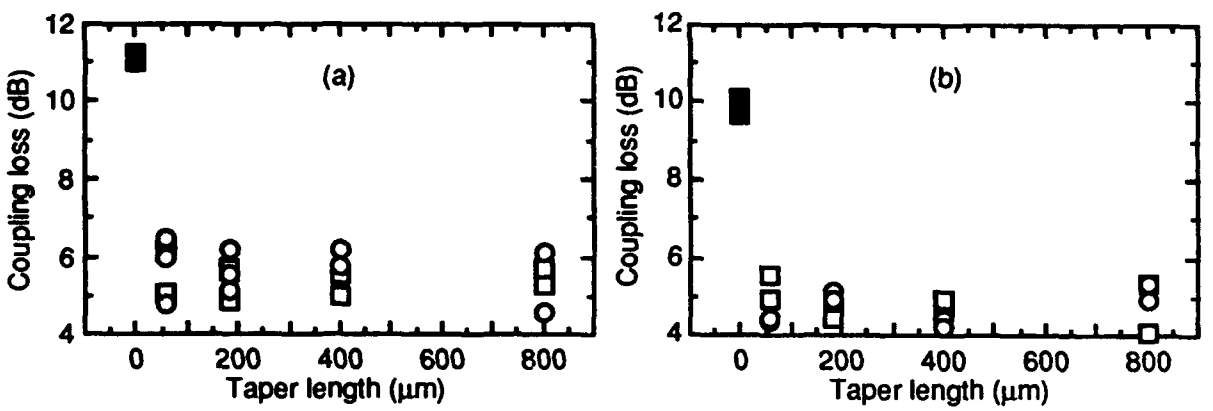

Fig 3. Coupling loss measured to 10 μm core cleaved fibre as a function of taper length measured at 50 mA drive current and 20 °C, for (a) 16 well unstrained and (b) 8 well strained MQW lasers. Where :-
■ 300 μm long untapered laser
□ Linear tapered device with 300 μm long untapered active and passive sections
○ 3 section tapered device with 300 μm long untapered active and passive sections

11:15am - 11:30am

W2.4 Narrow beam tapered thickness waveguide integrated BH MQW laser operation at high temperatures

H. Kobayashi, H. Soda, M. Ekawa, N. Okazaki, S. Ogita, and S. Yamazaki

Fujitsu Laboratories Ltd., 10-1 Morinosato-Wakamiya, Atsugi, Japan

High temperature operation of a tapered thickness waveguide BH MQW laser with a narrow beam divergence of 8° has been demonstrated by optimization of the current injection profile and BH structure.

A tapered thickness spot-size transformer integrated MQW-FP-LD[1] demonstrated a narrow beam divergence of ~10° and the low threshold current at room temperature. However, a notable increase in threshold current and Q-switching phenomena are often observed at high temperatures as shown in Fig. 1. We report on the high performance lasing characteristics of a tapered thickness waveguide laser at high temperatures which was optimized by current injection profile and BH structure.

Fig. 2 shows a schematic of the integrated BH laser. By using selective area MOVPE[2], we simultaneously grew the tapered thickness waveguide and 0.3%-compressively-strained MQW active layer. Fig. 3 shows the distribution of the measured total thickness of the MQW and guide layers from one chip. The total length of the device is 750 μm and the maximum thickness ratio was 4.2. Degradation of lasing characteristics at high temperatures are attributed to a saturable absorber in the uninjected tapered waveguide. To estimate the saturable absorber effect, we optimized the current injection by changing the electrode length from 400 μm to 550 μm. The 550 μm long electrode injects current over the entire tapered waveguide. Fig. 4 shows the electrode length dependence of the threshold current and slope efficiency at 25°C. The threshold current decrease monotonically with increasing length. On the other hand there is little reduction for slope efficiency. These experimental results indicate the saturable absorber is well compensated with the longer electrode.

Fig. 5 shows the L-I characteristics and differential efficiency for a laser with 550 μm long electrode at 25°C, 50°C and 70°C. As expected there is no significant increase in the threshold current and Q-switching operation up to 70°C. Observed lasing characteristics are comparable to those of conventional lasers. The narrowest radiation beam of 8.1° vertical and 6.4° lateral were obtained by reducing the active layer width to 1.0 μm. Even at high temperatures there was little change in the beam as shown in Fig. 6. Achieved lasing characteristics enables us to apply our lasers to laser modules which require superior performance even at high temperatures.

In conclusion, we have demonstrated high temperature operation of a narrow beam divergence tapered thickness waveguide integrated BH MQW lasers for the first time.

References

[1] H. Soda et al., Tech. Dig. IPR '94,San Francisco, USA, PD3.

[2] T. Kato et al., Tech. Dig. ECOC '91, Paris, France, paper WeB7-1.

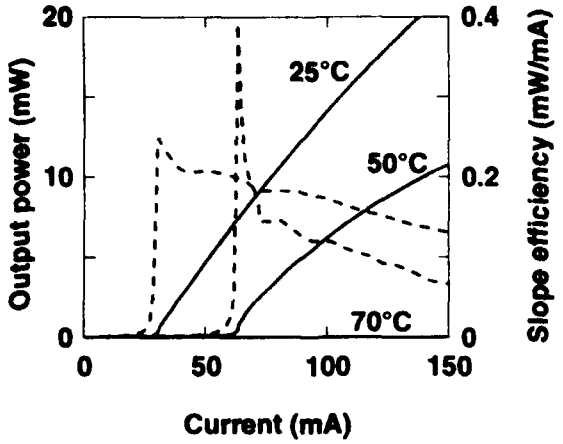

Fig. 1 Injection current dependence of output power and slope efficiency for a device with 400 μm long electrode.
Solid lines : Output power
Broken lines : Slope efficiency

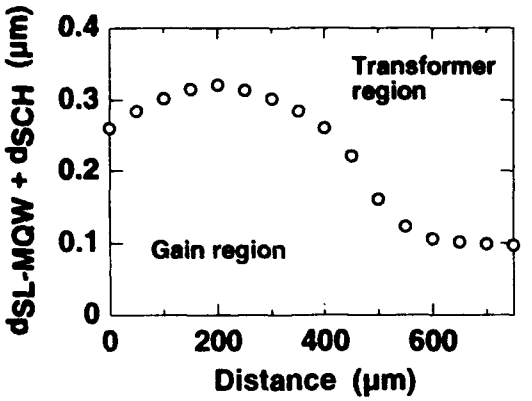

Fig. 3 Distribution of the measured total thickness of strained MQW layers and guide layers from one chip.

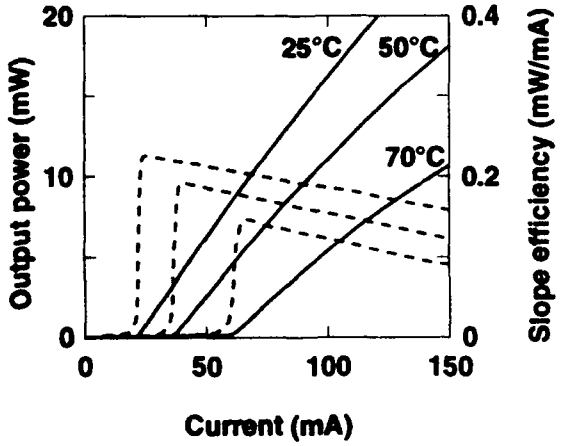

Fig. 5 Injection current dependence of output power and slope efficiency for a device with 550 μm long electrode.
Solid lines : Output power
Broken lines : Slope efficiency

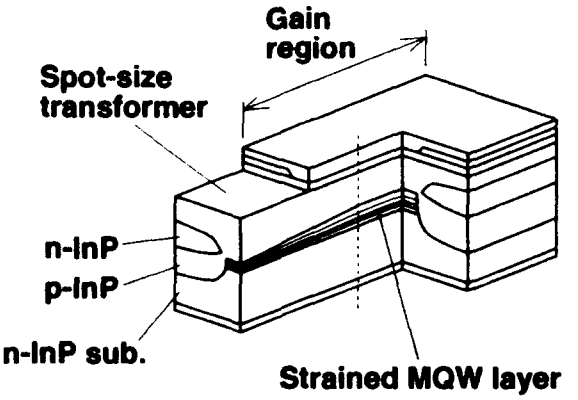

Fig. 2 A schematic of a tapered thickness BH MQW laser.

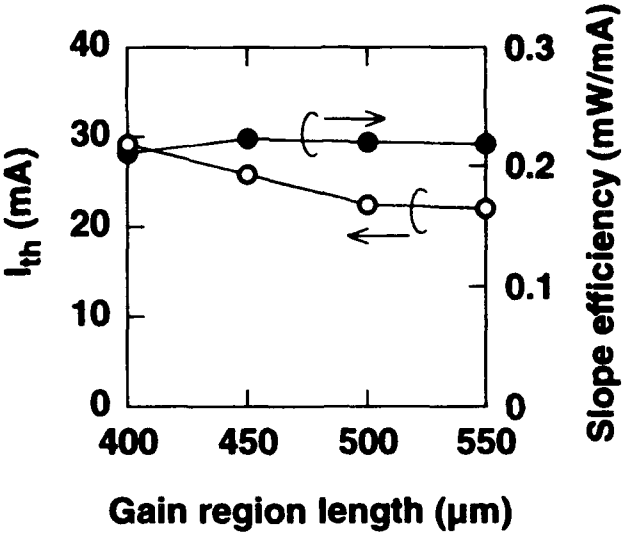

Fig. 4 Electrode length dependence of threshold current and slope efficiency.

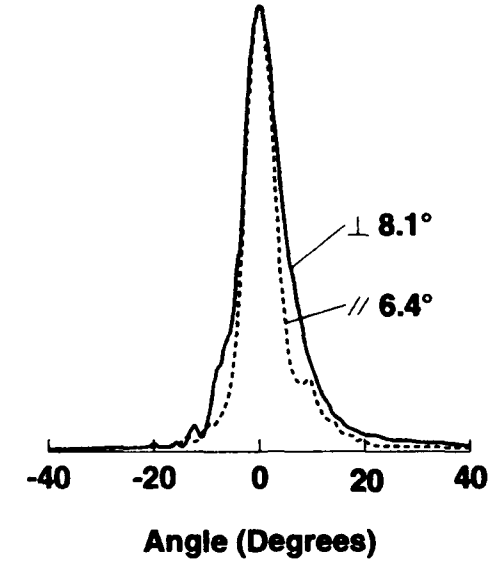

Fig. 6 Measured far-fiels from the front facet.

11:30am - 11:45am

W2.5 **Surface Emitting 1.3µm SL-QW InGaAsP/InP Ridge-Waveguide Laserdiodes with Monolithic Integrated Microlens**

B. Stegmüller, H. Westermeier and H. Hedrich

Siemens AG, Corporate R&D, Otto-Hahn-Ring 6, 81739 Munich, Germany

Abstract: 1.3µm strained-layer (SL) quantum well (QW) InGaAsP/InP ridge-waveguide (RWG) laserdiodes with a monolithic integrated microlens have been fabricated. At 25°C 27mA CW-threshold current and 10mW CW-emission perpendicular to the InP substrate are achieved using a 45° internal deflector.

Introduction: Surface emitting (SE) lasers with emission perpendicular to the substrate plane are of considerable interest for a variety of applications such as monolithic two-dimensional arrays and optical interconnects /1/. In SE laserdiodes using vertical cavity (VC) configuration high-reflectivity resonator mirrors and high-gain active regions are required for laser operation. Due to the high temperature sensitivity of the optical gain it is very difficult to achieve room temperature operation with long wavelength (1.3µm or 1.55µm) VCSEL`s /2/. In another configuration the optical cavity lies in the plane of the active layers and surface emission is obtained by deflecting the light perpendicular to the substrate plane /3/. Thereby conventional laser structures can be applied which are capable of high-temperature and high-power operation. For coupling the optical power efficiently to optical systems or fibers imaging lenses are used. The SE laserdiode configuration is very suitable for a monolithic integration of an optical lens.

In this contribution we report for the first time on 1.3µm SE-DFB-RWG laserdiodes with internal deflecting 45°-mirror and a monolithic integrated microlens.

Fabrication: The structure of the SE-DFB-RWG laserdiode is shown in Fig. 1. The undoped QW structure consists of six compressively strained (0.9%) quaternary wells (7nm thick), separated by five InGaAsP barriers (λ_{PL}=1.15µm, 10nm thick) and is sandwiched between two p- and n-doped SC layerstructures each consisting of a 35nm thick (λ_{PL}=1.15µm) and a 100nm thick (λ_{PL}=1.05µm) InGaAsP layer, respectively. The whole laserstructure was grown in two steps by low pressure MOVPE. A first order grating was formed into a quaternary (λ_{PL}=1.05µm) etch-stop layer by conventional holographic techniques. The RWG laserstructure was processed using wet chemical etching. By ion beam etching the 3.5µm deep 45° mirror trench was formed and coated by sputtering Al_2O_3. After thinning the substrate to a thickness of 70µm the microlens was fabricated by using a molten photoresist to form a spherical photoresist microlens that was then replicated into the underlying n-InP substrate by using a dry etching process /4/. The antireflection coated microlens is centered opposite to the 3µm wide ridge and the 45°-mirror. The devices were mounted episide-down on copper heatsinks with the cleaved facet positioned to the front edge of the heatsink.

Results: In Fig.2 the CW-light-current characteristic of a SE-DFB-RWG laserdiode with 290µm cavity length is shown. At 25°C the threshold current is 27mA. Due to the low lasermode reflectivity at the

microlens surface /5/ a high external efficiency of η_d=0.27W/A was obtained from the beam through the transparent substrate. From the output at the cleaved mirror facet η_d=0.1W/A was measured. With a diode current >40mA the sidemode suppression ratio (SSR) of the emission spectrum at 1308nm exceeds 40dB. The far-field distribution (Fig.3) demonstrates the effect of the microlens on the emission perpendicular to the substrate plane. The full width at half-power (FWHP) is $\Theta_{lat} = 8.8°$ and $\Theta_{tra} = 6.1°$, respectively. The corresponding values measured from the output beam at the cleaved mirror are $\Theta_{lat} = 20.5°$ and $\Theta_{tra} = 44.5°$. This difference in the far-field pattern results from the imaging effect of the microlens. An image of the cross-sectional lasermode profile at the deflecting mirror was found in a distance of 50±5μm from the front principal point microlens. Fig.4 shows the image spot profiles. From the FWHP of $w_{lat} = 10\mu m$ and $w_{tra} = 4$ respectively, a factor of magnification of about 3 can be estimated. This is also expected from the spherical microlens profile with an experimental aperture of 50μm and a sag of 8μm. As a consequence this may provide an efficient coupling of the laserlight into a singlemode fiber.

Acknowledgements: The authors gratefully acknowledge the technical assistance of B. Borchert, H. Michel and J. Rieger.

References:

/1/ K. Zürl et. al., Optical and Quantum Electronics, vol.24 (1992), pp. S405-S414.
/2/ T. Baba et. al., Jpn. J. Appl. Phys., vol. 32 (1993), pp. 1126-1127.
/3/ S. Wakabayashi et. al., Appl. Phys. Lett., vol. 61 (1992), pp. 1499-1501.
/4/ O. Wada, J. Electrochem. Soc., vol. 131 (1984), pp.2373-2380.
/5/ B. Stegmüller et. al., IEEE Photon. Technol. Lett., vol. 3 (1991), pp. 776-778.

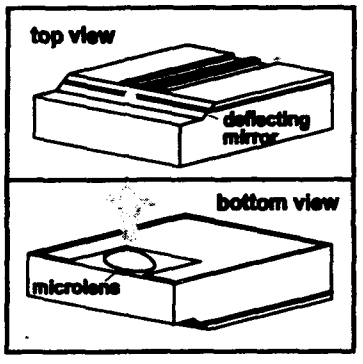

Fig.1: Structure of the SE-DFB-RWG laserdiode

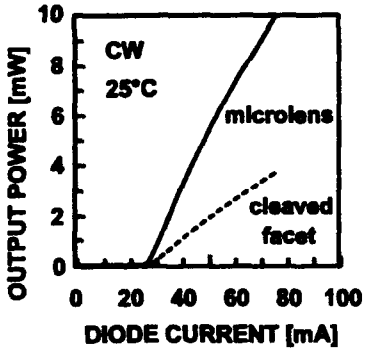

Fig.2: Light-current characteristics of a 290µm long SE-DFB-RWG laserdiode

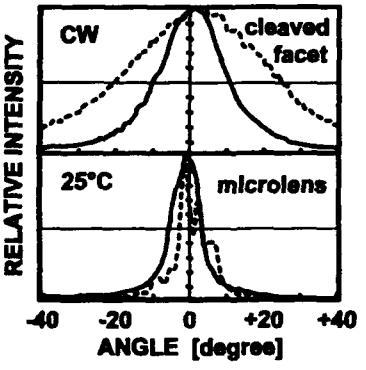

Fig.3: Far-field pattern
— lateral; -- transverse

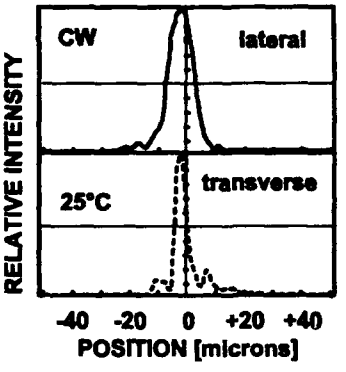

Fig.4: Image spot profiles at 50µm from microlens

11:45am - 12:00noon

W2.6

A Strained-Layer InGaAs-GaAs Buried Heterostructure Circular Ring Laser with Integrated Y-Coupled Passive Waveguide by Selective-Area Metalorganic Chemical Vapor Deposition

T.M. Cockerill, M.L. Osowski, R.M. Lammert and J.J. Coleman

Microelectronics Laboratory
Materials Research Laboratory
University of Illinois
208 N. Wright St.
Urbana, IL 61801
USA

A strained-layer InGaAs-GaAs buried heterostructure circular ring laser with an integrated Y-coupled passive waveguide is fabricated by selective-area growth. The device operates (300K cw) single mode with side mode suppression ≥ 24dB.

Ring lasers are an attractive source for optoelectronic integrated circuits due to cleave-free device operation. Most ring lasers are fabricated by etching through the active region of the device [1], leaving rough sidewalls which contribute to losses in the device due to surface recombination and optical scattering. These losses can be reduced substantially by utilizing a strained-layer buried heterostructure (BH) InGaAs-GaAs laser fabricated by selective-area MOCVD in which there are no etched surfaces and no regrowth over exposed AlGaAs [2]. These strongly index guided structures with smooth interfaces are ideal for ring laser operation.

Y-coupled waveguides have been shown to be an effective means of output coupling in semiconductor ring lasers [1]. A passive waveguide which does not significantly affect the ring laser operation is highly desirable. For most ring lasers, the waveguide section has the same active region structure as the laser and thus is not suitable as a passive waveguide. Selective-area epitaxy provides in-plane bandgap energy control in selected regions of the wafer and has been used to integrate a laser and passive waveguide [3]. Selective-area epitaxy utilizes growth inhibition of GaAs and $In_xGa_{1-x}As$ over a silicon dioxide mask for selective growth in the mask openings. This results in a growth rate enhancement which depends on the relative oxide and stripe opening widths due to the diffusion of reactants over the oxide mask into the stripe opening. For the same stripe opening, different quantum well thicknesses and hence different confined state energy levels result from different oxide widths, so the waveguide section can be made transparent to the light generated in the ring. In this talk, we present the design, fabrication and device results for strained-layer circular ring lasers with low threshold currents and good spectral characteristics.

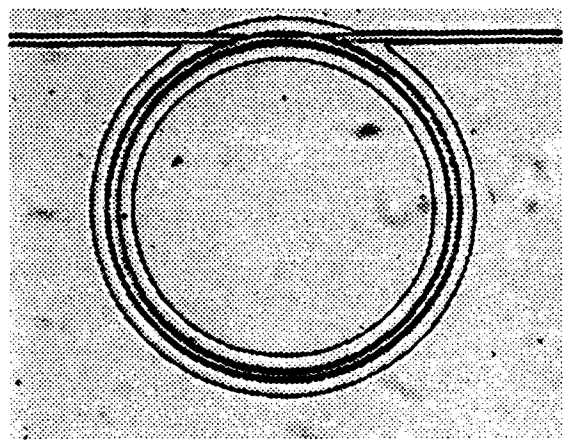

Figure 1. Top view of BH circular ring laser with integrated Y-coupled passive waveguide.

Figure 1 shows a photograph of the top view of the BH ring laser grown by selective-area MOCVD. The ring pattern consists of 14.5 μm wide twin oxide stripes separated by a 2 μm opening with a 200 μm radius. The Y-coupled passive waveguide is also 2 μm wide but has 4 μm wide twin oxide stripes. Since the oxide widths are much narrower for the waveguide section than for the ring section, the growth rate enhancement in the waveguide section is lower, resulting in a much thinner quantum well in the waveguide than in the laser. This makes the quantum well in the

waveguide transparent to the light generated in the ring laser. To isolate the contact to the ring section only, a wet etch is used to remove the highly doped GaAs contact layer except for over the ring itself. An oxide layer is then deposited and contact windows are opened only over the ring. The waveguide sections are not contacted. An antireflection (AR) coating was applied to the cleaved waveguide facets to minimize the effect of back reflections at the facet on the ring laser operation. The devices were tested both pulsed and cw for light output power versus current (L-I) and spectral properties.

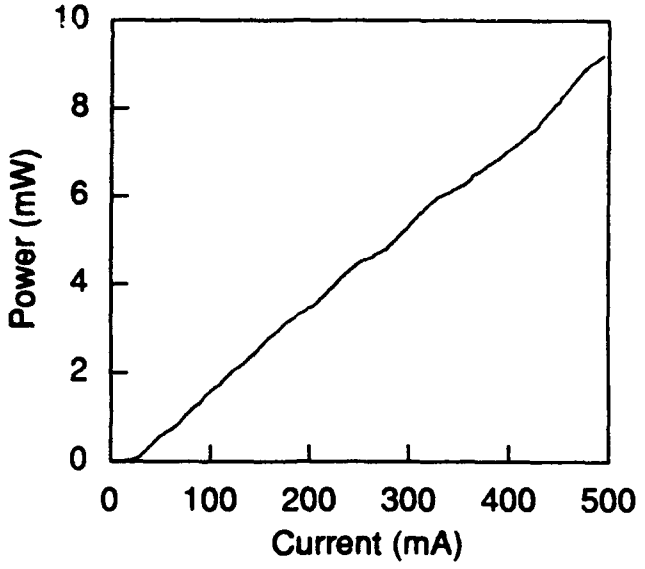

Figure 2. Light output power versus pulsed current for a BH circular ring laser with AR-coated output waveguide facets. The threshold current is 25 mA for a 200 μm ring radius.

Figure 2 is an L-I curve which shows a pulsed threshold current of 25 mA for a device with AR-coated cleaved facets. The ring lasers have a sharp turn-on and operate to relatively high powers. Threshold currents for uncoated devices are comparable to the AR-coated devices, indicating the facets have little effect on the ring laser operation. The kinks are associated with mode hops in the spectrum and are typical of semiconductor ring lasers. Figure 3 shows a single longitudinal mode spectrum for the same device operating cw at room temperature with a peak wavelength of 1.0057 μm. The side mode suppression is ≥ 24 dB.

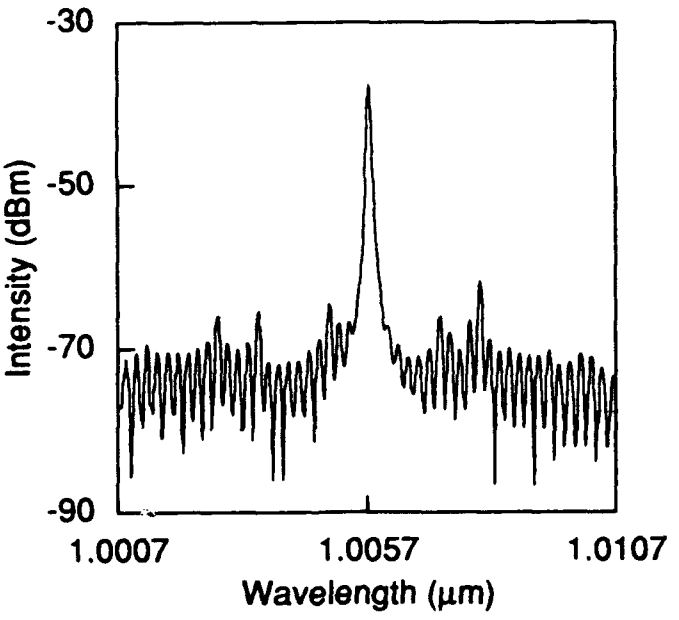

Figure 3. Single longitudinal mode spectrum for a BH circular ring laser operating cw at room temperature with a peak wavelength of 1.0057 μm. The sidemode suppression is ≥ 24 dB.

[1] J.P. Hohimer, D.C. Craft, G.R. Hadley, G.A. Vawter, and M.E. Warren, "Single-frequency continuous-wave operation of ring resonator diode lasers," *Appl. Phys. Lett.*, vol. 59, p. 3360, 1991.

[2] T.M. Cockerill, D.V. Forbes, J.A. Dantzig and J.J. Coleman, "Strained-layer InGaAs-GaAs-AlGaAs buried heterostructure quantum-well lasers by three-step selective-area metalorganic chemical vapor deposition," *IEEE J. Quantum Electron.*, vol. 30, 1994 (in press).

[3] T.M. Cockerill, D.V. Forbes, H. Han and J.J. Coleman, "Monolithic integration of a strained-layer InGaAs-GaAs-AlGaAs quantum-well laser with a passive waveguide by selective-area MOCVD," *IEEE Photon. Technol. Lett.*, vol. 4, p. 448, 1993.

High Temperature and High Power Operation of Dual Strained layer QW Visible laser diodes

A.Valster and C.J. van der Poel
Philips Optoelectronics Centre
PO Box 80000, 5600JA Eindhoven, The Netherlands

Very reliable, high performance monolithic dual visible light emitting laser diodes are described with $25\mu m$ centre to centre spacing. Record-low crosstalk of less than 3 % at T = 50^0C in the full output power range of 2-20 mW/channel is demonstrated. Crosstalk and Droop are related, both theoretically and experimentally, to lasing wavelength, output power and device geometry.

Individually addressable monolithic dual laser diodes with a lasing wavelength in the visible range are of interest for application in laser printing and high-density optical data storage. The stringent demands put on spot spacing, optical beam quality, crosstalk, droop and reliability needed for these applications can be met by employing the excellent performance of selectively buried-ridge GaInP/AlInGaP laser diodes with a disordered Strained Quantum Well active layer [1]. To separate the diodes, a groove is etched between the two stripes, thereby eliminating electrical crosstalk while minimizing thermal effects. To facilitate separate contacting, the diodes are mounted p-side up on a copper heatsink. At 25^0C, the lasing wavelength is 680 nm, the threshold current is i_{thr} = 22 mA and the external differential efficiency is $\eta = 0.4\ \frac{mW}{mA}$. The characteristic temperature, as measured between T = 25^0C and 50^0C amounts to T_0 = 165 K.

Crosstalk data as a function of output power are obtained by spatial filtering and subsequent selection of one of the two spots. An example of the data is shown in figure 1. In the figure the light output of spot "a" versus the injection current in spot "b", $P_a - i_b$, is given with spot "a" at powers ranging from 0-25 mW. The figure also displays the light-current characteristics , $P_a - i_a$, of spot "a" with spot "b" off and with spot "b" on at maximum output, respectively. The results are collected in figure 2. At a temperature of T = 50^0C record-low crosstalk of less than 3 % over an output power range of 2-20 mW is obtained.

It can be shown that the thermal crosstalk X in dual laser devices is given by

$$X \equiv \frac{\Delta P}{P_{op}} = -\frac{V R_{th}^{a-b}}{T_0} i_{thr}[1 + \frac{\eta i_{thr}}{P_{op}}],$$

where V and R_{th}^{a-b} are the operating voltage and thermal cross-resistance, respectively. The analysis shows that, given the separation geometry, a good figure of merit for crosstalk and droop in such devices is given by $\frac{i_{thr}}{T_0}$ and indicates how these parameters will depend on device geometry, centre to centre stripe spacing and laser biasing. The results stress the importance of a good single stripe index-guided laser design [2] . Also, by changing the active layer we have investigated the wavelength dependence of the device performance towards shorter wavelengths. These trends will be further discussed and compared with experimental results.

In figure 3 we demonstrate, for the first time, excellent reliability of dual diodes at T = 50^0C and at an output power of 10 mW/channel. After 4000h the dual lasers were remeasured with respect to crosstalk and droop. No differences with respect to data taken at t=0h were observed.

[1] A. Valster, C.J. van der Poel, M.N. Finke and M.J.B. Boermans, *Conference on Lasers and Electro-Optics (1992), Anaheim, Paper CMA5, Techn. Digest,p4*

[2] R.S.Geels, D.F.Welch, D.R.Scrifes, D.P.Bour, D.W.Treat and R.D. Bringans, *Electron. Letters 28 (1992), p1460.*

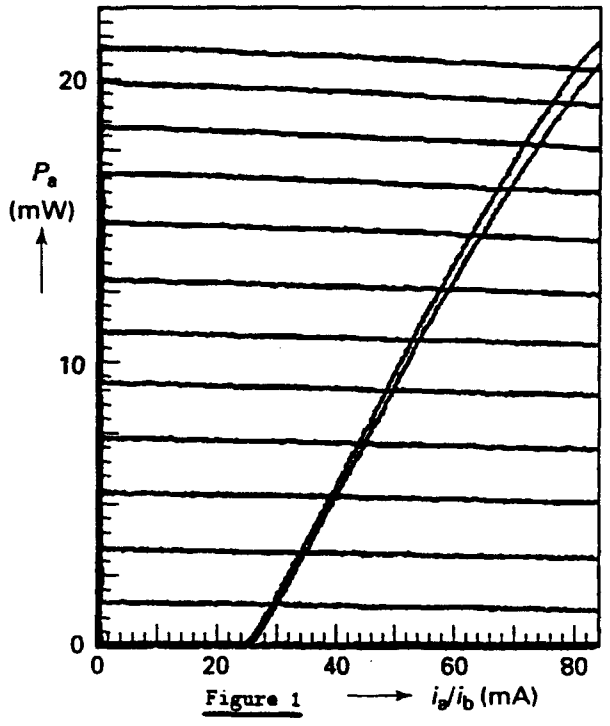

Figure 1

Spatially filtered Light-current characteristics of dual lasers at T= 50 C.

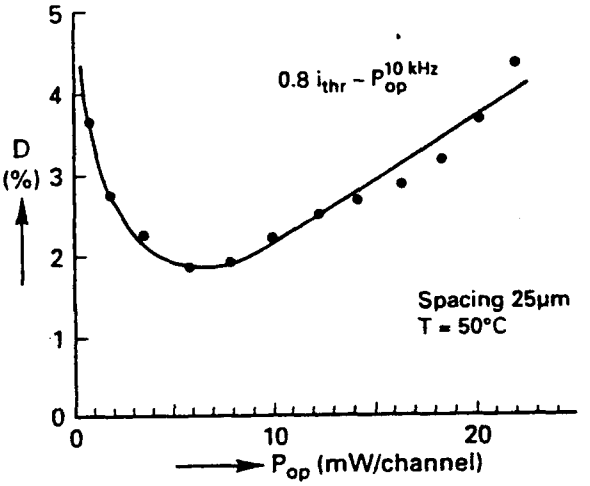

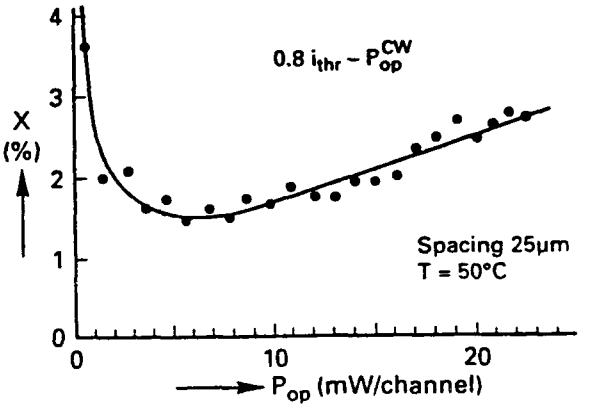

Figure 2

Droop D (10 kHz) and Crosstalk X (CW) of dual lasers at T= 50 C as function of laser output power.

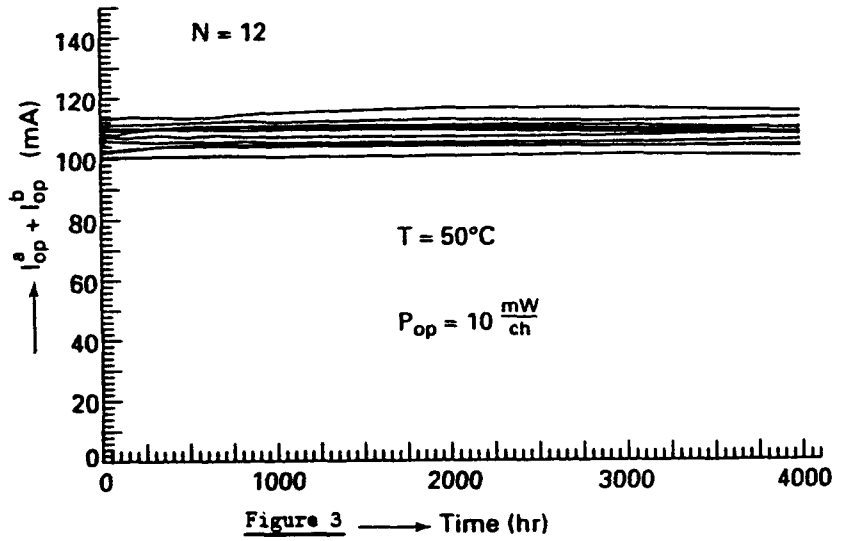

Figure 3

Lifetesting results of dual visible laser diodes at T= 50 C. Both channels are on at 10 mW/channel and the operating current is the total sum of the currents of the two separate diodes.

1:45pm - 2:00pm
W3.2

Low Voltage Carrier Injection in ZnSe-Based Blue-Green Laser Diodes on p-type GaAs substrates with InGaAlP Band Offset Reduction Layers

M. Ishikawa, Y. Nishikawa, S. Saito, M. Onomura, P. J. Parbrook
K. Nitta, J. Rennie and G. Hatakoshi

Materials and Devices Laboratory, Research and Development Center, Toshiba Corporation
1, Komukai Toshiba-cho, Saiwai-ku, Kawasaki 210, Japan

Abstract

A low voltage current injection is demonstrated theoretically and experimentally for ZnSe/CdZnSe blue-green lasers. Insertion of InGaAlP layers reduce the excess voltage drop, due to the large valence band offset between the p-type GaAs substrate and p-type ZnSe layer. The InGaAlP layers are also useful as high concentration p-type ZnSe layers can be grown on them.

A low voltage operation is indispensable for practical ZnSe-based blue-green laser diodes. Several contact techniques employing lattice mismatched contact layers for p-type ZnSe have been applied to laser structures fabricated on n-type GaAs substrates [1,2]. However, the observed excess voltage drops, due to the large Schottky- and/or hetero-barriers present, are not negligible. Recently, we have proposed a new ZnSe-based laser structure, which is fabricated on a p-type GaAs substrate with an InGaP band offset reduction layer [3]. The structure showed a significant reduction in operation voltage. In this paper, we discuss the current versus voltage characteristics of a ZnSe-based laser structure fabricated on a p-type GaAs substrate in detail. A low voltage current injection is demonstrated by using p-type InGaAlP band offset reduction layers between the p-type GaAs substrate and the p-type ZnSe cladding layer.

The InGaAlP material has an intermediate valence band depth between GaAs and ZnSe with a complete lattice matching to the GaAs substrate. Therefore, the enhancement of the hole thermionic emission current caused by the related reduction of the hetero-barrier can be expected to lower the excess voltage drop. This is similar to the use of InGaP intermediate layer between GaAs and InGaAlP [4]. Figure 1 shows theoretical calculation results of band structures and carrier distributions for the CdZnSe/ZnSe 3QW laser structures given in Fig. 2, in which Poisson's and current continuity equations were solved simultaneously with the finite difference method [5]. Hetero-spikes at the p-p iso-type interfaces are lowered and the hole depletion widths are narrowed by introducing a series of InGaAlP layers between the p-ZnSe and p-GaAs. The band offset reduction effect is enhanced by using a deeper valence band material, which, in this case, corresponds to the high Al composition InGaAlP layer, as shown in Fig. 3.

The laser structure was fabricated by a combination of MOCVD for the InGaAlP layers and MBE for the ZnSe-based II-VI layers . Experimentally measured operation voltages for p-n ZnSe/CdZnSe 3QW structures with and without an InGaP layer are also plotted in Fig. 3. The operation voltage at a current density of 0.1 A/cm^2 is reduced by 10 V by introducing the InGaP layer as predicted by the theoretical calculation. The calculated results indicate that the use of a combination of InAlP, InGaAlP and InGaP can reduce the excess voltage drop to 0.3 V even at the high injection levels required for laser operation, as shown in Fig.1 and Fig. 3.

A high concentration p-type ZnSe layer is essential to reduce the excess voltage drop at the hetero-interface as shown in Fig. 4. Figure 5 shows the net acceptor concentration profiles for p-type ZnSe layers grown on GaAs substrates with and without InGaP layers. The net acceptor concentration is higher near the interface for the layer grown on the InGaP layer than that directly grown on the GaAs substrate. The nitrogen concentration profiles determined by SIMS measurement were uniform through the layers for the both structures. This result indicates that the electrical activity of the p-type ZnSe is improved by growing on an InGaP band offset reduction layer. This improvement in the doping profile is also effective in reducing the operation voltage of the ZnSe-based blue-green laser diodes.

[1] A. Salokatve et al., Electron. Lett., Vol. 29 (1993) pp. 2192.
[2] N. Nakayama et al., Electron. Lett., Vol. 29 (1993) pp. 2194.
[3] M. Onomura et al., Electron. Lett., Vol. 29 (1993) pp. 2114.
[4] K. Itaya et al., Jpn. J. Appl. Phys., Vol. 32 (1993) pp. 1919.
[5] G. Hatakoshi et al., Trance IEICE Japan, Vol. 71 (1988) pp. 923.

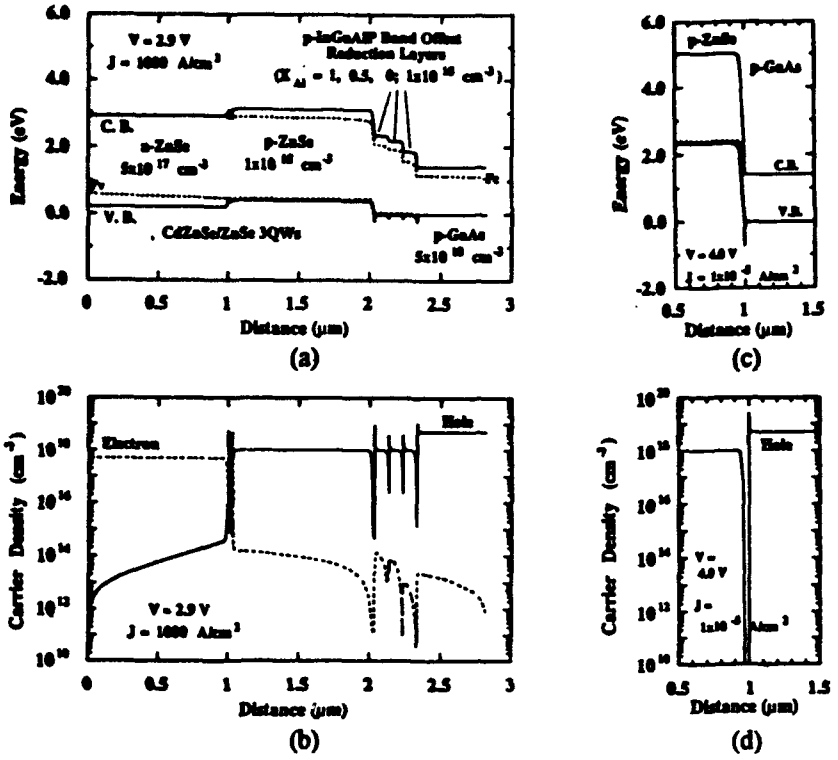

Fig. 1 Calculated band structures and carrier distributions for CdZnSe/ZnSe 3QW laser structures on p-type GaAs substrates with a series of InGaAlP band offset reduction layers (a), (b) , and without it (c), (d).

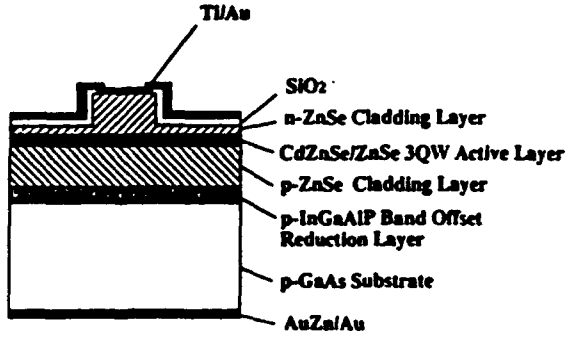

Fig. 2 Schematic structure of the CdZnSe/ZnSe 3QW structure fabricated on the p-type GaAs substrate.

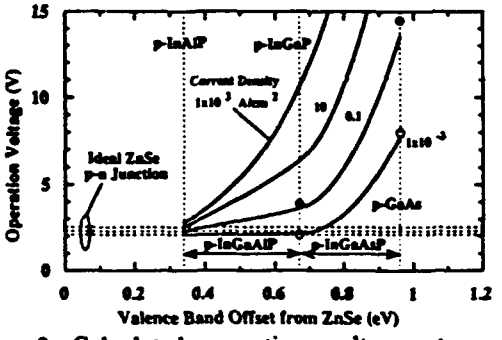

Fig. 3 Calculated operation voltage at several injection current density levels with InGaAlP and InGaAsP band offset reduction layers. Solid and open circles denote experimentally measured voltage results for p-n ZnSe/CdZnSe 3QW structure with and without an InGaP layer at current injection levels of 0.1 A/cm^2 and 1x10^{-3} A/cm^2 respectively.

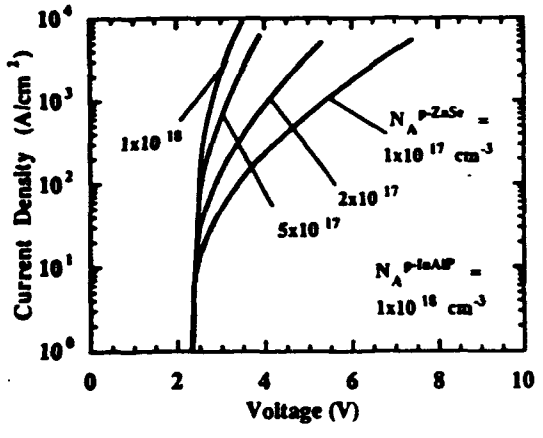

Fig. 4 Calculated current density versus voltage characteristics for several p-type ZnSe layer acceptor concentration levels.

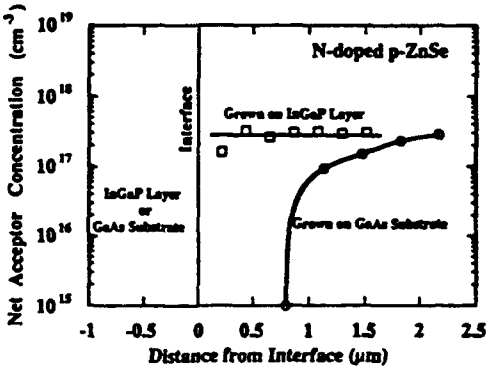

Fig. 5 Measured net acceptor concentration profiles of Nitrogen doped p-type ZnSe layers with and without an InGaP band offset reduction layer.

2:00pm - 2:15pm

W3.3 **New determination of the band structure of disordered AlGaInP and its influence on visible laser characteristics**

A.F. Phillips, A.T. Meney, A.D. Prins, J.L. Sly, E.P. O'Reilly, D.J. Dunstan and A.R. Adams
Physics Department, University of Surrey, Guildford, Surrey GU2 5XH, England
A. Valster
Philips Optoelectronic Centre, 5600 JA Eindhoven, The Netherlands

Using hydrostatic pressure, new energies for the X-minima, L-minima and band offsets in $(Al_xGa_{1-x})_{0.5}In_{0.5}P$ were obtained and correlated with temperature and pressure measurements on visible lasers using diffusion models.

The upper limit to the photon energy achievable in P and As based III-V semiconductor lasers is set by the energy of the indirect minima. Since hydrostatic pressure can increase the energy of the direct band gap until the material goes indirect, it provides an ideal tool to determine the positions of the satellite minima, the band-offsets and to probe their influence on laser characteristics. Here we report the results of high pressure measurements on the $(Al_xGa_{1-x})_{0.5}In_{0.5}P$ system and 655nm lasers and compare the results with theory.

In AlGaInP the pressure coefficients of the energy separations from the valence band maximum of the Γ, L and X minima are about 8meV/kbar, 4meV/kbar and -2meV/kbar respectively. Starting with a direct band gap alloy composition it is therefore possible to observe band crossing effects. This we have done using photoluminescence (PL) from a sample encapsulated in Helium in a diamond-anvil high pressure cell. The results taken at 2K for a 40Å unstrained GaInP well between $(Al_{0.3}Ga_{0.7})_{0.5}In_{0.5}P$ barriers are shown in figure 1. Only direct band gap luminescence is observed at 0kbar for the well and barrier giving their difference ΔE_g (with quantum confinement). The well and barrier band gaps are both observed to increase at 8.1meV/kbar. However, above 15kbar the character of the PL signal from the barrier was observed to change and to decrease in energy at -1.96meV/kbar. This is typical for the X-minima and so projecting back the curve as shown by the dotted line gives the energy of the X-valleys, E_x, to be 2.287 eV above the valence band at atmospheric pressure. The results on a series of samples, to be discussed in detail elsewhere [1], give $E_x = 2.258+0.085x$ eV (see figure 2) which is approximately 60meV lower than previously given [2]. At about 22 kbar the Γ minimum in the well also crosses with the X minima in the barrier so the separation of the X minima PL energies above this pressure is a direct measure of the valence band offset ΔE_v which in this case is 41meV, when corrected for quantum confinement. For this sample this gives a conduction band offset of 75% (see figure 3) which is larger than previously observed [2]. In a material where the L minima start closer to the Γ minimum than to the X minima, there may be an intermediate pressure range when the L minima are lowest [3], however we were unable to observe this in the present system, putting the L minima at least 125meV above the Γ minimum at atmospheric pressure.

Since pressure brings the Γ minimum in the well of a laser closer to the X minima in the barrier, as we have now accurately quantified, we can use it to study thermal loss of electrons from the active region of the device. This we have done using a laser diode consisting of an unstrained 800Å region of GaInP with cladding regions of $(Al_{0.7}Ga_{0.3})_{0.5}In_{0.5}P$ all grown in the disordered phase. Measurements were made in a copper-beryllium pressure cell with a sapphire window. The observed variation of the threshold current with pressure and temperature is shown in figure 4. As can be seen, the threshold current increases with increasing temperature and with increasing pressure and the temperature sensitivity is larger at higher pressures. This effect we have interpreted in terms of the band structure, radiative recombination and the thermal loss of carriers to the barrier regions.

The Γ-point band structure in the bulk active region was obtained using an 8-band *k.p* Hamiltonian which accounts for nonparabolicity. In this material system it is essential to include the split-off valence band due to the small spin-orbit energy. We take into account both Γ and

X minima in the cladding region using the $\Gamma - X$ energy separation obtained from figure 2. This separation is assumed to be independent of temperature. We obtain the diffusion parameters by scaling the known Γ-valley values according to the ratio of density-of-states masses, and further assume a constant diffusion length of 1μm for both minima. The X minima in the active region are experimentally determined to lie 275meV above Γ (figure 2) and are of little importance in this structure. The excess in the experimental current density over the radiative current density is taken as the leakage component. The calculated current density as a function of pressure was obtained from the bandstructure and the experimental pressure-dependence of the band gaps. The results are shown in figure 4. Although a simple theoretical model has been used, good agreement between experiment and theory is obtained.

This work is presently being extended to strained-layer quantum well lasers under the ESPRIT contract 'HIRED', and further results will be presented.

[1] A.D. Prins et al., in preparation.

[2] D.P. Bour, Chapter 9 of *Quantum Well Lasers*, ed. by P.S. Zory, Jr, (Academic Press 1993)

[3] R.J. Warburton et al.,Phys. Rev. **B43**, 4994 (1991).

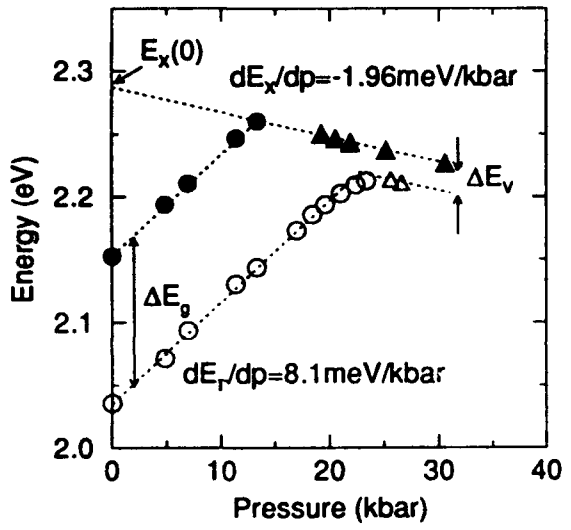

Figure 1. 2K photoluminescence transition energies of a 40Å unstrained GaInP quantum well in $(Al_{0.7}Ga_{0.3})_{0.5}In_{0.5}P$ barriers.

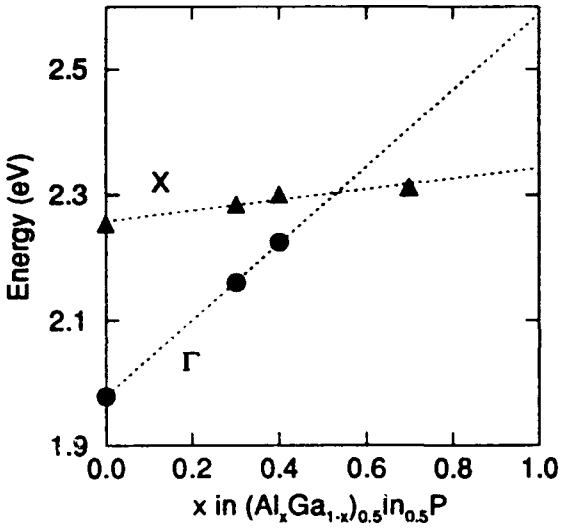

Figure 2. Composition dependence of bandgap energies for $(Al_xGa_{1-x})_{0.5}In_{0.5}P$ at 2K.

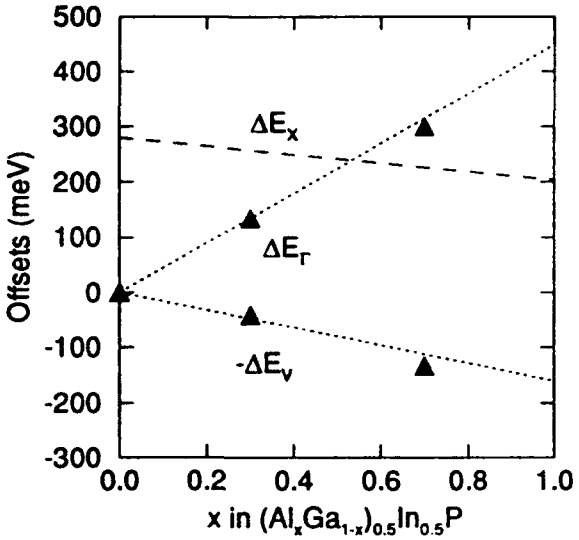

Figure 3. Composition dependence of band offsets in $Ga_{0.5}In_{0.5}P$ / $(Al_xGa_{1-x})_{0.5}In_{0.5}P$ at 2K. Dotted lines show ΔE_Γ=75%.

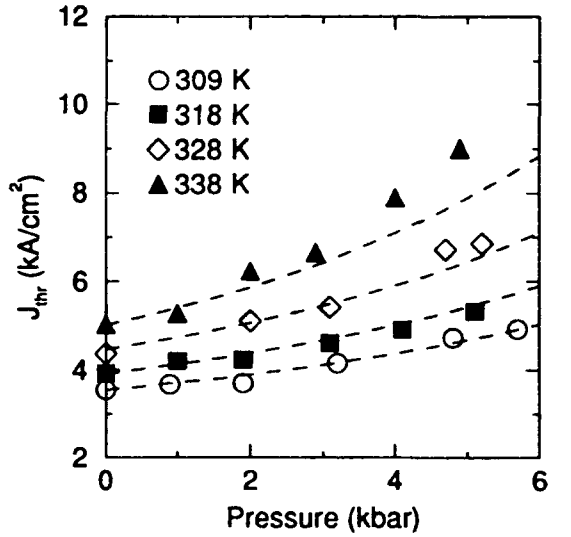

Figure 4. Temperature and pressure dependence of the threshold current density in bulk $Ga_{0.5}In_{0.5}P$ / $(Al_{0.7}Ga_{0.3})_{0.5}In_{0.5}P$ laser.

2:15pm - 2:30pm

W3.4 Uniform Hole Injection Resulting in Low Operating Current and Stable High Temperature CW Operation in 630 nm band AlGaInP Multi-Quantum Well Laser

Hitoshi Hotta, Fumito Miyasaka, Kentaro Tada and Kenichi Kobayashi
Opto-Electronics Research Laboratories, NEC Corporation
34, Miyukigaoka, Tsukuba, Ibaraki 305, Japan
Phone:+81-298-50-1151, Fax:+81-298-50-1106, E-mail:hotta@optd.cl.nec.co.jp

INTRODUCTION AlGaInP red emission lasers are anticipated as light sources for high-density optical disk systems. The laser characteristics have been improved by using MQW structures [1]. Problems associated with hole injection into MQWs have been reported for AlGaAs lasers [2] and InGaAsP lasers [3-5]. However, they have not been investigated for AlGaInP lasers. In this paper, we report the influence of distributing the injected holes uniformly for AlGaInP MQW lasers. This uniform distribution reduced the operating current, thereby allowing 630 nm band lasers to operate stably at 60°C, for the first time.

LASER STRUCTURE AND CRYSTAL GROWTH The device structure is shown in Fig. 1. Two different laser structures were applied with regard to stripe width W. One had a 50 μm mesa stripe and the other a 5 μm mesa stripe. Crystal layers were grown by MOVPE on (115)A GaAs substrates.

INFLUENCE OF HOLE INJECTION External differential quantum efficiencies η_d and threshold current densities J_{th} were examined as a function of the barrier height, the number of wells, and the barrier width, as shown in Figs. 2, 3 and 4, respectively. The efficiencies η_d decreased and the currents J_{th} increased with increases in the barrier height, the number of wells, or the barrier width. The reason was considered as follows.

With high or wide barriers, it is thought that hole transport time between wells increased, causing hole localization at the well near the p-cladding layer [3]. With a large number of wells, the hole localization was enhanced. This localization resulted in the current J_{th} increase because the wells near the n-cladding layer caused optical loss due to the smaller carrier concentration. The decrease in efficiency η_d was attributed to the spontaneous emission increase caused by the higher density of localized holes at the well near the p-cladding layer [5].

INDEX-GUIDED LASERS WITH UNIFORM HOLE INJECTION Index-guided lasers with optimized MQW structure, i.e. three tensile strained QWs which have barriers with an Al composion of 0.5 and a width of 4 nm, were examined under cw condition. As shown in Fig. 5, the threshold current at 25°C and the maximum cw temperature were 38 mA and 90°C, respectively. The lasing wavelength was 639 nm. These lasers operated stably for over 2,500 hours at 60°C as well as at 50°C, as shown in Fig. 6. The estimated MTTF was over 10,000 hours at 50°C, 5mW. These long lifetimes were due to low operating currents, which resulted from the uniform hole injection.

CONCLUSION The influence of hole injection was investigated for AlGaInP MQW lasers. By improving the unifromity of the hole injection, low operating currents were obtained for 630 nm band AlGaInP MQW lasers, with stable operation at 60°C, for the first time.

ACKNOWLEDGMENTS We would like to thank Kohroh Kobayashi and Ikuo Mito for their encouragement, and Masayasu Ueno and Hiroyuki Yamazaki for their useful discussions. We would also like to thank Kunihiro Hara for technical support.

REFERENCES

[1] A. Valster et al., Proc. 13th IEEE Int. Semiconductor Laser Conf., (1992) G-1.
[2] W. T. Tsang, Appl. Phys. Lett. **39** (1981) 786.
[3] N. Tessler and G. Eisenstein, Appl. Phys. Lett. **62** (1993) 10.
[4] Y. Sasaki et al., Extended Abstracts of The 40th Spring Meeting of The Japan Society of Applied Physics

and Related Societies (1993) 31a-C-5.
[5] H. Yamazaki et al., Extended Abstracts of The 54th Autumn Meeting of The Japan Society of Applied Physics (1993) 28p-H-7.

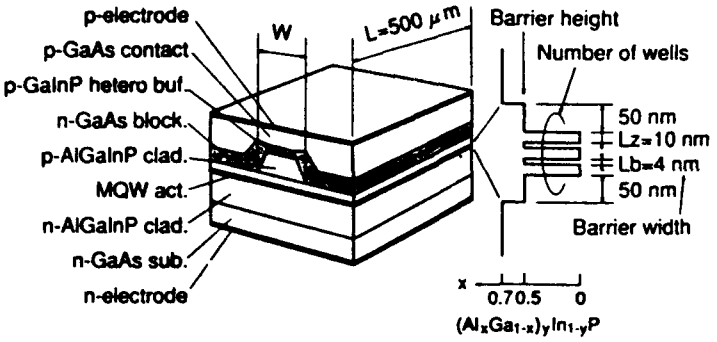

Fig. 1 Laser structure.

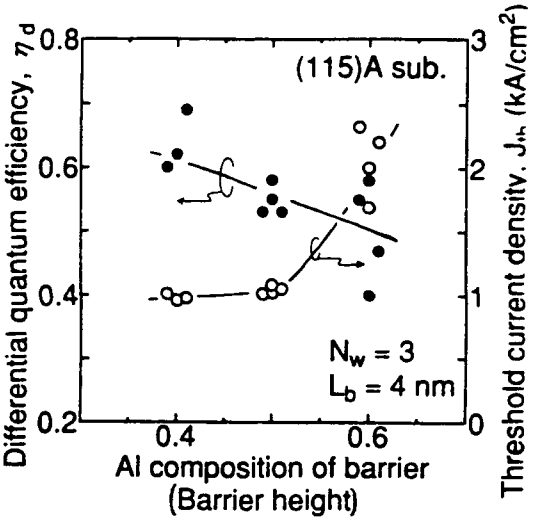

Fig. 2 Efficiency and threshold current as a function of barrier height for tensile strained QWs (10 nm thick).

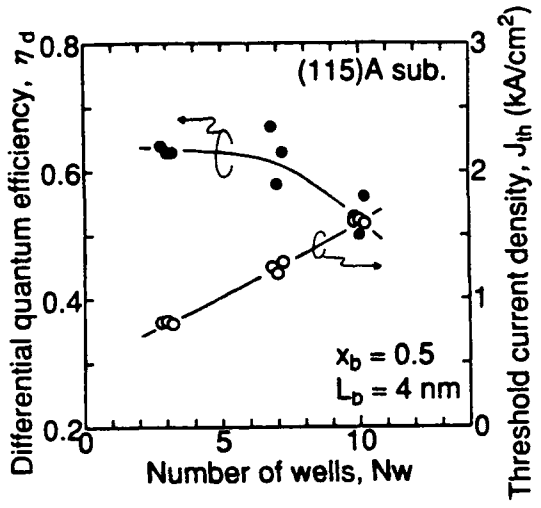

Fig. 3 Efficiency and threshold current as a function of the number of wells for non-strained QWs (6 nm thick).

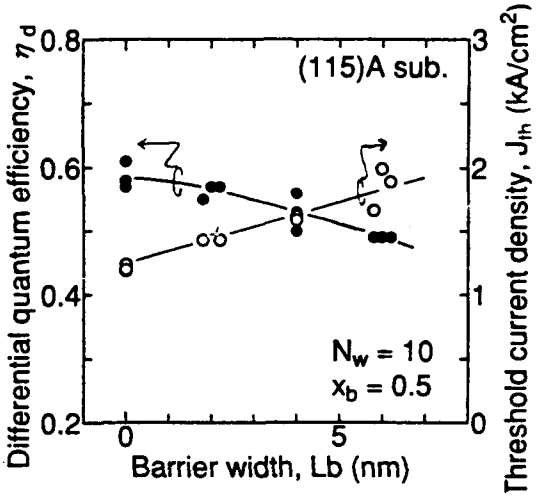

Fig. 4 Efficiency and threhold current as a function of barrier width for non-strained QWs (6 nm thick).

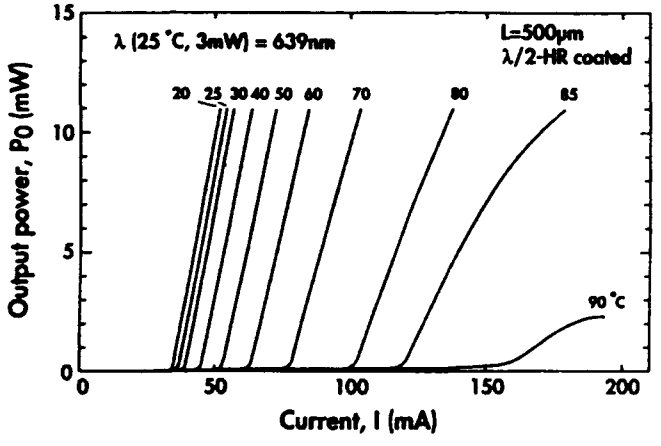

Fig. 5 Current-Light output characteristics of three tensile strained QWs (10 nm thick).

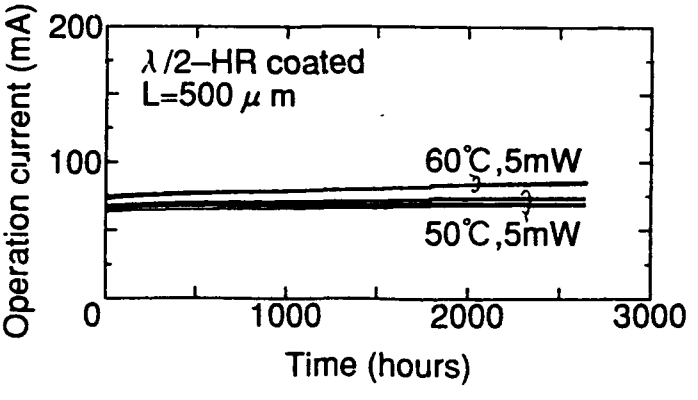

Fig. 6 Operation current transition of 630 nm lasers.

2:30pm - 2:45pm
W3.5

Strain-compensated Multiple Quantum Well 630-nm-band AlGaInP Laser Diodes

R. Hiroyama, Y. Bessho, H. Kase, T. Ikegami, S. Honda, M. Shono, K. Yodoshi, T. Yamaguchi and T. Niina

SANYO Electric Co., Ltd. Microelectronics Research Center
1-18-13 Hashiridani, Hirakata, Osaka 573, Japan

1) Abstract

Strain-compensated multiple quantum well 630-nm-band AlGaInP laser diodes were investigated for the first time. The lowest threshold current of 33mA and the highest maximum operating temperature of 90°C were achieved.

2) Summary

Recently, a low threshold 630-nm-band AlGaInP laser diode was developed by using a tensile strained single quantum well structure [1] [2]. However, there have been no reports of 630-nm-band laser diodes with both a low threshold current and a high maximum operating temperature. A multiple quantum well (MQW) structure is effective for obtaining good temperature characteristics. To realize a low threshold 630-nm-band laser diode with high maximum operating temperature, it is necessary to reduce the threshold current of the laser diode with an MQW active layer.

The strain-compensated MQW active layer with a compressively strained quantum barrier and a tensile strained quantum well offers some advantages for reducing the threshold current of MQW laser diodes. First, a larger tensile strain can be introduced into the quantum well because the amount of strain in the active layer is decreased. Furthermore, the holes are injected more uniformly to the quantum well because of the large diffusion velocity of holes due to the compressive strain in the quantum barrier. In this study, we fabricated 630-nm-band AlGaInP laser diodes with a strain-compensated structure in the active layer for the first time, and we realized 630-nm-band AlGaInP laser diodes with a low threshold current and a high maximum operating temperature.

The device structure is a buried ridge stripe structure. Epitaxial growth was carried out by a low-pressure MOCVD method on 9° misoriented substrates. The stripe width is 5 μm, the p-cladding layer under the blocking layer is 0.3 μm, and the cavity length is 350μm. The active layer consists of compressively strained AlGaInP quantum barriers (+0.3%) and tensile strained GaInP quantum wells. An MQB [3] is introduced in the p-cladding layer to suppress the carrier overflow.

Figure 1 shows the relationship between the tensile strain in the quantum well and the threshold current in the case of a strain-compensated MQW active layer, and in the case of a strain-uncompensated MQW active layer. In the case of the strain-compensated MQW active layer, the threshold current decreases up to the tensile strain of -1.1% ,while in the case of the strain-uncompensated MQW active layer, it decreases up to the tensile strain of -0.5%. Figure 2 shows the temperature dependence of the current-light output power (I-L curves) of the laser diodes with a strain-compensated MQW (well: -1.1%, barrier: +0.3%) active layer oscillating at 636 nm. The threshold current is 33 mA at 25°C and light output power of 3 mW is obtained up to 90°C. This threshold current is the lowest value of the 630-nm-band MQW laser diodes, to our knowledge. Figure 3 shows a life-test for laser diodes with 30%-30% facet coatings under 5 mW at 50°C. These devices have been operating reliably for more than 1200 hours.

In conclusion, we fabricated 630-nm-band AlGaInP laser diodes with a strain-compensated structure containing a compressively strained quantum barrier and a tensile

strained quantum well in the active layer for the first time. The threshold current at 25°C was 33 mA. Light output power of 3 mW was obtained up to 90°C. The laser diodes have been operating more than 1200 hours under 5 mW at 50°C without significant degradation.

References

[1] R. S. Geels et al.: 13th IEEE Int. Semiconductor Laser Conf., Takamatsu, paper no.G-3, pp.156-157, 1992
[2] T. Tanaka et al.: Electron. Lett., 29, pp.606-607, 1993
[3] K. Iga et al.: Electron. Lett., 22, pp.1008-1010, 1986

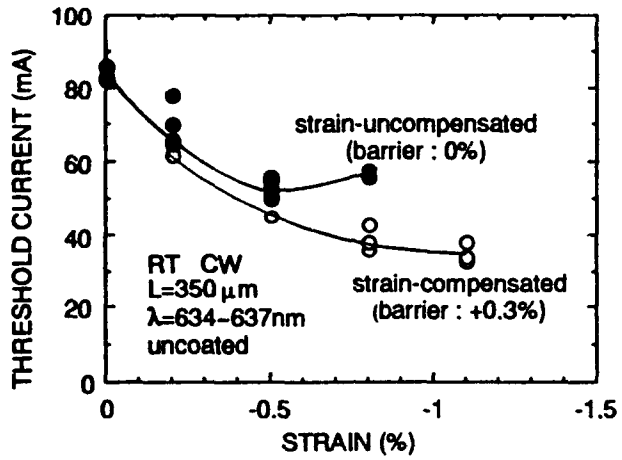

Figure 1 Relationship between the tensile strain and the threshold current

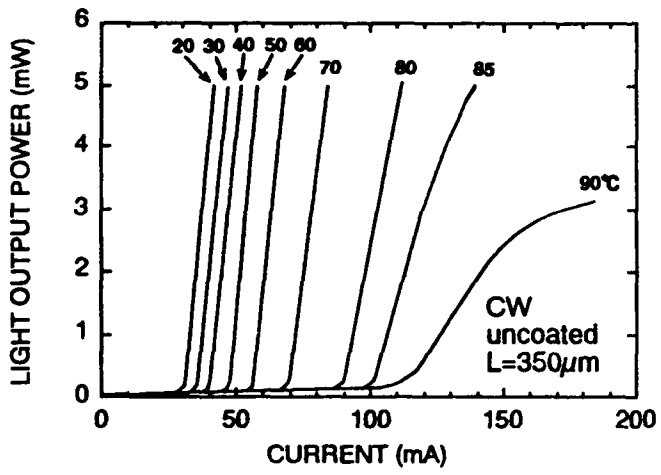

Figure 2 Temperature dependence of the I-L curves

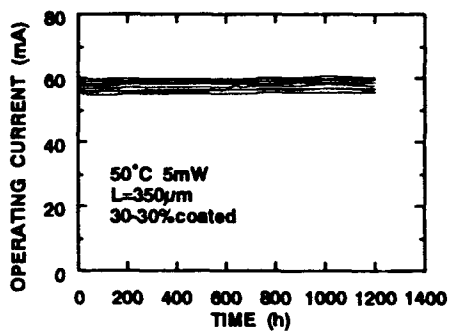

Figure 3 Life-test

2:45pm - 3:00pm
W3.6

Study of Strained Multiquantum Well AlGaInP Visible Lasers Using GaInAsP Well Layers

A. Furuya, C. Anayama, M. Kondo, Y. Kito, M. Sugano, H. Sudo, K. Domen, and T. Tanahashi

Fujitsu Laboratories Ltd.

10-1 Morinosato -Wakamiya, Atsugi 243-01, Japan

Using GaInAsP wells, we studied independently the effect of well thickness, oscillation wavelength and strain on the threshold current and its characteristic temperature of AlGaInP strained multiquantum well lasers. We obtained good characteristic temperature of 179K(15°C-50°C) and 120K(60°C-90°C) in optimized laser.

MO-disk memories require high-temperature and high-power operations of AlGaInP lasers. Use of a compressively strained GaInP multiquantum well (MQW) active layer has improved the temperature characteristics of AlGaInP visible lasers. The temperature characteristics depend on the well thickness, oscillation wavelength, and strain. Since these three factors are interdependent in the GaInP strained quantum well, the way to optimize the strained MQW is complicated. Introduction of quaternary material as the strained quantum well makes it possible to set these factors independently by changing the quaternary content[1]. In this work, we used strained GaInAsP quantum well to study independently the effects of those factors on the threshold current (I_{th}) and its characteristic temperature(T_o), and obtained good characteristic temperature of 179K(15°C-50°C) and 120K(60°C-90°C) in the optimized laser.

We used the self-aligned stepped substrate (S^3) laser [2]. The cavity was 700μm long. The front facet was anti-reflectively (7% - 13%) coated and the rear facet was high-reflectively (95%) coated. These experimental parameters were suitable for practical high power lasers. First, we examined the well thickness dependence (Fig. 1). To maintain almost constant optical confinement of 3.2%, we kept the total thickness of wells in this examination. And we maintained the strain and the oscillation wavelength to be 0.67% and 674 nm, respectively. We evaluated T_o between 15°C and 50°C, and plotted I_{th} at 27°C. As the well thickness decreased, T_o increased. I_{th} at 8.1 nm and that at 5.4 nm were almost the same, however, that at 4.1 nm was larger than these. These are due to the increase of density of states in quantum well with the decrease of well thickness. To obtain low I_{th} and high T_o, the well thickness of around 6nm was preferable. Next, we examined the oscillation wavelength dependence (Fig. 2). We maintained the well thickness and the strain to be 6nm and 0.73%, respectively. The As mole content of the well in the sample of 672 nm was zero, that is, well is GaInP. As the wavelength increased, T_o increased and I_{th} decreased monotonically. However, they began to saturate at wavelengths above 680 nm. This suggests that the carrier overflow is almost suppressed at wavelengths above 680 nm. Then, we examined the strain dependence (Fig. 3). We maintained the well thickness and the oscillation wavelength to be 6nm and around 690 nm, respectively. As the strain increased, T_o increased, and I_{th} decreased. This result shows the increase of strain still affects the characteristics when the well thickness is optimized and the oscillation wavelength is long enough to suppress the carrier overflow. In comparison with the effects of the three factors, the effect of the well thickness on the temperature characteristics was relatively large in our experiments. For high T_o and low I_{th} of the laser, the well thickness of around 6nm, the oscillation wavelength above 680 nm, and the high strain are important.

Fig. 4 shows the temperature dependence of light-current characteristics and threshold current for the optimized laser with the well thickness of 6nm, the oscillation wavelength of 688 nm, and the strain of 1.08%. The laser oscillated even at 110°C, and high characteristic temperature of 179K (15°C - 50°C) and 120K (60°C - 90°C) was obtained.

In summary, we used GaInAsP strained MQW to study independently the effect of the well thickness, the oscillation wavelength, and the strain on threshold current and its characteristic temperature. The well thickness of around 6nm, the oscillation wavelength above 680 nm, and the high strain are important for good characteristics. The optimized laser showed high characteristic temperature of 179K (15°C - 50°C) and 120K (60°C - 90°C).

References
[1] C. Anayama et. al.. Extended Abstract of the 1993 International Conference on Solid State Device and Materials, 1993, p.769
[2] C. Anayama et. al.. Appl. Phys. Lett., vol. 63, no. 13, pp. 1736-1738, 1993

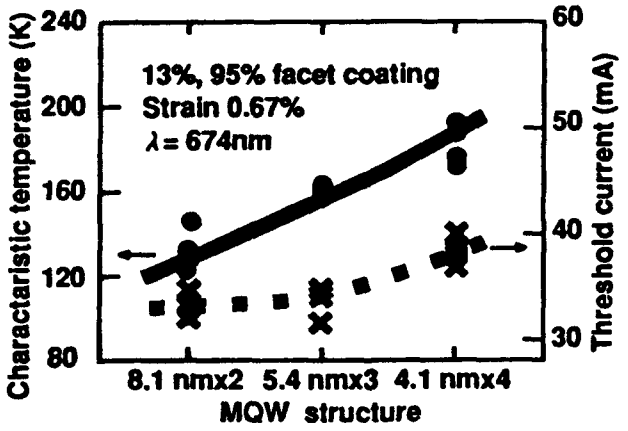

Fig. 1 Dependence of characteristic temperature and threshold current on well thickness. Strain and oscillation wavelength are 0.67% and 674 nm, respectively.

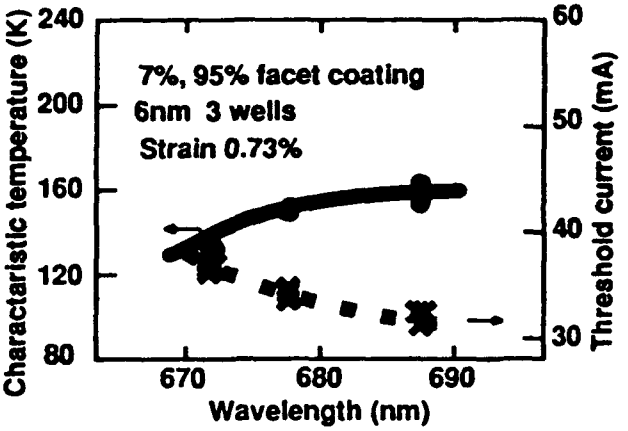

Fig. 2 Dependence of characteristic temperature and threshold current on oscillation wavelength. Strain and well thickness are 0.73% and 6 nm, respectively.

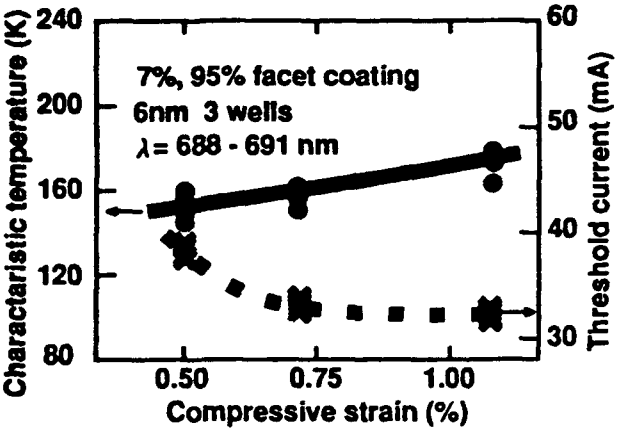

Fig. 3 Dependence of characteristic temperature and threshold current on strain. Well thickness and oscillation wavelength are 6nm and around 690 nm, respectively.

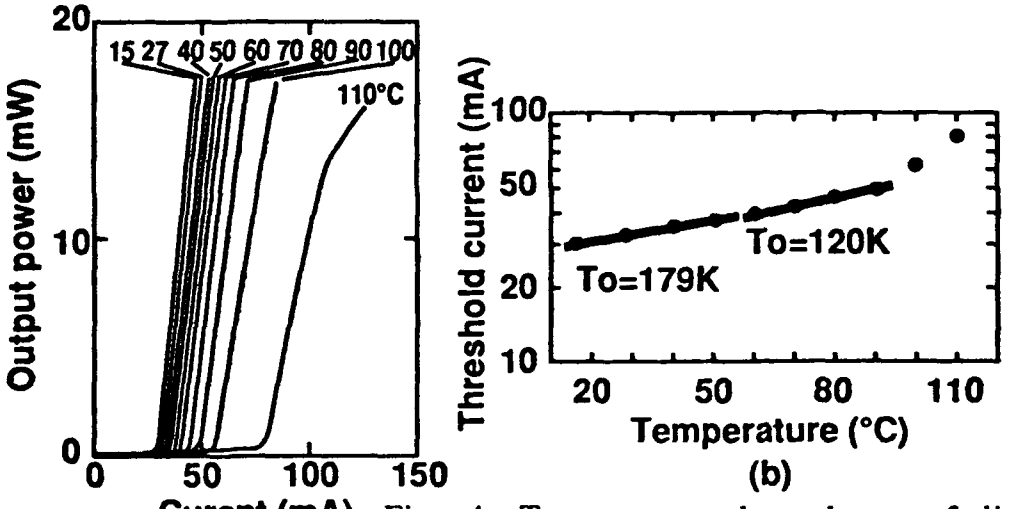

Fig. 4. Temperature dependence of light-current characteristics (a) and threshold current (b) for optimized laser.

Thursday
September 22, 1994

SESSION Th1
High-Speed Lasers I

SESSION Th2
High Speed Lasers II

SESSION Th3
New Structures and Characterization Approaches

SESSION Th4
High Power Edge and Surface Emitting Lasers

8:30am - 8:45am

Th1.1

Low-Bias-Current Direct Modulation up to 33 GHz in GaAs-Based Pseudomorphic MQW Ridge-Waveguide Lasers Suitable for Monolithic Integration

J.D. Ralston, K. Eisele, R.E. Sah, E.C. Larkins, S. Weisser, J. Rosenzweig, J. Fleissner, and K. Bender
Fraunhofer-Institut für Angewandte Festkörperphysik, Tullastrasse 72, D-79108 Freiburg, Germany

The successful application of direct laser modulation for very-high-speed digital transmission or microwave/millimeter-wave analog optical links requires a) reductions in the drive currents required to achieve high modulation bandwidths, b) increases in the maximum intrinsic modulation bandwidths, c) reductions in laser chirp under high-speed direct modulation, and d) high-speed laser structures which can be monolithically integrated with high-speed transistors. Due to the maturity of GaAs transistor and circuit fabrication technologies, we have pursued the development of GaAs-based MQW lasers which address all of the above requirements. By adding both p-doping and strained $In_{0.35}Ga_{0.65}As$/GaAs MQW's in the laser active region, we have previously demonstrated both very efficient high-speed modulation (20 GHz at a DC bias current of 50 mA) and the first semiconductor lasers to achieve a direct modulation bandwidth of 30 GHz (114 mA DC bias) [1]. In addition, the above devices show a factor of 2 reduction in the linewidth enhancement factor, α, compared with that of unstrained, undoped GaAs/AlGaAs MQW lasers [2].

More recently, we have investigated several additional modifications, both in the epitaxial growth sequence and in the device geometry, in order to further enhance the direct modulation characteristics and to further simplify the monolithic integration of GaAs-based MQW lasers. Extensive investigations have been carried out in order to clarify the relaxation limits and factors influencing defect generation and redistribution in MBE-grown pseudomorphic $In_yGa_{1-y}As$/GaAs MQW structures for laser active regions. Substantial improvements have been achieved by lowering the growth temperature of the high-Al-mole-fraction cladding layers. These cladding layers were implemented using GaAs/AlAs binary short-period-superlattices (instead of ternary $Al_xGa_{1-x}As$ layers) in order to reduce unintentional impurity incorporation. Lasers containing 4 undoped $In_{0.35}Ga_{0.65}As$/GaAs QW's in the active region show decreases in threshold current densities by more than a factor of 2, and an increase in internal quantum efficiency from 60% to 70% due to the lower temperature growth. We have also developed a Cl_2 + BCl_3 chemically-assisted ion-beam etching (CAIBE) process for dry-etching of the laser mirrors. This 2-component process relaxes several constraints previously reported in the dry-etching of $Al_xGa_{1-x}As$-containing optoelectronic device structures, is ideally suited for monolithic laser/transistor integration, and facilitates the reproducible fabrication of short-cavity lasers.

Utilizing a single epitaxial growth (HEMT + laser) and an air-bridged, coplanar electrode geometry (Fig. 1), a complete technological process has also been developed in our labs for the monolithic integration of vertically-compact [1] GaAs MQW ridge-waveguide (RWG) lasers with double pulse-doped GaAs/AlGaAs QW enhancement/ depletion HEMT electronics. Fully functional laser/driver chips have been fabricated and tested at data transmission rates up to 7.5 Gbit/s [3], limited by the bit-pattern generator. Substantial reductions in the drive currents required for high-speed modulation have been achieved by combining low-temperature MBE growth and CAIBE-etched short-cavity RWG structures in a 3-mesa coplanar-electrode geometry (Fig. 2). Fig. 3 shows the direct modulation response, at various bias currents, of a 3x100 μm^2 RWG laser containing 4 undoped $In_{0.35}Ga_{0.65}As$/GaAs QWs in the active region

(uncoated facets, I_{th}=6 mA). These devices demonstrate unprecedented high-speed performance, attaining a 3dB direct modulation bandwidth of 24 GHz at a dc bias of only 25 mA and a single facet output power of 5 mW. Higher frequency operation can be achieved in devices with p-doped active regions, due to the enhanced differential gain and reduced damping [1], as well as reduced carrier re-emission from the QWs [4]. As shown in Fig. 4, a 3dB bandwidth of 33 GHz at a dc bias of only 65 mA (P_o = 9 mW) has been achieved for a dry-etched 3x100 μm^2 RWG device containing 4 p-doped $In_{0.35}Ga_{0.65}As$/GaAs QWs in the active region (uncoated facets, I_{th}=13 mA). Both the undoped and p-doped lasers demonstrate modulation current efficiency factors (MCEF) of 5 GHz/$\sqrt{mA}$, matching the best reported results for a QW laser [5]. A key advantage of our MQW design is the absence of gain saturation in the above 3x100 μm^2 ridge lasers.

This work was supported by the Bundesministerium für Forschung und Technologie.

[1] J.D. Ralston et al, *IEEE J. Quantum Electron.*, **29**, 1648-1659, 1993.
[2] A. Schönfelder et al, *Electron. Lett.* **29**, 1685-1686, 1994.
[3] J. Hornung et al, *Electron. Lett.* **29**, 1694-1696, 1993.
[4] S. Weisser et al, 1993 *IEDM Technical Digest*, 601-604.
[5] T.R. Chen et al, *Electron. Lett.* **29**, 1525-1527, 1993

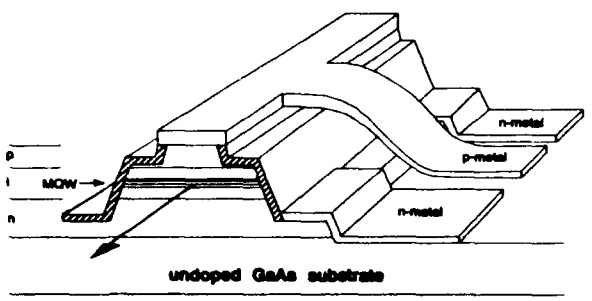

Fig. 1 MQW RWG laser layout with air-bridged coplanar electrodes for monolithic integration.

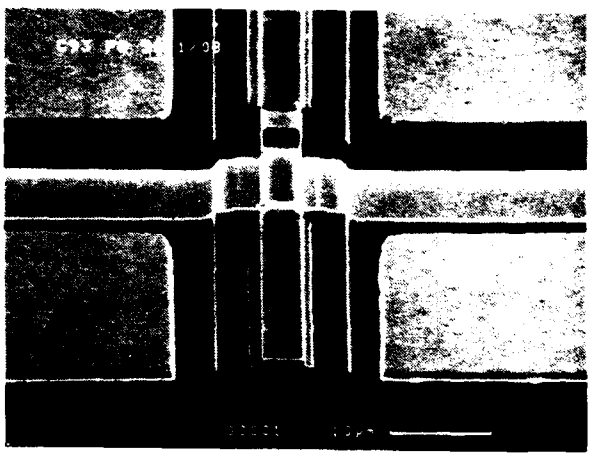

Fig. 2 High-speed MQW RWG laser with 3-mesa coplanar electrodes and dry-etched mirror.

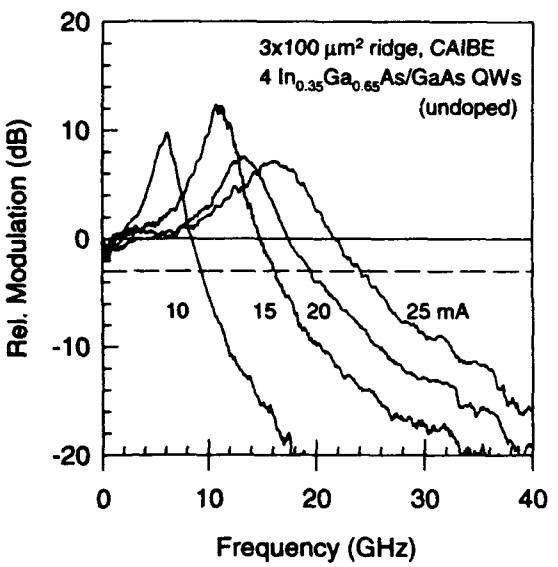

Fig. 3 Modulation response of low growth-temperature $In_{0.35}Ga_{0.65}As$/GaAs MQW RWG laser (uncoated facets, 25°C heat-sink).

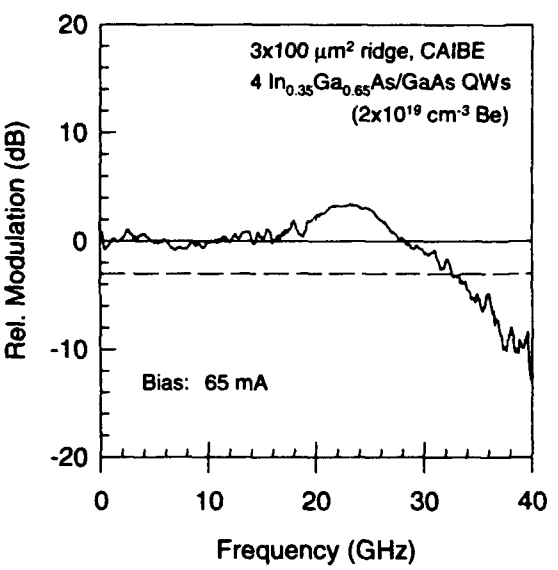

Fig. 4 33 GHz direct modulation of p-doped $In_{0.35}Ga_{0.65}As$/GaAs MQW RWG laser (65 mA dc bias current, uncoated facets, 25°C heat-sink).

8:45am - 9:00am

Th1.2

1.5μm InGaAsP/InP Multi-Gain-Levered -MQW-DFB-LD with high efficiency and large bandwidth FM response

Jong-In Shim*, Hiroyuki Yamazaki, Masayuki Yamaguchi, and Mitsuhiro Kitamura
*Dept. of Electronics Eng., Hanyang University, Ansan-si, Kyungki-do, 457-91,Korea
NEC Corporation, 34, Miyukigaoka, Tsukuba, Ibaraki, 305, Japan

It is essential to develop single frequency lasers with a high efficiency and large bandwidth FM response for high bit-rate FSK systems. In this paper, novel Multi-Gain-Levered(MGL)-MQW-DFB-LDs are proposed and fabricated by selective MOVPE. FM efficiency - bandwidth product of 20 GHz^2/mA, about 3 times larger than the best reported value for 1.5μm band single frequency LDs, has been achieved.

Figure 1 shows a schematic structure as well as a gain characteristics. The outer sections are connected to one electrode and the center section to another electrode which is the modulation region(1). The lasing mode will experience different gain spectra in different regions of the cavity formed by the selective MOVPE technique(2). By properly choosing the growth condition and the corrugation pitch, it is possible to achieve lasing between the gain spectra of the two adjacent regions. As a result, the lasing mode will have a negative detuning relative to the gain peak in the center section and a positive detuning in the outer sections, which in turn gives rise to a large differential gain difference between two regions. Therefore the device is expected to show an enhanced gain-levering effect, namely multi-gain-levering effects, compared to normal gain-levered lasers which only employs a variation in a differential gain due to the bias difference between two regions(3).

1.5μm InGaAsP/InP MGL-MQW-DFB-LD was grown by 2-step MOVPE selective epitaxy. The outer region length L_C and center region length L_O are 300 μm and 50 μm, respectively. Anti-reflection coating was employed on both facets. The $L_C/(L_C+2L_O)$ value and threshold current were measured around 3.5 and 25 mA, respectively. Figure 2 shows the measured EL spectra of the outer and center regions. The gain peak detuning between two regions was 40 nm and the lasing wavelength was found in between the two gain peaks as designed. Effective λ/4 phase shift in the center section was confirmed from measurement of below threshold spectrum.

Figure 3 shows a measured FM response of MGL-MQW-DFB-LD for different center region current and a constant outer section current of 100mA. The FM efficiency increases as the center region current decreases. Very flat and high FM efficiency of 10 GHz/mA was obtained above 2 GHz modulation bandwidth in a nonuniform bias condition. Even at a uniform bias condition it exceeds a value of 1 GHz/mA, which is resulted from a new gain-levering effect of the lasing wavelength detuning from the gain peaks.

Figure 4 shows the previously reported FM efficiency and bandwidth of single frequency lasers along with the results from this work denoted as open circles. The FM efficiency tends to decrease as the modulation bandwidth increases, in such a way that the FM efficency - bandwidth product can represent a figure of merit of the FM response charactersitics of single mode lasers. The highest value of FM efficiency and bandwidth product ever reported is 7.5 GHz^2/mA in a 3-electrode DFB-LD. MGL-MQW-DFB-LD shows over 20 GHz^2/mA, which is the highest reported to the best of our knowledge. We believe that this improved FM response is resulted from the multi-gain-levering effect introduced by the gain peak detuning and bias difference between two regions.

In conclusion, we have proposed and fabricated 1.5μm MGL-MQW-DFB-LD grown by MOVPE selective epitaxy. High and flat FM Efficiency value of 10 GHz/mA was realized up to 2 GHz modulation frequency by introducing a new concept of Multi-Gain-Levering effect.

Acknowledgement: The authors would like to express thanks to Dr. I. Mito and Dr. K. Kobayasi for fruitful discussion and to Mr. M.Yasuda and Ms. K. Ueda for experimental help.

References: (1).H.Olesen, J.I.Shim, M.Yamaguchi, and M.Kitamura, IEEE Photon. Tchnol. Lett., vol.5, no.6, pp.599-602,1993 (2)T.Sasaki, M.Kitamura, and I.Mito, J. Crystal Growth, 132, pp. 435-443, 1993 (3). K.Y.Lau, Appl. Phys. Lett., vol.57, pp. 2068-2070, 1990

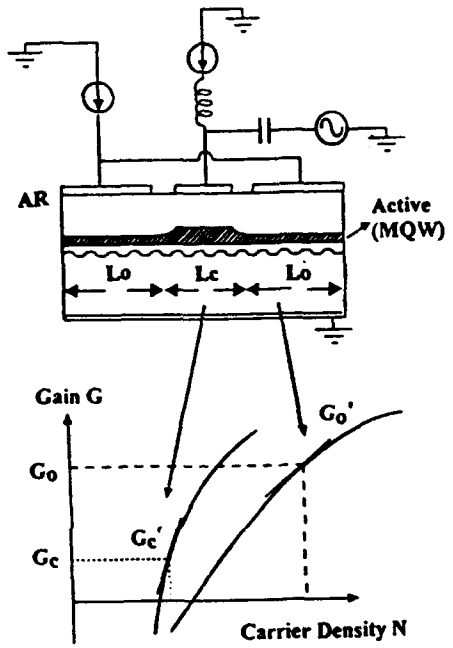

Fig. 1 Schematic diagram of MGL-MQW-DFB-LD The bottom part shows the gain vs carrier density curve.

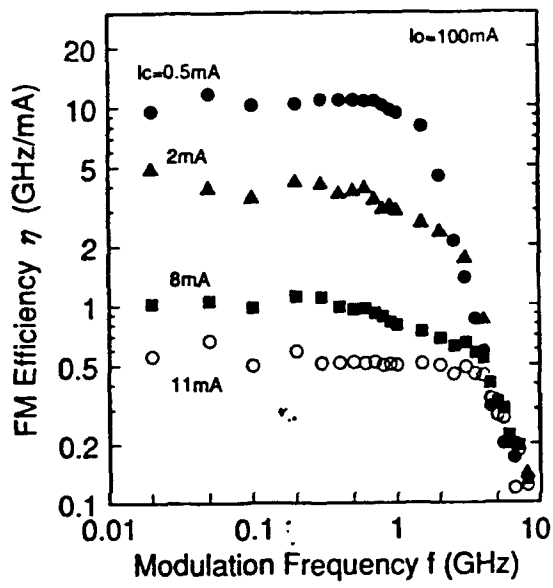

Fig.3 FM response of MGL-MQW-DFB-LD

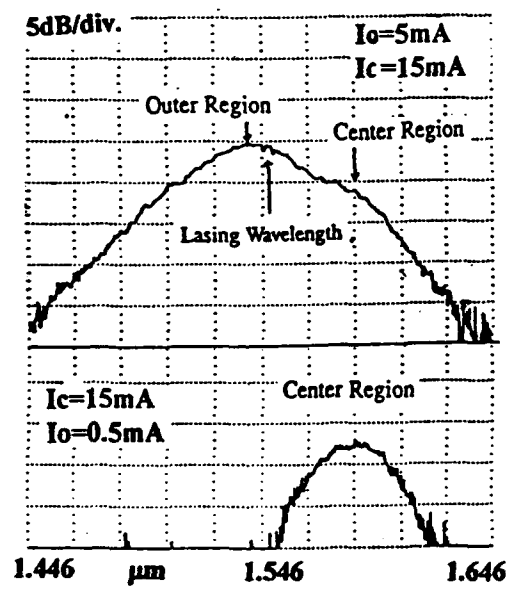

Fig. 2 Measured EL spectra from the two regions

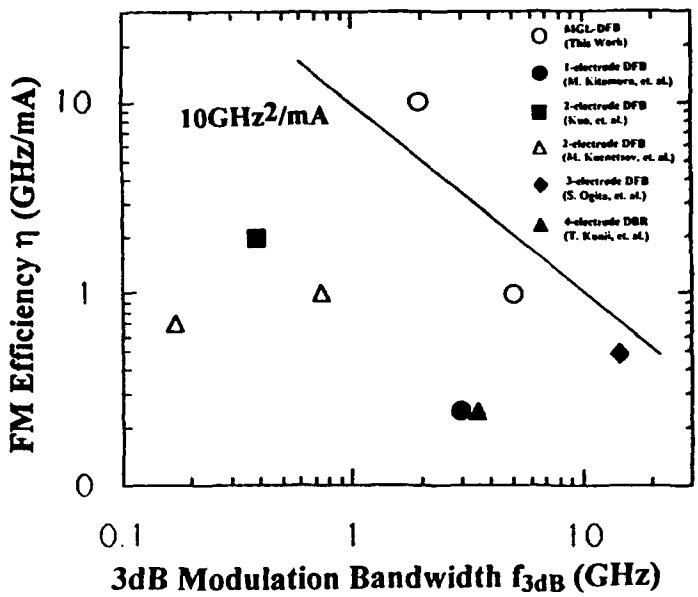

Fig. 4 FM Efficiency and Bandwidth of single frequency lasers

9:00am - 9:15am
Th1.3

High-Temperature Modulation Dynamics of 1.3 μm $Al_xGa_yIn_{1-x-y}As$/InP Compressive-Strained Multiple-Quantum-Well Lasers

C. E. Zah, M. C. Wang[a], R. Bhat, T. P. Lee, S. L. Chuang[a]
Z. Wang[b], D. Darby[b], D. Flanders[b], and J. J. Hsieh[b]
Bellcore, NVC3X361, 331 Newman Springs Rd., Red Bank, NJ 07701, USA
[a] Dept. of Electrical and Computer Engineering, Univ. of Illinois, Urbana-Champaign, IL 61801
[b] Lasertron, Burlington, MA 01803

Abstract: Intrinsic small-signal modulation responses of 1.3 μm $Al_xGa_yIn_{1-x-y}As$/InP compressive-strained multiple-quantum-well lasers with three different barrier layers are investigated. For the lasers with a barrier bandgap wavelength of 1.01 μm, *k* factors are determined to be 0.24-0.25 ns, and thermal-limited 3-dB bandwidths of 19.5, 15, and 13.9 GHz are measured at 25, 65 and 85 °C, respectively.

For loop applications, it is desirable to use uncooled semiconductor lasers that can perform well in an extreme temperature environment. They are more economical and reliable than the lasers requiring cooling against the variations in the ambient temperature. The conventional GaInAsP-based multiple-quantum-well lasers suffer from the compromise between poor electron confinement and nonuniform hole distribution resulting from the small band offset ratio (~40%) of the conduction band. It has been expected that the carrier confinement in the AlGaInAs-based lasers should be improved since the band offset ratio of the conduction band is about ~72% in this material system. Recently, we have demonstrated that the 1.3 μm $Al_xGa_yIn_{1-x-y}As$/InP compressive-strained multiple-quantum-well lasers have excellent light-current performance and high reliability over the temperature range from -40 to 85 °C.[1,2] In this work, we investigate the barrier height effects on the high-temperature modulation dynamics of $Al_xGa_yIn_{1-x-y}As$/InP compressive-strained multiple-quantum-well lasers for the first time.

The devices used in this study are three kinds of 1.3 μm $Al_xGa_yIn_{1-x-y}As$/InP compressive-strained five-quantum-well ridge-waveguide lasers, each employing five quantum-wells in the middle of the graded-index separate-confinement heterostructure (GRINSCH) region. Their structures are described in Table I. The bandgap wavelengths of the barrier layers are 0.94, 1.01 and 1.17 μm, respectively. On either side of the multiple-quantum-well region, a linearly graded AlGaInAs waveguide layer of 100 nm is grown, which begins at the barrier composition and ends at a quaternary layer of 0.96 μm bandgap wavelength for Device A or a ternary layer of $Al_{.48}In_{.52}As$ for Devices B and C. The fabrication details can be found in Ref. [3] and [4]. The cavity is 300 μm long and the rear facet is high-reflection coated with a reflectance of 70 %.

The intrinsic small-signal modulation responses are measured in the range of 0.1-20 GHz by a parasitic-free optical modulation technique. The 1.3 μm laser diode under test is optically modulated by injecting a 0.98 μm light externally modulated by an optical modulator inside a lightwave network analyzer. The output of the 1.3 μm laser diode is separated from the reflected 0.98 μm light by a WDM coupler.[3] The intrinsic small-signal modulation responses are measured at various bias currents and three heat sink temperatures. As shown in Fig. 1, the solid lines are the theoretical fittings to the measured data for Device B shown in dots. Its maximum intrinsic 3-dB bandwidths are measured to be of 19.5, 15, and 13.9 GHz at 25, 65 and 85 °C, respectively. Power roll-off caused by heating prevents further increase of the modulation bandwidth. The device characteristics are summarized in Table II. It includes the differential gain g_n, the nonlinear gain factor ε, and the *k* factor, derived from the relaxation resonance frequency f_r and the nonlinear damping factor γ which are obtained by fitting the experimental data.

A comparison made between Devices A, B and C suggests that the differential gain g_n is similar in Devices B and C, but lower in Device A. More importantly, the temperature sensitivity of Device A is also worse. By contrast, the nonlinear gain factor ε and its temperature sensitivity are found to be similar among the three devices, within experimental error. As a result, the *k* factor is larger in Device A, and increases faster as the temperature increases. To further understand the origin of the temperature sensitivity of the differential gain in these three lasers, spontaneous emission spectra were measured at high temperature (75 °C). The spontaneous emission was measured through a window on the back side of the chips. As shown in Figs. 2, three transition peaks can be identified in the spontaneous emission spectra of Device A at 18 mA bias current. They are attributed to the band to band transitions in the well, the heavy hole band to the conduction band (1.30 μm) and the light hole band to the conduction band (1.23 μm), and in the barrier (1.17 μm). At room temperature, the lasing mode is due to the transition between the heavy hole band and the conduction band which dominates the other two transitions. With the increase of the barrier height in Devices B and C, the separation between the heavy-hole and the light-hole

subbands increases. Most of the valence holes stay in the first heavy-hole state, which is confirmed by the clean spectra of Device C in Fig. 2

To reduce the temperature sensitivity of lasers, it is important to confine the carrier well at high temperature by adopting a sufficient high barrier and a large compressive-strain in the well such as Devie B. Device B has smaller k factor, higher differential gain and smaller nonlinear gain factor than the InGaAsP/InP multiple quantum well lasers over the temperature range from 25 to 85 °C.[5] This is attributed to the favorable band offset of $Al_xGa_yIn_{1-x-y}As$/InP materials system which enables the design of lasers with deep quantum wells. Therefore, $Al_xGa_yIn_{1-x-y}As$/InP materials system is a better choice for making high speed lasers.

[1] C. E. Zah, et al., *Tech. Dig. of Optical Fiber Comm.* ThG1, 204-205, San Jose, CA, February 20-25, 1994.

[2] Z. Wang, et al., *Tech. Dig. of Optical Fiber Comm.* Wl4, 144-145, San Jose, CA, February 20-25, 1994.

[3] C. E. Zah, et al., *J. Quantum Electron.*, **30**, February 1994.

[4] R. Bhat, et al., *7th Int. Conf. on MOVPE*, Yokohama, Japan, May 31-June 3, 1994.

[5] M. Ishikawa, et al., *Appl. Phys. Lett.*, **61** (4), 396-398, 1992.

Table I Compositions of 1.3 μm $Al_xGa_yIn_{1-x-y}As$ compressive-strained quantum wells

Device	A	B	C
Well Composition	$Al_{.17}Ga_{.157}In_{.673}As$	$Al_{.153}Ga_{.114}In_{.733}As$	$Al_{.143}Ga_{.106}In_{.751}As$
Strain	0.99 %	1.4 %	1.53 %
Well Thickness	7.1 nm	5.2 nm	6.2 nm
η_w	1.77 %	0.93 %	1.03 %
Barrier Composition	$Al_{.2}Ga_{.273}In_{.527}As$	$Al_{.303}Ga_{.165}In_{.532}As$	$Al_{.368}Ga_{.111}In_{.521}As$
Barrier Thickness	10.1 nm	10.0 nm	10.2 nm
λ_B	1.17 μm	1.01 μm	0.94 μm

λ_B: Barrier bandgap wavelength η_w: Optical confinement factor per well

Table II Device characteristics of 1.3 μm $Al_xGa_yIn_{1-x-y}As$ compressive-strained quantum well lasers

Device	T, °C	I_{th}, mA	λ, μm	α_i, cm-1	$\frac{f_r}{\sqrt{P_f}}$, $\frac{GHz}{\sqrt{mW}}$	k, ns	g_n, $10^{16}cm^2$	ε, 10^{-17} cm^3
A	25	16	1.29	11.6	1.56	0.31	3.35	1.36
	65	36	1.31	16.1	1.15	0.37	1.62	0.92
B	25	13	1.34	8.6	1.7	0.24	5.82	1.35
	65	21	1.36	10.7	1.49	0.24	4.18	1.04
	85	28	1.37	11.3	1.36	0.25	3.38	0.93
C	25	14	1.34	4	1.49	0.27	5.57	1.41
	65	24	1.36	4.34	1.34	0.27	4.38	1.12
	85	33	1.37	3.48	1.13	0.28	3.16	0.85

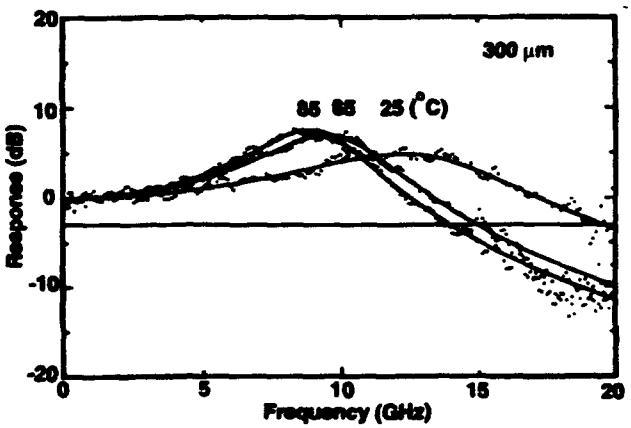

Fig. 1 Small-signal modulation responses of Device B at 25, 65 and 85 °C with bias currents of 153, 137 and 150 mA, respectively.

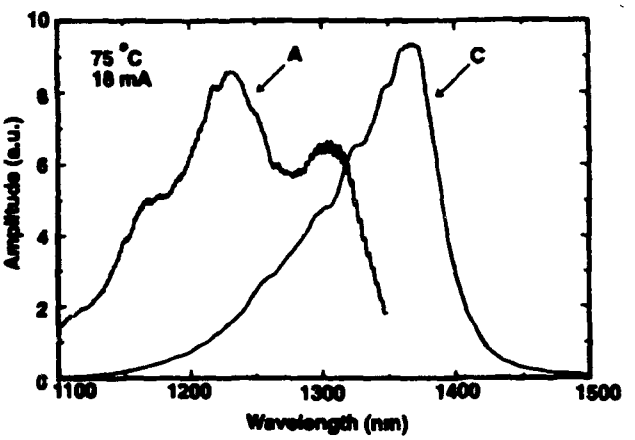

Fig. 2 Measured spontaneous emission spectra of Device A and C at 75 °C with a bias current of 18 mA.

9:15am - 9:30am

Th1.4 1.3 μ m Strained MQW-DFB Lasers with Extremely-Low-Intermodulation Distortion for 1.9GHz Analog Transmission

H.Watanabe, T.Aoyagi, A.Takemoto,T.Takiguchi,H.Tada,K.Isshiki and E.Omura
Mitsubishi Electric Corporation, Optoelectric & Microwave Devices Laboratory
4-1 Mizuhara, Itami, Hyogo 664, Japan FAX:+81-727-80-2696

[Abstract] The third order intermodulation distortion as low as -88dBc is achieved at high frequency of 1.9GHz in 1.3 μ m strained MQW-DFB lasers fabricated by all-MOCVD growth technique. High CNR over 80dB is also realized.

Recent outstanding progress in SCM (Subcarrier Multiplexing) system is expanding new applications for laser diodes such as fiber-optic microcellular radio communication system. LDs for those systems are required to have extremely low distortion and low noise at higher frequency than the conventional CATV band. It has been shown that the modulation distortion of LDs is caused by 1) the nonlinearity in L-I curve and 2) the nonlinear interaction of photons and electrons. In particular, the latter becomes the serious issue with increasing the modulation frequency depending on the resonance frequency f_r. Therefore realization of high f_r is quite important to suppress the intermodulation distortion at high frequency[1]. In this paper, we have demonstrated the significant reduction of the third order intermodulation distortion (IMD3) in 1.3 μ m strained MQW-DFB lasers by optimizing the MQW structure and applying all-MOCVD fabrication technique.

We have adopted 2-inch diameter wafer processing and all-MOCVD growth technology. Highly uniform characteristics and excellent reproductivity were demonstrated in comparison with the conventional small-size-wafer and LPE technologies[2),3)]. Furthermore, it was shown that the leakage current which causes the nonlinearity in the L-I curve was drastically reduced, because filling growth by MOCVD made it easy to control the leakage current gap between the active region and current blocking layers.

The MQW active region with compressively strain consists of 4nm thick InGaAsP(λ g =1.45 μ m) wells and 10nm thick InGaAsP(λ g=1.10 μ m) barriers. The cavity length is 300 μ m and the facets are AR/HR coated. The wavelength is detuned by 10nm shorter than the gain peak. The number of well/barrier is changed to investigate the well number dependence of f_r. Figure.1 shows relation between fr and optical confinement factor calculated from the structure parameters. Experimental results of f_r estimated from RIN spectrum are in good agreement with the calculation taking the strain effect into consideration. Maximum fr of 3.9GHz/mW$^{1/2}$(=2.15GHz/mA$^{1/2}$) is obtained for the LDs with 10wells.

The dependence of IMD3 on fr was examined by changing bias level for the samples with 5 and 10 wells under 2-tone test (f1=1900MHz, f2=1900.6MHz and optical modulation depth=20%) to clarify how effective to make f_r higher to achieve low distortion. Clear dependence on fr , which indicates that higher than 18GHz is needed to obtain IMD3<-80dBc, is observed as shown in Figure 2. Figure 3 shows a typical behavior of IMD3 in a 10-well sample at various bias current. Monotonous decrease of IMD3 with bias current is attributed to

increase in fr. The onset of the increase of IMD3 at high bias level is believed to be caused by the nonlinearity of L-I curve due to the high bias current. The IMD3 as low as -88dBc is achieved. Figure 4 shows RIN and CNR (@OMD=20%,BW=288kHz) characteristics at 1.9GHz. RIN less than -152dB/Hz or CNR more than 80dB is achieved in the range of enough low distortion.

In conclusion, we have developed 1.3 μ m strained MQW-DFB lasers with extremely low third order intermodulation distortion and low noise by means of improving resonance frequency and applying all-MOCVD fabrication technique. These are suitable for 1.9GHz analog transmission.

References

1) H.Yamada et al, Electron. Lett.,Vol.29, pp1944-1945 (1993)

2) T.Nishimura et al, SPIE, Vol.1849, pp272-279 (1993)

3) T.Nishimura et al, Tech. Dig. of OFC'94, pp101-102 (1994)

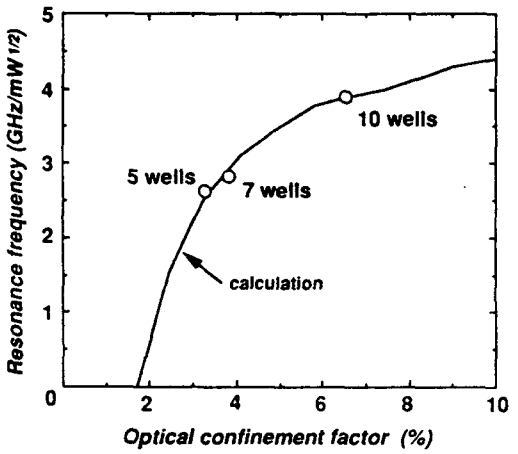

Fig.1 Dependence of resonance frequency on optical confinement factor with 5wells, 7wells and 10 wells samples

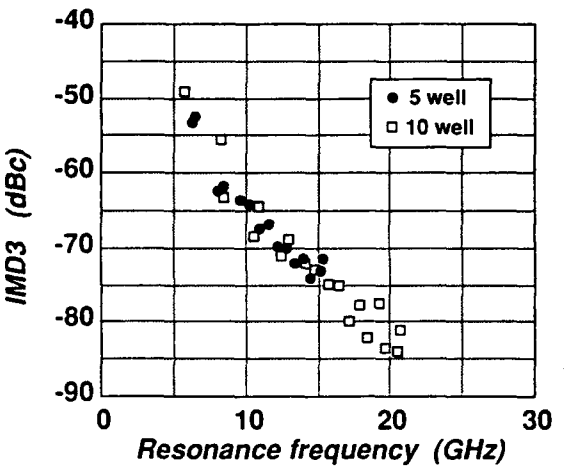

Fig. 2 Relation between IMD3 and resonance frequency (f1=1900MHz,f2=1900.6MHz,OMD=20%)

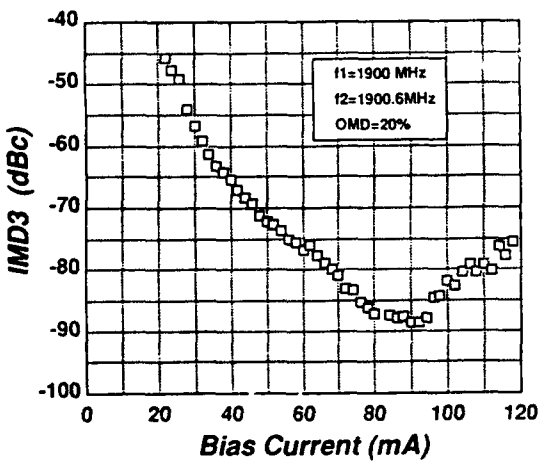

Fig.3 IMD3 characteristics with bias current in a 10-well sample

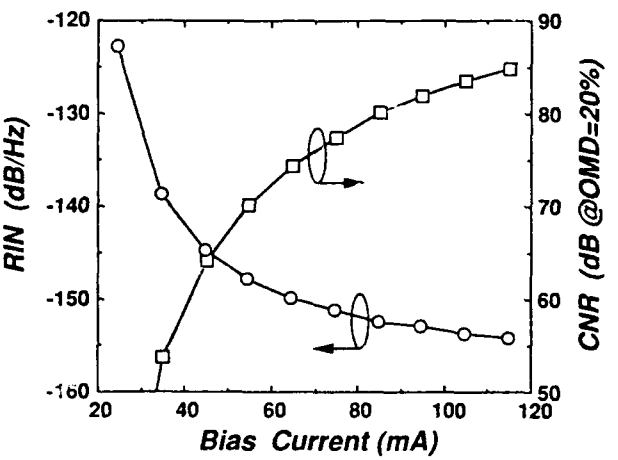

Fig.4 RIN and CNR (OMD=20%) characteristics with bias current

9:30am - 9:45am
Th1.5

Intra-Cavity Contacted Vertical Cavity Laser Arrays Optimized for Low Current, High Speed Interconnect Applications

J.W. Scott†, B.J. Thibeault, C.J. Mahon‡, F. H. Peters† , D. B. Young and L.A. Coldren
ECE Dept., University of California at Santa Barbara, Santa Barbara, California 93106, USA.

† Optical Concepts Incorporated, 432A Commerce Court, Lompoc, California 93436, USA
‡ Tele Danmark Research, Lyngsø Allé 2, 2970 Hørsholm, Denmark.

Abstract- Experimental measurements of the performance of intra-cavity contacted vertical cavity lasers for short haul Gigabit data link applications are presented. At an output power of 1 mW these top-surface-emitting, sub-milliamp threshold lasers have bandwidths above 7 GHz while consuming only 10 mW of electrical power.

In recent years there has been considerable interest in the development of vertical cavity lasers. Their geometry produces low divergence output beams and should lead to very low threshold currents and high density laser arrays. More recently, research has shown that vertical cavity lasers have the capability for high modulation efficiency and built-in temperature compensation [1,2]. In addition, their surface emission properties promise the development of wafer level testing and lower cost packaging. Realizing the above potentials in a single device structure has proven to be more elusive, however. Sub-milliamp threshold lasers have had very low output power and wallplug efficiencies. High density arrays require very low power lasers while high speed arrays for communications require low capacitance interconnect lines to be useful. We report here on arrays of high efficiency, sub-milliamp vertical cavity lasers on semi-insulating substrates which realize many of the potentials of this class of semiconductor lasers. These intra-cavity contacted, top-surface emitting vertical cavity lasers have shown output powers greater than 1mW, 3dB bandwiths in excess of 7 GHz and gigabit data rates at bias currents of only a few milliamps and power consumption below 10 mW. The advantages of semi-insulating substrates enabled all the laser characterization to be made with wafer level probing.

A micrograph of a 10 μm diameter intra-cavity contacted laser is shown in Fig. 1. The sample was grown by solid source MBE. Three mesas can be observed; the 10 μm diameter waveguide / top Bragg reflector in the center, the 20 μm diameter p-mesa and a semi-circular 40 μm diameter n-mesa. Underneath the surface is the undoped bottom Bragg reflector. Visible as a dark ring around the perimeter, a wet etch has been used to undercut the p-mesa and force the current into the optical waveguide. The p and n-type layers provide an electrical path for the current to pump the active region within the optical cavity. The doping and layer structure was designed to minimize current crowding effects at the perimeter of the waveguide by introducing a current levelling resistive layer between the conductive p layer and the active region. By using this intra-cavity contacted design, both contacts and emission can be made on the top surface. In addition, the electrical and optical designs have become separated, avoiding the tradeoffs of higher optical losses and thermal impedence made in Bragg reflectors optimized for low resistance.

The LI characteristics of various diameter $In_{0.2}Ga_{0.8}As$ lasers are shown in Fig. 2. Of particular interest are the 7 μm diameter lasers with threshold currents of 0.72 mA and thermally limited output powers of 2.1 mW. The drive voltage for the various lasers was near 3V at threshold and below 4V at peak power for all four device diameters, indicating significant room for improvement in future revisions. The inset shows the optical spectrum of the 7 μm laser at a bias of 3 mA. The spectral characteristics varied with device from more than 30 dB of mode suppression ratio (MSR) for the 5 μm diameter laser to 4 competing modes in the 15 μm diameter device. Depending on the application, single mode or multimode operation may be desirable. The modal properties can be determined simply by varying the waveguide diameter.

The power conversion efficiency of the various laser diameters are shown in Fig. 3 as a function of the input power. At a drive current of 3 mA, the 7 μm laser produces 1 mW of optical power for an input power of 10 mW, yielding a 10% power conversion efficiency. For high density array applications such as optically interconneted multi-chip modules or free space interconnects, it is critical to achieve these kinds of efficiencies at low power levels. Thermal management considerations require the minimum amount of heat generation. For computer interconnect applications, output powers near 1mW must be achieved at low current levels to enable the use of low capacitance driver circuits. These lasers have the potential for effective application in these areas.

The small modal volume of a vertical cavity laser should lead to high bandwidths at low current levels. Due to the decreasing diameter, the smaller devices have higher modulation efficiencies. The 7 μm laser achieves a bandwidth of 8.5 GHz at a bias of only 4 mA. It has a modulation efficiency of 5.7 GHz/√mA, higher than any in-plane laser reported to date. The low threshold currents and high modulation efficiencies of these lasers make them ideal for high

bit rate digital data links operating at low currents. Bit error rate (BER) curves were made at 2.488 Gbit/s for all four laser sizes. The measurements were made with 30 meters of graded index multimode fiber. Electrical and optical connections were made using Cascade microwave and lightwave probes. The lightwave probe held a lensed multimode fiber 50 - 100 μm above the laser surface. The results are shown in Fig. 4 along with a theoretical curve taking into account thermal noise, amplifier noise and an extinction ratio penalty of 1.4 dB. (All devices could be operated at 3 Gbit/s, the limiting bit rate of the test equipment used, with no additional penalty.) The bias conditions for the 7 μm device was 4mA/3.5V with a modulation signal of 1V peak to peak into 50Ω. No error floor was observed for any of the laser diameters.

In summary, we have presented measurements of intra-cavity contacted vertical cavity lasers on semi-insulating substrates. These laser arrays have shown the ideal characteristics for use in high density, high speed digital applications where low power consumption and ≈mW scale output powers are required. Measurements of the thermal and electrical properties indicate that significantly higher speeds and efficiencies will be achieved as the laser designs are improved. This work was supported in part by ARPA via the Optoelectronics Technology Center and the Office of Naval Research as well as the Ballistic Missile Defense Organization via the U.S. Army Research Office.

Figure 1. SEM of a 10 μm diameter vertical cavity laser. Emission and intra-cavity contacts are on the top surface.

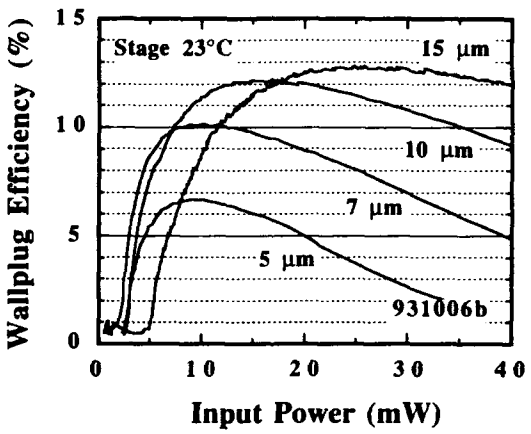

Figure 3. Power conversion efficiency for the four sizes. The 7 μm laser has an efficiency of 10% at an input of only 10 mW.

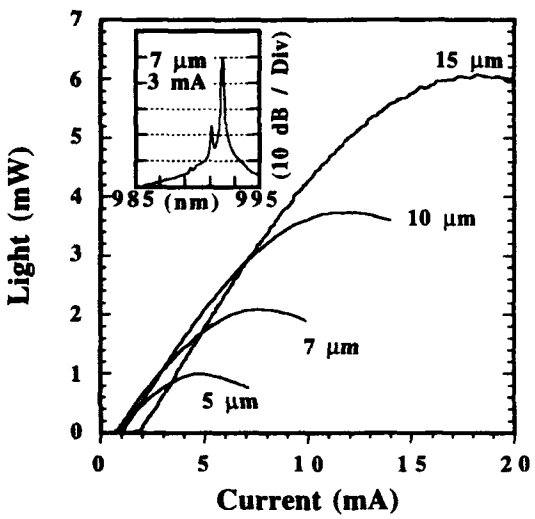

Figure 2. LI characteristics for the four sizes showing sub-milliamp threshold currents with high external efficiency.

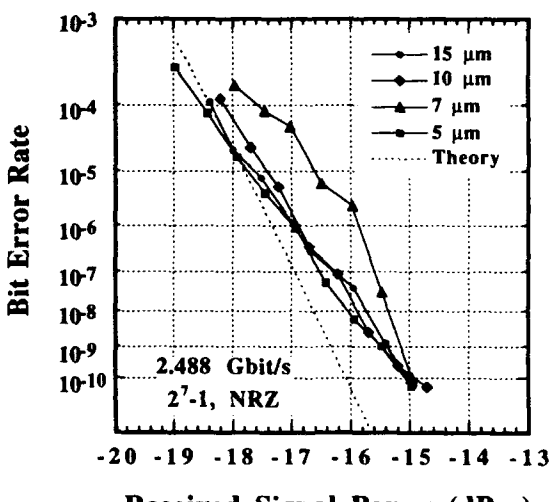

Figure 4. Bit error rate curves for the four sizes. Measurements were made on wafer using electrical and optical probes.

References

[1] D.Tauber, G. Wang, R.S. Geels, J. E. Bowers and L. A. Coldren, *Appl. Phys. Lett.*, **62** (4), 325-327 (1993)

[2] J. W. Scott, D. B. Young, S. W. Corzine and L. A. Coldren, *Appl. Phys. Lett.*, **62** (10) 1050-1052 (1993)

9:45am -10:00am
Th1.6

MULTI QUANTUM WELL 1.55 μm DFB LASERS WITH LOW THRESHOLD CURRENT, HIGH RESONANCE FREQUENCY AND BANDWIDTH AT LOW CURRENT INJECTION

O. Kjebon. U. Öhlander, S. Lourdudoss, J. Wallin, K. Streubel, S. Nilsson and T. Klinga
Royal Institute of Technology
Laboratory of Photonics and Microwave Engineering, Dept. of Electronics
Electrum 229, S-164 40 Kista, Sweden

Abstract

Multi quantum well DFB buried heterostructure lasers with low threshold, 3.4 mA, large slope of resonance frequency versus square root of current above threshold, 2.6 GHz/mA$^{1/2}$, and high maximum bandwidth, 21.7 GHz, have been fabricated.

Introduction: Lasers with low threshold current, high resonance frequency and low parasitics can yield large bandwidth at low current which reduces power consumption. Such lasers are desired for ultrahigh direct intensity modulation for optical communication systems and have been fabricated by e.g., Morton et al. [1]. The aim of this paper is to show an improvement in a 1.55 μm DFB laser by a proper combination of carefully optimised growth techniques and processing steps. From a large slope of the plot of resonance frequency versus square root of current above threshold we will show that we have obtained as high a value of 2.6 GHz/mA$^{1/2}$ which is to the authors knowledge the best value ever reported for a 1.55 μm DFB laser.

Laser design: The basic structure represented in Fig.1 consisted of an MOVPE grown multi quantum well (MQW) structure with 8 compressivily (1 %) strained quaternery wells and tensile (0.9 %) strained quaternery barriers, with zero net strain [2]. it also included a graded index separate confinement heterostructure (GRINSCH). The GRINSCH on the p-side and the wells were intentionally undoped. To avoid excessive diffusion of zinc into the quantum wells the 250 Å InP spacer layer between the grating layer and GRINSCH was low doped p=2 x 10^{17} cm^{-3}. After mesa formation by reactive etching, regrowth of 5 μm thick iron doped InP (Fe=1x10^{18} cm^{-3}) was performed in a hydride vapour phase epitaxy reactor [3]. A ground-signal-ground pattern to enable direct probing on the lasers with high frequency probes was formed on the lasers.

Measurements: Measurements were done on as cleaved lasers of length 100-240 μm. They were mounted epitaxial side up and small signal analysis was performed with an HP 8703 A light wave component analyzer via direct probing on the laser by a Cascade Microtech WPH-005-150 microprobe.

Results and discussion: The lasers exhibited very low threshold currents. The minimum value was 3.4 mA and the average value was 4.5 mA for the as cleaved lasers. The quantum efficiency from the front facet was in the range 20-30 %. The small signal analysis yielded both response and match measurements. The S_{11} parameter was used to fit a simple model of the laser with excellent agreement between experimental data and model [4]. This model yielded a parasitical 3dB bandwidth of 30 GHz. The highest 3dB bandwidth measured for the 140 μm long laser in Fig.2,3 was 18 GHz which was reached at 50 mA. The maximum bandwidth was reached at about half of maximum output power and it may be due to transport phenomena or spectral hole burning [5]. Regarding the resonance frequency, it is mainly affected by differential gain, g, ($g=\partial G/\partial n$ G=optical gain and n=carrier density), photon life time, τ_p, photon density, S and gain compression coefficient, ε [6]:

$$f_r = 1/2\pi(gS/\tau_p)^{1/2}(1-\varepsilon S)^{1/2}$$

At high power the curve f_r versus $S^{1/2}$ is sublinear due to gain compression. However at low power the $(1-\varepsilon S)^{1/2}$ term can be neglected and the slope of f_r versus $S^{1/2}$ together with the threshold current is a good measure of the ability to obtain high resonance frequency and high bandwidth at low power. From system point of view it is more interesting to look at the slope of f_r versus $(I-I_{th})^{1/2}$ than $S^{1/2}$. If the I-P curve is linear over threshold then S is proportional to $I-I_{th}$ and f_r proportional to $(I-I_{th})^{1/2}$. A plot of the resonance frequency versus $(I-I_{th})^{1/2}$ shows a slope of 2.6 GHz/mA$^{1/2}$ at low current which is to the authors knowledge the highest value published for lasers operating at 1.55 μm Fig. 2. Besides the resonance frequency reaches such high value as 11 GHz at only 25 mA. The low threshold currents are due to an optimisation of the growth of the quantum wells, an etching and regrowth process yielding few defects and low p-doping near the active layer. Low defects minimize the nonradiative recombination and low p-doping near the active layer gives low optical absorption. The low threshold currents in conjunction with large number of wells results in low band filling in the wells which gives a high differential gain. The combination of low threshold and high differential gain gives very high resonance frequency at low current. An

indication that the design for maximum bandwidth is different from that for maximum resonance frequency at low current is that a similiar structure with high p-doping $1x10^{18}$ cm^{-3} in the GRINSCH reached a maximum bandwidth of 21.7 GHz at 100 mA eventhough the threshold was higher, 14 mA, and the slope of f_r versus $(I-I_{th})^{1/2}$ was lower, 2.1 $GHz/mA^{1/2}$.

In conclusion we have fabricated an 1.55 μm MQW-DFB buried heterostructure laser with SI regrowth with an overall improved performance leading to a slope of 2.6 $GHz/mA^{1/2}$ for f_r versus $(I-I_{th})^{1/2}$.

Acknowledgement: This work was partly supported by the European RACE project R2069 "UFOS".

References

P. A. Morton et. al. Electron. Lett., vol. 29, No. 16, pp 1429-1430, 1994.

A. Mircea et. al., Indium phosphide and related materials'93, Paris, post-deadline, pp 41-44, 1993.

S. Lourdudoss et.al.,. Jour. Elect. Mat., 19 (9), pp. 981-987.

4, O. Kjebon et. al., ECOC'93, Montreaux, vol. 2, pp 201-204, 1993.

5. R. Nagarajan et. al., Appl. Phys. Lett. 59 (15) pp 1835-1837, 1991.

6. J.E. Bowers, Solid State Electron, 30, pp 1-11, 1987.

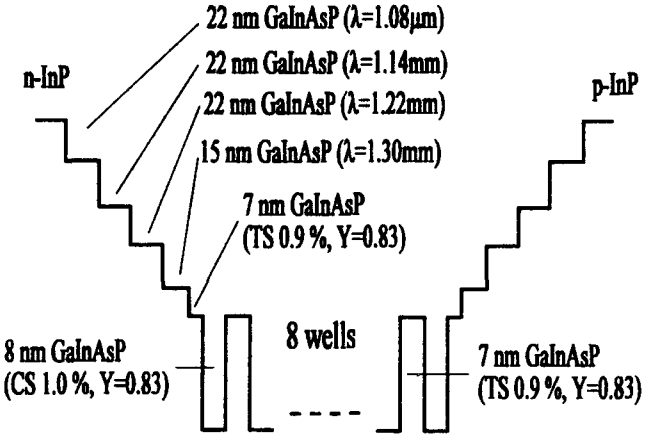

Fig. 1. The multi quantum structure and the GRINSCH

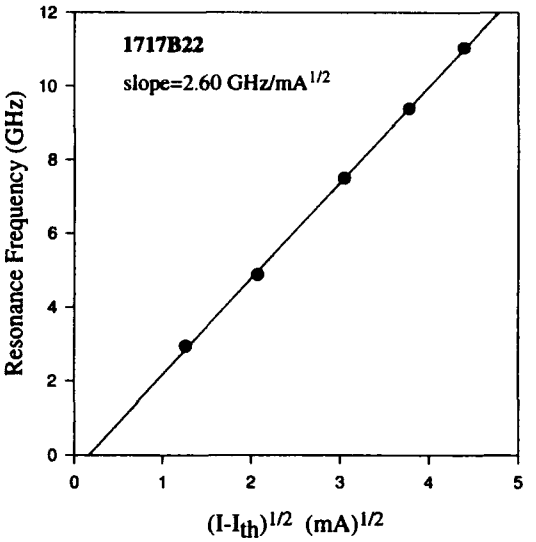

Fig. 2. Resonance frequency as a function of square root of current over threshold current.

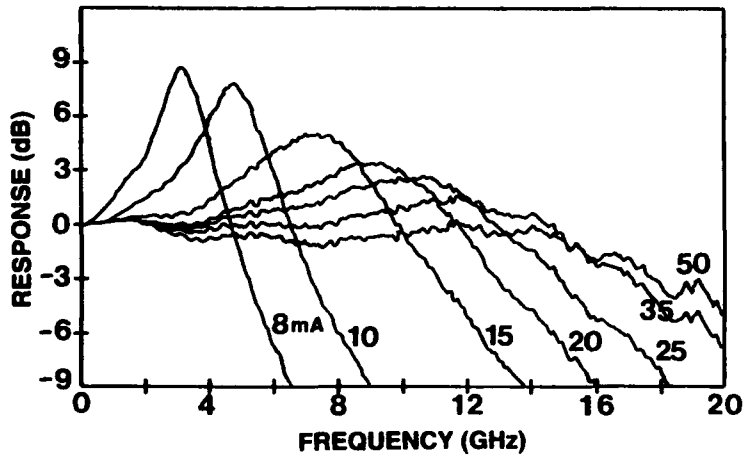

Fig. 3. Small signal response of a 140 mm long laser at different bias currents.

10:30am - 10:45am
Th2.1

Modulation Characteristics Of Short Cavity Distributed Bragg Reflection Lasers With A Narrow Band Bragg Mirror

N. Tessler, M. Margalit, G. Eisenstein Electrical Eng. Dept. TECHNION Haifa ISRAEL
U. Koren C. A. Burrus AT&T Bell Labs. Holmdel N.J. 07733
Tel. +972 4 294 694 FAX +972 4 323 041

ABSTRACT

We describe small and large signal modulation characteristics of distributed Bragg reflection lasers with a Bragg reflection bandwidth narrower than the cavity mode spacing.

SUMMARY

Distributed Bragg reflector (DBR) lasers usually operate with a Bragg reflection bandwidth which is several times wider than the cavity mode spacing. This paper describes characteristics of DBR lasers in which the Bragg reflection filter overlaps only one cavity mode at a time. This is obtained by using short gain sections in conjunction with Bragg filters whose bandwidth is narrower than the cavity mode spacing [1]. This laser enables efficient ***amplitude modulation*** by tuning the ***Bragg*** center wavelength. We concentrate here on the dynamic effects of tuning the Bragg reflection filter ***across*** the cavity mode in order to obtain that amplitude modulation. The special DBR laser which is shown schematically in Fig. 1 contains a 150μm long gain section and a 300μm long low coupling coefficient Bragg section with a bandwidth smaller than 1nm.

We first address the conceptual issues associated with modulation of the gain section or the Bragg center frequency. A rate equation model of the laser which includes the influence of the wavelength selective feedback reveals that for the case of gain section modulation, the narrowband Bragg Mirror introduces detuned loading like effects [2] that widen the bandwidth. Figure 2 shows such measured responses for different Bragg section biases, namely different detuning levels. The bandwidths shown are limited by conventional parasitics to about 4 GHz and the dependence on detuning level is consistent with the model.
Modulation of the Bragg center frequency is attractive since, compared to gain section modulation, the calculated response includes an additional zero which causes a bandwidth increase. The Bragg center frequency may be modulated by current injection. Such a measurement is shown in Fig. 3 which shows a low frequency roll off due to the long carrier lifetime of the passive Bragg section but also reveals a high frequency resonance at a few GHz. The low frequency roll of is not an inherent limitation since the Bragg center frequency may be modulated by means of the reverse biased electro optic effect which is very fast [3]. The result of Fig. 3 serves to demonstrate the conceptual advantage of modulating the Bragg center frequency.

Next we demonstrate a practical advantage of Bragg section modulation - high on/off ratio in the large signal regime with extremely low AC drive current. Figure 4 shows modulation with a pseudo random word. The drive current to the Bragg section was ± 1.5 mA at 100 Mb/s and the output on/off ratio was larger than 20 dB. Figure 5 shows the generation, by Bragg section modulation, of short Q - switched pulses. The AC power to the Bragg section was -15 dBm and the output pulse train consists of ~0.6 ns pulses also having an on/off ration larger than 20

dB. Both large signal cases are limited to ~200 MHz due to the bandwidth of the Bragg section. As mentioned above, this is not an inherent limitation and can be removed with a fast Bragg section center frequency modulation mechanism.

REFERENCES

[1] M. Margalit et. al., Optics Lett., 8, (1993) 610

[2] K. Vahala et. al., Appl. Phys. Lett., 46 (1985) 1025

[3] O. Mitomi et. al., Appl. Optics, 31, (1992), 2030

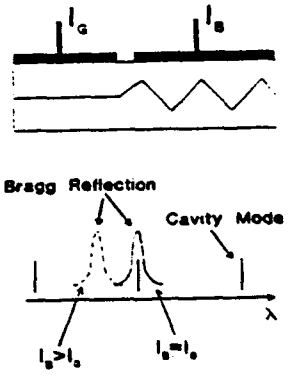

Fig. 1 - Schematic of the DBR laser

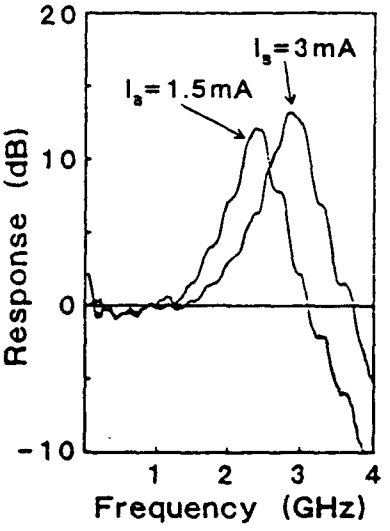

Fig. 2 - Small signal modulation of the gain section for different Bragg bias levels

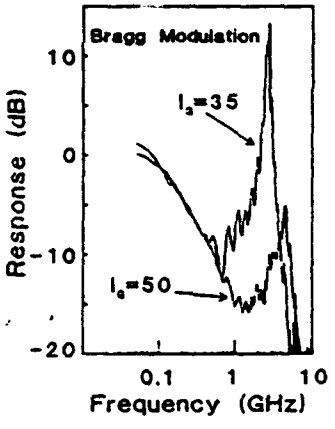

Fig. 3 - Small signal modulation of the Bragg section

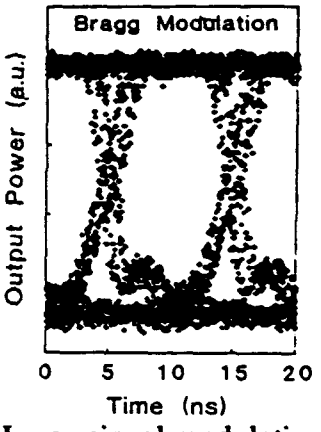

Fig. 4 - Large signal modulation at 100 Mb/s with ±1.5 mA Bragg section current

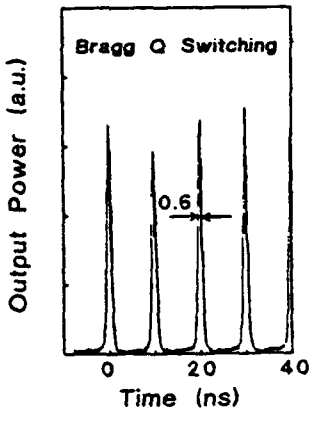

Fig. 5 - Q - switched pulses at 100 MHz with -15 dBm AC drive signal to the Bragg section.

10:45am - 11:00am
Th2.2

Ultra Fast Electro-Optical Distributed Bragg Reflector Laser for Optical Switching.

F. DELORME, B. ROSE, A. RAMDANE, B. PIERRE, H. NAKAJIMA.
France Telecom - CNET / PAB
196, Avenue H. Ravera, BP 107, 92225 Bagneux Cedex, France.

Introduction: Rapidly tunable transmitters are required as high speed light sources for high capacity **WDM** transmission and photonic switching systems. Different recent results on the tuning speed of the Distributed Bragg Reflector laser demonstrated the promising capacities of this device for such applications **[1-2]**. Nevertheless, the switching time of a **DBR** laser is limited by the carrier lifetime of the Bragg section, and increases with the wavelength jump. To overcome this problem, we fabricated a modified **DBR** laser including an electro-optical Bragg section waveguide on which a voltage is applied to tune the wavelength. Using this device, we measured the best switching time between the different wavelength channels ever reported on **DBR** laser: ***600 ps, independently of the wavelength shift.*** And this switching speed is only limited by the parasitic parameters of the Bragg section.

Electro-Optical DBR structure and fabrication.
The schematic structure of a 2-section Electro-Optical **DBR** is shown in Fig.1. A butt-jointed **DBR** structure is used to couple an amplifying section (MQW material with λ_p = 1.55 µm), grown during the first MOVPE epitaxy, to a passive Franz-Keldysh GaAsInP waveguide, realised by a Selective Area Epitaxy regrowth **[3]**, in which the grating is etched. The MQW structure consists on three 80 Å-thick InGaAs quantum wells and four 70 Å InGaAsP barriers, and two confinement 0.1 µm-thick 1.18 µm InGaAsP layers. And a 0.3 µm-thick 1.43 µm InGaAsP layer is used as Franz-Keldysh material. The choice of this material is determinated by the low absorption variation (0.3 dB/100 µm/V) compatible with a sufficient index variation at λ = 1.56 µm. In the active area, a Buried Ridge Structure **(BRS) [4]** is then used to achieve the lateral optical and electrical confinements of the Fabry-Perot laser. In the Bragg section, ridge waveguides of 3-µm width are formed by a combination of RIBE and wet etching. Low capacitance contact pads are realised on the thick lateral polyimide layer to limit the parasitic parameters of the Bragg section. And using the same technology, very high speed electroabsorption modulator have been realised **[5]**. To ensure a high electric isolation between the two sections, a proton implantation in a 12-µm width channel is used: with this technique, a 1 MΩ isolation resistor can be assumed.

Experimental results.
Under CW operation, the threshold currents of the devices, with active and Bragg lengths respectively equal to 850 µm and 370 µm are in the range 30-40 mA, and powers can be higher than 15 mW. A minimum linewidth as low as 315 kHz has been obtained at I_{active} = 130 mA. The coupling coefficient of the grating κ, determinated from sub-threshold spectra, is about 70 cm^{-1}.
This laser is discretely tunable by voltage applied to the DBR section, to 6 modes regularly spaced by 4Å over a tunable range of 25 Å around a wavelength of 1.56 µm **(Fig.2)**.
The measurement of the tuning speed of the **EO-DBR** laser is based on the Spectrally Resolved Time response (SRT) and has been described elsewhere **[6]**. **Fig.3** shows the switching curve obtained on the **EO-DBR** laser: the current injected in the active region is 100 mA, a -2 V voltage is applied to select the wavelength λ_1 , and a -2 V voltage pulse is used to switch to the wavelength λ_3. The rise time of the pulse is 100 ps, its duration is 15 ns and the repetition frequency is 100 kHz. The switching time between modes λ_1 and λ_2 is about 600 ps and is approximately equal to the switching time between λ_1 and λ_3. These results confirm that the switching time with electro-optical material is really short **(<<100ps)** and is only limited by parasitic elements of the Bragg section. On this wafer, the capacitance of the device is relatively high **(4.5 pF/100 µm)** and leads to this switching speed limitation of 600 ps. With lower capacitance, we hope to obtain switching time lower than 100 ps.

Conclusion: We realised a DBR laser with an electro-optical Bragg section using voltage to tune the wavelength. The tuning range is 25 Å for a 5 V drive voltage. And we measured on this device, the best switching time between the different accessible wavelength channels, ever reported on DBR laser: ***600 ps, independently of the wavelength shift*** . These results demonstrate the capability of the EO-DBR laser for ultra-high fast optical switching operation.

Acknowledgements: The authors would like to thank F. Devaux for useful discussion and P. Boulet, A. Gloukhian, S. Grosmaire and D. Robein for technical assistance. This work is partially supported by the EEC RACE 2039 ATMOS program.

References:

[1] **F. DELORME et al.**, Electron. Lett., Vol 29, N°1, p. 41-43, Jan. 1993.
[2] **B. GLANCE et al.**, IEEE Photonics Technol. Lett., Vol 4, N° 18, pp.1186 -1188, Oct. 1992.
[3] **B. ROSE et al.**, IPRM 94, Paper WP25, Santa Barbara, USA, March 27-31, 1994.
[4] **F. DELORME et al.**, Electron. Lett., Vol 27, (21), pp.1969 - 1971, 1991.
[5] **F. DEVAUX et al.**, IEEE Photonics Technol. Lett., Vol 5, N°11, pp.1288 - 1290, Nov. 1993.
[6] **S. CHERIF et al.**, Opto'94, Paris, 26-28 April 1994.

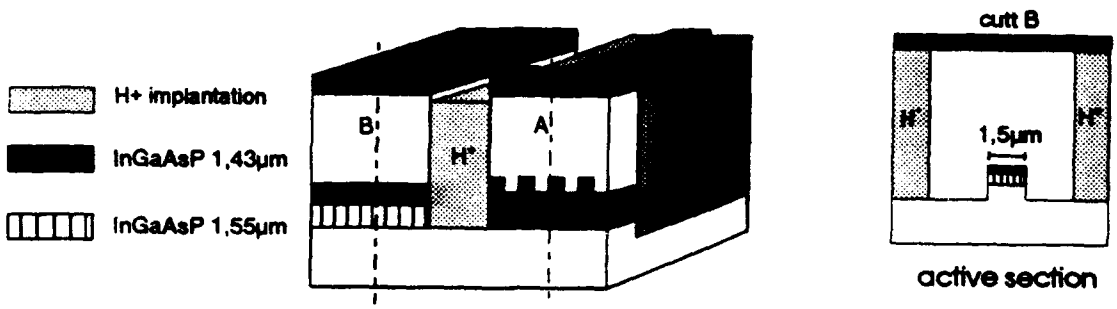

Fig.1: *Schematic structure of a 2-section Electro-optical DBR laser*

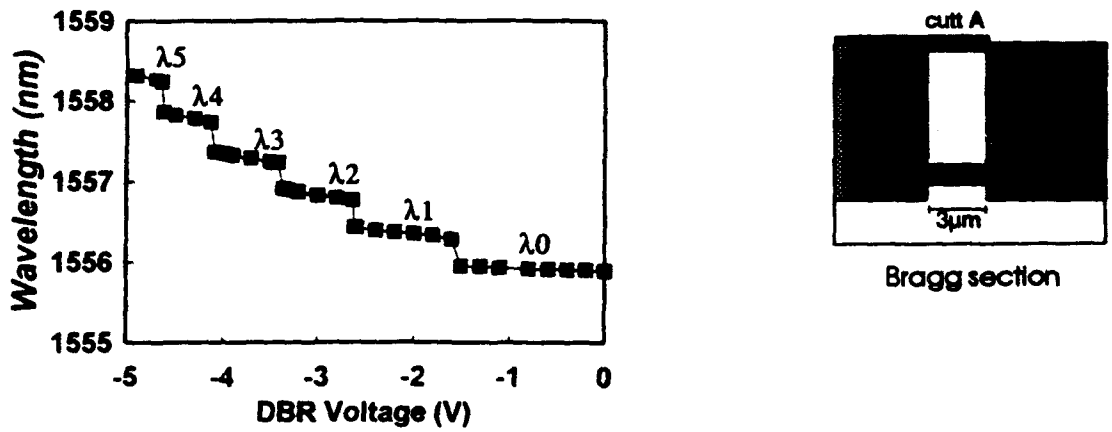

Fig.2: *Tuning of the E-O DBR laser versus the voltage applied to the Bragg section.*

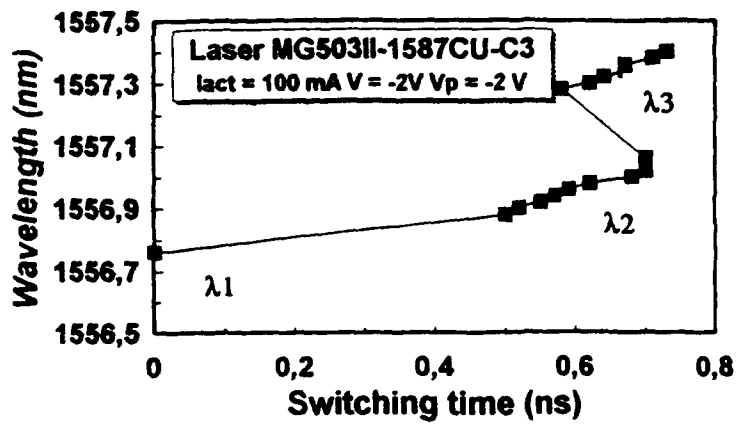

Fig.3: *Switching time of the E-O DBR laser for a jump between modes λ_1-λ_3*

11:00am - 11:15am

Th2.3 12 GHz to 64 GHz Continuous Frequency Tuning in Selfpulsating 1.55 μm Quantum Well DFB Lasers

U. Feiste, M. Möhrle, B. Sartorius, J. Hörer, R. Löffler
Heinrich-Hertz-Institut für Nachrichtentechnik Berlin GmbH, Berlin, Germany

Background: Selfpulsating DFB lasers represent single mode pulse sources which combine high speed operation and an electrically adjustable repetition rate. Continuous frequency tuning from 13GHz to 31GHz has been achieved in InGaAsP bulk DFB lasers /1/. The pulse trace emitted from the devices can be synchronized to an optically injected modulation, if the frequency mismatch is within a certain locking-range. Using such a selfpulsating DFB laser, all-optical clock recovery at 18Gbit/s has been demonstrated recently /2/. Clock recovery is indispensable for optical signal processing in future high speed telecommunication systems in the 40 to 100Gbit/s range. One main target of the device development is therefore to raise the pulsation frequencies.

Device development towards high pulsation frequencies: The selfpulsation in DFB lasers is based on dispersive self Q-switching /3/. Recent modeling results suggest that high pulsation frequencies in DFB lasers can be achieved in structures with high $\varkappa$-values and with high differential gain. For this purpose we optimized our DFB structures accordingly. Ridge waveguide DFB lasers were fabricated using an MOVPE grown heterostructure with eight 7nm thick InGaAs-wells, separated by 10nm thick 1.25μm-InGaAsP barriers. The active region was embedded in a 200nm thick 1.25μm-InGaAsP-waveguide. The first order DFB grating etched 70nm into the p-side waveguide has a coupling coefficient of about 300/cm. The device selected for the following investigations had section lengths of 250μm and 300μm. The facet at the longer section was AR coated.

Optical spectra: In Fig. 1 we show spectra when the current in the 300μm section is fixed to 50mA, and the current in the 250μm section is varied. The device emits in a single mode (SMS > 35dB) on the first DFB mode at longer wavelengths (stop band: flat spectrum). The splitting of the single mode emission line is caused by the onset of selfpulsation. With increasing current the spectra shift to longer wavelengths. Notice, that it is the center of the splitted line which shifts parallel to the observable higher DFB modes. The spectral characteristics turn out to be the same as in single mode pulsating bulk DFB lasers.

Electrical frequency tuning range: The pulsation frequency ν can be measured up to 26GHz using a fast detector and an RF spectrum analyzer. Higher frequencies ν are derived from the optical spectra by measuring the splitting of the emission line into sidebands $\Delta\lambda$ according to the equation $\nu = c \cdot \Delta\lambda/\lambda^2$. In Fig. 1 the splitting and the resulting frequencies belonging to the spectra are given. The whole frequency tuning range by varying the current in the 250μm section is shown in Fig.2. A record continuous electrical tuning range from 12 to 64GHz is achieved. These results demonstrate the unique tunability of this type of pulse sources.

80GHz pulsation proved by autocorrelation measurements: With increasing frequencies the splitting in the spectra becomes larger and its determination is easier. On the other hand, it becomes difficult to correlate the spectra unambiguously with selfpulsation and not with different higher DFB modes. For prooving the existence of selfpulsations at such high frequencies the analysis of pulse traces by autocorrelation measurements is performed. Fig.3 shows a result. For experimental reasons the pulse shape and the modulation depth could not be extracted from these first measurements. But we can clearly recognize the repetition time of 12.4ps corresponding to a frequency of 80 GHz.

Conclusion: A record selfpulsation frequency of 80 GHz and an extreme large continuous electrical frequency tuning range (12 - 64 GHz) were achieved. Regarding the earlier shown locking feature, the devices enable the generation of all-optically synchronized pulse trains at high and variable frequencies.

This work was supported by the Deutsche Bundespost Telekom.

References:

[1] U. Feiste, D.J. As and A. Ehrhardt: "18 GHz all-optical frequency locking and clock recovery using a selfpulsating two-section DFB laser", IEEE Photonics Technology Lett., vol 6, pp. 106-108, 1994

[2] A. Ehrhardt, D.J. As and U. Feiste, "All-Optical Clock Extraction at 18 Gbit/s by a Self-Pulsating Two-Section DFB-Laser", ECOC 1993, post-deadline paper ThP12.9

[3] U. Bandelow, H.J. Wünsche and H. Wenzel, "Theory of selfpulsations in two-section DFB lasers", IEEE Photonics Technology Lett., vol. 5, pp 1176-1179, 1993

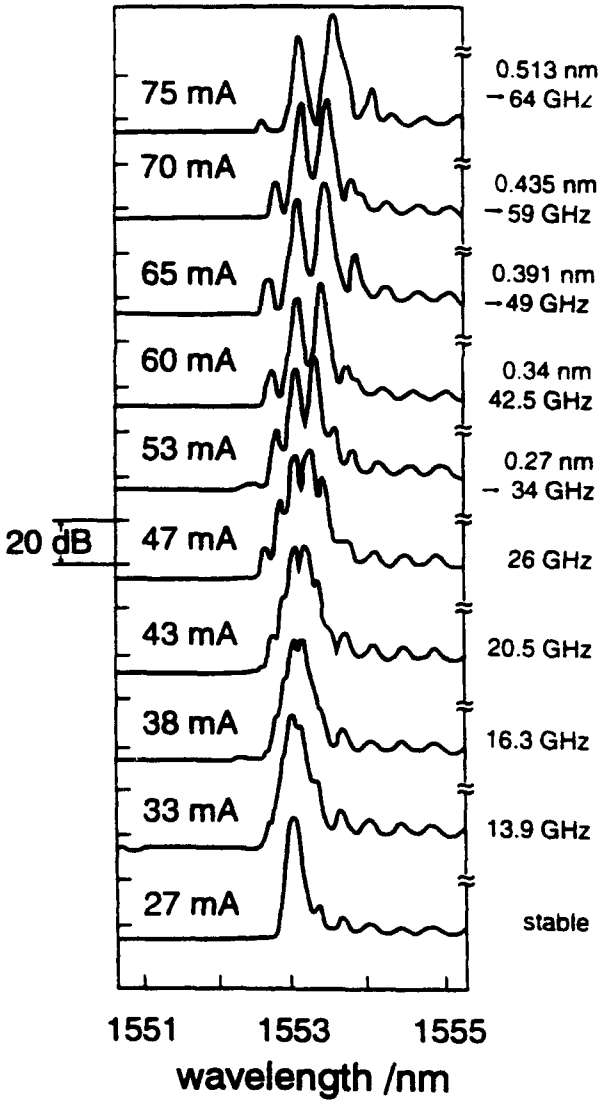

Fig.1
Optical spectra at various currents in the 250μm section. Current in the 300μm section: 50mA. Wavelength splittings and pulsation frequencies are noted.

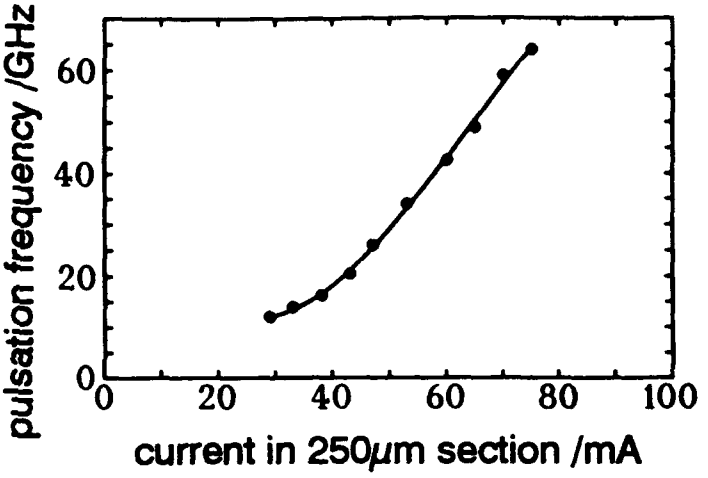

Fig.2
Frequency tuning by varying the current in the 250μm section. Current in 300μm section: 50mA.

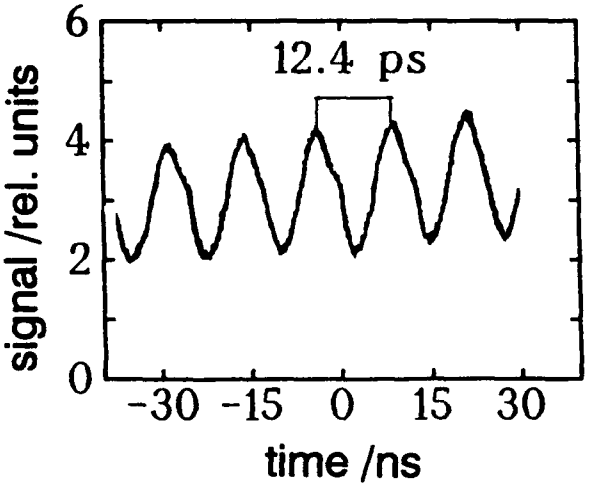

Fig.3
Autocorrelation trace. 80 GHz pulsation frequency detected.

Digital signal regeneration with side-injection-light-controlled bistable laser diode

Koji Nonaka, Yoshio Noguchi, Hiroyuki Tsuda, and Takashi Kurokawa
NTT Opto-Electronics Laboratories
3-1 Morinosato Wakamiya, Atsugi-shi, Kanagawa 243-01, Japan

Abstract
Digital optical signal regeneration with a SILC-BLD markedly improves the bit error rate of the degraded optical signals. The diode can not only regenerates the signal but also converts the signal wavelength at the same time without wavelength filters and isolators.

I.Introduction

All-optical switching nodes would degrade the optical signals in future optical communication networks due to optical path reconfiguration, burst signal ad-drop, wavelength conversion and so on. Using a linear optical amplifier, such as an EDFA, to compensate for system loss, can not improve the signal waveform sufficiently. All-optical signal regeneration devices are promising to construct simple regenerating circuits without O/E and E/O conversion.

We have developed a side-injection-light-controlled bistable laser diode (SILC-BLD) that works as wavelength converter as well as digital regeneration device due to its thresholding amplifier characteristics[1][2][3]. In this paper, we describe the signal regeneration demonstration of degraded optical signals with SILC-BLD.

II. Experiment and result

Figure 1 shows how the SILC-BLD is used to digitally regenerate optical signals with (i) low extinction, (ii) intensity fluctuation and (iii) waveform deformation. The SILC-BLD consists of a main-waveguide laser for output and an orthogonally crossed sub-waveguide for input. The sub-waveguide amplifies input light and conducts it to the saturable absorption region in the main laser cavity. The isolation between input and output is sufficiently large and the back reflection of signals is negligibly small, so no optical isolator and filters are necessary in the regeneration configuration. In this experiment, we used a pn-buried SILC-BLD whose modulation bandwidth is up to 3.6 GHz and switching optical power is around 50 μW. These values are about twice those of the ridge-SILC-BLD we previously reported[2]. The intensity and wavelength of the light input to SILC-BLD were around -4dBm and 1540 nm. The signal intensity was amplified up to 4 dB on fiber to fiber, and wavelength was simultaneously converted to 1553 nm.

Figure 2 shows typical input and output signal and extinction with SILC-BLD. The thresholding characteristics act as a discriminator, suppressing the noise level and amplifying the on-set signal to a constant level, so that output signal level is stable and signal extinction is improved to 17 dB for 622 Mb/s and 1 Gb/s of bit rate.

The effects of digital regeneration with SILC-BLD are shown by the improvements in bit error rate. Figure 3(a) shows typical signal bit error rate with and without SILC-BLD when the initial signal extinction is low(3dB) and when it is high (>13 dB). The SILC-BLD improves up to 4dB of power penalty. Figure 3(b) shows bit error rate with and without SILC-BLD when the initial signal level fluctuates (>1.1 dB) and when it is stable (0 dB). The unstably errorful signal is improved to error-free signals with all-optical regeneration. Both results show the SILC-BLD improves BER by regenerating the signal value from low extinction to high extinction and from an unstable level to stable level.

III. Conclusion

The thresholding amplifier characteristics of the SILC-BLD improves the extinction ratio from 3 dB to 17 dB and intensity fluctuation of optical signals from 1.1 dB to 0 dB. These effects were confirmed by improvement in bit error rates from signal regeneration with the SILC-BLD. The SILC-BLD is very useful because it can not only regenerate optical signals directly but also can convert the signal wavelength at the same time without isolators and filters.

[1] K.Nonaka, H.Tsuda, H. Uenohara, H. Iwamura, and T. Kurokawa, Photon. Technol. Lett.,5,2, 139- 141, 1993.
[2] H.Tsuda, K.Nonaka, K. Hirabayashi, H. Uenohara, H. Iwamura, and T. Kurokawa, Appl. Phys. Lett. 63 (23),6, 3116-3118, 1993.
[3] K. Nonaka, H. Tsuda, K. Hirabayashi and T. Kurokawa, ECOC'93, TuC6.3, 285-288, 1993.

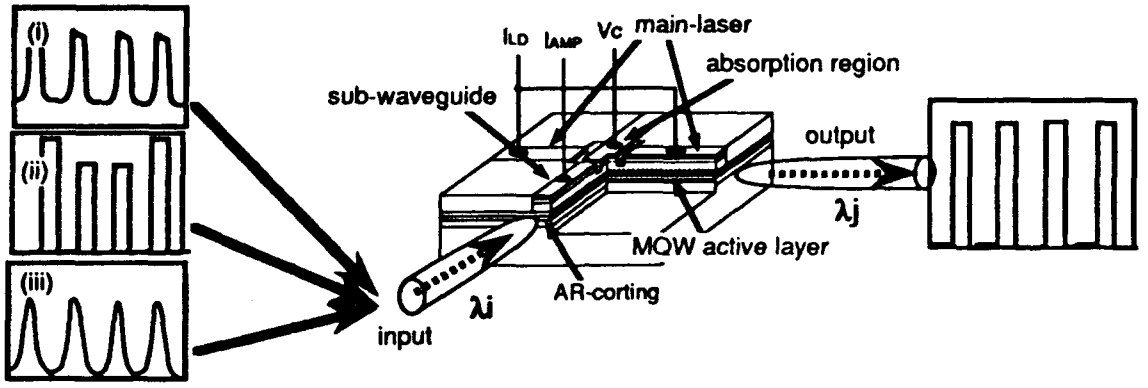

Fig.1: digital signal regeneration of (i)low-extinction (ii)level fluctuating (iii)deformed signals

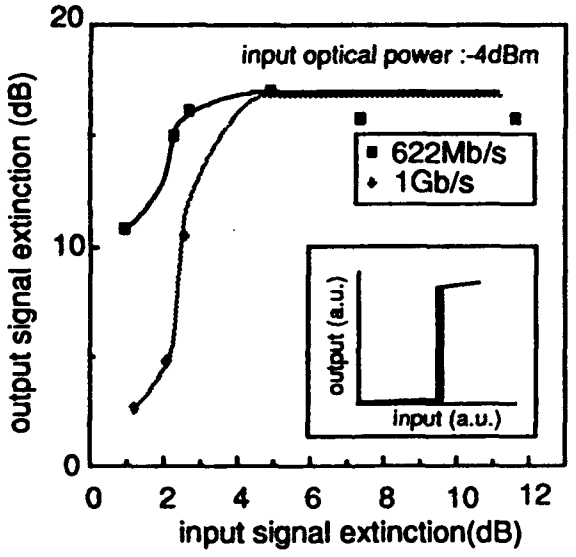

Fig. 2: extinction improvement with SILC-BLD
(inset: optical input and output)

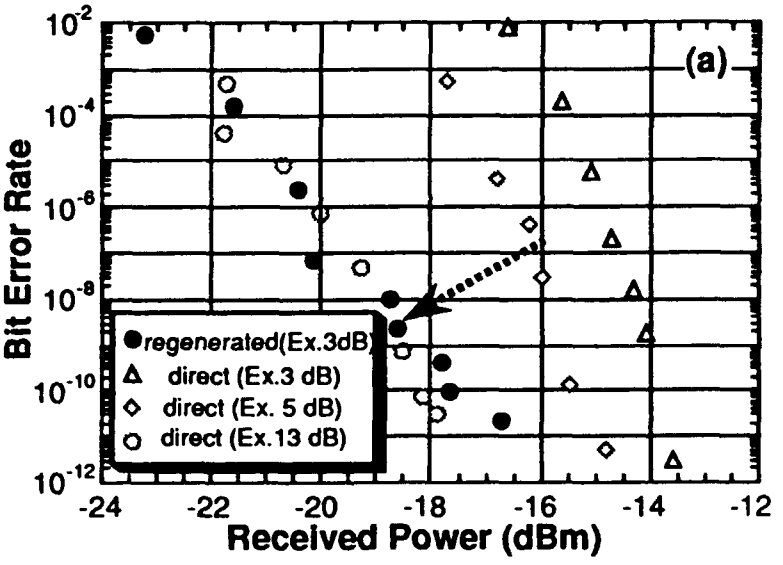

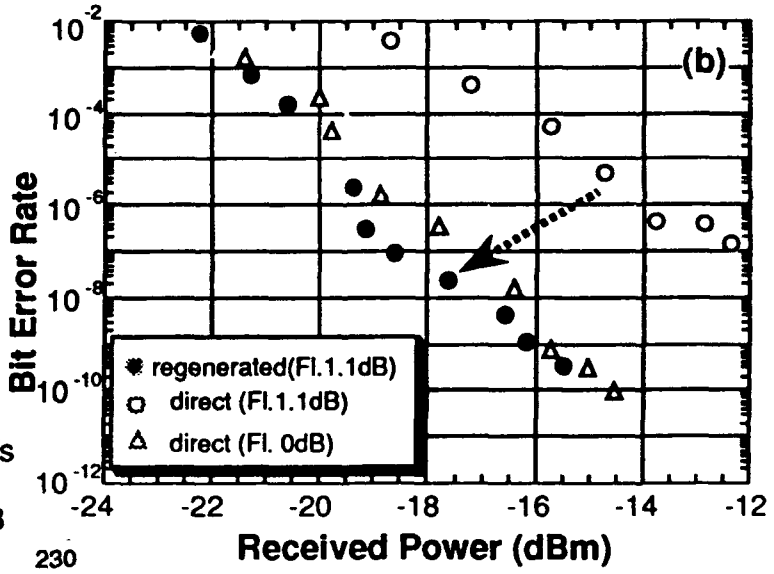

Fig. 3
bit error rate vs. received power for 622 Mb/s data with and without the SILC-BLD.
(a) input signal extinctions of 3 dB and 13dB
(b) input level fluctuation of 1.1 and 0 dB.

Packaged Hybrid Soliton Pulse Source Results and 270 Terabit.km/sec Soliton Transmission using Sliding-Frequency Guiding Filters

P. A. Morton, V. Mizrahi, G. Harvey, L. Mollenauer, T. Tanbun-Ek, R. A. Logan, H. M. Presby, T. Erdogan, A. M. Sergent, K. W. Wecht.

AT&T Bell Laboratories, 600 Mountain Ave., Murray Hill, NJ 07974

Abstract

A fully packaged Hybrid Soliton Pulse Source is described. Excellent stability and tuning characteristics are shown. Error free soliton transmission at 10 GBit/s is achieved over 27,000 km using sliding-frequency guiding filters.

For implementation of long distance soliton based transmission systems it is necessary to provide a simple and practical optical pulse source. This paper describes a fully packaged version of one major contender for this pulse source, together with initial system results on a soliton transmission recirculating loop using sliding-frequency guiding filters.

The Hybrid Soliton Pulse Source (HSPS) [1] is an excellent candidate for a practical pulse source for soliton transmission systems. This device (Fig. 1(a)) incorporates a semiconductor gain element which allows direct electrical pumping of the device, and a Bragg reflector written in a fiber cavity, which provides excellent wavelength and optical bandwidth control [2]. The precise wavelength control afforded by this passive grating is particularly appropriate for systems using sliding-frequency guiding filters [3], especially if wavelength division multiplexing is being used. The HSPS is very simple and easy to manufacture. The use of a linearly chirped Bragg reflector makes the device extremely stable, and allows operation over a very large range of modulation frequencies. This feature allows for manufacturing variations in fabricated cavity length, ensuring that the device will always work at the desired operating frequency.

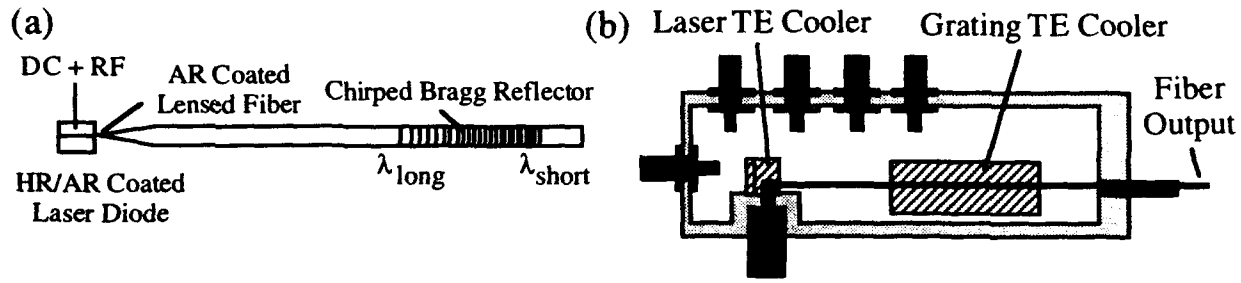

Fig. 1 (a) HSPS schematic and (b) package layout.

The packaged device described in this paper was designed to specifications set by soliton system designers. This ability to meet design parameters set by others is of paramount importance for a practical pulse source. The package layout is shown in Fig. 1(b). The full package is 9x2x1 cm, and includes temperature control of the passive grating to allow very fine wavelength control. Typical output pulses and optical spectra are shown in Fig. 2. The spectra show extremely high rejection of residual Fabry-Perot modes (>40 dB). Fig. 3 (a) shows the small variation in optical pulse-width for large changes in rf power and dc bias to the laser diode. The pulse-width stays consistently around the designed value of 20 ps, this being fixed by the grating bandwidth and chirp rate, together with the differential gain of the laser diode. Fig. 3 (b) shows the wide frequency range over which this device will operate, and the stability of the pulse-width over this large range. It is the smooth and large tuneability of this device over large ranges of drive parameters that make it a practical source. The wavelength is fixed with Å resolution during grating writing, and can be fine tuned with temperature to provide up to 1 nm tuning range.

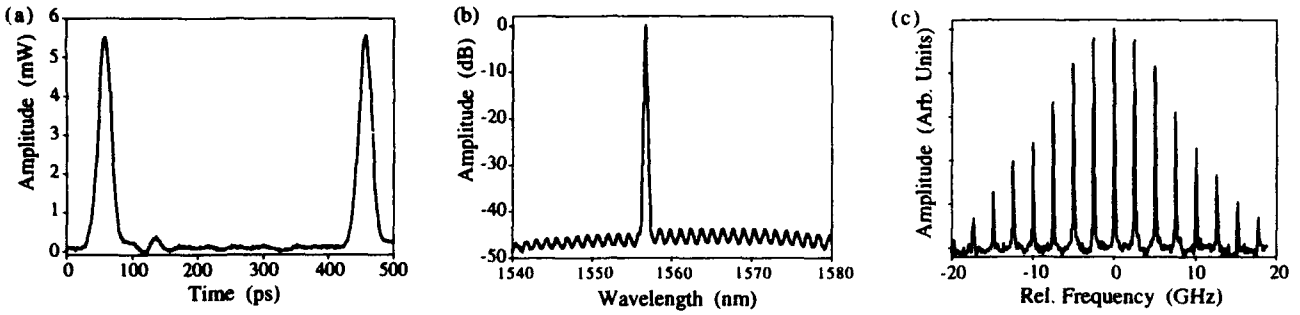

Fig. 2 (a) Typical pulse output, and (b,c) optical spectra

Transmission experiments were carried out on a recirculating loop soliton transmission system, including three sliding-frequency guiding filters, one per optical amplifier [3]. The center frequencies of the three filters are translated in time to provide a linear variation in center frequency versus transmission distance. The 2.5 Gbit/s pulse train is optically multiplexed to 10 GBit/s for transmission, then demultiplexed at the receiving end with a nonlinear loop mirror. Experiments using this soliton transmission setup produced the Bit Error Rate (BER) results shown in Fig. 4. These results show there is no error floor, and error free transmission (10^{-9} BER) is achieved for over 27,000 km transmission distance.

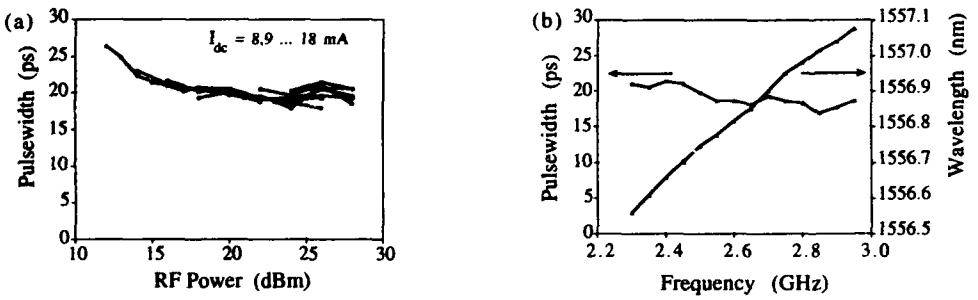

Fig. 3 (a) Pulse-width for various rf drives and dc biases and (b) effect of modulation frequency.

In conclusion, we have demonstrated a fully packaged Hybrid Soliton Pulse Source designed for soliton transmission using sliding-frequency guiding filters. The source is extremely stable and reliable, and produces the required output characteristics over large parameter ranges. The device operates over a large modulation frequency range, and can be fixed in wavelength with great accuracy. The 2.5 Gbit/s bit stream is optically multiplexed to 10 GBit/s. Error free soliton transmission over 27,000 km is achieved in a recirculating loop incorporating sliding-frequency guiding filters.

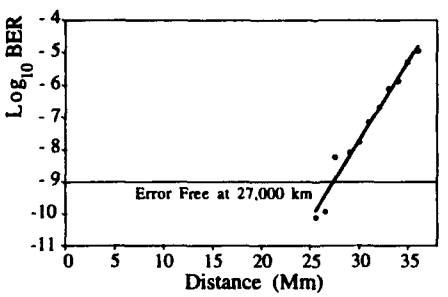

Fig. 4 BER measurements using sliding-frequency guiding filter recirculating loop.

References

[1] P. A. Morton et al., IEEE Phot. Tech. Lett., **5**, p28, 1993.
[2] V. Mizrahi and J. E. Sipe, J. Lightwave Tech. **11**, p1513, 1993.
[3] L. F. Mollenauer, J. P. Gordon, S. G. Evangelides, Optics Letters, **17**, p1575, 1992.

NON-LINEAR CHIRP COMPENSATION IN HIGH-POWER (>100W) BROAD SPECTRUM (~20 NM) PULSES FROM MODE-LOCKED ALGAAS LASERS

A. AZOUZ, N. STELMAKH, P. LANGLOIS, J-M. LOURTIOZ
Institut d'Electronique Fondamentale, URA 22 du CNRS, Bât. 220, Université Paris-Sud, 91405 Orsay Cedex, France, (Ph: 331 69 41 62 99, Fax 331 60 19 25 93)

P. GAVRILOVIC
Research Division, Polaroid Corporation, 21 Osborn Street, Cambridge, Massachusetts 02139, USA (Ph: 617 577 42 37 , Fax 617 494 8230)

Summary

Short-pulse high-power mode-locked laser diodes are of interest for many applications presently covered by conventional femtosecond lasers. Pulsewidths below 300 fs have been reported in recent experiments [1,2], but much smaller widths are expected when considering the large amplification bandwidth of laser diodes. In this paper, we show that very broad pulse spectra (20 nm) can be effectively obtained by active/hybrid mode-locking of long-stripe (1mm) high-power AlGaAs laser diodes, the spectral widths corresponding in principle to sub-100 fs pulses in the transform-limit situation. A novel technique is presented in order to analyze chirp non-linearities (i.e, high-order dispersion effects) in the laser pulses. Second- and third-order dispersion compensation is realized with an external compressor, leading to 160 fs pulses after compression with peak powers in excess of 100 W.

The AlGaAs lasers are separate-confinement single-quantum-well (SQW) lasers with standard ≈1% AR coating on one facet. The active layer is a 170 Å GaAs quantum well in the center of an $Al_{0.35}Ga_{0.75}As$ waveguide layer. Laser emission occurs in a single-transverse mode near 0.83 μm and an average power of ≈20 mW is currently available from the uncoated facet. Active mode-locking is achieved in an external cavity by applying a strong RF modulation (a few watts) near 650 MHz. A saturable absorber created by ion implantation can be added for hybrid mode-locking. Laser pulses are measured by autocorrelation and a streak camera is used for time-resolved spectroscopy.

Pulse chirp non-linearities are analyzed by using a four-pass grating compressor [3] equipped with a holographic grating; the compressor transmission exceeds 70% (fig.1). A precise calibration of the group velocity dispersion (GVD) is realized by interferometry. Third-order dispersion in the laser pulses can be compensated for by a mechanical S-deformation of the rear mirror. Non-linear chirp measurements actually consist in selecting small consecutive parts of the laser spectrum and determining for each part the linear dispersion required for optimal compression. An adjustable slit is introduced in the compressor for this purpose (fig.1). The overall chirp evolution is reconstructed from the different measurements corresponding to different spectral regions.

Fig.2 shows a typical mode-locked pulse spectrum measured under very strong RF modulation (45 dBm). The record spectral width (~20 nm) is related both to the SQW structure parameters and to the high circulating intensity (~100 MW/cm^2), which in turn leads to high gain- and high refractive-index non-linearities in the semiconductor medium. The time-bandwidth product of pulses is much larger than unity in these conditions. Fig.3 shows the chirp evolution deduced from our original method of measurement. As seen, not only second-

order, but also third- and fourth- order phase non-linearities are present in the laser pulses. Figs. 4a and 4b show the autocorrelation traces measured after second- and third- order compensation, respectively. The compressor dispersion is D≈0.7 ps/nm in fig.4a while a wavelength-dependent correction $\partial D/\partial\lambda$ =0.09 ps/nm^2 is introduced in fig.4b. As seen, most of the energy is emitted in one pulse, a strong reduction of side-lobes being achieved in the case of third-order dispersion compensation. The pulsewidth (~160 fs) and peak power (~150 W) evaluated in that case are to our knowledge among the best performances reported to date for a mode-locked laser diode.

(1) P.J. Delfyett et al., IEEE J. Quantum Electron., QE-28, pp. 2203-2219, (1992)
(2) N.Stelmakh et al., Electron. Lett. 29, pp. 160-161, (1993)
(3) O.E. Martinez, IEEE J. Quantum Electron., QE-23, pp. 59-64, (1987)

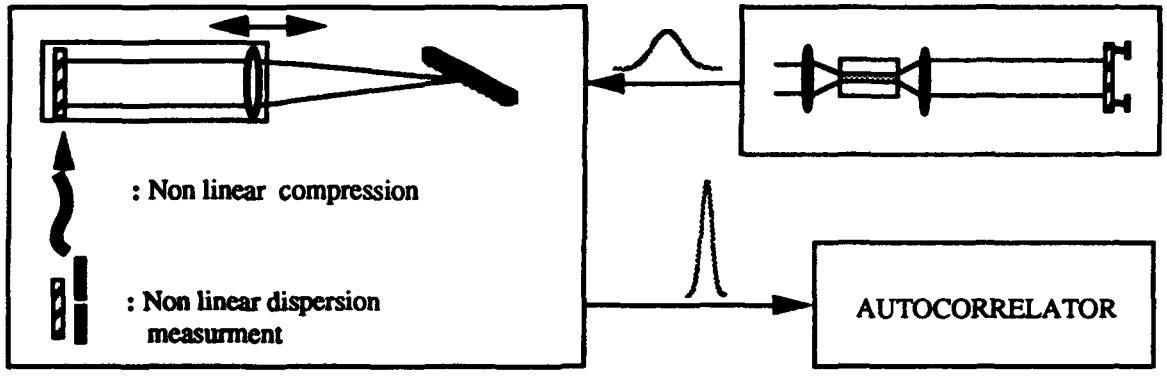

fig 1 Experimental set-up

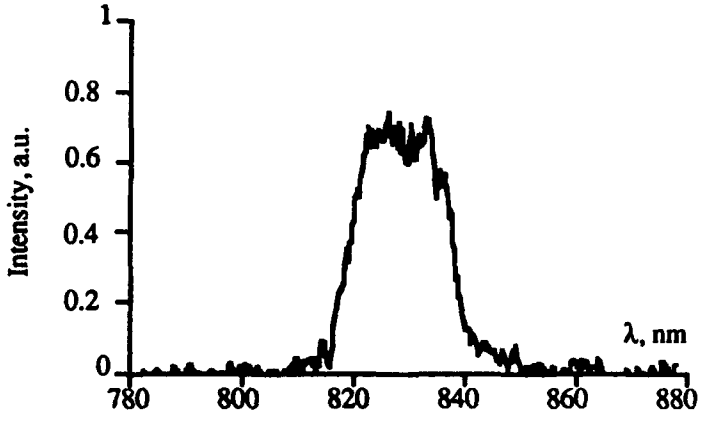

fig 2 Pulse spectrum

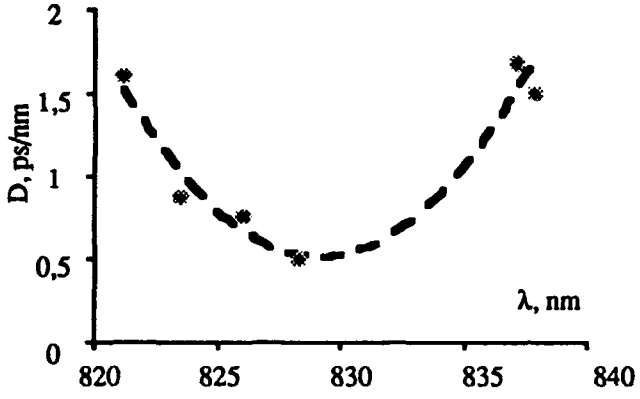

fig 3 GVD

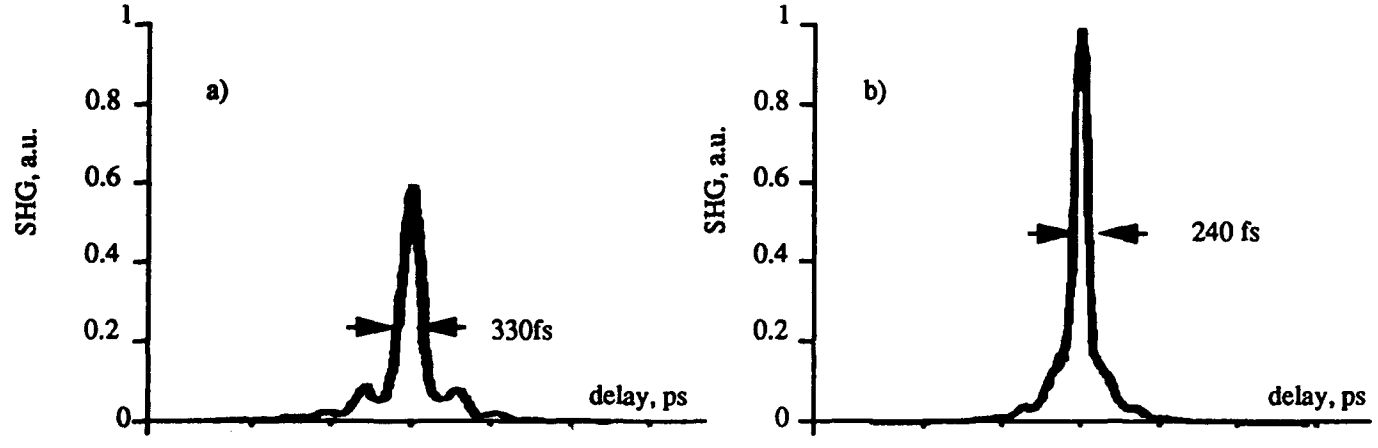

fig 4 Autocorrelation traces after: a) Linear compression
b) Non linear compression

1:30pm - 1:45pm

Th3.1

Sub-Micron Thermography of Laser Diodes by Charging Dielectric Coatings with an Electron Beam

A. Jakubowicz
IBM Research Division, Zurich Research Laboratory, Säumerstr. 4, CH-8803 Rüschlikon, Switzerland

Abstract: *Electron beam charging thermography, a novel scanning electron microscope-based technique featuring submicron resolution and high speed, has been applied to investigate the thermal behavior of laser diodes. Examples presented illustrate the complexity of thermal effects at and adjacent to laser mirrors.*

It is well known that heat effects determine the operation stability of semiconductor laser diodes. Heat production limits the laser's operation power. Thermal effects accelerate gradual degradation and are responsible for the catastrophic failure of these devices. Laser diodes are known to fail due to mirror degradation. Studies of this failure mode have led to the development of techniques to measure mirror temperatures and to image temperature distributions during laser operation ([1,2] and references therein). The resolution of thermographic methods is usually no better than 1 μm. As laser mirrors have lateral dimensions in the range of a few microns, and the entire thickness of the active region (consisting of various materials) is in the submicron range, there is a clear need for techniques offering better resolution.

To provide the capability of localizing heat sources precisely with respect to the laser structure, and to image the hot regions fast and with high resolution, a novel scanning electron microscope (SEM)-based technique, called electron beam charging thermography (EBCT), has recently been proposed [1]. EBCT entails charging a thin insulating film deposited on the laser by scanning the film with a low-energy electron beam in an SEM. Under electron irradiation, when the beam energy, beam current and scanning rate are appropriately selected, a stable charge state is obtained in the insulating film. This film serves as thermographic medium. The appearance of a hot region on the device surface modifies locally the charge in the insulator. This modified charge distribution, induced by device operation, changes the local secondary electron signal accordingly and produces a thermographic image. A detailed discussion of the EBCT technique is presented in [1]. The formation of EBCT contrast is demonstrated in Fig. 1. A thin-film Pt resistor structure was coated with a 0.3 μm thick aluminum oxide layer. The resistor contacts were left uncoated. Without current flow through the resistor no contrast is seen within the area covered by the insulating film. Under current flow, due to the generated heat, a contrast representing the thermographic image of the resistor appears.

Ridge-type GaAs/AlGaAs ([1,2] and references therein), InGaAs/AlGaAs [3], and GaInP/AlGaInP [4] quantum well lasers were investigated. Aluminum oxide and silicon nitride were employed as thermographic media. Figure 2 shows SEM images of the same laser mirror (a) when the laser is off and (b) in operation. During electron irradiation of the non-operating laser, the entire scanned field becomes negatively charged. Laser operation reduces this charge at the active region (arrow in Fig. 2b). This marked contrast represents the thermographic image of the mirror; it disappears when the laser is switched off.

Figure 3 demonstrates the potential of EBCT in terms of spatial resolution. It shows a thermographic image of a laser mirror when the laser operates in a pulsed mode (50 ns pulses with a 2 μs repetition period). The two hot spots are attributed to the two maxima of the laser's near-field emission. The curve in Fig. 3b represents a line-scan through the center of the hot region. From the width of the two peaks, measured at 75% of their height, the resolution is concluded to be 0.25 μm. It was possible to obtain this superior resolution since the pulses were shorter than the time needed to obtain thermal equilibrium in the semiconductor.

When operated in the SEM's TV mode, EBCT offers the unique ability to observe complete thermographic images continuously in time. This can be beneficial for studies of dynamic thermal effects. For example, the thermal drift prior to the thermal runaway at a laser mirror was investigated. At a high constant driving current, EBCT revealed first a large diffuse warm area with a maximum at the active region. In time, the EBCT contrast not only increased as a whole, it also increasingly concentrated on a small spot located in the active region. This behavior, illustrated in Fig. 4, is likely to have been caused by thermal focusing.

The attractivity of EBCT as a microscopy tool stems also from the unique ability to work simultaneously with standard SEM and related techniques such as EBIC (electron beam-induced current). For GaAs/AlGaAs lasers, a combined EBIC/EBCT investigation of cleaved mirrors and chemically assisted ion-beam-etched mirrors, with and without sulfur passivation, has been performed. In non-passivated devices, EBIC has revealed the occurance of laser operation-induced diffusion of beryllium from the *p*-type cladding. In devices with dry-etched mirrors passivated with sulfur, in-diffusion of sulfur from the mirror into the crystal has been detected. As both elements act in the bulk as shallow dopants, after some time of laser operation the active and adjacent regions at and behind the mirror become, respectively, *p*- or *n*-type doped. During this laser operation-induced mirror doping the *p-n* junction migrates towards the *n*-type or *p*-type cladding, respectively. Using EBCT, it has been demonstrated that this process can result in heat generation at laser mirrors.

A standard SEM investigation of the degradation of uncoated mirrors of GaInP/AlGaInP lasers with AlGaAs claddings [4] has revealed laser operation-induced modifications at the mirrors correlating with the

AlGaInP/AlGaAs interfaces in the claddings. Consistently, combined EBIC/EBCT observations have shown that the maxima of the hot areas are located not at the laser's active region, but correlate with the AlGaInP/AlGaAs interfaces.

In all previous examples EBCT was applied to investigate laser mirrors. However, this technique can also be used to investigate thermal effects along the laser's waveguide. Non-destructively, i.e. without removing the ridge metallization, the formation of hot regions several microns behind the laser mirror was observed during thermal roll-over experiments with InGaAs/AlGaAs lasers.

[1] A. Jakubowicz, J. Appl. Phys. 74, 6488 (1993).
[2] A. Jakubowicz, A. Oosenbrug, and Th. Forster, Appl. Phys. Lett. 63, 1185 (1993).
[3] A. Moser, A. Oosenbrug, E.E. Latta, Th. Forster, and M. Gasser, Appl. Phys. Lett. 59, 2642 (1991).
[4] P. Unger, G.-L. Bona, R. Germann, P. Roentgen, and D.J. Webb, IEEE J. Quantum Electron. 29, 1880 (1993).

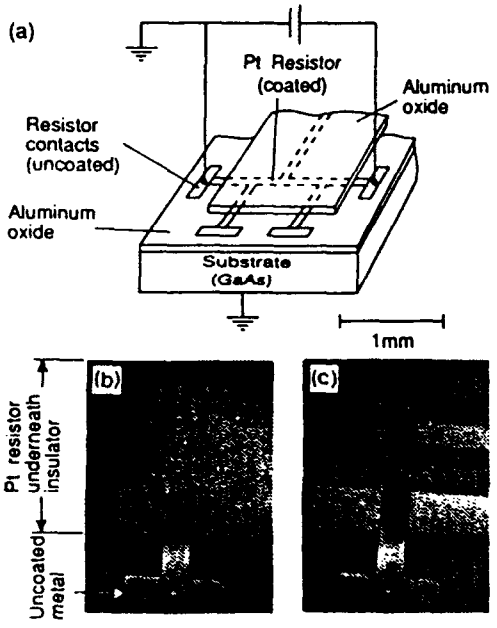

Fig. 1. Formation of EBCT contrast; (a) test sample, (b) SEM image without heating (resistor current: 0 mA), (c) same part of the resistor structure as in (b), taken at 200 mA (from [1]).

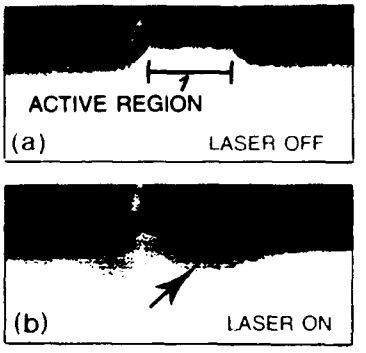

Fig. 2. Formation of EBCT contrast at a laser mirror; (a) laser off, (b) laser on (from [1]).

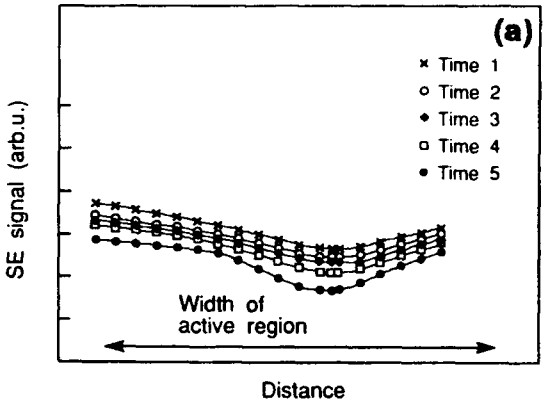

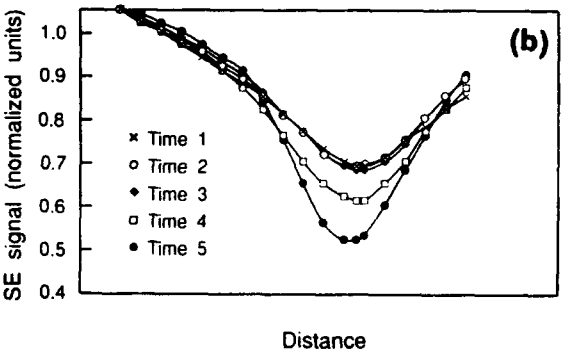

Fig. 4. SEM secondary electron signal profiles along the active region of the laser in Fig. 2, recorded with a time interval of 10 seconds (current: 160 mA) (from [1]).

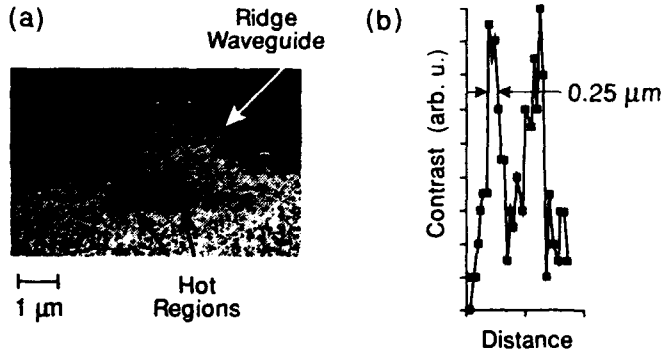

Fig. 3. (a) EBCT image of a laser mirror; (b) contrast at the center of the hot spots along the laser's active region (from [1]).

1:45pm - 2:00pm
Th3.2

New Insight Into the Temperature Sensitivity of the Threshold Current of Long Wavelength Semiconductor Lasers

J.D. Evans, and J.G. Simmons
McMaster University, Department of Engineering Physics, Hamilton, Ontario, Canada, L8S 4M1

Abstract

A new relationship describing the threshold current *vs.* temperature relation of InGaAsP/InP lasers is proposed. The commonly used characteristic temperature, T_o, is replaced by a new, temperature insensitive, parameter T_{max} which represents the lasers' maximum operating temperature.

In the past twenty years there has been considerable effort spent in attempting to explain the temperature dependence of the threshold current, I_{th}, of InGaAsP/InP based semiconductor lasers. This effort stems from the importance of these lasers for optical communications systems and the desire to achieve lasing of these lasers at high operating temperatures (>100°C) without the use of thermoelectric coolers.

An exponential relationship describing the temperature dependence of semiconductor lasers was first proposed by Pankove in 1968[1]. This relationship, which is given by:

$$I_{th} = I_o \exp(T/T_o), \tag{1}$$

where T_o and I_o are the characteristic temperature and current, respectively, was based on empirical observations, and has since become widely accepted. Due to the wide acceptance of this relationship, much of the effort to explain the temperature dependence of semiconductor lasers has centered on finding a single dominant physical mechanism, such as intervalence band absorption[2] or Auger recombination[3], that can affect the laser threshold condition with an exponential temperature dependence. This is particularly true for InGaAsP/InP lasers above room temperature. The wide use of Pankove's relation has even resulted in other laser parameters, such as the internal efficiency, the modal gain, the threshold carrier density and the transparency current density being ascribed an exponential temperature dependence[4], without any physical basis. It should be noted, however, that, although they are defined as characteristic parameters, *T_o and I_o actually vary with temperature* . In addition, in his original article Pankove indicated that "there [was] no explicit demonstration that an exponential dependence [of I_{th}] on temperature should be obtained." Other authors have also suggested that (1) needs to be re-examined or is inappropriate[5,6].

We have examined the temperature sensitivity of the threshold current density, J_{th}, for a variety of strained and unstrained MQW laser structures, in terms of the temperature rate of change of J_{th}, as given by:

$$\nabla_T J_{th} \equiv \frac{J_{i+1} - J_i}{T_{i+1} - T_i} \equiv \frac{\partial J}{\partial T}, \tag{2}$$

in relation to the threshold current density, J_{th}. As shown in Fig. 1, a previously unobserved strong correlation was found between $\nabla_T J_{th}$ and J_{th}. The quantity $\nabla_T J_{th}$ was found to be related to J_{th} by the power law expression:

$$J^m/(\nabla_T J_{th}) = C, \tag{3}$$

where, C, unlike T_o, is an essentially *temperature and length independent* constant that depends on the device active region structure, and m had a value of ≈3/2 for all devices studied. By treating the empirically determined expression of (1) as a mathematical relationship and integrating it, a new expression describing variation of the threshold current density with temperature has also been arrived at. This expression is given by:

$$J_{th} = \left[\frac{n}{C}(T_{max} - T)\right]^{-1/n}, \tag{4}$$

where $n = m-1$, and T_{max}, which represents the theoretical maximum operating temperature of the laser, is the constant of integration. Figure 2 shows fit of (4) to the J_{th} *vs.* T data for two strained MQW lasers of different lengths. Also shown in Fig. 2, for comparative purposes, is the fit of Pankove's equation, (1), to the data between -50°C and -30°C for one of the structures. Clearly (4) gives a much better fit (correlation factor R=0.9999) to the data than does Pankove's exponential relationship. In addition, an explanation of the results of Fig. 1 may lead to new physical insight into the cause of the threshold current temperature sensitivity of InGaAsP/InP based semiconductor lasers for use in optical communications systems.

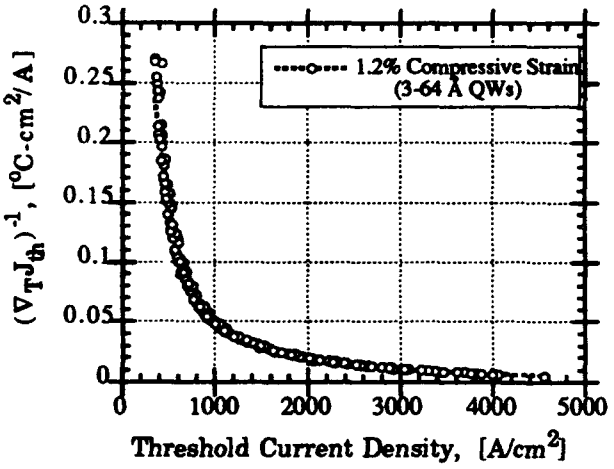

Figure 1: Inverse temperature sensitivity of threshold current density *vs.* J_{th} for compressively strained MQW laser structures of lengths ranging from 250-1500μm.

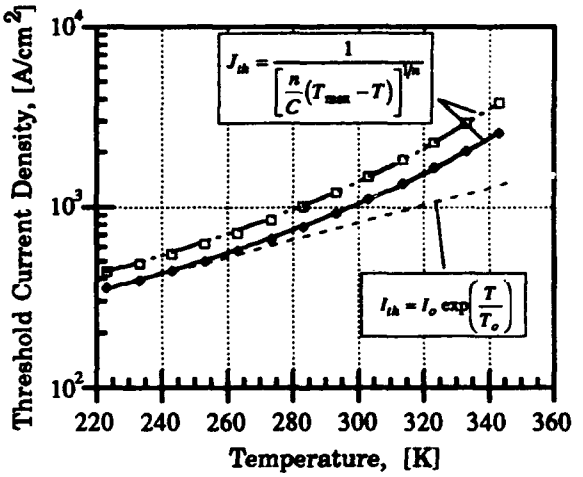

Figure 2: Comparison of fit of (4) and (1) to J_{th} *vs.* temperature data for two compressively strained MQW lasers of different lengths.

REFERENCES

[1] Pankove, J.I., IEEE J. Quantum Electron. **4**(4) pp.10-13, 1968.
[2] Asada, M., and Suematsu, Y., IEEE J. Quantum Electron. **19**(6), pp.917-923, 1983.
[3] Dutta, *et. al.* Appl. Phys. Lett. **58**(11), pp.1125-127, 1991.
[4] Zah, C.E., *et. al.* To be published, IEEE J. Quantum Electron. **30**(1), 1994.
[5] Leopold M.M., and Specht, A.P., Appl. Phys. Lett. **50**(20), pp. 1403-1404, 1987.
[6] O'Gorman *et. al.* Appl. Phys. Lett. **60**(2), pp.157-159, 1992.

Study of gain in determining T_0 of 1.3μm semiconductor lasers

D. A. Ackerman, P. A. Morton, R. F. Kazarinov, M. S. Hybertsen, G. E. Shtengel, T. Tanbun-Ek and R. A. Logan

AT&T Bell Laboratories
Murray Hill, New Jersey, USA 07974

Extensive measurements on 1.3μm semiconductor lasers show the dominant role of gain in threshold temperature dependence. Material gain is decomposed into two components using chemical potential in order to isolate deviation of theoretical predictions from experimental results.

Motivation

A high volume market exists for 1.3μm semiconductor lasers operating over a wide temperature range with reduced temperature sensitivity. This drives the search for understanding of T_0, a parameter describing the temperature dependence of threshold. Recently, gain has been determined as the dominant cause of low T_0 in 1.3μm strained multi-quantum well (MQW) and bulk lasers[1] and in 1.55μm strained MQW lasers[2]. In the present investigation, we focus experimentally and theoretically upon gain in 1.3μm semiconductor lasers. We seek to isolate a mechanism underlying the strong, observed temperature dependence.

Experiment

Several designs of 1.3μm compressively strained MQW as well as simple bulk active lasers were examined in the present study. All devices contained buried heterostructures laser cavities approximately 1μm in width surrounded on each side by InP current confining layers. Lasers tested were 250 to 300μm in length with uncoated facets bonded substrate-side down on ceramic submounts.

Net modal gain vs. photon energy was measured for temperatures between 25 and 85°C for each device as a function of sub-threshold current using a spectral fringe contrast method[3] which includes correction for spectrometer resolution. Material transparency as a function of current and temperature was determined by nulling voltage modulation across a device into which a small, tunable, single-frequency, ac probe signal was injected[4]. Measured transparency energies were checked against the crossing point of TE- and TM-polarized gain spectra[5]. Comparison of maximum net gain to loss at transparency gives a measure of total modal gain.

Differential carrier lifetime τ_d was determined as a function of sub-threshold current I and temperature by measuring the sub-threshold frequency response of spontaneous emission collected from a laser facet under small signal current modulation[6]. Internal efficiency η_i was estimated by comparing threshold external slope efficiency $L_{th}'(I)$ to the ratio of mirror to total loss. Carrier density was then determined by integrating τ_d over the product $(I \cdot \eta_i)$ assuming a current dependence of η_i extrapolated from that of above-threshold $L'(I)$. This treatment represents an extension of that described in reference 7.

Results

Gain and loss plotted against carrier density for various temperatures are shown in Figure 1 for a representative bulk active laser. The crossing of net gain and net loss curves occurs at threshold carrier density $n_{th}(T)$. Previous work[1,2] has demonstrated temperature insensitivity in the relationship of current vs. carrier density, suggesting that recombination processes are at most weakly temperature dependent. Thus, the temperature dependence of threshold current is primarily determined by that of threshold carrier density which is, in turn, determined by that of gain. In particular, the temperature dependence of differential gain dg/dn and transparency carrier density n_0 appears to determine $n_{th}(T)$ in both bulk active and MQW 1.3μm lasers[1].

To understand the origin of temperature dependence of material gain G, we examine the dependence of G on transparency energy, i.e. separation in quasi-Fermi levels or chemical potential μ. We separately examine the dependence of μ on carrier density.

Total material gain G (modal gain divided by calculated active layer confinement factor) is plotted against μ, in Figure 2 for the bulk active laser of Figure 1. We observe that curves for various temperatures are nearly parallel and offset by energies characteristic of bandgap shrinkage over the temperatures range. Slopes dG/dμ of curves in Figure 2 appear to be largely temperature independent decreasing only ~10% between 25 and 85°C. Following reference 1, we can assign to dG/dμ a negligibly high component of T_0 of ~550K.

Similar plots of μ vs. carrier density n for the same laser are shown in Figure 3 for the same temperatures. In contrast to the data of Figure 2, we observe ~35% decrease in dμ/dn at constant gain between 25 and 85°C. To dμ/dn, we can assign a T_0 component of 160K. Results such as shown in Figures 2 and 3 are observed for all 1.3μm MQW and bulk active lasers examined. Noting that differential gain is the product of the slopes pictured in Figures 2 and 3, we conclude that the temperature dependence of differential gain is dominated by that of dμ/dn.

Gain modeling

Material gain for bulk quaternary material with peak gain near 1.3μm was modeled using an eight band k·p

model to represent the energy bands and optical matrix elements[8] with standard literature values used as input parameters to the model. Non-parabolicity and warping of the hole bands are included naturally in this treatment. Three dimensional Brillouin zone integrations were performed to obtain spontaneous emission and material gain. The quasi-Fermi level separation was corrected for temperature and for many-body effects due to the electron-hole plasma.

We find ~7% drop in calculated dG/dμ between 25 and 85°C, in good agreement with data of Figure 2. However, calculated dμ/dn is considerably less temperature sensitive than that shown in Figure 3 decreasing by only ~14% between 25 and 85°C. The present eight band k·p model, although a good representation of the energy gands for intrinsic, bulk material, does not provide the degree of temperature sensitivity of gain observed in our experiments.

Conclusions

Measurements of gain, loss, internal efficiency, and chemical potential as functions of carrier density and temperature have been performed on 1.3μm MQW and bulk active lasers. We find that T_0 ~ 55K for all of the devices examined. This undesirably low value arises from a strong temperature dependence of gain. We have decomposed the gain-related components of T_0 to find that change in chemical potential with carrier density rather than change of gain with chemical potential determines the temperature dependence of differential gain.

References

1. D. A. Ackerman, P. A. Morton, R. F. Kazarinov, T. Tanbun-Ek and R. A. Logan, *Proc. InP and Related Materials Conf.*, Santa Barbara, CA, pp. 466-468,1994.
2. Y. Zou, J. S. Osinski, P. Grodzinski, P. D. Dapkus, W. C. Rideout, W. F. Sharfin, J. Schlafer and F. D. Crawford, *J. Quantum Electron.* **29**, pp. 1565-1575, 1993.
3. D. T. Cassidy, *J. Appl. Phys.* **56**, pp. 3096-3099, 1984.
4. P. A. Andrekson, N. A. Olsson, T. Tanbun-Ek, R. A. Logan, D. L. Coblentz and H. Temkin, *Electron. Lett.* **28**, pp. 171-172, 1992.
5. E. A. Avrutin, I. E. Chebunina, I. A. Eliachevitch, S. A. Gurevich, M. E. Portnoi and G. E. Shtengel, *Semicond. Sci. Technol.* **8**, pp. 80-87 (1993).
6. R. Olshansky, J. LaCourse, T. Chow and W. Powazinik, *Appl. Phys. Lett.* **50**, pp. 310-312, 1987.
7. G. H. B. Thompson, *Electron. Lett.* **19**, pp. 154-155, 1983.
8. D. Gershoni, C. H. Henry and G. A. Baraff, *J. Quantum Electron.* **29**, pp 2433-2450, 1993.

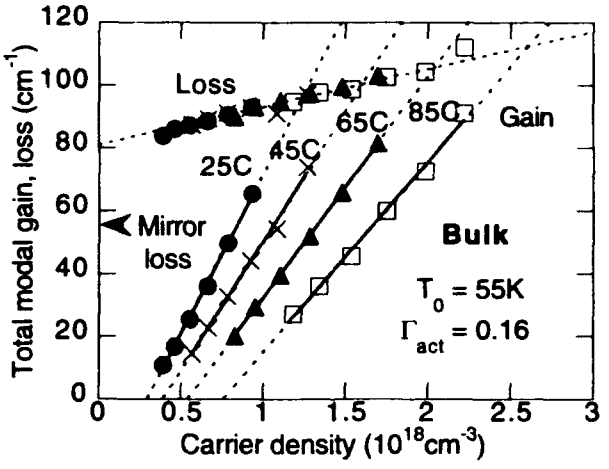

Figure 1. Modal gain and loss vs. carrier density and temperature for a representative bulk active laser. Gain slope dg/dn and transparency carrier density appear strongly temperature dependent.

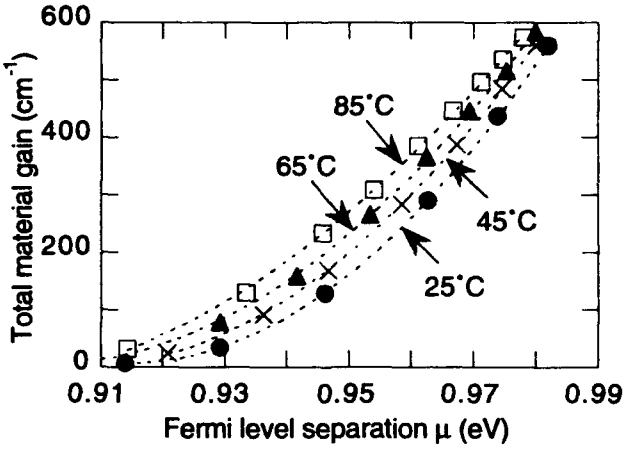

Figure 2. Total material gain versus Fermi level separation μ and temperature showing weak temperature dependence of dG/dμ.

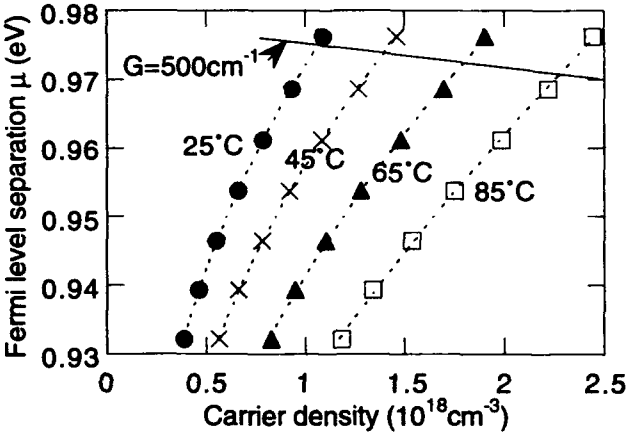

Figure 3. Fermi level separation μ versus carrier density and temperature including a contour of constant gain at (~80% of threshold) showing strong temperature dependence of dμ/dn.

Variation of Kink power with cavity length in weakly index guided semiconductor lasers

C.J. van der Poel, M.F.C. Schemmann and G.A. Acket
Philips Optoelectronics Centre
PO Box 80000, 5600JA Eindhoven, The Netherlands

A periodic dependence of kink power on laser length is observed and explained. Weakly index guided high power stripe lasers in the AlGaAs, InGaAlP and InGaAlAs material systems are studied and periods of 100 to 350 μm are found. The observations indicate that phase locked fundamental and first order modes exist at certain laser lengths. This new model fully explains the oscillatory behaviour of the kink power and the correlated changes in lateral far field distributions at the front and rear mirror facets.

For many applications it is required that narrow stripe high power laser diodes emit their power in a stable diffraction limited far field. As a result of mode instabilities and output power fluctuations at high injection currents, high power narrow stripe diodes appear limited in maximum diffraction limited output power. The transition from diffraction limited to non-diffraction limited operation is observed as a kink in the light versus current curve. In this paper, the limits on kink power are investigated for high power lasers in the wavelength range between 670 and 980 nm.

The waveguide structures studied here can be classified as weakly index guided. The designs however are quite different: for $\lambda = 780$ nm, a ridge-type waveguide structure with a bulk AlGaAs active layer, for $\lambda = 670$ nm a buried-ridge type structure with strongly absorbing GaAs current blocking layers and a double quantum well strained InGaP/AlInGaP active layer, and for $\lambda = 980$ nm a buried-ridge type structure with transparent InGaP current blocking layers and a double quantum well strained InGaAs/AlGaAs active layer are studied, respectively.

Figure 1 gives typical L/I and dL/dI curves of a 780 nm laser. Above the kink power level the far field is observed to shift. Figure 2 gives kink power data as a function of laser length for the 670, 780 and 980 nm devices, respectively. Clearly a periodic variation of kink power as a function of laser length is observed with periods of 350 μm, 110 μm and 100 μm, respectively. The data in figure 2 show a common systematic large variation of kink power level with laser length for very different waveguide geometries and material systems. The results indicate that the kink mechanism is of the same origin for all laser types. Such systematics and the corresponding kink mechanism have, up till now, not been reported in the literature.

A new model is proposed to explain the kink behaviour. This model assumes that phase locked fundamental and first order lateral modes propagate in a laser above the kink power level. A necesssary additional condition for phase locking is that both fundamental and first-order modes, with respective propagation constants β_0 and β_1, simultaneously have to satisfy the cavity roundtrip phase condition. The beat length $L = \frac{2\pi}{\beta_0 - \beta_1}$ therefore plays a decisive role in kink phenomena. More extended modelling results describing these

phenomena will be presented and compared with experimental data. Above the kink, the combination of fundamental and first order modes results in a hybrid mode zig-zagging periodically through the laser cavity along the laser length. Depending on the number of periods in the cavity the mode patterns at front and rear mirror should subsequently appear identical or be each others mirror image. The lateral far field shift directions at front and rear mirrors must therefore be correlated. In figure 3 the experimentally observed lateral far fields below and above the kink power level for a 670 nm wavelength laser are given at different laser lengths. The results are seen to confirm the model prediction.

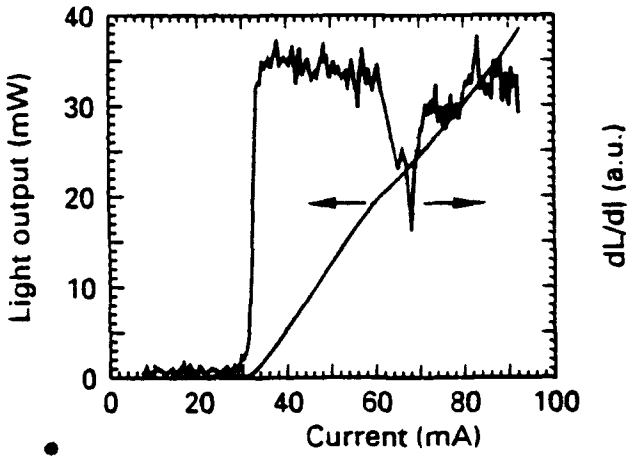

Figure 1

L/I and dL/dI curves of ridge waveguide laser with a kink at 20 mW.

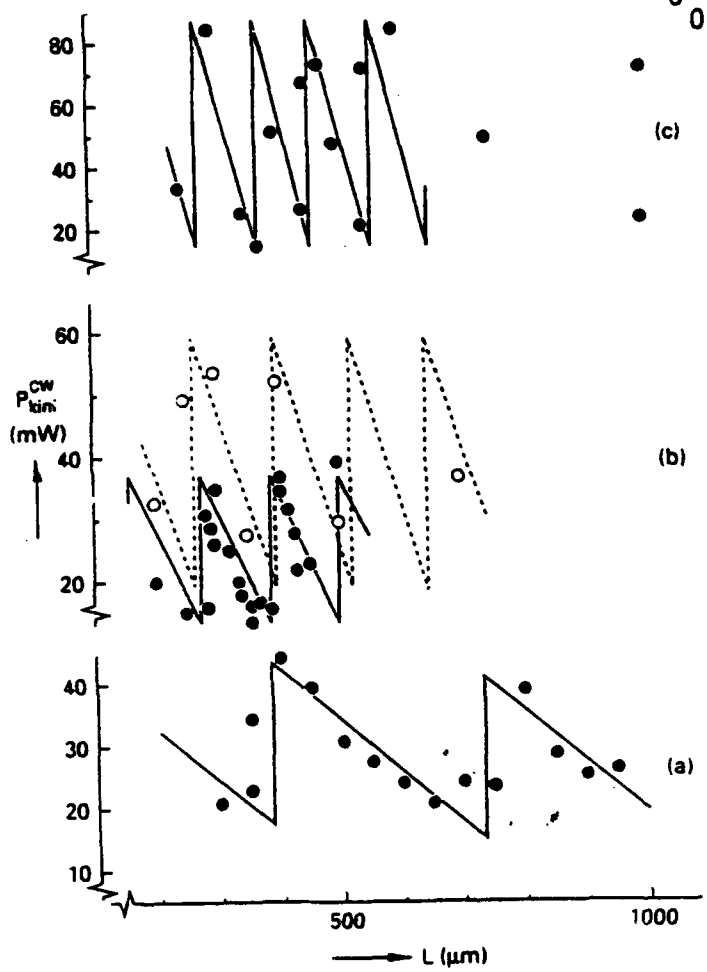

Figure 2

Kink Power versus laser length for devices with a wavelength of a) 670 nm, b) 780 nm and c) 980 nm.

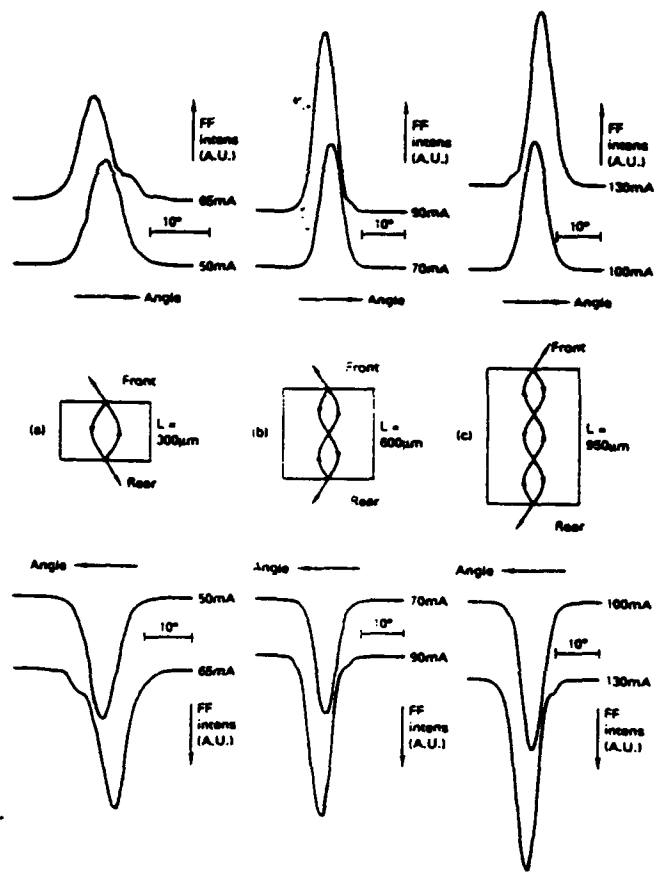

Figure 3

Front and backfacet Far Field for laser lengths of a) 300 um, b) 600 um and c) 950 um.

Real Index Guided AlGaInP Visible Laser with High Bandgap Energy AlInP Current Blocking Layer Grown by HCl-Assisted Metalorganic Vapor Phase Epitaxy

Ryuji Kobayashi, Hitoshi Hotta, Fumito Miyasaka, Kunihiro Hara and Kenichi Kobayashi
Opto-Electronics Research Laboratories, NEC Corporation
34 Miyukigaoka, Tsukuba, Ibaraki 305, JAPAN
PHONE +81-298-50-1151, FAX +81-298-50-1106

INTRODUCTION High power AlGaInP visible light lasers have been developed intensively for light sources in high density optical disk systems. A ridge stripe buried in a GaAs current blocking layer is used for the optical waveguide[1]. By replacing the GaAs layer to a high bandgap energy $Al_{0.5}In_{0.5}P$ layer, we take a great advantage of the optical loss reduction, resulting in laser characteristics improvement, because $Al_{0.5}In_{0.5}P$ is completely transparent for the laser light. However, it had been difficult to grow Al-contained semiconductor layers selectively by conventional MOVPE. Recently, Shimoyama et al. reported selective growth of AlGaAs by HCl-assisted MOVPE[2]. In this paper, we report, for the first time, 680 nm real index guided AlGaInP lasers with $Al_{0.5}In_{0.5}P$ current blocking layers, which were realized by selective growth of $Al_{0.5}In_{0.5}$.P using HCl-assisted MOVPE.

SELECTIVE GROWTH Figures 1(a), (b) show cross-section SEM images of AlInP layers grown on GaAs (001) mesa-substrates at 660℃ with and without HCl addition, respectively. The mesa top was covered by SiN_X. AlInP layers were selectively grown by a small amount of HCl addition (4.1×10^{-6} mol/min). The Al content X increased and the growth rate decreased with an increase in HCl mole ratio, as shown in Fig. 2. This is because In-chloride desorption was enhanced by HCl. Furthermore, Al contents were found to be different between at the ridge side and at the flat area. Therefore, mole ratio between HCl and source gasses were precisely controlled in order that AlInP blocking layers were lattice-matched to the substrate at both sides of the ridge stripe in the laser fabrication.

LASER STRUCTURE AND CHARACTERISTICS Figure 3 shows a schematic cross-section view of the real index guided AlGaInP high power laser (AlInP buried laser). The active layer consists of four 0.3% compressive strained 10 nm-thick $Ga_{0.47}In_{0.53}P$ wells, separated by three lattice-matched 5 nm-thick $(Al_{0.6}Ga_{0.4})_{0.5}In_{0.5}P$ barriers. Figure 4 shows light output power-current (L-I) curves comparing AlInP buried lasers with GaAs buried lasers. Remarkable threshold current reduction as well as slope efficiency increase were observed for AlInP buried lasers. The measured internal loss for a AlInP buried laser was 14 cm^{-1}, which was 40% smaller than that for a GaAs buried laser. An L-I curve under CW operation and far field patterns are shown in Fig. 5. Stable fundamental transverse mode operations were obtained. No kinks were observed up to 55 mW.

CONCLUSION Selective growth of high bandgap energy AlInP layers were established by HCl-assisted MOVPE and applied to real index guided AlGaInP high power lasers for the first time. Reduction in threshold current and increase in slope efficiency were obtained. CW operation over 50 mW without any kinks was achieved.

ACKNOWLEDGEMENTS The authors would like to thank Kohroh Kobayashi and Ikuo Mito for their encouragement, and to Kentaro Tada for useful discussions.

REFERENCES

1) Y. Ueno, H. Fujii, H. Sawano, K. Kobayashi, K. Hara, A. Gomyo and K. Endo: IEEE J. Quantum Electron. **29**(1993)1851.
2) K. Shimoyama, Y. Inoue, K. Fujii and H. Gotoh: J. Crystal Growth **124**(1992)235.

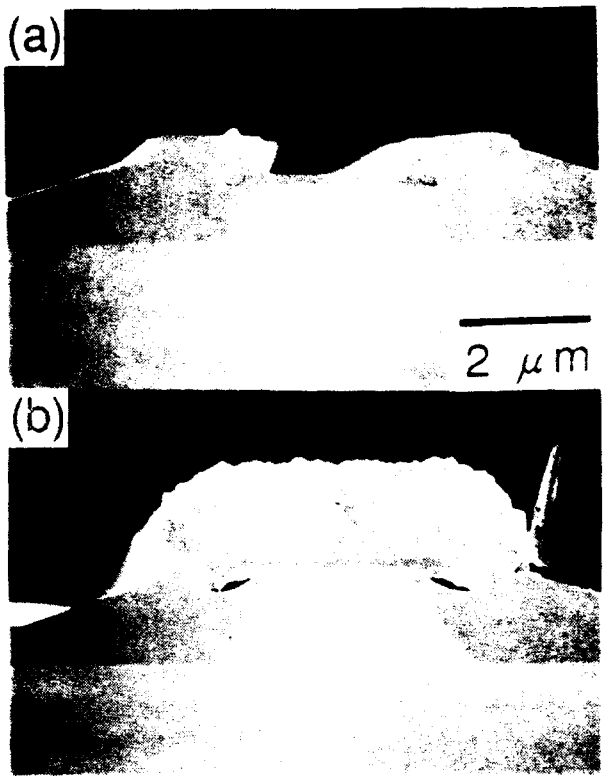

Fig. 1 Cross-section SEM images of AlInP grown on GaAs (001) mesa-substrate (a)with HCl (4.1×10^{-6} mol/min) and (b)without HCl addition.

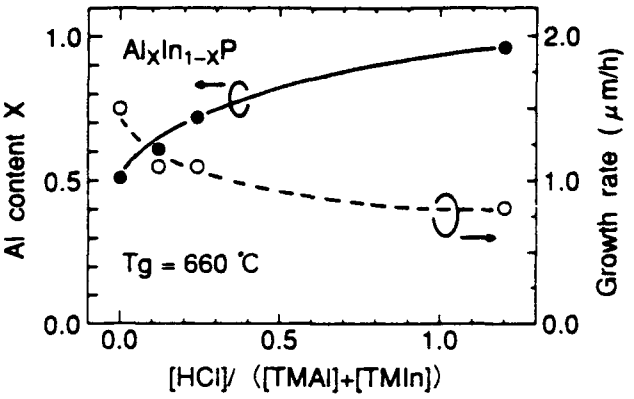

Fig. 2 Al content X and growth rate of AlInP versus HCl mole ratio. The mole fractions of TMAl and TMIn are kept to be 1.4×10^{-5} and 1.9×10^{-5} mol/min, respectively.

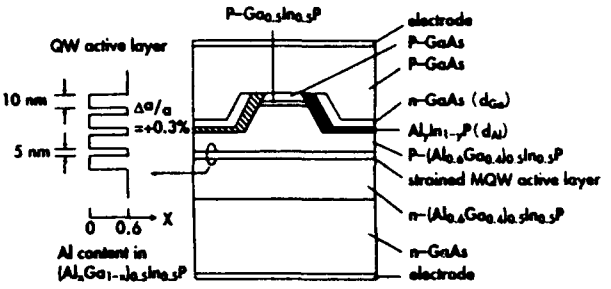

Fig. 3 Cross-section view of real index guided AlGaInP laser.

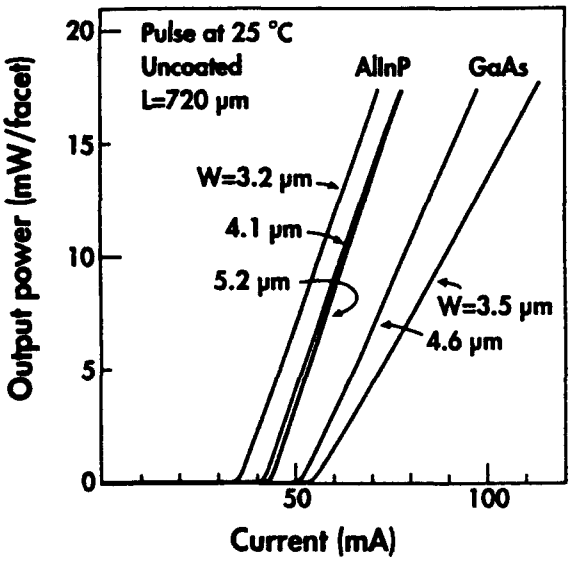

Fig. 4 L-I curves under pulse operation at 25°C. L-I Curves for GaAs buried lasers are also shown for comparison.

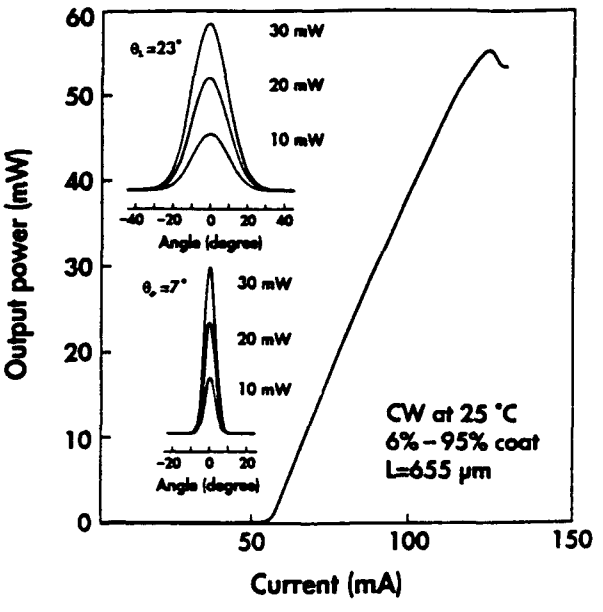

Fig. 5 L-I curve and far field patterns under CW operation. The front and rear facet reflectivities are 6% and 95%, respectively. The mesa bottom width is 5.2 μm.

2:45pm - 3:00pm
Th3.6

Tunable 2.7-3.7 um InAsSb(P)/InAsSbP low threshold diode lasers

Yu.P.Yakovlev, A.N.Baranov, A.N.Imenkov, V.V.Sherstnev

A.F.Ioffe Physical Technical Institute
194021, St.Petersburg, Polytechnicheskaya 26, Russia
Fax: (812) 247-1017, Tel.: (812) 247 9956

The main applications of mid-infrared diode lasers are the high resolution spectroscopy. Recently low threshold 3.3 um lasers on the base InAs solid solution was created for spectroscopy of methane [1]. This report is devoted to study the temperature dependence of the threshold current and laser tunability by current.

The laser structures were grown by LPE on InAs (100) substrate and consisted of two cladding layers of the InAsSbP alloy with InP mole fraction 0.35 (E_g = 0.59 eV, T = 77 K) and active layer which was made either of InAsSbP with a lower band gap or of the InAsSb solid solution. The active layer and the n-type cladding layer were undoped, the p-type cladding layer was doped with Zn up to 1×10 cm^{-3}. The diodes of deep mesa geometry were fabricated with a (10-30) um mesa width.

Lasing was obtained at 80 K at the discrete wavelengths in the range 2.7-3.05 um for the structures with the InAsSbP active layer of different compositions and with InAsSb active region for the range 3.1-3.7 um. The lowest values of threshold current was achieved up to 18 mA for 3.3 um laser. With increasing the emission wavelength from 3.3 to 3.7 the threshold current increased up to 70-100 mA, which is due, probably, to poorer crystalline quality of the structures. For the lasers with the InAsSbP active layers with increasing the Sb and P mole fractions electron confinement of injected carriers becomes worse and for this reason threshold current increase up to 70-120 mA at 2.7 um. The dependence of the threshold current on the cavity length shows a minimum at L = 250-300 um. At L < 200 um the threshold current sharply increases while the cavity length decreases and no lasing has been achieved for the lasers shorter than 100 um. The lasers with threshold current lower than 100 mA could operate in CW regime up to 100 K. The emission spectra of lasers contained 1-3 longitudinal modes depending on the current value and the cavity length.

Figure 1 shows the threshold current versus heatsink temperature for pulsed operation. The characteristic temperature T_0 was 30 K. The maximum temperature of lasing was achieved up to 180 K.

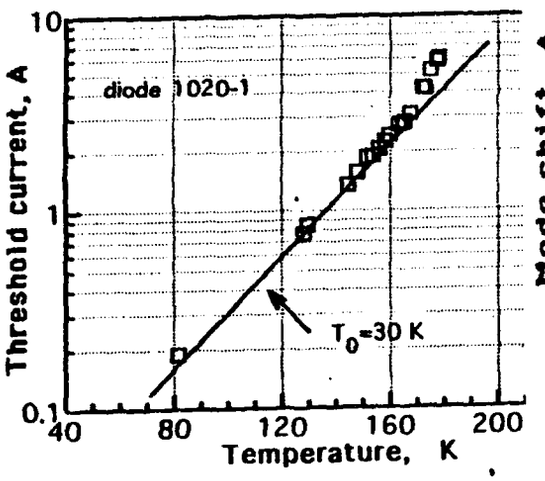

Fig.1. Temperature dependence of the threshold current of an InPAsSb laser.

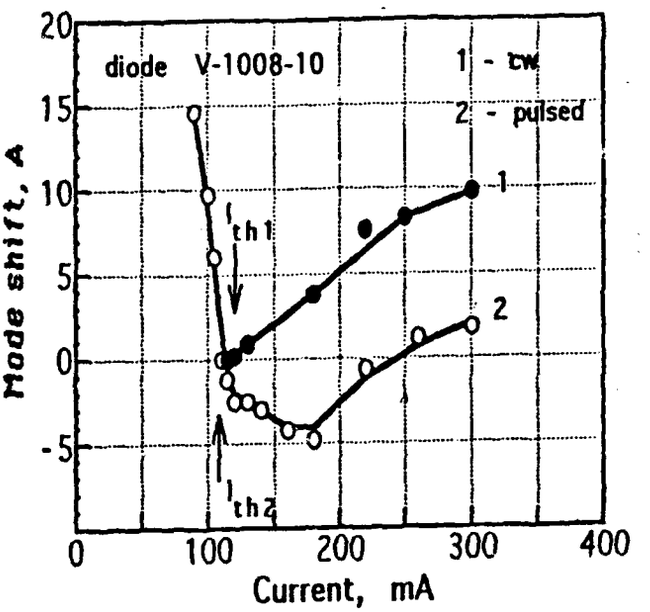

Fig.2. Dependence of the Fabry-Perot mode position on current.

The shift of the main lasing mode with current is shown in fig. 2 for pulsed and CW regimes. For CW operation above the threshold the mode position shifts continuously to the longer wavelength side, in pulsed regime the mode shifts to shorter wavelengths and then at higher currents it moves to the longwavelength side. The blue shift is explained by increasing the carrier density in the active region. The red shift is due to heating of laser structure at higher currents. Our experiments demonstrated that lasers can be successfully used for high resolution spectroscopy.

References

1. A.N.Baranov, A.N.Imenkov, V.V.Sherstnev, Yu.P.Yakovlev. Proc. 5th Int. Conf. on InP and Related mater., April 19-22, 1993, Paris, pp.660-662.

3:30pm - 3:45pm
Th4.1

800mW Peak Power Self-Sustained Pulsation GaAlAs Laser Diodes

T.Takayama, O.Imafuji, H.Sugiura, M.Yuri, H.Naito, M.Kume,
A.Yoshikawa, and K.Itoh
Electronics Research Laboratory, Matsushita Electronics Corporation
Takatsuki, Osaka 569, Japan

Abstract—We have developed a self-sustained pulsation laser whose peak power is as high as 0.8W for the first time, by using a new multiple-quantum-well (MQW) real refractive index guided structure with large saturable absorber.

Recently, a high power pulsed laser light is demanded for optical mesurements, optical computing, second harmonic generation (SHG), and so forth. Particularly, a high power pulsed infra-red laser light is strongly required for SHG[1] elements because SHG capability increases in proportion to the square of the input power. Various investigations of self-sustained pulsation laser diodes have been reported by using complex refractive index guided structure. However, so far reported maximum average output power with self-sustained pulsation is 40mW[2].

In this paper, we report a high-power self-sustained pulsation laser by using a new MQW real refractive index guided structure with large saturable absorber.

Figure 1 shows a schematic drawing of the present laser structure. In the structure, a GaAlAs optical-confinement layer gives a very small refractive index step[3] so that a lasing spot size becomes larger than the width of the current-injection stripe. In particular, narrower current injection stripe spreads optical field to the lateral direction widely, therefore, a large saturable absorber is formed in the active layer under the optical-confinement layer. Moreover, the MQW active layer is utilized for obtaining high optical gain, leading to attaining high peak power operation.

The saturable absorbing effect can be estimated by the difference between the maximum and minimum optical absorption in the active layer ($\Delta \alpha_A$) during the self-sustained pulsation. Figure 2 shows calculation results of $\Delta \alpha_A$ as a function of the stripe width. It is found that narrow stripe width is suitable for obtaining large saturable absorbing effect in the structure.

The front and rear facets of the laser are given reflectivities of 3% and 94% coated, respectively. The cavity length and stripe width are 800 μm and 1.0 μm, respectively. A high-power fundamental mode operation has been obtained over 250mW average power with lasing wavelength of 0.86 μm.

The light-current characteristics is shown in Fig.3. High-power operation over average power of 250mW is obtained. The optical pulse waveform at an average output power of 180mW is shown in Fig.4. The light pattern shows self-sustained pulsation with 125ps half width and 0.8W peak power.

In conclusion, a 0.8W peak power self-sustained pulsation laser is obtained for the first time, by using a new MQW real refractive index guided structure with large saturable absorber.

References

[1]M. Kume et al., Solid-State Electronics, Vol. 34, 1329(1991).
[2]T. Tanaka et al., Appl. Phys. Lett., vol. 53, 2471(1988).
[3]O. Imafuji et al., IEEE J. Quantum Electron., QE-29, 1889(1993).

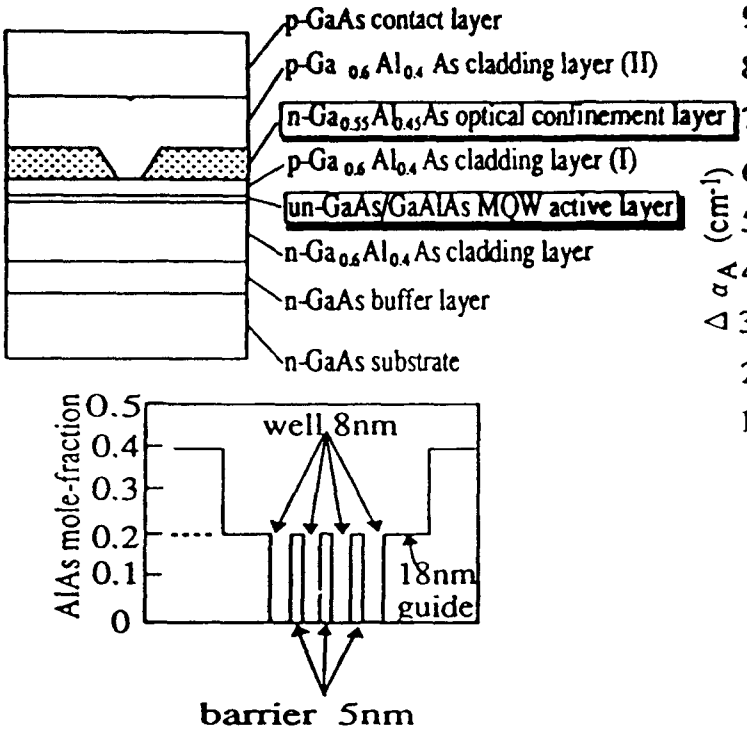

FIG.1. Schematic drawing of the present laser structure.

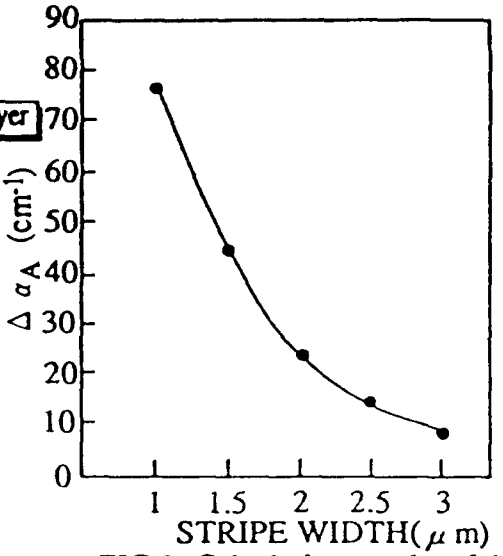

FIG.2. Calculation results of the relationship between the stripe width and the $\Delta \alpha_A$ in the self-sustained pulsation lasers.

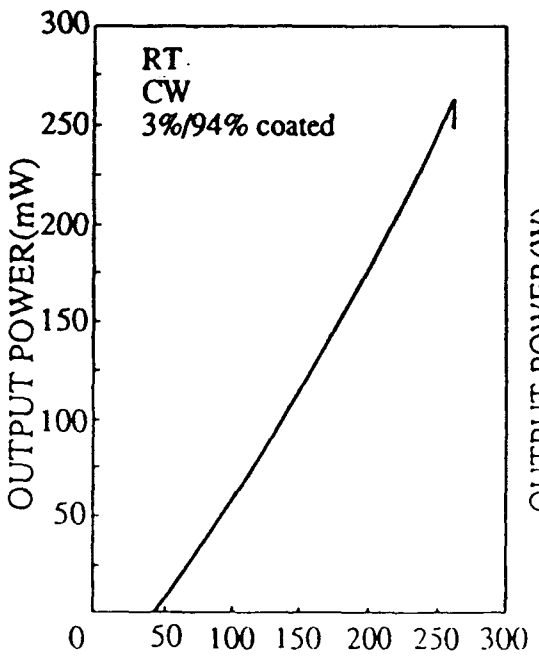

FIG.3. Light-current characteristics.

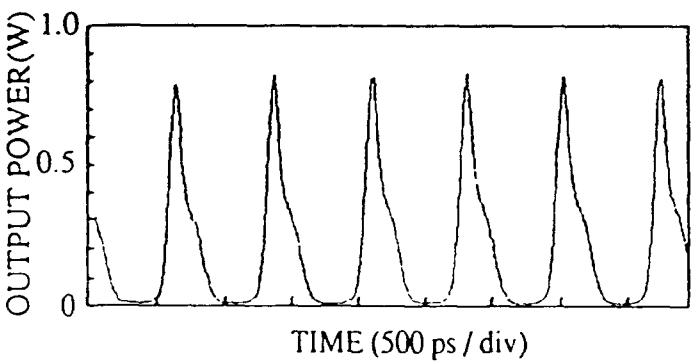

FIG.4. Measured pulse waveform at an average output power of 180mW.

3:45pm - 4:00pm
Th4.2

2.2 W cw Diffraction-Limited Monolithically Integrated Master Oscillator Power Amplifier at 854 nm

S. O'Brien, R. Lang, D. F. Welch, R. Parke, and D. Scifres
SDL, Inc., 80 Rose Orchard Way, San Jose, CA 95134 FAX (408) 943-1070

ABSTRACT

A monolithically integrated master oscillator amplifier power (M-MOPA) operating in a single longitudinal mode at 854 nm has been fabricated which produces 2.2 W cw with a single-lobed, diffraction-limited far field pattern. Additionally, the extinction ratio in the far field with the oscillator turned off is 26 dB.

SUMMARY

In this paper we demonstrate that over 2.2 W of cw power is achievable from a monolithically integrated master oscillator amplifier power (M-MOPA) at alternative wavelengths using the GaAs/AlGaAs material system. When compared to the InGaAs/GaAs material system, GaAs/AlGaAs materials present unique processing issues related to obtaining high quality regrowths on AlGaAs. Previously reported results with GaAs/AlGaAs M-MOPAs have been limited to 1.3 W cw, therefore the work described in this paper represents an improvement of almost 1 W.[1] High diffraction-limited power in the 830-870 nm range is important for several applications including free-space communications and frequency doubling into the blue. For example, for free-space communications, high power operation at a wavelength of 852.1 nm enables the use of an ultra-narrow bandpass cesium transmission filter which significantly improves system performance by strongly attenuating sunlight.

The M-MOPA design, presented in Figure 1 consists of a single spatial mode distributed Bragg reflector (DBR) laser followed by a flared amplifier which expands at an angle large enough to allow free diffraction of the injected beam. The width of the output aperture of the flared amplifier is approximately 280 μm. To minimize the internal losses, buried gratings are fabricated in AlGaAs to form the DBR laser.

An L-I curve showing the output power vs amplifier current for the M-MOPA is shown in Figure 2. The M-MOPA exhibits a smooth, linear behavior with a slope efficiency of 0.74 W/A. An optical emission spectrum taken at an output power of 2.2 W cw is shown as an inset in Figure 2. The output from the M-MOPA replicates that of the single frequency master oscillator and operates in a single longitudinal mode at 854.2 nm with a side mode suppression greater than 20 dB.

Far field patterns taken with an oscillator current of 150 mA and amplifier drive currents of 3.0, 3.5, 4.0, 4.5, and 5.0 A are shown in Figure 3. The full width at half maximum is 0.18°, the diffraction limit for the 280 μm wide emitting aperture. At all drive currents, the M-MOPA maintains the diffraction-limited, single-lobed far field intensity pattern. Additionally, the peak intensity grows linearly with drive current implying that the Strehl ratio is remaining approximately constant. Also shown in Figure 3 is the far field pattern, magnified by 10X, at an amplifier drive current of 5 A with the oscillator is turned off. With the oscillator turned off, the peak far field intensity is extinguished by 26 dB. Comprehensive modulation experiments have not yet been completed, however, results with similar M-MOPAs fabricated with the InGaAs/GaAs materials suggests that small signal modulation speeds in excess of 2 GHz can be expected from the present 855 nm M-MOPA design.

This work was supported by SDIO and managed by USAF-Rome Laboratories under research contract F30602-90-C-0104.

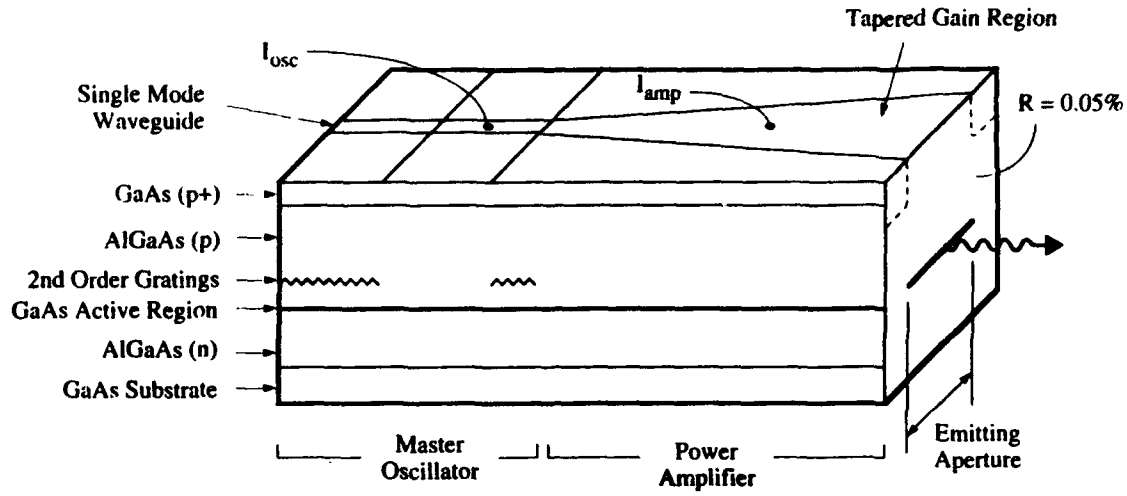

Figure 1 Schematic diagram of the M-MOPA

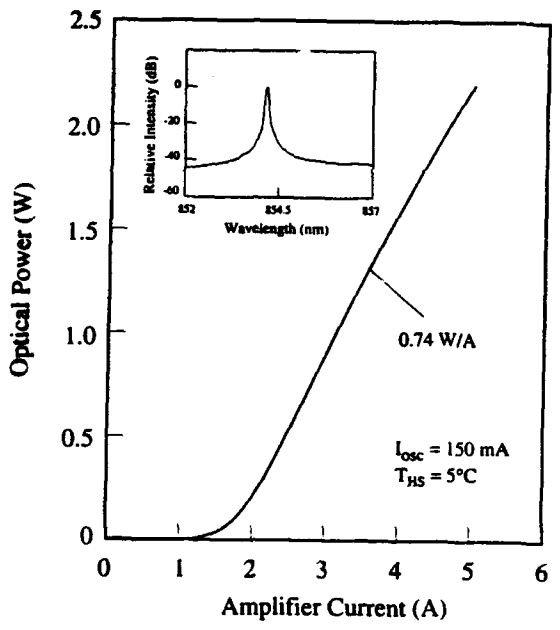

Fig. 2 CW output power vs amplifier current with 150 mA to the master oscillator. Shown as an inset is an optical emission spectrum taken at an output power of 2.2 W cw.

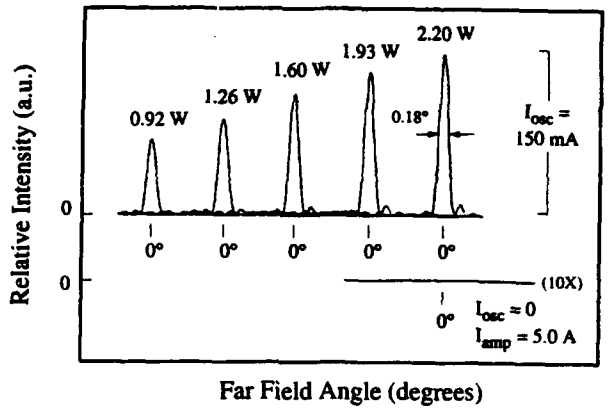

Fig. 3 Far field patterns taken at various CW output powers.

(1) S. O'Brien, D. Mehuys, J. Major, R. Lang, D.F. Welch, and D. Scifres, "1.3 W cw, diffraction-limited monolithically integrated master oscillator flared amplifier at 863 nm," Electron. Lett. 29, 2109 (1993).

4:00pm - 4:15pm
Th4.3

295 mW CW Maximum Output of AlGaInP Laser Diode with Windows Grown on Facets

Masanori Watanabe, Kentaro Tani, Kazuaki Sasaki, Hiroshi Nakatsu, Masahiro Hosoda, Sadayoshi Matsui, Osamu Yamamoto and Saburo Yamamoto

Opto-Electronic Devices Division, Sharp Corporation
2613-1, Ichinomoto, Tenri, Nara 632, Japan
Fax 07436-5-2475

Up to 295 mW kink-free CW maximum output, about twice as much as the conventional one, was achieved by implementing the WGF (Windows Grown on Facets) structure to AlGaInP laser diode.

High power operation of fundamental transverse mode AlGaInP laser is required for high-density optical data storage systems and other applications. However, AlGaInP lasers are very susceptible to facet degradation at high power operation. To overcome this problem, several window structures which reduce optical absorption near the facets have been reported[1,2]. Among these window structures, the WGF structure[3], previously implemented to AlGaAs laser, is rather simple; growing window layers on the cleaved facets. We think the WGF structure is the best technique to improve maximum optical output and to maintain performance because the proper window layers can be selected independent of the internal laser structure.

Figure 1 shows the WGF laser structure. The cavity length is 1200 μm, and the ridge width is 4 μm. The internal laser structure was fabricated by two-step molecular beam epitaxy (MBE)[4]. Because undoped GaInP strained active layer ($\Delta a/a$=+1%) and p-multi quantum barrier (MQB) were used, a kink-free 150 mW maximum output (Fig.2) was obtained without using the window structure.

On the front and the rear cleaved facets, undoped $(Al_{0.7}Ga_{0.3})_{0.5}In_{0.5}P$ thin layers were grown by low pressure metalorganic chemical vapor deposition (LP-MOCVD) using PH_3, trimethylaluminum, trimethylgallium and trimethylindium. The anti-reflective film (R_f=4%) and high-reflective film (R_r=90%) were coated on the front and the rear facets, respectively.

The laser oscillated at 680 nm. The current-to-optical output characteristics are shown in fig.2. The kink-free maximum output of 295 mW was obtained at room temperature, which was about twice as much as that of the conventional one. The threshold current (about 100 mA) and the slope efficiency under 150 mW (about 0.75W/A) were the same as those of the conventional one, which indicates that the window layers do not affect the properties. Figure 3 shows the far field patterns of the WGF laser. The fundamental transverse mode operation up to 150 mW was confirmed.

In summary, the WGF structure was first implemented to AlGaInP laser, and the kink-free 295 mW output was obtained. This result also suggests the good reliability for the practical power leveis.

[1] Y.Ueno, H.Fujii, K.Kobayashi, K.Endo, A.Gomyo, K.Hara, S.Kawata, T.Yuasa and T.Suzuki: Jpn. J. Appl. Phys. 29, 9, L1666-L1668 (1990)
[2] S.Arimoto, M.Yasuda, A.Shima, K.Kadoiwa, T.Kamizato, H.Watanabe, E.Omura M.Aiga, K.Ikeda and S.Mitsui: IEEE J. QE-29, 6, 1874-1878 (1993)
[3] K.Sasaki, M.Matsumoto, M.Kondo, T.Ishizumi, T.Takeoka, S.Yamamoto and T.Hijikata: Jpn. J. Appl. Phys. 30, 5B, L904-L906 (1991)
[4] K.Takahashi et al: to be presented in 8th Int'l Conf on MBE (Aug. 1994)

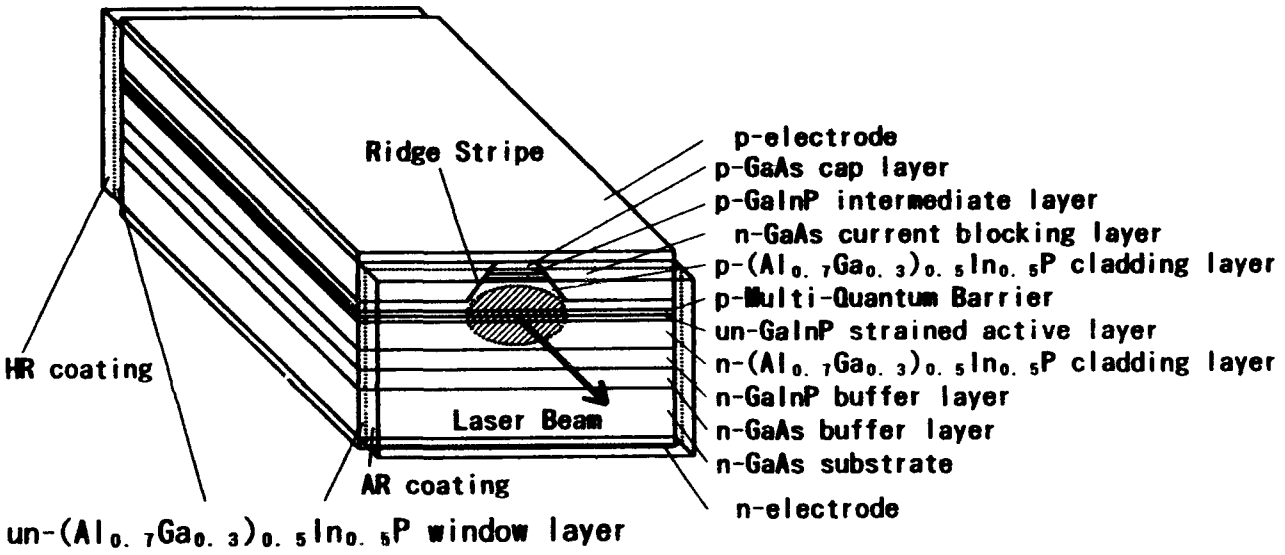

Fig. 1 Schematic view of the WGF laser

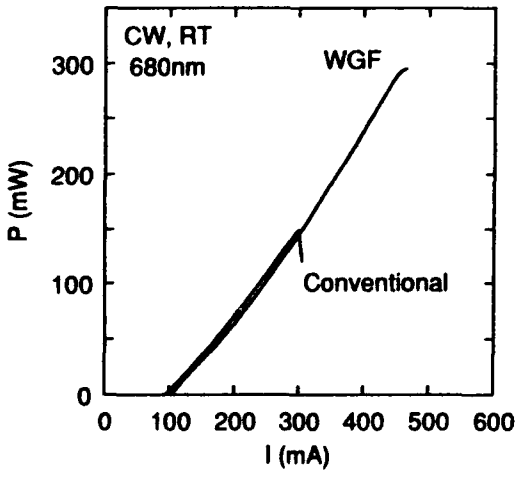

Fig. 2 I-L characteristics

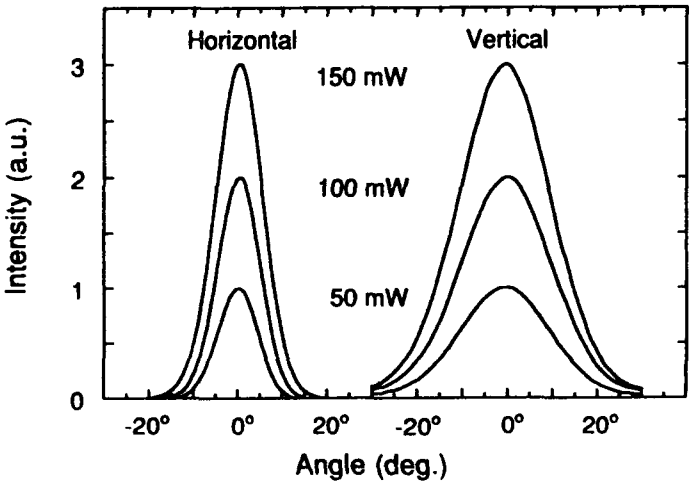

Fig. 3 Far field patterns

4:15pm - 4:30pm

Th4.4 Uniform and high-power characteristics of AlGaInP visible laser diodes and their four-element arrays fabricated on a 3-inch wafer

A.Shima, H.Nishiguchi, M.Kato, Y.Nagai, T.Motoda, T.Nishimura, E.Omura, and M.Otsubo
Optoelectronic & Microwave Devices Laboratory, Mitsubishi Electric Corporation
4-1, Mizuhara, Itami City, Hyogo, 664 Japan FAX:+81-727-80-2696

High-power, 680nm laser diodes (LD's) with uniform characteristics and 100μm-spaced, 4-element individually addressable LD arrays have been fabricated, for the first time, on a 3-inch GaAs substrate. The LD's have been operating for over 2,000 hours and the elements of the LD arrays have exhibited the uniform high-power and high-temperature characteristics.

Recently, demand has increased for high-power and highly reliable LD's lasing at the wavelength range of 670-690nm. This is due to an increase in the production of large memory capacity optical disks (made possible by using high density recording technique). Moreover, an individually addressable LD array is expected to be required since parallel data processing drastically improves the data-transfer-rate for such a large amount of information. In order to satisfy these requirements, it is necessary to be able to fabricate large numbers of LD elements with uniformly excellent high-power characteristics.

In this paper, we present, for the first time, the uniform high-power characteristics of visible LD's and their arrays, which are fabricated by using the 3-inch diameter wafer technology [1]. In order to attain these excellent high-power and high-temperature characteristics, a strained double-quantum-well (DQW) active layer [2] and a multi-quantum-barrier (MQB) [2,3] are applied to the buried-ridge loss-guided LD's. The growth conditions of the MOCVD (metalorganic chemical vapor deposition) have been optimized in conjunction with the uniformity and the quality for the multi-layers of AlGaInP/GaInP on the 3-inch diameter GaAs substrates [4]. For improvement of the uniformity and the controllability of the LD fabrication, we have utilized some wafer processing technologies widely used for IC's. The LD mirror is formed by the conventional cleaving process.

Fig.1 shows the distribution of the threshold currents (Ith's) and the operating currents (Iop's) at 20mW of the uncoated single element LD's in the pulsed condition. The width (W) of the LD chip and the cavity length (L) are 300μm and 650μm, respectively. We have measured the Ith's and the Iop's of 124 chips contained in a length of ~4cm along the gas flow direction of the MOCVD. Except for the 8 non-lasing LD's, the standard deviation of the Ith's and Iop's are 0.94mA (average: 33.6mA) and 2.23mA (average: 72.3mA), respectively. The coated (13%-90%) LD's randomly selected from the central region (broken oval) have been operating for over 2,000 hours, as shown in Fig.2.

The 100μm-spaced, 4-element individually addressable LD arrays are also fabricated in a part of the 3-inch wafer. The LD array chip (L=650μm) is mounted on a cubic-BN submount in a junction-up configuration. Fig.3 shows the light output power versus current (P-I) characteristics of the coated (13%-90%) LD array. The Ith's at 25℃ and the Ith's at 50℃ are 32.8-33.2mA and 40.9-41.6mA, respectively. The characteristic temperature (To) of each element is 111-116K. The Iop's at 25℃, 30mW and the Iop's at 50℃, 30mW are 40.9-41.6mA and 73.3-73.8mA, respectively. Even at 50℃, the linear P-I characteristics are obtained up to 40mW. The lasing wavelength of each element is in the range of 683.3-684.1nm. The full angles at half maximum power of the far-field-pattern (FFP) perpendicular to the junction plane ($\theta\perp$'s) and parallel ($\theta\parallel$'s) are typically 23° and 7°, respectively.

In summary, the visible LD's and the 4-element LD array fabricated on the 3-inch diameter wafer have shown the uniform high-power and high-temperature characteristics.

References
[1] Y.Nagai et al, Conference Digest of Large Area Wafer Growth and Processing for Electronic and Photonic Devices (1994), to be published.
[2] S.Arimoto et al, SPIE, Laser Diode Technology and Applications V, vol. 1850, p.262 (1993).
[3] K.Iga, et al, Electron. Lett., vol.22, p.1008 (1986).
[4] T.Motoda et al, Conference Digest of ICMOVPE VII (1994), to be published.

Single element LD (L=650μm, W=300μm)

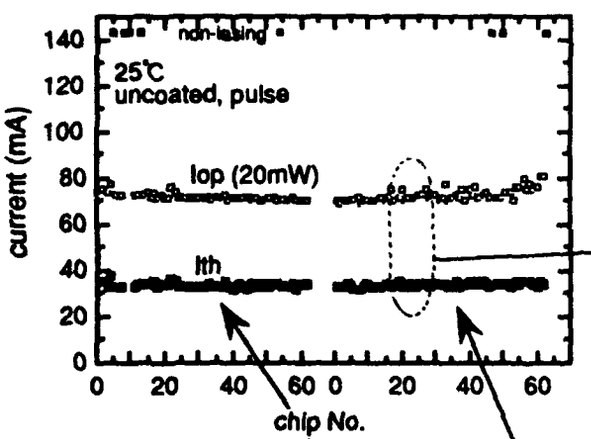

Fig.1 Distribution of the Ith's and the Iop's in the 3-inch wafer

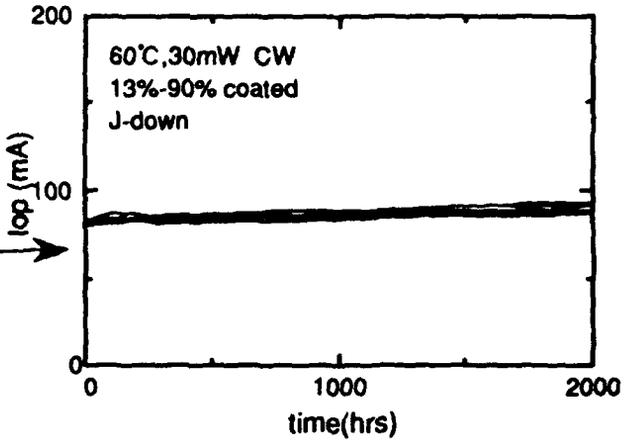

Fig.2 The aging test result of the LD's obtained from the 3-inch wafer

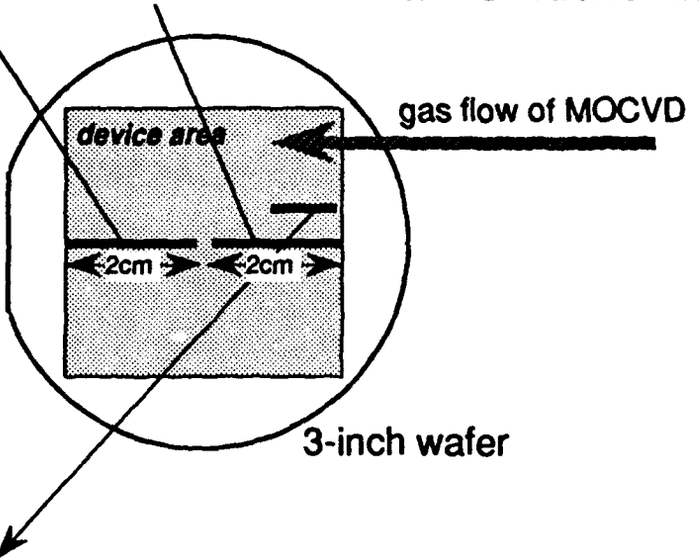

4-element LD array (L=650μm, Pitch=100μm)

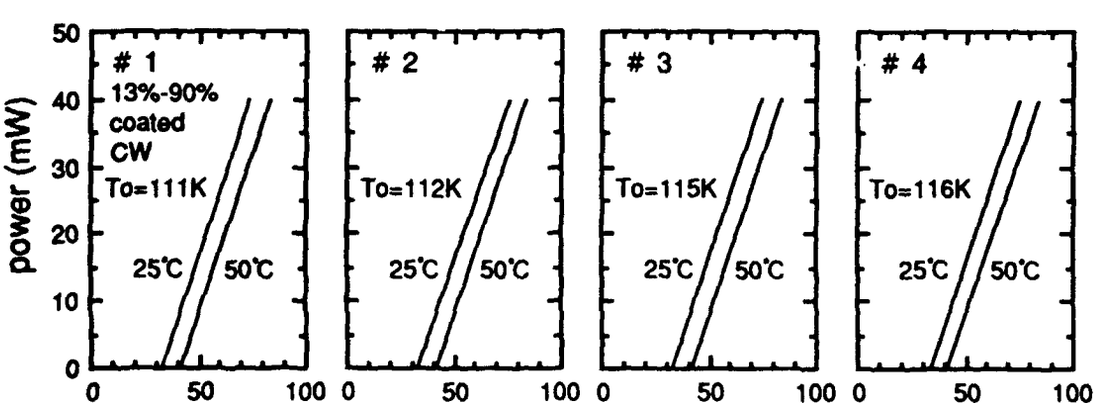

Fig.3 P-I characteristics of the 4-element LD array

4:30pm - 4:45pm
Th4.5

High-Power High-Temperature Operation of 0.98-μm S-SQW Lasers with InGaAsP (Eg: 1.61 eV) barriers

M. Sagawa, T. Toyonaka*, K. Hiramoto, K Shinoda and K. Uomi
Central Research Laboratory, Hitachi, Ltd., *Fiber Optics Division, Hitachi, Ltd.
1-280 Higashi-Koigakubo, Kokubunji, Tokyo 185, Japan

0.98 μm InGaAs strained quantum well (S-QW) lasers have been studied intensively to obtain high-power highly reliable operation of exciting sources for EDFAs. GaAs layers are usually used for the barriers[1-3]. However, the energy gap difference between a GaAs barrier and an InGaAs well is as small as 160 meV. Therefore, when the confinement factor is designed to be small in order to enlarge the spot size for higher power operation, the temperature characteristics deteriorate due to carrier overflow. Recently, a few studies have been made of 0.98 μm lasers with InGaAsP barriers[4-5]. In this paper, we systematically investigate the advantage of InGaAsP (Eg: 1.61 eV) barriers, which have the bandgap difference of 345 meV, against temperature characteristics, and compare them with conventional GaAs barriers. The excellent temperature characteristics of the laser with InGaAsP barriers results in high power operation at high temperatures.

Figure 1 shows the laser structure studied here. The GaAs waveguide layer, whose refractive index is higher than that of the InGaP cladding layers, provides a low-loss real-index waveguide. Two types of lasers with different active layers were fabricated. Type (a) has an active layer consisting of a 7-nm InGaAs S-QW sandwiched by 35-nm InGaAsP (Eg: 1.61 eV) barriers. The active layer of type (b) consists of a 7-nm InGaAs S-QW with 8-nm GaAs barriers sandwiched by 20-nm InGaAsP (Eg: 1.57 eV) SCH layers. The confinement factors of both lasers were designed to be the same.

The temperature dependence of both the lasers on threshold current (I_{th}) is shown in Fig. 2. Kinks in the lines were observed at temperatures (T_C) of 80°C for type (a) and 60 °C for type (b). The characteristic temperatures (T_0) are 156 K and 121 K for the type (a) and (b) laser, respectively. Above T_C, T_0 deteriorates due to carrier overflow into the barrier layers. The fact that T_C and T_0 of type (a) are higher clearly indicates the superiority of the InGaAsP barriers. The light output power versus current characteristics of the type (a) laser at 20-90°C are shown in Fig. 3. I_{th} at 20°C is 15.5 mA. Because of the high T_0, 200-mW operation was obtained even at 90 °C without any significant deterioration. Figure 4 shows the far field patterns of the same laser shown in Fig. 3 in the direction parallel to the junction plane at various operating currents at 25°C. Stable fundamental operation was achieved up to 235 mA, at which point the output power is 175 mW. Preliminary life test at an output power of 80 mW at 50°C has revealed that there is no significant deterioration for over 1000 hours.

It should be noted that it is essential to increase the output power at which point COD occurs (P_C) since the maximum output power (P_{max}) of the lasers is limited by the COD. We fabricated a structure of lasers with non-injection regions (NIR) near the facets in order to increase P_C. The active layer consists of two InGaAs QWs and three GaAs barriers. Figure 5 shows the light output power versus current characteristics of the lasers with and without NIR under CW operation at 25°C. Identical characteristics were obtained with I_{th} of 26.5 mA. However, P_{max} was 466 mW in the laser with NIR while COD took place at 386 mW in the laser without NIR. We believe that this is the highest CW output power obtained in the InGaAs/InGaAsP 0.98 μm lasers. P_{max} of the laser is limited by thermal saturation. This improvement is attributed to the suppression of the temperature rise at the facets due to the reduction of the non-radiative recombination. By introducing InGaAsP barriers, higher output power can be expected because of the improvement of the thermal characteristics. These lasers are being processed.

In summary, comparisons between S-SQW lasers with InGaAsP barriers and identical lasers with GaAs barriers confirm that lasers with InGaAsP barriers have better temperature characteristics. Maximum output power of 466 mW was obtained from the laser with NIR.

References [1] M. Sagawa et al., *Electron. Lett.*, 28, 1639 (1992) [2] S. Ishikawa et al., *IEEE J. of Quantum Electron.*, 29, 1936 (1993) [3] W. J. Gingac et al., ECOC '92, Mo B2.3 (1992) [4] H. Asonen et al., *IEEE Photonics Tech. Lett.*, 5, 589 (1993) [5] M. Ohkubo et al., *IEEE J. of Quantm Electron.*, 29, 1932 (1993)

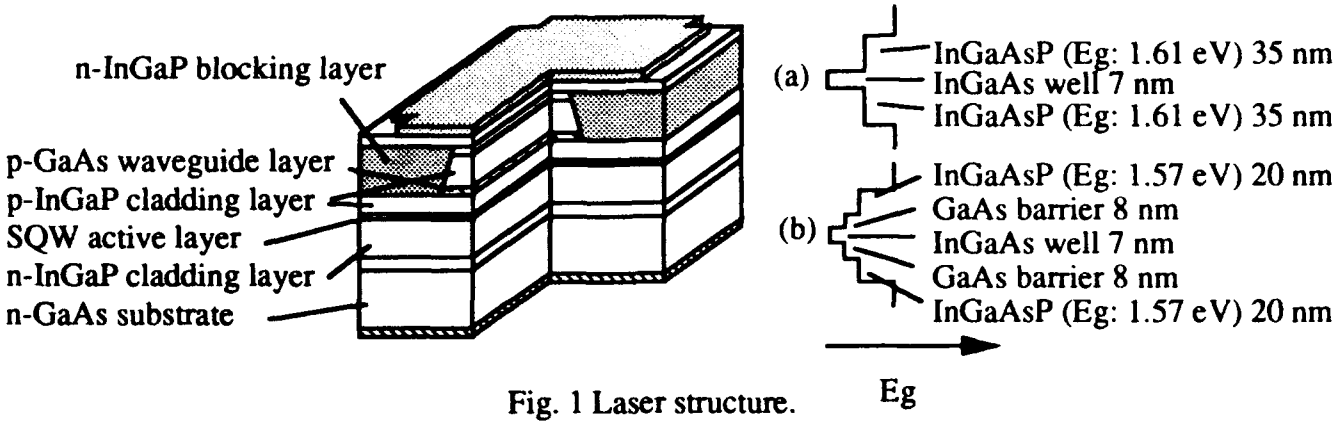

Fig. 1 Laser structure.

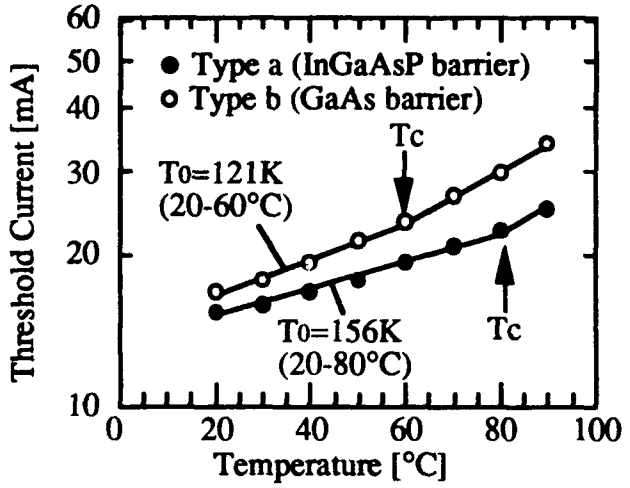

Fig. 2 Temperature dependence of the threshold current.

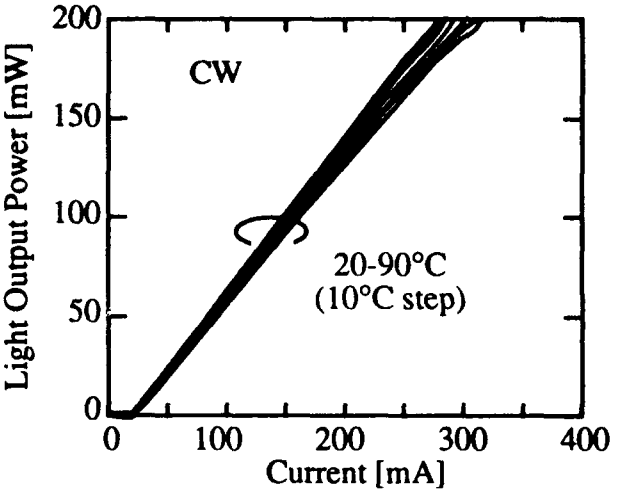

Fig. 3 Light output power vs. current characteristics of the type (a) laser at various temperatures.

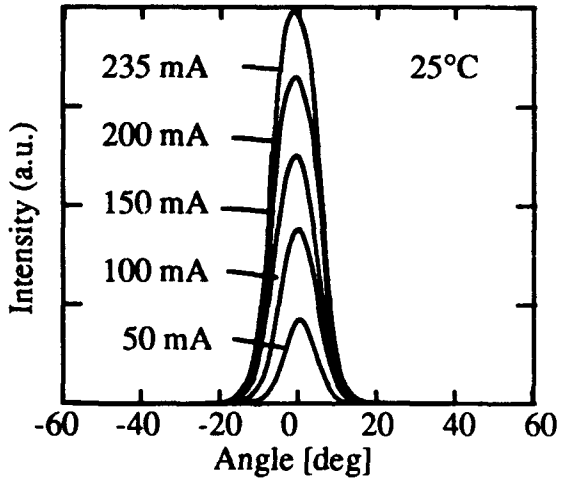

Fig. 4 Far field patterns of the type (a) laser at various operating currents.

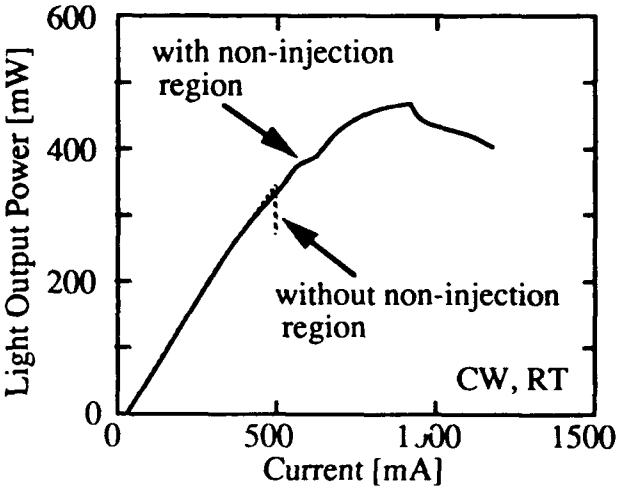

Fig. 5 Light output power vs. current characteristics of lasers with and without non-injection regions near the facets.

4:45pm - 5:00pm

Th4.6

High-Power, Coherent Phased Array of Monolithic Flared Amplifier–Master Oscillator Power Amplifiers

J. S. Osinski, D. Mehuys, D. F. Welch, K. M. Dzurko
R. Waarts, R. Lang, and J. S. Major, Jr.
SDL, Inc., 80 Rose Orchard Way, San Jose, CA 95134
(408) 943-9411 FAX (408) 943-1070

ABSTRACT: A coherent array of MFA-MOPAs is demonstrated by integrating a DBR laser, single-mode power distribution network, phase modulators, and flared amplifiers on a single chip. 39 W of coherent, pulsed output power is obtained.

High-power diffraction-limited semiconductor laser sources are useful for several key applications such as free-space communications and frequency doubling. Previously, greater than 2 W of continuous diffraction-limited power[1] has been demonstrated in a single monolithic flared amplifier–master oscillator/power amplifier (MFA-MOPA) configuration. Scaling of single devices to higher single-mode powers by increasing amplifier length is limited by considerations such as heat dissipation and filament formation that degrades beam quality. We demonstrate an alternate, scalable approach with an integrated array of MFA-MOPAs which is spectrally and spatially coherent, made by distributing the single-mode emission from a single DBR laser to a row of amplifiers. Integration of a phase-shifting region into each input waveguide of the amplifiers allows individual phase tuning to obtain mutual phase coherence and near-diffraction limited operation.

Figure 1 is a schematic of the device. Power is distributed from the DBR laser to a power splitter network consisting of a series of Y-junctions leading to curved, index-guided waveguides. This network provides roughly equal single-mode power injection into each element of the array. Following the distribution network, initial amplification is provided by a pre-amplifier region.

From the pre-amplifier, each waveguide enters a 500 μm long phase shifting region capable of individually tuning the phases by up to 4π using carrier injection. A 2π phase shift is generally obtained with less than 15 mA of pulsed current in these devices. The power exiting the phase shift region then enters each of the flared amplifiers that lead to exit apertures on 500 μm centers, AR coated to $R < 0.1\%$ reflectivity.

Figure 2 shows the pulsed power-current characteristics of an array of eight amplifiers, where the current scale corresponds to the total current delivered to all eight amplifiers driven in parallel. 60 W of total power is obtained, although separate measurements indicate that 65% of this occurs at the DBR signal wavelength with the remainder being amplified spontaneous emission (ASE) power. Therefore, approximately 39W of output is spectrally coherent.

The emitters can be phased by observing the fringe pattern obtained when their far-fields overlap in the Fourier-transform plane of a lens. For a 4-element array, this has been accomplished to a nearly ideal state at a total coherent, diffraction-limited power level of over 5 W. Using external optics to spatially overlap the far-field patterns from individual elements, the in- and out-of-phase conditions are evident in the resulting beam, as shown in Figure 3 for the case of two elements. Use of micro-optics or integrated lenses can therefore provide a near-diffraction limited far field pattern determined by the extended aperture of the array. These results suggest that this scalable architecture is capable of obtaining unprecedented levels of diffraction-limited, coherent power.

This work supported by Phillips Lab, Kirtland AFB, Albuquerque, NM 87117.

---

[1] R. Parke, D. F. Welch, A. Hardy, R. Lang, D. Mehuys, S. O'Brien, K. Dzurko, and D. Scifres, "2.0 W CW, Diffraction-Limited Operation of a Monolithically Integrated Master Oscillator Power Amplifier," *IEEE Phot. Tech. Lett.*, **5**, 297, 1993.

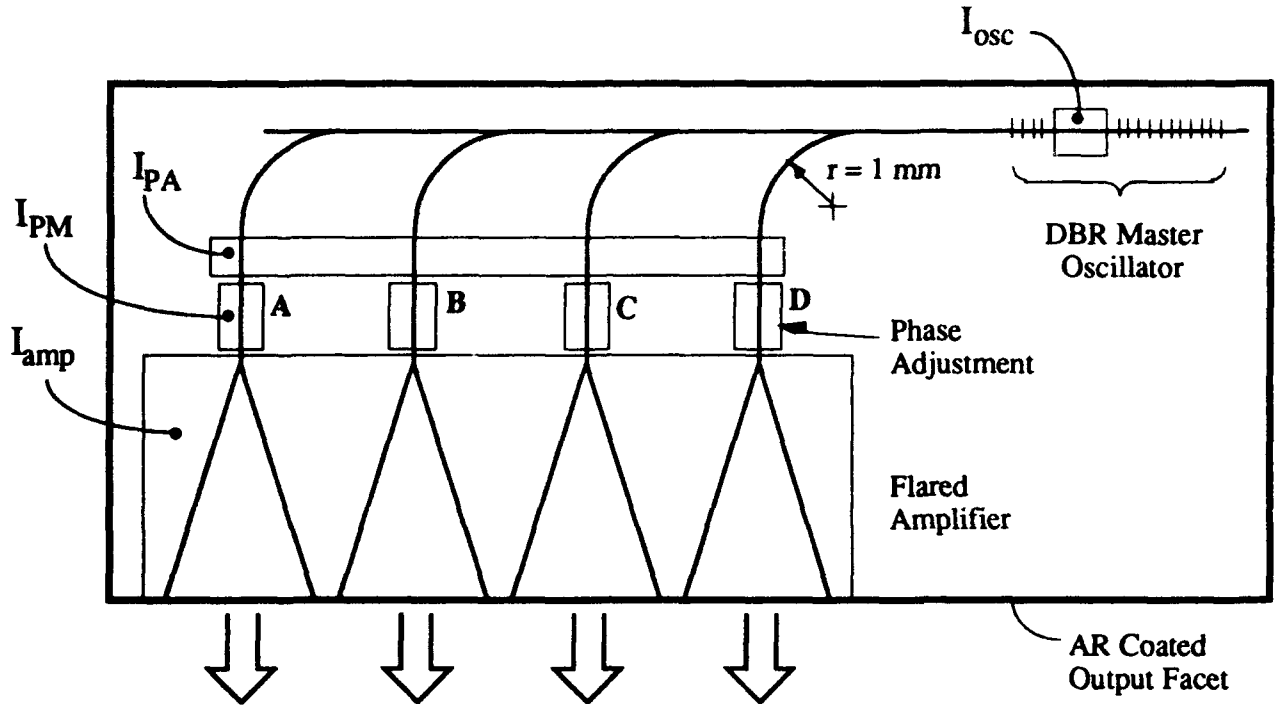

Fig. 1. Integrated phased array architecture of coherent MFA-MOPAs.

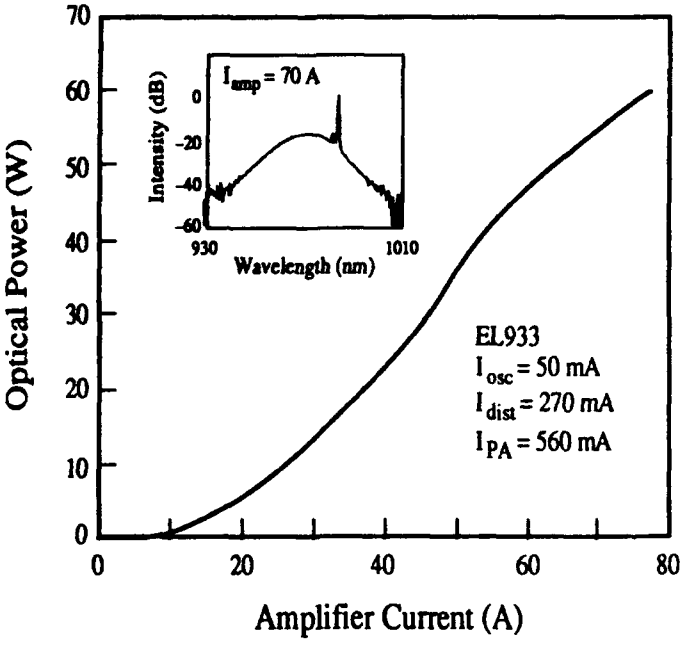

Fig. 2. Power-current and spectral characteristics of an 8-element array.

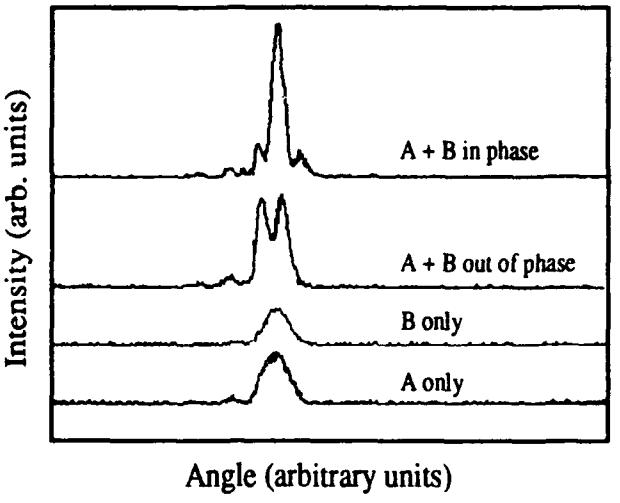

Fig. 3. Phased superposition of far field patterns from two adjacent elements. The individual far-fields are approximately 0.2° wide.

5:00pm - 5:15pm
Th4.7

Multiple-Quantum-Well Broad-Area Tapered Amplifier with a Monolithically Integrated Output Focusing Lens and 1 W CW Operation at 0.98 μm Wavelength

K.-Y. Liou, M. G. Young, E. C. Burrows, R. M. Jopson, G. Raybon, and C. A. Burrus

AT&T Bell Laboratories, Crawford Hill and Holmdel Laboratories, Holmdel, NJ 07733

ABSTRACT: We report a 0.98-μm wavelength tapered broad-area amplifier with a monolithically integrated waveguide lens. CW operation with 1 W output was measured with 10 mW input from a 0.98 μm diode laser. The amplifier output is focused to a single spot by the integrated waveguide lens.

Tapered semiconductor optical amplifiers have been used in the master-oscillator (MO) power amplifier (PA) configuration as a high-power diode source. MOPAs with adiabatically tapered single-mode waveguides have demonstrated up to 0.37 W output at 1.48 μm and 1.5 μm wavelengths [1,2]. The output from these devices is limited by the volume of the single mode guide. By using broad-area amplifiers that are tapered, without lateral guiding, to widths of about 250 μm, outputs of 1 W to 3 W have been reported for MOPAs [3,4] at 0.98 μm wavelengths. These broad-area diode sources are very attractive for free space applications. However, coupling to a single mode fiber may be difficult, because the optical field is emitted from a broad area slab waveguide and the phase front is curved. To resolve this problem, we reported previously a tapered broad-area amplifier with a monolithic waveguide lens [5], which focused the high-power quasi-cw output at 1.48 μm wavelength to a single spot. We report in this paper 1 W cw operation of a 0.98 μm strained InGaAs/GaAs tapered amplifier with a monolithically integrated aspherical lens. The integrated chip may be useful as a pump source for Er-doped fiber amplifiers.

Figure 1 shows the structure of the monolithic amplifier-lens chip. The device is fabricated by two-step MOVPE. The active region consists of an undoped GaAs guide layer, three 40 Å thick, compressively strained, $In_{0.3}Ga_{0.7}As$ quantum wells with GaAs barriers, which are surrounded by an n-type $Al_{0.5}GaAs$ bottom cladding layer and a p-type InGaP top cladding layer. The active MQW layers are removed from the passive region, where an undoped InGaP top cladding is used. The effective index change from the active to passive region is 2.3%, which is used for the lens design. The amplifier is tapered by a 5.7° angle and tilted by 7°. With the output facet AR coated and with optical input from a master oscillator, self-oscillation is completely eliminated. On finished chips, the distances from the input facet to the lens surface, and from the lens to the output facet, are 1300 μm and 1160 μm, respectively. The integrated chip is mounted p-side down on a copper heat sink for cw operation.

The beam propagation method is used for device modeling. Figure 2 shows an example of calculated intensity of an optical field propagating in a tapered amplifier-lens chip. The calculated focal distance from the input facet to the focal point is 2400 μm. For the experiment, a 0.98 μm diode laser with a single mode output fiber is used as a master oscillator. The input to the amplifier is TE polarized. Figure 3 shows the parallel near-field pattern (focused by the monolithic lens), and the perpendicular near-field pattern (guided by the multilayer slab guide), with 8 μm and 3.3 μm FWHM spot size, respectively. The resolution of the near-field measurement setup is ~3 μm. The measured focal point is in air at 200 μm from the facet (= 60 μm optical length in semiconductor). Comparing the experiment with theory, the measured focal distance (semiconductor) is 5% longer than calculations.

The cw output power from a monolithic lensed amplifier chip is shown in the L-I curves in Fig.4 with various input levels from a master oscillator. The output reaches 1 W at about 4.5 A amplifier current. The output spectrum consists mainly of the amplified input at 0.98 μm wavelength. Figure 4 shows that the output gain saturates as the input is increased to 10 mW, indicating that the lensed amplifier can be designed to operate with less than 10 mW master oscillator power, while a high output power can still be attained by increasing the amplifier length.

In conclusion, we have demonstrated 1 W cw operation of a monolithic tapered amplifier-lens chip at 0.98 μm wavelength. The integrated lens can be designed for lateral wave guiding in broad-area MOPAs to achieve either a flat phase front output or a focused output for mode matching to a single mode fiber.

REFERENCES:

[1] U. Koren, et. al., Appl. Phys. Lett., vol. 59, pp.2351-2353, 1991.
[2] P. A. Yazaki, et. al., IEEE Photon. Tech.. Lett., vol.5, pp.1060-1063, 1991.
[3] J. N. Walpole, E. S. kintzer, S. R. Chinn, C. A. Wang, and L. J. Missaggia, Appl. Phys. Lett., vol. 61, pp.740-742, 1992.
[4] D. Welch, R. Parke, D. Mehuys, A. Hardy, R. Lang, S. O'Brien, and D. Scifres, IEEE Photon. Tech. Lett., vol.5, pp.297-300,1993.
[5] F. Koyama, K.-Y. Liou, A. G. Dentai, T. Tanbun-ek, and C. A. Burrus, IEEE Photon. Tech. Lett., vol.5, pp. 916-919, 1993.

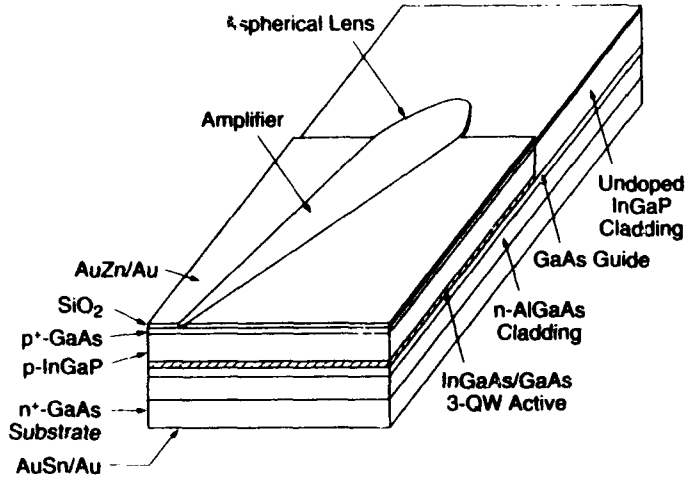

Fig.1 Schematic structure of the monolithic amplifier-lens chip.

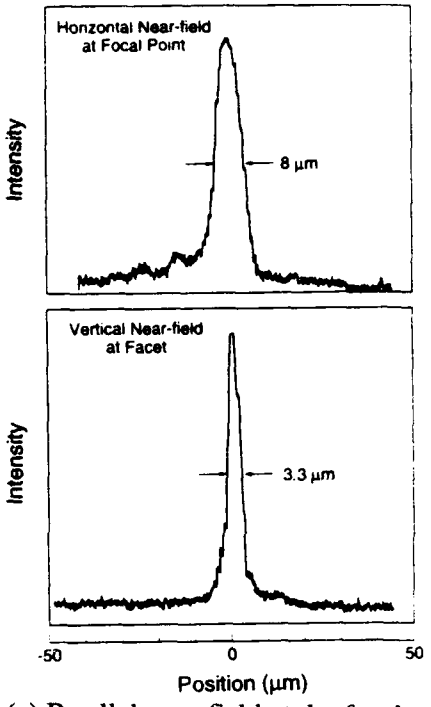

Fig.3 (a) Parallel near-field at the focal point, and (b) perpendicular near-field at the facet.

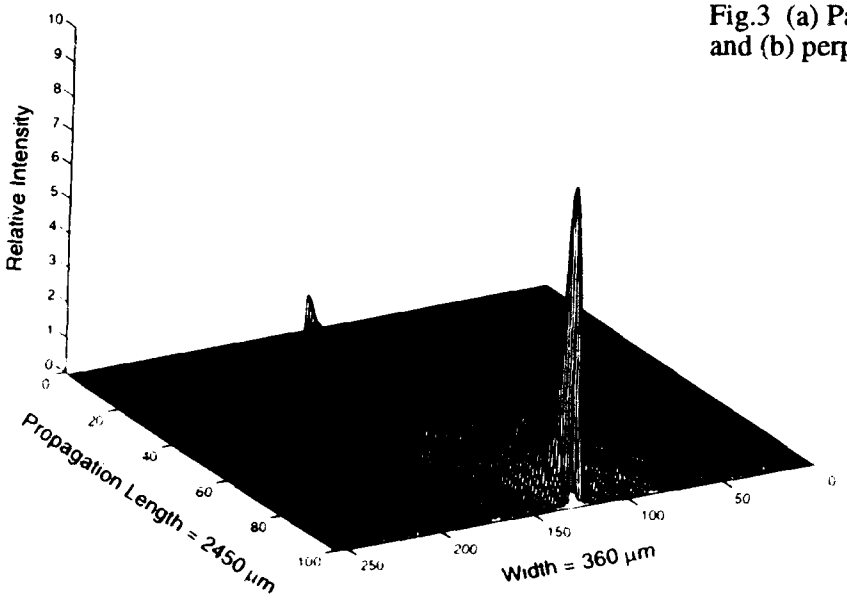

Fig.2 Calculated intensity of optical field propagating in a monolithic tapered amplifier-lens structure.

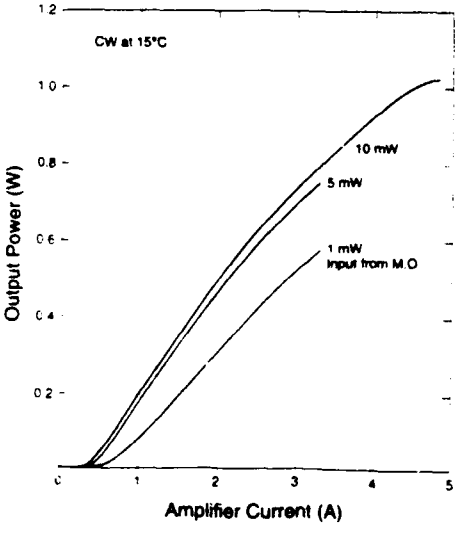

Fig.4 L-I curves of an amplifier-lens chip with inputs from a 0.98 μm master oscillator.

5:15pm - 5:30pm
Th4.8

132 W Monolithic Two-Dimensional Surface Emitting Laser Arrays

D.W. Nam, S. Sanders, R. G. Waarts, and D. F. Welch

SDL, Inc.
80 Rose Orchard Way
San Jose, CA 95134-1356
(408) 943-9411, Fax (408) 943-1070

Abstract

We have demonstrated output powers of 3.4 W CW and 132 W Q-CW from a single element and a monolithic 4 x 12 element surface emitting lasers with ion milled 45° and 90° facets, respectively.

Summary

Monolithic two-dimensional (2-D) surface emitting laser (SEL) arrays have attracted great deal of interest for their potential optoelectronic and high power applications. Monolithic 2-D arrays can be used in high-power applications such as pumps for solid state lasers and possibly hybrid 2-D pump source (stacked bars) replacements. For pumping solid state materials, output powers of 1-3 W per element or 50-100 W total power are required. Previously, we have demonstrated 50 W CW total power from a monolithic 2-D (16 x 94) surface emitting single mode laser arrays with ion milled 90° and 45° facets that are suitable for optoeletronic applications[1]. In this presentation, we report the operation of high power monolithic 2-D SEL arrays utilizing an in-plane gain cavity with ion milled 90° and 45° facets that are applicable for pumping of solid state materials. We have achieved 3.4 W CW and greater than 130 W Q-CW power from a single element and a monolithic 4 x 12 array of surface emitter lasers with ion milled facets, respectively.

The basic structure of the SEL is presented in a schematic form in Fig. 1. The horizontal gain cavity consists of 150 μm wide x 1000 μm long gain guided InGaAs-$Al_xGa_{1-x}As$ quantum well heterostructure with ion milled 90° and 45° facets. A superlattice designed for ≈5 % reflectivity, located below the InGaAs-$Al_xGa_{1-x}As$ active region, provides the feedback for laser operation. The SELs are spaced on 750 μm x 1150 μm centers. The laser emission exits through the anti-reflective coated GaAs substrate.

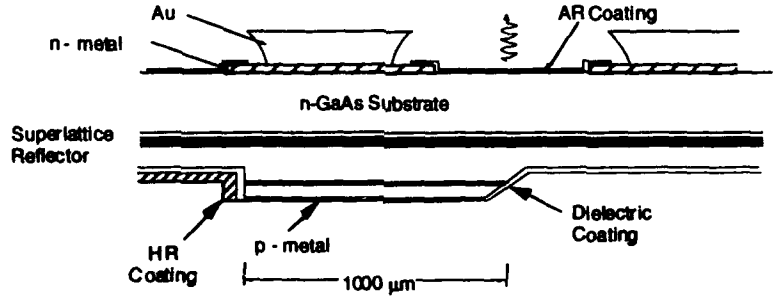

Figure 1: Schematic diagram of surface emitting laser (SEL).

The CW light output versus current characteristic of a typical single-element SEL bonded p-down (junction side) on a Cu heatsink is presented in Fig. 2(a). A CW threshold current of ≈500 mA ($J_{th} \approx 333$ A/cm^2) and a differential efficiency of 47 % (0.6 W/A) are measured until heating effects cause the efficiency of the device to decrease. We have obtained 3.4 W CW output power is from the SEL at 973 nm. The full-width at half maximum (FWHM) of the perpendicular far field is measured as 28°. The output power achieved from the SEL is comparable to that of commercially available Fabry-Parot broad area lasers (≈1-3 W).

The monolithic 2-D SEL arrays consisting of 4 x12 elements (0.5 cm x 1 cm) are bonded p-side down on a heatsink for the array characterization under Q-CW condition (100 μs pulses 50 Hz). The Q-CW L-I characteristic of the 4 x 12 SEL array is presented in Fig. 2(b). The Q-CW threshold and differential quantum efficiency of the SEL array are 22.5 A (470 mA/device) and 47 %, respectively. The total peak output power of 132 W Q-CW (2.75 W/element) is achieved from the 2-D array that corresponds to an optical power density of 264 W/cm^2. The total power output from the 4 x 12 SEL array was limited by the current supply. The peak of the 2-D SEL array spectral output is at 973 nm with FWHM of 7.5 nm. These result represents the highest optical power and the highest optical power density from a surface emitting laser array. The high output power, spectral output, and good uniform characteristics of the 2-D SEL array make this array an excellent choice as a pump for solid state materials in many different configurations. The work presented in this letter has been supported by ARPA under contract MDA972-92-C-0047.

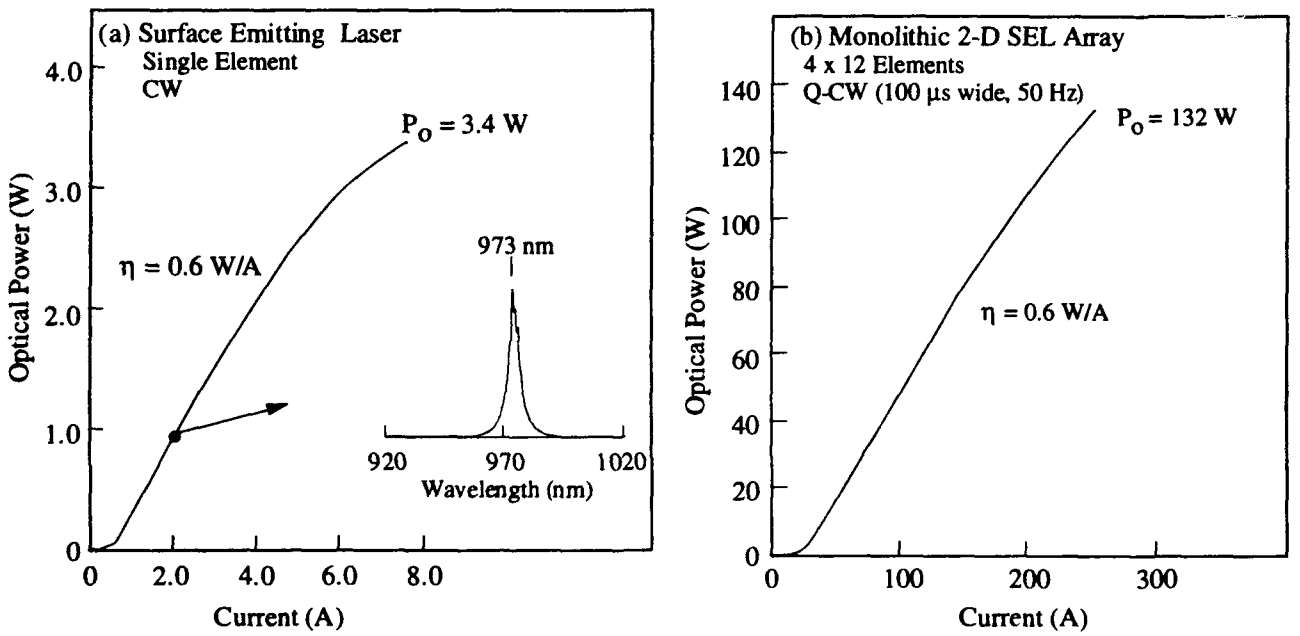

Figure 2: (a) CW L-I from a single element SEL. (b) Q-CW L-I from a monolithic 2-D 4 x 12 array of SEL.

1. D. W. Nam, R. G. Waarts, D. F. Welch, J. S. Major, Jr., and D. R. Scifres, "Operating characteristics of high continuous power (50W) two-dimensional surface-emitting laser array," *IEEE Photonics Technol. Lett.*, **5**, (7), pp. 281-284 (1993).

Author Index

Author Index

Author Index

Author Index